

CEREBRAL SMALL VESSEL DISEASES: FROM VESSEL ALTERATIONS TO CORTICAL PARENCHYMAL INJURY

EDITED BY: Andreas Charidimou, Eric Jouvent and Susanne J. Van Veluw
PUBLISHED IN: Frontiers in Neurology





frontiers

Frontiers eBook Copyright Statement

The copyright in the text of individual articles in this eBook is the property of their respective authors or their respective institutions or funders. The copyright in graphics and images within each article may be subject to copyright of other parties. In both cases this is subject to a license granted to Frontiers.

The compilation of articles constituting this eBook is the property of Frontiers.

Each article within this eBook, and the eBook itself, are published under the most recent version of the Creative Commons CC-BY licence.

The version current at the date of publication of this eBook is CC-BY 4.0. If the CC-BY licence is updated, the licence granted by Frontiers is automatically updated to the new version.

When exercising any right under the CC-BY licence, Frontiers must be attributed as the original publisher of the article or eBook, as applicable.

Authors have the responsibility of ensuring that any graphics or other materials which are the property of others may be included in the CC-BY licence, but this should be checked before relying on the CC-BY licence to reproduce those materials. Any copyright notices relating to those materials must be complied with.

Copyright and source acknowledgement notices may not be removed and must be displayed in any copy, derivative work or partial copy which includes the elements in question.

All copyright, and all rights therein, are protected by national and international copyright laws. The above represents a summary only. For further information please read Frontiers' Conditions for Website Use and Copyright Statement, and the applicable CC-BY licence.

ISSN 1664-8714

ISBN 978-2-88963-587-0

DOI 10.3389/978-2-88963-587-0

About Frontiers

Frontiers is more than just an open-access publisher of scholarly articles: it is a pioneering approach to the world of academia, radically improving the way scholarly research is managed. The grand vision of Frontiers is a world where all people have an equal opportunity to seek, share and generate knowledge. Frontiers provides immediate and permanent online open access to all its publications, but this alone is not enough to realize our grand goals.

Frontiers Journal Series

The Frontiers Journal Series is a multi-tier and interdisciplinary set of open-access, online journals, promising a paradigm shift from the current review, selection and dissemination processes in academic publishing. All Frontiers journals are driven by researchers for researchers; therefore, they constitute a service to the scholarly community. At the same time, the Frontiers Journal Series operates on a revolutionary invention, the tiered publishing system, initially addressing specific communities of scholars, and gradually climbing up to broader public understanding, thus serving the interests of the lay society, too.

Dedication to Quality

Each Frontiers article is a landmark of the highest quality, thanks to genuinely collaborative interactions between authors and review editors, who include some of the world's best academicians. Research must be certified by peers before entering a stream of knowledge that may eventually reach the public - and shape society; therefore, Frontiers only applies the most rigorous and unbiased reviews.

Frontiers revolutionizes research publishing by freely delivering the most outstanding research, evaluated with no bias from both the academic and social point of view. By applying the most advanced information technologies, Frontiers is catapulting scholarly publishing into a new generation.

What are Frontiers Research Topics?

Frontiers Research Topics are very popular trademarks of the Frontiers Journals Series: they are collections of at least ten articles, all centered on a particular subject. With their unique mix of varied contributions from Original Research to Review Articles, Frontiers Research Topics unify the most influential researchers, the latest key findings and historical advances in a hot research area! Find out more on how to host your own Frontiers Research Topic or contribute to one as an author by contacting the Frontiers Editorial Office: researchtopics@frontiersin.org

CEREBRAL SMALL VESSEL DISEASES: FROM VESSEL ALTERATIONS TO CORTICAL PARENCHYMAL INJURY

Topic Editors:

Andreas Charidimou, Massachusetts General Hospital, Harvard Medical School, United States

Eric Jouvent, Lariboisière Hospital, Assistance-Publique Hôpitaux de Paris and Université de Paris, France

Susanne J. Van Veluw, Massachusetts General Hospital, Harvard Medical School, United States

Citation: Charidimou, A., Jouvent, E., Van Veluw, S. J., eds. (2020). Cerebral Small Vessel Diseases: From Vessel Alterations to Cortical Parenchymal Injury. Lausanne: Frontiers Media SA. doi: 10.3389/978-2-88963-587-0

Table of Contents

- 05 Editorial: Cerebral Small Vessel Diseases: From Vessel Alterations to Cortical Parenchymal Injury**
Susanne J. van Veluw, Eric Jouvent and Andreas Charidimou
- 07 Spatial Signature of White Matter Hyperintensities in Stroke Patients**
Markus D. Schirmer, Anne-Katrin Giese, Panagiotis Fotiadis, Mark R. Etherton, Lisa Cloonan, Anand Viswanathan, Steven M. Greenberg, Ona Wu and Natalia S. Rost
- 17 Characterization of White Matter Hyperintensities in Large-Scale MRI-Studies**
Benedikt M. Frey, Marvin Petersen, Carola Mayer, Maximilian Schulz, Bastian Cheng and Götz Thomalla
- 33 The Altered Reconfiguration Pattern of Brain Modular Architecture Regulates Cognitive Function in Cerebral Small Vessel Disease**
Renyuan Liu, Haifeng Chen, Ruomeng Qin, Yucheng Gu, Xin Chen, Junhui Zou, YongCheng Jiang, Weikai Li, Feng Bai, Bing Zhang, Xiaoying Wang and Yun Xu
- 44 Decreased CSF Levels of β -Amyloid in Patients With Cortical Superficial Siderosis**
Cihan Catak, Marialuisa Zedde, Rainer Malik, Daniel Janowitz, Vivian Soric, Anna Seegerer, Alexander Krebs, Marco Düring, Christian Opherk, Jennifer Linn and Frank A. Wollenweber
- 51 Cortical Microinfarcts and White Matter Connectivity in Memory Clinic Patients**
Doeschka Ferro, Rutger Heinen, Bruno de Brito Robalo, Hugo Kuijf, Geert Jan Biessels, and Yael Reijmer On behalf of the Utrecht VCI study group
- 61 Basal Ganglia-Cortical Circuit Disruption in Subcortical Silent Lacunar Infarcts**
Haiyan Zhu, Wenxiao Wang, He Li, Kewei Chen, Peng Li, Xin Li, Junying Zhang, Dongfeng Wei and Yaojing Chen
- 70 Cerebral Small Vessel Disease and Enlarged Perivascular Spaces-Data From Memory Clinic and Population-Based Settings**
Bibek Gyanwali, Henri Vrooman, Narayanaswamy Venketasubramanian, Tien Yin Wong, Ching-Yu Cheng, Christopher Chen and Saima Hilal
- 78 HTRA1 Mutations Identified in Symptomatic Carriers Have the Property of Interfering the Trimer-Dependent Activation Cascade**
Masahiro Uemura, Hiroaki Nozaki, Akihide Koyama, Naoko Sakai, Shoichiro Ando, Masato Kanazawa, Taisuke Kato and Osamu Onodera
- 84 Effects of Isosorbide Mononitrate and/or Cilostazol on Hematological Markers, Platelet Function, and Hemodynamics in Patients With Lacunar Ischaemic Stroke: Safety Data From the Lacunar Intervention-1 (LACI-1) Trial**
Jason P. Appleton, Gordon W. Blair, Katie Flaherty, Zhe Kang Law, Jane May, Lisa J. Woodhouse, Fergus Doubal, Nikola Sprigg, Philip M. Bath and Joanna M. Wardlaw

- 90** *Alteration of the Cortex Shape as a Proxy of White Matter Swelling in Severe Cerebral Small Vessel Disease*
François De Guio, David Germanaud, Julien Lefèvre, Clara Fischer, Jean-François Mangin, Hugues Chabriat and Eric Jouvent
- 99** *Spatial Gradient of Microstructural Changes in Normal-Appearing White Matter in Tracts Affected by White Matter Hyperintensities in Older Age*
Susana Muñoz Maniega, Rozanna Meijboom, Francesca M. Chappell, Maria del C. Valdés Hernández, John M. Starr, Mark E. Bastin, Ian J. Deary and Joanna M. Wardlaw
- 113** *Total Small Vessel Disease Burden Predicts Functional Outcome in Patients With Acute Ischemic Stroke*
Ying-chao Huo, Qi Li, Wen-yu Zhang, Ning Zou, Rui Li, Si-yuan Huang, Hui-qi Wang, Kai-yi Song, Rong-rong Zhang and Xin-yue Qin
- 121** *Correlation Between the Number of Lenticulostriate Arteries and Imaging of Cerebral Small Vessel Disease*
Yuan-Chang Chen, Xiao-Er Wei, Jing Lu, Rui-Hua Qiao, Xue-Feng Shen and Yue-Hua Li
- 129** *Enlarged Perivascular Spaces and Cerebral Small Vessel Disease in Spontaneous Intracerebral Hemorrhage Patients*
Xin Wang, Hao Feng, Yu Wang, Jian Zhou and Xingquan Zhao
- 138** *Enhanced Effective Connectivity From Ipsilesional to Contralesional M1 in Well-Recovered Subcortical Stroke Patients*
Yanmin Peng, Jingchun Liu, Minghui Hua, Meng Liang and Chunshui Yu
- 146** *Cerebral Amyloid Angiopathy Related Inflammation With Prominent Meningeal Involvement. A Report of 2 Cases*
Agnès Aghetti, Damien Sène, Marc Polivka, Natalia Shor, Sarah Lechtman, Hugues Chabriat, Eric Jouvent and Stéphanie Guey
- 150** *Effects of Dabigatran in Mouse Models of Aging and Cerebral Amyloid Angiopathy*
Neethu Michael, Mher Mahoney Grigoryan, Kelley Kilday, Rachita K. Sumbria, Vitaly Vasilevko, Joanne van Ryn, David H. Cribbs, Annlia Paganini-Hill and Mark J. Fisher
- 158** *Underlying Small Vessel Disease Associated With Mixed Cerebral Microbleeds*
Clemence Blanc, Alain Viguier, Lionel Calviere, Mélanie Planton, Jean François Albucher, Vanessa Rousseau, Agnès Sommet, Fabrice Bonneville, Jérémie Pariente, Jean Marc Olivot and Nicolas Raposo
- 166** *Risk Profile of Ischemic Stroke Caused by Small-Artery Occlusion vs. Deep Intracerebral Hemorrhage*
Zimo Chen, Jinglin Mo, Jie Xu, Haiqiang Qin, Huaguang Zheng, Yuesong Pan, Xia Meng, Jing Jing, Xianglong Xiang and Yongjun Wang
- 174** *Application of an Imaging-Based Sum Score for Cerebral Amyloid Angiopathy to the General Population: Risk of Major Neurological Diseases and Mortality*
Pinar Yilmaz, Mohammad Arfan Ikram, Mohammad Kamran Ikram, Wiro J. Niessen, Anand Viswanathan, Andreas Charidimou and Meike W. Vernooij



Editorial: Cerebral Small Vessel Diseases: From Vessel Alterations to Cortical Parenchymal Injury

Susanne J. van Veluw^{1*}, Eric Jouvent^{2,3,4} and Andreas Charidimou^{1,5}

¹ Department of Neurology, Massachusetts General Hospital and Harvard Medical School, Boston, MA, United States,

² Department of Neurology, APHP, Lariboisière Hospital, Paris, France, ³ Univ Paris Diderot, Sorbonne Paris Cité, Paris, France, ⁴ UMR-S 1141 INSERM, Paris, France, ⁵ Boston Medical Center, Boston University, Boston, MA, United States

Keywords: small vessel disease, cerebral amyloid angiopathy, perivascular spaces, MRI, animal models

Editorial on the Research Topic

Cerebral Small Vessel Diseases: From Vessel Alterations to Cortical Parenchymal Injury

Cerebral small vessel disease (CSVD) encompasses a group of (mostly) age-related and vascular risk factor-driven processes affecting the small vessels of the brain. The two most common forms of CSVD are sporadic hypertension-related microangiopathies and cerebral amyloid angiopathy (CAA) (Aghetti et al.; Yilmaz et al.), which can both result in ischemic or hemorrhagic damage including clinically overt strokes (Blanc et al.; Chen Z. et al.; Wang et al.). During life, CSVD is recognized by its manifestations on magnetic resonance imaging (MRI) scans, including white matter hyperintensities, lacunes, cerebral microbleeds, microinfarcts, cortical superficial siderosis, and MRI-visible perivascular spaces (Yilmaz et al.; Appleton et al.; Chen Z. et al.; Catak et al.; Ferro et al.; Frey et al.; Gyanwali et al.; Muñoz Maniega et al.; Schirmer et al.). These manifestations of CSVD might collectively contribute to cognitive decline in older individuals (Huo et al.; Liu et al.; Yilmaz et al.). Currently, there are no specific therapies or prevention strategies that can slow down the progression of cognitive impairment in these patients. Some of the major existing challenges in the field, that have hampered the identification and development of therapeutic targets are the following: (1) conventional MRI does not capture the entire spectrum of CSVD manifestations nor does it directly show the smallest blood vessels in the brain, (2) the histopathological features underlying some of the CSVD manifestations on MRI are not fully understood, (3) it is unclear how changes to the small vessels result in parenchymal tissue injury either locally or in remote (including cortical) structures, and (4) it is poorly understood how CSVD manifestations contribute to clinical and cognitive deficits in older individuals (and appears context dependent). Recent advancements in neuroimaging techniques have fueled scientific research into these knowledge gaps. The aim of this topic was to bring together novel studies in this area, and to highlight different yet complementary approaches and techniques to advance our understanding of CSVD.

The large number of contributions made to this special issue underscores the growing interest in CSVD research, and at the same time the complexity of these processes. The studies covered a wide range of topics, between novel image analysis approaches and the identification of new neuroimaging signatures with relevance to CSVD (Chen Y. C. et al.; De Guio et al.; Frey et al.; Liu et al.; Muñoz Maniega et al.; Peng et al.), to the uncovering of etiologies and potential mechanisms underlying tissue injury (Blanc et al.; De Guio et al.; Ferro et al.; Uemura et al.; Zhu et al.). Notably, several contributions zoomed in on MRI-visible perivascular spaces, the spaces surrounding long penetrating arterioles of the brain (Gyanwali et al.; Huo et al.; Wang et al.; Yilmaz et al.). Perivascular spaces are believed to be related to clearance of waste products from the brain, and when enlarged, may implicate impaired perivascular drainage as a potential mechanism. In particular, impaired

OPEN ACCESS

Edited and reviewed by:

Jean-Claude Baron,
University of Cambridge,
United Kingdom

*Correspondence:

Susanne J. van Veluw
svanveluw@mgh.harvard.edu

Specialty section:

This article was submitted to
Stroke,
a section of the journal
Frontiers in Neurology

Received: 16 December 2019

Accepted: 27 January 2020

Published: 14 February 2020

Citation:

van Veluw SJ, Jouvent E and
Charidimou A (2020) Editorial:
Cerebral Small Vessel Diseases: From
Vessel Alterations to Cortical
Parenchymal Injury.
Front. Neurol. 11:92.
doi: 10.3389/fneur.2020.00092

perivascular clearance of Amyloid β from the cortex has been implicated in the pathophysiology of Alzheimer's disease and dementia. This pathway may therefore represent an interesting target to direct the development of therapeutic or prevention strategies. In this scenario, MRI-visible perivascular spaces may be a useful biomarker in future clinical trials. MRI-visible perivascular spaces in the basal ganglia have been linked to hypertension, whereas in the cerebral white matter (centrum semiovale) the presence of perivascular spaces suggests advanced CAA in the overlying cortex. Whether both patterns are related to faulty waste clearance from subcortical or cortical parts of the brain respectively, is currently not completely clear, and requires further experimental investigations (Wang et al.)

Despite some of the latest advancements in CSVD research, there is still a great unmet need for the development of better disease models for experimental studies to unravel the pathophysiological mechanisms involved in CSVD (Michael et al.) Due to the scarcity of relevant animal models to recapitulate several of the aspects of small vessel injury and

the formation of spontaneous lesions, we have an imperfect understanding of the disease pathways. Future studies are warranted to take on this challenge with the hope to bridge the gap from the bench to the bed side and improve clinical outcome in patients affected with CSVD.

AUTHOR CONTRIBUTIONS

SV drafted the editorial. EJ and AC made substantial revisions.

Conflict of Interest: The authors declare that the research was conducted in the absence of any commercial or financial relationships that could be construed as a potential conflict of interest.

Copyright © 2020 van Veluw, Jouvent and Charidimou. This is an open-access article distributed under the terms of the Creative Commons Attribution License (CC BY). The use, distribution or reproduction in other forums is permitted, provided the original author(s) and the copyright owner(s) are credited and that the original publication in this journal is cited, in accordance with accepted academic practice. No use, distribution or reproduction is permitted which does not comply with these terms.



Spatial Signature of White Matter Hyperintensities in Stroke Patients

Markus D. Schirmer^{1,2,3*}, Anne-Katrin Giese^{1,4}, Panagiotis Fotiadis¹, Mark R. Etherton¹, Lisa Cloonan¹, Anand Viswanathan¹, Steven M. Greenberg¹, Ona Wu⁵ and Natalia S. Rost¹

¹ Department of Neurology, Massachusetts General Hospital, Harvard Medical School, Boston, MA, United States,

² Computer Science and Artificial Intelligence Lab, MIT, Cambridge, MA, United States, ³ Department of Population Health Sciences, German Centre for Neurodegenerative Diseases (DZNE), Bonn, Germany, ⁴ Program in Medical and Population Genetics, Broad Institute of MIT and Harvard, Cambridge, MA, United States, ⁵ Department of Radiology, Athinoula A. Martinos Center for Biomedical Imaging, Massachusetts General Hospital, Boston, MA, United States

Purpose: White matter hyperintensity (WMH) is a common phenotype across a variety of neurological diseases, particularly prevalent in stroke patients; however, vascular territory dependent variation in WMH burden has not yet been identified. Here, we sought to investigate the spatial specificity of WMH burden in patients with acute ischemic stroke (AIS).

Materials and Methods: We created a novel age-appropriate high-resolution brain template and anatomically delineated the cerebral vascular territories. We used WMH masks derived from the clinical T2 Fluid Attenuated Inverse Recovery (FLAIR) MRI scans and spatial normalization of the template to discriminate between WMH volume within each subject's anterior cerebral artery (ACA), middle cerebral artery (MCA), and posterior cerebral artery (PCA) territories. Linear regression modeling including age, sex, common vascular risk factors, and TOAST stroke subtypes was used to assess for spatial specificity of WMH volume (WMHv) in a cohort of 882 AIS patients.

Results: Mean age of this cohort was 65.23 ± 14.79 years, 61.7% were male, 63.6% were hypertensive, 35.8% never smoked. Mean WMHv was 11.58 ± 13.49 cc. There were significant differences in territory-specific, relative to global, WMH burden. In contrast to PCA territory, age (0.018 ± 0.002 , $p < 0.001$) and small-vessel stroke subtype (0.212 ± 0.098 , $p < 0.001$) were associated with relative increase of WMH burden within the anterior (ACA and MCA) territories, whereas male sex (-0.275 ± 0.067 , $p < 0.001$) was associated with a relative decrease in WMHv.

Conclusions: Our data establish the spatial specificity of WMH distribution in relation to vascular territory and risk factor exposure in AIS patients and offer new insights into the underlying pathology.

Keywords: acute ischemic stroke, white matter hyperintensity, spatial, vascular territory, template

INTRODUCTION

White matter hyperintensity (WMH) is an important and widely studied radiographic phenotype (1). Even though WMH burden has been linked to both incidence and outcomes of stroke (2), spatial specificity of WMH has not been fully explored. WMH is commonly assessed on axial T2 Fluid Attenuated Inverse Recovery (FLAIR) magnetic resonance (MR) images and total WMH

OPEN ACCESS

Edited by:

Eric Jouvent,
Université Sorbonne Paris Cité, France

Reviewed by:

Saima Hilal,
Erasmus University Rotterdam,
Netherlands
Richard Beare,
Monash University, Australia
Laurent Puy,
Centre Hospitalier Régional et
Universitaire de Lille, France

*Correspondence:

Markus D. Schirmer
mschirmer1@mgh.harvard.edu

Specialty section:

This article was submitted to
Stroke,
a section of the journal
Frontiers in Neurology

Received: 30 October 2018

Accepted: 18 February 2019

Published: 19 March 2019

Citation:

Schirmer MD, Giese A-K, Fotiadis P,
Etherton MR, Cloonan L,
Viswanathan A, Greenberg SM, Wu O
and Rost NS (2019) Spatial Signature
of White Matter Hyperintensities in
Stroke Patients. *Front. Neurol.* 10:208.
doi: 10.3389/fneur.2019.00208

burden can be summarized as WMH volume (WMHv) (1–3). Importantly, it has been shown, that WMHv presents an accurate and uniform way of quantifying this phenotype in clinical populations, such as acute ischemic stroke (AIS) patients (4). However, summarizing the burden on such a high level, i.e., total WMHv, eliminates potential spatial specificity, which in turn may provide insight with regard to underlying vascular pathology and disease progression.

While other studies have explored spatial WMH patterns in diseased and healthy populations (5–7), prior studies exploring the extent of WMH on a voxel-based level in AIS patients with respect to varying risk factors, such as hypertension (8), were limited due to high dimensionality. For WMH, as a prototypical small vessel disease (9), a spatial differentiation may be based on supplying arteries, as previously established for stroke lesions (10). In the human brain, we distinguish between the anterior and posterior circulation. The anterior supratentorial circulation is comprised of the anterior (ACA) and middle cerebral artery (MCA), while the posterior cerebral artery (PCA) supplies the posterior supratentorial vascular area. Infratentorial structures receive their blood supply through the posterior circulation. Moreover, large-scale analysis of WMH burden for each vascular territory is limited, as manual assessment and differentiation of individual vascular territories is time consuming and results in inter-rater variations.

In general, medical image analysis is prone to inter-subject variability. It is common practice to reduce this variability by normalizing images to a common coordinate system (11). In addition to allowing reproducible assessment of disease phenotypes across subjects with respect to their spatial location, it furthermore allows comparison across studies. Moreover, computational costs can be reduced by utilizing prior information such as brain or tissue segmentation. However, for WMH analysis in AIS patients, an age-appropriate T2 FLAIR template for spatial normalization with outlined vascular territories is currently missing.

Here, we examined the distribution of WMH, differentiated by supratentorial cerebral vascular territories in clinically acquired axial T2 FLAIR images of patients with AIS. In order to assess spatial distribution, we first created an age appropriate brain template, including T1, T2, and 3D-FLAIR sequences based on high-resolution MR images, and delineate all 5 bi-lateral vascular territories. We utilized these vascular territories, by spatially normalizing each subject's axial T2 FLAIR image to the 3D-FLAIR template. Finally, we investigated WMHv for each of the supratentorial vascular territories with respect to the common clinical WMH risk factors, while accounting for territory size, in a multivariate analysis.

MATERIALS AND METHODS

Study Design and Patient Population

Patients were enrolled as part of the Genes Associated with Stroke Risk and Outcomes Study (GASROS) between 2003 and 2011 (4). Patients presenting to the Massachusetts General Hospital Emergency Department (ED) within 12 h of AIS symptom onset and who were >18 years of age, were eligible

TABLE 1 | Study cohort characterization. Smoking is assessed based on past or current history of smoking (ever/never).

	AIS
<i>n</i>	882
Age (mean (sd); <i>n</i> missing)	65.23 (14.79; 4)
Sex = Male (%; <i>n</i> missing)	542 (61.7; 4)
Smoking (%; <i>n</i> missing)	559 (64.2; 11)
HTN (%; <i>n</i> missing)	558 (63.6; 5)
DM2 (%; <i>n</i> missing)	173 (19.7; 5)
HLD (%; <i>n</i> missing)	362 (41.3; 5)
SV (%; <i>n</i> missing)	85 (11.8; 162)
CE (%; <i>n</i> missing)	263 (36.5; 162)
LA (%; <i>n</i> missing)	164 (22.8; 162)
Other (%; <i>n</i> missing)	167 (23.2; 162)
TIA (%; <i>n</i> missing)	68 (7.8; 6)
Prior stroke (%; <i>n</i> missing)	138 (15.7; 4)
WMHv (mean (sd); <i>n</i> missing)	11.58 (13.49)
DWIv (mean (sd); <i>n</i> missing)	13.52 (28.61; 238)

to enroll. Each patient was evaluated by a vascular neurologist and clinical variables, including age, sex, common vascular risk factors (history of hypertension (HTN), diabetes mellitus (DM2), hyperlipidemia (HLD), tobacco smoking), and TOAST stroke subtypes [CE: cardioembolic, LA: large-artery atherosclerosis, SV: small-vessel occlusion, Other: other determined etiology; (12)] were recorded. Each patient underwent standard clinical imaging protocol within 48 h of admission, including axial T2 FLAIR imaging (TR 5,000 ms, minimum TE of 62 to 116 ms, TI 2,200 ms, FOV 220–240 mm). This study was carried out in accordance with the recommendations of Partners Institutional Review Board with written informed consent from all subjects. All subjects gave written informed consent in accordance with the Declaration of Helsinki. The protocol was approved by the Partners Institutional Review Board.

We identified 882 subjects with manual WMH outlines (4) and most complete phenotypic information available for this analysis (Table 1). Manual WMH outlines were performed using MRICro software for computer-assisted determination of WMHv (9). Maps were created using axial T2 FLAIR sequences, based on a previously published semi-automated method with high inter-rater reliability (13). Each subject's DWI sequence was utilized to exclude acute ischemia, edema, and chronic infarcts. Additionally, out of the 882 subjects with confirmed DWI lesions, 586 subjects had lesions manually outlined, using a semi-automated algorithm (14), by reader blinded to the admission stroke severity and 90-day outcome, measured by the modified Rankin Scale.

In addition to the AIS cohort, 16 subjects were recruited between 2016 and 2017 at Massachusetts General Hospital, to generate a high-resolution template. The template cohort selection aimed to match characteristics (age and sex) of the elderly adults presenting to the ED with pre-existing cerebrovascular pathology and incident AIS. Twelve stroke-free, non-demented patients with the sporadic form

of cerebral amyloid angiopathy (CAA), a known cerebral small vessel disorder and similarly-aged healthy controls ($n = 4$) underwent high-resolution MRI as part of a separate study at our hospital. MR scans were manually assessed to exonerate any gross pathology, such as hemorrhage or silent brain infarcts.

High-resolution structural brain MRI sequences were acquired with a Siemens Magnetom Prisma 3T scanner (using a 32-channel head coil). The standardized protocol included a Multiecho T1-weighted (voxel size: $1 \times 1 \times 1 \text{ mm}^3$; Repetition Time [TR]: 2,510 ms), a 3D-FLAIR (voxel size: $0.9 \times 0.9 \times 0.9 \text{ mm}^3$; TR: 5,000 ms; TE: 356 ms), and a T2-weighted Turbo Spin Echo (voxel size: $0.5 \times 0.5 \times 2.0 \text{ mm}^3$; TR: 7,500 ms; TE: 84 ms) sequence.

Template Creation

We employed Advanced Normalization Tools (ANTs) for image processing, a well-established tool for image registration and template creation (15, 16). Utilizing the 16 high-resolution images, we created a brain template based on multimodal information using T1, T2, and 3D-FLAIR sequences. After template creation was completed, and due to the relatively low number of subjects, we smoothed the resulting templates (FSL; Gaussian smoothing, $\sigma = 1$). Finally, we registered the resulting templates into MNI space using ANTs (16).

Additionally, manual brain extraction was performed on all subjects based on their 3D-FLAIR sequences. Binary manual masks were warped into template space and averaged. For each voxel, majority voting was performed and an average brain mask was generated based on the voxels where more than

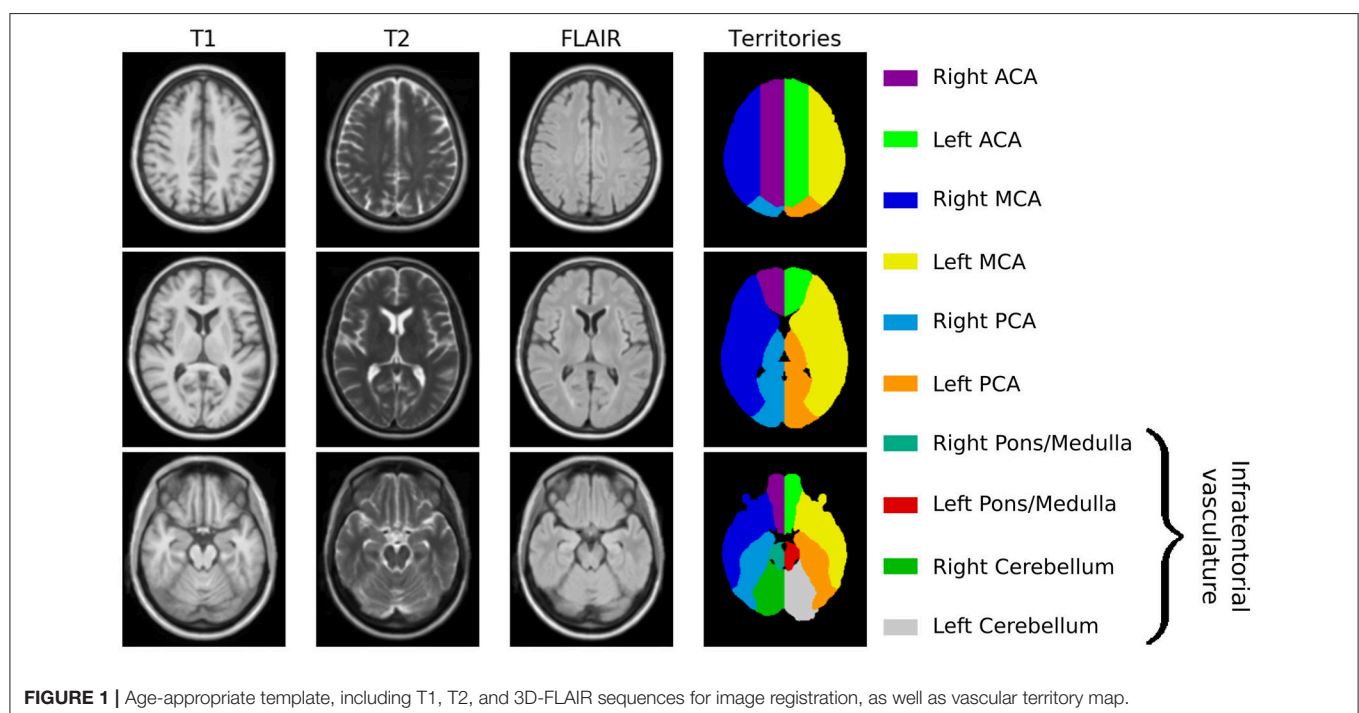
50% of the subjects agreed, providing an initial brain mask, which was manually assessed and corrected on a per-slice basis where necessary.

Vascular territories were outlined on the right hemisphere in the T1-weighted atlas image by an expert neurologist (A.K.G.). Vascular territories included anatomically validated ACA, MCA, and PCA territories supratentorially. We also created the anterior territory (ANT), a combined ACA and MCA territory named after the “anterior” circulation vs. “posterior” supratentorial circulation supplied by the PCA. The outline was then mirrored onto the left hemisphere and subsequently combined to create a full-brain vascular territory map. This map was manually assessed and corrected where necessary. Additionally, WMHv and ventricular size were manually determined on the atlas, to ensure that the template is representative of subjects in this age category.

Neuroimage Analysis of WMH Burden

Each axial T2 FLAIR image was first skull-stripped using an in-house skull-stripper for clinical quality scans (17) and then non-linearly registered to the high-resolution 3D-FLAIR template using ANTs (16). Subsequently, the vascular territory map was warped into subject space, allowing us to calculate both the volume of each vascular territory in subject space, as well as the WMH burden for each territory. Finally, we normalized each territorial WMHv by the total WMHv, to describe a relative burden per territory (WMHv_{rel}).

Each subject's vascular territory map was manually assessed for gross registration errors, such as midline shift. Furthermore, we identified potential outliers using the modified z-score (18) for each set of territorial volumes of the cohort. Subjects with



registration errors and those deemed outliers were removed from analysis.

Additionally, we registered all 586 subjects non-linearly with manual DWI lesion outlines to the 3D-FLAIR template. This allowed us, with the addition of WMH outlines being mapped to the same template, to create incidence maps of both the chronic WMH disease burden, as well as the acute lesion locations.

Statistical Analysis

First, we transformed the relative WMH disease burden in each territory using a logit transformation, to avoid potential issues due to the response variables in the models being bound between 0 and 1. We then assessed WMH burden for each territory based on a univariate analysis, where each phenotype was used in a linear model (continuous) or Mann-Whitney U test (categorical) for each of the transformed relative WMH burden. This was followed by a multivariate analysis, where all factors were included in the model,

given by

$$\text{WMH}_{\text{rel}} \sim \text{Age} + V_{\text{terr}} + \text{Sex} + \text{SV} + \text{CE} + \text{LA} + \text{Other} + \text{DM2} + \text{HLD} + \text{HTN} + \text{Smoking}, \quad (1)$$

including age, volume of the territory in subject space (V_{terr}), sex, TOAST subtypes (yes/no) (including SV, LA, CE, Other), DM2, HLD, HTN, and smoking (ever/never) status. The undetermined TOAST subgroup was not investigated in this analysis. To reduce the statistical burden of utilizing 11 independent variables in the model, we used a backward selection approach to simultaneously refine all 4 territorial models, i.e., MCA, ACA, PCA, and ANT, by removing the variable with the highest p -value above 0.1 iteratively, where p -values were summarized as the minimum p -value for the variable across the models.

As a comparison, we also investigate the efficacy of this model, compared to a baseline model, where the WMH_{rel} is solely explained by V_{terr} , given by

$$\text{WMH}_{\text{rel}} \sim V_{\text{terr}}. \quad (2)$$

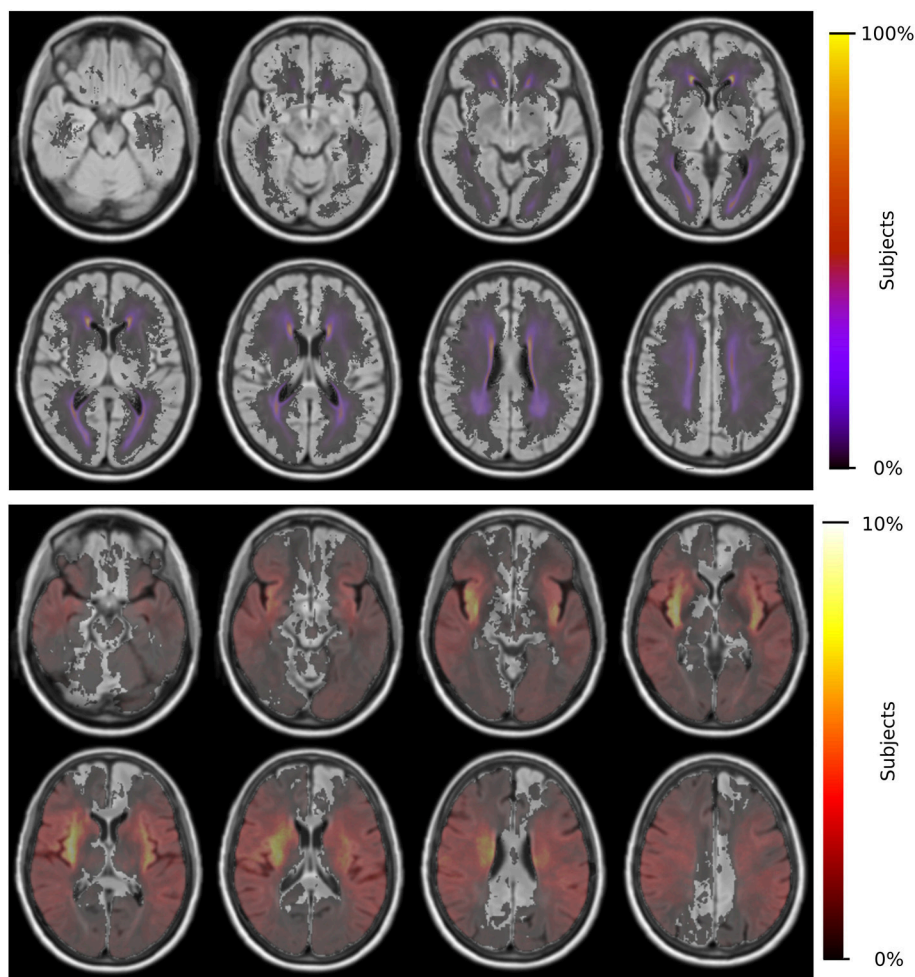
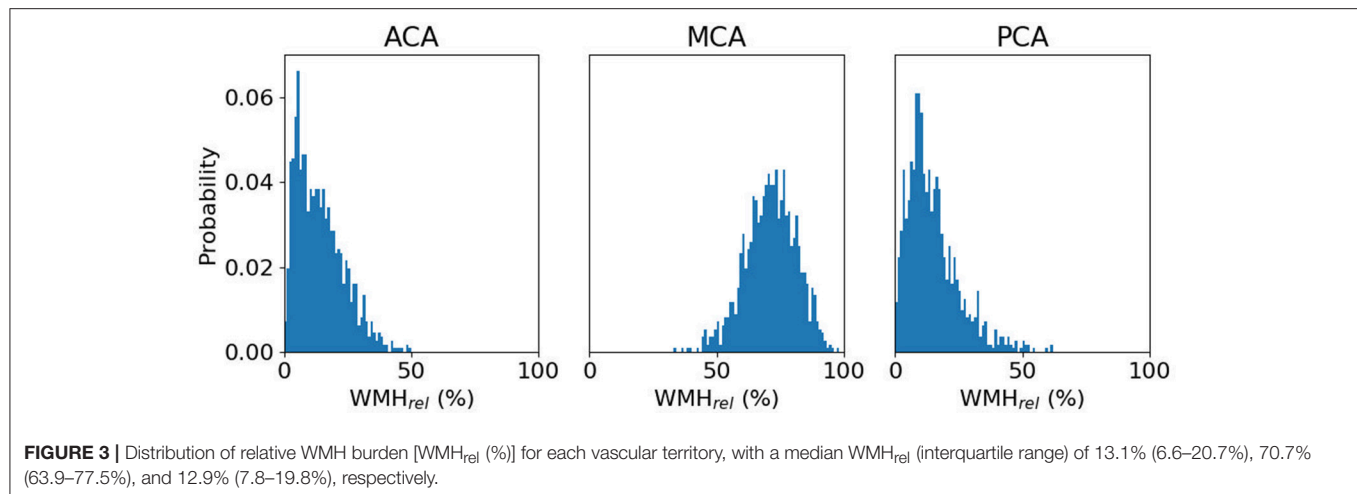


FIGURE 2 | Distributions of WMH burden (top) and acute lesion location (bottom) for 865 patients and 586 patients, respectively.



Both models are compared using a χ^2 test.

Statistical analysis was conducted using the computing environment R (19).

Data Availability

The utilized template will be made available upon acceptance to facilitate reproducibility of our findings. The authors agree to make available to any researcher the data, methods used in the analysis, and materials used to conduct the research for the express purposes of reproducing the results and with the explicit permission for data sharing by the local institutional review board.

RESULTS

Template and Territorial Map

Utilizing ANTs, we created a multimodal template from the 16 subjects with high-resolution MR images. **Figure 1** shows axial slices of the T1, T2, and 3D-FLAIR template, after registration to MNI space. Additionally, it shows the vascular territory map, which was delineated on the template's T1 sequence. Within this template, WMH and ventricular volume were manually assessed, with 13.2cc and 34.4cc, respectively.

Neuroimage Analysis of WMH Burden

Final Cohort and Territorial WMH Burden Characterization

Each subject is non-linearly registered to the 3D-FLAIR template and the vascular territory map transformed into low-resolution subject space. We assessed each subject for registration errors, leading to 17 subjects being excluded. Utilizing the modified z-score for each territory's volumes did not lead to further exclusions. Registering the DWI volumes to the 3D-FLAIR template did not lead to any of the 586 subjects being excluded. **Figure 2** shows the spatial distribution of WMH burden and acute lesion location within the template.

For the remaining 865 subjects with WMH outlines, ACA, MCA and PCA volumes (mean \pm standard deviation) were estimated to be 334.7 ± 40.7 cc, 671.5 ± 79.8 cc, and $253.9 \pm$

31.9cc, respectively. WMHv within each of the bi-lateral ACA, MCA, and PCA territories were calculated for each subject and normalized by the subject's total WMHv, resulting in a relative WMHv_{rel} for each territory. **Figure 3** shows WMHv_{rel} for each vascular territory. Additionally, we combined both ACA and MCA to represent the combined anterior (ANT) territory. Out of the remaining 865 subjects, 162 did not have a stroke subtype classification available and were subsequently excluded from analysis.

Clinical Determinants of Territorial WMHv: Univariate Analysis

Univariate analysis showed that age and territorial volume were significant correlates of relative WMH burden for all territories ($p < 0.001$), while only HTN and sex (male) were found significant for ACA, PCA, and ANT territories ($p \leq 0.001$). **Table 2** includes the complete set of univariate analyses.

Clinical Determinants of Territorial WMHv: Multivariate Analysis

10/30/18 2:57:00 PMWe used the relative WMH burden as dependent variable and estimated the model parameters of the linear model, given by equation (1). This led to the removal (p -values for MCA, ACA, PCA, and ANT, respectively) of territorial volume ($p = 0.615, 0.813, 0.583, 0.974$), CE ($p = 0.565, 0.506, 0.982, 0.982$), LA ($p = 0.817, 0.813, 1.000, 1.000$), other ($p = 0.418, 0.787, 0.497, 0.497$), and diabetes ($p = 0.708, 0.199, 0.877, 0.877$), refining the model to

$$WMH_{v_{rel}} \sim Age + SV + HTN + Sex + HLD + Smoking. \quad (3)$$

The results are summarized in **Table 3** and diagnostic regression plots are shown in **Figure 4**. These results show that each phenotype modulates individual aspects of the spatial patterns of WMH burden in our cohort. In the ACA territory, age, SV stroke subtype, hypertensive status, HLD, and smoking were found statistically significant, where HLD decrease the relative burden in ACA. The only phenotype found statistically significant in MCA is age, where an increase in age is associated

with the relatively lower WMH burden in MCA. All phenotypes, except for hypertensive status, HLD, and smoking, were found statistically significant in PCA, as well as ANT.

Assumptions of the linear models, i.e., mean residual equals 0, no correlation between residuals and dependent variables, positive variability, homoscedasticity, and no multicollinearity (defined as variance inflation factors <2), were fulfilled. However, autocorrelation of the residuals was significant for MCA, PCA, and ANT models. By removing the influential data points for the model fit using Cook's distance for outlier detection (threshold 4/703), we identified 81 subjects (see **Table 4**) significantly younger and with larger WMH burden in the MCA territory. All assumptions for the linear models were fulfilled after removal of these subjects. **Table 5** summarizes the difference in model fit before and after exclusion of the 81 subjects, showing a loss of significance in the stroke subtype for all models, and reveals significance of sex (male) in the ACA territory, as well as hypertensive status and hyperlipidemia in the PCA and ANT territories.

TABLE 2 | Univariate analysis of phenotypes with respect to relative WMH burden for each territory.

	MCA	<i>p</i>	ACA	<i>p</i>	PCA	<i>p</i>	ANT	<i>p</i>
Age	0.013	<0.001	-0.028	<0.001	-0.030	<0.001	0.030	<0.001
V _{terr}	0.001	<0.001	-0.006	<0.001	-0.008	<0.001	0.002	<0.001
SV	-0.012	0.620	-0.094	0.435	0.149	0.204	-0.149	0.204
CE	0.005	0.863	0.011	0.742	-0.011	0.942	0.011	0.942
LA	-0.019	0.899	-0.035	0.717	-0.004	0.858	0.004	0.858
Other	0.063	0.099	-0.099	0.089	0.011	0.958	-0.011	0.958
HTN	0.065	0.086	-0.486	<0.001	0.320	<0.001	-0.320	<0.001
Sex (male)	0.031	0.470	0.218	0.001	-0.347	<0.001	0.347	<0.001
DM2	0.009	0.897	-0.092	0.420	0.006	0.994	-0.006	0.994
HLD	-0.010	0.927	-0.029	0.724	0.019	0.642	-0.019	0.642
Smoking	-0.002	0.722	-0.089	0.377	-0.016	0.946	0.016	0.946

Continuous variables were assessed using a linear model (reported beta and *p*-value), whereas categorical variables (maximum of two categories per variable) were assessed using a Mann-Whitney U Test (reported differences of the mean and *p*-value). Statistically significant correlations ($p < 0.05$) are shown in bold.

Comparing the models summarized in **Table 3** to their corresponding baseline models given by equation (2), we find that the reduction of residual deviation of the observed data is statistically significant in each case ($p < 0.001$).

DISCUSSION

In this work, we investigated the relative WMH disease burden per established cerebral vascular territory in AIS patients and how it is affected by common vascular risk factors, including age and sex. To allow automated characterization of WMH burden per vascular territory, we introduced an age-appropriate template with a 3D-FLAIR sequence for registration. Both WMH and ventricular volume of the template were representative of the disease burden in our AIS cohort and ventricular size of that found in healthy elderly (20). Moreover, this template allowed us to delineate vascular territories. We used this territorial map to elucidate relative spatial WMHv distributions in 865 patients with clinical 3D-FLAIR sequences, while accounting for size differences in the vascular territories.

Spatially specific effects of each investigated phenotype were identified in our cohort. Age shows a relative increase in the ACA and ANT with a relative decrease in the MCA and PCA territories. Age is known to be one of the most robust predictors of the overall WMH burden (4). Our data suggest furthermore that an effect between the anterior and posterior vascular territory exists, where older patients accumulate more WMH burden in the ACA territory. A similar, but greater effect can be observed in case of patients with small-vessel stroke subtypes. While the exact biology of the underlying disease processes that drive these differences is unclear, spatial pathology distribution differences with posterior predominance were noted in patients with genetically defined small-vessel disease phenotypes such as CAA (21, 22), which manifest early as impaired vascular reactivity and later as WMH and cerebral microbleeds. In these patient populations enriched for specific genetic mutations, small vessel dysfunction occurs early in life and appears to affect posterior circulation vessels first. Anterior circulation preponderance of the WMH burden seen in our study may imply that, by the time these

TABLE 3 | Parameter estimate for the linear model fit using R.

	ACA		MCA		PCA		ANT	
	Estimate	<i>p</i>	Estimate	<i>p</i>	Estimate	<i>p</i>	Estimate	<i>p</i>
Intercept	-4.340 ± 0.136	<0.001	1.423 ± 0.098	<0.001	-0.825 ± 0.163	<0.001	0.825 ± 0.163	<0.001
Age	0.034 ± 0.002	<0.001	-0.007 ± 0.001	<0.001	-0.018 ± 0.002	<0.001	0.018 ± 0.002	<0.001
SV	0.171 ± 0.082	0.037	0.007 ± 0.059	0.910	-0.212 ± 0.098	0.031	0.212 ± 0.098	0.031
HTN	0.191 ± 0.061	0.002	-0.011 ± 0.044	0.811	-0.138 ± 0.073	0.061	0.138 ± 0.073	0.061
Sex (male)	-0.085 ± 0.056	0.127	-0.066 ± 0.040	0.099	0.275 ± 0.067	<0.001	-0.275 ± 0.067	<0.001
HLD	-0.183 ± 0.057	0.001	0.046 ± 0.041	0.258	0.098 ± 0.068	0.149	-0.098 ± 0.068	0.149
Smoking	0.153 ± 0.056	0.007	0.005 ± 0.041	0.900	-0.064 ± 0.068	0.341	0.064 ± 0.068	0.341

Statistically significant parameters ($p < 0.05$) are highlighted.

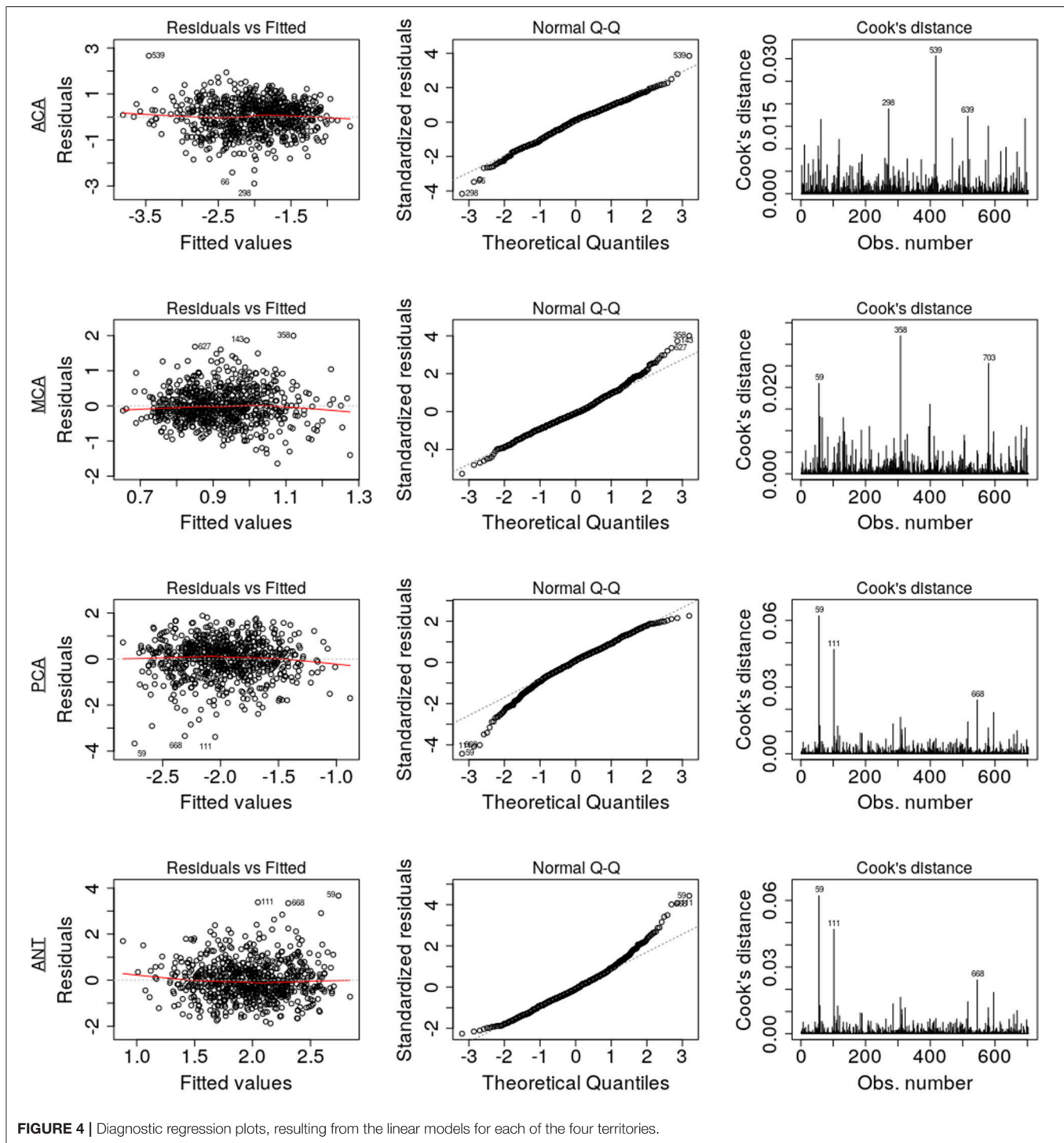


FIGURE 4 | Diagnostic regression plots, resulting from the linear models for each of the four territories.

patients present with a symptomatic event, their sporadic cerebral microangiopathy is diffuse and without predilection for posterior territory.

Smoking status shows a modifying effect on WMH burden with a relative increase in the ACA territory alone. Ghatan et al. (23) observed a reduced regional cerebral blood flow in the anterior cingulate cortex, among other

regions. While there are no definite explanations as to the cause of the increased WMH burden yet, our findings, combined with those of Ghatan et al. may suggest chronic ischemia related to smoking leading to leukoaraiosis (24). Sex (male) demonstrated the opposite effect, where larger relative burden were found in the posterior territory, similar but to a lesser extent than that of hyperlipidemia. There

are no known biological mechanisms yet to explain these spatial differences.

In addition to smoking, hypertensive status shows an increase of relative WMH burden in the ACA territory, while a corresponding increase in ANT and decrease in the PCA territory only appeared after the subset analysis. There was no effect on the MCA territory, implying that the effect is driven by the spatial distribution of WMH in the ACA territory predominantly. The general lack of significance in modifying risk factors in MCA may be the result of the stroke lesions being predominantly in the MCA territory, thereby introducing uncertainty in identifying underlying disease burden (see **Figure 2**). The difference between ACA and PCA, however, may be due to differences between the small vessel architecture in both territories. Detailed investigations into those differences are urgently needed.

TABLE 4 | Characteristics of excluded subjects based on Cook's distance threshold (4/703), compared to the remainder (included; significant differences in bold).

	Excluded	Included	p
n	81	622	
Age [mean (sd)]	58.22 (15.74)	65.83 (14.09)	<0.001
MCA_vol [mean (sd)]	682.13 (70.07)	671.00 (75.48)	0.209
MCA [mean (sd)]	1.22 (0.88)	0.88 (0.43)	<0.001
ACA_vol [mean (sd)]	338.47 (34.89)	334.04 (38.91)	0.331
ACA [mean (sd)]	-2.61 (1.20)	-1.94 (0.79)	<0.001
PCA_vol [mean (sd)]	255.55 (29.45)	253.96 (30.34)	0.655
PCA [mean (sd)]	-2.45 (1.57)	-1.91 (0.75)	<0.001
ANT_vol [mean (sd)]	1,020.60 (102.57)	1,005.05 (112.83)	0.239
ANT [mean (sd)]	2.45 (1.57)	1.91 (0.75)	<0.001
SV (%)	22 (27.2)	62 (10.0)	<0.001
CE (%)	29 (35.8)	226 (36.3)	1
LA (%)	15 (18.5)	148 (23.8)	0.358
Other (%)	11 (13.6)	151 (24.3)	0.044
HTN (%)	43 (53.1)	409 (65.8)	0.034
Sex (%)	47 (58.0)	386 (62.1)	0.562
DM2 (%)	13 (16.0)	123 (19.8)	0.516
HLD (%)	33 (40.7)	258 (41.5)	0.994
Tobacco (%)	46 (56.8)	412 (66.2)	0.12

TABLE 5 | Parameter comparison of those significant (bold) in at least one of the four models using the full data set and the subset, after 81 had been excluded based on Cook's distance.

	ACA		MCA		PCA		ANT	
	Full	Subset	Full	Subset	Full	Subset	Full	Subset
Intercept	-4.340 ± 0.136	-4.330 ± 0.127	1.423 ± 0.098	1.443 ± 0.089	-0.825 ± 0.163	-0.765 ± 0.148	0.825 ± 0.163	0.765 ± 0.148
Age	0.034 ± 0.002	0.035 ± 0.002	-0.007 ± 0.001	-0.009 ± 0.001	-0.018 ± 0.002	-0.018 ± 0.002	0.018 ± 0.002	0.018 ± 0.002
SV	0.171 ± 0.082	0.116 ± 0.079	—	—	-0.212 ± 0.098	-0.090 ± 0.093	0.212 ± 0.098	0.090 ± 0.093
HTN	0.191 ± 0.061	0.181 ± 0.055	—	—	-0.138 ± 0.073	-0.168 ± 0.064	0.138 ± 0.073	0.168 ± 0.064
Sex (male)	-0.085 ± 0.056	-0.134 ± 0.050	—	—	0.275 ± 0.067	0.226 ± 0.059	-0.275 ± 0.067	-0.226 ± 0.059
HLD	-0.183 ± 0.057	-0.163 ± 0.050	—	—	0.098 ± 0.068	0.124 ± 0.059	-0.098 ± 0.068	-0.124 ± 0.059
Smoking	0.153 ± 0.056	0.159 ± 0.051	—	—	—	—	—	—

There are several limitations to our study. In general, spatial normalization of clinical low-resolution images is a non-trivial task, in particular in AIS patients, where biological responses to stroke, such as mass effects, can play an important role. In this study, we manually assessed the registration, leading to 17 subjects being excluded from final analysis due to gross registration errors. Nonetheless, small registration errors may be important for assessing WMHv within vascular territories. However, using an age-appropriate FLAIR template is a first step to mitigate the resulting uncertainties. Furthermore, using the template developed from MRI scans of age- and sex-matched individuals, who are stroke-free but with known intrinsic cerebrovascular pathology (CAA), has its advantage due its similarity to the average stroke patient brain. Although we demonstrated spatially discriminative changes of relative WMH burden, the underlying etiology needs to be further elucidated. In fact, accounting for common vascular risk factors that contribute to various ischemic stroke subtypes as well as adjusting for these TOAST subtypes further narrowed down pathophysiological contributions to WMH burden accumulation in the anterior vs. posterior circulation. By removing influential data points before model fit we demonstrated the consistency of the presented trends. The majority of model parameters before and after excluding the 81 subjects from analysis fall within one standard deviation of another. However, small vessel occlusion become non-significant, whereas sex (ACA model), HTN (PCA and ANT model), and HLD (PCA and ANT model) become significant. While removing influential data points before model fit can bias the data, our results suggest that the risk factors with changing levels of significance should be interpreted with care. An additional limitation to our study was the lack of phenotype availability as related to other characteristics of small vessel disease such as chronic lacunes, cerebral microrbleeds, and dilated perivascular spaces. Future use of these phenotypes may further characterize underlying brain pathology that contributes to variability in WMH accumulation by vascular territories and other anatomical distributions. While beyond the scope of this work, additional investigation into the capillary densities and networks of each vascular territory would also further this line of research. Another promising direction to delineate underlying WMH pathologies is to assess the effect of territorial mapping to border zone ("watershed") areas between ACA-MCA and MCA-PCA

territories. Given the hypothesis of diminished cerebral blood flow contribution to pathophysiology of WMH, a future study that develops and validates a concept of border zone through pathological-radiographic correlation would provide further insights on the role of chronic hypoxia-hypoperfusion etiology of WMH.

Other types of analyses will also be considered in future work. One promising, hypothesis free approach is the use of voxel-based lesion symptom mapping. While such analysis may reveal interesting correlates of the presentation of WMH in our cohort, its hypothesis free nature makes it difficult to directly interpret the results. By relying on a hypothesis-driven approach in this analysis, however, we are able to attribute the WMH burden to the individual supplying arteries.

The strengths of this analysis include (a) development of a novel FLAIR-based vascular territory template for clinical image registration in patients with stroke; (b) utilization of a large, thoroughly ascertained hospital-based cohort of AIS patients with detailed neuroimaging analysis; and (c) use of the validated methodologies for image processing and analysis.

In this work, we demonstrated that vascular risk factors influence spatial specificity of WMH, one of the most important radiographic manifestations of chronic cerebral ischemia. Here, we illustrated that WMH burden does not develop homogeneously throughout the supratentorial brain. These findings of spatial specificity of WMH in relation to vascular territory and risk factor exposure in AIS patients open the path for new investigations into underlying pathology of this common vascular disease and its associated risk factors, and ultimately into its connection with stroke.

REFERENCES

- Debette S, Markus HS. The clinical importance of white matter hyperintensities on brain magnetic resonance imaging: systematic review and meta-analysis. *BMJ*. (2010) 341:c3666. doi: 10.1136/bmj.c3666
- Kuller LH, Longstreth WT, Arnold AM, Bernick C, Bryan RN, Beauchamp NJ. White matter hyperintensity on cranial magnetic resonance imaging: a predictor of stroke. *Stroke*. (2004) 35:1821–5. doi: 10.1161/01.STR.0000132193.35955.69
- Giese A-K, Schirmer MD, Donahue KL, Cloonan L, Irie R, Winzeck S, et al. Design and rationale for examining neuroimaging genetics in ischemic stroke The MRI-GENIE study. *Neurol Genet*. (2017) 3:e180. doi: 10.1212/NXG.0000000000000180
- Zhang CR, Cloonan L, Fitzpatrick KM, Kanakis AS, Ayres AM, Furie KL, et al. Determinants of white matter hyperintensity burden differ at the extremes of ages of ischemic stroke onset. *J Stroke Cerebrovasc Dis*. (2015) 24:649–54. doi: 10.1016/j.jstrokecerebrovasdis.2014.10.016
- Griffanti L, Jenkinson M, Suri S, Soldos E, Mahmood A, Filippini N, et al. Classification and characterization of periventricular and deep white matter hyperintensities on MRI: a study in older adults. *NeuroImage*. (2017) 170:174–81. doi: 10.1016/j.neuroimage.2017.03.024
- Holland CM, Smith EE, Csapo I, Gurol ME, Brylka DA, Killiany RJ, et al. Spatial distribution of white-matter hyperintensities in Alzheimer disease, cerebral amyloid angiopathy, and healthy aging. *Stroke*. (2008) 39:1127–33. doi: 10.1161/STROKEAHA.107.497438
- Kim KW, MacFall JR, Payne ME. Classification of white matter lesions on magnetic resonance imaging in elderly persons. *Biol Psychiatry*. (2008) 64:273–80. doi: 10.1016/j.biopsych.2008.03.024
- Yoshita M, Fletcher E, Harvey D, Ortega M, Martinez O, Mungas DM, et al. Extent and distribution of white matter hyperintensities in normal aging, MCI, and AD. *Neurology*. (2006) 67:2192–8. doi: 10.1212/01.wnl.0000249119.95747.1f
- Rost NS, Rahman RM, Biffi A, Smith EE, Kanakis A, Fitzpatrick K, et al. White matter hyperintensity volume is increased in small vessel stroke subtypes. *Neurology*. (2010) 75:1670–7. doi: 10.1212/WNL.0b013e3181fc279a
- Ng YS, Stein J, Ning M, Black-Schaffer RM. Comparison of clinical characteristics and functional outcomes of ischemic stroke in different vascular territories. *Stroke*. (2007) 38:2309–14. doi: 10.1161/STROKEAHA.106.475483
- Mandal PK, Mahajan R, Dinov ID. Structural brain atlases: design, rationale, and applications in normal and pathological cohorts. *J Alzheimers Dis*. (2012) 31:S169–S188. doi: 10.3233/JAD-2012-120412
- Adams HP, Bendixen BH, Kappelle LJ, Biller J, Love BB, Gordon DL, et al. Classification of subtype of acute ischemic stroke. Definitions for use in a multicenter clinical trial. TOAST. Trial of Org 10172 in Acute Stroke Treatment. *Stroke*. (1993) 24:35–41. doi: 10.1161/01.STR.24.1.35
- Chen YW, Gurol ME, Rosand J, Viswanathan A, Rakich SM, Groover TR, et al. Progression of white matter lesions and hemorrhages in cerebral amyloid angiopathy. *Neurology*. (2006) 67:83–7. doi: 10.1212/01.wnl.0000223613.57229.24
- Mocking S, Garg P, Chutinet A, Copen W, Sorensen A, Wu O. Accuracy and execution speed of automatic voxel-based algorithms for segmenting stroke

DATA AVAILABILITY

The datasets generated for this study are available on request to the corresponding author for the express purposes of reproducing the results and with the explicit permission for data sharing by the local institutional review board.

AUTHOR CONTRIBUTIONS

MS, A-KG, OW, and NR: conceptualization; MS and NR: methodology and writing—original draft; MS, A-KG, PF, ME, LC, AV, SG, OW, and NR: investigation and writing—review and editing; MS: formal analysis and visualization; NR: supervision. All authors had full access to all the data in the study and take responsibility for the integrity of the data and the accuracy of the data analysis.

FUNDING

This project has received funding from the European Union's Horizon 2020 research and innovation programme under the Marie Skłodowska-Curie grant agreement No 753896 (MS). This study was supported by the NIH-National Institute of Neurological Disorders and Stroke (K23NS064052, R01NS082285, and R01NS086905), American Heart Association/Bugher Foundation Centers for Stroke Prevention Research, and Deane Institute for Integrative Study of Atrial Fibrillation and Stroke.

- lesions in clinical DWI imaging. In: *19th International Society for Magnetic Resonance in Medicine. ISMRM 2011*. Quebec, QC: ISMRM (2011).
15. Avants BB, Yushkevich P, Pluta J, Minkoff D, Korczykowski M, Detre J, et al. The optimal template effect in hippocampus studies of diseased populations. *Neuroimage*. (2010) 49:2457–66. doi: 10.1016/j.neuroimage.2009.09.062
 16. Avants BB, Tustison NJ, Song G, Cook PA, Klein A, Gee JC. A reproducible evaluation of ANTs similarity metric performance in brain image registration. *Neuroimage*. (2011) 54:2033–44. doi: 10.1016/j.neuroimage.2010.09.025
 17. Schirmer MD, Dalca AV, Sridharan R, Giese AK, Donahue KL, Nardin MJ, et al. White matter hyperintensity quantification in large-scale clinical acute ischemic stroke cohorts-the MRI-GENIE study. *bioRxiv*. [Preprint]. (2019). doi: 10.1101/552844
 18. Iglewicz, B., and Hoaglin, D. C. (1993). *How to detect and handle outliers*. ASQC Quality Press Milwaukee, WI.
 19. R Core Team. *R: A Language and Environment for Statistical Computing*. Vienna (2013).
 20. Ambarki K, Israelsson H, Wahlin A, Birgander R, Eklund A, Malm J. Brain ventricular size in healthy elderly: comparison between Evans index and volume measurement. *Neurosurgery*. (2010) 67:94–9. doi: 10.1227/01.NEU.0000370939.30003.D1
 21. Grabowski TJ, Cho HS, Vonsattel JPG, Rebeck GW, Greenberg SM. Novel amyloid precursor protein mutation in an Iowa family with dementia and severe cerebral amyloid angiopathy. *Ann Neurol Off J Am Neurol Assoc Child Neurol Soc*. (2001) 49:697–705. doi: 10.1002/ana.1009
 22. Smith EE, Vijayappa M, Lima F, Delgado P, Wendell L, Rosand J, et al. Impaired visual evoked flow velocity response in cerebral amyloid angiopathy. *Neurology*. (2008) 71:1424–30. doi: 10.1212/01.wnl.0000327887.64299.a4
 23. Ghatan PH, Ingvar M, Eriksson L, Stone-Elander S, Serrander M, Ekberg K, et al. Cerebral effects of nicotine during cognition in smokers and non-smokers. *Psychopharmacology*. (1998) 136:179–89. doi: 10.1007/s002130050554
 24. O'sullivan M, Lythgoe DJ, Pereira AC, Summers PE, Jarosz JM, Williams SCR, et al. Patterns of cerebral blood flow reduction in patients with ischemic leukoaraiosis. *Neurology*. (2002) 59:321–6. doi: 10.1212/WNL.59.3.321

Conflict of Interest Statement: The authors declare that the research was conducted in the absence of any commercial or financial relationships that could be construed as a potential conflict of interest.

Copyright © 2019 Schirmer, Giese, Fotiadis, Etherton, Cloonan, Viswanathan, Greenberg, Wu and Rost. This is an open-access article distributed under the terms of the Creative Commons Attribution License (CC BY). The use, distribution or reproduction in other forums is permitted, provided the original author(s) and the copyright owner(s) are credited and that the original publication in this journal is cited, in accordance with accepted academic practice. No use, distribution or reproduction is permitted which does not comply with these terms.



Characterization of White Matter Hyperintensities in Large-Scale MRI-Studies

Benedikt M. Frey^{*†}, Marvin Petersen[†], Carola Mayer, Maximilian Schulz, Bastian Cheng and Götz Thomalla

Department of Neurology, University Medical Center Hamburg-Eppendorf, Hamburg, Germany

OPEN ACCESS

Edited by:

Andreas Charidimou,
Massachusetts General Hospital and
Harvard Medical School,
United States

Reviewed by:

Anne-Katrin Giese,
Massachusetts General Hospital and
Harvard Medical School,
United States

Loes C. A. Rutten-Jacobs,
University of Cambridge,
United Kingdom

*Correspondence:

Benedikt M. Frey
b.frey@uke.de

[†]These authors have contributed
equally to this work

Specialty section:

This article was submitted to
Stroke,
a section of the journal
Frontiers in Neurology

Received: 26 October 2018

Accepted: 22 February 2019

Published: 26 March 2019

Citation:

Frey BM, Petersen M, Mayer C,
Schulz M, Cheng B and Thomalla G
(2019) Characterization of White
Matter Hyperintensities in Large-Scale
MRI-Studies. *Front. Neurol.* 10:238.
doi: 10.3389/fneur.2019.00238

Background: White matter hyperintensities of presumed vascular origin (WMH) are a common finding in elderly people and a growing social malady in the aging western societies. As a manifestation of cerebral small vessel disease, WMH are considered to be a vascular contributor to various sequelae such as cognitive decline, dementia, depression, stroke as well as gait and balance problems. While pathophysiology and therapeutical options remain unclear, large-scale studies have improved the understanding of WMH, particularly by quantitative assessment of WMH. In this review, we aimed to provide an overview of the characteristics, research subjects and segmentation techniques of these studies.

Methods: We performed a systematic review according to the PRISMA statement. One thousand one hundred and ninety-six potentially relevant articles were identified via PubMed search. Six further articles classified as relevant were added manually. After applying a catalog of exclusion criteria, remaining articles were read full-text and the following information was extracted into a standardized form: year of publication, sample size, mean age of subjects in the study, the cohort included, and segmentation details like the definition of WMH, the segmentation method, reference to methods papers as well as validation measurements.

Results: Our search resulted in the inclusion and full-text review of 137 articles. One hundred and thirty-four of them belonged to 37 prospective cohort studies. Median sample size was 1,030 with no increase over the covered years. Eighty studies investigated in the association of WMH and risk factors. Most of them focussed on arterial hypertension, diabetes mellitus type II and Apo E genotype and inflammatory markers. Sixty-three studies analyzed the association of WMH and secondary conditions like cognitive decline, mood disorder and brain atrophy. Studies applied various methods based on manual (3), semi-automated (57), and automated segmentation techniques (75). Only 18% of the articles referred to an explicit definition of WMH.

Discussion: The review yielded a large number of studies engaged in WMH research. A remarkable variety of segmentation techniques was applied, and only a minority referred to a clear definition of WMH. Most addressed topics were risk factors and secondary clinical conditions. In conclusion, WMH research is a vivid field with a need for further standardization regarding definitions and used methods.

Keywords: white matter hyperintensities, white matter lesions, systematic review, large-scale studies, white matter hyperintensity segmentation, segmentation, cerebral small vessel disease

INTRODUCTION

Cerebrovascular disease represents a major burden on an individual as well as societal level, with growing importance in the aging western societies. Stroke as the most prominent example is the second most frequent cause of death in the world and the most frequent cause of acquired permanent disability (1). Vascular dementia represents another manifestation of cerebrovascular disease and is the second most frequent type of dementia following Alzheimer's disease (2). In Alzheimer's disease, cerebrovascular pathology is also a frequent finding (3). Among other causes, these disease entities are considered to be associated with cerebral small vessel disease (CSVD). CSVD comprises different structural changes observed in post-mortem or *in-vivo* brain imaging, all of them related to alterations of small brain arteries. These include small subcortical infarcts, lacunes, dilated perivascular spaces, cerebral microbleeds, and particularly white matter hyperintensities of presumed vascular origin (WMH).

According to the *Standards for Reporting Vascular changes on nEuroimaging* (STRIVE)—an international consensus on the definition of cerebral small vessel disease—WMH are hyperintensities on T2-weighted magnetic resonance images (MRIs), which are located in the white matter and of varying size (4). Affecting preferentially the elderly, WMH are associated with cognitive impairment, mortality, increased risk of stroke and play a role in the development of late-onset depression (5–7). They are further considered to worsen gait (8), balance (9), and urinary function (10). Common cardiovascular risk factors associated with WMH (11), include hypertension (12), smoking (13), and diabetes (14). Nevertheless, the exact etiology and pathogenesis of WMH, as well as their role in neurodegeneration, is not fully understood. Therefore, further research on WMH is necessary to clarify these questions and guide future treatment and preventive interventions.

For epidemiological research, quantitative assessment of WMH is a crucial requirement for adequate analysis of associated risk factors and clinical deficits. Semi-quantitative assessments using visual rating scales (15, 16) carry certain disadvantages such as limited accuracy, high intra- and inter-rater-variation (17), low comparability (18), and inadequate depiction of longitudinal changes (19). Moreover, visual rating scales usually do not reflect precise localization of observed WMH. Although correlating with visual rating scales (20), quantitative measurements based on WMH segmentation offer a more reliable, sensitive, and objective alternative (21), which also enables the anatomical analysis. Technically, WMH segmentation is the process of subdividing image voxels into subgroups based on predefined features such as signal intensity. **Figure 1** illustrates representative results of different segmentation techniques for exemplary purposes. Since segmenting brain lesions by hand is a highly demanding process, the vivid research field produced various automated and semi-automated segmentation techniques (24). Nevertheless, there are no standardized approaches to quantitative or semi-quantitative WMH segmentations. Also, inconsistent definitions of WMH (4) and differing standards for the qualitative

evaluation and quantitative comparison of the results to a so-called gold standard exist, not to mention the reporting of these. The research community has recognized these problems and addressed them over the last years, with the STRIVE as a major milestone achieved in 2013: in this position paper, experts in the field provided an unification of cerebral small vessel disease definitions including a clear definition of white matter hyperintensities of presumed vascular origin (4).

Currently, there is accumulating evidence pointing to a clinical relevance of WMH, substantially driven by large-scale studies. Thus, standardization of methodological approaches for WMH characterization in these studies is of crucial importance. In this systematic review, we provide an overview of large-scale studies assessing WMH quantitatively over the past 14 years. We describe their characteristics, research subjects, approaches on WMH segmentation, and the study-specific and general development of segmentation techniques. Furthermore, we continue the discussion about the heterogeneity issues in this particular field of research. By this, we aim to contribute to the unification work of the field started previously by other research groups.

METHODS

We conducted a systematic review according to the Preferred Reporting Items for Systematic Reviews and Meta-Analysis (PRISMA) Statement (25). The review protocol was not registered in advance, the completed PRISMA checklist can be found in the **Supplementary Material**.

Search Strategy and Study Selection

The methods of study selection, including searched data sources and selection criteria, were determined in advance. Two reviewers (BF, MP) carried out the literature research in December 2018 by searching the online-database Pubmed for eligible records. Search terms and applied filters are presented in the **Supplementary Material**.

Study selection was performed by both reviewers independently by screening abstracts or if necessary full-text papers for exclusion criteria. Exclusion criteria were specified as follows: (1) sample size <500, (2) a publication date earlier than 01.01.2005, (3) age <18 years, (4) written in another language than English, (5) no WMH segmentation has been performed, (6) review articles, (7) investigation of WMH of non-vascular origin (studies on WMH occurring in inflammatory or neurodegenerative conditions like multiple sclerosis, lupus, Sneddon syndrome, Huntington-like diseases, neurofibromatosis, leukodystrophies, cerebral autosomal dominant arteriopathy with subcortical infarcts and leukoencephalopathy, Fabry disease, sickle cell disease, progressive multifocal leukoencephalopathy, cerebral amyloid angiopathy, posterior leukoencephalopathy syndrome). Studies were included if no exclusion criteria were met.

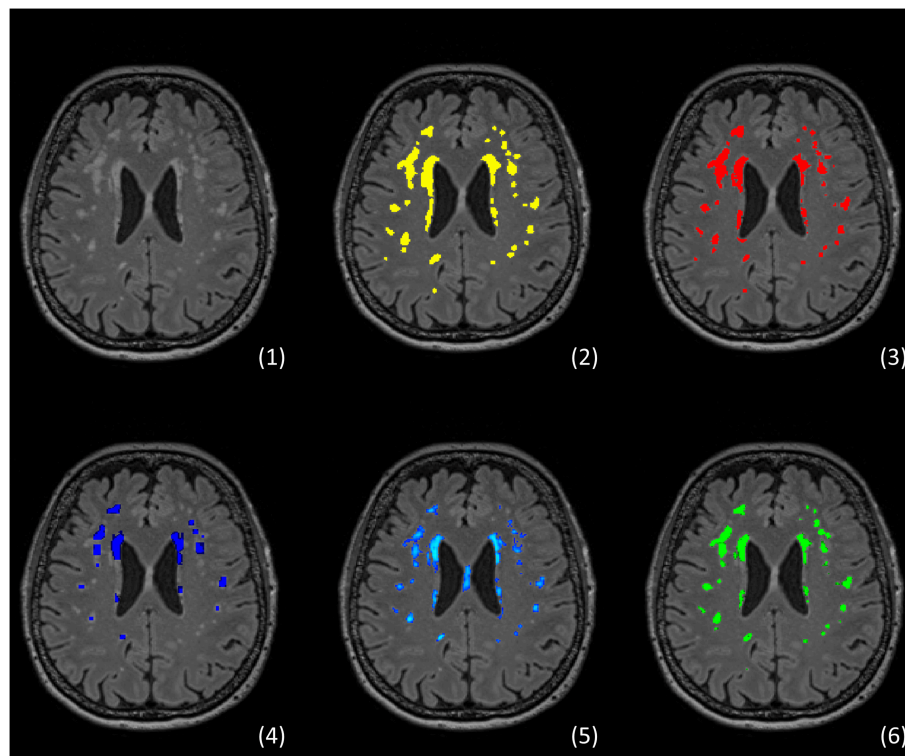


FIGURE 1 | Example of segmentation of white matter hyperintensities (WMH) using different approaches. The figure shows an example from an own unpublished dataset: (1) FLAIR showing typical distribution of WMH, (2) manual segmentation rater 1 (MP), (3) manual segmentation rater 2 (CM), (4) automated segmentation via Lesion growth algorithm (LGA) of LST toolbox version 2.0.15 (22), (5) automated segmentation via Lesion prediction algorithm (LPA) also of LST toolbox, (6) automated segmentation via the Brain Intensity AbNormality Classification Algorithm (BIANCA) implemented in FSL (23).

Data Extraction and Analysis

Data extraction was conducted independently by both reviewers reading the full-text articles. Resulting data were cross-checked afterwards. Extracted information included the name of the population study the articles belong to, year of publication, sample size, mean age of subjects in the study, the cohort included, and segmentation details like the definition of WMH, the segmentation method, reference to methods papers as well as validation measurements. Additionally, referenced methods papers were surveyed for further details on segmentation methods. All descriptive results are given by the mean \pm the standard error of the mean. Data that was not available is reported as missing as long as there was no possibility to compute it.

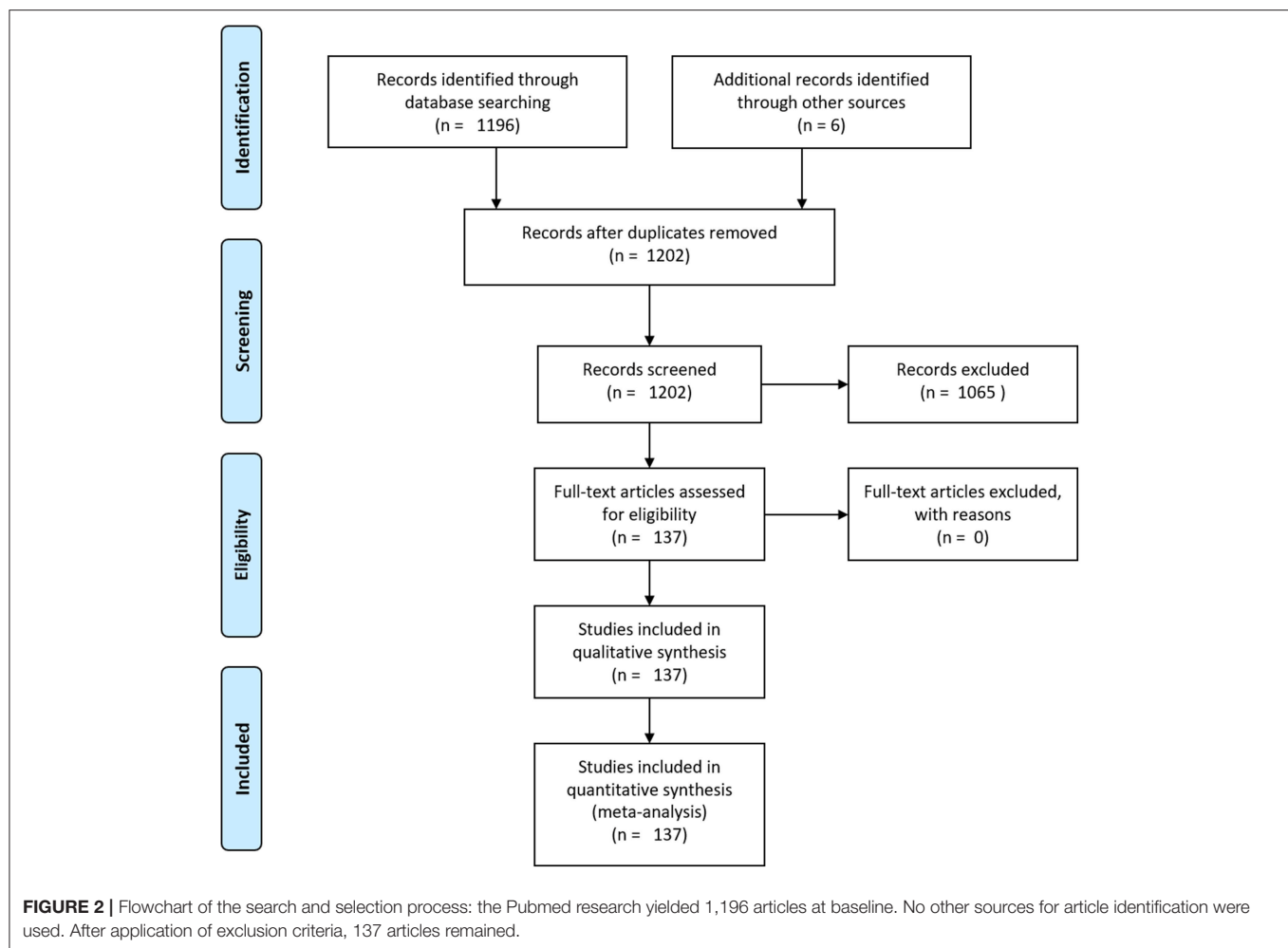
In accordance with previous work in this field, the methods underlying the image segmentation were categorized into manual, semi-automated, and automated (24). A method was considered “manual” if the researcher annotates all lesion voxels himself; “semi-automated,” if the researcher intervenes in certain situations and “automated,” if there is no necessity of human intervention in the computing process. The latter was again classified in supervised and unsupervised depending on whether or not the classification algorithm requires a previously produced reference segmentation dataset, defining the affiliation of voxels to a particular group, e.g., WMH or non-WMH.

Furthermore, papers were characterized by the type of the underlying research question related to WMH, i.e., whether they studied the association of risk factors and WMH, the influence of WMH on a certain pathology, both directions of causation, or neither of them. All research subjects (e.g., *IL-6* or *CRP*) were extracted and assigned to subcategories defined by umbrella terms (e.g., *Inflammatory markers*). Since age and sex are regularly control variables, they are not mentioned as distinct research subjects.

RESULTS

Search Results

A flowchart summarizing the search and selection process is provided in **Figure 2**. Applying the aforementioned search terms and filters, the PubMed search yielded 1,196 potentially relevant records. We ruled out 1,065 of them as they met the exclusion criteria. Six further articles classified as relevant were added manually. A total of 137 articles fitting the criteria remained and were included in this systematic review. An overview of the six studies with most included articles is also part of the results section, encompassing study characteristics and their segmentation approach.



Study Characteristics

The main characteristics of the studies incorporated in this review are shown in **Table 1**. 137 articles were included, whereas 134 belonged to 37 large-scale prospective cohort studies **Box 1** delineates the 5 cohort studies that contributed the most articles to this review. The median sample size was 1,030, ranging from 501 to 9,361. Mean study sample size did not increase over the 14 years investigated (**Figure 3**). The mean age of subjects in the studies ranged from 46 to 83 years with a total mean of 67 ± 0.8 years. Regarding sample characteristics, 88 of the 137 studies described investigations in a standard population, while 32 included patients with a specific pathology. Seventeen studies compared their pathological cohort with a healthy control group. Concerning the underlying research question, 80 studies analyzed the relationship of risk factors and WMH, which could be categorized into 50 different thematic groups (**Table 2**). Sixty-four studies examined the link of WMH to diseases and vice versa, covering 25 different thematic groups (**Table 3**). Two papers did not fit this way of categorization. Their research subjects were “White matter hyperintensities and normal-appearing white matter integrity in the aging brain” (121) and “Incidental Findings on MRI” (122). Two

studies, the Leukoaraiosis And DISability Study (LADIS) and the Genetics of Microangiopathic Brain Injury (GMBI) study, were originally established especially for research in WMH and their associations, not for other or more general topics.

Segmentation

Definition of White Matter Hyperintensities

Only 24 (17.5%) articles contained an explicit definition of WMH. The remaining studies either gave an implicit explanation through their segmentation method or had no specific definition of WMH. Of the studies included in our review, 72 were published since 2014, i.e., after publication of the STRIVE paper. Of these, 15 defined WMH explicitly, 10 of them according to STRIVE. Forty-seven studies did not refer to any explicit definition of WMH at all.

Segmentation Types and Segmentation Techniques

The largest proportion of studies applied automated segmentation techniques: supervised and unsupervised segmentation were used in 60 and 15 articles, respectively. Fifty-seven articles described a semi-automated segmentation technique, while only 3 papers relied on manual segmentation

TABLE 1 | Characteristics of large-scale study-samples incorporated in this review.

Cohort study	Incorporated articles	Years published	Mean sample size	Mean age	Sample	Segmentation method	Gold standard	Methods paper
3C	15	2008–2017	1493	72	HS	Bayesian classifier, supervised, intensity thresholding, semi-automated	Visual rating scales, none	(26, 27)
ADNI	3	2010–2015	752	75	MS: MCI/AD	Markov random field, semi-automated	Semi-automated segmentation	(28)
AGES-Reykjavik	7	2009–2015	3975	76	HS	Artificial neural network, supervised	Manual segmentation	(29)
ARIC MRI	4	2013–2016	1193	65	HS	Intensity thresholding, unsupervised	Manual segmentation	(30)
ARIC-NCS	1	2017	1713	75	MS: Atherosclerosis Risk	Intensity thresholding, unsupervised	Manual segmentation	(30)
ASPS	1	2016	762	65	HS	Intensity thresholding, semi-automated	None	None
ASPS/ASPFs	1	2014	584	67	HS	Region growing, semi-automated	None	None
CDOT	1	2013	713	70	MS: DM II	Watershed transformation, unsupervised	Manual segmentation	(31)
CHAP	2	2010–2014	573	80	MS: dementia	Intensity thresholding, semi-automated	Manual segmentation	(32, 33)
CHARGE	1	2011	9361	70	MS:	Miscellaneous	None	None
EVA	1	2011	780	69	HS	Bayesian classifier, supervised	Visual rating scales	(27)
FHS	1	2017	1527	60	HS	Intensity thresholding, semi-automated	Manual segmentation	(32, 33)
FOS	13	2007–2018	1398	62	HS	Intensity thresholding, semi-automated	Manual segmentation	(32, 33)
FOS/FHS	1	2005	2081	62	HS	Intensity thresholding, semi-automated	Manual segmentation	(32, 33)
GEN III	1	2016	1995	46	HS	Intensity thresholding, semi-automated	Manual segmentation	(32, 33)
GeneSTAR	2	2014–2015	654	51	MS: Relatives of early onset CHD patients	Manual segmentation	None	None
GENOA/GMBI	4	2007–2017	1182	62	MS: Siblings of hypertensive patients, antihypertensive medication	Intensity thresholding, unsupervised	Manual segmentation	(30)
HUNT MRI	1	2018	862	59	HS	Manual segmentation and freesurfer	None	None
ILAS	1	2018	802	59	HS	Region growing, unsupervised	None	(22)
LADIS	5	2007–2016	594	74	PS: WMH	Region growing, semi-automated	None	(18)
LBC 1936	6	2014–2018	676	73	HS	Multispectral coloring modulation and variance identification, unsupervised	Semi-automated segmentation	(34)
MCSA	1	2016	1044	78	HS	Region growing, semi-automated	None	(35)
NACC UDS (Databank)	1	2018	694	73	MS: AD, MCI	Intensity thresholding, semi-automated	Manual segmentation	(32, 33)
No specific cohort study	3	2010–2016	1703	65	MS, PS: Stroke	Intensity thresholding, semi-automated	None	(26, 36, 37)
NOMAS	7	2011–2018	1216	70	HS	Intensity thresholding, semi-automated	Manual segmentation	(32, 33) None

(Continued)

TABLE 1 | Continued

Cohort study	Incorporated articles	Years published	Mean sample size	Mean age	Sample	Segmentation method	Gold standard	Methods paper
PoP/Sunnybrook	1	2018	820	71	MS: AD, MCI, Dementia	Adaptive local thresholding	None	(38)
PROSPER	2	2006	541	75	PS: Vascular disease or high cardiovascular risk	Fuzzy inference system, unsupervised	None	(39)
RS	10	2007–2018	2378	62	HS	k-Nearest neighbor, supervised	Manual segmentation	(40, 41)
SHIP	1	2016	2367	52	HS	Support vector machine, supervised	Manual segmentation	(42)
SHIP/BLSA	1	2018	2143	74	HS	Not specified	None	None
SMART-MR	22	2008–2015	818	58	PS: Symptomatic atherosclerotic disease	k-Nearest neighbor, supervised	Manual segmentation	(43, 44)
SNAC-K	1	2016	501	71	HS	Manual segmentation	None	None
TASCOG/Sydney-MAS	1	2014	655	75	HS	Intensity thresholding, unsupervised	Visual rating scales	(45)
UK Biobank	2	2018	8439	62	HS, PS: WMH	k-Nearest neighbor, supervised	Manual segmentation	(23)
WHICAP	10	2008–2018	831	77	HS	Intensity thresholding, semi-automated, fuzzy inference system, unsupervised, region growing, unsupervised	Manual segmentation, Semi-automated segmentation	(46–48)
WHICAP/ESPRIT	1	2014	1233	81	HS	Region growing, unsupervised	Semi-automated segmentation	(47)
WHIMS-MRI	1	2014	729	83	HS	Support vector machine, supervised	Manual segmentation	(42)

3C, Three-City Study; ADNI, Alzheimer's Disease Neuroimaging Initiative; AGES-Reykjavik, Age, Gene/Environment Susceptibility-Reykjavik Study; ARIC, Atherosclerosis Risk in Communities; ARIC-NCS, Atherosclerosis Risk in Communities Neurocognitive Study; ASPS, Austrian Stroke Prevention Study; ASPFS, Austrian Stroke Prevention Family Study; BLSA, Baltimore Longitudinal Study of Aging; CDOT, Cognition and Diabetes in Older Tasmanians; CHAP, Chicago Health and Aging Project; CHARGE, Multiple studies in CHARGE Consortium; ESPRIT, European/Australasian Stroke Prevention in Reversible Ischemia Trial; EVA, Epidemiology of Vascular Aging; FOS, Framingham Offspring Study; FHS, Framingham Heart Study; GEN III, Third Generation Cohort; GeneSTAR, Genetic Study of Aspirin Responsiveness; GENOA, Genetic Epidemiology Network of Arteriopathy; GMBI, Genetics of Microangiopathic Brain Injury; HUNT, Nord-Trøndelag Health study; LADIS, Leukoaraiosis and Disability Study; LBC1936, Lothian Birth Cohort 1936; MCSA, Mayo Clinic Study of Aging; NACC UDS, National Alzheimer Coordinating Center databank; NOMAS, Northern Manhattan Study; PoP, proof-of-principle cohort; PROSPER, PROspective Study of Pravastatin in the Elderly at Risk of cardiovascular disease; RS, Rotterdam Study; SHIP, Study of Health in Pomerania; SMART-MR, Second Manifestations of Arterial Disease-Magnetic Resonance; SNAC-K, Swedish National study on Aging and Care in Kungsholmen; Sunnybrook, Sunnybrook Dementia study; Sydney-MAS, Sydney Memory and aging study; TASCOG, Tasmanian Study of Cognition and Gait; Sydney MAS, Sydney Memory and Aging Study; WHICAP, Washington Heights-Hamilton Heights-Inwood Community Aging Project; WHIMS, Women's Health Initiative Memory Study; mean age in years; SP, Standard Population; MS, Mixed Sample; PS, Patient Sample; CHD, Coronary heart Disease.

and 2 papers described a miscellaneous approach. Studies using fully automated methods had a significantly higher sample size ($p = 0.002$; Student's t -test) compared to semi-automated methods (mean 1017.0 vs. 1650.8). **Figure 3** shows the distribution of the segmentation types over the years. The peak of published articles on WMH was in 2014. We identified 17 different segmentation techniques used in the studies included in our review (**Table 1**). **Box 2** delivers an introductory explanation for the 5 most employed techniques.

Validation Methods

Methodological validation was done by application of accuracy and reproducibility measurements. Of 60 articles with semi-automated or manual segmentation techniques, 18 (30.0%) validated their results with reproducibility metrics, namely the intraclass-correlation coefficient and intra-rater repeatability. Of 132 articles using semi-automated and automated segmentation techniques, 112 (84.8%) reported accuracy metrics like Dice

similarity index, intraclass-correlation coefficient, mean absolute error, Pearson's correlation, Cronbach's alpha, Spearman's correlation coefficient, ANOVA, and ANCOVA to validate their results. The gold standard the segmentation techniques were tested against was manual segmentation in 84 studies, while 16 and 13 tested against visual rating scales and semi-automated techniques, respectively.

DISCUSSION

In this systematic review, we identified 137 papers from large-scale studies applying a quantitative analysis of WMH over the past 14 years. With 134 of these being part of a longitudinal prospective cohort study, this indicates to the relevance of these studies in this particular field of research. The large number of studies included in this review reflects the current scientific relevance of WMH in cerebrovascular research. The sample size of these studies ranged from 501 to more than 9,000,

BOX 1 | The Big 5: Cohort studies with the most contributing articles in this work.**SMART-MR**

With 22 articles the Second Manifestations of ARterial disease—Magnetic Resonance Study (SMART-MR) made up the biggest proportion of all included studies. Localized in the Netherlands, SMART-MR had initially been designed to investigate the brain changes on MRI in patients with symptomatic atherosclerotic disease, namely, manifest coronary artery disease, cerebrovascular disease, peripheral artery disease, and abdominal aortic aneurysm. Recruitment took place from May 2001 until December 2005 and resulted in a baseline sample size of 1,309 subjects (49, 50).

3C

Established in the three French cities Bordeaux, Dijon, and Montpellier, the objective of the 3C-study was the assessment of risk of dementia and cognitive impairment attributable to vascular factors. 9294 older adults form the original sample size, recruited from March 1999 to March 2001 (51).

Framingham Offspring Cohort

The Framingham Offspring Cohort contains the offspring of participants from the original Framingham Heart Study. Founded in requirement of a young study sample, the enrolment phase in 1971 supplied an initial study sample of 5,124. The study's purpose is described as the identification of common factors contributing to cardiovascular disease (52, 53).

WHICAP

The Washington/Hamilton Heights-Inwood Columbia Aging Project, located in New York, investigates in Alzheimer's Dementia and Aging in a cohort of multiple ethnicities. The original cohorts size counts 3,452 members (54).

Rotterdam Study

Situated in the Netherlands, the enrolment of the Rotterdam study started in 1990 with the baseline sample size of 7,983 participants. Having a broader approach, the study covers multiple diseases of elderly people in its investigations, i.e., cardiovascular, neurological, ophthalmological, endocrinological, and psychiatric diseases (55).

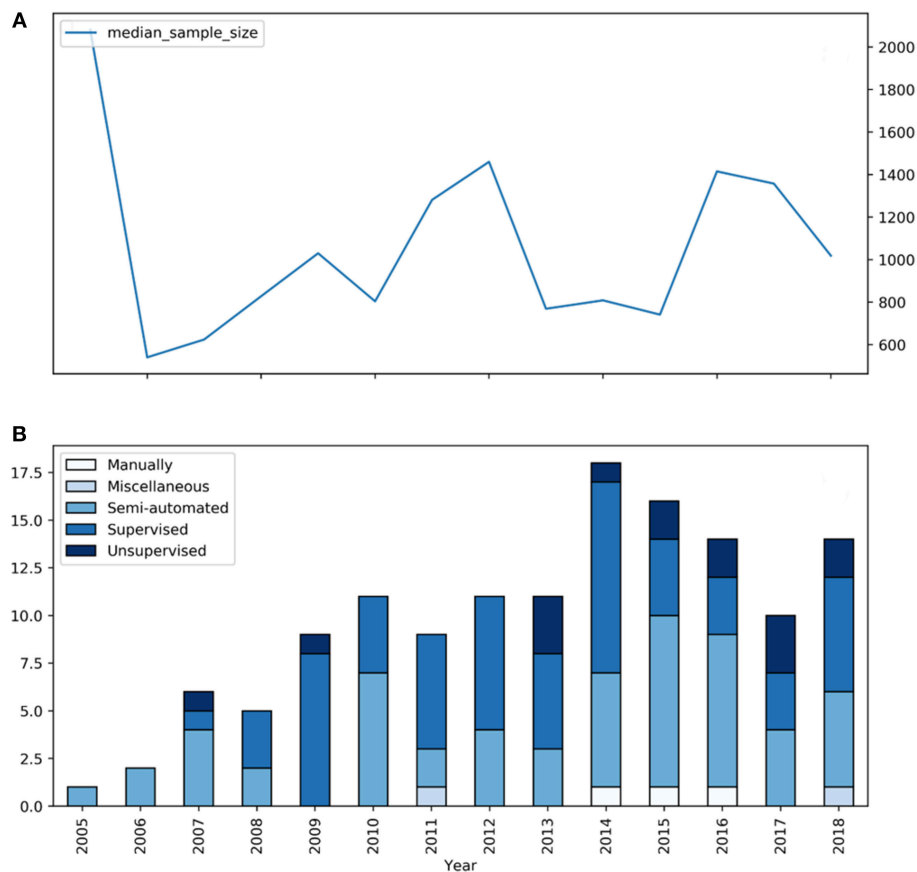


FIGURE 3 | Segmentation types and mean sample size of studies on WMH between 2005 and 2018. **(A)** The blue graph represents the median sample size of the according studies. **(B)** The blue bars represent the number of large-scale studies for each year included in our review with the specific segmentation type.

which demonstrates the feasibility of WMH segmentation in large samples resulting from the scalability of largely automated image analysis techniques. However, although the past years have

brought ongoing improvements in automated image analysis techniques, we did not observe a clear increase of sample size over time. This may either reflect the typical delay until new analysis

TABLE 2 | Overview of supposed risk factors for WMH in large-scale studies.

Risk factors	Studies
Ad-genetics	(56)
Adiposity	(58)
Angiotension converting enzyme	(59)
Antihypertensive treatment	(60)
Aortic stiffness	(61)
ApoE genotype	(148, 178, 182, 74, 91, 58)
Arterial stiffness	(191, 132, 171, 141)
Atherosclerosis	(183, 49, 179)
Atrial fibrillation	(138, 163)
Blood pressure variability	(62)
Cardiac stress markers	(63)
Cardiovascular risk factors	(143, 158, 56)
Common risk factors	(152, 98, 187, 135, 176, 193, 79)
Conjugated equine estrogen	(64)
Diabetes mellitus type II	(136, 165, 192, 175, 14, 153, 144)
Diet quality	(167, 150)
Dysglycemia	(65)
Exhaled carbon monoxide	(66)
Extracellular vesicle protein levels	(67)
FGF23 elevation	(68)
Folate	(69)
Genetic loci	(70, 71)
Hba1C	(72)
Homocystein	(69, 72, 142, 161)
Hyperlipidemia	(73)
Hypertension	(75, 182, 173, 187, 132, 149, 174, 146)
Inflammatory markers	(115, 85, 159, 186, 168, 57)
Leisure activity	(74)
Lipoproteins	(75)
Metabolic syndrome	(76)
Metalloproteinases	(77)
Midlife obesity	(78)
Nocturnal blood pressure	(79)
Parathyroid hormon	(80)
Parental longevity	(81)
Parental stroke	(82)
Perceived stress	(83)
Physical activity	(84)
Plasma beta-amyloid	(85, 86)
Red blood cell omega-3 fatty acid	(87)
S100B	(88)
Sleep duration	(89)
Sulfur amino acids	(69)
Thyroid function	(90)
Tomm40 523 genotype	(91)
Uric acid	(92)
VCAN snps	(93)
Vitamin B12	(69)
Vitamin D	(94)
Vo2Max	(95)

Common risk factors are age, sex, gender, and ethnicity. Significant associations with WMH indicated in bold.

TABLE 3 | Overview of supposed sequelae of WMH in large-scale studies.

Sequelae	Studies
Alzheimer's disease	(96–99)
Antidepressant Use	(100, 101)
Apathy symptoms	(102)
Brain atrophy	(181, 182, 184, 56, 172, 145)
Brain volumetric changes	(32, 162, 189)
Callosum atrophy	(103, 104)
Cerebral blood flow	(105)
Cognitive function	(21, 56, 62, 95, 153, 79, 104, 134, 140, 143, 155, 156, 160, 164, 166, 169, 170, 180, 188–190, 194, 195)
Death	(106)
Depressive symptoms	(100, 101, 154, 133, 147, 151, 177, 139)
Falls	(107)
Functional status	(108)
Grief	(109)
Headache	(110–112)
Immobility	(57)
Manual dexterity	(113)
Migraine	(110, 112)
Mild cognitive impairment	(98, 137, 185, 157)
Olfactory function	(114)
Perivascular spaces	(115)
Restless-Legs-syndrome	(116)
Retinal Microvasculature	(117)
Study-drop-out	(118)
Subjective memory impairment	(119)
Tract Integrity	(120)

Significant associations with WMH indicated in bold.

methods are implemented in large epidemiological studies, which usually are running over a long period. This may also be explained by other factors limiting sample size in large-scale studies beyond factors related to image analysis, e.g., recruitment, or limited capacity of study centers for clinical or imaging studies. Mean age of study subjects across all studies was 67 years, which is likely due to the fact of cerebrovascular diseases being aggregated primarily in the elderly.

The research questions addressed in the studies included in our review could be divided into two groups: the association of risk factors with WMH and supposed clinical or other consequences of WMH. The five most frequently investigated risk factors studied with regards to their association with WMH were hypertension, common risk factors, diabetes, ApoE genotype and inflammatory markers. The majority represents risk factors or markers of atherosclerosis (123).

With regard to clinical manifestations of WMH, there were two areas of interest in the focus of the reviewed studies: a large number of studies looked at WMH in the context of cognitive decline, mild cognitive impairment, or brain volumetric changes and brain atrophy, which are considered as

BOX 2 | Top 5 most used methods for WMH-segmentation in large-scale studies.**Intensity thresholding—DeCarli et al. (32, 35)**

The semi-automated method is based on the work of DeCarli et al. Taking the dataset with unclassified voxels, the examiner models a gaussian curve based on the voxel intensity values. Afterwards a threshold value of 3.5 standard deviations above the mean is set. Every voxel with an intensity value higher than the threshold value is defined as a white matter hyperintensity voxel.

Region Growing—Brickman et al. (47)

Similar to the approach by DeCarli, the approach by Brickman and colleagues starts with an intensity thresholding step (2.5 standard deviations) to determine seed voxels for each hemisphere. The seeds are the origin of region growing processes. Every seed voxel intensity value serves as calculation base of an interval ($\pm 5\%$). The algorithm determines class membership of every adjacent voxel by looking whether its intensity value falls into that interval. The algorithm moves further by considering every new WMH defined voxel as a seed with its own interval.

k-Nearest Neighbors—Anbeek et al. (43, 44) and de Boer et al. (40)

Utilized by the Rotterdam study as well as SMART-MR, k-NN is a supervised machine learning algorithm that aims to classify objects based on multiple features, e.g., voxel intensities in T1-w, IR, PD, T2-w, and FLAIR as well as spatial information. For every preclassified voxel a certain location in a multi-dimensional feature space is calculated. Subsequently, a probability is allocated to every voxel of unknown classification based on the labels of its k nearest neighbors in the feature space.

Naïve Bayesian Classifier—Maillard et al. (27)

The Naïve Bayesian Classifier is a machine learning algorithm utilizing Bayesian statistics. As a learning step a preclassified dataset is consigned. The algorithm takes this dataset and calculates its baseline probabilities: simple probabilities like the likelihood of choosing a WMH through a random pick $[P(\text{WMH})]$ and conditional probabilities like the likelihood of a choosing a WMH through a random pick under the assumption of certain features $[P(\text{WMH}|\text{Features})]$. Next, unclassified voxels are handed over to the algorithm. Based on the baseline probabilities the algorithm delivers probability values of group membership given certain features for every voxel. Finally, those membership values are compared and the voxel is assigned to the group with the highest (24).

Artificial Neural networks—Zijdenbos et al. (29)

Artificial neural networks are algorithms inspired by the architecture of biological neural networks, containing neurons and in-between connections. The network established by Zijdenbos and colleagues consists of three layers: an input layer counting consisting of six nodes/neurons where the spatial and intensity information is handed over to the algorithm, a hidden layer with 10 nodes that processes information the input layer delivers and an output layer with two nodes determining the classification of non-WMH and WMH.

biomarkers of neurodegeneration. This research focus appears obvious, as cerebral small vessel disease is a known risk factor for vascular cognitive impairment and vascular dementia (3). Depressive symptoms were the second clinical focus, as well-thematized in multiple studies. This is in line with the vascular depression hypothesis which proposes an association between the disruption of frontostriatal pathways by WMH and late-life depression (124, 125).

The lack of studies addressing e.g., the association of WMH and ischemic stroke and intracerebral hemorrhage (37, 126) might represent a bias in our search criteria.

Our review focused on the methods utilized for WMH characterization. To some parts, the heterogeneity and lack of standardization seem not only to be a problem of imaging analysis but also of the definition and nomenclature of findings related to cerebral small vessel disease. In an analysis of 1,144 studies dealing with WMH research, 275 used a variant term to “white matter hyperintensity” in their titles or abstracts (4). Efforts to overcome this lack of consensus on terminology and definition of white matter hyperintensities led to publishing the STRIVE consensus criteria in 2013, defining standards for research into cerebral small vessel disease (4). We also wanted to see, whether this initiative and publication of research standards had an impact on scientific studies of WMH in large cohorts. Still, a lot of unifying potential remains here, harboring the problem of arbitrary WMH segmentation and contributing another aspect to the discussion. These numbers suggest that there is still much room for the unification of scientific standards in this research area. In line with this, a recent contribution to the discussion suggested that the descriptive nature of most definitions of white matter hyperintensities is accountable for low-quality segmentation (127). The authors propose a statistical definition as a solution

due to its better measurability and provide competitive results with it.

Virtually all studies relied on either semi-automated or fully-automated techniques for WMH segmentation. This finding reflects the trend toward segmentation automation resulting from the acknowledgment of limitations of manual segmentation: it is laborious, thus expensive; is prone to errors; subjective and shows high intra-rater and inter-rater variability (36). Since semi-automated segmentation techniques succumb automated ones regarding human intervention while showing similar segmentation quality, a further trend from semi-automated segmentation methods to fully automated techniques was assumable. Although automated segmentation techniques constituted the largest proportion over the past 14 years from observation of the time course of our data a clear trend toward automated segmentation was not derivable. The significantly higher sample size of studies using automated methods compared to studies using semi-automated methods can be explained by the fact that with higher sample size approaches requiring interaction with a human observer become less feasible.

One striking result of our review is the manifoldness of segmentation techniques used. Almost every cohort study identified had its own segmentation approach. Our review was not designed to answer the question, whether any of the segmentation methods is superior for WMH segmentation. Due to the inherent complexity of the segmentation task, the research field's demand for one proper automated segmentation technique remains unresolved. However, the diversity of segmentation approaches used in large-scale studies is remarkable, which in turn reflect the total lack of any consensus or agreed methodological standard for WMH segmentation.

The existence of a large variety of segmentation techniques is not inherently harmful to the field of research, as it may

also be interpreted as a reflection of its vividness. However, the multiplicity of methods used for segmentation and quantification of WMH represents a scientific problem, because it leads to potential incoherence and incomparability between studies. Crucial results such as the overall WMH extent may differ in significant ways depending on the methods used for WMH segmentation.

As a relevant example of how to address cross-study heterogeneity, the NeuroCHARGE Consortium (70) used results of 7 different large-scale prospective cohort studies for a genome-wide association study (GWAS). Before conducting their analysis, they assessed the results for comparability, encompassing WMH segmentation and visual rating scale data, by examining their quality individually via comparison with a reference standard. In addition, utilized visual scoring and volumetric methods were performed on standard image data sets to test agreement.

Automated segmentation was primarily based on machine learning algorithms: for instance, k-nearest neighbors, naive Bayesian classifiers, artificial neural networks and support vector machines were successfully employed to serve the problem of quantitative WMH delineation. Since deep learning, namely convolutional neural networks (CNN), proved themselves for computer vision tasks they are also a hot contender in the WMH segmentation problem. First studies and the WMH segmentation challenge at MICCAI 2017 (<http://wmh.isi.uu.nl/>) delivered promising results (128–130).

In the publications analyzed in our review, some validated their segmentation results against a gold-standard—usually manual segmentation. This “gold standard,” however, has a lot of inherent limitations, resulting in a significant degree of subjectivity in the validation process. This, again, contributes to incomparability between different methods due to the fact they have been validated on hardly comparable gold standards. Moreover, the methods used for validation, also show some heterogeneity. Many studies use different parameters than the most common metrics like the Dice similarity index and thereby contribute to the overall heterogeneity and lead to aggravated comparison. Again, standardization might provide a solution. The study field could consent, just in the manner of the STRIVE, to specific parameters for validation measures including guidelines of subset selection for specific segmentation tasks (131).

Regardless of the already discussed problems, there are further contributors to variation in WMH quantification. In the end, the quality of the segmentation process depends strongly on the quality of the underlying MRI-images. Especially clinical scans are often very heterogeneous in terms of available MRI-sequences, manufacturer, field strength, signal-to-noise ratio,

additional pathologies visible in the scan like stroke lesions or tumors, overall quality assurance protocols and sequence parameters like voxel dimensions, slice gaps, contrast and automated distortion correction. Therefore, the application of the discussed algorithms in the clinical routine might be only possible to a limited extent.

In conclusion, the vast number of large-scale studies reporting the results of segmentation and quantification of WMH reflects the fact that cerebral small vessel disease is a research topic of great interest, especially within the context of epidemiological studies or large patient cohorts. Both, risk factors associated with the presence and extent of WMH and possible behavioral or clinical sequelae are in the focus of research. Approaches to WMH segmentation used in these studies with large samples rely on semi-automated or fully automated algorithms. A multiplicity of methods is used, and clear definitions of WMH are only provided in a minority of studies, which limits comparability and reproducibility of results. New technical developments in segmentation methods may further improve automated lesion segmentation in the near future. In addition to technical advancements, there is a clear need for creating and adhering to reporting guidelines covering both definition of WMH and description of segmentation approach.

DATA AVAILABILITY

The datasets generated for this study are available on request to the corresponding author.

AUTHOR CONTRIBUTIONS

BF, MP, and GT contributed to the conception and design of the review and to the writing of the manuscript. BF and MP performed the PubMed search and extracting of relevant studies. All authors contributed to the analysis of the results, to manuscript revision, read and approved the submitted version. GT supervised the project.

FUNDING

This work has been supported by DFG, SFB936/project C2. The funding sources were not involved in the organization and report of this work.

SUPPLEMENTARY MATERIAL

The Supplementary Material for this article can be found online at: <https://www.frontiersin.org/articles/10.3389/fneur.2019.00238/full#supplementary-material>

REFERENCES

1. Feigin VL, Norrving B, Mensah GA. Global burden of stroke. *Circ Res.* (2017) 120:439–48. doi: 10.1161/CIRCRESAHA.116.308413
2. Fitzpatrick AL, Kuller LH, Ives DG, Lopez OL, Jagust W, Breitner JCS, et al. Incidence and prevalence of dementia in the cardiovascular health study. *J Am Geriatr Soc.* (2004) 52:195–204. doi: 10.1111/j.1532-5415.2004.52058.x
3. Gorelick PB, Counts SE, Nyenhuis D. Vascular cognitive impairment and dementia. *Biochim Biophys Acta Mol Basis Dis.* (2016) 1862:860–8. doi: 10.1016/j.bbdis.2015.12.015
4. Wardlaw JM, Smith EE, Biessels GJ, Cordonnier C, Fazekas F, Frayne R, et al. Neuroimaging standards for research into small vessel disease and its contribution to ageing and neurodegeneration. *Lancet Neurol.* (2013) 12:822–38. doi: 10.1016/S1474-4422(13)70124-8

5. Debette S, Markus HS. The clinical importance of white matter hyperintensities on brain magnetic resonance imaging: systematic review and meta-analysis. *BMJ*. (2010) 341:1–9. doi: 10.1136/bmj.c3666
6. Herrmann LL, Le Masurier M, Ebmeier KP. White matter hyperintensities in late life depression: a systematic review. *J Neurol Neurosurg Psychiatry*. (2008) 79:619–24. doi: 10.1136/jnnp.2007.124651
7. Murray A, McNeil C, Salarirad S, Deary I, Phillips L, Whalley L, et al. Brain hyperintensity location determines outcome in the triad of impaired cognition, physical health and depressive symptoms: a cohort study in late life. *Arch Gerontol Geriatr*. (2016) 63:49–54. doi: 10.1016/j.archger.2015.10.004
8. van der Holst HM, Tuladhar AM, Zerbi V, van Uden IWM, de Laat KF, van Leijns EMC, et al. White matter changes and gait decline in cerebral small vessel disease. *NeuroImage Clin*. (2018) 17:731–8. doi: 10.1016/j.nicl.2017.12.007
9. Baezner H, Blahak C, Poggesi A, Pantoni L, Inzitari D, Chabriat H, et al. Association of gait and balance disorders with age-related white matter changes: the LADIS study. *Neurology*. (2008) 70:935–42. doi: 10.1212/01.wnl.0000305959.46197.e6
10. Poggesi A, Pracucci G, Chabriat H, Erkinjuntti T, Fazekas F, Verdelho A, et al. Urinary Complaints in nondisabled elderly people with age-related white matter changes: the leukoaraiosis and disability (LADIS) Study. *J Am Geriatr Soc*. (2008) 56:1638–43. doi: 10.1111/j.1532-5415.2008.01832.x
11. Longstreth WT, Manolio TA, Arnold A, Burke GL, Bryan N, Jungreis CA, et al. Clinical correlates of white matter findings on cranial magnetic resonance imaging of 3301 elderly people. *Stroke*. (1996) 27:1274–82. doi: 10.1161/01.STR.27.8.1274
12. Maillard P, Seshadri S, Beiser A, Himali JJ, Au R, Fletcher E, et al. Effects of systolic blood pressure on white-matter integrity in young adults in the Framingham Heart Study: a cross-sectional study. *Lancet Neurol*. (2012) 11:1039–47. doi: 10.1016/S1474-4422(12)70241-7
13. Gons RAR, van Norden AGW, de Laat KF, van Oudheusden LJB, van Uden IWM, Zwiers MP, et al. Cigarette smoking is associated with reduced microstructural integrity of cerebral white matter. *Brain*. (2011) 134:2116–24. doi: 10.1093/brain/awr145
14. Schneider ALC, Selvin E, Sharrett AR, Griswold M, Coresh J, Jack CR, et al. Diabetes, prediabetes, and brain volumes and subclinical cerebrovascular disease on MRI: the atherosclerosis risk in communities neurocognitive study (ARIC-NCS). *Diab Care*. (2017) 40:1514–21. doi: 10.2337/dc17-1185
15. Fazekas F, Chawluk J, Alavi A, Hurtig H, Zimmerman R. MR signal abnormalities at 1.5 T in Alzheimer's dementia and normal aging. *Am J Roentgenol*. (1987) 149:351–6. doi: 10.2214/ajr.149.2.351
16. Scheltens P, Barkhof F, Leys D, Pruvo J, Nauta JJP, Vermersch P, et al. A semiquantitative rating scale for the assessment of signal hyperintensities on magnetic resonance imaging. *J Neurol Sci*. (1993) 114:7–12. doi: 10.1016/0022-510X(93)90041-V
17. Wardlaw JM, Ferguson KJ, Graham C. White matter hyperintensities and rating scales? observer reliability varies with lesion load. *J Neurol*. (2004) 251:584–90. doi: 10.1007/s00415-004-0371-x
18. van Straaten ECW, Fazekas F, Rostrup E, Scheltens P, Schmidt R, Pantoni L, et al. Impact of white matter hyperintensities scoring method on correlations with clinical data. *Stroke*. (2006) 37:836–40. doi: 10.1161/01.STR.0000202585.26325.74
19. Prins ND, van Straaten ECW, van Dijk EJ, Simoni M, van Schijndel RA, Vrooman HA, et al. Measuring progression of cerebral white matter lesions on MRI: visual rating and volumetrics. *Neurology*. (2004) 62:1533–9. doi: 10.1212/01.WNL.0000123264.40498.B6
20. Valdés Hernández M, del C, Morris Z, Dickie DA, Royle NA, Muñoz Maniega S, et al. Close correlation between quantitative and qualitative assessments of white matter lesions. *Neuroepidemiology*. (2013) 40:13–22. doi: 10.1159/000341859
21. van den Heuvel DMJ, ten Dam VH, de Craen AJM, Admiraal-Behloul F, van Es ACGM, Palm WM, Spilt A, et al. Measuring longitudinal white matter changes: comparison of a visual rating scale with a volumetric measurement. *Am J Neuroradiol*. (2006) 27:875–78. doi: 10.1136/jnnp.2005.070193
22. Schmidt P, Gaser C, Arsic M, Buck D, Förschler A, Berthele A, et al. An automated tool for detection of FLAIR-hyperintense white-matter lesions in multiple sclerosis. *Neuroimage*. (2012) 59:3774–83. doi: 10.1016/j.neuroimage.2011.11.032
23. Griffanti L, Zamboni G, Khan A, Li L, Bonifacio G, Sundaresan V, et al. BIANCA (Brain Intensity AbNormality Classification Algorithm): a new tool for automated segmentation of white matter hyperintensities. *Neuroimage*. (2016) 141:191–205. doi: 10.1016/j.neuroimage.2016.07.018
24. Caligiuri ME, Perrotta P, Augimeri A, Rocca F, Quattrone A, Cherubini A. Automatic detection of white matter hyperintensities in healthy aging and pathology using magnetic resonance imaging: a review. *Neuroinformatics*. (2015) 13:261–76. doi: 10.1007/s12021-015-9260-y
25. Moher D, Liberati A, Tetzlaff J, Altman DG. preferred reporting items for systematic reviews and meta-analyses: the PRISMA statement. *PLoS Med*. (2009) 6:e1000097. doi: 10.1371/journal.pmed.1000097
26. Guro ME, Irizarry MC, Smith EE, Raju S, Diaz-Arrastia R, Bottiglieri T, et al. Plasma -amyloid and white matter lesions in AD, MCI, and cerebral amyloid angiopathy. *Neurology*. (2006) 66:23–9. doi: 10.1212/01.wnl.0000191403.95453.6a
27. Maillard P, Delcroix N, Crivello F, Dufouil C, Gicquel S, Joliet M, et al. An automated procedure for the assessment of white matter hyperintensities by multispectral (T1, T2, PD) MRI and an evaluation of its between-centre reproducibility based on two large community databases. *Neuroradiology*. (2008) 50:31–42. doi: 10.1007/s00234-007-0312-3
28. Schwarz C, Fletcher E, DeCarli C, Carmichael O. Fully-automated white matter hyperintensity detection with anatomical prior knowledge and without FLAIR. *Inf Process Med Imag*. (2009) 21:239–51.
29. Zijdenbos AP, Forghani R, Evans AC. Automatic “pipeline” analysis of 3-D MRI data for clinical trials: application to multiple sclerosis. *IEEE Trans Med Imag*. (2002) 21:1280–91. doi: 10.1109/TMI.2002.806283
30. Jack CR, O'Brien PC, Retman DW, Shiung MM, Xu Y, Muthupillai R, et al. FLAIR histogram segmentation for measurement of leukoaraiosis volume. *J Magn Reson Imag*. (2001) 14:668–76. doi: 10.1002/jmri.10011
31. Beare R, Srikanth V, Chen J, Phan TG, Stapleton J, Lipshut R, et al. Development and validation of morphological segmentation of age-related cerebral white matter hyperintensities. *Neuroimage*. (2009) 47:199–203. doi: 10.1016/j.neuroimage.2009.03.055
32. DeCarli C, Massaro J, Harvey D, Hald J, Tullberg M, Au R, et al. Measures of brain morphology and infarction in the framingham heart study: establishing what is normal. *Neurobiol Aging*. (2005) 26:491–510. doi: 10.1016/j.neurobiolaging.2004.05.004
33. DeCarli C, Miller BL, Swan GE, Reed T, Wolf PA, Garner J, et al. Predictors of brain morphology for the men of the NHLBI twin study. *Stroke*. (1999) 30:529–36. doi: 10.1161/01.STR.30.3.529
34. Valdés Hernández M, del C, Ferguson KJ, Chappell FM, Wardlaw JM. New multispectral MRI data fusion technique for white matter lesion segmentation: method and comparison with thresholding in FLAIR images. *Eur Radiol*. (2010) 20:1684–91. doi: 10.1007/s00330-010-1718-6
35. Raz L, Jayachandran M, Tosakulwong N, Lesnick TG, Wille SM, Murphy MC, et al. Thrombotic microvesicles and white matter hyperintensities in postmenopausal women. *Neurology*. (2013) 80:911–8. doi: 10.1212/WNL.0b013e3182840c9f
36. Grimaud J, Lai M, Thorpe J, Adeleine P, Wang L, Barker GJ, et al. Quantification of MRI lesion load in multiple sclerosis: a comparison of three computer-assisted techniques. *Magn Reson Imag*. (1996) 14:495–505.
37. Rost NS, Rahman RM, Biffi A, Smith EE, Kanakis A, Fitzpatrick K, et al. White matter hyperintensity volume is increased in small vessel stroke subtypes. *Neurology*. (2010) 75:1670–7. doi: 10.1212/WNL.0b013e3181f279a
38. Ramirez J, Gibson E, Qudus A, Lobaugh NJ, Feinstein A, Levine B, et al. Lesion Explorer: A comprehensive segmentation and parcellation package to obtain regional volumetrics for subcortical hyperintensities and intracranial tissue. *Neuroimage*. (2011) 54:963–73. doi: 10.1016/j.NEUROIMAGE.2010.09.013
39. van der Flier WM, Middelkoop HAM, Weverling-Rijnsburger AWE, Admiraal-Behloul F, Spilt A, Bollen ELEM, et al. Interaction of medial temporal lobe atrophy and white matter hyperintensities in AD. *Neurology*. (2004) 62:1862–4. doi: 10.1212/01.WNL.0000125337.65553.8A
40. de Boer R, Vrooman HA, van der Lijn F, Vernooij MW, Ikram MA, van der Lugt A, et al. White matter lesion extension to automatic

- brain tissue segmentation on MRI. *Neuroimage*. (2009) 45:1151–61. doi: 10.1016/j.neuroimage.2009.01.011
41. Vrooman HA, Cocosco CA, van der Lijn F, Stokking R, Ikram MA, Vernooij MW, et al. Multi-spectral brain tissue segmentation using automatically trained k-Nearest-Neighbor classification. *Neuroimage*. (2007) 37:71–81. doi: 10.1016/j.neuroimage.2007.05.018
 42. Lao Z, Shen D, Liu D, Jawad AF, Melhem ER, Launer LJ, et al. Computer-Assisted Segmentation of white matter lesions in 3d mr images using support vector machine. *Acad Radiol*. (2008) 15:300–13. doi: 10.1016/j.acra.2007.10.012
 43. Anbeek P, Vincken KL, van Bochove GS, van Osch MJP, van der Grond J. Probabilistic segmentation of brain tissue in MR imaging. *Neuroimage*. (2005) 27:795–804. doi: 10.1016/j.neuroimage.2005.05.046
 44. Anbeek P, Vincken KL, van Osch MJP, Bisschops RHC, van der Grond J. Probabilistic segmentation of white matter lesions in MR imaging. *Neuroimage*. (2004) 21:1037–44. doi: 10.1016/j.neuroimage.2003.10.012
 45. Wen W, Sachdev P. The topography of white matter hyperintensities on brain MRI in healthy 60- to 64-year-old individuals. *Neuroimage*. (2004) 22:144–54. doi: 10.1016/j.neuroimage.2003.12.027
 46. Admiraal-Behloul F, van den Heuvel DMJ, Olofsen H, van Osch MJP, van der Grond J, van Buchem MA, et al. Fully automatic segmentation of white matter hyperintensities in MR images of the elderly. *Neuroimage*. (2005) 28:607–17. doi: 10.1016/j.NEUROIMAGE.2005.06.061
 47. Brickman AM, Sneed JR, Provenzano FA, Garcon E, Johnert L, Muraskin J, et al. Quantitative approaches for assessment of white matter hyperintensities in elderly populations. *Psychiatry Res Neuroimag*. (2011) 193:101–6. doi: 10.1016/j.psychres.2011.03.007
 48. DeCarli C, Fletcher E, Ramey V, Harvey D, Jagust WJ. Anatomical Mapping of White Matter Hyperintensities (WMH). *Stroke*. (2005) 36:50–5. doi: 10.1161/01.STR.0000150668.58689.f2
 49. Geerlings MI, Appelman APA, Vincken KL, Algra A, Witkamp TD, Mali WPTM, et al. Brain volumes and cerebrovascular lesions on MRI in patients with atherosclerotic disease. *The SMART-MR study Atherosclerosis*. (2010) 210:130–6. doi: 10.1016/j.ATHEROSCLEROSIS.2009.10.039
 50. Simons PCG, Algra A, Eikelboom BC, Grobbee DE, van der Graaf Y, SMART study group. Carotid artery stenosis in patients with peripheral arterial disease: the SMART study. *J Vasc Surgery*. (1999) 30:519–25. doi: 10.1016/S.0741-5214(99)70079-0
 51. 3C Study Group M, Pugliatti M, Hubbard R, Britton J, Sotgiu S, Sadovnick AD, et al. Vascular factors and risk of dementia: design of the three-city study and baseline characteristics of the study population. *Neuroepidemiology*. (2003) 22:316–25. doi: 10.1159/000072920
 52. Feinleib M, Kannel WB, Garrison RJ, McNamara PM, Castelli WP. The framingham offspring study. Design and preliminary data. *Prev Med*. (1975) 4:518–25. doi: 10.1016/0091-7435(75)90037-7
 53. Kannel WB, Feinleib M, McNamara PM, Garrison RJ, Castelli WP. An investigation of coronary heart disease in families. The Framingham offspring study. *Am J Epidemiol*. (1979) 110:281–90. doi: 10.1093/oxfordjournals.aje.a112813
 54. Tang MX, Cross P, Andrews H, Jacobs DM, Small S, Bell K, et al. Incidence of AD in African-Americans, Caribbean Hispanics, and Caucasians in northern Manhattan. *Neurology*. (2001) 56:49–56. doi: 10.1212/WNL.56.1.49
 55. Hofman A, Grobbee DE, de Jong PT, van den Ouweland FA. Determinants of disease and disability in the elderly: the Rotterdam Elderly Study. *Eur J Epidemiol*. (1991) 7:403–22. doi: 10.1007/BF00145007
 56. Habes M, Sotiras A, Erus G, Toledo JB, Janowitz D, Wolk DA, et al. White matter lesions Spatial heterogeneity, links to risk factors, cognition, genetics, and atrophy. *Neurol*. (2018) 91:964–75. doi: 10.1212/WNL.0000000000006116
 57. Windham BG, Wilkening SR, Lirette ST, Kullo IJ, Turner ST, Griswold ME, et al. Associations between inflammation and physical function in african americans and european americans with prevalent cardiovascular risk factors. *J Am Geriatr Soc*. (2016) 64:1448–55. doi: 10.1111/jgs.14229
 58. Zade D, Beiser A, McGlinchey R, Au R, Seshadri S, Palumbo C, et al. Apolipoprotein Epsilon 4 allele modifies waist-to-hip ratio effects on cognition and brain structure. *J Stroke Cerebrovasc Dis*. (2013) 22:119–25. doi: 10.1016/j.jstrokecerebrovasdis.2011.06.020
 59. Jochemsen HM, Geerlings MI, Grool AM, Vincken KL, Mali WP, van der Graaf Y, et al. Angiotensin-converting enzyme and progression of white matter lesions and brain atrophy – the SMART-MR Study. *J Alzheimer's Dis*. (2012) 29:39–49. doi: 10.3233/JAD-2012-111772
 60. Godin O, Tzourio C, Maillard P, Mazoyer B, Dufouil C. Antihypertensive treatment and change in blood pressure are associated with the progression of white matter lesion volumes. *Circulation*. (2011) 123:266–73. doi: 10.1161/CIRCULATIONAHA.110.961052
 61. Pase MP, Himali JJ, Mitchell GF, Beiser A, Maillard P, Tsao C, et al. Association of aortic stiffness with cognition and brain aging in young and middle-aged adults. *Hypertension*. (2016) 67:513–9. doi: 10.1161/HYPERTENSIONAHA.115.06610
 62. Tully PJ, Debette S, Tzourio C. The association between systolic blood pressure variability with depression, cognitive decline and white matter hyperintensities: the 3C Dijon MRI study. *Psychol Med*. (2018) 48:1444–53. doi: 10.1017/S0033291717002756
 63. Andersson C, Preis SR, Beiser A, DeCarli C, Wollert KC, Wang TJ, et al. Associations of circulating growth differentiation factor-15 and ST2 concentrations with subclinical vascular brain injury and incident Stroke. (2015) 46:2568–75. doi: 10.1161/STROKEAHA.115.009026
 64. Coker LH, Espeland MA, Hogan PE, Resnick SM, Bryan RN, Robinson JG, et al. Change in brain and lesion volumes after CEE therapies: the WHIMS-MRI studies. *Neurology*. (2014) 82:427–34. doi: 10.1212/WNL.0000000000000079
 65. Reitz C, Guzman VA, Narkhede A, DeCarli C, Brickman AM, Luchsinger JA. Relation of Dysglycemia to structural brain changes in a multiethnic elderly cohort. *J Am Geriatr Soc*. (2017) 65:277–85. doi: 10.1111/jgs.14551
 66. Naylor M, Enserro DM, Beiser AS, Cheng S, DeCarli C, Vasan RS, et al. Association of exhaled carbon monoxide with stroke. incidence and subclinical vascular brain injury. *Stroke*. (2016) 47:383–9. doi: 10.1161/STROKEAHA.115.010405
 67. Kanhai DA, de Kleijn DPV, Kappelle LJ, Uiterwaal CSPM, van der Graaf Y, Pasterkamp G, et al. Extracellular vesicle protein levels are related to brain atrophy and cerebral white matter lesions in patients with manifest vascular disease: the SMART-MR study. *BMJ Open*. (2014) 4:e003824. doi: 10.1136/bmjopen-2013-003824
 68. Wright CB, Shah NH, Mendez AJ, DeRosa JT, Yoshita M, Elkind MSV, et al. Fibroblast growth factor 23 is associated with subclinical cerebrovascular damage. *Stroke*. (2016) 47:923–8. doi: 10.1161/STROKEAHA.115.012379
 69. Hooshmand B, Mangialasche F, Kalpouzos G, Solomon A, Kåreholt I, Smith AD, et al. Association of vitamin b₁₂, folate, and sulfur amino acids with brain magnetic resonance imaging measures in older adults. *JAMA Psychiatry*. (2016) 73:606. doi: 10.1001/jamapsychiatry.2016.0274
 70. Fornage M, Debette S, Bis JC, Schmidt H, Ikram MA, Dufouil C, et al. Genome-wide association studies of cerebral white matter lesion burden: the CHARGE consortium. *Ann Neurol*. (2011) 69:928–39. doi: 10.1002/ana.22403
 71. Traylor M, Zhang CR, Adib-Samii P, Devan WJ, Parsons OE, Lanfranconi S, et al. Genome-wide meta-analysis of cerebral white matter hyperintensities in patients with stroke. *Neurology*. (2016) 86:146–53. doi: 10.1212/WNL.0000000000002263
 72. Cloonan L, Fitzpatrick KM, Kanakis AS, Furie KL, Rosand J, Rost NS. Metabolic determinants of white matter hyperintensity burden in patients with ischemic stroke. *Atherosclerosis*. (2015) 240:149–53. doi: 10.1016/j.atherosclerosis.2015.02.052
 73. Jimenez-Conde J, Biffi A, Rahman R, Kanakis A, Butler C, Sonni S, et al. Hyperlipidemia and reduced white matter hyperintensity volume in patients with ischemic Stroke. (2010) 41:437–42. doi: 10.1161/STROKEAHA.109.563502
 74. Hafsteinsdottir SH, Eiriksdottir G, Sigurdsson S, Aspelund T, Harris TB, Launer LJ, et al. Brain tissue volumes by APOE genotype and leisure activity—the AGES-Reykjavik Study. *Neurobiol Aging*. (2012) 33:829.e1–829.e8. doi: 10.1016/j.neurobiolaging.2011.06.028
 75. Chung C-P, Chou K-H, Peng L-N, Liu L-K, Lee W-J, Chen L-K, et al. Associations between low circulatory low-density lipoprotein cholesterol level and brain health in non-stroke non-demented subjects. *Neuroimage*. (2018) 181:627–34. doi: 10.1016/j.neuroimage.2018.07.049

76. Tiehuis AM, van der Graaf Y, Mali WPTM, Vincken K, Muller M, Geerlings MI. Metabolic syndrome, prediabetes, and brain abnormalities on mri in patients with manifest arterial disease: The SMART-MR Study. *Diab Care*. (2014) 37:2515–21. doi: 10.2337/dc14-0154
77. Romero JR, Vasan RS, Beiser AS, Au R, Benjamin EJ, DeCarli C, et al. Association of matrix metalloproteinases with MRI indices of brain ischemia and aging. *Neurobiol Aging*. (2010) 31:2128–35. doi: 10.1016/j.neurobiolaging.2008.11.004
78. Dettie S, Beiser A, Hoffmann U, DeCarli C, O'Donnell CJ, Massaro JM, et al. Visceral fat is associated with lower brain volume in healthy middle-aged adults. *Ann. Neurol.* (2010) 68:136–44. doi: 10.1002/ana.22062
79. Yano Y, Butler KR, Hall ME, Schwartz GL, Knopman DS, Lirette ST, et al. Associations of nocturnal blood pressure with cognition by self-identified race in middle-aged and older adults: the GENOA (Genetic Epidemiology Network of Arteriopathy) Study. *J Am Heart Assoc.* (2017) 6:e007022. doi: 10.1161/JAHA.117.007022
80. Korada SKC, Zhao D, Gottesman RF, Guallar E, Lutsey PL, Alonso A, et al. Parathyroid hormone and subclinical cerebrovascular disease: the atherosclerosis risk in communities brain magnetic resonance imaging study. *J Stroke Cerebrovasc Dis.* (2016) 25:883–93. doi: 10.1016/j.jstrokecerebrovasdis.2015.12.029
81. Murabito JM, Beiser AS, DeCarli C, Seshadri S, Wolf PA, Au R. Parental longevity is associated with cognition and brain ageing in middle-aged offspring. *Age Ageing*. (2014) 43:358–63. doi: 10.1093/ageing/afu175
82. Weinstein G, Beiser AS, Au R, DeCarli C, Wolf PA, Seshadri S. Association of Parental Stroke with brain injury and cognitive measures in offspring. *Stroke*. (2013) 44:812–5. doi: 10.1161/STROKEAHA.112.680520
83. Aggarwal NT, Clark CJ, Beck TL, Mendes de Leon CF, DeCarli C, Evans DA, et al. Perceived stress is associated with subclinical cerebrovascular disease in older adults. *Am J Geriatr Psychiatry*. (2014) 22:53–62. doi: 10.1016/j.jagp.2012.06.001
84. Kooistra M, Boss HM, van der Graaf Y, Kappelle LJ, Biessels GJ, Geerlings MI. Physical activity, structural brain changes and cognitive decline. SMART-MR study. *Atherosclerosis*. (2014) 234:47–53. doi: 10.1016/j.atherosclerosis.2014.02.003
85. Hilal S, Ikram MA, Verbeek MM, Franco OH, Stoops E, Vanderstichele H, et al. C-Reactive protein, plasma amyloid- β levels, and their interaction with magnetic resonance imaging markers. *Stroke*. (2018) 49:2692–8. doi: 10.1161/STROKEAHA.118.022317
86. Kaffashian S, Tzourio C, Soumare A, Dufouil C, Zhu Y, Crivello F, et al. Plasma -amyloid and MRI markers of cerebral small vessel disease: Three-City Dijon Study. *Neurology*. (2014) 83:2038–45. doi: 10.1212/WNL.0000000000001038
87. Tan ZS, Harris WS, Beiser AS, Au R, Himali JJ, Dettie S, et al. Red blood cell omega-3 fatty acid levels and markers of accelerated brain aging. *Neurology*. (2012) 78:658–64. doi: 10.1212/WNL.0b013e318249f6a9
88. Cox SR, Allerhand M, Ritchie SJ, Muñoz Maniega S, Valdés Hernández M, Harris SE, et al. Longitudinal serum S100 β and brain aging in the Lothian Birth Cohort 1936. *Neurobiol Aging*. (2018) 69:274–82. doi: 10.1016/j.neurobiolaging.2018.05.029
89. Ramos AR, Dong C, Rundek T, Elkind MSV, Boden-Albala B, Sacco RL, et al. Sleep duration is associated with white matter hyperintensity volume in older adults: the Northern Manhattan Study. *J Sleep Res*. (2014) 23:524–30. doi: 10.1111/jsr.12177
90. Chaker L, Wolters FJ, Bos D, Korevaar TIM, Hofman A, van der Lugt A, et al. Thyroid function and the risk of dementia. *Neurology*. (2016) 87:1688–95. doi: 10.1212/WNL.0000000000003227
91. Lyall DM, Muñoz Maniega S, Harris SE, Bastin ME, Murray C, Lutz MW, et al. APOE/TOMM40 Genetic Loci, white matter hyperintensities, and cerebral microbleeds. *Int J Stroke*. (2015) 10:1297–300. doi: 10.1111/ijs.12615
92. Latourte A, Soumaré A, Bardin T, Perez-Ruiz F, Dettie S, Richette P. Uric acid and incident dementia over 12 years of follow-up: a population-based cohort study. *Ann Rheum Dis*. (2018) 77:328–35. doi: 10.1136/annrheumdis-2016-210767
93. Ruten-Jacobs LCA, Tozer DJ, Duering M, Malik R, Dichgans M, Markus HS, et al. Genetic Study of white matter integrity in uk biobank (n=8448) and the overlap with stroke, depression, and dementia. *Stroke*. (2018) 49:1340–7. doi: 10.1161/STROKEAHA.118.020811
94. Michos ED, Carson KA, Schneider ALC, Lutsey PL, Xing L, Sharrett AR, et al. Vitamin D and Subclinical cerebrovascular disease. *JAMA Neurol.* (2014) 71:863. doi: 10.1001/jamaneurol.2014.755
95. Freudenberger P, Petrovic K, Sen A, Töglhofer AM, Fixa A, Hofer E, et al. Fitness and cognition in the elderly. *Neurology*. (2016) 86:418–24. doi: 10.1212/WNL.0000000000002329
96. Brickman AM, Tosto G, Gutierrez J, Andrews H, Gu Y, Narkhede A, et al. An MRI measure of degenerative and cerebrovascular pathology in Alzheimer disease. *Neurology*. (2018) 91:e1402–12. doi: 10.1212/WNL.000(0000)000006310
97. Brickman AM, Zahodne LB, Guzman VA, Narkhede A, Meier IB, Griffith EY, et al. Reconsidering harbingers of dementia: progression of parietal lobe white matter hyperintensities predicts Alzheimer's disease incidence. *Neurobiol Aging*. (2015) 36:27–32. doi: 10.1016/j.neurobiolaging.2014.07.019
98. Burke SL, Hu T, Fava NM, Li T, Rodriguez MJ, Schuldiner KL, et al. Sex differences in the development of mild cognitive impairment and probable Alzheimer's disease as predicted by hippocampal volume or white matter hyperintensities. *J Women Aging*. (2018) 31:140–64. doi: 10.1080/08952841.2018.1419476
99. Lo RY, Jagust WJ. Vascular burden and Alzheimer disease pathologic progression. *Neurology*. (2012) 79:1349–55. doi: 10.1212/WNL.0b013e31826c1b9d
100. Geerlings MI, Brickman AM, Schupf N, Devanand DP, Luchsinger JA, Mayeux R, et al. Depressive symptoms, antidepressant use, and brain volumes on mri in a population-based cohort of old persons without dementia. *J Alzheimer's Dis*. (2012) 30:75–82. doi: 10.3233/JAD-2012-112009
101. Grool AM, van der Graaf Y, Mali WPTM, Geerlings MI. Location of cerebrovascular and degenerative changes, depressive symptoms and cognitive functioning in later life: the SMART-Medea study. *J Neurol Neurosurg Psychiatry*. (2011) 82:1093–100. doi: 10.1136/jnnp.2010.232413
102. Grool AM, Geerlings MI, Sigurdsson S, Eiriksdottir G, Jonsson PV, Garcia ME, et al. Structural MRI correlates of apathy symptoms in older persons without dementia: AGES-Reykjavik Study. *Neurology*. (2014) 82:1628–35. doi: 10.1212/WNL.0000000000000378
103. Ryberg C, Rostrup E, Sjöstrand K, Paulson OB, Barkhof F, Scheltens P, et al. White Matter Changes Contribute to Corpus Callosum Atrophy in the Elderly: The LADIS Study. *Am J Neuroradiol*. (2008) 29:1498–504. doi: 10.3174/ajnr.A1169
104. Ryberg C, Rostrup E, Stegmann MB, Barkhof F, Scheltens P, van Straaten ECW, et al. Clinical significance of corpus callosum atrophy in a mixed elderly population. *Neurobiol Aging*. (2007) 28:955–63. doi: 10.1016/j.neurobiolaging.2006.04.008
105. van der Veen PH, Muller M, Vincken KL, Hendrikse J, Mali WPTM, van der Graaf Y, et al. Longitudinal relationship between cerebral small-vessel disease and cerebral blood flow: the second manifestations of arterial disease-magnetic resonance study. *Stroke*. (2015) 46:1233–8. doi: 10.1161/STROKEAHA.114.008030
106. Wiegman AF, Meier IB, Provenzano FA, Schupf N, Manly JJ, Stern Y, et al. Regional white matter hyperintensity volume and cognition predict death in a multiethnic community cohort of older adults. *J Am Geriatr Soc*. (2013) 61:2246–8. doi: 10.1111/jgs.12568
107. Callisaya ML, Srikanth VK, Lord SR, Close JC, Brodaty H, Sachdev PS, et al. Sub-Cortical Infarcts and the risk of falls in older people: combined results of TASCOC and Sydney MAS Studies. *Int J Stroke*. (2014) 9:55–60. doi: 10.1111/ijs.12279
108. Dhamoon MS, Cheung Y-K, Moon Y, DeRosa J, Sacco R, Elkind MSV, et al. Cerebral white matter disease and functional decline in older adults from the Northern Manhattan Study: A longitudinal cohort study. *PLoS Med*. (2018) 15:e1002529. doi: 10.1371/journal.pmed.1002529
109. Saavedra Pérez HC, Ikram MA, Direk N, Prigerson HG, Freak-Poli R, Verhaaren BFJ, et al. Cognition, structural brain changes and complicated grief. A population-based study. *Psychol Med*. (2015) 45:1389–99. doi: 10.1017/S0033291714002499
110. Hamedani AG, Rose KM, Peterlin BL, Mosley TH, Coker LH, Jack CR, et al. Migraine and white matter hyperintensities: The ARIC MRI study. *Neurology*. (2013) 81:1308–13. doi: 10.1212/WNL.0b013e3182a8235b

111. Honningsvåg L-M, Håberg AK, Hagen K, Kvistad KA, Stovner LJ, Linde M. White matter hyperintensities and headache: A population-based imaging study (HUNT MRI). *Cephalalgia*. (2018) 38:1927–39. doi: 10.1177/0333102418764891
112. Kurth T, Mohamed S, Maillard P, Zhu Y-C, Chabriat H, Mazoyer B, et al. Headache, migraine, and structural brain lesions and function: population based Epidemiology of Vascular Ageing-MRI study. *BMJ*. (2011) 342:c7357–c7357. doi: 10.1136/bmj.c7357
113. Nyquist PA, Yanek LR, Bilgel M, Cuzzocreo JL, Becker LC, Chevalier-Davis K, et al. Effect of white matter lesions on manual dexterity in healthy middle-aged persons. *Neurology*. (2015) 84:1920–6. doi: 10.1212/WNL.0000000000001557
114. Devanand DP, Tabert MH, Cuasay K, Manly JJ, Schupf N, Brickman AM, et al. Olfactory identification deficits and MCI in a multi-ethnic elderly community sample. *Neurobiol Aging*. (2010) 31:1593–1600. doi: 10.1016/j.neurobiolaging.2008.09.008
115. Aribisala BS, Wiseman S, Morris Z, Valdés-Hernández MC, Royle NA, Maniega SM, et al. Circulating inflammatory markers are associated with magnetic resonance imaging-visible perivascular spaces but not directly with white matter hyperintensities. *Stroke*. (2014) 45:605–7. doi: 10.1161/STROKEAHA.113.004059
116. Rist PM, Tzourio C, Elbaz A, Soumaré A, Dufouil C, Mazoyer B, et al. Structural brain lesions and restless legs syndrome: a cross-sectional population-based study. *BMJ Open*. (2014) 4:e005938. doi: 10.1136/bmjopen-2014-005938
117. Mutlu U, Cremers LGM, de Groot M, Hofman A, Niessen WJ, van der Lugt A, et al. Retinal microvasculature and white matter microstructure. *Neurology*. (2016) 87:1003–10. doi: 10.1212/WNL.0000000000003080
118. Glymour MM, Chene G, Tzourio C, Dufouil C. Brain MRI markers and dropout in a longitudinal study of cognitive aging: The Three-City Dijon Study. *Neurology*. (2012) 79:1340–8. doi: 10.1212/WNL.0b013e31826cd62a
119. Stewart R, Godin O, Crivello F, Maillard P, Mazoyer B, Tzourio C, et al. Longitudinal neuroimaging correlates of subjective memory impairment: 4-year prospective community study. *Br J Psychiatry*. (2011) 198:199–205. doi: 10.1192/bjp.bp.110.078683
120. Seiler S, Fletcher E, Hassan-Ali K, Weinstein M, Beiser A, Himali JJ, et al. Cerebral tract integrity relates to white matter hyperintensities, cortex volume, and cognition. *Neurobiol Aging*. (2018) 72:14–22. doi: 10.1016/j.neurobiolaging.2018.08.005
121. Maniega SM, Valdés Hernández MC, Clayden JD, Royle NA, Murray C, Morris Z, et al. White matter hyperintensities and normal-appearing white matter integrity in the aging brain. *Neurobiol Aging*. (2015) 36:909–18. doi: 10.1016/j.neurobiolaging.2014.07.048
122. Vernooij MW, Ikram MA, Tanghe HL, Vincent AJPE, Hofman A, Krestin GP, et al. Incidental findings on brain MRI in the general population. *N Engl J Med*. (2007) 357:1821–8. doi: 10.1056/NEJMoa070972
123. Weber C, Noels H. Atherosclerosis: current pathogenesis and therapeutic options. *Nat Med*. (2011) 17:1410–22. doi: 10.1038/nm.2538
124. Aizenstein HJ, Baskys A, Boldrini M, Butters MA, Diniz BS, Jaiswal MK, et al. Vascular depression consensus report – a critical update. *BMC Med*. (2016) 14:161. doi: 10.1186/s12916-016-0720-5
125. Taylor WD, Aizenstein HJ, Alexopoulos GS. The vascular depression hypothesis: mechanisms linking vascular disease with depression. *Mol Psychiatry*. (2013) 18:963–74. doi: 10.1038/mp.2013.20
126. Kaffashian S, Tzourio C, Zhu Y-C, Mazoyer B, Debette S. Differential effect of white-matter lesions and covert brain infarcts on the risk of ischemic stroke and intracerebral Hemorrhage. *Stroke*. (2016) 47:1923–5. doi: 10.1161/STROKEAHA.116.012734
127. Damangir S, Westman E, Simmons A, Vrenken H, Wahlund L-O, Spulber G. Reproducible segmentation of white matter hyperintensities using a new statistical definition. *Magn Reson Mater Phys Biol Med*. (2017) 30:227–37. doi: 10.1007/s10334-016-0599-3
128. Ghafoorian M, Karssemeijer N, Heskes T, van Uden IWM, Sanchez CI, Litjens G, et al. Location sensitive deep convolutional neural networks for segmentation of white matter hyperintensities. *Sci Rep*. (2017) 7:5110. doi: 10.1038/s41598-017-05300-5
129. Guerrero R, Qin C, Oktay O, Bowles C, Chen L, Joules R, et al. White matter hyperintensity and stroke lesion segmentation and differentiation using convolutional neural networks. *NeuroImage Clin*. (2018) 17:918–34. doi: 10.1016/j.nicl.2017.12.022
130. Moeskops P, de Bresser J, Kuijff HJ, Mendrik AM, Biessels GJ, Pluim JPW, et al. Evaluation of a deep learning approach for the segmentation of brain tissues and white matter hyperintensities of presumed vascular origin in MRI. *NeuroImage Clin*. (2018) 17:251–62. doi: 10.1016/j.nicl.2017.10.007
131. Taha AA, Hanbury A. Metrics for evaluating 3D medical image segmentation: analysis, selection, and tool. *BMC Med Imag*. (2015) 15:29. doi: 10.1186/s12880-015-0068-x
132. Poels MMF, Zaccari K, Verwoert GC, Vernooij MW, Hofman A, van der Lugt A, et al. Arterial stiffness and cerebral small vessel disease. *Stroke*. (2012) 43:2637–42. doi: 10.1161/STROKEAHA.111.642264
133. Grool AM, Graaf Y, Vincken KL, Witkamp TD, Mali WPTM, Geerlings MI. Antidepressant use is related to larger white matter lesion volume in patients with symptomatic atherosclerotic disease: the SMART-MR study. *J Neurol*. (2013) 260:197–206. doi: 10.1007/s00415-012-6616-1
134. Glazer H, Dong C, Yoshita M, Rundek T, Elkind MSV, Sacco RL, et al. Subclinical cerebrovascular disease inversely associates with learning ability: The NOMAS. *Neurology*. (2015) 84:2362–7. doi: 10.1212/WNL.0000000000001657
135. Nyquist PA, Bilgel MS, Gottesman R, Yanek LR, Moy TF, Becker LC, et al. Extreme deep white matter hyperintensity volumes are associated with african american race. *Cerebrovasc Dis*. (2014) 37:244–50. doi: 10.1159/000358117
136. Kooistra M, Geerlings MI, Mali WPTM, Vincken KL, van der Graaf Y, Biessels GJ. Diabetes mellitus and progression of vascular brain lesions and brain atrophy in patients with symptomatic atherosclerotic disease. SMART-MR study. *J Neurol Sci*. (2013) 332:69–74. doi: 10.1016/j.jns.2013.06.019
137. Huey ED, Manly JJ, Tang M-X, Schupf N, Brickman AM, Manoochehri M, et al. Course and etiology of dysexecutive MCI in a community sample. *Alzheimer's Dement*. (2013) 9:632–9. doi: 10.1016/j.jalz.2012.10.014
138. Stefansdottir H, Arnar DO, Aspelund T, Sigurdsson S, Jonsdottir MK, Hjaltason H, et al. Atrial fibrillation is associated with reduced brain volume and cognitive function independent of cerebral infarcts. *Stroke*. (2013) 44:1020–5. doi: 10.1161/STROKEAHA.12.679381
139. Versluis CE, van der Mast RC, van Buchem MA, Bollen ELEM, Blauw GJ, Eekhof JAH, et al. Progression of cerebral white matter lesions is not associated with development of depressive symptoms in elderly subjects at risk of cardiovascular disease. The PROSPER Study *Int J Geriatr Psychiatry*. (2006) 21:375–81. doi: 10.1002/gps.1477
140. Swardfager W, Cogo-Moreira H, Masellis M, Ramirez J, Herrmann N, Edwards JD, et al. The effect of white matter hyperintensities on verbal memory. *Neurology*. (2018) 90:e673–e682. doi: 10.1212/WNL.0000000000004983
141. Tsao CW, Himali JJ, Beiser AS, Larson MG, DeCarli C, Vasan RS, et al. Association of arterial stiffness with progression of subclinical brain and cognitive disease. *Neurology*. (2016) 86:619–26. doi: 10.1212/WNL.0000000000002368
142. Kloppenborg RP, Geerlings MI, Visseren FL, Mali WPTM, Vermeulen M, van der Graaf Y, et al. Homocysteine and progression of generalized small-vessel disease: The SMART-MR Study. *Neurology*. (2014) 82:777–83. doi: 10.1212/WNL.0000000000000168
143. Carmichael O, Schwarz C, Drucker D, Fletcher E, Harvey D, Beckett L, et al. Longitudinal changes in white matter disease and cognition in the first year of the alzheimer disease neuroimaging initiative. *Arch Neurol*. (2010) 67:1370. doi: 10.1001/archneurol.2010.284
144. Tiehuis AM, van der Graaf Y, Visseren FL, Vincken KL, Biessels GJ, Appelman APA, et al. Diabetes increases atrophy and vascular lesions on brain mri in patients with symptomatic arterial disease. *Stroke*. (2008) 39:1600–3. doi: 10.1161/STROKEAHA.107.506089
145. Kloppenborg RP, Nederkoorn PJ, Grool AM, Vincken KL, Mali WPTM, Vermeulen M, et al. Cerebral small-vessel disease and progression of brain atrophy: The SMART-MR study. *Neurology*. (2012) 79:2029–36. doi: 10.1212/WNL.0b013e3182749f02

146. Vlek A, Visseren F, Kappelle L, Witkamp T, Vincken K, Mali W, et al. Blood Pressure and white matter lesions in patients with vascular disease: The SMART-MR Study. *Curr Neurovasc Res.* (2009) 6:155–62. doi: 10.2174/156720209788970027
147. Tully PJ, Debette S, Mazoyer B, Tzourio C. White matter lesions are associated with specific depressive symptom trajectories among incident depression and dementia populations: three-city dijon MRI Study. *Am J Geriatr Psychiatry.* (2017) 25:1311–21. doi: 10.1016/j.jagp.2017.06.003
148. Brickman AM, Schupf N, Manly JJ, Stern Y, Luchsinger JA, Provenzano FA, et al. APOE $\epsilon 4$ and risk for alzheimer's disease: do regionally distributed white matter hyperintensities play a role? *Alzheimer's Dement.* (2014) 10:619–29. doi: 10.1016/j.jalz.2014.07.155
149. Schwartz GL, Bailey KR, Mosley T, Knopman DS, Jack CR, Canzanello VJ, et al. Association of ambulatory blood pressure with ischemic brain injury. *Hypertension.* (2007) 49:1228–34. doi: 10.1161/HYPERTENSIONAHA.106.078691
150. Gardener H, Scarmeas N, Gu Y, Boden-Albala B, Elkind MSV, Sacco RL, et al. Mediterranean diet and white matter hyperintensity volume in the northern manhattan study. *Arch Neurol.* (2012) 69:251. doi: 10.1001/archneurol.2011.548
151. Teodorczuk A, O'Brien JT, Firbank MJ, Pantoni L, Poggesi A, Erkinjuntti T, et al. White matter changes and late-life depressive symptoms. *Br J Psychiatry.* (2007) 191:212–7. doi: 10.1192/bjp.bp.107.036756
152. Brickman AM, Schupf N, Manly JJ, Luchsinger JA, Andrews H, Tang MX, et al. Brain morphology in older african americans, caribbean hispanics, and whites from northern manhattan. *Arch Neurol.* (2008) 65:1053. doi: 10.1001/archneur.65.8.1053
153. Tiehuis AM, Mali WPTM, van Raamt AF, Visseren FLJ, Biessels GJ, van Zandvoort MJE, et al. Cognitive dysfunction and its clinical and radiological determinants in patients with symptomatic arterial disease and diabetes. *J Neurol Sci.* (2009) 283:170–4. doi: 10.1016/j.jns.2009.02.337
154. Godin O, Dufouil C, Maillard P, Delcroix N, Mazoyer B, Crivello F, et al. White Matter Lesions as a predictor of depression in the elderly: the 3c-dijon study. *Biol Psychiatry.* (2008) 63:663–9. doi: 10.1016/j.biopsycho.2007.09.006
155. Aggarwal NT, Wilson RS, Bienias JL, De Jager PL, Bennett DA, Evans DA, et al. The association of magnetic resonance imaging measures with cognitive function in a biracial population sample. *Arch Neurol.* (2010) 67:475–82. doi: 10.1001/archneurol.2010.42
156. Vernooij MW, Ikram MA, Vrooman HA, Wielopolski PA, Krestin GP, Hofman A, et al. White Matter Microstructural Integrity and Cognitive Function in a General Elderly Population. *Arch Gen Psychiatry.* (2009) 66:545. doi: 10.1001/archgenpsychiatry.2009.5
157. Ritchie K, Ancelin M-L, Beaino E, Portet F, Brickman AM, Dartigues J-F, et al. Retrospective Identification and characterization of mild cognitive impairment from a prospective population cohort. *Am J Geriatr Psychiatry.* (2010) 18:692–700. doi: 10.1097/JGP.0b013e3181df4897
158. Debette S, Seshadri S, Beiser A, Au R, Himali JJ, Palumbo C, et al. Midlife vascular risk factor exposure accelerates structural brain aging and cognitive decline. *Neurology.* (2011) 77:461–8. doi: 10.1212/WNL.0b013e318227b227
159. Jefferson AL, Massaro JM, Wolf PA, Seshadri S, Au R, Vasan RS, et al. Inflammatory biomarkers are associated with total brain volume: The Framingham Heart Study. *Neurology.* (2007) 68:1032–8. doi: 10.1212/01.wnl.0000257815.20548.df
160. Lorus N, Locascio JJ, Rentz DM, Johnson KA, Sperling RA, Viswanathan A, et al. Vascular disease and risk factors are associated with cognitive decline in the alzheimer disease spectrum. *Alzheimer Dis Assoc Disord.* (2015) 29:18–25. doi: 10.1097/WAD.0000000000000043
161. Kloppenborg RP, Nederkoorn PJ, van der Graaf Y, Geerlings MI. Homocysteine and cerebral small vessel disease in patients with symptomatic atherosclerotic disease. The SMART-MR study. *Atherosclerosis.* (2011) 216:461–6. doi: 10.1016/j.atherosclerosis.2011.02.027
162. Sigurdsson S, Aspelund T, Forsberg L, Fredriksson J, Kjartansson O, Oskarsdottir B, et al. Brain tissue volumes in the general population of the elderly. *Neuroimage.* (2012) 59:3862–70. doi: 10.1016/j.neuroimage.2011.11.024
163. Graff-Radford J, Madhavan M, Vemuri P, Rabinstein AA, Cha RH, Mielke MM, et al. Atrial fibrillation, cognitive impairment, and neuroimaging. *Alzheimer's Dement.* (2016) 12:391–8. doi: 10.1016/j.jalz.2015.08.164
164. Biesbroek JM, Kuijf HJ, van der Graaf Y, Vincken KL, Postma A, Mali WPTM, et al. Association between subcortical vascular lesion location and cognition: a voxel-based and tract-based lesion-symptom mapping study. The SMART-MR Study. *PLoS ONE.* (2013) 8:e60541. doi: 10.1371/journal.pone.0060541
165. Liu J, Rutten-Jacobs L, Liu M, Markus HS, Traylor M. Causal impact of type 2 diabetes mellitus on cerebral small vessel disease: a mendelian randomization analysis. *Stroke.* (2018) 49:1325–31. doi: 10.1161/STROKEAHA.117.020536
166. Duering M, Gesierich B, Seiler S, Pirpamer L, Gonik M, Hofer E, et al. Strategic white matter tracts for processing speed deficits in age-related small vessel disease. *Neurology.* (2014) 82:1946–50. doi: 10.1212/WNL.0000000000000475
167. Croll PH, Voortman T, Ikram MA, Franco OH, Schoufour JD, Bos D, et al. Better diet quality relates to larger brain tissue volumes. *Neurology.* (2018) 90:e2166–73. doi: 10.1212/WNL.0000000000005691
168. Shoamanesh A, Preis SR, Beiser AS, Vasan RS, Benjamin EJ, Kase CS, et al. Inflammatory biomarkers, cerebral microbleeds, and small vessel disease: framingham heart study. *Neurology.* (2015) 84:825–32. doi: 10.1212/WNL.0000000000001279
169. Zahodne L, Manly J, Narkhede A, Griffith E, DeCarli C, Schupf N, et al. Structural MRI predictors of late-life cognition differ across african americans, hispanics, and whites. *Curr Alzheimer Res.* (2015) 12:632–9. doi: 10.2174/1567205012666150530203214
170. Godin O, Tzourio C, Rouaud O, Zhu Y, Maillard P, Pasquier F, et al. Joint effect of white matter lesions and hippocampal volumes on severity of cognitive decline: The 3C-Dijon MRI Study. *J Alzheimer's Dis.* (2010) 20:453–63. doi: 10.3233/JAD-2010-1389
171. Rundek T, Della-Morte D, Gardener H, Dong C, Markert MS, Gutierrez J, et al. Relationship between carotid arterial properties and cerebral white matter hyperintensities. *Neurology.* (2017) 88:2036–42. doi: 10.1212/WNL.0000000000003951
172. Habes M, Erus G, Toledo JB, Zhang T, Bryan N, Launer LJ, et al. White matter hyperintensities and imaging patterns of brain ageing in the general population. *Brain.* (2016) 139:1164–79. doi: 10.1093/brain/aww008
173. Maillard P, Crivello F, Dufouil C, Tzourio-Mazoyer N, Tzourio C, Mazoyer B. Longitudinal follow-up of individual white matter hyperintensities in a large cohort of elderly. *Neuroradiology.* (2009) 51:209–20. doi: 10.1007/s00234-008-0489-0
174. Verhaaren BFJ, Vernooij MW, de Boer R, Hofman A, Niessen WJ, van der Lugt A, et al. High blood pressure and cerebral white matter lesion progression in the general population. *Hypertension.* (2013) 61:1354–9. doi: 10.1161/HYPERTENSIONAHA.111.00430
175. Saczynski JS, Sigurdsson S, Jonsson PV, Eiriksdottir G, Olafsdottir E, Kjartansson O, et al. Glycemic status and brain injury in older individuals: the age gene/environment susceptibility-reykjavik study. *Diab Care.* (2009) 32:1608–13. doi: 10.2337/dc08-2300
176. Ritchie SJ, Tucker-Drob EM, Cox SR, Dickie DA, del C, Valdés Hernández M, et al. Risk and protective factors for structural brain ageing in the eighth decade of life. *Brain Struct. Funct.* (2017) 222:3477–90. doi: 10.1007/s00429-017-1414-2
177. van Sloten TT, Sigurdsson S, van Buchem MA, Phillips CL, Jonsson PV, Ding J, et al. Cerebral small vessel disease and association with higher incidence of depressive symptoms in a general elderly population: the ages-reykjavik study. *Am J Psychiatry.* (2015) 172:570–8. doi: 10.1176/appi.ajp.2014.14050578
178. Godin O, Tzourio C, Maillard P, Alperovitch A, Mazoyer B, Dufouil C. Apolipoprotein E genotype is related to progression of white matter lesion load. *Stroke.* (2009) 40:3186–90. doi: 10.1161/STROKEAHA.109.555839
179. Vidal J-S, Sigurdsson S, Jonsdottir MK, Eiriksdottir G, Thorgeirsson G, Kjartansson O, et al. Coronary artery calcium, brain function and structure. *Stroke.* (2010) 41:891–7. doi: 10.1161/STROKEAHA.110.579581
180. Knopman DS, Griswold ME, Lirette ST, Gottesman RF, Kantarci K, Sharrett AR, et al. Vascular imaging abnormalities and cognition. *Stroke.* (2015) 46:433–40. doi: 10.1161/STROKEAHA.114.007847

181. Appelman AP, van der Graaf Y, Vincken KL, Tiehuis AM, Witkamp TD, Mali WP, et al. Total cerebral blood flow, white matter lesions and brain atrophy: the SMART-MR Study. *J Cereb Blood Flow Metab.* (2008) 28:633–9. doi: 10.1038/sj.jcbfm.9600563
182. Godin O, Maillard P, Crivello F, Rovitch A, Mazoyer B, Tzourio C, et al. Association of white-matter lesions with brain atrophy markers: the three-city dijon MRI study. *Cerebrovasc Dis.* (2009) 28:177–84. doi: 10.1159/000226117
183. Aparicio HJ, Petrea RE, Massaro JM, Manning WJ, Oyama-Manabe N, Beiser AS, et al. Association of descending thoracic aortic plaque with brain atrophy and white matter hyperintensities: the framingham heart study. *Atherosclerosis.* (2017) 265:305–11. doi: 10.1016/j.atherosclerosis.2017.06.919
184. Appelman APA, Vincken KL, van der Graaf Y, Vlek ALM, Witkamp TD, Mali WPTM, et al. White matter lesions and lacunar infarcts are independently and differently associated with brain atrophy: the SMART-MR study. *Cerebrovasc Dis.* (2010) 29:28–35. doi: 10.1159/000255971
185. Luchsinger JA, Brickman AM, Reitz C, Cho SJ, Schupf N, Manly JJ, et al. Subclinical cerebrovascular disease in mild cognitive impairment. *Neurology.* (2009) 73:450–6. doi: 10.1212/WNL.0b013e3181b1636a
186. Satizabal CL, Zhu YC, Mazoyer B, Dufouil C, Tzourio C. Circulating IL-6 and CRP are associated with MRI findings in the elderly: The 3C-Dijon Study. *Neurology.* (2012) 78:720–7. doi: 10.1212/WNL.0b013e318248e50f
187. Marcus J, Gardener H, Rundek T, Elkind MSV, Sacco RL, DeCarli C, et al. Baseline and Longitudinal Increases in diastolic blood pressure are associated with greater white matter hyperintensity volume. *Stroke.* (2011) 42:2639–41. doi: 10.1161/STROKEAHA.111.617571
188. Muller M, Appelman APA, van der Graaf Y, Vincken KL, Mali WPTM, Geerlings MI. Brain atrophy and cognition: interaction with cerebrovascular pathology? *Neurobiol Aging.* (2011) 32:885–93. doi: 10.1016/j.neurobiolaging.2009.05.005
189. Ritchie SJ, Dickie DA, Cox SR, Valdes Hernandez M, del C, Corley J, et al. Brain volumetric changes and cognitive ageing during the eighth decade of life. *Hum Brain Mapp.* (2015) 36:4910–25. doi: 10.1002/hbm.22959
190. Vibha D, Tiemeier H, Mirza SS, Adams HHH, Niessen WJ, Hofman A, et al. Brain volumes and longitudinal cognitive change. *Alzheimer Dis Assoc Disord.* (2018) 32:43–9. doi: 10.1097/WAD.0000000000000235
191. Jochemsen HM, Muller M, Bots ML, Scheltens P, Vincken KL, Mali WPTM, et al. Arterial stiffness and progression of structural brain changes: the SMART-MR study. *Neurology.* (2015) 84:448–55. doi: 10.1212/WNL.0000000000001201
192. Moran C, Phan TG, Chen J, Blizzard L, Beare R, Venn A, et al. Brain Atrophy in Type 2 Diabetes: Regional distribution and influence on cognition. *Diab Care.* (2013) 36:4036–42. doi: 10.2337/dc13-0143
193. van der Veen PH, Muller M, Vincken KL, Witkamp TD, Mali WPTM, van der Graaf Y, et al. Longitudinal changes in brain volumes and cerebrovascular lesions on MRI in patients with manifest arterial disease: the SMART-MR study. *J Neurol Sci.* (2014) 337:112–8. doi: 10.1016/j.jns.2013.11.029
194. Jokinen H, Melkas S, Madureira S, Verdelho A, Ferro JM, Fazekas F, et al. Cognitive reserve moderates long-term cognitive and functional outcome in cerebral small vessel disease. *J Neurol Neurosurg Psychiatry.* (2016) 87:1296–302. doi: 10.1136/jnnp-2016-313914
195. Geerlings MI, Appelman APA, Vincken KL, Mali WPTM. Association of white matter lesions and lacunar infarcts with executive functioning: the SMART-MR study. *Am J Epidemiol.* (2009) 170:1147–55. doi: 10.1093/aje/kwp256

Conflict of Interest Statement: The authors declare that the research was conducted in the absence of any commercial or financial relationships that could be construed as a potential conflict of interest.

Copyright © 2019 Frey, Petersen, Mayer, Schulz, Cheng and Thomalla. This is an open-access article distributed under the terms of the Creative Commons Attribution License (CC BY). The use, distribution or reproduction in other forums is permitted, provided the original author(s) and the copyright owner(s) are credited and that the original publication in this journal is cited, in accordance with accepted academic practice. No use, distribution or reproduction is permitted which does not comply with these terms.



The Altered Reconfiguration Pattern of Brain Modular Architecture Regulates Cognitive Function in Cerebral Small Vessel Disease

Renyuan Liu^{1,2,3†}, Haifeng Chen^{1,2,3†}, Ruomeng Qin^{1,2,3}, Yucheng Gu^{1,2,3}, Xin Chen^{1,2,3}, Junhui Zou^{1,2,3}, YongCheng Jiang^{1,2,3}, Weikai Li⁴, Feng Bai^{1,2,3}, Bing Zhang⁵, Xiaoying Wang⁶ and Yun Xu^{1,2,3*}

¹ Department of Neurology, Drum Tower Hospital, Medical School and The State Key Laboratory of Pharmaceutical Biotechnology, Institute of Brain Science, Nanjing University, Nanjing, China, ² Jiangsu Province Stroke Center for Diagnosis and Therapy, Nanjing, China, ³ Nanjing Neuropsychiatry Clinic Medical Center, Nanjing, China, ⁴ College of Computer Science and Technology, Nanjing University of Aeronautics and Astronautics, Nanjing, China, ⁵ Department of Radiology, Drum Tower Hospital, Medical School of Nanjing University, Nanjing, China, ⁶ Departments of Neurology, Harvard Medical School, Massachusetts General Hospital, Charlestown, MA, United States

OPEN ACCESS

Edited by:

Eric Jouvent,
Université Sorbonne Paris Cité, France

Reviewed by:

Anil Man Tuladhar,
Radboud University Nijmegen Medical
Centre, Netherlands
Tommaso Gilli,
IMT School for Advanced Studies
Lucca, Italy

*Correspondence:

Yun Xu
xuyun20042001@aliyun.com

[†]These authors have contributed
equally to this work

Specialty section:

This article was submitted to
Stroke,
a section of the journal
Frontiers in Neurology

Received: 02 December 2018

Accepted: 15 March 2019

Published: 05 April 2019

Citation:

Liu R, Chen H, Qin R, Gu Y, Chen X,
Zou J, Jiang Y, Li W, Bai F, Zhang B,
Wang X and Xu Y (2019) The Altered
Reconfiguration Pattern of Brain
Modular Architecture Regulates
Cognitive Function in Cerebral Small
Vessel Disease. *Front. Neurol.* 10:324.
doi: 10.3389/fneur.2019.00324

Background: Cerebral small vessel disease (SVD) is a common cause of cognitive dysfunction. However, little is known whether the altered reconfiguration pattern of brain modular architecture regulates cognitive dysfunction in SVD.

Methods: We recruited 25 cases of SVD without cognitive impairment (SVD-NCI) and 24 cases of SVD with mild cognitive impairment (SVD-MCI). According to the Framingham Stroke Risk Profile, healthy controls (HC) were divided into 17 subjects (HC-low risk) and 19 subjects (HC-high risk). All individuals underwent resting-state functional magnetic resonance imaging and cognitive assessments. Graph-theoretical analysis was used to explore alterations in the modular organization of functional brain networks. Multiple regression and mediation analyses were performed to investigate the relationship between MRI markers, network metrics and cognitive performance.

Results: We identified four modules corresponding to the default mode network (DMN), executive control network (ECN), sensorimotor network and visual network. With increasing vascular risk factors, the inter- and intranetwork compensation of the ECN and a relatively reserved DMN itself were observed in individuals at high risk for SVD. With declining cognitive ability, SVD-MCI showed a disrupted ECN intranetwork and increased DMN connection. Furthermore, the intermodule connectivity of the right inferior frontal gyrus of the ECN mediated the relationship between periventricular white matter hyperintensities and visuospatial processing in SVD-MCI.

Conclusions: The reconfiguration pattern of the modular architecture within/between the DMN and ECN advances our understanding of the neural underpinning in response to vascular risk and SVD burden. These observations may provide novel insight into the underlying neural mechanism of SVD-related cognitive impairment and may serve as a potential non-invasive biomarker to predict and monitor disease progression.

Keywords: small vessel disease, cognitive impairment, network reconfiguration, compensation, visuospatial processing

INTRODUCTION

Cerebral small vessel disease (SVD) is a significant contributor to cognitive dysfunction (1). It is characterized by white matter hyperintensities (WMH), lacunar infarcts (LI), microbleeds and the Virchow-Robin space in MRI (1). Although the mechanism is still incompletely understood, SVD is generally considered to be the result causes of aging and vascular risk factors including hypertension, diabetes, and smoking (2). More vascular risk factors create an easier path to SVD (3). The Framingham Stroke Risk Profile (FSRP) is a composite risk index of vascular risk factors and has been used to identify the population at high risk for SVD (4, 5).

Early identification of individuals at risk for cognitive decline is important to the development of effective therapies for cognitive decline or dementia in SVD. Previous publications have indicated that the progression or location of WMH could induce cognitive decline (6, 7). Currently, a promising brain functional imaging technique, that is, resting-state fMRI has been widely used in the human brain functional network researches, which can show the metabolism in the different areas, spontaneous activity in different mode regions, and intra- or inter-regional connectivity among different brain networks (8).

Functional connectivities are not homogeneously distributed across the whole network, but gather into subnetworks (i.e., modules) that are densely connected internally but only weakly coupled externally (8). Overall, modular organization may be conducive to the greater robustness and adaptability of the brain network responding to internal and external changes (8). Previous studies have observed modular reconfiguration of brain networks. In patients with subcortical vascular mild cognitive impairment, the executive control network (ECN) module was notably rearranged; i.e., the posterior parietal regions were separate from ECN as a new module (9). A gene-connectome study demonstrated that APOE $\epsilon 4$ in patients with Alzheimer's disease led to the reconfiguration of the posterior default mode network (pDMN) and ECN correlated with cognitive performance (10). Furthermore, a task-state MRI study revealed that normal individuals showed dynamic integration between specialized brain modules at different cognitive loads (11). Therefore, modularity analysis could provide further insights into the SVD-related cognitive impairment.

In this study, we applied graph-theoretical modularity analysis to resting-state functional MRI data and characterized the brain modular network organization in subjects with SVD or those at risk. Furthermore, we explored the relationship among SVD burden, modular measures and cognitive performance. We hypothesize that reconfiguration of modular architecture emerges during the progression of SVD and mediates the relationship between SVD burden and cognitive function.

MATERIALS AND METHODS

Participants

This is hospital-based Cross-study (Clinical Trial: ChiCTR-OOC-17010562), which consists of 85 Han Chinese participants (49 SVD subjects and 36 matched healthy controls [HC]) aged

between 50 and 80 years. SVD divided into SVD-non cognitive impairment (SVD-NCI, $n = 25$) and SVD-mild cognitive impairment (SVD-MCI $n = 24$) based on neuropsychological assessment. HC was split up into HC-low risk (risk $<15\%$, $n = 17$) and HC-high risk (risk $>15\%$, $n = 19$), following Stroke Risk Prediction Model (12). SVD criteria was defined by the presence on neuroimaging: WMH (Fazekas scale 2 or higher) with or without lacunar infarct (13, 14). Exclusion criteria included intracranial hemorrhage; non-SVD-related WMH mimics (e.g., multiple sclerosis); cardioembolic source (e.g., atrial fibrillation); intra/extracranial large artery stenosis $>50\%$; dementia [Mini-Mental State Examination (MMSE) ≤ 23] and other neurological or psychiatric disorders (15). This research was approved by the Ethics Committee of Nanjing Drum Tower Hospital, and signed informed consent was obtained from all participants.

Stroke Risk Prediction Model

FSRP is a clinical and composite risk score of vascular risk factors that predicts 10-year probability of stroke for individuals who are free of stroke at baseline (12). This model is based on the following risk factors: age, systolic blood pressure, use of hypertensive medication, diabetes mellitus, cigarette smoking, atrial fibrillation, cardiovascular heart disease, and left ventricular hypertrophy. A higher FSRP indicates a higher risk of developing a stroke event (12). The score ranges from 1 to 27 points for women and 1–30 points for men. In this study, participants with atrial fibrillation were excluded due to cardioembolic source. So, we excluded points assigned for atrial fibrillation. The sex-specific score is then converted to 10-year probability of strokes ranging from 1 to 84% for women and 3–88% for men (12).

Neuropsychological Assessment

All participants underwent a standardized neuropsychological evaluation protocol, which included the general cognitive examination and multiple cognitive domain assessments performed by an experienced neuropsychologist. General cognitive function was evaluated by MMSE and Beijing version of the Montreal Cognitive Assessment (MoCA-BJ). In this study, we used MoCA-BJ to detect SVD-MCI. Since education is the strongest non-cognitive factor influencing the assessment of MoCA-BJ, the optimal cutoff points are determined according to education level (or years of education). For subjects with no formal education, the MoCA-BJ cutoff was 13/14; for subjects with 1–6 years of education, the MoCA-BJ cutoff was 19/20; and for subjects with 7 or more years of education, it was 24/25. The raw examination scores were transformed to Z-scores so as to calculate each cognitive domain performance. Episodic memory is a compound score that includes the mean of the Z-scores of Auditory Verbal Learning Test-delayed recall (AVLT-DR) and Wechsler Memory Scale Visual Reproduction-delayed recall (WMS-VR-DR). Visuospatial function (VPF) was calculated as the mean of the Z-scores of Clock Drawing Test (CDT) and Visual Reproduction-copy (VR-C). Information processing speed (IPS) is a compound score of the average Z-scores of Trail Making Test-A (TMT-A), Stroop Color and Word Tests A and B (Stroop A and B). Language consisted of Category Verbal Fluency (CVF) and Boston Naming Test (BNT). Executive

Function was calculated as the average Z-scores of Digit Span Test-backward (DST-backward), TMT-B, and Stroop C.

MRI Scanning

All of the subjects were scanned by a Philips 3.0-T scanner (Philips Medical Systems, The Netherlands) with a homogeneous birdcage head coil in order to reduce head movements. Prior to the scan, all subjects were instructed to keep their eyes closed but not fall asleep, think of nothing, and move as little as possible during data acquisition. Finally, a simple questionnaire indicated that all of the subjects had not fallen asleep during the scan. The high-resolution T1-weighted sagittal images covering the whole brain acquired by turbo fast echo acquisition as follows: repetition time (TR) = 9.8 ms, echo time (TE) = 4.6 ms, flip angle (FA) = 8°, acquisition matrix = 256×256 , number of slices = 192, thickness = 1.0 mm, FOV = 250×250 mm². The 3D fluid-attenuated inversion recovery (FLAIR) images were acquired by the sequence: TR = 4,500 ms, TE = 333 ms, time interval (TI) = 1,600 ms, acquisition matrix = 270×260 , voxel size = $0.95 \times 0.95 \times 0.95$ mm³, number of slices = 200. The resting-state functional scans covering 230 volumes were obtained with a gradient-recalled echoplanar imaging sequence: TR = 2,000 ms, TE = 30 ms, FA = 90°, acquisition matrix = 64×64 , number of slices = 35, thickness = 4.0 mm, FOV = 240×240 mm². WMH automated segmentation and volume quantification was processed in the Wisconsin White Matter Hyperintensities Segmentation Toolbox version 1.3 (W2MHS v1.3, <https://sourceforge.net/projects/w2mhs>) based on FLAIR and T1 images. The total WMH included periventricular-WMH (PWMH) and deep-WMH (DWMH). Intracranial volume was calculated as a sum of gray matter (GM), white matter and cerebrospinal fluid volume using automated segmentation on T1 images in Statistical Parametric Mapping (SPM8, <http://www.fil.ion.ucl.ac.uk/spm>). WMH volume was normalized to the intracranial volume (16). Lacunes of presumed vascular origin were defined as hypointense areas (>3 mm and ≤15 mm in diameter) on FLAIR and T1 images, distinguished from enlarged perivascular spaces and infraputamina pseudolacunes (1). Lacunes were counted by two trained raters blinded to the participants' clinical information.

Image Preprocessing

The resting-state fMRI data was preprocessed by the Graph Theoretical Network Analysis Toolbox version 2.0 (GRETNA v2.0, <http://www.nitrc.org/projects/gretna/>) based on SPM8. After removing the first 10 volumes, the remaining functional images were corrected for intravolume time offsets and intervolumetric geometrical displacements. No subjects performed a displacement >2 mm or an angular rotation >2° in any direction. Next, the obtained images were spatially normalized to the Montreal Neurological Institute (MNI) space and resampled to $3 \times 3 \times 3$ mm voxels. The resulting images were further band-pass filtered within the frequency range of 0.01–0.08 Hz to reduce the low-frequency drift and high frequency physiological noise (17). Linear trends were also removed. Finally, several nuisance signals were regressed out, including the Friston 24-motion parameter model (six head motion parameters, six head motion

parameters one time point before, and the 12 corresponding squared items), global mean, white matter and cerebrospinal fluid signals (18).

Network Construction

In this study, functional brain networks were constructed at the large-scale level with nodes for brain regions and edges for interregional functional connectivity (FC). To define the network nodes, we divided the brain into 1024 contiguous and uniform regions of interest (ROIs) based on a high resolution, randomly partitioning brain atlas (19). To define network edge, we calculated Pearson correlation coefficients for each pair of 1024 ROIs between the regional mean time series. To improve the normality, these correlation coefficients were translated to z values by Fisher's r-to-z transform. We restricted our analysis to positive correlations because of the ambiguous interpretation of negative correlations (20). As described in the previous study, brain networks were not fully connected at lower sparsity threshold and were less likely to remain small-world architecture at higher sparsity threshold (11). In this study, the matrix was thresholded at a set of sparsity (ranging from 0.10 to 0.30, with steps of 0.01) to obtain a binary undirected network (21).

Modularity

A module is referred to as a collection of nodes that are densely connected with each other but less connected with other nodes. And the modularity Q of a network quantifies the efficacy of segmenting a network into modules, which was defined as follows:

$$Q = \sum_{i=1}^{N_m} \left[l_i/L - (d_i/2L)^2 \right] \quad (1)$$

where N_m is the number of modules, L is the total number of edges in the network, l_i is the number of within-module edges in the module i and d_i is the sum of the linked edges at each node in the module i . In this study, we used a spectral optimization algorithm to detect the modular community structure, which was proposed by Newman (22). In practice, the network modularity Q with a powerful modular structure typically ranges from 0.3 to 0.7 (23). Given that the sparsity threshold could have an effect on modular partitioning, we performed the modularity analysis on group-level brain networks, applying a threshold of 20% sparsity at each group (9). According to prior investigations associated with cognition (11, 24), DMN and ECN modules, which were identified from the module partitioning at each group by visual inspection, were of particular interest in our study. Notably, to ensure comparability, we apply the module partitioning of HC-low risk group as the unified standard in the following analyses at module and nodal levels.

At the module level, we measured intramodule connectivity density (D_s) and intermodule connectivity density ($D_{s,t}$) as follows:

$$D_s = \frac{2 \sum_{i,j \in s} \varepsilon_{i,j}}{N_s(N_s - 1)} \quad (2)$$

where N_s is the number of nodes within module s , and $\varepsilon_{i,j}$ are the existing edges within module s .

$$D_{s,t} = \frac{\sum_{i \in s, j \in t} \varepsilon_{i,j}}{N_s * N_t} \quad (3)$$

where N_s is the number of nodes within module s and N_t is the number of nodes within module t , and $\varepsilon_{i,j}$ are the existing edges between module s and module t .

At the nodal level, within-module degree (WD) and participation coefficient (PC) were calculated as follows (25):

$$WD_i = \frac{e_i - \bar{e}_s}{\sigma_s} \quad (4)$$

where e_i is the nodal degree of a node i within module s and \bar{e}_s is the average nodal degree of all nodes in module s , and σ_s is the standard deviation of the within module nodal degree of all nodes in module s .

$$PC_i = 1 - \sum_{s=1}^{N_m} \left(\frac{k_{i,s}}{k_i} \right)^2 \quad (5)$$

Where N_m is the number of modules and $k_{i,s}$ is the number of connections between the node i and module s . k_i is the total number of connections of node i to all other nodes in the N_m modules.

Statistical Analysis

Differences between groups in demographic, neuroimaging characteristics and cognitive assessment were analyzed using a Chi-squared (χ^2) test or one-way analysis of variance (ANOVA) in SPSS version 22 (IBM Corp., Armonk, NY). The significance level was set at $P < 0.05$.

For module level metrics, we used ANOVA to investigate whether there were significant group differences in modularity, intramodule connectivity density and intermodule connectivity density. The significant level was set at $P < 0.05$. For nodal-wise measures (i.e., WD and PC), we applied GRENA to investigate the significantly different brain regions between groups, and false discovery rate (FDR) was performed at an α level of 0.01 to correct for multiple comparisons. Then, a *post hoc* test was used to determine the change pattern of nodal-wise metrics in differential regions. In all analyses, age, gender, education level, GM volume, and number of lacunes or WMH volume were controlled for as confounding covariates.

To investigate the relationship among MRI markers, network metrics and cognitive performance, a multiple regression analysis and mediation analysis were performed by using SPSS while controlling for relevant covariates (age, sex, education level, GM, and number of lacunes or WMH volume).

RESULTS

Demographic and Clinical Characteristics

Demographic and clinical data for the HC subgroups (HC-low risk and HC-high risk) and SVD subgroups (SVD-NCI and SVD-MCI) are summarized in **Table 1**. There were no significant differences in gender and years of education between four groups. However, HC-low risk group showed significantly lower age compared with other groups. In subsequent analyses, we controlled for the age as a confounding covariate. WMH and PWMH volume significantly differed among groups ($P < 0.001$). Both of SVD subgroups had a higher WMH and PWMH volume compared to each HC subgroup. The SVD-MCI group exhibited poorer performances on MoCA-BJ ($P < 0.001$), episodic memory ($P < 0.001$), VPF ($P = 0.017$), IPS ($P = 0.002$), language function ($P = 0.028$) and executive function ($P < 0.001$) than other groups (details of cognitive domain assessment in **Table 1**).

Brain Module Identification

All groups almost exhibited high modularity Q across the sparsity range (0.1–0.3), showing a powerful modular structure of brain network organization (**Supplementary Figure 1**). We further conducted the following analyses on functional networks constructed at the 20% sparsity threshold. We identified four modules that corresponded to DMN, ECN, sensorimotor network (SMN) and visual network (VN) detected from group-averaged brain networks (**Figure 1**).

Module-Wise Alterations and its Relationship With Cognition

We found the significant differences of intra-module connectivity density within DMN among the four groups ($F = 4.919$, $p = 0.004$) (**Figure 2A**). The further analysis indicated that SVD-MCI exhibited higher connectivity density than SVD-NCI ($p = 0.004$), while there was no significant difference between HC-low risk and HC-high risk (**Figure 2B**). Moreover, we found that IPS was positively associated with functional connectivity density within DMN ($\beta = 0.501$, $P = 0.022$) in SVD-NCI (**Supplementary Figure 2A**).

The group differences of intra-module connectivity density within ECN was also observed ($F = 66.169$, $p < 0.001$). In the HC group, the functional connectivity density within ECN remarkably enhanced with the increase of risk for SVD ($p < 0.001$), whereas in SVD group, the functional connectivity density notably decreased as the appearance of cognitive decline ($p < 0.001$) (**Figure 2C**). Multiple regression analyses indicated that IPS was negatively related to functional connectivity density within ECN ($\beta = -0.432$, $P = 0.036$) in SVD-NCI (**Supplementary Figure 2B**).

The inter-module connectivity density between DMN and ECN significantly differed in four groups ($F = 3.671$, $p = 0.016$). The HC-high risk group showed the more closely connected coupling between DMN and ECN compared with the HC-low risk group ($p = 0.002$) (**Figure 2D**). In contrast, there was no statistical difference between SVD groups. The FC density between DMN and ECN correlated negatively with DST ($\beta = -0.587$, $P = 0.006$) in HC-high risk (**Supplementary Figure 2C**).

TABLE 1 | Demographic and neuropsychological data.

Items	HC		CSVD		F/ χ^2 /H	p
	Low-risk (n = 17)	High-risk (n = 19)	NCI (n = 25)	MCI (n = 24)		
DEMOGRAPHICS						
Age (years)	55.47 ± 4.23	68.16 ± 5.32	64.52 ± 10.65	65.92 ± 9.11	8.260	<0.001 ^{b*}
Education (years)	11.47 ± 4.09	11.84 ± 3.63	11.16 ± 4.11	12.67 ± 3.38	0.694	0.559 ^b
Gender (male/female)	7/10	14/5	12/13	11/13	–	0.179 ^a
NEUROIMAGING CHARACTERISTICS						
GMV(cm ³)	540.88 ± 56.93	541.77 ± 46.88	539.75 ± 38.88	538.08 ± 51.44	0.023	0.995 ^b
WMV(cm ³)	505.66 ± 53.69	467.19 ± 52.91	460.83 ± 44.00	463.95 ± 59.47	0.709	0.550 ^b
WMH(mm ³)	470.97 (184.91, 651.34)	719.00 (147.29, 892.00)	2978.46 (762.74, 4019.20)	4826.16 (760.99, 5639.67)	20.220	<0.001 ^{c*}
PVWMH	287.38 (111.46, 500.42)	547.20 (107.91, 786.85)	2091.44(468.66, 2913.88)	3633.38 (317.13, 4862.83)	21.266	<0.001 ^{c*}
DWMH	97.93 (31.34, 173.13)	41.25 (17.50, 283.61)	298.69 (54.30, 980.61)	431.76 (14.55, 1149.31)	6.056	0.109
Lacunes, number (%)	–	–	7 (28%)	13 (54%)	–	–
GENERAL COGNITION						
MMSE	28.71 ± 1.26	28.58 ± 1.39	28.44 ± 1.29	27.75 ± 2.07	1.624	0.19 ^b
MoCA-BJ	25.47 ± 0.60	25.73 ± 0.54	26.10 ± 0.45	21.41 ± 0.46	21.789	<0.001 ^{b*}
COMPOSITION Z SCORES OF EACH COGNITIVE DOMAIN						
Episodic memory	0.60 ± 0.54	−0.10 ± 0.56	0.11 ± 0.54	−0.53 ± 0.91	9.762	<0.001 ^{b*}
AVLT-DR	6.53 ± 1.46	5.47 ± 1.47	5.52 ± 1.85	3.75 ± 2.05	9.061	<0.001 ^{b*}
VR-DR (WMS)	8.65 ± 3.26	6.37 ± 2.79	7.08 ± 2.68	5.83 ± 3.58	2.964	0.037 ^{b*}
Visuospatial processing function	0.18 ± 0.24	0.14 ± 0.21	0.26 ± 0.18	−0.503 ± 0.18	3.584	0.017 ^{b*}
CDT	3.96 ± 0.16	3.82 ± 0.14	3.99 ± 0.12	3.35 ± 0.12	5.529	0.002 ^{b*}
VR-C	13.71 ± 0.46	13.91 ± 0.41	13.88 ± 0.34	12.98 ± 0.35	1.514	0.217 ^b
Information processing speed	0.36 ± 0.75	0.09 ± 0.89	0.18 ± 0.78	−0.51 ± 0.58	5.538	0.002 ^{b*}
TMT-A	50.27 ± 5.74	51.15 ± 5.15	46.30 ± 4.27	68.67 ± 4.40	5.014	0.003 ^{b*}
Stroop A	16.51 ± 2.15	14.63 ± 1.93	17.66 ± 1.60	24.14 ± 1.65	5.749	<0.001 ^{b*}
Stroop B	20.45 ± 2.25	23.25 ± 2.02	19.97 ± 1.67	25.18 ± 1.72	1.816	0.151 ^b
Language	0.26 ± 0.20	0.12 ± 0.18	0.12 ± 0.15	−0.4 ± 0.15	3.207	0.028 ^{b*}
CVF	17.40 ± 1.01	17.17 ± 0.91	17.43 ± 0.75	15.55 ± 0.77	1.279	0.287 ^b
BNT	52.31 ± 1.62	50.77 ± 1.45	50.33 ± 1.20	46.79 ± 1.24	2.999	0.036 ^{b*}
Executive function	0.31 ± 0.53	0.36 ± 0.82	−0.12 ± 0.64	−0.38 ± 0.56	6.437	<0.001 ^{b*}
DST-backward	5.29 ± 0.38	5.69 ± 0.35	4.80 ± 0.29	4.66 ± 0.29	2.231	0.091 ^b
TMT-B	81.39 ± 12.06	79.22 ± 10.83	107.13 ± 8.98	131.21 ± 9.25	6.124	<0.001 ^{b*}
Stroop C	29.33 ± 2.67	28.90 ± 2.39	33.47 ± 1.98	36.77 ± 2.04	2.885	0.041 ^{b*}

Values are presented as the mean ± standard error (SE), median (interquartile ranges) or number (percentage).

^athe *p*-value was obtained by χ^2 test.

^bthe *p*-value was obtained by one-way ANOVA and ^cthe *p*-value was obtained by Kruskal-Wallis one-way ANOVA.

*indicates a statistical difference between groups, *p* < 0.05.

HC, health control; CSVD, cerebral small vessel disease; NCI, non-cognitive impairment; MCI, mild cognitive impairment; GMV, gray matter volume; WMV, white matter volume; WMH, white matter hyperintensities. PVWMH, periventricular-white matter hyperintensities; DWMH, deep-white matter hyperintensities; MMSE, mini mental state examination; MoCA-BJ, beijing version of the montreal cognitive assessment; AVLT-DR, auditory verbal learning test-delayed recall; VR-DR, visual reproduction-delay recall; WMS, wechsler memory scale; CDT, clock drawing test; VR-C, visual reproduction-copy; CVF, category verbal fluency; BNT, Boston Naming Test; DST, digit span test; TMT-A and TMT-B, trail making test-A and B; Stroop A, B and C, stroop color and word tests A, B, and C.

The alteration pattern of SMN and VN could be seen in **Supplementary Figure 6**.

Nodal-Wise Alterations and its Relationship With Cognition

Next, we investigate whether and how the node properties within DMN and ECN were altered in SVD. The spatial distribution of PC and WD in group-averaged network were shown in **Figure 3** and **Supplementary Figure 3**. Significant effects of vascular burden on PC were observed in the

DMN (such as bilateral superior frontal gyrus [SFG], inferior parietal lobule [IPL], and left posterior cingulate cortex [PCC], medial orbitofrontal cortex [mOFC]) and the ECN (such as bilateral inferior frontal gyrus [IFG] and right midcingulate cortex [MCC]) (*P* < 0.01, FDR corrected) (**Figure 3B**). The *post hoc* tests revealed that PC in the DMN mostly tended to increase in subjects at high risk and decrease in SVD-MCI, whereas the alterations of PC in the ECN showed the increased pattern in SVD-MCI (**Supplementary Figure 4**). Interestingly, PC in the left mOFC (i.e., anterior DMN

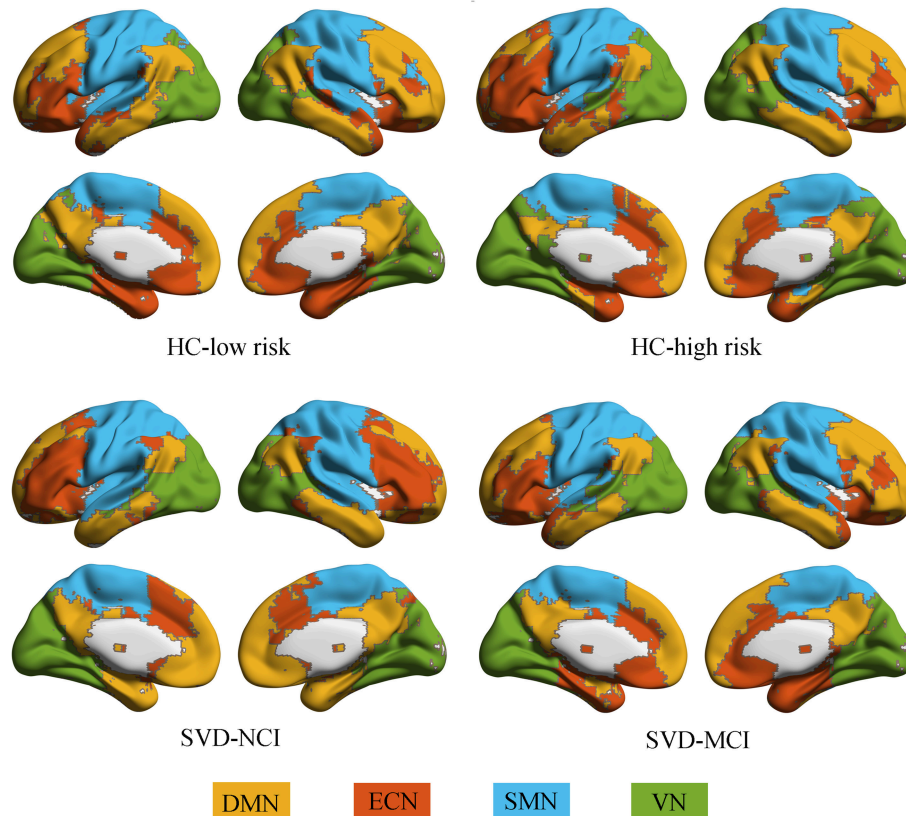


FIGURE 1 | Modular architecture for each group. In each group, four modules were found in the mean functional brain network: the default mode network (yellow), the executive control network (orange), the sensorimotor network (blue), and the visual network (green). HC, healthy control; SVD, small vessel disease; NCI, non-cognitive impairment; MCI, mild cognitive impairment; DMN, default mode network; ECN, executive control network; SMN, sensorimotor network; VN, visual network.

[aDMN]) only exhibited the increased pattern in SVD-MCI (**Supplementary Figure 4A**).

Group comparisons revealed that the WD was significantly regulated in the regions of the DMN (such as bilateral mOFC, middle temporal gyrus [MTG], and the right IPL) and the ECN (such as bilateral ACC, IFG, and anterior insula [AI]) ($P < 0.01$, FDR corrected) (**Figure 3D**). The *post-hoc* tests determined that WD did not homogeneously change within DMN and ECN. WD in the right IPL (i.e., pDMN) tended to increase, while WD in the bilateral mOFC and MTG (i.e., aDMN) decreased in SVD-MCI (**Supplementary Figure 5A**). In the ECN, WD of the bilateral IFG showed the similar pattern with the ECN module, whereas WD in bilateral ACC and AI had the increased tendency in SVD-MCI (**Supplementary Figure 5B**). We further found that WD of the right IPL negatively correlated with IPS ($\beta = -0.494$, $P = 0.030$) in HC-high risk (**Supplementary Figure 2D**). In SVD-MCI, WD of left AI was positively associated with IPS ($\beta = 0.410$, $P = 0.028$) (**Supplementary Figure 2E**).

Right IFG Mediates PWMH-Induced Visuospatial Function Decline

We then further investigated the relationship among MRI markers, network metrics and cognitive performance. WMH volumes, PWMH volumes, DWMH volumes, and numbers of

lacunes were selected as MRI markers for further mediation analysis. In SVD-NCI, the PWMH positively correlated with PC in the left PCC ($\beta = 0.449$, $P = 0.001$). In SVD-MCI, the mediation analysis suggested that the PWMH was associated with PC in the right IFG ($a = -0.541$, $P = 0.019$) and VPF ($c = -0.778$, $P < 0.001$; $c' = -0.560$, $P = 0.007$) and PC of right IFG was related to VPF ($b = 0.403$, $P = 0.039$) (**Figure 4**).

DISCUSSION

This study used graph-theoretical modularity for the first time to indicate that: (1) there was a high FC density in both the inter- and intra-network of the ECN and the DMN in the high risk individuals for SVD; (2) SVD-MCI patients showed a disrupted ECN intra-network and increased DMN connections; and (3) inter-module connectivity of the left IFG mediated the relationship between PWMH and visuospatial processing. These findings have important implications for the further understanding of the neural mechanism of SVD-related cognitive deficits.

Firstly, we wondered whether and how the brain modular architecture was altered in a population at high risk for SVD. Both DMN and ECN networks were chosen. The

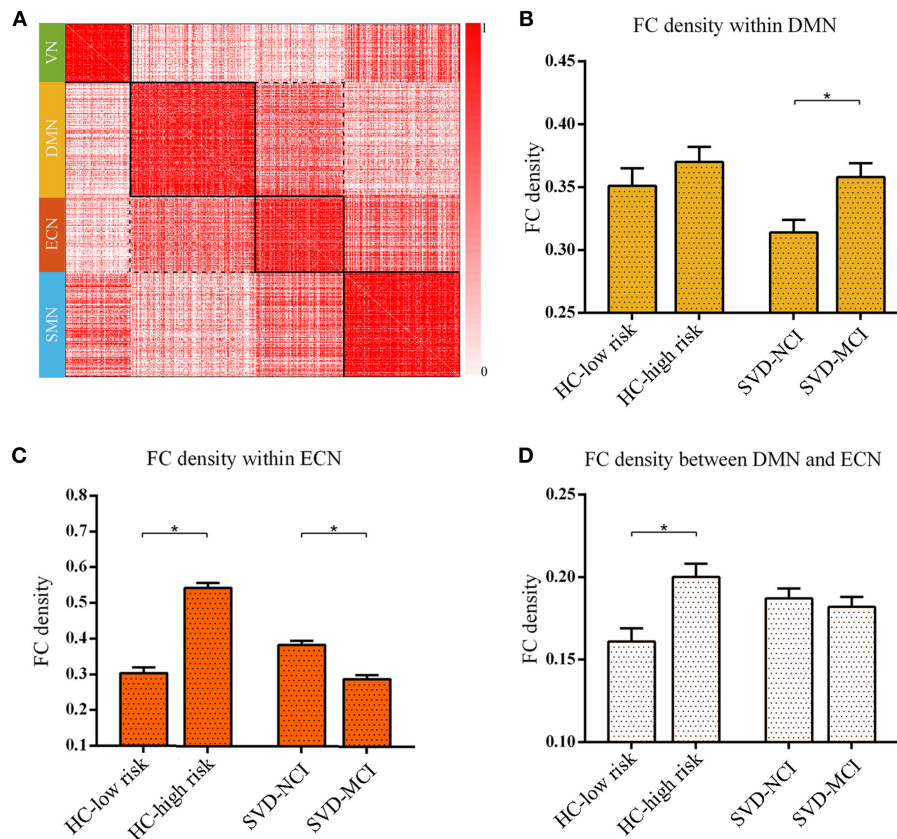


FIGURE 2 | The reorganized pattern of intramodule and intermodule connectivity density within/between DMN and ECN. **(A)** The matrix showed the four modules and interactions between these modules. The darker color mean the higher connectivity density (uncorrected). **(B)** The FC density within DMN in SVD-MCI was significantly higher than it in SVD-NCI ($p = 0.004$). **(C)** The FC density within ECN increased in HC-high risk compared with HC-low risk ($p < 0.001$), whereas it significantly decreased in SVD-MCI compared with SVD-NCI ($p < 0.001$). **(D)** The FC density between DMN and ECN in HC-high risk showed an higher pattern than it in HC-low risk ($p = 0.002$). HC, healthy control; SVD, small vessel disease; NCI, non-cognitive impairment; MCI, mild cognitive impairment; DMN, default mode network; ECN, executive control network; SMN, sensorimotor network; VN, visual network; FC, functional connectivity.

DMN (deactivated during tasks) is primarily involved in episodic memory and self-monitoring processing, while the ECN (activated during tasks) engages in the mediation of working memory, cognitive control and decision making. At the module level, our results revealed that connectivity density within the ECN increased in a high-risk population for SVD, but it did not within the DMN, which indicated that ECN (frontoparietal network) may be more susceptible to the vascular burden than the DMN and elucidated that the ECN supported cognitive processes by increasing its own integration (11). We also found increased intermodule connectivity density between the DMN and ECN that correlated negatively with DST (subcomponent of executive function), suggesting that the modular organization could increase flexibility and facilitate adaptation in response to environmental changes (8). By the evolutionary computation approach, hyperconnectivity between the DMN and ECN during recovery from traumatic brain injury reflected positive functional plasticity (26).

Next, we investigated the brain functional network of SVD-MCI patients. The results showed that the functional connectivity

density within the ECN was significantly decreased. This hints that the frontoparietal network was particularly vulnerable to SVD-related damages, and SVD could hamper network function and impair cognition via a “disconnection syndrome” (27, 28). A combined functional and structural imaging study indicated that disrupted functional connectivity in the frontoparietal network mediated the impact of reduced white matter integrity in the bilateral superior longitudinal fasciculus on executive dysfunction in hypertensive patients with WMH (29). These functional alterations were closely associated with WMH and specific neuropsychological deficits.

Furthermore, increased functional connectivity within the DMN happened in SVD-MCI, which was positively associated with IPS. These findings may also reflect that the DMN and ECN played distinct roles in the progression of SVD, in which the ECN had a compensatory effect in the early stage of disease, and the DMN played a compensatory role in the late stage. The differential associations of DMN and ECN on cognition performance were also observed in other diseases. A resting-state fMRI study demonstrated that depressed participants showed

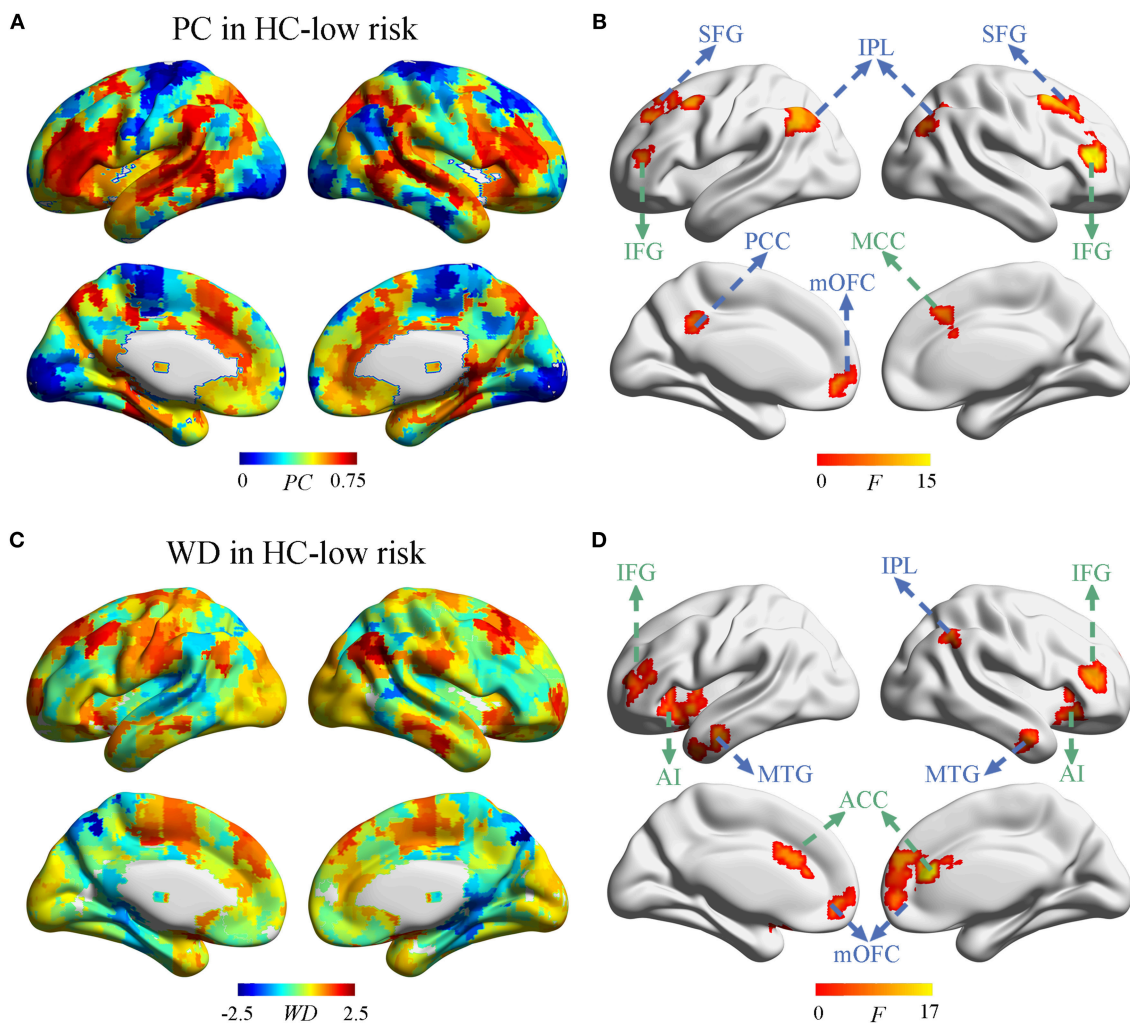
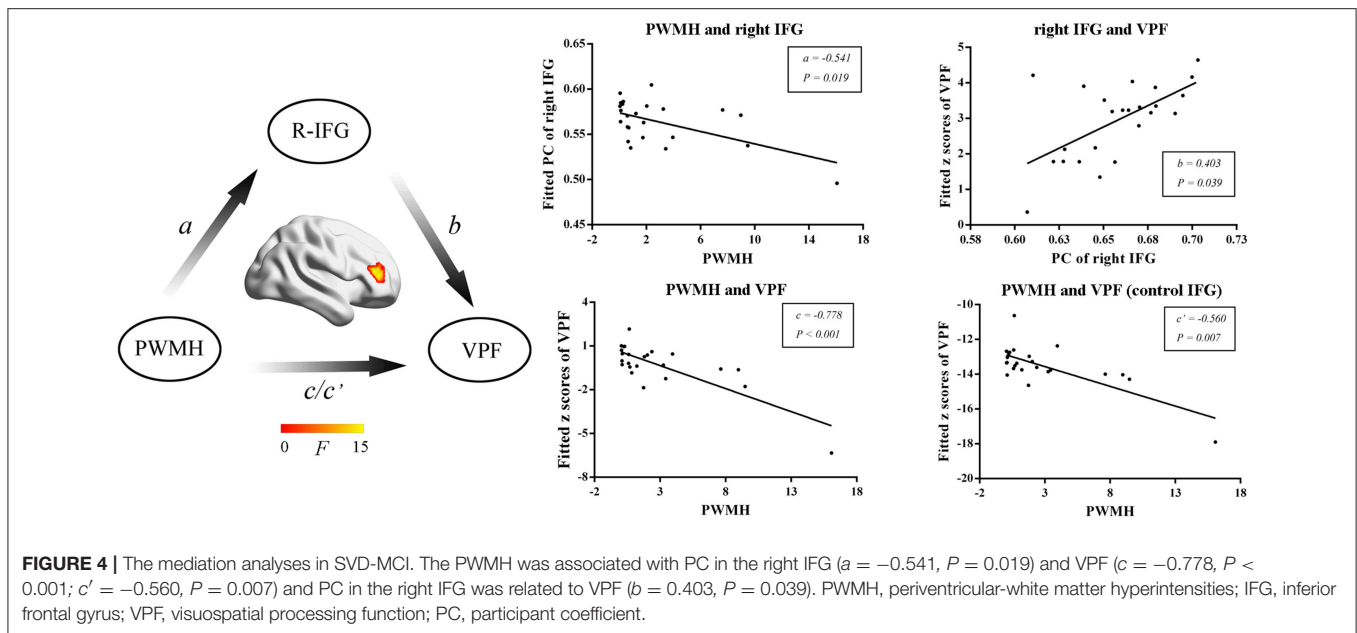


FIGURE 3 | The distribution of PC and WD in the whole brain. **(A)** The PC distribution in HC-low risk. **(B)** Significant effects of vascular burden on PC were observed in the DMN (such as bilateral superior frontal gyrus [SFG], inferior parietal lobule [IPL], and left posterior cingulate cortex [PCC], medial orbitofrontal cortex [mOFC]) and the ECN (such as bilateral inferior frontal gyrus [IFG] and right midcingulate cortex [MCC]) ($P < 0.01$, FDR corrected). **(C)** The WD distribution in HC-low risk. **(D)** The WD was significantly regulated in the regions of DMN (such as bilateral mOFC, middle temporal gyrus [MTG], and the right IPL) and the ECN (such as bilateral ACC, IFG, and anterior insula [AI]) ($P < 0.01$, FDR corrected). HC, healthy control; PC, participant coefficient; WD, within module degree.

decreased connectivity in the ECN and increased connectivity in the DMN compared to non-depressed participants and that these distinctive patterns of connectivity were associated with worse cognitive performance. In more detail, functional connectivity within the ECN was negatively associated with episodic memory performance while connectivity within the DMN was positively associated with episodic memory performance in the non-depressed participants (30). This highlights the potential importance of the DMN and ECN to adapt upon cognitive demands at different stages of the disease.

Excitingly, we found that some nodes, such as the bilateral ACC, AI, IFG, and right MCC within the ECN, exhibited increased intra- and inter-module functional connectivity in patients with SVD-MCI. However, regression analysis revealed that only the intra-module connectivity of the left AI was

positively associated with IPS. Notably, we observed that, at the nodal level, PC and WD did not homogeneously change across the DMN; regions of the aDMN showed increased inter-module connectivity, whereas regions of the pDMN exhibited increased intra-module connectivity in SVD-MCI. Acutely, the aDMN is often involved in perception or self-referential processing, and the pDMN is more commonly related to episodic memory retrieval (31). Based on modularity analysis, the pDMN exhibited decreased intra-module connectivity in the apolipoprotein E $\epsilon 4$ carriers compared to that in the noncarriers, but the aDMN showed no significant alterations (10). Patients with schizophrenia showed increased posterior and decreased anterior connectivity within the DMN compared with healthy controls (32). Notwithstanding, the neurobiological mechanism behind the differentiated pattern requires further investigation. Overall,



our results suggested that patients with SVD-MCI displayed complicated modular interactions with a parallel pattern of disruption and compensation in the ECN and DMN.

To further explore the relationship between vascular burden, network metrics and cognitive performance, mediation analysis was applied. The result suggested that PWMH induced VPF dysfunction regulated by the right IFG. VPF has been proposed to be susceptible to age-related decline and is preferentially disrupted in normal aging (33, 34). The visual processing-related regions can be divided into ventral and dorsal streams. The dorsal stream is involved in three major pathways, including the parieto-prefrontal, parieto-medial temporal, and parieto-premotor pathways (35). The parieto-prefrontal pathway is an important component of the dorsal stream in visuospatial processing (35). It sends input to the dorsal prefrontal region, which is essential for top-down executive control in visuospatial processing (35). The right IFG may play a central role in promoting the global processing of visuospatial perception (36). During the visuospatial working memory task, the fractional anisotropy and axial diffusivity of the white matter bundles connecting the IFG and fusiform were associated with processing speed (37). In subjects with autism spectrum disorder, poorer VPF was correlated with a disrupted white matter microstructure in the right inferior fronto-occipital fasciculus (38). Additionally, most of the investigations have revealed that the increasing burden of PWMH, not DWMH, may play an independent role in the decline of cognition (39). This evidence further supports our result that PWMH could result in the decline of visuospatial processing mediated by prefrontal functional connectivity in SVD.

Several issues in our study need to be noted. First, as a cross-sectional study, the data could not directly elucidate the relationship between imaging characteristics and SVD-related performance. Therefore, it is necessary to replicate

our findings in future longitudinal studies. Second, the connectivity within/between different modules was binary undirected matrices. Thus, weighted matrices might provide more detailed information about network alterations. Third, our functional data preprocessing steps included global signal regression and we were only concerned with the positive correlations in the subsequent analyses. Further exploration of the effect of non-global signal regression and negative correlations on modular alterations in SVD participants is needed. Fourth, several modularity algorithms are currently available with different advantages. Different algorithms need to estimate the repeatability of our results. Finally, we only examined functional brain networks in the current study. It might be worth applying multimodal imaging techniques (e.g., arterial spin labeling) to explore the correlation between structural and functional networks.

CONCLUSION

The modular architecture showed an altered reconfiguration pattern within/between the DMN and ECN and might have a mediation effect during the progression of SVD. These observations may provide novel insight into the underlying neural network mechanism of cerebral SVD-related cognitive impairment.

AUTHOR CONTRIBUTIONS

YX: conceived and designed the experiments. RQ, YG, XC, XW, JZ, and YJ: performed the experiments. RL, HC, and WL: analyzed the data. FB and BZ: contributed materials/analysis tools.

ACKNOWLEDGMENTS

This work was supported by the National Key Research and Development Program of China (2016YFC1300500-504 and 2016YFC0901004), National Natural Science Foundation of China (81230026; 81630028), Natural Science Foundation of Jiangsu Province (BE2016610;), Jiangsu Provincial Key Medical Discipline (ZDXKA2016020).

SUPPLEMENTARY MATERIAL

The Supplementary Material for this article can be found online at: <https://www.frontiersin.org/articles/10.3389/fneur.2019.00324/full#supplementary-material>

Supplementary Figure 1 | The modularity Q across the sparsity range (0.1–0.3) in each group. HC, healthy control; SVD, small vessel disease; NCI, non-cognitive impairment; MCI, mild cognitive impairment.

Supplementary Figure 2 | The significant relationship between modular indexes and cognitive assessments. **(A)** IPS was positively associated with functional connectivity density within DMN ($\beta = 0.501$, $P = 0.022$) in SVD-NCI. **(B)** IPS was negatively related to functional connectivity density within ECN ($\beta = -0.432$, $P = 0.036$) in SVD-NCI. **(C)** The FC density between DMN and ECN correlated negatively with DST ($\beta = -0.587$, $P = 0.006$) in HC-high risk. **(D)** WD of the right IPL negatively correlated with IPS ($\beta = -0.494$, $P = 0.030$) in HC-high risk. **(E)** WD of left AI was positively associated with IPS ($\beta = 0.410$, $P = 0.028$) in SVD-MCI. HC, healthy control; SVD, small vessel disease; NCI, non-cognitive impairment; MCI, mild cognitive impairment; WD, within module degree; FC, functional

connectivity; DMN, default mode network; ECN, executive control network; IPS, information processing speed; DST, digit span test; IPL, inferior parietal lobe; AI, anterior insula.

Supplementary Figure 3 | The distribution of PC and WD in HC-high risk, SVD-NCI, and SVD-MCI. HC, healthy control; SVD, small vessel disease; NCI, non-cognitive impairment; MCI, mild cognitive impairment; PC, participant coefficient; WD, within module degree.

Supplementary Figure 4 | The *post-hoc* tests of PC in significantly differentiated brain regions involved in DMN **(A)** and ECN **(B)**. HC, healthy control; SVD, small vessel disease; NCI, non-cognitive impairment; MCI, mild cognitive impairment; PC, participant coefficient; SFG, superior frontal gyrus; IPL, inferior parietal lobe; PCC, posterior cingulate cortex; mOFC, medial orbitofrontal cortex; IFG, inferior frontal gyrus; MCC, right midcingulate cortex.

Supplementary Figure 5 | The *post-hoc* tests of WD in significantly differentiated brain regions involved in DMN **(A)** and ECN **(B)**. HC, healthy control; SVD, small vessel disease; NCI, non-cognitive impairment; MCI, mild cognitive impairment; WD, within module degree; MTG, middle temporal gyrus; IPL, inferior parietal lobe; mOFC, medial orbitofrontal cortex; IFG, inferior frontal gyrus; ACC, anterior cingulate cortex; AI, anterior insula.

Supplementary Figure 6 | FC density within the visual network and sensorimotor network. **(A)** The FC density within the visual network showed a significant group difference ($p = 0.041$, ANOVA, controlled age, sex, and years of education). The FC density within the visual network in HC-high risk was significantly decreased compared to HC-low risk ($p = 0.005$). **(B)** There was no significant difference in FC density within the sensorimotor network. FC, functional connectivity; HC, healthy control; CSVD, cerebral small vessel disease; NCI, non-cognitive impairment; CI, cognitive impairment.

REFERENCES

- Wardlaw JM, Smith EE, Biessels GJ, Cordonnier C, Fazekas F, Frayne R, et al. Neuroimaging standards for research into small vessel disease and its contribution to ageing and neurodegeneration. *Lancet Neurol.* (2013) 12:822–38. doi: 10.1016/S1474-4422(13)70124-8
- Wardlaw JM, Smith C, Dichgans M. Mechanisms underlying sporadic cerebral small vessel disease: insights from neuroimaging. *Lancet Neurol.* (2013) 12:483–97. doi: 10.1016/S1474-4422(13)70060-7
- Joutel A, Chabriat H. Pathogenesis of white matter changes in cerebral small vessel diseases: beyond vessel-intrinsic mechanisms. *Clin Sci.* (2017) 13:635–51. doi: 10.1042/CS20160380
- Hajjar I, Yang F, Sorond F, Jones RN, Milberg W, Cupples LA, et al. A novel aging phenotype of slow gait, impaired executive function, and depressive symptoms: relationship to blood pressure and other cardiovascular risks. *J Gerontol A Biol Sci Med Sci.* (2009) 64:994–1001. doi: 10.1093/gerona/glp075
- Uiterwijk R, Staals J, Huijts M, de Leeuw PW, Kroon AA, van Oostenbrugge RJ. Framingham Stroke Risk Profile is related to cerebral small vessel disease progression and lower cognitive performance in patients with hypertension. *J Clin Hypertens.* (2018) 20:240–5. doi: 10.1111/jch.13175
- Pavlovic AM, Pekmezovic T, Tomic G, Trajkovic JZ, Sternic N. Baseline predictors of cognitive decline in patients with cerebral small vessel disease. *J Alzheimers Dis.* (2014) 42:S37–43. doi: 10.3233/JAD-132606
- Jokinen H, Gouw AA, Madureira S, Ylikoski R, van Straaten EC, van der Flier WM, et al. Incident lacunes influence cognitive decline: the LADIS study. *Neurology.* (2011) 76:1872–8. doi: 10.1212/WNL.0b013e31821d752f
- Sporns O, Betzel RF. Modular brain networks. *Annu Rev Psychol.* (2016) 67:613–40. doi: 10.1146/annurev-psych-122414-033634
- Yi LY, Liang X, Liu DM, Sun B, Ying S, Yang DB, et al. Disrupted topological organization of resting-state functional brain network in subcortical vascular mild cognitive impairment. *CNS Neurosci Ther.* (2015) 21:846–54. doi: 10.1111/cns.12424
- Wang J, Wang X, He Y, Yu X, Wang H, He Y. Apolipoprotein E $\epsilon 4$ modulates functional brain connectome in Alzheimer's disease. *Hum Brain Mapp.* (2015) 36:1828–46. doi: 10.1002/hbm.22740
- Liang X, Zou Q, He Y, Yang Y. Topologically reorganized connectivity architecture of default-mode, executive-control, and salience networks across working memory task loads. *Cereb Cortex.* (2016) 26:1501–11. doi: 10.1093/cercor/bhu316
- D'Agostino RB, Wolf PA, Belanger AJ, Kannel WB. Stroke risk profile: adjustment for antihypertensive medication. The Framingham study. *Stroke.* (1994) 25:40–3.
- Kwon HM, Lynn MJ, Turan TN, Derdeyn CP, Fiorella D, Lane BE, et al. Frequency, risk factors, and outcome of coexistent small vessel disease and intracranial arterial stenosis. *JAMA Neurol.* (2016) 73:36–42. doi: 10.1001/jamaneurol.2015.3145
- Tuladhar AM, van Dijk E, Zwiers MP, van Norden AG, de Laat KF, Shumskaya E, et al. Structural network connectivity and cognition in cerebral small vessel disease. *Hum Brain Mapp.* (2016) 37:300–10. doi: 10.1002/hbm.23032
- Tuladhar AM, van Uden IW, Rutten-Jacobs LC, Lawrence A, van der Holst H, van Norden A, et al. Structural network efficiency predicts conversion to dementia. *Neurology.* (2016) 86:1112–9. doi: 10.1212/WNL.0000000000002502
- Tuladhar AM, Lawrence A, Norris DG, Barrick TR, Markus HS, de Leeuw FE. Disruption of rich club organisation in cerebral small vessel disease. *Hum Brain Mapp.* (2017) 38:1751–66. doi: 10.1002/hbm.23479
- Liu F, Zhu C, Wang Y, Guo W, Li M, Wang W, et al. Disrupted cortical hubs in functional brain networks in social anxiety disorder. *Clin Neurophysiol.* (2015) 126:1711–6. doi: 10.1016/j.clinph.2014.11.014
- Li W, Wang Z, Zhang L, Qiao L, Shen D. Remodeling pearson's correlation for functional brain network estimation and autism spectrum disorder identification. *Front Neuroinform.* (2017) 11:55. doi: 10.3389/fninf.2017.00055
- Zalesky A, Fornito A, Harding IH, Cocchi L, Yücel M, Pantelis C, et al. Whole-brain anatomical networks: does the choice of nodes matter? *Neuroimage.* (2010) 50:970–83. doi: 10.1016/j.neuroimage.2009.12.027
- Murphy K, Birn RM, Handwerker DA, Jones TB, Bandettini PA. The impact of global signal regression on resting state correlations: are anti-correlated networks introduced? *Neuroimage.* (2010) 44:893–905. doi: 10.1016/j.neuroimage.2008.09.036

21. Chang TY, Huang KL, Ho MY, Ho PS, Chang CH, Liu CH, et al. Graph theoretical analysis of functional networks and its relationship to cognitive decline in patients with carotid stenosis. *J Cereb Blood Flow Metab.* (2016) 36:808–18. doi: 10.1177/0271678X15608390
22. Newman ME. Finding community structure in networks using the eigenvectors of matrices. *Phys Rev E Stat Nonlin Soft Matter Phys.* (2006) 74:036104. doi: 10.1103/PhysRevE.74.036104
23. Newman ME. Modularity and community structure in networks. *Proc Natl Acad Sci USA.* (2006) 103:8577–82. doi: 10.1073/pnas.0601602103
24. Ng KK, Lo JC, Lim JKW, Chee MWL, Zhou J. Reduced functional segregation between the default mode network and the executive control network in healthy older adults: a longitudinal study. *Neuroimage.* (2016) 133:321–30. doi: 10.1016/j.neuroimage.2016.03.029
25. Guimerà R, Nunes Amaral LA. Functional cartography of complex metabolic networks. *Nature.* (2005) 433:895–900. doi: 10.1038/nature03288
26. Roy A, Campbell C, Bernier RA, Hillary FG. An evolutionary computation approach to examine functional brain plasticity. *Front Neurosci.* (2016) 10:146. doi: 10.3389/fnins.2016.00146
27. Lawrence AJ, Chung AW, Morris RG, Markus HS, Barrick TR. Structural network efficiency is associated with cognitive impairment in small-vessel disease. *Neurology.* (2014) 83:304–11. doi: 10.1212/WNL.0000000000000612
28. De Laat KF, Tuladhar AM, van Norden AG, Norris DG, Zwiers MP, de Leeuw FE. Loss of white matter integrity is associated with gait disorders in cerebral small vessel disease. *Brain.* (2011) 134:73–83. doi: 10.1093/brain/awq343
29. Li X, Liang Y, Chen Y, Zhang J, Wei D, Chen K, et al. Disrupted frontoparietal network mediates white matter structure dysfunction associated with cognitive decline in hypertension patients. *J Neurosci.* (2015) 35:10015–24. doi: 10.1523/JNEUROSCI.5113-14.2015
30. Albert KM, Potter GG, Boyd BD, Kang H, Taylor WD. Brain network functional connectivity and cognitive performance in major depressive disorder. *J Psychiatr Res.* (2019) 110:51–6. doi: 10.1016/j.jpsychires.2018.11.020
31. Uddin LQ, Kelly AM, Biswal BB, Castellanos FX, Milham MP. Functional connectivity of default mode network components: correlation, anticorrelation, and causality. *Hum Brain Mapp.* (2009) 30:625–37. doi: 10.1002/hbm.20531
32. Mannell MV, Franco AR, Calhoun VD, Cañive JM, Thoma RJ, Mayer AR. Resting state and task-induced deactivation: a methodological comparison in patients with schizophrenia and healthy controls. *Hum Brain Mapp.* (2010) 31:424–37. doi: 10.1002/hbm.20876
33. Drag LL, Bieliauskas LA. Contemporary review 2009: cognitive aging. *J Geriatr Psychiatry Neurol.* (2010) 23:75–93. doi: 10.1177/0891988709358590
34. Drag LL, Light SN, Langenecker SA. Patterns of frontoparietal activation as a marker for unsuccessful visuospatial processing in healthy aging. *Brain Imaging Behav.* (2016) 10:686–96. doi: 10.1007/s11682-015-9428-y
35. Kravitz DJ, Saleem KS, Baker CI, Mishkin M. A new neural framework for visuospatial processing. *Nat Rev Neurosci.* (2011) 12:217–30. doi: 10.1038/nrn3008
36. Chen P, Hartman AJ, Priscilla Galarza C, DeLuca J. Global processing training to improve visuospatial memory deficits after right-brain stroke. *Arc Clin Neuropsychol.* (2012) 27:891–905. doi: 10.1093/arclin/acs089
37. Sala-Llanch R, Palacios EM, Junqué C, Bargalló N, Vendrell P. Functional networks and structural connectivity of visuospatial and visuo-perceptual working memory. *Front Hum Neurosci.* (2015) 9:340. doi: 10.3389/fnhum.2015.00340
38. McGrath J, Johnson K, O'Hanlon E, Garavan H, Gallagher L, Leemans A. White matter and visuospatial processing in autism: a constrained spherical deconvolution tractography study. *Autism Res.* (2013) 6:307–19. doi: 10.1002/aur.1290
39. Lee HK, Lee YM, Park JM, Lee BD, Moon ES, Chung YI. Amnesic multiple cognitive domains impairment and periventricular white matter hyperintensities are independently predictive factors progression to dementia in mild cognitive impairment. *Int J Geriatr Psychiatry.* (2014) 29:526–32. doi: 10.1002/gps.4035

Conflict of Interest Statement: The authors declare that the research was conducted in the absence of any commercial or financial relationships that could be construed as a potential conflict of interest.

Copyright © 2019 Liu, Chen, Qin, Gu, Chen, Zou, Jiang, Li, Bai, Zhang, Wang and Xu. This is an open-access article distributed under the terms of the Creative Commons Attribution License (CC BY). The use, distribution or reproduction in other forums is permitted, provided the original author(s) and the copyright owner(s) are credited and that the original publication in this journal is cited, in accordance with accepted academic practice. No use, distribution or reproduction is permitted which does not comply with these terms.



Decreased CSF Levels of β -Amyloid in Patients With Cortical Superficial Siderosis

Cihan Catak^{1†}, Marialuisa Zedde^{2†}, Rainer Malik¹, Daniel Janowitz¹, Vivian Soric¹, Anna Seegerer¹, Alexander Krebs³, Marco Düring¹, Christian Opherke⁴, Jennifer Linn⁵ and Frank A. Wollenweber^{1*}

¹ Institute for Stroke and Dementia Research, University Hospital, LMU Munich, Munich, Germany, ² Neurology Unit, Stroke Unit, Arcispedale Santa Maria Nuova, Azienda Unità Sanitaria Locale-IRCCS Reggio Emilia, Reggio Emilia, Italy, ³ MVZ Labor PD Dr. Volkmann und Kollegen, Gesellschaft Bürgerlichen Rechts, Karlsruhe, Germany, ⁴ Klinik für Neurologie, SLK-Kliniken Heilbronn GmbH, Heilbronn, Germany, ⁵ Institut und Poliklinik für Neuroradiologie, University Hospital Carl Gustav Carus, Dresden, Germany

OPEN ACCESS

Edited by:

Eric Jouvent,
Université Sorbonne Paris Cité, France

Reviewed by:

Alessandro Biffi,
Harvard Medical School,
United States
Yael D. Reijmer,
University Medical Center
Utrecht, Netherlands

*Correspondence:

Frank A. Wollenweber
frank.wollenweber@
med.uni-muenchen.de

[†]These authors have contributed
equally to this work as co-first authors

Specialty section:

This article was submitted to
Stroke,
a section of the journal
Frontiers in Neurology

Received: 22 February 2019

Accepted: 10 April 2019

Published: 26 April 2019

Citation:

Catak C, Zedde M, Malik R,
Janowitz D, Soric V, Seegerer A,
Krebs A, Düring M, Opherke C, Linn J
and Wollenweber FA (2019)
Decreased CSF Levels of β -Amyloid in
Patients With Cortical Superficial
Siderosis. *Front. Neurol.* 10:439.
doi: 10.3389/fneur.2019.00439

Background: Cortical superficial siderosis (cSS) represents a key neuroimaging marker of cerebral amyloid angiopathy (CAA) that is associated with intracranial hemorrhages and cognitive impairment. Nevertheless, the association between cSS and core cerebrospinal fluid (CSF) biomarkers for dementia remain unclear.

Methods: One hundred and one patients with probable (79%, 80/101) or possible (21%, 21/101) CAA according to the modified Boston criteria and mild cognitive impairment according to Petersen criteria were prospectively included between 2011 and 2016. CSF analyses of β -amyloid 42, β -amyloid 40, total tau and phosphorylated tau were performed using sandwich-type enzyme-linked immunosorbent-assay. All patients received MRI and Mini-Mental-State Examination (MMSE). Logistic regression analysis was used to adjust for possible confounders.

Results: cSS was present in 61% (62/101). Of those, 53% (33/62) had disseminated cSS and 47% (29/62) focal cSS. β -amyloid 42 was lower in patients with cSS than in patients without cSS (OR 0.2; 95% CI 0.08–0.6; $p = 0.0052$) and lower in patients with disseminated cSS than in those with focal cSS (OR 0.02; 95% CI 0.003–0.2; $p = 0.00057$). Presence of cSS had no association with regard to β -amyloid 40, total tau and phosphorylated tau.

Conclusions: Our results demonstrate that the presence and extent of cSS are associated with reduced CSF β -amyloid 42 levels. Further studies are needed to investigate the underlying mechanisms of this association.

Keywords: cerebral amyloid angiopathy, cortical superficial siderosis, cerebrospinal fluid, cerebral microbleeds, neuroimaging

INTRODUCTION

Cerebral amyloid angiopathy (CAA)—characterized by the deposition of β -amyloid in the walls of leptomeningeal vessels—is a common cerebral small vessel disease and a major cause of intracerebral hemorrhage in the elderly (1–3). Furthermore, it has become evident that CAA is associated with cognitive impairment (4). Specifically, it has been shown that CAA patients perform

worse in executive functioning, perceptual speed, and episodic memory compared with normative values (5).

The various CAA-related MRI structural lesions essentially represent vascular-mediated brain damage, rather than abnormalities of CAA-laden vessels themselves. CSF biomarkers that are typically altered in AD [β -amyloid 42 (A β 42), β -amyloid 40 (A β 40), total tau (t-tau) and phosphorylated tau (p-tau)] may offer another approach to understand underlying mechanisms and courses of patients with CAA (6). While A β 42 can be detected in both senile plaques of AD patients and capillaries of CAA patients, A β 40 deposition is supposed to appear preferentially in the walls of leptomeningeal arteries of CAA patients (7, 8).

More recently, it has been suggested that CAA-related cognitive impairment is more pronounced in a subgroup of CAA patients that demonstrate the MRI marker “cortical superficial siderosis” (cSS), which most likely reflect blood residues in the subarachnoid space (9). In line with this, patients from memory clinic populations have a higher cSS prevalence of 2–6% (10–12) compared to the general population at around 1% (13).

We hypothesized that differences between cSS positive and cSS negative patients might also be reflected in different CSF biomarker profiles. Since cSS patients are regarded to be of a higher risk for future neurovascular events and for cognitive dysfunction, we hypothesized that cSS positive patients would demonstrate lower levels of A β 40 and A β 42 together with elevated tau levels. Hence, we analyzed the core CSF biomarker profile in a prospective cohort of patients with mild cognitive impairment and the diagnosis of a possible or probable CAA.

METHODS

Subjects

Screening took place in the outpatient clinics of the university hospitals in Reggio Emilia (Italy) and LMU Munich (Germany). Three hundred and forty-five patients with subjective cognitive impairment and the MRI based suspicion of a CAA were screened. Of those 71% (244/345) did not undergo lumbar puncture because of (a) normal objective cognitive testing ($n = 134$), (b) patient decline ($n = 90$) or (c) intake of oral anticoagulation ($n = 20$). The remaining 101 patients entered the final analysis. Seventy-nine percent (80/101) had a probable CAA and 21% (21/101) a possible CAA according to the modified Boston criteria (2). All patients in the final analysis had the diagnosis of mild cognitive impairment based on the Petersen criteria (14). The reasons for the initial presentation at the outpatient clinics were distributed as follows: past intracranial hemorrhage 34% (34/101), memory complaints 39% (39/101), past ischemic stroke or TIA 14% (14/101), transient focal neurological episodes (TFNE) or presumed focal seizure 4%

(4/101), dizziness, headache or other unspecific neurological complaints 10% (10/101). Patients not included into the study did not differ in terms of age gender and cardiovascular risk factors (**Supplementary Table 3**). Informed consent were obtained from each patient according to the Declaration of Helsinki. Ethics approval was obtained from the regional ethics board.

MRI

MR images in Munich were acquired on a 3 Tesla MRI scanner (Signa HDxt, GE Healthcare), in Reggio Emilia on a 1.5 Tesla scanner (Achieva, Philips Healthcare). Cortical superficial siderosis was identified on T2*-weighted gradient-echo sequence (GRE) or susceptibility-weighted imaging (SWI) by two trained raters (FAW and CC). Disagreement in two cases was resolved by consensus read (interrater $\kappa = 0.97$). Cerebral microbleeds (CMB) were defined according to the STRIVE criteria (15). CMB were manually marked on lesion masks, which were then normalized to 1 mm Montreal Neurological Institute (MNI) standard space and automatically rated as described before (16). CMB were categorized in 4 groups (0 CMB, 1 CMB, 2–4 CMB and ≥ 5 CMB) according to the recent literature (17, 18).

CSF

CSF samples were obtained by lumbar puncture within 6 weeks after MRI, collected in 10 mL polypropylene tubes and centrifuged within 2 h, and then frozen until analysis. A β 42, A β 40, t-tau and p-tau were measured using sandwich type enzyme linked immunosorbent assays; A β 42 was measured with Innotech β -amyloid (42), A β 40 was measured with Innotech β -amyloid (40), t-tau with Innotech hTau-Ag, and p-tau with Innotech Phospho-tau (181 P) (Innogenetics, 9,052 Gent, Belgium, www.fujirebio-europe.com). The unit used for biomarkers is pg/mL.

The inter lot variation coefficient between the centers were A β 42 5.15%, A β 40 7.87%, t-tau 14.01%, p-tau 16.2% and A β 42 5.7%, A β 40 8.2%, t-tau 7.5, p-tau 16.4. Further, there were no significant differences between the median levels of core CFS markers between the two centers, indicating a good comparability of the CSF assays (**Supplementary Table 4**).

Statistical Analysis

Baseline characteristics and risk factors were compared using chi-square tests, Fisher's exact tests and student's t -tests where appropriate. Logistic regression analyses corrected for age, sex and CMB category was performed using the cSS groups as dependent variables. To use the binary cSS status as the dependent variable in the logistic regression, the analysis was inverted. All CSF marker levels were log-transformed for regression analysis and are presented as median with interquartile range to account for the non-normal distribution. Logistic regression analyses with MMSE as the dependent variable were performed using logistic regression corrected for age, sex, hypertension, diabetes and hypercholesterinemia. MRI field strength and T2*-weighted method (GRE vs. SWI) were tested as a variable in univariate analysis. Therefore, it was not included into the logistic regression model. The relationship between cSS and the categories of CMB and CSF markers was

Abbreviations: CAA, Cerebral amyloid angiopathy; cSS, Cortical superficial siderosis; CSF, Cerebrospinal fluid; A β 42, β -amyloid 42; A β 40, β -amyloid 40; t-tau, total tau; p-tau, phosphorylated tau; MMSE, Mini-Mental State Examination; AD, Alzheimer's disease; CMB, Cerebral microbleeds; SD, Standard deviation; OR, odds ratio; CI, confidence interval; y, years; DM, Diabetes mellitus; ApoE, Apolipoprotein E; IQR, interquartile range; HCHWA-D, hereditary cerebral hemorrhage with amyloidosis of the Dutch type.

TABLE 1 | Baseline characteristics stratified for the presence of cSS.

	CAA (<i>n</i> = 101)	CAA with cSS (<i>n</i> = 62)	CAA without cSS (<i>n</i> = 39)	<i>p</i>
Sex, male, <i>n</i> (%)	59 (58)	37 (60)	22 (56)	0.8
Age, mean, \pm SD	76 \pm 7	76 \pm 7	75 \pm 7	0.3
Hypertension, <i>n</i> (%)	69 (68)	40 (65)	29 (74)	0.4
Hypercholesterolemia, <i>n</i> (%)	41 (41)	23 (37)	18 (46)	0.4
Diabetes mellitus, <i>n</i> (%)	5 (5)	3 (5)	2 (5)	1
APOE ϵ 2, <i>n</i> (%)	12 (12)	8 (13)	4 (10)	0.8
APOE ϵ 4, <i>n</i> (%)	13 (13)	6 (10)	7 (18)	0.2
MMSE, median (IQR)	24 (18–28)	23 (17–26)	27 (21–29)	0.4
Number of CMB, <i>n</i> (%)				0.03
0	16 (16)	9 (15)	7 (18)	
1	12 (12)	8 (13)	4 (10)	
2–4	27 (27)	11 (18)	16 (41)	
\geq 5	39 (39)	30 (48)	9 (23)	

cSS, cortical superficial siderosis; ApoE, Apolipoprotein E; CMB, cerebral microbleeds; SD, standard deviation.

tested using ordinal logistic regression under a proportional odds assumption. For the additional model, we applied a backward stepwise regression analysis optimizing on Akaike Information Criterion (AIC) to statistically select for relevant covariates. As a result, hypertension was selected as the only parameter. All analyses was performed using R (R version 3.5.1: A language and environment for statistical computing; R Foundation for Statistical Computing, Vienna, Austria).

RESULTS

CSS was present in 61% (62/101). Patients with and without cSS were well balanced with regard to age, sex, and cardiovascular risk factors. MRI field strength and T2*-weighted method (GRE vs SWI) did not show any significant effect on the presence and extent of cSS (all $p > 0.4$). Detailed baseline characteristics are shown in **Tables 1, 2**.

Presence of cSS and MMSE

CAA patients with cSS had numerically lower median MMSE values than CAA patients without cSS (23 vs. 27, **Table 1**). However, this difference did not reach statistical significance, neither without adjustment (0.4), nor in a model adjusting for sex, age and cardiovascular risk factors ($p = 0.05$) nor in a model adjusting for hypertension only ($p = 0.1$).

Presence of cSS and CSF Markers

In logistic regression analyses, A β 42 was significantly lower in patients with cSS compared to those without (OR 0.2; 95% CI 0.08–0.7; $p = 0.0052$, **Figure 1** and **Table 3**). Further, the A β 42/40 ratio was significant lower in patients with cSS than in patients without cSS (OR 0.3; 95% CI 0.08–0.7; $p = 0.0091$). Patients with and without cSS did not show significantly different CSF levels of A β 40 (OR 0.8; 95% CI 0.3–2.6; $p = 0.77$), t-tau (OR 1.9; 95% CI 0.8–4.5; $p = 0.12$), and p-tau (OR 2.1; 95% CI 0.8–5.3; $p = 0.12$).

TABLE 2 | Baseline characteristics stratified for extent of cSS.

	Disseminated cSS (<i>n</i> = 33)	Focal cSS (<i>n</i> = 29)	<i>P</i>
Sex, male, <i>n</i> (%)	18 (55)	19 (66)	0.4
Age, mean, <i>y</i>	76 \pm 8	76 \pm 5	0.3
Hypertension, <i>n</i> (%)	19 (58)	21 (72)	0.3
Hypercholesterolemia, <i>n</i> (%)	10 (30)	13 (45)	0.3
Diabetes mellitus, (%)	1 (3)	2 (7)	0.6
APOE ϵ 2, <i>n</i> (%)	5 (15)	3 (10)	0.7
APOE ϵ 4, <i>n</i> (%)	4 (12)	2 (7)	0.7
MMSE, median (IQR)	22 (15–26)	24 (19–27)	0.09
Number of CMB, <i>n</i> (%)			0.1
0	2 (6)	7 (24)	
1	3 (9)	5 (17)	
2–4	8 (24)	3 (10)	
\geq 5	17 (52)	13 (45)	

cSS, cortical superficial siderosis; ApoE, Apolipoprotein E; CMB, cerebral microbleeds; SD, standard deviation.

Extent of cSS and CSF Markers

Out of the overall cohort, 33% (33/101) had disseminated (i. e. affecting >3 cortical sulci) cSS and 29% (29/101) had focal (affecting ≤ 3 sulci) cSS. CSF levels of A β 42 and A β 40 were significantly lower in patients with disseminated cSS than in focal cSS (OR 0.02; 95% CI 0.002–0.2; $p = 0.00057$ and OR 0.01; 95% CI 0.0003–0.3; $p = 0.0069$, please see **Figure 1** and **Table 4**).

CMB and CSF Marker

Eighty-four percent (85/101) of all patients had any CMB. Using Chi-Square test, there was a significant difference regarding the number of CMB in patients with and without cSS stratified for groups ($p = 0.03$). While patients with cSS less often had 2–4 CMB than patients without cSS (18%, 11/62 and 41%,

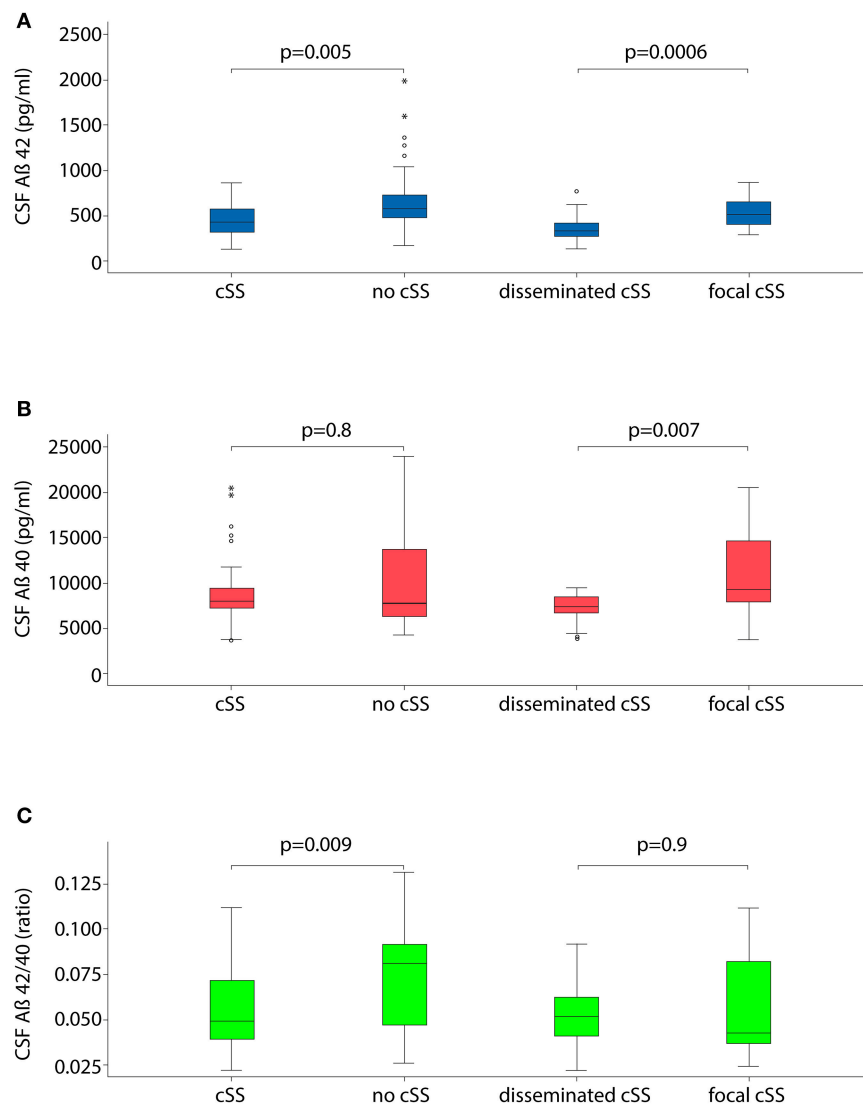


FIGURE 1 | Boxplots illustrating cerebrospinal fluid (CSF) markers for dementia stratified for the presence and extent of cortical superficial siderosis (cSS). **(A)** CSF level of Aβ42; **(B)** CSF level of Aβ40; and **(C)** ratio of Aβ42 to Aβ40.

16/39), cSS patients were overrepresented in the group of >5 CMB (48%, 30/62 and 23%, 9/39). The number of CMB did not differ between patients with disseminated and focal cSS ($p = 0.1$).

In ordinal logistic regression analysis adjusting for age, sex and cardiovascular risk factors, there was no significant correlation between the number of CMB and all tested CSF parameters (all $p > 0.05$).

cSS and CSF Markers in Subgroups

We repeated the logistic regression analyses restricted to patients with probable CAA according to the modified Boston criteria (Supplementary Tables 1, 2). In that analysis, Aβ42 remained lower in patients with cSS compared to those without (OR 0.3; 95% CI 0.07–0.9; $p = 0.05$). Further, the Aβ42/40 ratio was significantly lower in patients with cSS than in patients without

cSS (OR 0.3; 95% CI 0.07–0.9; $p = 0.04$). Also patients with disseminated cSS still showed significantly lower levels of Aβ42 (OR 0.02; 95% CI 0.002–0.3; $p = 0.003$) and lower levels of Aβ40 (OR 0.0004; 95% CI 0.0000006–0.3; $p = 0.01$).

DISCUSSION

The main results from this cohort study of 101 patients with a possible or probable CAA and CSF samples are that (1) CSF Aβ42 is significantly lower in patients with cSS than in patients without cSS, and (2) CSF Aβ42 is significantly lower in patients with disseminated cSS (>3 sulci) than in CAA patients with focal cSS.

The current results indicate that both the presence and the extent of cSS are associated with lower Aβ42 CSF levels. Since accumulating evidence suggests that the presence and extent of cSS might be a marker of CAA severity with higher recurrence

TABLE 3 | CSF marker stratified for presence of cSS.

	Total (n = 101)	cSS (n = 62)	No cSS (n = 39)	P	OR (95% CI)
Aβ42 (pg/ml), median (IQR)	474 (352–629)	400 (326–566)	575 (474–730)	0.005	0.2 [0.08–0.7]
Aβ40 (pg/ml), median (IQR)	8,079 (6,803–10,603) (n = 79)	8,170 (7,284–9,534) (n = 44)	7,906 (6,410–13,917) (n = 35)	0.8	0.8 [0.3–2.6]
T-tau (pg/ml), median (IQR)	322 (242–431)	319 (251–436)	331 (216–429)	0.1	1.9 [0.8–4.5]
P-tau (pg/ml), median (IQR)	58 (43–75)	60 (51–86)	50 (36–72)	0.1	2.1 [0.8–5.3]
Aβ42/40 ratio, median (IQR)	0.06 (0.04–0.08) (n = 79)	0.05 (0.04–0.07) (n = 44)	0.08 (0.04–0.09) (n = 35)	0.009	0.3 [0.08–0.7]

Logistic regression with adjustment for age, sex, number of cerebral microbleeds, MMSE, cholesterol, diabetes, and hypertension. All CSF marker levels were log-transformed for regression analysis. Odds Ratios correspond to one unit increase in log-transformed levels. Where data were missing, the number of subjects for which data were available is indicated within parentheses. SD, standard deviation; t-tau, total tau; p-tau, phosphorylated tau; Aβ42, β-amyloid 1–42; Aβ40, β-amyloid 1–40; cSS, cortical superficial siderosis; CSF, Cerebrospinal fluid; MMSE, Mini Mental State Examination; OR, odds ratio; CI, confidence interval. Significant values are indicated in bold.

TABLE 4 | CSF marker stratified for extent of cSS.

	Disseminated cSS (n = 33)	Focal cSS (n = 29)	P-value	OR (95% CI)
Aβ42 (pg/ml), median (IQR)	332 (269–421)	435 (367–679)	0.0006	0.02 [0.002–0.2]
Aβ40 (pg/ml), median (IQR)	7,506 (6,784–8,901) (n = 23)	9,418 (7,986–14,621) (n = 21)	0.007	0.01 [0.0003–0.3]
T-tau (pg/ml), median (IQR)	322 (245–431)	309 (248–1214)	0.6	0.8 [0.3–2]
P-tau (pg/ml), median (IQR)	60 (51–67)	60 (51–90)	0.2	0.5 [0.1–1.6]
Aβ42/40 ratio, median (IQR)	0.05 (0.04–0.06) (n = 23)	0.04 (0.04–0.08) (n = 21)	0.9	1.1 [0.2–4.9]

Logistic regression with adjustment for age, sex, number of cerebral microbleeds, MMSE, cholesterol, diabetes and hypertension. All CSF marker levels were log-transformed for regression analysis. Odds Ratios correspond to one unit increase in log-transformed levels. Where data were missing, the number of subjects for which data were available is indicated within parentheses. SD, standard deviation; t-tau, total tau; p-tau, phosphorylated tau; Aβ42, β-amyloid 1–42; Aβ40, β-amyloid 1–40; cSS, cortical superficial siderosis; CSF, Cerebrospinal fluid; MMSE, Mini Mental State Examination; OR, odds ratio; CI, confidence interval. Significant values are indicated in bold.

rates of intracerebral hemorrhage (3, 16), it may be possible that Aβ42 may also act as a biomarker of CAA severity. Previous data on Aβ42 CSF levels in patients with CAA are relatively rare and limited in power. A recent meta-analysis on the topic identified five heterogeneous CAA cohorts that included overall 60 patients (6).

The underlying mechanism of the presumed association between cSS and Aβ42 remain to be elucidated. However, our results are consistent with neuropathological studies that found Aβ42 trapped in the cerebral vessels of CAA patients and therefore hampers the transport of Aβ42 toward the cerebrospinal fluid. Also, *in vitro* data and PET studies suggest, that low Aβ42 in CSF of CAA patients is related to β-amyloid deposition in the vessel walls and the adjacent brain parenchyma (19, 20). Further, experimental studies and neuropathological findings have demonstrated a high co-incidence between CAA and Alzheimer's disease (AD) (21, 22). Therefore, it may be speculated that the demonstrated reduced Aβ42 levels may partly be explained by a higher rate of a co-incident AD in patients with cSS. However, we did not detect higher tau levels in cSS patients contradicting this hypothesis. Hence neuropathological studies are needed to disentangle the complex interplay between cSS and AD.

Patients with disseminated cSS had significantly lower Aβ40 levels than those with focal cSS in our cohort. We are not aware

of any other study that investigated the extent of cSS and its association with Aβ40. However, this result is in line with a case series of 15 patients with hereditary cerebral hemorrhage with amyloidosis–Dutch type (HCHWA-D) that detected decreased CSF Aβ40 levels in HCHWA-D patients in comparison to healthy controls (23). Further, it is in accordance with neuropathological reports demonstrating deposition of Aβ40 within the vessel walls of CAA patients (19). Since patients with disseminated cSS most probably represent a group of more severely affected CAA patients, they may harbor more Aβ40 depositions within the vessel wall and consecutively demonstrate lower CSF Aβ40 levels.

The MMSE values of patients with cSS were numerically lower than in patients without cSS as hypothesized by previous findings that detected a higher prevalence of cSS patients in memory clinics (10, 11). However, this difference did not reach statistical significance. Hence, the results of the current study prevent meaningful conclusions on the extent and etiology of cognitive impairment in patients with cSS. Longitudinal studies with repeated extensive neuropsychological testing and cSS lesion-volume mapping are needed to disentangle the complex interplay of vascular pathology and β-amyloid-pathology in cSS and CAA.

Of note, there was no consistent association between the presence of cSS and Aβ40 in the current study, which may relate to the experimental finding that Aβ42 deposits earlier in the vessel wall than Aβ40 (23–25). Alternatively, it might

be speculated from the odds ratio of 0.8 that slight A β 40 CSF levels differences are present, but the association did not reach statistical significance due to a lack of statistical power. We did not formally compare patients with focal cSS and no cSS due to the small sample sized within subgroups, but it also may be speculated that the effect of lower A β 40 values in cSS is primarily driven by the subgroup of patients with disseminated cSS rather than those with focal cSS. Further studies with larger sample size are needed to fully capture the effect of cSS subgroups and A β 40.

Interestingly, our results did not show an association between the number of CMB and reduced levels of A β 42 or A β 40 in contrast to other reports (23, 26, 27). This discrepancy may partly be related to differences in cohort characteristics since the prevalence of CMB was very high with 84% in this cohort resulting in a potential ceiling effect of the association.

Our study has several strengths including the prospective design, the standardized CSF sampling and analysis as well as the central MR imaging. Limitations include the use of two different MR scanners with different field strengths (3.0 or 1.5 Tesla), that may have had an impact on the number of CMB and potentially the extent of cSS. However, we included MRI field strength and the effect of T2*-weighted method (GRE vs. SWI) as a variable in univariate analysis were it did not show a significant association with CSF markers which makes a strong effect very unlikely. Further, there are no pathological proven CAA cases included. However, 79% of patients were diagnosed with probable CAA according to the modified Boston criteria, which have demonstrated an excellent sensitivity and specificity for CAA (2). Additionally, we repeated the logistic regression analysis on core CSF markers restricted to the subgroup of patients fulfilling the diagnosis of probable CAA with stable results. Finally, differences in medical history between patients might have confounded results in CSF analysis. However, in the backward stepwise regression analysis, only hypertension resulted relevant and a subgroup analysis stratified for differences in medical history was regarded not meaningful due to the limited sample sizes.

REFERENCES

- Wollenweber FA, Opherk C, Zedde M, Catak C, Malik R, Duering M, et al. Prognostic relevance of cortical superficial siderosis in cerebral amyloid angiopathy. *Neurology*. (2019) 92:e792–801. doi: 10.1212/WNL.0000000000006956
- Linn J, Halpin A, Demaerel P, Ruhland J, Giese AD, Dichgans M, et al. Prevalence of superficial siderosis in patients with cerebral amyloid angiopathy. *Neurology*. (2010) 74:1346–50. doi: 10.1212/WNL.0b013e3181dad605
- Charidimou A, Linn J, Vernooij MW, Opherk C, Akoudad S, Baron JC, et al. Cortical superficial siderosis: detection and clinical significance in cerebral amyloid angiopathy and related conditions. *Brain*. (2015) 138:2126–39. doi: 10.1093/brain/awv162
- Wermer MJH, Greenberg SM. The growing clinical spectrum of cerebral amyloid angiopathy. *Curr Opin Neurol*. (2018) 31:28–35. doi: 10.1097/WCO.0000000000000510
- Case NE, Charlton A, Zwiers A, Batool S, McCreary CR, Hogan DB, et al. Cerebral amyloid angiopathy is associated with executive dysfunction and mild cognitive impairment. *Stroke*. (2016) 47:2010–6. doi: 10.1161/STROKEAHA.116.012999
- Charidimou A, Friedrich JO, Greenberg SM, Viswanathan A. Core cerebrospinal fluid biomarker profile in cerebral amyloid angiopathy: a meta-analysis. *Neurology*. (2018) 90:e754–62. doi: 10.1212/WNL.0000000000005030
- Herzig MC, Winkler DT, Burgermeister P, Pfeifer M, Kohler E, Schmidt SD, et al. Abeta is targeted to the vasculature in a mouse model of hereditary cerebral hemorrhage with amyloidosis. *Nat Neurosci*. (2004) 7:954–60. doi: 10.1038/nn1302
- Thal DR, Griffin WS, de Vos RA, Ghebremedhin E. Cerebral amyloid angiopathy and its relationship to Alzheimer's disease. *Acta Neuropathol*. (2008) 115:599–609. doi: 10.1007/s00401-008-0366-2
- Lummel N, Wollenweber FA, Demaerel P, Bochmann K, Malik R, Opherk C, et al. Clinical spectrum, underlying etiologies and radiological

CONCLUSIONS

The present study demonstrates for the first time that presence and extent of cSS are associated with lower A β 42 CSF levels. Our data suggest that A β 42 may act as an additional marker of CAA severity. Nevertheless, further studies are needed to proof these findings and to investigate its underlying mechanisms.

DATA AVAILABILITY

All datasets generated for this study are included in the manuscript and/or the **Supplementary Files**.

CONSENT FOR PUBLICATION

All authors approved the final manuscript and consent to its publication.

ETHICS STATEMENT

Informed consent was obtained from each patient according to the Declaration of Helsinki. Ethics approval was obtained from the regional ethics board (Ethikkommission LMU Munich). Written informed consent was obtained from all patients.

AUTHOR CONTRIBUTIONS

CC and FW designed the study. CC, MZ, DJ, and VS acquired clinical, neuropsychological and CSF data. RM analyzed the data. AK, JL, CO, and MD interpreted the manuscript. CC and FW interpreted and drafted the manuscript. FW supervised and revised the manuscript. All authors read and approved the final manuscript.

SUPPLEMENTARY MATERIAL

The Supplementary Material for this article can be found online at: <https://www.frontiersin.org/articles/10.3389/fneur.2019.00439/full#supplementary-material>

- characteristics of cortical superficial siderosis. *J Neurol.* (2015) 262:1455–62. doi: 10.1007/s00415-015-7736-1
10. Wollenweber FA, Buerger K, Mueller C, Ertl-Wagner B, Malik R, Dichgans M, et al. Prevalence of cortical superficial siderosis in patients with cognitive impairment. *J Neurol.* (2014) 261:277–82. doi: 10.1007/s00415-013-7181-y
 11. Zonneveld HI, Goos JD, Wattjes MP, Prins ND, Scheltens P, van der Flier WM, et al. Prevalence of cortical superficial siderosis in a memory clinic population. *Neurology.* (2014) 82:698–704. doi: 10.1212/WNL.0000000000000150
 12. Inoue Y, Nakajima M, Uetani H, Hirai T, Ueda M, Kitajima M, et al. Diagnostic significance of cortical superficial siderosis for Alzheimer disease in patients with cognitive impairment. *AJNR Am J Neuroradiol.* (2016) 37:223–7. doi: 10.3174/ajnr.A4496
 13. Vernooij MW, Ikram MA, Hofman A, Krestin GP, Breteler MM, van der Lugt A. Superficial siderosis in the general population. *Neurology.* (2009) 73:202–5. doi: 10.1212/WNL.0b013e3181ae7c5e
 14. Petersen RC. Mild cognitive impairment as a diagnostic entity. *J Intern Med.* (2004) 256:183–94. doi: 10.1111/j.1365-2796.2004.01388.x
 15. Wardlaw JM, Smith EE, Biessels GJ, Cordonnier C, Fazekas F, Frayne R, et al. Neuroimaging standards for research into small vessel disease and its contribution to ageing and neurodegeneration. *Lancet Neurol.* (2013) 12:822–38. doi: 10.1016/S1474-4422(13)70124-8
 16. Wollenweber FA, Baykara E, Zedde M, Gesierich B, Achmuller M, Jouvent E, et al. Cortical superficial siderosis in different types of cerebral small vessel disease. *Stroke.* (2017) 48:1404–7. doi: 10.1161/STROKEAHA.117.016833
 17. Charidimou A, Boulouis G, Roongpiboonsopit D, Auriel E, Pasi M, Haley K, et al. Cortical superficial siderosis multifocality in cerebral amyloid angiopathy: a prospective study. *Neurology.* (2017) 89:2128–35. doi: 10.1212/WNL.00000000000004665
 18. Charidimou A, Martinez-Ramirez S, Reijmer YD, Oliveira-Filho J, Lauer A, Roongpiboonsopit D, et al. Total magnetic resonance imaging burden of small vessel disease in cerebral amyloid angiopathy: an imaging-pathologic study of concept validation. *JAMA Neurol.* (2016) 73:994–1001. doi: 10.1001/jamaneurol.2016.0832
 19. Vinters HV. Emerging concepts in Alzheimer's disease. *Annu Rev Pathol.* (2015) 10:291–319. doi: 10.1146/annurev-pathol-020712-163927
 20. Na HK, Park JH, Kim JH, Kim HJ, Kim ST, Werring DJ, et al. Cortical superficial siderosis: a marker of vascular amyloid in patients with cognitive impairment. *Neurology.* (2015) 84:849–55. doi: 10.1212/WNL.0000000000001288
 21. Thal DR, Ghebremedhin E, Orantes M, Wiestler OD. Vascular pathology in Alzheimer disease: correlation of cerebral amyloid angiopathy and arteriosclerosis/lipohyalinosis with cognitive decline. *J Neuropathol Exp Neurol.* (2003) 62:1287–301. doi: 10.1093/jnen/62.12.1287
 22. Verbeek MM, Kremer BP, Rikkert MO, Van Domburg PH, Skehan ME, Greenberg SM. Cerebrospinal fluid amyloid beta(40) is decreased in cerebral amyloid angiopathy. *Ann Neurol.* (2009) 66:245–9. doi: 10.1002/ana.21694
 23. van Etten ES, Verbeek MM, van der Grond J, Zielman R, van Rooden S, van Zwet EW, et al. beta-amyloid in CSF: biomarker for preclinical cerebral amyloid angiopathy. *Neurology.* (2017) 88:169–76. doi: 10.1212/WNL.0000000000003486
 24. Shinkai Y, Yoshimura M, Ito Y, Odaka A, Suzuki N, Yanagisawa K, et al. Amyloid beta-proteins 1-40 and 1-42(43) in the soluble fraction of extra- and intracranial blood vessels. *Ann Neurol.* (1995) 38:421–8. doi: 10.1002/ana.410380312
 25. Natte R, Yamaguchi H, Maat-Schieman ML, Prins FA, Neeskens P, Roos RA, et al. Ultrastructural evidence of early non-fibrillar Abeta42 in the capillary basement membrane of patients with hereditary cerebral hemorrhage with amyloidosis, Dutch type. *Acta Neuropathol.* (1999) 98:577–82. doi: 10.1007/s004010051121
 26. Kester MI, Goos JD, Teunissen CE, Benedictus MR, Bouwman FH, Wattjes MP, et al. Associations between cerebral small-vessel disease and Alzheimer disease pathology as measured by cerebrospinal fluid biomarkers. *JAMA Neurol.* (2014) 71:855–62. doi: 10.1001/jamaneurol.2014.754
 27. Shams S, Granberg T, Martola J, Li X, Shams M, Fereshtehnejad SM, et al. Cerebrospinal fluid profiles with increasing number of cerebral microbleeds in a continuum of cognitive impairment. *J Cereb Blood Flow Metab.* (2016) 36:621–8. doi: 10.1177/0271678X15606141

Conflict of Interest Statement: The authors declare that the research was conducted in the absence of any commercial or financial relationships that could be construed as a potential conflict of interest.

Copyright © 2019 Catak, Zedde, Malik, Janowitz, Soric, Seegerer, Krebs, Düring, Opherke, Linn and Wollenweber. This is an open-access article distributed under the terms of the Creative Commons Attribution License (CC BY). The use, distribution or reproduction in other forums is permitted, provided the original author(s) and the copyright owner(s) are credited and that the original publication in this journal is cited, in accordance with accepted academic practice. No use, distribution or reproduction is permitted which does not comply with these terms.



Cortical Microinfarcts and White Matter Connectivity in Memory Clinic Patients

Doeschka Ferro ^{1†}, Rutger Heinen ^{1†}, Bruno de Brito Robalo ¹, Hugo Kuijf ², Geert Jan Biessels ¹, and Yael Reijmer ¹ On behalf of the Utrecht VCI study group

¹ Brain Center, University Medical Center Utrecht, Department of Neurology, University Medical Center Utrecht, University Utrecht, Utrecht, Netherlands, ² Image Sciences Institute, University Medical Center Utrecht, University Utrecht, Utrecht, Netherlands

OPEN ACCESS

Edited by:

Eric Jouvent,
Université Sorbonne Paris Cité, France

Reviewed by:

Anil Man Tuladhar,
Radboud University Nijmegen Medical
Centre, Netherlands
Frank Arne Wollenweber,
Institute for Stroke and
Dementia Research, Germany

*Correspondence:

Doeschka Ferro
d.a.ferro@umcutrecht.nl

[†]These authors have contributed
equally to this work

Specialty section:

This article was submitted to
Stroke,
a section of the journal
Frontiers in Neurology

Received: 07 February 2019

Accepted: 15 May 2019

Published: 05 June 2019

Citation:

Ferro D, Heinen R, de Brito Robalo B,
Kuijf H, Biessels GJ and Reijmer Y
(2019) Cortical Microinfarcts and
White Matter Connectivity in Memory
Clinic Patients. *Front. Neurol.* 10:571.
doi: 10.3389/fneur.2019.00571

Background and purpose: Cerebral microinfarcts (CMIs) are associated with cognitive impairment and dementia. CMIs might affect cognitive performance through disruption of cerebral networks. We investigated in memory clinic patients whether cortical CMIs are clustered in specific brain regions and if presence of cortical CMIs is associated with reduced white matter (WM) connectivity in tracts projecting to these regions.

Methods: 164 memory clinic patients with vascular brain injury with a mean age of 72 ± 11 years (54% male) were included. All underwent 3 tesla MRI, including a diffusion MRI and cognitive testing. Cortical CMIs were rated according to established criteria and their spatial location was marked. Diffusion imaging-based tractography was used to reconstruct WM connections and voxel based analysis (VBA) to assess integrity of WM directly below the cortex. WM connectivity and integrity were compared between patients with and without cortical CMIs for the whole brain and regions with a high CMI burden.

Results: 30 patients (18%) had at least 1 cortical CMI [range 1–46]. More than 70% of the cortical CMIs were located in the superior frontal, middle frontal, and pre- and postcentral brain regions (covering 16% of the cortical surface). In these high CMI burden regions, presence of cortical CMIs was not associated with WM connectivity after correction for conventional neuroimaging markers of vascular injury. WM connectivity in the whole brain and WM voxels directly underneath the cortical surface did not differ between patients with and without cortical CMIs.

Conclusion: Cortical CMIs displayed a strong local clustering in highly interconnected frontal, pre- and postcentral brain regions. Nevertheless, WM connections projecting to these regions were not disproportionately impaired in patients with compared to patients without cortical CMIs. Alternative mechanisms, such as focal disturbances in cortical structure and functioning, may better explain CMI associated cognitive impairment.

Keywords: microinfarcts, cerebral small vessel disease, vascular cognitive impairment, white matter connectivity, diffusion tensor imaging

INTRODUCTION

Cerebral microinfarcts (CMIs) are small (<5 mm) ischemic lesions that are increasingly recognized as a clinically relevant marker in stroke and dementia (1). Besides post-mortem detection at autopsy, CMIs can now also be detected *in vivo* on MRI as *chronic cortical* CMIs on T1-weighted MRI and *acute* CMIs on diffusion-weighted MRI (2).

Both pathology and MRI studies have found a consistent association between CMI presence and cognitive impairment, also after adjustments for the presence of co-occurring Alzheimer's disease (3) and conventional neuroimaging markers of vascular injury (4–7). Although these findings suggest that CMIs play a causative role in the process of cognitive decline, the exact mechanism by which CMIs and cognitive impairment are linked is not yet clear.

Several manifestations of cerebral small vessel disease (SVD), such as white matter hyperintensities (WMHs), lacunes, and cerebral microbleeds have been suggested to affect cognitive functioning by disruption of the WM network (8–12). It appears that the severity and location of these SVD lesions determine their impact on the brain network and consequently cognition (12, 13). Disruption of WM connectivity may also play a role in the relation between cortical CMIs and cognitive impairment. We hypothesized that cortical CMIs exert their effect on the brain network by secondary degeneration of connecting WM pathways. A small study with cerebral amyloid angiopathy (CAA) patients showed that acute subcortical CMIs were indeed associated with changes in the surrounding local WM microstructural integrity (14). Whether similar effects on WM connectivity occur in relation to chronic cortical CMIs is unknown.

We have previously reported that presence of CMIs in memory clinic patients with vascular brain injury is associated with other neuroimaging markers of vascular injury, a diagnosis of vascular dementia and reduced performance in multiple cognitive domains (4). In the present study we investigated whether cortical CMIs in this cohort predominantly occur in specific brain regions and if presence of cortical CMIs is associated with impaired WM connectivity in tracts projecting to these regions.

METHODS

Study Population

This study involved patients from the TRACE-VCI cohort of the University Medical Center (UMC) Utrecht, an observational prospective cohort study of memory clinic patients with vascular brain injury (i.e., possible VCI) recruited between September 2009 and December 2013 [details described previously (4, 15)]. Patients were included in the cohort if they presented with cognitive complaints at the memory clinic, and had evidence of vascular brain injury on MRI, operationalized as: (1) WMHs with a Fazekas scale grade ≥ 2 (16); (2) ≥ 1 lacunar or non-lacunar infarcts; (3) ≥ 1 cerebral microbleeds; (4) ≥ 1 intracerebral hemorrhage(s) or (5) Fazekas scale grade 1 combined with ≥ 2 vascular risk factors (15). In line with proposed VCI criteria, patients with possible co-existing neurodegenerative disorders (such as Alzheimer's disease) were included in this study cohort, but patients with primary non-vascular or non-neurodegenerative causes of cognitive dysfunction (e.g., brain tumors, depression) were excluded (15). All patients ($n = 196$) underwent a standardized clinical assessment and 3 tesla brain MRI. Patients were included for the present study if they had complete MRI data, including a diffusion weighted scan ($n = 177$), another 13 patients were excluded due to poor quality of

the MRI ($n = 3$) or DTI ($n = 9$, including 2 network outliers) and 1 failure to co-register the AAL-template, resulting in a study population of 164.

Ethical approval was provided by the institutional review board of the UMC Utrecht. All procedures were in accordance with the ethical standards of the responsible committee on human experimentation (institutional and national) and with the Helsinki Declaration of 1975, as revised in 2013. Written informed consent was obtained from all participants prior to any research related procedures.

Clinical Diagnosis of Cognitive Impairment

Educational level was rated according to the 7-point Verhage scale (17). The Clinical Dementia Rating scale (CDR; range: 0–3) was used to assess the severity of cognitive symptoms and functional deficits (18). The mini-mental state examination (MMSE) in Dutch was used as a global measure of cognitive performance (19).

Severity of cognitive impairment was classified at a multidisciplinary consensus meeting. *No objective cognitive impairment* (NOCI) was defined as cognitive complaints, but without objective cognitive impairment on neuropsychological testing. *Mild cognitive impairment* (MCI) was defined as complaints or deterioration from prior functioning and objective impairment in at least one cognitive domain, but with no or mild impairment of activities in daily living. *Dementia* was defined as deficits in two or more cognitive domains at neuropsychological testing and who experienced interference of these deficits in daily living. Further etiological diagnoses of dementia were made based on internationally established diagnostic criteria (without knowledge of CSF biomarkers) into *vascular dementia* (VaD) (20), *Alzheimer's disease* (AD) (21), or other (i.e., dementia such as Lewy body, primary progressive aphasia, cortical basal syndrome, unknown etc (15)).

MRI

All patients were scanned on a 3 tesla MRI scanner (Philips Achieva or Philips Ingenia [Philips Medical Systems, Best, the Netherlands]). The standardized MRI protocol included a 3D T1-weighted sequence (192 slices, voxel size: $1.00 \times 1.00 \times 1.00 \text{ mm}^3$, repetition time (TR)/echo time (TE): 7.9/4.5 ms); the following transversal 2D sequences (48 slices, voxel size: $0.96 \times 0.96 \times 3.00 \text{ mm}^3$): T2-weighted turbo spin echo (TSE; TR/TE: 3198/140 ms), T2*-weighted (TR/TE: 1653/20 ms), and fluid-attenuated inversion recovery (FLAIR; TR/TE/inversion time: 11000/125/2800 ms); and diffusion-weighted imaging [DWI; 48 slices, voxel size: $1.72 \times 1.72 \times 2.50 \text{ mm}^3$, TR/TE: 6600/73 ms, 45 gradient directions with a b -value of $1,200 \text{ s/mm}^2$ and one with a b -value of 0 s/mm^2 (3 averages)].

Neuroimaging Markers

The following neuroimaging markers were rated according to the STRIVE criteria (22) by or under supervision of a neuroradiologist, who was blinded to the clinical condition of the participants: (1) WMHs on the Fazekas scale (16); (2) Lacunes (presence and number); (3) Cerebral microbleeds (presence and number); (4) Medial temporal lobe atrophy (MTA) using the Scheltens scale averaged for both hemispheres (23).

Brain Volume Measurements

The following semi-automated workflow was used to obtain brain volumes: (1) automated WMH segmentation of 2D FLAIR images using kNN-TTP (24); (2) lesion-filling of 3D T1 images using SLF toolbox (<http://atc.udg.edu/nic/slfToolbox/index.html>) for Statistical Parametric Mapping 12 (SPM Wellcome Department of Cognitive Neurology, Institute of Neurology, Queen Square London) with default settings (25, 26); (3) default settings were used to obtain probabilistic segmentations for gray matter, WM, and CSF. Total brain volume was defined as the sum of the gray and WM volume. Brain volumes were expressed as a percentage of the total intracranial volume.

Rating of Cortical CMIs

Cortical CMIs were rated by visual inspection according to previously proposed criteria (2, 27). Cortical CMIs were rated on 3 tesla MRI and were hypointense on T1-weighted imaging, hyper- or isointense on FLAIR or T2-weighted imaging and isointense on T2*-weighted imaging. Lesions had to be strictly intracortical and ≤ 4 mm in the greatest dimension on T1. If the lesions measured substantially larger than 4 mm on T2-weighted imaging or within 1 cm proximity of a larger stroke, it was disregarded as the lesion was considered part of a larger stroke. The lesion had to be visible in two viewing planes of the brain (e.g., sagittal, transversal, or coronal plane) and distinct from other structures and lesions such as arteries, veins, enlarged perivascular spaces and cerebral microbleeds. Rating were carried out using MeVisLab (MeVis medical solutions, Bremen, Germany) (28), while the rater was blinded to the clinical condition of the subjects. There was a good intra-rater and interrater (both intra-class correlation coefficient > 0.95) agreement, details regarding the intra- and interrater reliability were published previously (4).

Cortical CMI Spatial Mapping

Cortical CMI locations from all patients were registered to Montreal Neurological Institute (MNI) space. The automated anatomic labeling (AAL) template (29) was used as overlay on this sample-averaged CMI map. The number of CMIs within each AAL region was determined to assess whether CMIs predominantly occurred in specific brain regions. The AAL regions with a relatively high number of CMI were defined as *high CMI burden regions*, other AAL regions were defined as *low CMI burden regions*. The threshold for high vs. low CMI burden regions was arbitrarily set at > 5 CMIs (For a histogram of the CMI numbers per AAL region, see **Supplementary Figure 1**). For 3D rendering of the spatial distribution of cortical CMIs see **Figure 1**. The volume per AAL region was calculated using automated segmentation using CAT12 after registering the AAL template to the T1 image in patient space.

Diffusion MRI Processing and Network Reconstruction

Diffusion tensor imaging (DTI) scans were preprocessed as previously described (12, 30) using ExploreDTI version 4.8.6

(www.exploredti.com) and included subject motion correction, unwarping of eddy current and EPI induced distortions and a robust tensor estimation (including adjustment of the B-matrix) (31–33). Next, whole brain deterministic WM tractography was performed using constrained spherical deconvolution (CSD)-based tractography, which is different from standard tensor-based tractography, as it allows reconstruction of crossing fiber pathways (34–36). Reconstruction of fiber tracts was performed by using uniformly distributed starting seed samples throughout the brain's WM at every voxel with a fiber orientation distribution (FOD) > 0.1 (indicating WM) at a $2 \times 2 \times 2$ mm³ resolution. Fiber reconstruction was terminated if either a deflection in an angle of more than 45 degrees occurred or if a fiber entered a voxel with a FOD of < 0.1 (indicating no WM). An additional terminating mask was not applied. Brain network nodes were defined using the same AAL template as used for the cortical CMI mapping described above, consisting of 90 cortical and subcortical gray matter regions. The AAL template is a commonly used atlas to define nodes in clinical network studies (8, 9, 11). The atlas has the advantage that the gray matter regions also contain a small portion of WM, which allows streamlines that terminate just before the gray-white matter border to be included in the network, thereby reducing the chance of false negative connections. Nodes were considered to be connected if two end points of a reconstructed fiber bundle lay within those nodes, resulting in a 90×90 binary connectivity matrix. This matrix was then weighted by multiplying each connection by the mean fractional anisotropy (FA) or mean diffusivity (MD) of that connection, resulting in two weighted-connectivity matrices for each patient. To reduce partial volume effects in WM connections a threshold of FA > 0.2 was applied to all the connectivity matrices. See **Figure 2** (upper part A-D) for a graphical representation of this workflow.

Measures of Whole Brain and Regional WM Connectivity

The Brain Connectivity Toolbox (<http://www.brain-connectivity-toolbox.net>) was used to calculate network properties, including nodal degree (i.e., number of WM connections per node) and nodal strength (here defined as the mean FA or MD of all WM connections to that node) (37). For this study we used the following constructs: *Whole brain WM connectivity* was assessed by the average FA and MD-weighted nodal strength of all network nodes. *WM connectivity in high and low CMI burden regions* was assessed by the average FA- and MD-weighted nodal strength of the high and low CMI burden regions, respectively, (see paragraph 2.7, for an overview of regions see **Figure 1**).

Voxel-Based WM Diffusion Analysis

In addition to the network-based connectivity analyses we also performed a WM voxel-based analysis to assess differences in mean FA and MD. Although we assume that secondary degeneration affects the whole axon running from the cortex to the deep WM, one may speculate that the WM *directly*

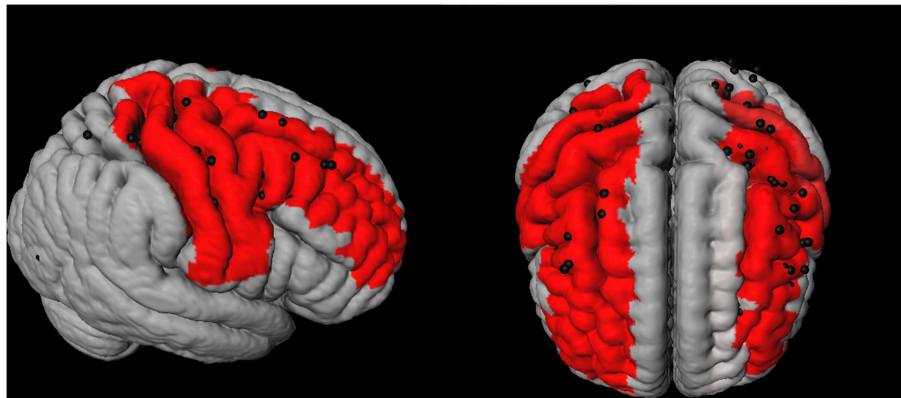


FIGURE 1 | 3D representation of the spatial distribution of cortical microinfarcts (CMIs; represented as black dots) across the brain in the cohort. The red areas represent the Automated Anatomical Labeling (AAL)-atlas regions with a high CMI burden (i.e., the 7 brain regions which contained 75% of all the cortical CMIs).

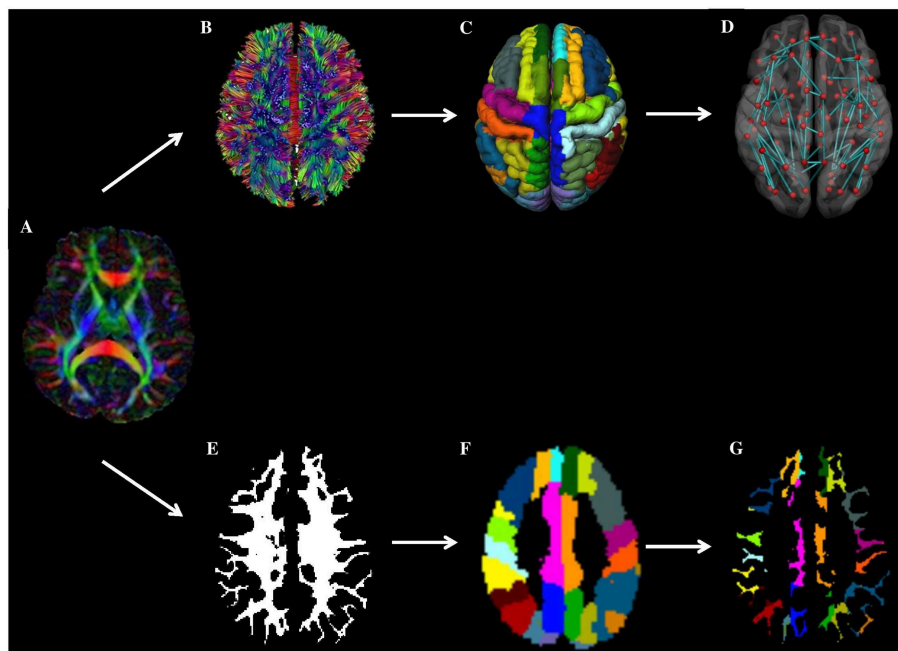


FIGURE 2 | Overview of workflow. In the top panel (network-based approach): from a patients' DTI images (A), WM connections are reconstructed using fiber tractography (B). Next, brain network nodes were defined using the cortical parcellation using the AAL template (C). Subsequently, the structural brain network was reconstructed (D). Weighting of the network was done by multiplying each connection by the mean fractional anisotropy (FA) or mean diffusivity (MD). Finally, the mean FA and MD of connections towards high and low cortical microinfarcts (CMI) burden regions were compared between patients with and without CMIs. In the bottom panel (voxel-based approach), the patient's DTI image (A) is combined with the patient's WM segmentation results (E) and AAL template (F) to assess diffusion properties of the WM voxels in the AAL region (i.e. directly underneath the cortex) (G).

underneath the CMI containing cortical (i.e., juxtacortical) surface is primarily affected. As can be seen in **Figure 2** (lower part) AAL regions mainly consist of GM, but also contain a small WM section in close proximity to the cortical surface. Therefore, we also calculated the mean FA and MD of the WM voxels within each AAL region (using a WM mask with a WM probability threshold of 75). The FA and MD was averaged across all AAL regions for the high and low CMI

burden regions respectively, see **Figure 2** (lower part E-G) for a graphical representation).

Statistical Analysis

Differences in baseline characteristics between patients with and without cortical CMIs were analyzed using independent sample *t*-tests (for continuous normally distributed data), χ -square test (for proportions), and Mann-Whitney *U*-test (for continuous,

non-normally distributed data). Differences in volume and connectivity strength between brain regions that were identified as high and low CMI burden regions were compared using a paired sample *t*-test (regardless of CMI presence).

The association between the presence of cortical CMIs (predictor) and FA- and MD-weighted WM connectivity (outcome) was analyzed using linear regression and included sex and age (Model 1) and sex, age and conventional neuroimaging markers (WMH Fazekas scale grade 3, presence of lacunar and non-lacunar infarcts) (Model 2) as covariates. Beta values are reported with 95% confidence interval (CI) and corresponding *t*-values and degrees of freedom (df). These analyses were carried out separately for whole brain, high and low CMI burden regions. Within the group of patients with cortical CMIs, patients with 1 vs. patients with multiple cortical CMIs (predictor) were compared on WM connectivity (outcome) using an independent *t*-tests and corresponding df. Using a voxel based approach, the association between cortical CMI presence (predictor) and the mean FA and MD of WM voxels in close proximity to the cortex (outcome) was analyzed using linear regression, adjusted for age and sex. A possible interaction effect between cortical CMI presence and clinical diagnosis on WM connectivity was explored in a regression analysis with *post hoc* Helmert contrasts, where each clinical diagnosis (except the first) was compared to the main effect of all previous diagnoses. *Post-hoc* power analysis was carried out using G*Power (Heinrich-Heine-University, Düsseldorf, Germany) (38). All analyses were carried out using IBM SPSS statistics (version 22). A *p*-value of <0.05 was considered significant, *p*-values were not adjusted for multiple comparisons, as all analyses were planned (not *post-hoc*).

Data Availability Statement

Any data on the VCI cohort used in these analyses that is not published within this article is available by request from any qualified investigator.

RESULTS

Baseline Characteristics of Patients With and Without Cortical CMIs

The 164 patients had a mean age of 72 (± 11) years and 88 (54%) were male. A total of 134 cortical CMIs were detected in 30 (18%) of the 164 patients. The number of cortical CMIs per patient ranged between 1 and 46, 14 patients had 1 cortical CMI and 16 patients had 2 or more cortical CMIs. Baseline characteristics of patients with and without cortical CMIs are presented in **Table 1**. We have previously published the detailed cognitive profile of patients with cortical CMIs in this specific cohort (4). In short patients with cortical CMIs were more often male, had more non-lacunar infarcts and were more often diagnosed with vascular dementia (all *p* < 0.05).

Characteristics of High and Low CMI Burden Regions

The spatial location of the cortical CMIs was highly clustered, as more than 70% (*n* = 99) of all cortical CMIs were located within 7 AAL regions (*High CMI burden regions*: middle

TABLE 1 | Characteristics of patients with and without cortical CMIs.

	Cortical CMI absent (<i>N</i> = 134)	Cortical CMI present (<i>N</i> = 30)
DEMOGRAPHICS		
Age (years)	72 \pm 11	71 \pm 11
Sex (males)	67 (50)	21 (70)*
Level of education (7 categories)	5 [4-6]	5 [4-6]
Cognitive Performance		
MMSE (<i>n</i> = 161)	26 \pm 3	25 \pm 3
CDR	0.5 [0.5-1]	0.5 [0.5-1]
Clinical diagnosis (<i>n</i> = 154)		
NOCI	24 (19)	3 (11)
MCI	49 (39)	7 (25)
Alzheimer's dementia	48 (38)	13 (46)
Vascular dementia	5 (4)	5 (18)*
Other ^a	8 (6)	2 (7)
NEUROIMAGING MARKERS		
Total brain volume (% of TIV)	68 \pm 4	67 \pm 3
Gray matter volume (% of TIV)	36 \pm 2	35 \pm 2
WMH (Fazekas scale)	2 [1-2]	2 [1-2]
Presence of non-lacunar infarcts	26 (19)	19 (63)‡
Presence of lacunar infarcts	43 (32)	12 (40)
Presence of cerebral microbleeds	46 (35)	10 (35)

CMI, Cortical microinfarct; MMSE, mini-mental state examination; CDR, Clinical dementia rating scale; NOCI, No objective cognitive impairment; MCI, Mild cognitive impairment; TIV, total intracranial volume; WMH, White matter hyperintensities.

^aOther: includes dementia such as Lewy body, primary progressive aphasia, cortical basal syndrome, unknown etc.

Data presented as mean \pm SD, *n* (percentages) or median [interquartile range]. **p* < 0.05
‡*p* < 0.0001.

frontal and pre- and postcentral regions of both hemispheres and the right superior frontal region; **Figure 1**). The other 83 supratentorial brain regions (i.e., *low CMI burden region*) contained the remaining 37 cortical CMIs. The mean volume of the high CMI burden regions was 68 \pm 8.5 ml (16% of total cortical GM volume) compared to 349 \pm 41 ml of the low CMI burden regions. Network analyses showed that the high CMI burden regions were more highly connected to the rest of the network than the low CMI burden regions. This was reflected in a higher nodal degree (high burden: 27.2 \pm 4.1 vs. low burden: 24.0 \pm 2.8), higher FA-weighted nodal strength (high burden: 0.300 \pm 0.020 vs. low burden: 0.293 \pm 0.016) and higher MD-weighted nodal strength (high burden: 0.940 $\times 10^{-3}$ mm²/s \pm 0.059 vs. low burden: 0.985 $\times 10^{-3}$ mm²/s \pm 0.059 all comparisons *p* < 0.0001).

Association Between Cortical CMI Presence and WM Connectivity

The presence of cortical CMIs was not associated with whole brain FA- and MD-weighted WM connectivity (**Table 2**). Within the group of patients with cortical CMIs, the number of cortical CMIs (cortical CMI=1 vs. cortical CMI \geq 2) also was not related to whole brain FA- ($t_{(df=28)} = -0.71$, *p* = 0.485) or MD-weighted WM connectivity ($t_{(df=28)} = 0.05$, *p* = 0.964). Regional

TABLE 2 | Association between cortical CMI presence and whole brain and regional FA- and MD-weighted WM connectivity in high and low CMI burden regions.

Cortical CMI absent (N = 134)		Cortical CMI present (N = 30)	Model 1			Model 2		
			Beta [95% CI]	t-value	p	Beta [95% CI]	t-value	p
WHOLE BRAIN								
FA	0.294 ± 0.017	0.290 ± 0.017	−0.093 [−0.256;0.070]	−1.19	0.234	−0.052 [−0.234;0.104]	−0.69	0.490
MD ^a	0.979 ± 0.057	0.993 ± 0.061	0.087 [−0.047;0.228]	1.27	0.208	0.018 [−0.108;0.138]	0.26	0.795
HIGH CORTICAL CMI BURDEN REGIONS								
FA	0.301 ± 0.020	0.296 ± 0.021	−0.109 [−0.254;0.036]	−1.40	0.165	−0.059 [−0.216;0.098]	−0.78	0.440
MD ^a	0.936 ± 0.057	0.958 ± 0.066	0.136 [−0.013;0.285]	1.82	0.071	0.030 [−0.102;0.162]	0.41	0.683
LOW CORTICAL CMI BURDEN REGIONS								
FA	0.294 ± 0.016	0.290 ± 0.016	−0.091 [−0.228;0.068]	−1.16	0.247	−0.051 [−0.204;0.102]	−0.67	0.501
MD ^a	0.983 ± 0.058	1.000 ± 0.063	0.082 [−0.050;0.208]	1.20	0.231	0.017 [−0.102;0.130]	0.24	0.808

CMI, Cerebral microinfarct; FA, Fractional anisotropy-weighted WM connectivity; MD, Mean diffusivity-weighted WM connectivity. Lower FA and higher MD indicated impaired WM connectivity.

^aMD values × 10^{−3} mm²/s.

Model 1: Covariates age and sex (degrees of freedom = 160).

Model 2: Covariates sex, age, WMH Fazekas grade 3, presence of lacunar and non-lacunar infarct (degrees of freedom = 157).

analyses showed that in the high CMI burden regions, patients with cortical CMIs had marginally higher MD-weighted WM connectivity (reflecting greater WM disruption), although not statistically significant ($p = 0.071$) while a similar FA-weighted connectivity was observed (Table 2). These association remained non-significant when conventional neuroimaging markers of vascular injury were entered as covariates in the model (Model 2; Table 2). Within the low CMI burden regions, cortical CMI presence was not associated with FA or MD-weighted WM connectivity (Table 2).

Since not all cortical CMIs were located in the high burden regions, a sensitivity analysis was performed between patients who had CMIs *exclusively* in the high burden regions ($n = 20$) and patients without CMIs, which yielded similar results.

A *post-hoc* power analysis for CMI presence in high CMI burden regions indicated a power of 0.24 for FA- and 0.44 for MD-weighted connectivity.

Voxel-Based WM Analysis

Limiting our analysis to WM voxels in close proximity to the cortex showed similar results, i.e., the presence of cortical CMIs was not associated with abnormal mean FA and MD in high CMI burden regions [FA: $t_{(df=158)} = -1.01$, $p = 0.314$; MD: $t_{(df=158)} = 0.753$, $p = 0.452$] or in low CMI burden regions [FA: $t_{(df=158)} = -0.97$, $p = 0.336$; MD: $t_{(df=158)} = 1.28$, $p = 0.204$].

Association Between Clinical Diagnosis, WM Connectivity and Cortical CMI Presence

Clinical diagnosis (NOCI, MCI, AD, or VaD) was a significant predictor of whole brain FA- [$F_{(df=4,152)} = 13.9$, $p = 0.005$] and MD-weighted WM connectivity [$F_{(df=4,152)} = 10.2$, $p = 0.008$]. *Post-hoc* analyses revealed that this effect was driven by the patients with the most severe clinical diagnosis, i.e., patients with AD and VaD had abnormal WM connectivity compared to the other groups (Figure 3). No significant interaction was observed between cortical CMI presence and clinical diagnosis

on FA- or MD-weighted WM connectivity [$F_{(df=4,152)} = 0.42$, $p = 0.783$] or MD [$F_{(df=4,152)} = 0.67$, $p = 0.700$], indicating that the association between cortical CMI presence and WM connectivity did not differ across the various clinical diagnoses. In a sensitivity analysis of patients without dementia ($n = 83$) presence of cortical CMIs was also not associated with whole brain FA [$t_{(df=79)} = 0.43$, $p = 0.667$] or MD [$t_{(df=79)} = -0.92$, $p = 0.359$].

DISCUSSION

This study shows that cortical CMIs in memory clinic patients vascular brain injury display a strong spatial clustering, as more than 70% of the cortical CMIs were located in frontal, precentral, and postcentral brain regions covering only 16% of the cortical surface. These high CMI burden regions proved to be strongly connected with the rest of the network. However, we found no evidence that the actual presence of cortical CMIs was related to disruption of WM connections to either the high CMI burden regions or within the whole brain.

Cortical CMIs showed a strong predilection for the frontal, precentral, and postcentral brain regions. A similar pattern of CMIs has been found in memory clinic patients (6), but also in patients with ischemic stroke (7, 39), Alzheimer's disease (40) and even in patients with CAA, where vessels are typically affected in the posterior brain regions (41). This preferential lesion location is likely to be of etiological significance. A similar predilection for frontal, pre- and postcentral brain regions was observed in patients with post-stroke cognitive impairment, where a thromboembolic origin has been suggested (42). Future research is encouraged to further explore the relation between lesion location and the pathophysiological origin of cortical CMIs using larger study samples.

We hypothesized that cortical CMIs might affect cognitive performance by disruption of cerebral networks. We have previously reported a relationship between cortical CMIs

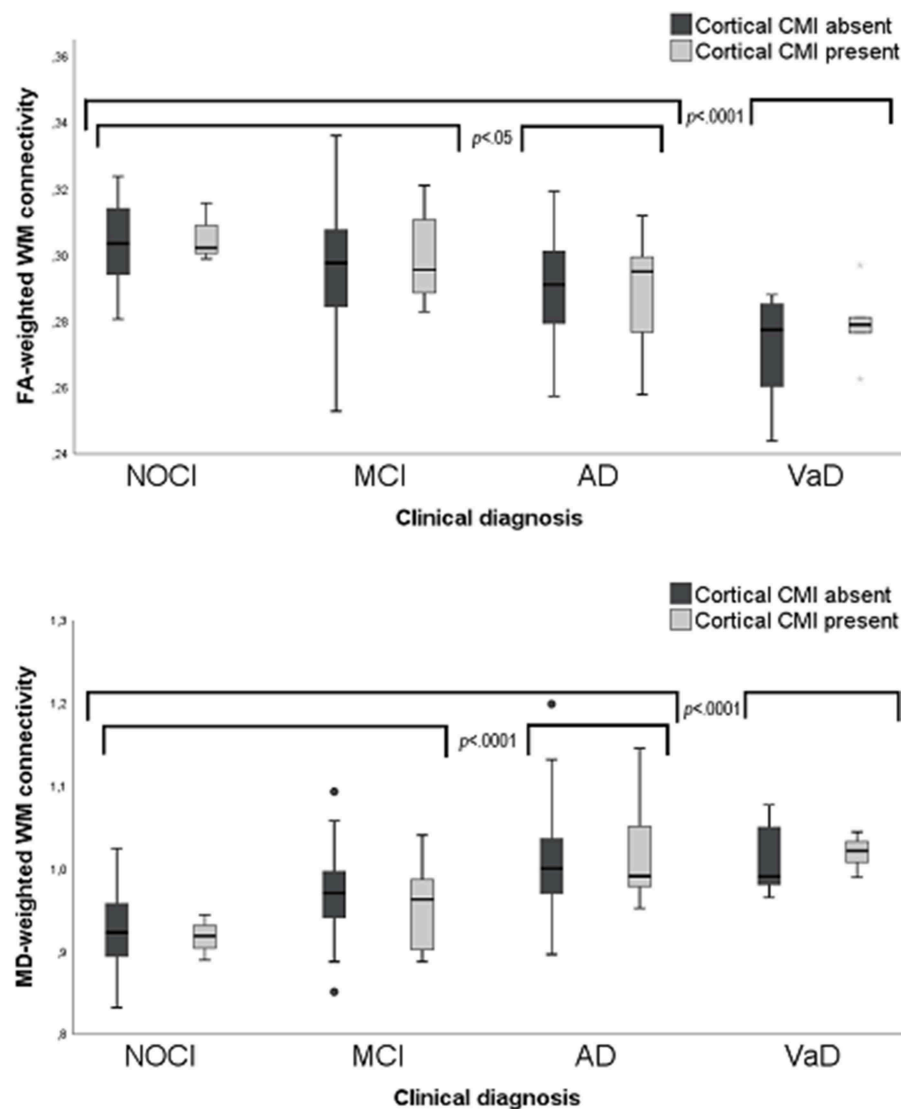


FIGURE 3 | Box plots of FA-(upper) and MD-(lower) weighted WM connectivity between patients with and without cortical CMIs (labels) clinical diagnosis (X-axis). MD values $\times 10^{-3}$ mm²/s. CMI, Cortical microinfarct; NOCI, No objective cognitive impairment; MCI, Mild cognitive impairment; AD, Alzheimer's disease; VaD, Vascular dementia.

and reduced cognitive performance on multiple domains in this same cohort (4). In the current study we investigated impaired WM connectivity as possible underlying mechanism. As lesion location could be crucial for its effect on the cerebral network (13), regions with high and low CMI burden were compared. We established no convincing relationship between cortical CMIs and WM connectivity, as the association between cortical CMIs and impaired WM connectivity in high CMI burden regions disappeared after correcting for conventional neuroimaging markers of vascular injury. These findings were in line with our voxel based analysis, showing no local disturbances in the WM directly below the cortical surface of high CMI burden regions. Independent of CMI presence, we did find that patients with dementia, especially VaD, presented with impaired WM connectivity, which corresponds to the

known association between network disruption and cognitive deficits (43).

Previous studies in patients with SVD found a disruptive effect of SVD MRI- manifestations, such as WMHs and lacunes, on WM connectivity (8–10, 12, 14, 44–46). Our study is the first to assess the effect of cortical CMIs and did not observe an effect on WM connectivity. This contrasting finding could be explained by the fact that these subcortical manifestations of SVD have a more direct impact on WM integrity, while cortical CMIs are thought to exert their effect indirectly through secondary degeneration. The limited size of the cortical CMIs could also account for the lack of association, as for macroscopic cortical infarcts the size of the lesion is directly correlated to the extent of the axonal injury (47). Considering the average lesion volume of cortical CMIs on 3-T MRI is max 0.1 ml, their effect on

WM connectivity could indeed be modest and not of major clinical relevance.

Since cortical CMIs were not related to WM connectivity, other underlying mechanisms should be considered to explain how cortical CMIs affect cognitive impairment. Our earlier work showed that the cortical CMIs were mainly associated with deficits in “cortical” cognitive domains, including visuoconstruction and language (4, 6) suggesting that cortical CMIs potentially affect cognition by disruption of local cortical processes. This notion is supported by a mouse study, that found diminished neural activity and neurovascular coupling in the cortical tissue surrounding the CMI (48). An alternative explanation is that cortical CMIs are a marker of more widespread vascular brain damage that affects cognitive performance (1, 2). As cortical CMIs smaller than 1 mm escape detection on 3 tesla MRI, larger visible cortical CMIs probably only represent the tips of the iceberg. Moreover, it is important to clarify the etiological underpinning of both the detectable as well as these smaller cortical CMIs in order to develop therapeutic strategies that counter cognitive decline.

The strength of our study includes the use of high quality imaging and clinical data of this memory clinic cohort and the systematic approach in cortical CMI rating. Moreover, this study utilized two different DTI approaches to assess the relation with cortical CMIs; a network-based analysis and a voxel-based analysis. However, this study also has some limitations. Firstly, the sample size of cortical CMI cases in our cohort was small, since MRI detectable cortical CMIs occur only in approximately a quarter of memory clinic patients (6). Based on our *post-hoc* power analysis for the observed effect sizes in our study, it would be recommended to replicate results in a larger cohort. Another possible limitation concerns the heterogeneity of the cohort, which includes memory clinic patients with different etiologies, severity of cognitive dysfunction and with large variation in cortical CMI burden. Although this reflects daily clinical practice, it may have reduced our sensitivity to detect abnormalities in WM connectivity due to cortical CMIs.

CONCLUSION

We showed that cortical CMIs in memory clinic patients displayed a strong local clustering in frontal and central brain regions, which warrants further investigations into their etiology. Nevertheless, the WM connections projecting to these regions were not impaired in patients with cortical CMIs. This does not support the hypothesis that cortical CMIs affect the brain's integrity through disturbance of WM connections, although further studies, also in larger cohorts with high burden of cortical CMIs, are recommended to confirm our observations.

ETHICS STATEMENT

Ethical approval was provided by the institutional review board of the UMC Utrecht. All procedures were in accordance

with the ethical standards of the responsible committee on human experimentation (institutional and national) and with the Helsinki Declaration of 1975, as revised in 2013. Informed consent was obtained from all participants prior to any research related procedures.

AUTHOR CONTRIBUTIONS

DF and RH contributed equally to study concept and design, data collection and interpretation, and drafting the manuscript. BdB contributed in data analysis and critical revision of manuscript. HK contributed to image processing and critical revision of manuscript. GB and YR contributed to study concept and design, obtaining funding, interpretation of data, revising the manuscript for important intellectual content.

FUNDING

This study is supported by Vidi grant 917.11.384 and Vici Grant 918.16.616 from ZonMw, The Netherlands, Organisation for Health Research and Development, and grant 2010T073 from the Dutch Heart Association to GB Biessels.

YD Reijmer receives funding from Alzheimer Nederland and ZonMw/Memorabel (grant # 733050503) and a Young Talent Fellowship from the Brain Center Rudolf Magnus, University Medical Center Utrecht.

We acknowledge the support from the Netherlands CardioVascular Research Initiative: the Dutch Heart Foundation (CVON 2012-06 Heart Brain Connection), Dutch Federation of University Medical Centers, the Netherlands Organisation for Health Research and Development, and the Royal Netherlands Academy of Sciences.

ACKNOWLEDGMENTS

We would like to thank Hamed Yousefi Mesri MSc for technical support in the voxel-based analysis.

Members of the Utrecht VCI Study Group

Members of the Utrecht Vascular Cognitive Impairment (VCI) Study group involved in the present study (in alphabetical order by department): University Medical Center Utrecht, the Netherlands, Department of Neurology: E. van den Berg, J.M. GB, M. Brundel, W.H. Bouvy, L.G. Exalto, C.J.M. Frijns, O. Groeneveld, S.M. Heringa, N. Kalsbeek, L.J. Kappelle, Y.D. Reijmer, J. Verwer; Department of Radiology/Image Sciences Institute: J. de Bresser, HK, A. Leemans, P.R. Luijten, M.A. Viergever, K.L. Vincken, J.J.M. Zwanenburg; Department of Geriatrics: H.L. Koek; Hospital Diaconessenhuis Zeist, the Netherlands: M. Hamaker, R. Faaij, M. Pleizier, E. Vriens.

SUPPLEMENTARY MATERIAL

The Supplementary Material for this article can be found online at: <https://www.frontiersin.org/articles/10.3389/fneur.2019.00571/full#supplementary-material>

REFERENCES

- Smith EE, Schneider JA, Wardlaw JM, Greenberg SM. Cerebral microinfarcts: the invisible lesions. *Lancet Neurol.* (2012) 11:272–82. doi: 10.1016/S1474-4422(11)70307-6
- Van Veluw SJ, Shih AY, Smith EE, Chen C, Schneider JA, Wardlaw JM, et al. Detection, risk factors, and functional consequences of cerebral microinfarcts. *Lancet Neurol.* (2017) 16:730–40. doi: 10.1016/S1474-4422(17)30196-5
- Arvanitakis Z, Leurgans SE, Barnes LL, Bennett DA, Schneider JA. Microinfarct pathology, dementia, and cognitive systems. *Stroke.* (2011) 42:722–7. doi: 10.1161/STROKEAHA.110.595082
- Ferro DA, van Veluw SJ, Koek HL, Exalto LG, Biessels GJ. Cortical cerebral microinfarcts on 3 tesla MRI in patients with vascular cognitive impairment. *J Alzheimer's Dis.* (2017) 60:1443–50. doi: 10.3233/JAD-170481
- Hilal S, Sikking E, Shaik MA, Chan QL, van Veluw SJ, Vrooman H, et al. Cortical cerebral microinfarcts on 3T MRI. *Neurology.* (2016) 87:1583–90. doi: 10.1212/WNL.0000000000003110
- Van Veluw SJ, Hilal S, Kuijff HJ, Ikram MK, Xin X, Yeow TB, et al. Cortical microinfarcts on 3T MRI: Clinical correlates in memory-clinic patients. *Alzheimer's Dement.* (2015) 11:1500–9. doi: 10.1016/j.jalz.2014.12.010
- Wang Z, van Veluw SJ, Wong A, Liu W, Shi L, Yang J, et al. Risk factors and cognitive relevance of cortical cerebral microinfarcts in patients with ischemic stroke or transient ischemic attack. *Stroke.* (2016) 47:2450–55. doi: 10.1161/STROKEAHA.115.012278
- Lawrence AJ, Chung AW, Morris RG, Markus HS, Barrick TR. Structural network efficiency is associated with cognitive impairment in small-vessel disease. *Neurology.* (2014) 83:304–11. doi: 10.1212/WNL.0000000000000612
- Tuladhar AM, van Dijk E, Zwiers MP, van Norden AGW, de Laat KF, Shumskaya E, et al. Structural network connectivity and cognition in cerebral small vessel disease. *Hum Brain Mapp.* (2016) 37:300–10. doi: 10.1002/hbm.23032
- D'Souza MM, Gorthi S, Vadwala K, Trivedi R, Vijayakumar C, Kaur P, et al. Diffusion tensor tractography in cerebral small vessel disease: correlation with cognitive function. *Neuroradiol J.* (2018) 31:83–9. doi: 10.1177/1971400916682753
- Reijmer YD, Fotiadis P, Martinez-Ramirez S, Salat DH, Schultz A, Shoamanesh A, et al. Structural network alterations and neurological dysfunction in cerebral amyloid angiopathy. *Brain.* (2015) 138:179–88. doi: 10.1093/brain/awu316
- Heinen R, Vlegels N, de Bresser J, Leemans A, Biessels GJ, Reijmer YD. The cumulative effect of small vessel disease lesions is reflected in structural brain networks of memory clinic patients. *NeuroImage Clin.* (2018) 19:963–9. doi: 10.1016/j.nicl.2018.06.025
- Reijmer YD, Fotiadis P, Piantoni G, Boulouis G, Kelly KE, Gurol ME, et al. Small vessel disease and cognitive impairment: The relevance of central network connections. *Hum Brain Mapp.* (2016) 37:2446–54. doi: 10.1002/hbm.23186
- Auriel E, Edlow BL, Reijmer YD, Fotiadis P, Ramirez-Martinez S, Ni J, et al. Microinfarct disruption of white matter structure: a longitudinal diffusion tensor analysis. *Neurology.* (2014) 83:182–8. doi: 10.1212/WNL.0000000000000579
- Boomsma JMF, Exalto LG, Barkhof F, van den Berg E, de Bresser J, Heinen R, et al. Vascular cognitive impairment in a memory clinic population: rationale and design of the "utrecht-amsterdam clinical features and prognosis in vascular cognitive impairment" (TRACE-VCI) study. *JMIR Res Protoc.* (2017) 6:e60. doi: 10.2196/resprot.6864
- Fazekas F, Chawluk J, Alavi A, Hurtig H, Zimmerman R. MR signal abnormalities at 1.5 T in Alzheimer's dementia and normal aging. *Am J Roentgenol.* (1987) 149:351–6. doi: 10.2214/ajr.149.2.351
- Verhage F. *Intelligentie en Leefstijl: Onderzoek bij Nederlanders Van Twaalf tot Zevenenzeventig Jaar.* Van Gorcum (1964).
- Hughes CP, Berg L, Danziger WL, Coben LA, Martin RL. A new clinical scale for the staging of dementia. *Br J Psychiatry.* (1982) 140:566–72. doi: 10.1192/bjp.140.6.566
- Folstein MF, Folstein SE, McHugh PR. "Mini-mental state." *J Psychiatr Res.* (1975) 12:189–98. doi: 10.1016/0022-3956(75)90026-6
- Román GC, Tatemichi TK, Erkinjuntti T, Cummings JL, Masdeu JC, Garcia JH, et al. Vascular dementia: diagnostic criteria for research studies. report of the NINDS-AIREN international workshop. *Neurology.* (1993) 43:250–60. doi: 10.1212/WNL.43.2.250
- McKhann G, Drachman D, Folstein M, Katzman R, Price D, Stadlan EM. Clinical diagnosis of Alzheimer's disease: report of the NINCDS-ADRDA Work Group under the auspices of Department of Health and Human Services Task Force on Alzheimer's Disease. *Neurology.* (1984) 34:939–44. doi: 10.1212/WNL.34.7.939
- Wardlaw JM, Smith EE, Biessels GJ, Cordonnier C, Fazekas F, Frayne R, et al. Neuroimaging standards for research into small vessel disease and its contribution to ageing and neurodegeneration. *Lancet Neurol.* (2013) 12:822–38. doi: 10.1016/S1474-4422(13)70124-8
- Scheltens P, Launer LJ, Barkhof F, Weinstein HC, van Gool WA. Visual assessment of medial temporal lobe atrophy on magnetic resonance imaging: interobserver reliability. *J Neurol.* (1995) 242:557–60. doi: 10.1007/BF00868807
- Steenwijk MD, Pouwels PJW, Daams M, van Dalen JW, Caan MWA, Richard E, et al. Accurate white matter lesion segmentation by k nearest neighbor classification with tissue type priors (kNN-TTPs). *NeuroImage Clin.* (2013) 3:462–9. doi: 10.1016/j.nicl.2013.10.003
- Valverde S, Oliver A, Roura E, Pareto D, Vilanova JC, Ramió-Torrentà L, et al. Quantifying brain tissue volume in multiple sclerosis with automated lesion segmentation and filling. *NeuroImage Clin.* (2015) 9:640–7. doi: 10.1016/j.nicl.2015.10.012
- Valverde S, Oliver A, Lladó X. A white matter lesion-filling approach to improve brain tissue volume measurements. *NeuroImage Clin.* (2014) 6:86–92. doi: 10.1016/j.nicl.2014.08.016
- Van Veluw SJ, Zwanenburg JJM, Engelen-Lee J, Spliet WGM, Hendrikse J, Luijten PR, et al. *In vivo* detection of cerebral cortical microinfarcts with high-resolution 7T MRI. *J Cereb Blood Flow Metab.* (2013) 33:322–9. doi: 10.1038/jcbfm.2012.196
- Ritter F, Boskamp T, Homeyer A, Laue H, Schwier M, Link F, et al. Medical image analysis. *IEEE Pulse.* (2011) 2:60–70. doi: 10.1109/MPUL.2011.942929
- Tzourio-Mazoyer N, Landeau B, Papathanassiou D, Crivello F, Etard O, Delcroix N, et al. Automated anatomical labeling of activations in SPM using a macroscopic anatomical parcellation of the MNI MRI single-subject brain. *Neuroimage.* (2002) 15:273–89. doi: 10.1006/nimg.2001.0978
- Reijmer YD, Leemans A, Caeyenberghs K, Heringa SM, Koek HL, Biessels GJ. Disruption of cerebral networks and cognitive impairment in Alzheimer disease. *Neurology.* (2013) 80:1370–7. doi: 10.1212/WNL.0b013e31828c2ee5
- Leemans A, Jones DK. The B-matrix must be rotated when correcting for subject motion in DTI data. *Magn Reson Med.* (2009) 61:1336–49. doi: 10.1002/mrm.21890
- Veraart J, Sijbers J, Sunaert S, Leemans A, Jeurissen B. Weighted linear least squares estimation of diffusion MRI parameters: strengths, limitations, and pitfalls. *Neuroimage.* (2013) 81:335–46. doi: 10.1016/j.neuroimage.2013.05.028
- Tax CMW, Otte WM, Viergever MA, Dijkhuizen RM, Leemans A. REKINDLE: robust extraction of kurtosis INDices with linear estimation. *Magn Reson Med.* (2015) 73:794–808. doi: 10.1002/mrm.25165
- Jeurissen B, Leemans A, Jones DK, Tournier JD, Sijbers J. Probabilistic fiber tracking using the residual bootstrap with constrained spherical deconvolution. *Hum Brain Mapp.* (2011) 32:461–79. doi: 10.1002/hbm.21032
- Tax CMW, Jeurissen B, Vos SB, Viergever MA, Leemans A. Recursive calibration of the fiber response function for spherical deconvolution of diffusion MRI data. *Neuroimage.* (2014) 86:67–80. doi: 10.1016/j.neuroimage.2013.07.067
- Tournier JD, Calamante F, Connelly A. Robust determination of the fibre orientation distribution in diffusion MRI: non-negativity constrained super-resolved spherical deconvolution. *Neuroimage.* (2007) 35:1459–72. doi: 10.1016/j.neuroimage.2007.02.016
- Rubinov M, Sporns O. Complex network measures of brain connectivity: uses and interpretations. *Neuroimage.* (2010) 52:1059–69. doi: 10.1016/j.neuroimage.2009.10.003
- Faul F, Erdfelder E, Lang A-G, Buchner A. G*Power: A flexible statistical power analysis program for the social, behavioral, and biomedical

- sciences. *Behav Res Methods*. (2007) 39:175–91. doi: 10.3758/BF03193146
39. Fu R, Wang Y, Wang Y, Liu L, Zhao X, Wang DZ, et al. The development of cortical microinfarcts is associated with intracranial atherosclerosis: data from the Chinese intracranial atherosclerosis study. *J Stroke Cerebrovasc Dis*. (2015) 24:2447–54. doi: 10.1016/j.jstrokecerebrovasdis.2015.03.011
 40. Suter OC, Sunthorn T, Kraftsik R, Straubel J, Darekar P, Khalili K, et al. Cerebral hypoperfusion generates cortical watershed microinfarcts in Alzheimer disease. *Stroke*. (2002) 33:1986–92. doi: 10.1161/01.STR.0000024523.82311.77
 41. van den Brink H, Zwiers A, Switzer AR, Charlton A, McCreary CR, Goodyear BG, et al. Cortical Microinfarcts on 3T magnetic resonance imaging in cerebral amyloid angiopathy. *Stroke*. (2018) 49:1899–905. doi: 10.1161/STROKEAHA.118.020810
 42. Zhao L, Biesbroek JM, Shi L, Liu W, Kuijf HJ, Chu WWC, et al. Strategic infarct location for post-stroke cognitive impairment: a multivariate lesion-symptom mapping study. *J Cereb Blood Flow Metab*. (2017) 38:1299–311. doi: 10.1177/0271678X17728162
 43. Palesi F, De Rinaldis A, Vitali P, Castellazzi G, Casiraghi L, Germani G, et al. Specific patterns of white matter alterations help distinguishing Alzheimer's and vascular dementia. *Front Neurosci*. (2018) 12:274. doi: 10.3389/fnins.2018.00274
 44. Heringa SM, Reijmer YD, Leemans A, Koek HL, Kappelle LJ, Biessels GJ. Multiple microbleeds are related to cerebral network disruptions in patients with early Alzheimer's disease. *J Alzheimer's Dis*. (2014) 38:211–21. doi: 10.3233/JAD-130542
 45. Papma JM, de Groot M, de Koning I, Mattace-Raso FU, van der Lugt A, Vernooij MW, et al. Cerebral small vessel disease affects white matter microstructure in mild cognitive impairment. *Hum Brain Mapp*. (2014) 35:2836–51. doi: 10.1002/hbm.22370
 46. Kim HJ, Im K, Kwon H, Lee JM, Kim C, Kim YJ, et al. Clinical effect of white matter network disruption related to amyloid and small vessel disease. *Neurology*. (2015) 85:63–70. doi: 10.1212/WNL.0000000000001705
 47. Mark VW, Taub E, Perkins C, Gauthier LV, Uswatte G, Ogorek J. Poststroke cerebral peduncular atrophy correlates with a measure of corticospinal tract injury in the cerebral hemisphere. *Am J Neuroradiol*. (2008) 29:354–8. doi: 10.3174/ajnr.A0811
 48. Summers PM, Hartmann DA, Hui ES, Nie X, Deardorff RL, McKinnon ET, et al. Functional deficits induced by cortical microinfarcts. *J Cereb Blood Flow Metab*. (2017) 37:3599–614. doi: 10.1177/0271678X16685573

Conflict of Interest Statement: The authors declare that the research was conducted in the absence of any commercial or financial relationships that could be construed as a potential conflict of interest.

Copyright © 2019 Ferro, Heinen, de Brito Robalo, Kuijf, Biessels and Reijmer. This is an open-access article distributed under the terms of the Creative Commons Attribution License (CC BY). The use, distribution or reproduction in other forums is permitted, provided the original author(s) and the copyright owner(s) are credited and that the original publication in this journal is cited, in accordance with accepted academic practice. No use, distribution or reproduction is permitted which does not comply with these terms.



Basal Ganglia-Cortical Circuit Disruption in Subcortical Silent Lacunar Infarcts

Haiyan Zhu^{1†}, Wenxiao Wang^{2,3†}, He Li^{3,4†}, Kewei Chen⁵, Peng Li⁶, Xin Li^{2,3}, Junying Zhang^{3,4}, Dongfeng Wei^{3,4} and Yaojing Chen^{2,3*}

¹ Institute for Cardiovascular Disease, Dongzhimen Hospital Affiliated to Beijing University of Chinese Medicine, Beijing, China, ² State Key Laboratory of Cognitive Neuroscience and Learning, Beijing Normal University, Beijing, China, ³ BABRI Centre, Beijing Normal University, Beijing, China, ⁴ Institute of Basic Research in Clinical Medicine, China Academy of Chinese Medical Sciences, Beijing, China, ⁵ Computational Image Analysis Lab, Banner Alzheimer's Institute, Phoenix, AZ, United States, ⁶ The Laboratory Research Center of Xiyuan Hospital, China Academy of Chinese Medical Sciences, Beijing, China

OPEN ACCESS

Edited by:

Eric Jouvent,
Université Sorbonne Paris Cité, France

Reviewed by:

Maurice Giroud,
Centre Hospitalier Régional
Universitaire De Dijon, France
Michele Romoli,
University of Perugia, Italy

*Correspondence:

Yaojing Chen
luckychen1989@gmail.com

[†]These authors have contributed
equally to this work

Specialty section:

This article was submitted to
Stroke,
a section of the journal
Frontiers in Neurology

Received: 23 March 2019

Accepted: 05 June 2019

Published: 25 June 2019

Citation:

Zhu H, Wang W, Li H, Chen K, Li P,
Li X, Zhang J, Wei D and Chen Y
(2019) Basal Ganglia-Cortical Circuit
Disruption in Subcortical Silent
Lacunar Infarcts.
Front. Neurol. 10:660.
doi: 10.3389/fneur.2019.00660

To investigate the alterations of basal ganglia (BG)-cortical structural and functional connectivity induced by subcortical silent lacunar infarct (SLI), and their associations with cognitive impairment in SLI subjects. All participants were recruited from communities, including 30 subcortical SLIs and 30 age-, gender-, and education-matched healthy controls. The structural and functional connectivity of BG-cortical circuits using diffusion and resting-state functional magnetic resonance imaging data were obtained. Diffusion abnormalities of the white matter tracts connecting the BG and cortical areas were observed in SLI subjects, including the BG-lateral frontal, BG-orbital frontal, and BG-insula tracts. Multiple regions showed a reduced BG-cortical functional connectivity in SLI patients, including direct connectivities with the BG, such as the BG-limbic, BG-insula, and BG-frontal connectivities, and others that showed no direct causation with the BG, such as the insula-limbic, insula-parietal, and frontal-parietal connectivities. Coupling of structural and functional BG-cortical connectivity was observed in healthy controls but not in SLI patients. Significant correlations between structural and functional BG-cortical connectivity and cognitive performance were demonstrated in SLI patients, indicating the potential use of BG-cortical connectivities as MRI biomarkers to assess cognitive impairment. These findings suggest that subcortical SLIs can impair BG-cortical circuits, and these changes may be the pathological basis of cognitive impairment in SLI patients.

Keywords: silent lacunar infarct, basal ganglia-cortical circuit, cognition, structural connectivity, functional connectivity

HIGHLIGHTS

- White matter and functional basal ganglia-cortical circuit disruption in silent lacunar infarcts.
- Focal lesions may spread beyond the sites of initial injury to remote regions throughout specific interconnected networks even at very early and asymptomatic stage.
- Reduced structural and functional BG-cortical connectivity significantly correlated with cognitive performance.

INTRODUCTION

The prevalence of subcortical silent lacunar infarcts (SLIs) has been well-documented. SLIs mainly appear in the basal ganglia (BG) and occur in 11–25% of individuals older than age 65 without psychiatric symptoms or neurological disorders (1, 2). Due to the lack of clinical signs, the danger of SLI is often underestimated. A subcortical SLI is a significant damaging factor to cognition and a key contributor to dementia; in fact, it is considered part of the deleterious dementia pathology despite lacking clinical symptoms (3–5).

Stroke can induce injuries ranging from a single neuron or synapse (at a microscale level) or adjunct neuronal tissues or connections (at a mesoscale level) to different brain regions or even a module composed of multiple brain regions or connections among these modules (at a macroscale level) (6, 7). Through advances in both technology and analysis, brain connectome studies have provided great understanding of the structural and functional disruptions after stroke using multiple measures at various scales in the human brain (7, 8). Brain connectivity disruptions can be observed by the time a stroke is fully diagnosed, however the alterations of connectivity patterns in SLIs in the absence of clinical symptoms remains largely unknown. Recent studies support the assumption that brain functions rely on the connections within network among different brain regions. For SLI patients, an initial subtle impairment to a single brain region may gradually lead to more severe and even irreversible damages to a local or global brain network, along with advancement of the pathological process. Across the whole pathological process, low or partly functioning brain regions with SLI may tend to keep communicating or interacting with the remaining parts of the brain network and gradually spread their harmful functions to adjacent areas (9).

Previous studies have described the anatomy and function of BG-cortical circuits that contribute to human primary and advanced cognitive functions (10, 11). In particular, neuroimaging studies have proven that BG-cortical circuits play an essential role in cognitive function, including executive function and planning and working memory (12, 13). We hypothesized that the disruption in the BG-cortical network is the underlying mechanism of cognitive impairments in SLI patients with BG pathology. This current study, therefore, is designed to determine the cognitive specific BG-cortical structural and functional dysconnectivity in elderly patients with SLI around the BG.

METHODS

Participants

A total of 60 (30 SLI patients and 30 controls) right-handed, native Chinese participants were used in this study (14). The data were obtained from the Beijing Aging Brain Rejuvenation Initiative (BABRI) database. The Ethics Committee and institutional review board of Beijing Normal University's Imaging Centre for Brain Research approved this study, and all participants gave written informed consent. To be included in this study, participants had to meet the following three

additional criteria: (1) a score of at least 24 on the Mini-Mental Status Examination (MMSE); (2) no history of coronary disease, diabetes, nephritis, tumors, gastrointestinal disease or psychiatric illness; and (3) no history of psychoactive medication use. The participants' medical histories and scans were separately reviewed by two experienced neurologists. Clinical judgment of cerebral small vessel disease harmonized with STRIVE criteria (15) when using these standards in clinical practice. We defined lacunar infarcts as round or ovoid lesions of increased signal relative to white matter on T2-weighted or T2-FLAIR images or as decreased attenuation similar to cerebrospinal fluid (CSF)-filled cavities on T1-weighted images that were 3–15 mm in diameter (16). All of the patients had lacunar infarcts around the BG territory, which included the caudate nucleus ($n = 4$), putamen ($n = 12$), globus pallidus ($n = 2$), internal capsule ($n = 13$), and thalamus ($n = 7$). In present study, we recruited elderly subjects from communities, which could decrease the bias of a clinical referral study that tends to recruit patients with more severe impairments. To exclude the confounding effects of white-matter lesions, we therefore only recruited patients with pure lacunar infarcts in the present study.

Neuropsychological Testing

All participants received a battery of neuropsychological tests assessing general mental status and several cognitive domains. The general mental status was assessed with MMSE [the Mini-Mental-Status Examination-Chinese version, (17)]. The comprehensive neuropsychological battery included the following five cognition domains: (a) Memory function [the Auditory Verbal Learning Test [AVLT] (18), and the Rey-Osterrieth Complex Figure test [ROCF] (recall) (19)]; (b) Visuo-spatial [ROCF-copy (19) and the Clock-Drawing Test [CDT] (20)]; (c) Language [the Category Verbal Fluency Test [CVFT] and the Boston Naming Test [BNT] (21)]; (d) Attention [the Trail Making Test [TMT-A] (22), and the Symbol Digit Modalities Test [SDMT] (23)], and (e) Executive function [the Trail Making Test [TMT-B], (22) and the Stroop Color and Word Test C [SCWT-C] (21)].

The neuropsychological characteristics for each group are presented in **Table 1**.

Image Acquisition

The MRI data were acquired on a 3.0T Siemens Trio Tim MRI scanner at the Imaging Center for Brain Research, Beijing Normal University. Each participant laid in the supine position with the head snugly fixed by a belt and foam pads to minimize head motion. The following procedures were employed to acquire each set of MRI images. (1) T2-weighted images (TR = 5,000 ms, TE = 105 ms, slice thickness = 3 mm, flip angle = 150°, number of slices = 33) and T2-FLAIR images (TR = 9,000 ms, TE = 81 ms, slice thickness = 3 mm, flip angle = 150°, number of slices = 25) were acquired. (2) T1-weighted, sagittal 3D magnetization-prepared rapid gradient echo (MP-RAGE) sequences were acquired and covered the entire brain [176 sagittal slices, repetition time (TR) = 1,900 ms, echo time (TE) = 3.44 ms, slice thickness = 1 mm, flip angle = 9°, inversion time = 900 ms, field of view (FOV) = 256 ×

TABLE 1 | Demographic and neuropsychological measurements.

	SLI (n = 30)	HC (n = 30)	T-value (χ^2)	P-value
Age	65.96 ± 6.17	63.53 ± 6.10	1.951	0.056
Women (%)	10 (33.3%)	18 (60%)	4.286 ^a	0.069
Education	12.10 ± 3.30	10.56 ± 2.73	1.142	0.258
Hypertention (%)	9(30%)	6(20%)	0.800 ^a	0.552
Smoking				
non/past/current	24/1/5	27/0/3	1.676 ^a	0.241
GENERAL MENTAL STATUS				
MMSE	26.43 ± 2.37	27.93 ± 1.55	-2.897	0.005
Memory function				
AVLT-delay recall	3.50 ± 2.77	5.10 ± 2.00	-2.559	0.013
AVLT- total	22.03 ± 9.9	29.16 ± 7.18	-3.194	0.002
ROCF-delay recall	12.73 ± 8.53	13.20 ± 5.28	-0.255	0.799
Digit Span	11.77 ± 2.31	11.70 ± 2.12	0.116	0.908
Visuo-spatial				
ROCF-Copy	32.50 ± 5.66	33.53 ± 2.62	-0.906	0.369
CDT	24.06 ± 4.14	24.56 ± 3.78	-0.488	0.627
Language				
CVFT	40.30 ± 9.48	45.70 ± 11.53	-1.980	0.052
BNT	24.06 ± 3.52	24.13 ± 3.53	-0.073	0.942
Attention				
SDMT	30.83 ± 12.79	37.86 ± 9.55	-2.413	0.019
SCWT-B Time(s)	44.66 ± 13.37	38.50 ± 9.48	2.061	0.044
TMT-A time (s)	65.60 ± 26.51	61.80 ± 25.06	0.571	0.571
Executive function				
SCWT C-B Time(s)	40.63 ± 23.11	41.83 ± 26.43	-0.187	0.852
TMT-B time(s)	192.83 ± 71.06	188.83 ± 63.54	0.230	0.819

Values are mean ± SD or Nos. of participants (percentage). The comparisons of neuropsychological scores between the two groups were performed with independent two-sample t-tests.

^aThe p value for gender, hypertension and smoking ratio were obtained using a Chi-square test.

MMSE, Mini-Mental State Examination; AVLT, Auditory Verbal Learning Test; ROCF, Rey-Osterrieth Complex Figure Test; TMT, Trail Making Test; SDMT, Symbol Digit Modalities Test; SCWT, Stroop Color and Word Test; CDT, Clock-Drawing Test; CVFT, Category Verbal Fluency Test; BNT, Boston Naming Test.

256 mm², acquisition matrix = 256 × 256]. (3) Two sets of diffusion tensor imaging (DTI) data scans were acquired for every subject and then averaged during the data processing. DTI images covering the whole brain were acquired using a single-shot, twice-refocused, diffusion-weighted echo planar imaging sequence [TR = 9,500 ms; TE = 92 ms; 30 diffusion-weighted directions with a b-value of 1,000 s/mm², and a single image with a b-value of 0 s/mm²; slice thickness = 2 mm; no inter-slice gap; 70 axial slices; matrix size = 128 × 128; FOV = 256 × 256 mm²; voxel size = 2 × 2 × 2 mm³]. (4) During the single-run resting acquisition, subjects were instructed to stay awake, relax with their eyes closed and remain as motionless as possible. Resting functional images were collected using an echo-planar imaging sequence (TE = 30 ms, TR = 2,000 ms, flip angle = 90°, 33 axial slices, slice thickness = 3.5 mm, acquisition matrix = 64 × 64, FOV = 200 × 200 mm²). The resting acquisition lasted for 8 min, and 240 image volumes were obtained.

Data Preprocessing

The DTI data preprocessing and fiber tracking were performed using DTI Studio (<http://cmrm.med.jhmi.edu>). The preprocessing comprised the following steps: eddy current and motion artifact correction of DTI data, estimation of diffusion tensor, fractional anisotropy (FA) calculation, and diffusion tensor tractography.

Functional data were preprocessed and statistically analyzed using SPM8 package (<http://www.fil.ion.ucl.ac.uk/spm/software/>). Preprocessing procedures included slice timing, within-subject interscan realignment to correct possible movement, spatial normalization to a standard brain template in the Montreal Neurological Institute coordinate space, resampling to 3 × 3 × 3 mm³, and smoothing with an 8 mm full-width half-maximum Gaussian kernel. Finally, the functional data were high-pass filtered with a cutoff frequency of 0.01 Hz, whereas resting functional imaging data were processed with linear detrending and 0.01–0.08 Hz bandpass filtering.

Structural Connectivity Analyses

Fiber tracking was performed using the Fiber Assignment by Continuous Tracking algorithm (24). The tracking procedure was stopped with an FA threshold of 0.2 and a track turning angle threshold of 45°. The fibers of interest were selected by designating manually defined ROIs and using the three logical operators AND, OR, and NOT. Our analysis of white matter structure was focused on tracts connecting the BG and cortical regions. As a result, the individual cerebrum in the native space were remerged into bilateral BG and 22 cortical and subcortical regions according to an automated anatomical labeling atlas (11 regions for each hemisphere; **Table S1**). For each hemisphere, we studied the structural connections between the BG and each of 11 ipsilateral regions. The average FA value for each fiber bundle of interest was calculated.

Functional Connectivity Analysis

Most previous studies showed that patients with SLI in the BG, although clinically normal, already exhibited cognitive decline. The cognitive impairment resulting from SLI is a complex process; we mainly focused on the changes in the organization of the cognitive specific BG-cortical network from a previous meta-analysis (25). The regions of interest (ROI) included 20 regions as detailed in **Table S2**, such as the caudate head (Cau.head), the thalamus (Tha), the red nucleus (RN), the insula (INS), the cingulate gyrus (CG), the precentral gyrus (PreCG), the inferior frontal gyrus (IFG), the superior parietal lobule (SPL), the inferior parietal lobule (IPL), and Brodmann areas 6, 9, and 46, which are portions of the middle frontal gyrus (MFG.BA6, MFG.BA9, and MFG.BA46). For each subject, the time series in each ROI was obtained by averaging the functional MRI time series across all voxels over a given ROI. To regress out the nuisance covariates, time series were corrected for patient movement, the global mean signal, the white matter signal and the cerebrospinal fluid signal. The Pearson's correlation coefficient of the ROI signal time course in the brain was computed. Specifically, we defined the functional connectivity between two regions as the weight of the network edges. Thus,

for each participant, we constructed the weighted BG-cortical network that was represented by a symmetric 20×20 matrix.

Statistical Analysis

Demographic and Neuropsychological Measurements

Between-group comparisons were performed using a χ^2 or two-sample independent *t*-test, depending on the variable type and distribution.

Structural Connectivity

For the BG-cortical tract alterations, we performed a two-sample *t*-test to compare the FA value between groups for each tracked fiber.

Functional Connectivity

Prior to group comparisons, the correlation coefficients were converted to *z*-scores using the Fisher *r*-to-*z* transformation. To test the between-group differences, two-sample *t*-tests were performed on each transformed *z*-value. For the multiple nodal efficiencies, we applied the false discovery rate (FDR) procedure to correct the multiple comparisons at a *q*-value of 0.05.

Finally, we investigated the relationship between structural and functional BG-cortical connectivity and between BG-cortical connectivity and cognitive performance for SLI and control groups, respectively. Of note, the correlation analyses were performed only among the structural connectivity, functional connectivity, and cognitive scores.

RESULTS

Demographic and Clinical Data

There were no significant differences in age, years of education, smoking habits, or medical history of hypertension between SLI and healthy groups. In the SLI patients, cognitive function in the domains of general mental status, memory, and attention were significantly worse than controls (Table 1).

Structural BG-Cortical Connectivity

Multiple white matter tracts connecting nodes between BG and cortical regions showed significantly lower FA values in SLI patients, especially for the connections between the BG and the bilateral lateral frontal area, left orbital frontal cortex, and right insula (Figure 1).

Functional BG-Cortical Network Connectivity

We investigated cognitive specific BG-cortical network connectivity between SLI patients and healthy controls. As shown in Figure 2A, BG-cortical intrinsic FC was decreased in SLI patients compared to controls. The majority of BG-cortical network FCs were significantly lower in SLI patients with BG lesions, including decreases within BG areas (Cau.head.L-RN.R, Cau.head.L-Tha.L, Cau.head.R-Tha.L), between the BG and limbic regions (Tha.L-CG.L, Tha.R-CG.L), between the BG and insula (RN.R-INS.L), and between the BG and frontal regions (RN.R-PreCG.L, RN.R-MFG.BA9.R1,

RN.R-MFG.BA9.R02, RN.R-MFG.BA46.R), and connectivity showed no direct causation with the BG, including the insula and limbic region (INS.L-CG.L), between the insula and parietal region (INS.L-IPL.R), between the frontal and parietal regions (MFG.BA9.R2-IPL.L, MFG.BA9.R2-IPL.R), within the insula (INS.L-INS.R), and within the frontal regions (MFG.BA9.R1-IFG.L; Figures 2B,C, FDR-corrected, $q < 0.05$).

Relationship Between Structural and Functional BG-Cortical Connectivity

We found significant positive correlations between BG-cortical white matter integrity and functional connectivity in controls, but not in the SLI patients (Table 2). The significant correlation results can be corrected for multiple comparisons and therefore should be regarded as exploratory in nature.

Correlation With Cognitive Function

The structural and functional BG-cortical connectivity measures were correlated with the performance on neuropsychologic tests. For structural connectivity, correlation analyses indicated that the FA value of the BG-Insul.R was positively correlated with the symbol digit modalities test (SDMT) performance and that the FA in the BG-Lateral Frontal.L was significant associated with performance on the auditory verbal learning test (AVLT)-delay recall, the AVLT-total, and the Stroop color and word test part B (SCWT-B) in the SLI patients but not in the controls (Table 3). In addition, higher functional BG-cortical connectivity was significantly correlated with better test performance on the MMSE, the AVLT-delay recall, the AVLT-total, the SCWT-B, and the SDMT in both SLI patients and controls.

DISCUSSION

The focus of this study was to evaluate small lesion-induced changes in structural and functional connectivity and network topology in the BG-cortical system in patients with subcortical SLI. SLI disrupted the structural integrity of the BG-cortical tracts, including the BG-frontal areas and the BG-insula integrity. We found that SLI leads to damage of direct functional connectivity with BG regions, such as between the BG and frontal, limbic regions and insula connectivity, and remote connectivity, such as to the frontal and parietal areas. Moreover, structural and functional BG-cortical connectivity were correlated in controls but not in SLI patients. We also found a significant association between structural and functional BG-cortical connectivity and several cognitive scores, including performance on the MMSE, the AVLT-delay recall, the AVLT-total, the SCWT-B, and SDMT. Therefore, studying the BG in SLI patients provides an opportunity to investigate the impact of information exchange in the BG-cortical network on cognitive decline.

BG, as an important structural region of the brain, is mainly involved in motor control and cognitive function (26, 27). However, due to the complexity of the molecular and anatomical structure of the BG, neurons in the BG region are more vulnerable to ischemia and toxicity injury (28). In particular, our previous study showed gray matter volume loss in insula,

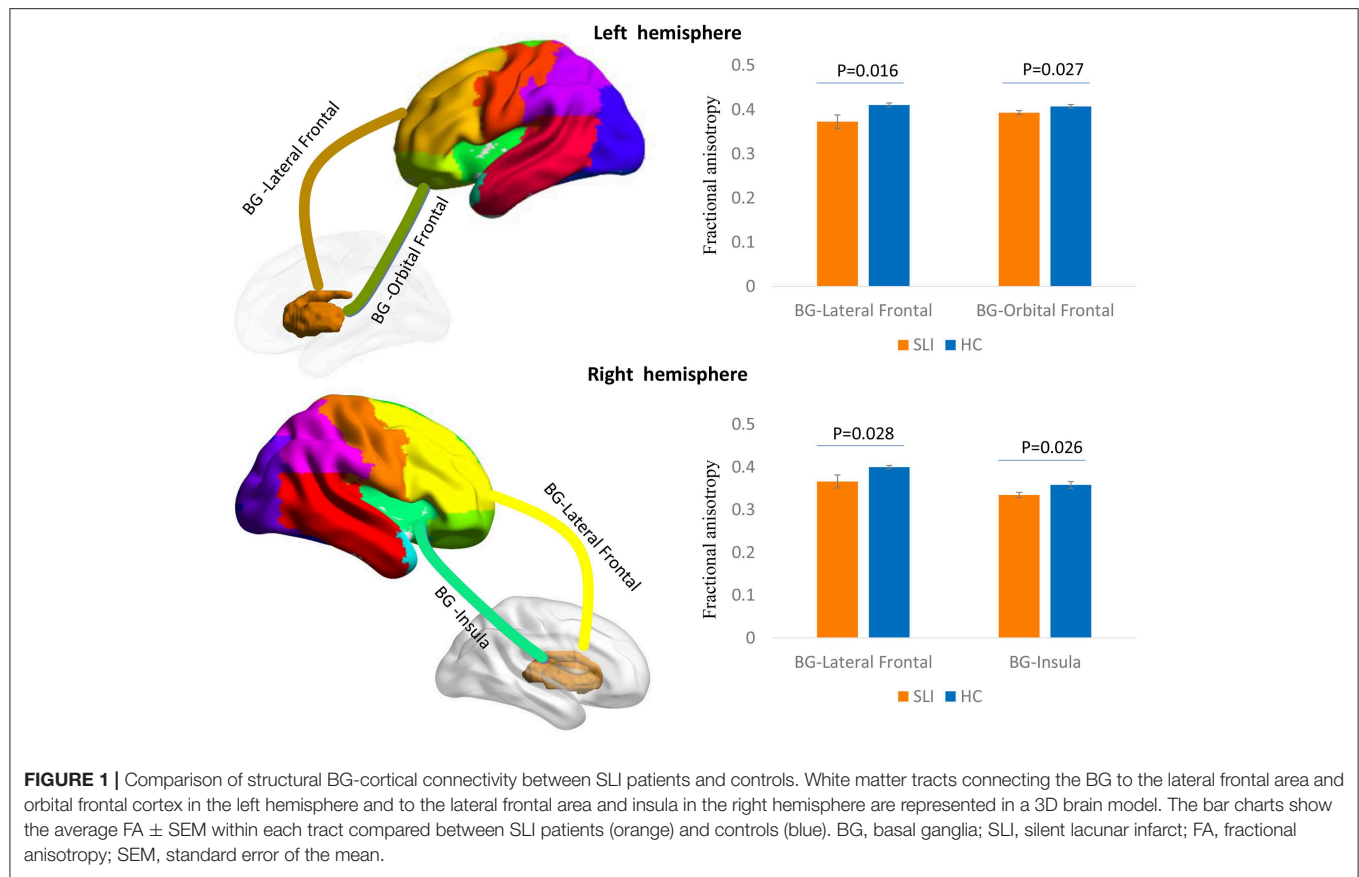


FIGURE 1 | Comparison of structural BG-cortical connectivity between SLI patients and controls. White matter tracts connecting the BG to the lateral frontal area and orbital frontal cortex in the left hemisphere and to the lateral frontal area and insula in the right hemisphere are represented in a 3D brain model. The bar charts show the average FA \pm SEM within each tract compared between SLI patients (orange) and controls (blue). BG, basal ganglia; SLI, silent lacunar infarct; FA, fractional anisotropy; SEM, standard error of the mean.

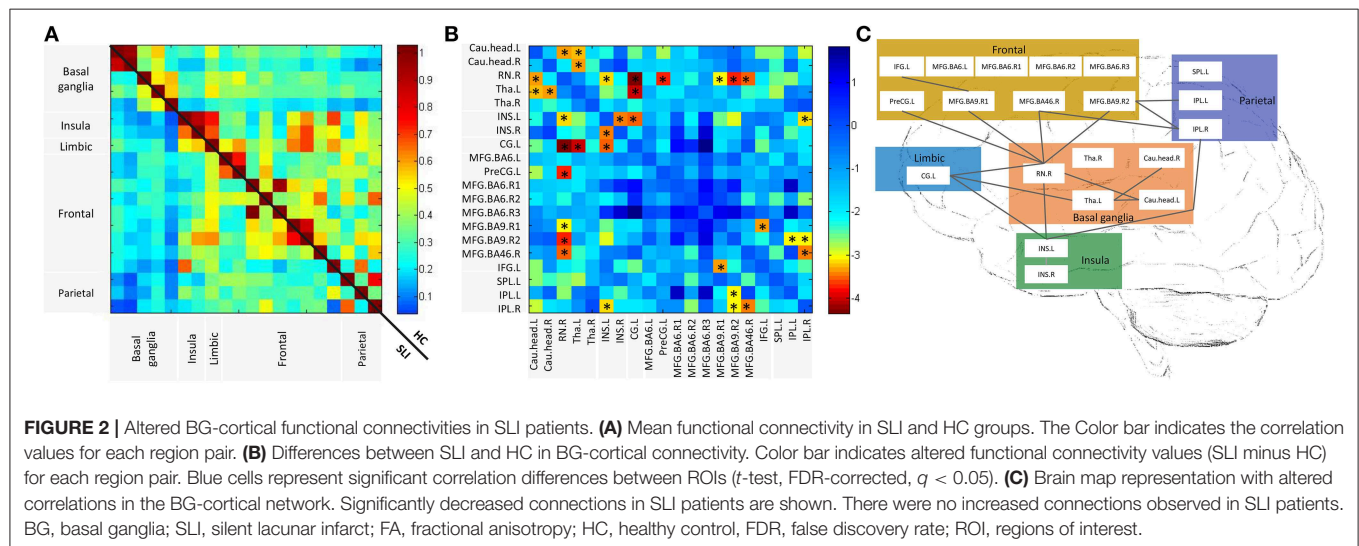


FIGURE 2 | Altered BG-cortical functional connectivities in SLI patients. **(A)** Mean functional connectivity in SLI and HC groups. The Color bar indicates the correlation values for each region pair. **(B)** Differences between SLI and HC in BG-cortical connectivity. Color bar indicates altered functional connectivity values (SLI minus HC) for each region pair. Blue cells represent significant correlation differences between ROIs (t -test, FDR-corrected, $q < 0.05$). **(C)** Brain map representation with altered correlations in the BG-cortical network. Significantly decreased connections in SLI patients are shown. There were no increased connections observed in SLI patients. BG, basal ganglia; SLI, silent lacunar infarct; FA, fractional anisotropy; HC, healthy control, FDR, false discovery rate; ROI, regions of interest.

anterior cingulate cortex, caudate and superior temporal pole and connectivity reduced in SLI patients (14). All these evidence provide a solid theoretical basis for this study on SLI patients located in the BG region.

Patients with lacunar infarcts have more severe white matter changes than patients with non-lacunar infarcts among patients with ischemic stroke (29), which is associated with executive

dysfunction. Our previous studies have reported that SLIs in the BG region led to local and remote white matter integrity damages (30) and topological alterations of the whole brain white matter network (31), suggesting that BG-frontal and BG-insula integrity are influenced by SLIs. Augustine and colleagues have shown that the BG in primates and humans has efferent and afferent fibers with the insula and prefrontal

TABLE 2 | Structural and functional BG-cortical connectivity correlations.

			Functional connectivity					
			Cau.head.L- Tha.L	Cau.head.R- Tha.L	RN.R- MFG.BA9.R1	INS.L-INS.R	MFG.BA9.R1- IFG.L	MFG.BA9.R2- IPL.R
White matter integrity	BG-Lateral Frontal.L	SLI	$r = -0.17$ $p = 0.396$	$r = 0.143$ $p = 0.485$	$r = 0.069$ $p = 0.736$	$r = -0.34$ $p = 0.094$	$r = -0.095$ $p = 0.646$	$r = 0.178$ $p = 0.385$
		HC	$r = 0.058$ $p = 0.763$	$r = 0.086$ $p = 0.653$	$r = 0.098$ $p = 0.607$	$r = 0.440$ $p = 0.014$	$r = 0.390$ $p = 0.033$	$r = 0.406$ $p = 0.026$
	BG-Lateral Frontal.R	SLI	$r = -0.12$ $p = 0.573$	$r = 0.067$ $p = 0.744$	$r = -0.034$ $p = 0.869$	$r = -0.106$ $p = 0.607$	$r = 0.011$ $p = 0.958$	$r = 0.127$ $p = 0.535$
		HC	$r = -0.197$ $p = 0.297$	$r = -0.070$ $p = 0.714$	$r = -0.081$ $p = 0.670$	$r = 0.386$ $p = 0.034$	$r = 0.165$ $p = 0.382$	$r = 0.021$ $p = 0.911$
	BG-Insul.R	SLI	$r = -0.042$ $p = 0.835$	$r = -0.182$ $p = 0.363$	$r = -0.227$ $p = 0.255$	$r = 0.189$ $p = 0.343$	$r = -0.172$ $p = 0.391$	$r = -0.212$ $p = 0.289$
		HC	$r = 0.374$ $p = 0.04$	$r = 0.441$ $p = 0.014$	$r = 0.383$ $p = 0.037$	$r = 0.0143$ $p = 0.450$	$r = -0.225$ $p = 0.232$	$r = 0.093$ $p = 0.626$

Cau.head, Caudate head; Tha, Thalamus (medial dorsal nucleus); RN, Red nucleus; TMT, Trail Making Test; MFG, Middle frontal gyrus; INS, Insula; IFG, Inferior frontal gyrus; IPL, Inferior parietal lobule; L, Left hemisphere; R, Right hemisphere; BA, Brodmann area. Bold values indicate Functional connectivity.

cortex (32). Additionally, the prefrontal areas consist of a number of modules, which seem to provide multiple subloops of the BG-thalamocortical connections in non-human primates (33, 34). Several investigators have demonstrated that BG lesions impair several cognitive deficits associated with prefrontal activity (35, 36).

We also assessed the intrinsic connectivity within the cognitive specific BG-cortical network. In SLI, a majority of connectivities including the BG-limbic, BG-insula, BG-frontal, insula-limbic, insula-parietal, frontal-parietal connectivities, and the connectivity between BG areas showed disconnection. By applying a longitudinal and lesion-restricted approach, a recent study observed secondary neurodegeneration in remote cortices after a subcortical stroke (37). Considering the network perspective, the BG could modulate advanced cognitive function through cognitive-related functional networks (14). Furthermore, surgery that targets the BG-thalamic cortical loop can restore normal cortical activity associated with behavioral and mood disorders (38, 39). Beneficial attempts to treat psychiatric disease by modulating BG-cortical loops suggested that neurological and psychiatric diseases share essential neurobiological mechanisms. This theory can explain why damage to the BG and related nuclei always affects those brain regions that belonging to the same non-motor BG-cortical loops. Our findings also supported the notion that subcortical SLI not only affected adjacent regions but also the regions in BG-cortical circuits.

Significant correlations between structural and functional BG-cortical connectivity in controls, supporting the notion “functional connectivity reflects anatomical connectivity.” The decoupling of structural and functional connectivity were observed in SLI patients may due to several pathological changes. Decreased perfusion in penetrating arteries may lead to an SLI (40). Feng et al. have shown that SLIs tend to occur in the radiation crown and the BG (41). In the early stages of lacunar infarction, acute ischemic changes can occur in neurons. Then,

an influx of macrophages occurs in the subacute stages, followed by neuronal death and glial cell proliferation. In addition, SLI also may have distant effects, such as Wallerian, retrograde or post-synaptic degeneration (42). The pathological damage caused by the combination of neuronal death, gliosis and degeneration are not synchronized and not limited to the lesion itself. Structural and functional connectivity was decoupled in SLI patients.

A recent study in a stroke cohort showed that advanced cognitive functions such as visual and verbal memory deficits are better predicted by functional connectivity than by the lesion location, and primary functions such as visual and motor deficits are better predicted by the lesion location than by functional connectivity (43). This finding may support the notion that stroke is a disease of brain connectivity, which is being supported by an increasing number of studies (44–46). There was a significant correlation between BG-cortical connectivity and general mental status, memory, and attention performance. Robust evidence has shown that the existence of BG-cortical loops achieves connectivity of the BG to the cerebral cortex and can be subdivided into motor, associative, and limbic domains (47). Therefore, the dysfunction of these BG-based circuits can lead to movement disorders, cognitive impairment, and emotional disorders. It is worth noting that the BG and its dopaminergic projections participate in some cognitive activities. A BG injury could potentially induce changes in these circuits and gradually result in cognitive impairment.

Despite the interesting findings in the present study, a few limitations need to be addressed. First, a longitudinal dataset is highly desired to verify the current results. Next, the heterogeneity of lesion location may result in different cognitive impairment and functional disconnection patterns. Therefore, stratification of patients according to lesion location should be considered for future work.

In summary, this study demonstrated a structural and functional disconnectivity of the BG-cortical network in the elderly with silent small lesions around the BG. Focal lesions

TABLE 3 | Correlation between BG-cortical connectivity and cognitive function.

			Cognitive function				
			MMSE	AVLT-delay recall	AVLT-total	SDMT	SCWT-B Time
White matter integrity	BG-Lateral Frontal.L	SLI	$r = -0.27$ $p = 0.18$	$r = -0.47$ $p = 0.01$	$r = -0.04$ $p = 0.03$	$r = -0.33$ $p = 0.10$	$r = 0.45$ $p = 0.02$
		HC	$r = 0.08$ $p = 0.67$	$r = 0.32$ $p = 0.08$	$r = 0.12$ $p = 0.53$	$r = 0.09$ $p = 0.64$	$r = -0.21$ $p = 0.27$
	BG-Insul.R	SLI	$r = 0.16$ $p = 0.44$	$r = 0.19$ $p = 0.35$	$r = 0.19$ $p = 0.33$	$r = 0.40$ $p = 0.04$	$r = -0.15$ $p = 0.45$
		HC	$r = -0.28$ $p = 0.14$	$r = 0.21$ $p = 0.27$	$r = 0.12$ $p = 0.52$	$r = 0.33$ $p = 0.08$	$r = -0.18$ $p = 0.33$
Functional connectivity	Cau.head.L-RN.R	SLI	$r = 0.22$ $p = 0.25$	$r = 0.31$ $p = 0.10$	$r = 0.29$ $p = 0.12$	$r = 0.06$ $p = 0.76$	$r = -0.09$ $p = 0.63$
		HC	$r = 0.38$ $p = 0.03$	$r = 0.35$ $p = 0.06$	$r = 0.26$ $p = 0.17$	$r = 0.05$ $p = 0.78$	$r = -0.17$ $p = 0.36$
	Cau.head.L-Tha.L	SLI	$r = 0.23$ $p = 0.22$	$r = 0.23$ $p = 0.23$	$r = 0.27$ $p = 0.15$	$r = 0.08$ $p = 0.69$	$r = -0.27$ $p = 0.16$
		HC	$r = 0.62$ $p < 0.0001$	$r = 0.14$ $p = 0.45$	$r = 0.17$ $p = 0.36$	$r = 0.01$ $p = 0.94$	$r = -0.10$ $p = 0.58$
	Cau.head.R-Tha.L	SLI	$r = 0.08$ $p = 0.68$	$r = -0.05$ $p = 0.81$	$r = -0.04$ $p = 0.82$	$r = -0.23$ $p = 0.23$	$r = 0.10$ $p = 0.61$
		HC	$r = 0.52$ $p = 0.002$	$r = 0.03$ $p = 0.87$	$r = -0.02$ $p = 0.93$	$r = -0.04$ $p = 0.85$	$r = -0.13$ $p = 0.50$
	RN.R-CG.L	SLI	$r = 0.35$ $p = 0.06$	$r = -0.05$ $p = 0.78$	$r = 0.03$ $p = 0.87$	$r = -0.05$ $p = 0.78$	$r = -0.01$ $p = 0.97$
		HC	$r = 0.51$ $p = 0.003$	$r = 0.26$ $p = 0.17$	$r = 0.12$ $p = 0.51$	$r = -0.06$ $p = 0.74$	$r = -0.002$ $p = 1.0$
	RN.R-PreCG.L	SLI	$r = 0.17$ $p = 0.38$	$r = -0.02$ $p = 0.91$	$r = -0.05$ $p = 0.79$	$r = 0.11$ $p = 0.57$	$r = -0.08$ $p = 0.68$
		HC	$r = 0.38$ $p = 0.04$	$r = 0.02$ $p = 0.92$	$r = 0.03$ $p = 0.89$	$r = 0.02$ $p = 0.92$	$r = -0.29$ $p = 0.13$
	RN.R-MFG.BA46.R	SLI	$r = 0.43$ $p = 0.02$	$r = 0.18$ $p = 0.35$	$r = 0.07$ $p = 0.69$	$r = 0.12$ $p = 0.51$	$r = 0.04$ $p = 0.85$
		HC	$r = 0.26$ $p = 0.16$	$r = 0.12$ $p = 0.53$	$r = -0.08$ $p = 0.69$	$r = 0.06$ $p = 0.75$	$r = -0.33$ $p = 0.08$
	Tha.L-CG.L	SLI	$r = 0.12$ $p = 0.53$	$r = 0.10$ $p = 0.59$	$r = 0.15$ $p = 0.43$	$r = 0.02$ $p = 0.91$	$r = -0.25$ $p = 0.18$
		HC	$r = 0.42$ $p = 0.02$	$r = 0.03$ $p = 0.89$	$r = 0.19$ $p = 0.33$	$r = 0.13$ $p = 0.49$	$r = -0.18$ $p = 0.33$
	INS.L- INS.R	SLI	$r = 0.35$ $p = 0.06$	$r = 0.31$ $p = 0.10$	$r = 0.30$ $p = 0.11$	$r = 0.31$ $p = 0.09$	$r = -0.37$ $p = 0.04$
		HC	$r = 0.1$ $p = 0.33$	$r = 0.38$ $p = 0.04$	$r = 0.25$ $p = 0.19$	$r = 0.36$ $p = 0.05$	$r = -0.401$ $p = 0.03$
	INS.L-CG.L	SLI	$r = 0.29$ $p = 0.12$	$r = 0.53$ $p = 0.002$	$r = 0.58$ $p = 0.0008$	$r = 0.27$ $p = 0.15$	$r = -0.41$ $p = 0.02$
		HC	$r = 0.13$ $p = 0.48$	$r = 0.03$ $p = 0.88$	$r = 0.12$ $p = 0.53$	$r = 0.08$ $p = 0.66$	$r = -0.16$ $p = 0.41$
	INS.L-IPL.R	SLI	$r = 0.32$ $p = 0.09$	$r = 0.33$ $p = 0.08$	$r = 0.35$ $p = 0.06$	$r = 0.41$ $p = 0.02$	$r = -0.30$ $p = 0.11$
		HC	$r = 0.24$ $p = 0.20$	$r = -0.07$ $p = 0.72$	$r = 0.01$ $p = 0.94$	$r = 0.03$ $p = 0.89$	$r = -0.19$ $p = 0.31$
	MFG.BA9.R2-IPL.L	SLI	$r = -0.06$ $p = 0.75$	$r = 0.02$ $p = 0.92$	$r = 0.04$ $p = 0.84$	$r = 0.10$ $p = 0.60$	$r = -0.25$ $p = 0.17$
		HC	$r = -0.003$ $p = 0.98$	$r = 0.02$ $p = 0.91$	$r = 0.10$ $p = 0.61$	$r = 0.34$ $p = 0.07$	$r = -0.43$ $p = 0.02$

MMSE, Mini-Mental State Examination; AVLT, Auditory Verbal Learning Test; SDMT, Symbol Digit Modalities Test; SCWT, Stroop Color and Word Test; Cau.head, Caudate head; Tha, Thalamus (medial dorsal nucleus); RN, Red nucleus; TMT, Trail Making Test; MFG, Middle frontal gyrus; INS, Insula; IFG, Inferior frontal gyrus; IPL, Inferior parietal lobule; L, Left hemisphere; R, Right hemisphere; BA, Brodmann area. Bold values indicate Functional connectivity.

can spread beyond the sites of initial injury to remote regions throughout specific interconnected networks. Both structural and functional BG-cortical connectivity strength were predictive of cognitive dysfunction. Taken together, the study opens up a new avenue for investigating lesion-induced network dysfunction, highlighting the importance of early damage to the structural and functional connectivity as a potential manifestation of preclinical small vessel disease.

DATA AVAILABILITY

All datasets generated for this study are included in the manuscript and/or the **Supplementary Files**.

ETHICS STATEMENT

This study was carried out in accordance with the recommendations of the institutional review board of BNU imaging center for brain research, national key laboratory of cognitive neuroscience and learning, BNU with written informed consent from all subjects. All subjects gave written informed consent in accordance with the Declaration of Helsinki. The protocol was approved by the institutional review board of BNU imaging center for brain research, national key laboratory of cognitive neuroscience and learning, BNU.

AUTHOR CONTRIBUTIONS

HZ, WW, and HL designed the entire study and contributed to the study equally. HZ also analyzed the cognitive data.

WW and HL analyzed the neuroimage data and wrote the main part of the manuscript. KC guided the data analysis and participated in the revision of the article. PL and XL participated in data analysis and discussion. JZ and DW wrote part of the article. YC participated in the coordination of the study and reviewed the manuscript. All authors read and approved the final manuscript.

FUNDING

This work was supported by National Science Fund for Distinguished Young Scholars (grant number 81625025), Funds for International Cooperation and Exchange of the National Natural Science Foundation of China (grant number 81820108034), National Key Research and Development Project of China (grant number 2018YFC1315200), State Key Program of National Natural Science of China (grant number 81430100), National Natural Science Foundation of China (grant number 31700997), and the Fundamental Research Funds for the Central Universities (grant number 2017XTCX04).

ACKNOWLEDGMENTS

We thank all the volunteers for their participation in the study.

SUPPLEMENTARY MATERIAL

The Supplementary Material for this article can be found online at: <https://www.frontiersin.org/articles/10.3389/fneur.2019.00660/full#supplementary-material>

REFERENCES

- Jellinger KA, Attems J. Incidence of cerebrovascular lesions in Alzheimer's disease: a postmortem study. *Acta Neuropathol.* (2003) 105:14–7. doi: 10.1007/s00401-002-0634-5
- Roman GC, Erkinjuntti T, Wallin A, Pantoni L, Chui HC. Subcortical ischaemic vascular dementia. *Lancet Neurol.* (2002) 1:426–36. doi: 10.1016/S1474-4422(02)00190-4
- Gold G, Kovari E, Herrmann FR, Canuto A, Hof PR, Michel JP, et al. Cognitive consequences of thalamic, basal ganglia, and deep white matter lacunes in brain aging and dementia. *Stroke.* (2005) 36:1184–8. doi: 10.1161/01.STR.0000166052.89772.b5
- Jellinger KA. The pathology of “vascular dementia”: a critical update. *J Alzheimers Dis.* (2008) 14:107–23. doi: 10.3233/JAD-2008-14110
- Schneider JA, Boyle PA, Arvanitakis Z, Bienias JL, Bennett DA. Subcortical infarcts, Alzheimer's disease pathology, and memory function in older persons. *Ann Neurol.* (2007) 62:59–66. doi: 10.1002/ana.21142
- Grefkes C, Fink GR. Reorganization of cerebral networks after stroke: new insights from neuroimaging with connectivity approaches. *Brain.* (2011) 134(Pt 5):1264–76. doi: 10.1093/brain/awr033
- Silasi G, Murphy TH. Stroke and the connectome: how connectivity guides therapeutic intervention. *Neuron.* (2014) 83:1354–68. doi: 10.1016/j.neuron.2014.08.052
- Grefkes C, Fink GR. Connectivity-based approaches in stroke and recovery of function. *Lancet Neurol.* (2014) 13:206–16. doi: 10.1016/S1474-4422(13)70264-3
- Kucyeski A, Kamel H, Navi BB, Raj A, Iadecola C. Predicting future brain tissue loss from white matter connectivity disruption in ischemic stroke. *Stroke.* (2014) 45:717–22. doi: 10.1161/STROKEAHA.113.003645
- McNab F, Klingberg T. Prefrontal cortex and basal ganglia control access to working memory. *Nat Neurosci.* (2008) 11:103–7. doi: 10.1038/nn2024
- Smith Y, Bevan MD, Shink E, Bolam JP. Microcircuitry of the direct and indirect pathways of the basal ganglia. *Neuroscience.* (1998) 86:353–87.
- Bostan AC, Dum RP, Strick PL. Cerebellar networks with the cerebral cortex and basal ganglia. *Trends Cogn Sci.* (2013) 17:241–54. doi: 10.1016/j.tics.2013.03.003
- Voytek B, Knight RT. Prefrontal cortex and basal ganglia contributions to visual working memory. *Proc Natl Acad Sci USA.* (2010) 107:18167–72. doi: 10.1073/pnas.1007277107
- Chen Y, Wang J, Zhang J, Zhang T, Chen K, Fleisher A, et al. Aberrant functional networks connectivity and structural atrophy in silent lacunar infarcts: relationship with cognitive impairments. *J Alzheimers Dis.* (2014) 42:841–50. doi: 10.3233/JAD-140948
- Wardlaw JM, Smith EE, Biessels GJ, Cordonnier C, Fazekas F, Frayne R, et al. Neuroimaging standards for research into small vessel disease and its contribution to ageing and neurodegeneration. *Lancet Neurol.* (2013) 12:822–38. doi: 10.1016/S1474-4422(13)70124-8
- Fisher CM. Lacunes: small, deep cerebral infarcts. 1965. *Neurology.* (1998) 50:841 and 811 pages following. doi: 10.1212/WNL.50.4.841-a
- Zhang MY, Katzman R, Salmon D, Jin H, Cai GJ, Wang ZY, et al. The prevalence of dementia and Alzheimer's disease in Shanghai, China: impact of age, gender, and education. *Ann Neurol.* (1990) 27:428–37. doi: 10.1002/ana.410270412
- Rosenberg SJ, Ryan JJ, Prifitera A. Rey Auditory-Verbal Learning Test performance of patients with and without memory impairment. *J Clin*

- Psychol.* (1984) 40:785–7. doi: 10.1002/1097-4679(198405)40:3<785::AID-JCLP2270400325>3.0.CO;2-4
19. Rey A. L'examen psychologique dans le cas d'encephalopathie traumatique. *Arch Psychol.* (1941) 28:215–85.
 20. Rouleau I, Salmon DP, Butters N, Kennedy C, McGuire K. Quantitative and qualitative analyses of clock drawings in Alzheimer's and Huntington's disease. *Brain Cognit.* (1992) 18:70–87. doi: 10.1016/0278-2626(92)90112-Y
 21. Guo QH, Hong ZN, Chuan-Zhen LU, Zhou Y, Jun-Chao LU. Application of Stroop color-word test on Chinese elderly patients with mild cognitive impairment and mild Alzheimer's dementia. *Chinese J Neuromed.* (2005) 4:701–4.
 22. Reitan RM. Validity of the trail making test as an indicator of organic brain damage. *Percept Motor Skills.* (1958) 8:271–6. doi: 10.2466/pms.1958.8.3.271
 23. Sheridan LK, Fitzgerald HE, Adams KM, Nigg JT, Martel MM, Puttler LI, et al. Normative Symbol Digit Modalities Test performance in a community-based sample. *Arch Clin Neuropsychol.* (2006) 21:23–8. doi: 10.1016/j.acn.2005.07.003
 24. Mori S, Crain BJ, Chacko VP, van Zijl PC. Three-dimensional tracking of axonal projections in the brain by magnetic resonance imaging. *Ann Neurol.* (1999) 45:265–9. doi: 10.1002/1531-8249(199902)45:2<265::AID-ANA21>3.0.CO;2-3
 25. Robinson JL, Laird AR, Glahn DC, Blangero J, Sanghera MK, Pessoa L, et al. The functional connectivity of the human caudate: an application of meta-analytic connectivity modeling with behavioral filtering. *Neuroimage.* (2012) 60:117–29. doi: 10.1016/j.neuroimage.2011.12.010
 26. Calabresi P, Picconi B, Tozzi A, Ghiglieri V, Di Filippo M. Direct and indirect pathways of basal ganglia: a critical reappraisal. *Nat Neurosci.* (2014) 17:1022–30. doi: 10.1038/nn.3743
 27. Rosin B, Nevet A, Elias S, Rivlin-Etzion M, Israel Z, Bergman H. Physiology and pathophysiology of the basal ganglia-thalamo-cortical networks. *Parkinsonism Relat Disord.* (2007) 13(Suppl. 3):S437–9. doi: 10.1016/S1353-8020(08)70045-2
 28. Tambasco N, Romoli M, Calabresi P. Selective basal ganglia vulnerability to energy deprivation: experimental and clinical evidences. *Prog Neurobiol.* (2018) 169:55–75. doi: 10.1016/j.pneurobio.2018.07.003
 29. Mantyla R, Aronen HJ, Salonen O, Pohjasvaara T, Korpelainen M, Peltonen T, et al. Magnetic resonance imaging white matter hyperintensities and mechanism of ischemic stroke. *Stroke.* (1999) 30:2053–8. doi: 10.1161/01.STR.30.10.2053
 30. Chen Y, Wang A, Tang J, Wei D, Li P, Chen K, et al. Association of white matter integrity and cognitive functions in patients with subcortical silent lacunar infarcts. *Stroke.* (2015) 46:1123–6. doi: 10.1161/STROKEAHA.115.008998
 31. Tang J, Zhong S, Chen Y, Chen K, Zhang J, Gong G, et al. Aberrant white matter networks mediate cognitive impairment in patients with silent lacunar infarcts in basal ganglia territory. *J Cereb Blood Flow Metab.* (2015) 35:1426–34. doi: 10.1038/jcbfm.2015.67
 32. Augustine JR. Circuitry and functional aspects of the insular lobe in primates including humans. *Brain Res Rev.* (1996) 22:229–44. doi: 10.1016/S0165-0173(96)00011-2
 33. Groenewegen HJ, Wright CI, Uylings HB. The anatomical relationships of the prefrontal cortex with limbic structures and the basal ganglia. *J Psychopharmacol.* (1997) 11:99–106. doi: 10.1177/026988119701100202
 34. Nakano K. Neural circuits and topographic organization of the basal ganglia and related regions. *Brain Dev.* (2000) 22(Suppl. 1):S5–16. doi: 10.1016/S0387-7604(00)00139-X
 35. Damasio AR, Damasio H, Chui HC. Neglect following damage to frontal lobe or basal ganglia. *Neuropsychologia.* (1980) 18:123–32. doi: 10.1016/0028-3932(80)90058-5
 36. Levy R, Dubois B. Apathy and the functional anatomy of the prefrontal cortex-basal ganglia circuits. *Cereb Cortex.* (2006) 16:916–28. doi: 10.1093/cercor/bhj043
 37. Cai J, Ji Q, Xin R, Zhang D, Na X, Peng R, et al. Contralateral cortical structural reorganization contributes to motor recovery after sub-cortical stroke: a longitudinal voxel-based morphometry study. *Front Hum Neurosci.* (2016) 10:393. doi: 10.3389/fnhum.2016.00393
 38. Helie S, Ell SW, Ashby FG. Learning robust cortico-cortical associations with the basal ganglia: an integrative review. *Cortex.* (2015) 64:123–35. doi: 10.1016/j.cortex.2014.10.011
 39. Krack P, Hariz MI, Baunez C, Guridi J, Obeso JA. Deep brain stimulation: from neurology to psychiatry? *Trends Neurosci.* (2010) 33:474–84. doi: 10.1016/j.tins.2010.07.002
 40. Caplan LR. Lacunar infarction and small vessel disease: pathology and pathophysiology. *J Stroke.* (2015) 17:2–6. doi: 10.5853/jos.2015.17.1.2
 41. Feng C, Bai X, Xu Y, Hua T, Liu XY. The 'silence' of silent brain infarctions may be related to chronic ischemic preconditioning and nonstrategic locations rather than to a small infarction size. *Clinics.* (2013) 68:365–9. doi: 10.6061/clinics/2013(03)OA13
 42. Jellinger KA. Neuropathologic substrates of ischemic vascular dementia. *J Neuropathol Exp Neurol.* (2001) 60:658–9. doi: 10.1093/jnen/60.6.658
 43. Siegel JS, Ramsey LE, Snyder AZ, Metcalf NV, Chacko RV, Weinberger K, et al. Disruptions of network connectivity predict impairment in multiple behavioral domains after stroke. *Proc Natl Acad Sci USA.* (2016) 113:E4367–76. doi: 10.1073/pnas.1521083113
 44. Baldassarre A, Ramsey L, Rengachary J, Zinn K, Siegel JS, Metcalf NV, et al. Dissociated functional connectivity profiles for motor and attention deficits in acute right-hemisphere stroke. *Brain.* (2016) 139(Pt 7):2024–38. doi: 10.1093/brain/aww107
 45. Carter AR, Shulman GL, Corbetta M. Why use a connectivity-based approach to study stroke and recovery of function? *Neuroimage.* (2012) 62:2271–80. doi: 10.1016/j.neuroimage.2012.02.070
 46. Lim DH, LeDue JM, Mohajerani MH, Murphy TH. Optogenetic mapping after stroke reveals network-wide scaling of functional connections and heterogeneous recovery of the peri-infarct. *J Neurosci.* (2014) 34:16455–66. doi: 10.1523/JNEUROSCI.3384-14.2014
 47. Alexander GE, DeLong MR, Strick PL. Parallel organization of functionally segregated circuits linking basal ganglia and cortex. *Annu Rev Neurosci.* (1986) 9:357–81. doi: 10.1146/annurev.ne.09.030186.002041

Conflict of Interest Statement: The authors declare that the research was conducted in the absence of any commercial or financial relationships that could be construed as a potential conflict of interest.

Copyright © 2019 Zhu, Wang, Li, Chen, Li, Li, Zhang, Wei and Chen. This is an open-access article distributed under the terms of the Creative Commons Attribution License (CC BY). The use, distribution or reproduction in other forums is permitted, provided the original author(s) and the copyright owner(s) are credited and that the original publication in this journal is cited, in accordance with accepted academic practice. No use, distribution or reproduction is permitted which does not comply with these terms.



Cerebral Small Vessel Disease and Enlarged Perivascular Spaces-Data From Memory Clinic and Population-Based Settings

Bibek Gyanwali^{1,2}, Henri Vrooman³, Narayanaswamy Venketasubramanian⁴, Tien Yin Wong⁵, Ching-Yu Cheng⁵, Christopher Chen^{1,2} and Saima Hilal^{1,2,6*}

¹ Memory Aging and Cognition Centre, National University Health System, Singapore, Singapore, ² Department of Pharmacology, National University of Singapore, Singapore, Singapore, ³ Departments of Radiology and Medical Informatics, Erasmus University Medical Center, Rotterdam, Netherlands, ⁴ Raffles Neuroscience Centre, Raffles Hospital, Singapore, Singapore, ⁵ Singapore National Eye Center, Singapore Eye Research Institute, Singapore, Singapore, ⁶ Departments of Epidemiology and Radiology and Nuclear Medicine, Erasmus University Medical Center, Rotterdam, Netherlands

OPEN ACCESS

Edited by:

Andreas Charidimou,
Massachusetts General Hospital,
Harvard Medical School,
United States

Reviewed by:

Duangnapa Roongpiboonsopit,
Naresuan University, Thailand
Ellis van Etten,
Leiden University Medical
Center, Netherlands

*Correspondence:

Saima Hilal
phchs@nus.edu.sg

Specialty section:

This article was submitted to
Stroke,
a section of the journal
Frontiers in Neurology

Received: 26 March 2019

Accepted: 07 June 2019

Published: 25 June 2019

Citation:

Gyanwali B, Vrooman H,
Venketasubramanian N, Wong TY,
Cheng C-Y, Chen C and Hilal S (2019)
Cerebral Small Vessel Disease and
Enlarged Perivascular Spaces-Data
From Memory Clinic and
Population-Based Settings.
Front. Neurol. 10:669.
doi: 10.3389/fneur.2019.00669

Background: Enlarged perivascular spaces (ePVS) are common finding on magnetic resonance imaging (MRI) in elderly. ePVS are thought to be associated with cerebral small vessel disease (SVD) such as white matter hyperintensities (WMH), lacunes, and cerebral microbleeds (CMBs). However, the different location of SVD and its relationship to ePVS distribution requires further investigation.

Objective: To study the association between location and severity of SVD with ePVS from memory clinic and population-based settings.

Methods: This study includes patients from an ongoing memory clinic based case-control study and participants from the population-based: Epidemiology of Dementia in Singapore study (EDIS). All participants underwent a comprehensive standardized evaluation including physical, medical and neuropsychological assessment and a brain MRI. CMBs and lacune location were categorized into strictly lobar, strictly deep and mixed, and ePVS location into centrum semiovale and basal ganglia. WMH volume was automatically segmented and was classified into anterior and posterior distribution. Negative binomial regression models were constructed to analyse associations between SVD and ePVS and the rate ratios (RR) and 95% confidence intervals (CI) were reported.

Results: Of 375 patients (median age = 73 years) from memory clinic and 583 participants (median age = 70 years) from EDIS, the median total ePVS count was 17.0 and 7.0, respectively. Increased severity of SVD was not associated with total ePVS counts in both memory clinic and EDIS study. Analysis with the location of SVD and ePVS also showed similar results. However, in EDIS study, presence of ≥ 2 lacunes [RR = 1.61, 95% CI = 1.3, 2.30, $p = 0.009$], presence of ≥ 2 CMBs [RR = 1.40, 95% CI = 1.08, 1.83, $p = 0.012$], and higher volume of WMH [RR = 1.41, 95% CI = 1.10, 1.81, $p = 0.006$] were associated with basal ganglia ePVS independent of age, gender and vascular risk factors.

Conclusion: In this study, we found that the ePVS were not associated with the location and severity of SVD in the memory-clinic patients. However, only severity of SVD was associated with basal ganglia ePVS in the population-based setting. Our findings will need to be studied further in different cohorts so as to understand the mechanism underlying different SVD types in subclinical and clinical phases as well as for predicting cognitive decline.

Keywords: enlarged perivascular spaces, cerebral small vessel disease, memory clinic, population-based, magnetic resonance imaging

INTRODUCTION

Cerebral small vessel disease (SVD) is considered as one of the leading causes of cognitive decline, physical disability and dementia in the elderly population (1, 2). SVD represents a group of pathological processes affecting the small arteries, arterioles, venules, and capillaries in the brain, resulting in various ischemic, hemorrhagic, and inflammatory damage (1, 3). White matter hyperintensities (WMH), lacunes, and cerebral microbleeds (CMBs) are MRI signatures of SVD and have been extensively studied in relation to cognition, clinical outcome and associations with other markers of SVD (4–6). In recent years, enlarged perivascular spaces (ePVS) have emerged as another feature of SVD, however their occurrence may also be non-pathogenic as they appear during normal aging (7).

Perivascular spaces are thought to be interstitial fluid-filled spaces surrounding the penetrating vessels in the brain. Physiologically, perivascular spaces are important for the drainage of interstitial fluid and regulating immune response (7). When enlarged, these perivascular spaces are commonly observed on MRI of elderly people (8). ePVS are mainly seen in the centrum semiovale and basal ganglia but may also appear in the hippocampus and the brain stem (9).

Previous studies have shown that ePVS are not only associated with other SVD markers such as WMH, lacunes, and CMBs (7, 10–12) but also with aging and vascular risk factors such as hypertension (13–16). By contrast, a few recent studies have shown that ePVS are not associated with WMH (16) and other cardiovascular risk factors (7). Furthermore, it is suggested that different location of ePVS may indicate different pathophysiological mechanisms such as cerebral amyloid angiopathy and hypertensive arteriopathy (7, 12). Previous studies have examined centrum semiovale and basal ganglia ePVS in relation to lobar and deep CMBs (12, 15). However, very few studies have taken into account the association between the location of lacunes and WMH with the location of ePVS (10, 17).

We aim to investigate the association between different locations and severity of SVD markers such as WMH, lacunes, and CMBs with different locations of ePVS (centrum semiovale and basal ganglia) in a spectrum of diseased patients (memory-clinic) to a population-based (Epidemiology of Dementia in Singapore study) setting.

MATERIALS AND METHODS

Study Population

In this study, participants were recruited from two studies in Singapore. The first is a memory-clinic based case-control study, where patients (age ≥ 50 years) were recruited from memory clinics at the National University Hospital from August 2010 to December 2016. Cases were participants with subjective memory complaints and impairment on neuropsychological assessment and were diagnosed with cognitive impairment no dementia (CIND) and dementia. CIND was defined as impairment in at least one cognitive domain on comprehensive neuropsychological test, but did not meet the criteria for dementia according to Diagnostic and Statistical Manual for Mental Disorder-Fourth Edition (DSM-IV). Dementia was diagnosed according to the DSM-IV criteria. The controls were individuals who had no objective cognitive impairment on comprehensive neuropsychological tests or any functional decline and were diagnosed as No Cognitive Impairment (NCI).

Of the total 501 patients from the memory clinics, 18 had incomplete or poor quality scan, 12 did not undergo MRI scans (3 were claustrophobic, 1 refused, 2 were uncooperative or could not follow instructions, and 6 had contraindications for MRI), and 96 had no ePVS grading (because the primary sequences required for ePVS grading i.e., T1 and T2-weighted images were missing and/or had motion artifacts which restricted our grading), leaving a final sample of 375 cases for analysis.

The second is the Epidemiology of Dementia in Singapore study (EDIS), which recruited multi-ethnic (Chinese, Indian, and Malay) participants from the Singapore Epidemiology of Eye Disease (SEED) study (18). SEED is a large population based study among Chinese [Singapore Chinese Eye Study (SCES)], Malay [Singapore Malay Eye Study (SiMES-2)], and Indians [Singapore Indian Eye Study (SINDI-2)]. Participants from the SEED study who were ≥ 60 years and were screened-positive on the Abbreviated Mental Test (AMT) or self-reported progressive forgetfulness (PF) were invited to participate in the EDIS study from August 2010 to July 2015 (19). EDIS study also used similar diagnostic criteria as memory clinic, where participants were diagnosed as NCI (individuals who had no objective cognitive impairment on comprehensive neuropsychological tests or any functional decline), CIND (individuals with impairment in at least one cognitive domain on comprehensive neuropsychological test, but did not meet

the criteria for dementia according to DSM-IV), and Dementia (diagnosed according to the DSM-IV criteria).

A total of 300 Chinese and 323 Malay screen-positive participants agreed to take part in the second phase of this study, which included an extensive neuropsychological test battery and brain MRI. The present analysis was restricted to Chinese and Malay as the ePVS data was only available in these two ethnicities. Of the 623 participants, 36 had no MRI scans and 4 had poor quality MRI scans, leaving 583 (284 Chinese and 299 Malays) cases for the final analysis.

The memory clinic study was approved by the National Healthcare Group Domain-Specific Review Board. For the EDIS study, ethics approval was obtained from both the Singapore Eye Research Institute and National Healthcare Group Domain-Specific Review Board. This study is conducted in accordance with the Declaration of Helsinki. A written informed consent was obtained from all participants or their caregivers prior to the recruitment for this study.

Demographics and Vascular Risk Factors

All participants were administered a detailed questionnaire to collect information on age, gender, years of formal education, and smoking history. Previous medical history of hypertension, diabetes, and hyperlipidemia was noted and subsequently verified by medical records. Hypertension was defined as systolic blood pressure ≥ 140 mmHg and/or diastolic blood pressure ≥ 90 mmHg during the examination, or previous diagnosis of hypertension, or the use of antihypertensive medications. Hyperlipidemia was defined as total cholesterol level ≥ 4.14 mmol/l during the examination or previous diagnosis of hyperlipidemia, or the use of lipid-lowering medications. Diabetes mellitus was defined as glycated hemoglobin $\geq 6.5\%$ during the examination, or previous diagnosis of diabetes mellitus, or the use of glucose-lowering medications.

Neuroimaging

MRI scans of all the participants from both EDIS study and the memory clinics were performed at the Clinical Imaging Research Centre of the National University of Singapore, using a 3T Siemens Magnetom Trio Tim Scanner system with a 32-channel head coil. The standardized neuroimaging protocol in this study included a three dimensional T1-weighted sequence, a T2-weighted sequence, fluid-attenuated inversion recovery (FLAIR), and a susceptibility weighted image (SWI). Quantitative MRI analyses were performed using automated segmentation procedures at the Department of Medical Informatics, Erasmus University Medical Center, the Netherlands, using a model-based methodology (FreeSurfer, v.5.1.0) on T1 weighted images (TR = 7.2 ms, TE = 3.3 ms, matrix = $256 \times 256 \times 180$ mm³). For each participant, the following MRI-based markers were analyzed:

- CMBs were graded on SWI sequence according to the Brain Observer Micro Bleed Scale (20). CMBs were manually classified in both lobes (left and right) into two different locations: lobar (cortex/gray-white junction, subcortical white matter) and deep (basal ganglia, thalamus, internal and external capsule, brainstem, and cerebellum). CMBs were

then further divided into three groups: strictly lobar CMBs (presence of CMBs exclusively in lobar region), strictly deep CMBs (presence of CMBs exclusively in deep region), and mixed CMBs (CMBs distributed in both lobar and deep locations). The total number of CMBs in each location was recorded and calculated as the sum of strictly lobar, strictly deep, and mixed CMBs. Total CMBs was further categorized into three groups according to CMBs burden: 0 CMB, presence of 1 CMB, and presence of ≥ 2 CMBs (21).

- Lacunes were defined as round or ovoid lesions involving the subcortical regions, 3–15 mm in diameter, with a low signal on T1-weighted images and FLAIR, a high signal on T2-weighted images and a hyperintense rim with a center following the cerebrospinal fluid intensity (22). Similarly, lacunes were classified into two different locations: lobar (when located in frontal, parietal, temporal, occipital, insula, and centrum semiovale) and deep (when located in basal ganglia, thalamus, internal, and external capsule) (23). Lacunes were further divided into three groups: strictly lobar lacunes (presence of lacunes exclusively in lobar region), strictly deep lacunes (presence of lacunes exclusively in deep region), and mixed lacunes (presence of lacunes distributed in both lobar and deep locations). The total number of lacunes in each location was recorded and was calculated as sum of strictly lobar, strictly deep, and mixed lacunes. Total lacunes were further categorized into three groups according to lacunes burden: 0 lacune, presence of 1 lacune, and presence of ≥ 2 lacunes.
- ePVS were defined as round or linear hypointense lesions on T1 weighted and hyperintense lesion on T2 weighted images. When lesion is ≥ 1 mm, it is considered as dilated. In this study, ePVS were visually counted in four different regions of the brain: centrum semiovale, basal ganglia, mesencephalon, and hippocampus. Centrum semiovale EPVS were graded in the slice 10 mm above the lateral ventricle, whereas basal ganglia EPVS were graded to the level of the anterior commissure. ePVS in mesencephalon and hippocampus, were graded in all slices (24). Total ePVS was calculated as sum of centrum semiovale, basal ganglia, hippocampus, and mesencephalon ePVS. Due to the small number of ePVS in mesencephalon and hippocampus, we did not use these regions in further analysis.
- WMH volume was quantified using T1 and T2 weighted images. The image preprocessing steps and the tissue classification algorithm have been described elsewhere (25). Briefly, a k-nearest-neighbor (kNN) classifier technique was used to classify voxels into cerebrospinal fluid (CSF), gray matter, normal white matter and WMH. Volumes (ml) were calculated for all biomarkers from these segmentations. Region-specific WMH volume was calculated for frontal, parietal, occipital, and temporal lobes. Total WMH volume was calculated as the sum of WMH volumes in the above mentioned five regions. In this study, frontal WMH volume was classified as anterior and sum of parietal and occipital WMH volume as posterior (26–28). Total WMH volume was further categorized into tertiles to represent severity of WMH.

Intra-rater agreement for lacunes, CMBs, and ePVS was good to excellent, which has been published previously (8, 29).

Statistical Analysis

CMBs and lacunes were treated as counts and categorical variables. For categorical data, we classify CMB and lacunes as: presence vs. absence and 1 vs. 0, ≥ 2 vs. 0, and by location (strictly lobar vs. no, strictly deep vs. no, and mixed vs. no). WMH volumes were logarithmically transformed due to skewed distribution and were divided into tertiles (second tertile vs. first tertile and third tertile vs. first tertile). We chose to present the results with ePVS as count variable in this study because the numbers of participants with no ePVS were too few in binary category. SVD markers were treated as determinants and ePVS as outcomes. In our secondary analysis, we divided our study subjects into two groups i.e., NCI group which included NCI and cognitive impairment group which included CIND and Dementia. In order to analyze the association between location and severity of SVD markers with ePVS counts, negative binomial regression was constructed with rate ratios (RR) and 95% confidence intervals (CI). All models were adjusted for age, gender, hypertension, hyperlipidemia, and diabetes. Results were considered significant at $p < 0.05$. In view of multiple testing performed between SVD and ePVS, we used Bonferroni correction to obtain revised statistical significance level of $0.05/2 \sim 0.025$. All the data were analyzed using SPSS software package (version 25).

RESULTS

The characteristics of the study population from the memory clinic and EDIS study is shown in **Table 1**. Patients from memory clinic were older. EDIS participants had burden of hypertension where as participants from memory clinic had higher SVD burden. The median number (interquartile range) of total ePVS in memory clinic was 17.0 (11.0) and in EDIS, 7.0 (8.0).

The association between severity of SVD with total and region-specific ePVS in the memory clinic population is shown in **Table 2**. Increased severity of CMBs, lacunes and WMH was not associated with increased number of ePVS. Region-specific analysis also showed that increased severity of SVD was not associated with centrum semiovale ePVS and basal ganglia ePVS. Similarly, stratifying CMBs and lacunes into 0, 1, and ≥ 2 and WMH volume into tertiles did not change the results.

The association between locations of SVD with ePVS in memory clinic population is shown in **Table 3**. Increased number of lobar, deep, and mixed CMBs as well as lacunes and higher volumes of anterior and posterior WMH were not associated with ePVS (total ePVS, centrum semiovale ePVS, and basal ganglia ePVS). When treating CMBs and lacunes as categorical data (presence vs. absence) in regression analysis, no association was again observed (**Supplementary Table 1**).

The association between severity of SVD with ePVS in EDIS participants is shown in **Table 4**. Increased numbers of CMBs, lacunes, and increased severity of WMH volume were not associated with increased number of ePVS. Furthermore, region-specific analysis of ePVS as centrum semiovale ePVS and basal ganglia ePVS also did not show any significant association with SVD. However, on stratifying CMBs and lacunes into 1 vs. 0 and

TABLE 1 | Characteristics of study participants.

Baseline variables	Memory clinic (n = 375)	EDIS (n = 583)
Demographic factors		
Age, median (IQR)	73 (12)	70 (11)
Gender (Female), n (%)	199 (53.1)	319 (54.7)
Cardiovascular determinants		
Hypertension, n (%)	264 (70.4)	485 (83.2)
Hyperlipidemia, n (%)	273 (72.8)	412 (70.7)
Diabetes, n (%)	132 (35.2)	176 (30.2)
MRI markers		
Presence of Lacunes, n (%)	106 (28.3)	106 (18.2)
Strictly lobar lacunes, n (%)	32 (8.5)	50 (8.6)
Strictly deep lacunes, n (%)	43 (11.5)	27 (4.6)
Mixed lacunes, n (%)	31 (8.3)	29 (5.0)
Presence of CMBs, n (%)	156 (41.6)	215 (36.5)
Strictly lobar CMBs, n (%)	81 (21.6)	110 (18.9)
Strictly deep CMBs, n (%)	30 (8.0)	32 (5.5)
Mixed CMBs, n (%)	45 (12.0)	73 (12.5)
Total WMH volume, ml, median (IQR)	3.5 (11.0)	2.1 (6.0)
Anterior WMH volume, ml, median (IQR)	0.7 (3.3)	0.3 (1.4)
Posterior WMH volume, ml, median (IQR)	0.5 (3.1)	0.3 (1.5)
Total ePVS, median (IQR)	17.0 (11)	7.0 (8.0)
Centrum semiovale ePVS, median (IQR)	10.0 (9.0)	3.0 (5)
Basal ganglia ePVS, median (IQR)	3.0 (3)	2.0 (3)

SD, standard deviation; IQR, inter quartile range; WMH, white matter hyperintensity; ePVS, enlarged perivascular spaces; EDIS, Epidemiology of Dementia in Singapore.

TABLE 2 | Association between severity of SVD and ePVS (Memory clinic).

SVD markers	Total ePVS RR (95% CI)	Centrum semiovale ePVS RR (95% CI)	Basal ganglia ePVS RR (95% CI)
Total CMBs	1.00 (0.99, 1.01)	1.00 (0.98, 1.01)	1.01 (0.99, 1.02)
1 CMB	0.96 (0.71, 1.30)	1.00 (0.74, 1.36)	0.96 (0.69, 1.33)
≥ 2 CMBs	1.06 (0.83, 1.36)	1.02 (0.80, 1.31)	1.04 (0.79, 1.37)
Total lacunes	1.04 (0.93, 1.16)	0.98 (0.87, 1.01)	1.10 (0.98, 1.25)
1 lacune	1.13 (0.84, 1.51)	1.13 (0.84, 1.52)	0.98 (0.71, 1.36)
≥ 2 lacunes	1.17 (0.76, 1.49)	0.88 (0.62, 1.24)	1.37 (0.96, 1.97)
Total WMH volume	1.00 (0.94, 1.00)	1.00 (0.99, 1.00)	1.00 (0.99, 1.00)
Second tertile	1.04 (0.80, 1.35)	1.06 (0.82, 1.39)	0.96 (0.72, 1.28)
Third tertile	1.09 (0.83, 1.43)	1.07 (0.82, 1.41)	1.02 (0.75, 1.37)

RR, rate ratio; CI, confidence interval; CMBs, cerebral microbleeds; ePVS, enlarged perivascular spaces; WMH, white matter hyperintensity. All values adjusted for age, gender, hypertension, hyperlipidemia, and diabetes.

≥ 2 vs. 0; presence of ≥ 2 lacunes [RR = 1.61, 95% CI = 1.3, 2.30, $p = 0.009$] and presence of ≥ 2 CMBs [RR = 1.40, 95% CI = 1.08, 1.83, $p = 0.012$] were associated with basal ganglia ePVS. Higher volume of WMH in third tertile was associated with basal ganglia ePVS [RR = 1.41, 95% CI = 1.10, 1.81, $p = 0.006$]. Moreover, presence of ≥ 2 lacunes was found to be associated with reduced

TABLE 3 | Association between location of SVD and ePVS (Memory clinic).

SVD markers	Total ePVS RR (95% CI)	Centrum semiovale ePVS RR (95% CI)	Basal ganglia ePVS RR (95% CI)
Strictly lobar CMBs	1.00 (0.98, 1.02)	0.99 (0.97, 1.01)	1.01 (0.99, 1.03)
Strictly deep CMBs	1.01 (0.88, 1.15)	0.99 (0.86, 1.12)	1.02 (0.87, 1.20)
Mixed CMBs	1.00 (0.99, 1.02)	1.00 (0.98, 1.01)	1.01 (0.99, 1.02)
Strictly lobar lacunes	0.99 (0.76, 1.29)	0.93 (0.71, 1.23)	1.03 (0.78, 1.35)
Strictly deep lacunes	1.00 (0.79, 1.27)	0.98 (0.77, 1.25)	0.92 (0.71, 1.18)
Mixed lacunes	1.05 (0.92, 1.19)	1.00 (0.88, 1.14)	1.15 (1.00, 1.32)
Anterior WMH volume	1.00 (0.98, 1.01)	0.99 (0.98, 1.01)	1.00 (0.98, 1.02)
Posterior WMH volume	1.00 (0.99, 1.01)	1.00 (0.99, 1.01)	1.00 (0.99, 1.01)

RR, rate ratio; CI, confidence interval; CMBs, cerebral microbleeds; ePVS, enlarged perivascular spaces; WMH, white matter hyperintensity. All values adjusted for age, gender, hypertension, hyperlipidemia, and diabetes.

TABLE 4 | Association between severity of SVD and ePVS (EDIS).

SVD markers	Total ePVS RR (95% CI)	Centrum semiovale ePVS RR (95% CI)	Basal ganglia ePVS RR (95% CI)
Total CMBs*	1.00 (0.99, 1.01)	0.99 (0.98, 1.00)	1.00 (0.99, 1.01)
1 CMB	1.04 (0.84, 1.30)	0.93 (0.73, 1.18)	1.09 (0.85, 1.40)
≥2 CMBs	1.18 (0.93, 1.51)	1.00 (0.78, 1.29)	1.40 (1.08, 1.83)*
Total lacunes	1.07 (0.93, 1.22)	0.89 (0.76, 1.04)	1.21 (0.70, 1.92)
1 lacune	1.33 (1.00, 1.76)	1.43 (1.06, 1.92)	1.14 (1.00, 1.48)
≥2 lacunes	1.05 (0.75, 1.47)	0.61 (0.42, 0.88)*	1.61 (1.13, 2.30)*
Total WMH volume	1.00 (0.99, 1.12)	1.00 (0.99, 1.00)	1.00 (0.99, 1.00)
Second tertile	0.97 (0.78, 1.20)	0.90 (0.72, 1.14)	1.15 (0.90, 1.47)
Third tertile	1.07 (0.85, 1.34)	0.81 (0.63, 1.03)	1.41 (1.10, 1.81)*

RR, rate ratio; CI, confidence interval; CMBs, cerebral microbleeds; ePVS, enlarged perivascular spaces; WMH, white matter hyperintensity; EDIS, Epidemiology of Dementia in Singapore. All values adjusted for age, gender, hypertension, hyperlipidemia, and diabetes. Bold values represents statistically significant associations at $p < 0.05$.

*Statistically significant after Bonferroni correction ($0.05/2 \sim 0.025$).

centrum semiovale ePVS counts [RR = 0.61, 95% CI = 0.42, 0.88, $p = 0.009$]. These associations survived multiple testing.

The association between locations of SVD with ePVS in EDIS participants is shown in **Table 5**. Location-specific analysis of SVD did not show any significant association with total ePVS counts. On repeating this analysis with region-specific ePVS counts, increased number of lobar, deep and mixed CMBs, and lacunes were not associated with centrum semiovale ePVS. However, there was borderline association between increased number of strictly lobar lacunes [RR = 1.27, 95% CI = 1.00, 1.62, $p = 0.055$] and mixed lacunes [RR = 1.16, 95% CI = 0.99, 1.36, $p = 0.070$] with basal ganglia ePVS. Higher anterior and posterior WMH volumes were not associated with centrum semiovale ePVS or with basal ganglia ePVS.

In EDIS participants, when treating CMBs and lacunes as categorical data (presence vs. absence), no significant association was again observed between presence of SVD and ePVS.

TABLE 5 | Association between location of SVD and ePVS (EDIS study).

SVD markers	Total ePVS RR (95% CI)	Centrum semiovale ePVS RR (95% CI)	Basal ganglia ePVS RR (95% CI)
Total CMBs	1.00 (0.99, 1.01)	0.99 (0.98, 1.00)	1.00 (0.99, 1.01)
Strictly lobar CMBs	0.98 (0.83, 1.16)	0.92 (0.78, 1.10)	1.10 (0.92, 1.32)
Strictly deep CMBs	1.22 (0.84, 1.77)	1.27 (0.86, 1.88)	0.88 (0.57, 1.35)
Mixed CMBs	1.00 (0.99, 1.01)	0.99 (0.98, 1.00)	1.00 (0.99, 1.01)
Strictly lobar lacunes	1.12 (0.88, 1.42)	1.04 (0.80, 1.36)	1.27 (1.00, 1.62)
Strictly deep lacunes	1.23 (0.86, 1.75)	1.21 (0.83, 1.77)	1.25 (0.85, 1.83)
Mixed lacunes	1.00 (0.86, 1.16)	0.78 (0.63, 0.94)	1.16 (0.99, 1.36)
Anterior WMH volume	1.00 (0.99, 1.01)	1.00 (0.99, 1.01)	1.01 (0.99, 1.02)
Posterior WMH volume	1.00 (0.99, 1.01)	1.00 (0.99, 1.01)	1.00 (0.99, 1.01)

RR, rate ratio; CI, confidence interval; CMBs, cerebral microbleeds; ePVS, enlarged perivascular spaces; WMH, white matter hyperintensity; EDIS, Epidemiology of Dementia in Singapore. All values adjusted for age, gender, hypertension, hyperlipidemia, and diabetes.

However, there was border line association between presence of CMBs [RR = 1.23, 95% CI = 0.99, 1.51, $p = 0.058$] and lacunes [RR = 1.29, 95% CI = 0.97, 1.91, $p = 0.056$] with basal ganglia ePVS. Region-specific analysis of CMBs and lacunes showed border line association between mixed CMBs [RR = 1.18, 95% CI = 0.94, 1.09, $p = 0.057$], and mixed lacunes [RR = 1.36, 95% CI = 0.74, 2.27, $p = 0.054$] with basal ganglia ePVS (**Supplementary Table 2**).

On performing secondary analysis among cognitive impairment and NCI groups, we found location and severity of SVD markers were not associated with ePVS counts in memory clinic and population-based setting. However, in EDIS study, presence of ≥ 2 lacunes [RR = 1.59, 95% CI = 1.09, 2.31, $p = 0.015$], ≥ 2 CMBs [RR = 1.40, 95% CI = 1.08, 1.98, $p = 0.014$], and higher volume of WMH in third tertile [RR = 1.45, 95% CI = 1.08, 1.94, $p = 0.012$] were associated with basal ganglia ePVS in cognitively impaired group only. Moreover, among individuals with NCI in EDIS study, increased number of strictly lobar lacunes [RR = 0.37, 95% CI = 0.17, 0.77, $p = 0.008$] and higher WMH volume in third tertile [RR = 0.48, 95% CI = 0.29, 0.78, $p = 0.003$], more specifically anterior [RR = 0.07, 95% CI = 0.66, 0.90, $p = 0.001$] and posterior WMH volume [RR = 0.76, 95% CI = 0.66, 0.88, $p < 0.001$] were associated with lower centrum semiovale ePVS counts [data not shown].

DISCUSSION

This study demonstrated that increased severity of SVD markers were not associated with total ePVS counts in memory clinic and population-based settings. Region specific analysis did not change these results. However, in EDIS study presence of ≥ 2 lacunes, ≥ 2 CMBs, and higher volume of WMH were associated with basal ganglia ePVS independent of age, gender, and vascular risk factors. We did not find an association between location of SVD with ePVS in centrum semiovale and basal ganglia.

Till date, this is the first study to examine the association between location and severity of SVD with total and region specific ePVS counts. Previous studies have shown that lobar CMBs were associated with centrum semiovale ePVS and deep CMBs with basal ganglia ePVS (12, 15). Furthermore, higher WMH volume was associated with basal ganglia ePVS (12). However, in this study we found that total and region specific ePVS counts were not associated with location of SVD in both memory clinic and population-based settings. This might be due to the fact that first, ePVS are considered as an early MRI feature in the spectrum of SVD markers (16). Previous studies have shown that the WMH, CMBs, ePVS, and lacunes co-occur suggesting a common pathophysiological mechanism underlying these lesions (30). Second, during the different stages of cognitive impairment, other factors such as inflammation, amyloid, tau may attenuate the effect the traditional cardiovascular risk factors such as hypertension, hyperlipidemia, and diabetes (31, 32). Third, cerebral amyloid angiopathy and hypertensive arteriopathy may be due to two separate mechanisms in preclinical stages, but at the advanced stage, they co-occur and manifest as mixed pathology (30). Since the participants of the memory clinic have a higher burden of cardiovascular risk factors, we speculate that they might already be in more advanced stage of cerebrovascular damage and hence a ceiling effect is likely to be observed (8), which may explain the lack of association between location and severity of SVD with ePVS. Moreover, there might be differences in study population (hospital/memory clinic vs. population-based), different MRI modalities i.e., field strength (1.5T vs. 3T vs. 7T), methods in ePVS grading (whole brain vs. particular slice vs. particular hemisphere), sequences used and variation in risk factor profile as well as the inclusion criteria of the study population. It has been shown that, perivascular spaces are present in abundance throughout the healthy brain (7) and when enlarged can be visualized on MRI (8). It is possible that ePVS differ from other markers of SVD and may represent a non-pathological process of aging with no clinical consequences.

The prevalence of SVD has been suggested to differ among ethnicities due to differences in vascular risk factors, genetic, and environmental susceptibility (29). It is reported that the burden of SVD is higher in Asians compared to Caucasians due to higher prevalence of cardiovascular risk factors (33). Hence, we speculate that Asians with higher SVD burden would have higher number of ePVS compared to Caucasians. By contrast, the ePVS counts in both memory clinics and EDIS study were lower than previous studies (7, 10, 17, 34, 35). This difference may be attributed to different grading method for ePVS. Similar results were also mentioned in a recent meta-analysis which included EDIS and other community-based samples from Austria, Hong Kong, Netherlands, and Germany. Despite using a harmonized method to grade ePVS in each study, Asians had lower number of ePVS, especially lowest in Hong Kong (mean ePVS = 2.1) compared to other cohorts in that study [Austria; mean ePVS = 30.8, Netherlands; mean ePVS = 16.7, Germany; mean ePVS = 8.2] (8).

Previous neuropathological studies have shown co-occurrence of ePVS with other SVD markers such as CMBs, WMH, and

lacunes. However, it is difficult to conclude the chronological order of the occurrence of these markers as post-mortem samples are obtained at later stage of life when there is significant SVD burden. It is not clear that ePVS precede, follow or co-occur together with other SVD. We cannot exclude the possibility that ePVS of ≥ 1 mm may be non-pathogenic and may not have any significant effect on SVD. It has been shown that large perivascular spaces (≥ 3 mm in diameter) were associated with MRI markers of SVD and increased risk of dementia (36). We postulate that smaller ePVS are non-pathological and hence are not associated with SVD in this study.

Interestingly, in EDIS study, we found that the presence of ≥ 2 lacunes, CMBs, and higher WMH volume were associated with basal ganglia ePVS. We only found this association in population-based setting but not in memory-clinic study. Although no direct conclusion can be drawn from this study with respect to the association between ePVS and SVD, these results should be interpreted with caution. Notably, EDIS participants were relatively younger and had lower burden of vascular risk factors especially lower diabetes and hyperlipidemia hence, they may be at early stage of disease, whereas memory clinic participants were older and had higher burden of vascular risk factors and are at later stage of cognitive impairment. Furthermore, EDIS participants had a higher burden of hypertension compared to memory clinic subjects, which might have influenced the association however, previous studies on association between vascular risk factors and ePVS are controversial. It has been shown ePVS were associated with vascular risk factors such as hypertension (13–16) but a recent study did not report such findings (7). Hence, this finding leads us to further confirm that ePVS may be early marker of SVD. However, these results should be interpreted with caution. Interestingly in EDIS study, we found that the presence of ≥ 2 lacunes was associated with lower ePVS counts in centrum semiovale. In subgroup analysis, among the individuals with NCI in EDIS study increased number of strictly lobar lacunes was associated with lower ePVS count in centrum semiovale. The possible reason might be, due to similar MRI characteristics of ePVS and lacunes, where several ePVS may have been mis-graded as lacunes or vice versa and thus we might have underestimated the exact numbers of ePVS (22, 37–39). Similarly, in subjects with NCI in EDIS study, higher WMH volume were associated with lower counts of centrum semiovale ePVS. This might be explained by the fact that extensive WMH obscures ePVS grading especially in centrum semiovale and hence under estimates PVS counting in that region.

Our study has some limitations. First, as this is a cross-sectional study, we were unable to determine the cause-effect relationship and also the chronological order of SVD and temporal change of SVD over time. Second, even though we adjusted for several risk factors such as age, gender, hypertension, diabetes, and hyperlipidemia, we cannot ignore the possibility of residual confounding. Third, ePVS were graded at one particular slice for basal ganglia and centrum semiovale, we may have missed other possible ePVS. However, this method has shown strong correlation with whole brain grading approach (9). Fourth, as this study was conducted in Asian population, our results are not generalizable to other ethnicities. Fifth,

the data on ≥ 3 mm ePVS is only present in EDIS study. There were only 25 subjects with ePVS ≥ 3 mm in this study. With this small number of cases, we were unable to find any association. Hence we are unable to perform analysis comparing the association of ePVS and SVD in small ePVS (≥ 1 mm) and large ePVS (≥ 3 mm). Strength of this study include, use of 2 different population i.e., memory clinic and population-based with different risk factor profile and SVD burden. All MRIs were done on 3T scanner and SVD markers were graded blinded to clinical history following similar protocol.

Our findings demonstrated that ePVS counts were not associated with markers of SVD in memory clinic and population-based settings in Asia. However, in population-based setting presence of ≥ 2 lacunes, ≥ 2 CMBs, and higher WMH volume were associated with basal ganglia ePVS. Our results need to be studied further in large cohorts with cross-sectional and longitudinal designs using consistent and harmonized methods for ePVS so as to understand the underlying mechanism of different SVD markers in subclinical and clinical phases as well as for predicting cognitive decline.

DATA AVAILABILITY

All datasets generated for this study are included in the manuscript and/or the **Supplementary Files**.

ETHICS STATEMENT

The memory clinic study was approved by the National Healthcare Group Domain-Specific Review Board. For the EDIS study, ethics approval was obtained from both the Singapore Eye Research Institute and National Healthcare Group Domain-Specific Review Board. This study is conducted in accordance

with the Declaration of Helsinki. A written informed consent was obtained from all participants or their caregivers prior to the recruitment for this study.

AUTHOR CONTRIBUTIONS

BG participated in data acquisition, performed analysis, drafted, and revised manuscript. HV participated in MRI segmentation and revised manuscript. NV was responsible for provided intellectual advice and revised manuscript. TW and C-YC revised the manuscript. CC and SH were responsible for study design and concept, obtaining funding, overall supervision, and revised the manuscript.

FUNDING

Memory clinic study was supported by the National Medical Research Council grants; NMRC/CG/NUHS/2010-R-184-005-184-511, NMRC/CG/013/2013, NMRC/CIRG/1446/2016. EDIS study was supported by the National Medical Research Council grants; NMRC/CG/NUHS/2010, NMRC/CSA/038/2013, and NMRC/CG/013/2013.

ACKNOWLEDGMENTS

We acknowledge all the Memory Aging and Cognition Centre coordinators for their contribution to subject recruitment and data acquisition.

SUPPLEMENTARY MATERIAL

The Supplementary Material for this article can be found online at: <https://www.frontiersin.org/articles/10.3389/fneur.2019.00669/full#supplementary-material>

REFERENCES

- Pantoni L. Cerebral small vessel disease: from pathogenesis and clinical characteristics to therapeutic challenges. *Lancet Neurol.* (2010) 9:689–701. doi: 10.1016/S1474-4422(10)70104-6
- De Laat KF, Tuladhar AM, Van Norden AG, Norris DG, Zwiers MP, De Leeuw FE. Loss of white matter integrity is associated with gait disorders in cerebral small vessel disease. *Brain.* (2011) 134:73–83. doi: 10.1093/brain/awq343
- Wardlaw JM, Smith C, Dichgans M. Mechanisms of sporadic cerebral small vessel disease: insights from neuroimaging. *Lancet Neurol.* (2013) 12:483–97. doi: 10.1016/S1474-4422(13)70060-7
- Debette S, Markus HS. The clinical importance of white matter hyperintensities on brain magnetic resonance imaging: systematic review and meta-analysis. *BMJ.* (2010) 341:c3666. doi: 10.1136/bmj.c3666
- Schmidt R, Seiler S, Loitfelder M. Longitudinal change of small-vessel disease-related brain abnormalities. *J Cereb Blood Flow Metab.* (2016) 36:26–39. doi: 10.1038/jcbfm.2015.72
- Smith EE, Beaudin AE. New insights into cerebral small vessel disease and vascular cognitive impairment from MRI. *Curr Opin Neurol.* (2018) 31:36–43. doi: 10.1097/WCO.0000000000000513
- Bouvy WH, Zwanenburg JJ, Reinink R, Wisse LE, Luijten PR, Kappelle LJ, et al. Perivascular spaces on 7 Tesla brain MRI are related to markers of small vessel disease but not to age or cardiovascular risk factors. *J Cereb Blood Flow Metab.* (2016) 36:1708–17. doi: 10.1177/0271678X16648970
- Hilal S, Tan CS, Adams HHH, Habes M, Mok V, Venketasubramanian N, et al. Enlarged perivascular spaces and cognition: a meta-analysis of 5 population-based studies. *Neurology.* (2018) 91:e832–42. doi: 10.1212/WNL.00000000000006079
- Adams HHH, Hilal S, Schwingenschuh P, Wittfeld K, Van Der Lee SJ, Decarli C, et al. A priori collaboration in population imaging: The Uniform Neuro-Imaging of Virchow-Robin Spaces Enlargement consortium. *Alzheimers Dement.* (2015) 1:513–20. doi: 10.1016/j.dadm.2015.10.004
- Doubal FN, MacLulich AM, Ferguson KJ, Dennis MS, Wardlaw JM. Enlarged perivascular spaces on MRI are a feature of cerebral small vessel disease. *Stroke.* (2010) 41:450–4. doi: 10.1161/STROKEAHA.109.564914
- Charidimou A, Boulouis G, Haley K, Auriel E, Van Etten ES, Fotiadis P, et al. White matter hyperintensity patterns in cerebral amyloid angiopathy and hypertensive arteriopathy. *Neurology.* (2016) 86:505–11. doi: 10.1212/WNL.0000000000002362
- Charidimou A, Boulouis G, Pasi M, Auriel E, Van Etten ES, Haley K, et al. MRI-visible perivascular spaces in cerebral amyloid angiopathy and hypertensive arteriopathy. *Neurology.* (2017) 88:1157–64. doi: 10.1212/WNL.0000000000003746
- Rouhl RP, Van Oostenbrugge RJ, Knottnerus IL, Staals JE, Lodder J. Virchow-Robin spaces relate to cerebral small vessel disease severity. *J Neurol.* (2008) 255:692–6. doi: 10.1007/s00415-008-0777-y
- Klarenbeek P, Van Oostenbrugge RJ, Rouhl RP, Knottnerus IL, Staals J. Ambulatory blood pressure in patients with lacunar stroke: association with

- total MRI burden of cerebral small vessel disease. *Stroke*. (2013) 44:2995–9. doi: 10.1161/STROKEAHA.113.002545
15. Martinez-Ramirez S, Pontes-Neto OM, Dumas AP, Auriel E, Halpin A, Quimby M, et al. Topography of dilated perivascular spaces in subjects from a memory clinic cohort. *Neurology*. (2013) 80:1551–6. doi: 10.1212/WNL.0b013e31828f1876
 16. Francis F, Ballerini L, Wardlaw JM. Perivascular spaces and their associations with risk factors, clinical disorders and neuroimaging features: a systematic review and meta-analysis. *Int J Stroke*. (2019). doi: 10.1177/1747493019830321. [Epub ahead of print].
 17. Potter GM, Doubal FN, Jackson CA, Chappell FM, Sudlow CL, Dennis MS, et al. Enlarged perivascular spaces and cerebral small vessel disease. *Int J Stroke*. (2015) 10:376–81. doi: 10.1111/ijvs.12054
 18. Hilal S, Xin X, Ang SL, Tan CS, Venketasubramanian N, Niessen WJ, et al. Risk factors and consequences of cortical thickness in an Asian population. *Medicine*. (2015) 94:e852. doi: 10.1097/MD.0000000000000852
 19. Hilal S, Ikram MK, Saini M, Tan CS, Catindig JA, Dong YH, et al. Prevalence of cognitive impairment in Chinese: epidemiology of dementia in Singapore study. *J Neurol Neurosurg Psychiatry*. (2013) 84:686–92. doi: 10.1136/jnnp-2012-304080
 20. Cordonnier C, Potter GM, Jackson CA, Doubal F, Keir S, Sudlow CL, et al. Improving interrater agreement about brain microbleeds: development of the Brain Observer MicroBleed Scale (BOMBS). *Stroke*. (2009) 40:94–9. doi: 10.1161/STROKEAHA.108.526996
 21. Hilal S, Saini M, Tan CS, Catindig JA, Koay WI, Niessen WJ, et al. Cerebral microbleeds and cognition: the epidemiology of dementia in Singapore study. *Alzheimer Dis Assoc Disord*. (2014) 28:106–12. doi: 10.1097/WAD.0000000000000015
 22. Wardlaw JM, Smith EE, Biessels GJ, Cordonnier C, Fazekas F, Frayne R, et al. Neuroimaging standards for research into small vessel disease and its contribution to ageing and neurodegeneration. *Lancet Neurol*. (2013) 12:822–38. doi: 10.1016/S1474-4422(13)70124-8
 23. Pasi M, Boulouis G, Fotiadis P, Auriel E, Charidimou A, Haley K, et al. Distribution of lacunes in cerebral amyloid angiopathy and hypertensive small vessel disease. *Neurology*. (2017) 88:2162–8. doi: 10.1212/WNL.0000000000004007
 24. Adams HH, Cavalieri M, Verhaaren BF, Bos D, Van Der Lugt A, Enzinger C, et al. Rating method for dilated Virchow-Robin spaces on magnetic resonance imaging. *Stroke*. (2013) 44:1732–5. doi: 10.1161/STROKEAHA.111.000620
 25. Vrooman HA, Cocosco CA, Van Der Lijn F, Stokking R, Ikram MA, Vernooij MW, et al. Multi-spectral brain tissue segmentation using automatically trained k-Nearest-Neighbor classification. *Neuroimage*. (2007) 37:71–81. doi: 10.1016/j.neuroimage.2007.05.018
 26. Marquie MJ, Attix DK, Goldstein LB, Samsa GP, Payne ME, Chelune GJ, et al. Differential patterns of cognitive decline in anterior and posterior white matter hyperintensity progression. *Stroke*. (2010) 41:1946–50. doi: 10.1161/STROKEAHA.110.587717
 27. Polvikoski TM, Van Straaten ECW, Barkhof F, Sulkava R, Aronen HJ, Niinistö L, et al. Frontal lobe white matter hyperintensities and neurofibrillary pathology in the oldest old. *Neurology*. (2010) 75:2071–8. doi: 10.1212/WNL.0b013e318200d6f9
 28. Zhu YC, Chabriat H, Godin O, Dufouil C, Rosand J, Greenberg SM, et al. Distribution of white matter hyperintensity in cerebral hemorrhage and healthy aging. *J Neurol*. (2012) 259:530–6. doi: 10.1007/s00415-011-6218-3
 29. Gyanwali B, Shaik MA, Tan BY, Venketasubramanian N, Chen C, Hilal S. Risk factors for and clinical relevance of incident and progression of cerebral small vessel disease markers in an Asian memory clinic population. *J Alzheimers Dis*. (2019) 67:1209–19. doi: 10.3233/JAD-180911
 30. Akoudad S, Ikram MA, Koudstaal PJ, Hofman A, Niessen WJ, Greenberg SM, et al. Cerebral microbleeds are associated with the progression of ischemic vascular lesions. *Cerebrovasc Dis*. (2014) 37:382–8. doi: 10.1159/000362590
 31. Van Dijk EJ, Prins ND, Vermeer SE, Vrooman HA, Hofman A, Koudstaal PJ, et al. C-reactive protein and cerebral small-vessel disease: the Rotterdam Scan Study. *Circulation*. (2005) 112:900–5. doi: 10.1161/CIRCULATIONAHA.104.506337
 32. Shoamanesh A, Preis SR, Beiser AS, Vasan RS, Benjamin EJ, Kase CS, et al. Inflammatory biomarkers, cerebral microbleeds, and small vessel disease: Framingham Heart Study. *Neurology*. (2015) 84:825–32. doi: 10.1212/WNL.0000000000001279
 33. Hilal S, Mok V, Youn YC, Wong A, Ikram MK, Chen CL. Prevalence, risk factors and consequences of cerebral small vessel diseases: data from three Asian countries. *J Neurol Neurosurg Psychiatry*. (2017) 88:669–74. doi: 10.1136/jnnp-2016-315324
 34. Zhu YC, Dufouil C, Mazoyer B, Soumare A, Ricolfi F, Tzourio C, et al. Frequency and location of dilated Virchow-Robin spaces in elderly people: a population-based 3D MR imaging study. *AJNR Am J Neuroradiol*. (2011) 32:709–13. doi: 10.3174/ajnr.A2366
 35. Loos CMJ, Klarenbeek P, Van Oostenbrugge RJ, Staals J. Association between perivascular spaces and progression of white matter hyperintensities in lacunar stroke patients. *PLoS ONE*. (2015) 10:e0137323. doi: 10.1371/journal.pone.0137323
 36. Ding J, Sigurdsson S, Jonsson PV, Eiriksdottir G, Charidimou A, Lopez OL, et al. Large perivascular spaces visible on magnetic resonance imaging, cerebral small vessel disease progression, and risk of dementia: the age, gene/environment Susceptibility-Reykjavik Study. *JAMA Neurol*. (2017) 74:1105–12. doi: 10.1001/jamaneurol.2017.1397
 37. Benjamin P, Trippier S, Lawrence AJ, Lambert C, Zeestraten E, Williams OA, et al. Lacunar infarcts, but not perivascular spaces, are predictors of cognitive decline in cerebral small-vessel disease. *Stroke*. (2018) 49:586–93. doi: 10.1161/STROKEAHA.117.017526
 38. Rudie JD, Rauschecker AM, Nabavizadeh SA, Mohan S. Neuroimaging of dilated perivascular spaces: from benign and pathologic causes to mimics. *J Neuroimaging*. (2018) 28:139–49. doi: 10.1111/jon.12493
 39. Meyers CW, Berg MJ. Benign MRI findings and their pathologic mimics. *Neurol Clin Pract*. (2013) 3:155–60. doi: 10.1212/CPJ.0b013e31828d9f02

Conflict of Interest Statement: The authors declare that the research was conducted in the absence of any commercial or financial relationships that could be construed as a potential conflict of interest.

Copyright © 2019 Gyanwali, Vrooman, Venketasubramanian, Wong, Cheng, Chen and Hilal. This is an open-access article distributed under the terms of the Creative Commons Attribution License (CC BY). The use, distribution or reproduction in other forums is permitted, provided the original author(s) and the copyright owner(s) are credited and that the original publication in this journal is cited, in accordance with accepted academic practice. No use, distribution or reproduction is permitted which does not comply with these terms.



HTRA1 Mutations Identified in Symptomatic Carriers Have the Property of Interfering the Trimer-Dependent Activation Cascade

Masahiro Uemura¹, Hiroaki Nozaki², Akihito Koyama^{1,3}, Naoko Sakai¹, Shoichiro Ando¹, Masato Kanazawa¹, Taisuke Kato⁴ and Osamu Onodera^{1*}

¹ Department of Neurology, Brain Research Institute, Niigata University, Niigata, Japan, ² Department of Medical Technology, Graduate School of Health Sciences, Niigata University, Niigata, Japan, ³ Division of Legal Medicine, Niigata University, Niigata, Japan, ⁴ Department of System Pathology for Neurological Disorders, Brain Research Institute, Niigata University, Niigata, Japan

OPEN ACCESS

Edited by:

Andreas Charidimou,
Massachusetts General Hospital and
Harvard Medical School,
United States

Reviewed by:

Alessandra Rufa,
University of Siena, Italy
Hidetoshi Kasuya,
Tokyo Women's Medical University
Medical Center East, Japan

*Correspondence:

Osamu Onodera
onodera@bri.niigata-u.ac.jp

Specialty section:

This article was submitted to
Stroke,
a section of the journal
Frontiers in Neurology

Received: 21 March 2019

Accepted: 13 June 2019

Published: 28 June 2019

Citation:

Uemura M, Nozaki H, Koyama A, Sakai N, Ando S, Kanazawa M, Kato T and Onodera O (2019) HTRA1 Mutations Identified in Symptomatic Carriers Have the Property of Interfering the Trimer-Dependent Activation Cascade. *Front. Neurol.* 10:693. doi: 10.3389/fneur.2019.00693

Background: Mutations in the *high-temperature requirement A serine peptidase 1* (HTRA1) cause cerebral autosomal recessive arteriopathy with subcortical infarcts and leukoencephalopathy (CARASIL). Most carriers for HTRA1 mutations are asymptomatic, but more than 10 mutations have been reported in symptomatic carriers. The molecular differences between the mutations identified in symptomatic carriers and mutations identified only in CARASIL patients are unclear. HTRA1 is a serine protease that forms homotrimers, with each HTRA1 subunit activating the adjacent HTRA1 via the sensor domain of loop 3 (L3) and the activation domain of loop D (LD). Previously, we analyzed four HTRA1 mutant proteins identified in symptomatic carriers and found that they were unable to form trimers or had mutations in the LD or L3 domain. The mutant HTRA1s with these properties are presumed to inhibit trimer-dependent activation cascade. Indeed, these mutant HTRA1s inhibited wild-type (WT) protease activity. In this study, we further analyzed 15 missense HTRA1s to clarify the molecular character of mutant HTRA1s identified in symptomatic carriers.

Methods: We analyzed 12 missense HTRA1s identified in symptomatic carriers (hetero-HTRA1) and three missense HTRA1s found only in CARASIL (CARASIL-HTRA1). The protease activity of the purified recombinant mutant HTRA1s was measured using fluorescein isothiocyanate-labeled casein as substrate. Oligomeric structure was evaluated by size-exclusion chromatography. The protease activities of mixtures of WT with each mutant HTRA1 were also measured.

Results: Five hetero-HTRA1s had normal protease activity and were excluded from further analysis. Four of the seven hetero-HTRA1s and one of the three CARASIL-HTRA1s were unable to form trimers. The other three hetero-HTRA1s had mutations in the LD domain. Together with our previous work, 10 of 11 hetero-HTRA1s

and two of six CARASIL-HTRA1s were either defective in trimerization or had mutations in the LD or L3 domain ($P = 0.006$). By contrast, eight of 11 hetero-HTRA1s and two of six CARASIL-HTRA1 inhibited WT protease activity ($P = 0.162$).

Conclusions: HTRA1 mutations identified in symptomatic carriers have the property of interfering the trimer-dependent activation cascade of HTRA1.

Keywords: heritability, vascular dementia, mutations, HTRA1, carriers, CARASIL

INTRODUCTION

Loss-of-function mutations in the *high-temperature requirement A serine peptidase 1* (*HTRA1*) gene cause cerebral autosomal recessive arteriopathy with subcortical infarcts and leukoencephalopathy (CARASIL) (1, 2). HTRA1 is a serine protease that forms a homotrimer. The sensor domain of loop 3 (L3) and the activation domain of loop D (LD) play essential roles in trimer-mediated activation of the neighboring HTRA1 (3, 4).

Recently, symptomatic carriers have been reported for several *HTRA1* mutant alleles (5–9). We analyzed four *HTRA1* alleles identified in symptomatic carriers and found that the proteins inhibited WT protease activity (6). In contrast, two of three missense HTRA1s observed only in CARASIL patients did not inhibit WT protease activity. Therefore, we proposed that the missense HTRA1s identified in symptomatic carriers have unique molecular characteristics (6). However, these characteristics have not been evaluated in other missense HTRA1s identified in symptomatic carriers or in homozygous CARASIL patients. The prediction of the pathogenicity of HTRA1 mutation in carriers is important to relatives of homozygous CARASIL patients, and carriers for variant *HTRA1* alleles. In this study, we have evaluated an additional 15 missense HTRA1 mutants identified in symptomatic carriers and CARASIL patients.

METHODS

Mutation Selection

From a literature search performed up to December 2017, we retrieved 12 missense *HTRA1* alleles identified in symptomatic carriers: S121R, A123S, R133G, R166C, R166L, A173P, S284G, S284R, P285Q, F286V, G295R, and D450H; and 3 missense *HTRA1* alleles reported only in CARASIL patients: A173T, A321T, and L364P (5, 8–12). Clinical characteristics of the symptomatic carriers are summarized in **Supplemental Table 1**. This study was approved by the Niigata University institutional review board.

Measurement of HTRA1 Protease Activity

An expression plasmid for each variant *HTRA1* cDNA was generated using the GENEART® Site-Directed Mutagenesis System (Invitrogen, Carlsbad, CA). The WT-*HTRA1* cDNA tagged with a C-terminal myc-His₆ was subcloned into the pcDNA 3.1 vector (Invitrogen) was the substrate for mutagenesis. The concentration of each plasmid was measured using the Quant-iT™ PicoGreen dsDNA Assay Kit (Thermo Fisher

Scientific, Waltham, MA, USA). The *HTRA1* cDNA plasmid vectors were transfected into FreeStyle 293 cells (Thermo Fisher Scientific) and incubated for 72 h. After incubation, secreted HTRA1 protein was purified from the culture medium using a HisTrap FF crude column (GE Healthcare, Cleveland, OH, USA). The concentration of recombinant HTRA1 proteins was

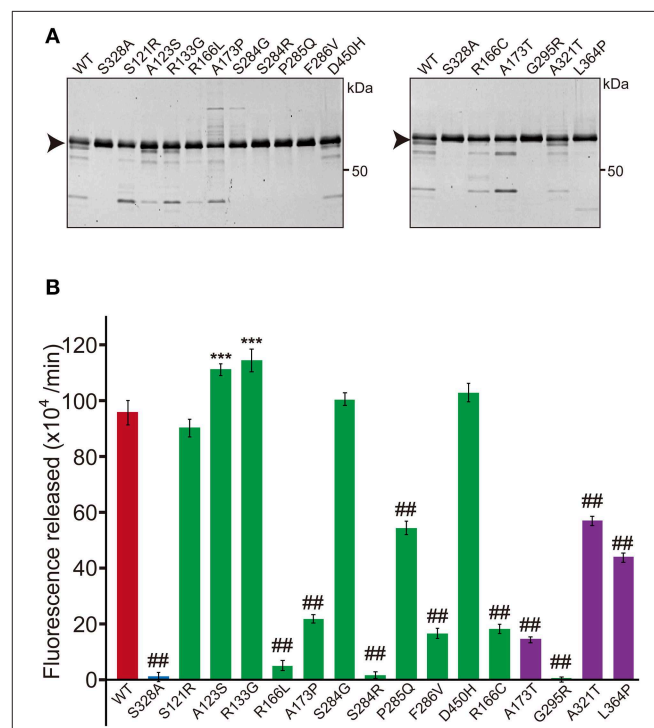


FIGURE 1 | Protease activity of missense HTRA1s identified in symptomatic carriers. **(A)** SDS-PAGE of WT and missense mutant HTRA1 proteins used in the protease assay. Black arrows indicate the full-length band of HTRA1 tagged with myc-His₆. **(B)** Protease activities of missense HTRA1s identified in symptomatic carriers and CARASIL patients. Activities were calculated from the slope of the linear portion of the normalized fluorescence vs. time (30, 60, 90 min) plots. Mean values from 3 independent experiments are shown. Red and blue bars indicate protease activities of WT and S328A, the positive and negative controls, respectively. Green bars indicate protease activities of missense HTRA1s identified in symptomatic carriers. Purple bars indicate protease activities of missense HTRA1s identified only in CARASIL patients. I-bars indicate standard errors (SE). Statistical comparisons of protease activities between WT and each missense HTRA1 protein were performed with one-way analysis of variance followed by the Dunnett's *post hoc* test. *** $P < 0.0001$ for protease activities of each HTRA1 relative to WT. ## $P < 0.0001$ for protease activities of HTRA1 relative to WT.

measured using a Bicinchoninic Acid (BCA) Protein Assay Kit (Wako, Osaka, Japan). After pre-incubating 1 μ g of the recombinant HTRA1 protein, protease activities were evaluated at 37°C using fluorescein isothiocyanate (FITC)-labeled casein as a substrate (Fluorescent Protease Assay Kit; Pierce, Rockford, IL, USA) (2, 6). WT was used as the positive control and S328A, which is deficient in protease activity, was used as the negative control. Fluorescence was measured using a FilterMax F5 Multi-Mode Microplate Reader (Molecular Devices, Sunnyvale, CA, USA). Protease activities were calculated from the slope of the linear portion of the normalized fluorescence vs. time plots at 30, 60, and 90 min using MATLAB® R2017b (9.3.0.713579). The amount of each HTRA1 protein was analyzed by sodium dodecyl sulfate polyacrylamide gel electrophoresis (SDS-PAGE), stained by SYPRO® Ruby Protein Gel Stain (Thermo Fisher Scientific). Five mutations, S121R, A123S, R133G, S284G, and D450H, were excluded from further analysis because the protease activities of these mutations were normal (**Figure 1B**); two of these five mutations were appeared to be benign (A123S and R133G) (5).

Analysis of Oligomerization of HTRA1 Proteins

Oligomerization was evaluated by size-exclusion chromatography using a Superdex 200 10/300 GL column (GE Healthcare, Chicago, IL, USA) on an AKTA FPLC workstation equilibrated with Tris-buffered saline (100 mM Tris-HCl, pH 8.0 and 150 mM NaCl). After pre-incubation at

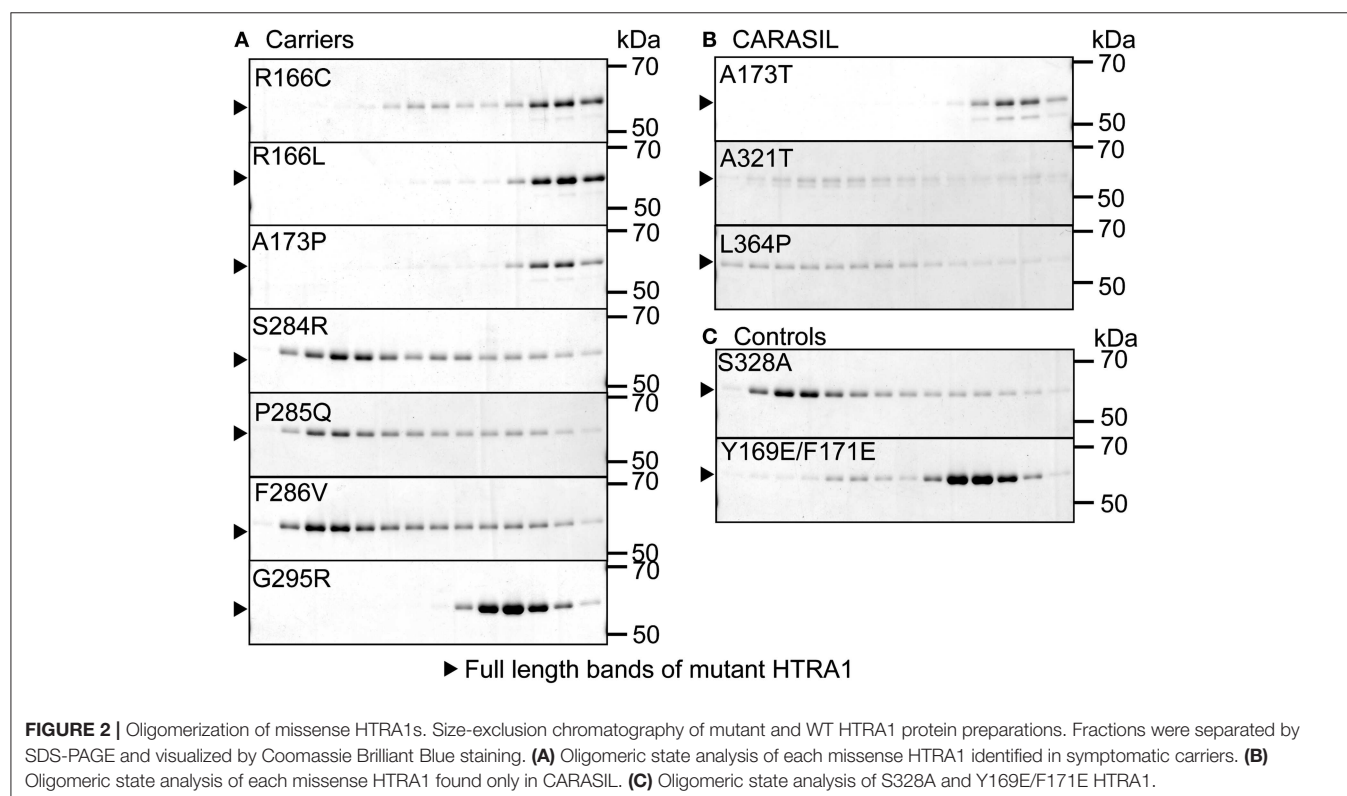
37°C for 30 min, each HTRA1 protein sample was injected at 500 ng/ μ l. Y169E/F171E HTRA1, an artificial, known monomeric HTRA1, was used as the reference monomer and S328A HTRA1 was used as a reference trimer (**Figure 2C**) (4, 6). SDS-PAGE was used to evaluate fractions from size-exclusion chromatography (6).

Evaluation of Dominant-Negative Effects of HTRA1 Mutants on Wild-Type HTRA1

Each *HTRA1* variant vector was cotransfected with an equal amount of WT vector into FreeStyle 293 cells. Purification of the mixed HTRA1 proteins and evaluation of their protease activity were performed as described above. We compared the protease activities of the mixtures of WT with each variant HTRA1 to that of a mixture of WT and S328A, an artificially inactive HTRA1 that forms a trimer with WT and does not have a dominant-negative effect; this was used as a reference to adjust the protein concentration in the reaction mixture (6). The mixtures of G283E with WT and A252T with WT were used as positive and negative controls for dominant-negative effects, respectively (6).

Statistical Analysis

Statistical analyses were performed using R 3.2.2. Groups were compared using one-way analysis of variance (ANOVA) for independent samples, followed by Dunnett's multiple-comparison test when overall *P* was < 0.05. Fisher's exact test was used to compare the frequencies of mutant HTRA1s



with dominant-negative effect between symptomatic carriers and CARASIL.

RESULTS

Oligomerization of Missense HTRA1 Mutant Proteins

Five missense HTRA1s (S121R, A123S, R133G, S284G, and D450H) showed normal protease activity, thus we excluded these HTRA1s from further analysis (**Figures 1A,B**). Protease activities of other HTRA1s were significantly decreased relative to WT activity. We assayed trimerization of the other HTRA1s and found that four hetero-HTRA1s (R166C, R166L, A173P, and G295R) and one CARASIL-HTRA1 (A173T) were unable to form trimers (**Figures 2A,B**). Among mutant HTRA1s form trimers, all hetero-HTRA1s had mutations in the LD domain (residues 284–290) or L3 loop domain, (residues 301–314) while two CARASIL-HTRA1s had mutations in the protease domain (residues 204–356) (**Table 1**).

Inhibition of WT Protease Activity

Next we investigated whether these missense HTRA1s have dominant-negative. To serve as a control for this assay,

the half dose of WT was not suitable because protein and substrate concentrations in the reaction mixture differ from those expressing WT and each mutant HTRA1 (6). Therefore, we used a mixture of WT and S328A, an artificial inactive HTRA1 that trimerizes, as a control (3, 4) and compared the protease activities of the mixtures of WT and each mutant HTRA1 with that of the control. dominant-negative was then defined as a protease activity less than that of the control. Four of six hetero-HTRA1s and one of four CARASIL-HTRA1 showed dominant-negative (**Figure 3** and **Supplemental Figure 1**).

Molecular Characteristics of Missense HTRA1 Mutant Proteins in Symptomatic Carriers

The results showed the possibility that the HTRA1 mutant proteins identified in the symptomatic carriers cannot form trimers or have mutations in the LD or L3 domain. Therefore, we examined the frequency of mutant HTRA1s with these characteristics between missense mutations identified in symptomatic carriers and only in CARASIL. Combined with our previous results, all missense HTRA1s identified in symptomatic carriers were defective in trimerization or had mutations in

TABLE 1 | Summary information of previously-reported *HTRA1* mutations identified in symptomatic carriers and CARASIL patients.

	Amino acid substitution	Location (Domain)	Trimerization	Dominant-negative	References
Reported in symptomatic carriers hetero-HTRA1s	R166L	Other	Defective	+	(5)
	R166C	Other	Defective	–	(8)
	A173P	Other	Defective	+	(5)
	G283E*	Protease	Defective	+	(6)
	G295R	Protease	Defective	+	(9)
	T319I*	Protease	Defective	+	(6)
	S284R	LD	Trimer	+	(5)
	P285L*	LD	Trimer	+	(6)
	P285Q	LD	Trimer	–	(5)
	F286V	LD	Trimer	–	(5)
	R302Q*	L3	Trimer	+	(6)
	<i>R302X</i>	L3	u.d.	u.d.	(7)
	A173T	Other	Defective	+	(12)
	R274Q*	Protease	Defective	+	(6)
Reported only in CARASIL CARASIL-HTRA1s	A252T*	Protease	Trimer	–	(6)
	V297M*	Protease	Trimer	–	(6)
	A321T	Protease	Trimer	–	(11)
	L364P	Protease	Trimer	–	(10)
	<i>E42Dfs</i>	IGFBP	u.d.	u.d.	(11)
	<i>G56Afs</i>	IGFBP	u.d.	u.d.	(13)
	<i>K168X</i>	Other	u.d.	u.d.	(14)
	<i>E247Rfs</i>	Protease	u.d.	u.d.	(14)
	<i>E277Vfs</i>	Protease	u.d.	u.d.	(14)
	<i>R370X</i>	Protease	u.d.	u.d.	(2)

Asterisks: mutant HTRA1s evaluated in our previous report (6). Bold font: mutant HTRA1s analyzed in this study. Italics: frameshift or non-sense mutations. IGFBP, insulin-like growth factor binding protein domain. Protease, protease domain outside the LD or L3 domain. LD, loop D domain; L3, loop 3 domain. u.d., undetermined. The mRNA of these mutants was degraded. +, present and –, absent.

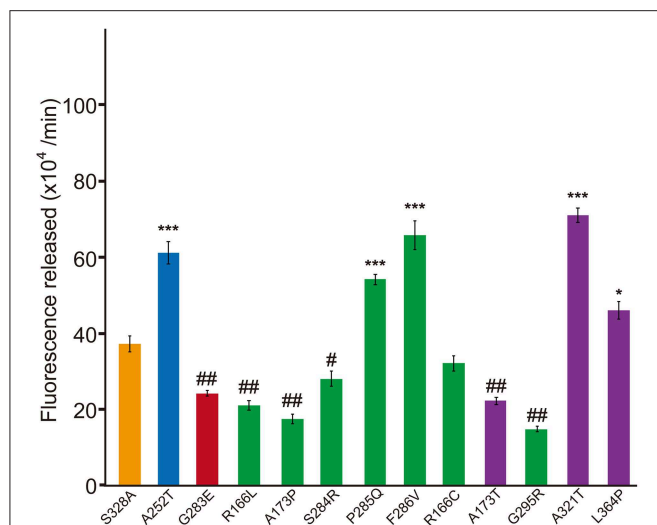


FIGURE 3 | Dominant-negative effects of missense HTRA1s identified in symptomatic carriers. Protease activities of mixtures of each missense HTRA1 with WT calculated from the slope of the linear portion of normalized fluorescence vs. time (30, 60, and 90 min) plots. Orange, S328A/WT, a positive control for a dominant-negative effect. Blue and red bars indicate protease activities of A252T/WT and G283E/WT, respectively, negative and positive controls for dominant-negative effect, respectively. Green bars, missense HTRA1s identified in symptomatic carriers. Purple bars, missense HTRA1s found only in CARASIL patients. I-bars indicate standard errors (SE). Statistical comparisons of protease activities between each mutant HTRA1/WT and S328A/WT were performed with one-way analysis of variance followed by Dunnett's *post hoc* test. *** $P < 0.0001$; * $P < 0.05$ for increases in protease activities for each HTRA1/WT relative to S328A/WT. ## $P < 0.0001$; # $p < 0.05$ for differences for HTRA1/WT mixtures relative to S328A/WT.

the LD or L3 domain, but only two of six missense HTRA1s found only in CARASIL patients were defective in trimerization and none had mutations in the LD or L3 domain ($P = 0.006$; **Table 1**). In contrast, the frequency of mutant HTRA1s with dominant-negative effects in symptomatic carriers was not significantly higher than that in CARASIL patients (72.7 vs. 33.3%, $P = 0.162$; **Table 1**).

DISCUSSION

In this study, we found that missense HTRA1 mutations identified in symptomatic carriers display two characteristics: defective trimerization or mutations in the LD or L3 domain. We newly identified that four HTRA1 missense mutants identified in symptomatic carriers were defective trimerization (R166C, R166L, A173P, and G295R). We also demonstrated that monomeric HTRA1 inhibits WT protease activity (6). Thus, these mutants have a more deleterious effect on carriers relative to mutants that did not inhibit WT protease activity, resulting in a symptomatic carrier. Although A173T and R274Q were also defective trimerization, no symptomatic carriers with A173T or and R274Q have been identified to date (12, 15), carriers with these mutations should be carefully evaluated for cerebral small vessel disease (CSVD).

Among the other missense HTRA1s observed in the symptomatic carriers, four of the five missense HTRA1s had a mutation in the LD domain. The simulation analysis revealed that these mutations induced an instability in the helical structure of the LD loop (16). For the L3 domain, R302 is the only portion observed in the symptomatic carrier. R302 is essential for inter-monomer communication and substrate binding (16). Thus, a mutation in the LD or L3 domain that interferes with signal transduction between the monomers result in inhibition of the WT activity.

Regarding the molecular pathogenesis in symptomatic carriers, we hypothesized that these mutations inhibit the WT protease activity by interfering with the trimer-dependent activation cascade, resulting in <50% of protease activity in symptomatic carriers (6). However, the data from this study show that not all mutations identified in symptomatic carriers showed <50% of protease activity. Moreover, symptomatic carriers with non-sense or frameshift mutations have also been reported (7, 17). Thus, we consider that the residual HTRA1 protease activity might correlate with the risk for developing CSVD. To elucidate the precise correlation between HTRA1 protease activity and risk of CSVD, we and others must identify and evaluate additional carriers for HTRA1 mutations.

Our study has several limitations. First, protease activity was measured by using casein, a non-physiological substrate. Several substrates, including fibronectin and transforming growth factor-beta binding protein 1 have been reported (18, 19). Thus, results of protease assays may be different if other substrates are used. Second, the pathogenicity of mutations outside the protease domain remains unknown. Several studies have investigated the role of the Kazal-like and PDZ domains in regulating the protease activity of HTRA1s (20–22). The Kazal-like domain has been implicated in autolysis (21), and mutations in this domain could influence its expression. Thus, the possibility that a mutation may decrease the amount of protein *in vivo* by decreasing stability or secretion to the extracellular matrix cannot be excluded.

CONCLUSION

We found that a either a deficiency in trimerization or location of the amino-acid mutation in the LD or L3 domain was highly observed in individual missense HTRA1 alleles in symptomatic carriers. Our findings will have significant utility for improving genetic counseling both for the relatives of CARASIL patients and for carriers with HTRA1 variants with sporadic CSVDs.

DATA AVAILABILITY

The raw data supporting the conclusions of this manuscript will be made available by the authors, without undue reservation, to any qualified researcher.

AUTHOR CONTRIBUTIONS

MU: draft of manuscript, study concept and design, acquisition of data and analysis. HN: revision of manuscript,

interpretation of data, and study supervision. NS, SA, and MK: revision of manuscript and interpretation of data. AK and TK: acquisition of data and interpretation of data. OO: revision of the manuscript, study concept and design, and study supervision.

FUNDING

This study was funded by a grant-in-aid for Scientific Research on Innovative Areas (Brain Protein Aging and Dementia Control; 26117006) from MEXT; a grant-in-aid for Practical Research Project for Rare/Intractable Diseases (17928469) from AMED; a grant-in-aid for Scientific Research (A) (16804840); a grant-in-aid for Medical Research from the Takeda Science Foundation;

and a grant-in-aid for Research on Intractable Diseases from the Japanese Ministry of Health, Labor, and Welfare.

SUPPLEMENTARY MATERIAL

The Supplementary Material for this article can be found online at: <https://www.frontiersin.org/articles/10.3389/fneur.2019.00693/full#supplementary-material>

Supplemental Figure 1 | Mixtures of missense HTRA1 proteins with WT protein. Mixture of each missense HTRA1 and WT protein evaluated by SDS-PAGE stained with SYPRO[®] Ruby. Broken arrows indicate the full-length band of missense HTRA1s tagged with myc-His₆. Arrowheads indicate the full-length band of WT HTRA1 tagged with His₆.

Supplemental Table 1 | Summary of the clinical features of symptomatic heterozygotes with HTRA1 mutations.

REFERENCES

- Fukutake T, Hirayama K. Familial young-adult-onset arteriosclerotic leukoencephalopathy with alopecia and lumbago without arterial hypertension. *Eur Neurol.* (1995) 35:69–79. doi: 10.1159/000117096
- Hara K, Shiga A, Fukutake T, Nozaki H, Miyashita A, Yokoseki A, et al. Association of HTRA1 mutations and familial ischemic cerebral small-vessel disease. *N Engl J Med.* (2009) 360:1729–39. doi: 10.1056/NEJMoa0801560
- Clausen T, Kaiser M, Huber R, Ehrmann M. HTRA proteases: regulated proteolysis in protein quality control. *Nat Rev Mol Cell Biol.* (2011) 12:152–62. doi: 10.1038/nrm3065
- Truebestein L, Tennstaedt A, Monig T, Krojer T, Canellas F, Kaiser M, et al. Substrate-induced remodeling of the active site regulates human HTRA1 activity. *Nat Struct Mol Biol.* (2011) 18:386–8. doi: 10.1038/nsmb.2013
- Verdura E, Herve D, Scharrer E, Amador Mdel M, Guyant-Marechal L, Philippi A, et al. Heterozygous HTRA1 mutations are associated with autosomal dominant cerebral small vessel disease. *Brain.* (2015) 138:2347–58. doi: 10.1093/brain/awv155
- Nozaki H, Kato T, Nihonmatsu M, Saito Y, Mizuta I, Noda T, et al. Distinct molecular mechanisms of HTRA1 mutants in manifesting heterozygotes with CARASIL. *Neurology.* (2016) 86:1964–74. doi: 10.1212/WNL.0000000000002694
- Tateoka T, Onda H, Hirota K, Kasuya H, Shinohara T, Kinouchi H, et al. Unusual case of cerebral small vessel disease with a heterozygous nonsense mutation in HTRA1. *J Neurol Sci.* (2016) 362:144–6. doi: 10.1016/j.jns.2016.01.037
- Bougea A, Velonakis G, Spantideas N, Anagnostou E, Paraskevas G, Kapaki E, et al. The first Greek case of heterozygous cerebral autosomal recessive arteriopathy with subcortical infarcts and leukoencephalopathy: an atypical clinico-radiological presentation. *Neuroradiol J.* (2017) 30:583–5. doi: 10.1177/1971400917700168
- Di Donato I, Bianchi S, Gallus GN, Cerase A, Taglia I, Pescini F, et al. Heterozygous mutations of HTRA1 gene in patients with familial cerebral small vessel disease. *CNS Neurosci Ther.* (2017) 23:759–65. doi: 10.1111/cns.12722
- Wang XL, Li CF, Guo HW, Cao BZ. A novel mutation in the HTRA1 gene identified in Chinese CARASIL pedigree. *CNS Neurosci Ther.* (2012) 18:867–9. doi: 10.1111/j.1755-5949.2012.00373.x
- Bianchi S, Di Palma C, Gallus GN, Taglia I, Poggiani A, Rosini F, et al. Two novel HTRA1 mutations in a European CARASIL patient. *Neurology.* (2014) 82:898–900. doi: 10.1212/WNL.0000000000000202
- Khaleeli Z, Jaunmuktane Z, Beaufort N, Houlden H, Haffner C, Brandner S, et al. A novel HTRA1 exon 2 mutation causes loss of protease activity in a Pakistani CARASIL patient. *J Neurol.* (2015) 262:1369–72. doi: 10.1007/s00415-015-7769-5
- Cai B, Zeng J, Lin Y, Lin Y, Lin W, Lin W, et al. A frameshift mutation in HTRA1 expands CARASIL syndrome and peripheral small arterial disease to the Chinese population. *Neurol Sci.* (2015) 36:1387–91. doi: 10.1007/s10072-015-2121-5
- Preethish-Kumar V, Nozaki H, Tiwari S, Vengalil S, Bhat M, Prasad C, et al. CARASIL families from India with 3 novel null mutations in the HTRA1 gene. *Neurology.* (2017) 89:2392–4. doi: 10.1212/WNL.0000000000004710
- Nishimoto Y, Shibata M, Nihonmatsu M, Nozaki H, Shiga A, Shirata A, et al. A novel mutation in the HTRA1 gene causes CARASIL without alopecia. *Neurology.* (2011) 76:1353–5. doi: 10.1212/WNL.0b013e318215281d
- Cabrera AC, Melo E, Roth D, Topp A, Delobel F, Stucki C, et al. HtrA1 activation is driven by an allosteric mechanism of inter-monomer communication. *Sci Rep.* (2017) 7:14804. doi: 10.1038/s41598-017-14208-z
- Lee YC, Chung CP, Chao NC, Fuh JL, Chang FC, Soong BW, et al. Characterization of heterozygous HTRA1 mutations in Taiwanese patients with cerebral small vessel disease. *Stroke.* (2018) 49:1593–601. doi: 10.1161/STROKEAHA.118.021283
- Tiaden AN, Richards PJ. The emerging roles of HTRA1 in musculoskeletal disease. *Am J Pathol.* (2013) 182:1482–8. doi: 10.1016/j.ajpath.2013.02.003
- Beaufort N, Scharrer E, Kremmer E, Lux V, Ehrmann M, Huber R, et al. Cerebral small vessel disease-related protease HtrA1 processes latent TGF-beta binding protein 1 and facilitates TGF-beta signaling. *Proc Natl Acad Sci USA.* (2014) 111:16496–501. doi: 10.1073/pnas.1418087111
- Eigenbrot C, Ultsch M, Lipari MT, Moran P, Lin SJ, Ganesan R, et al. Structural and functional analysis of HtrA1 and its subdomains. *Structure.* (2012) 20:1040–50. doi: 10.1016/j.str.2012.03.021
- Risor MW, Poulsen ET, Thomsen LR, Dyrland TF, Nielsen TA, Nielsen NC, et al. The autolysis of human HtrA1 is governed by the redox state of its N-terminal domain. *Biochemistry.* (2014) 53:3851–7. doi: 10.1021/bi401633w
- Poepsel S, Sprengel A, Sacca B, Kaschani F, Kaiser M, Gatsogiannis C, et al. Determinants of amyloid fibril degradation by the PDZ protease HTRA1. *Nat Chem Biol.* (2015) 11:862–9. doi: 10.1038/nchembio.1931

Conflict of Interest Statement: OO has received speaking honoraria from Kyowa Hakko Kirin Co., Ltd., Bristol-Myers Squibb, Ono Pharmaceutical Co., Ltd., Mitsubishi Tanabe Pharm, Takeda, Daiichi-Sankyo, FUJIFILM, SANOFI, and FP-pharm.

The remaining authors declare that the research was conducted in the absence of any commercial or financial relationships that could be construed as a potential conflict of interest.

Copyright © 2019 Uemura, Nozaki, Koyama, Sakai, Ando, Kanazawa, Kato and Onodera. This is an open-access article distributed under the terms of the Creative Commons Attribution License (CC BY). The use, distribution or reproduction in other forums is permitted, provided the original author(s) and the copyright owner(s) are credited and that the original publication in this journal is cited, in accordance with accepted academic practice. No use, distribution or reproduction is permitted which does not comply with these terms.



Effects of Isosorbide Mononitrate and/or Cilostazol on Hematological Markers, Platelet Function, and Hemodynamics in Patients With Lacunar Ischaemic Stroke: Safety Data From the Lacunar Intervention-1 (LACI-1) Trial

OPEN ACCESS

Edited by:

Andreas Charidimou,
Massachusetts General Hospital,
Harvard Medical School,
United States

Reviewed by:

Vincent Chung Tong Mok,
The Chinese University of
Hong Kong, China
Joan Marti Fabregas,
Hospital de la Santa Creu i Sant
Pau, Spain

*Correspondence:

Joanna M. Wardlaw
joanna.wardlaw@ed.ac.uk

† These authors have contributed
equally to this work

Specialty section:

This article was submitted to
Stroke,
a section of the journal
Frontiers in Neurology

Received: 08 April 2019

Accepted: 18 June 2019

Published: 03 July 2019

Citation:

Appleton JP, Blair GW, Flaherty K,
Law ZK, May J, Woodhouse LJ,
Doubal F, Sprigg N, Bath PM and
Wardlaw JM (2019) Effects of
Isosorbide Mononitrate and/or
Cilostazol on Hematological Markers,
Platelet Function, and Hemodynamics
in Patients With Lacunar Ischaemic
Stroke: Safety Data From the Lacunar
Intervention-1 (LACI-1) Trial.
Front. Neurol. 10:723.
doi: 10.3389/fneur.2019.00723

Jason P. Appleton^{1,2†}, Gordon W. Blair^{3,4,5†}, Katie Flaherty¹, Zhe Kang Law^{1,2,6}, Jane May¹,
Lisa J. Woodhouse¹, Fergus Doubal^{3,4,5}, Nikola Sprigg^{1,2}, Philip M. Bath^{1,2†} and
Joanna M. Wardlaw^{3,4,5*†}

¹ Stroke Trials Unit, Division of Clinical Neuroscience, University of Nottingham, Nottingham, United Kingdom, ² Stroke, Nottingham University Hospitals NHS Trust, Nottingham, United Kingdom, ³ Brain Research Imaging Centre, Centre for Clinical Brain Sciences, University of Edinburgh, Edinburgh, United Kingdom, ⁴ Edinburgh Dementia Research Centre in the UK Dementia Research Initiative, Edinburgh, United Kingdom, ⁵ Edinburgh Imaging, University of Edinburgh, Edinburgh, United Kingdom, ⁶ Department of Medicine, National University of Malaysia, Kuala Lumpur, Malaysia

Background: Cilostazol and isosorbide mononitrate (ISMN) are candidate treatments for cerebral small vessel disease and lacunar ischaemic stroke. As both drugs may influence hemoglobin and platelet count, and hemodynamics, we sought to assess their effects in the lacunar intervention-1 (LACI-1) trial.

Methods: Fifty-seven lacunar ischaemic stroke patients were randomized to immediate ISMN, cilostazol, or their combination for 9 weeks in addition to guideline stroke prevention. A fourth group received both drugs with a delayed start. Full blood count, platelet function, peripheral blood pressure (BP), heart rate and central hemodynamics (Augmentation index, Buckberg index) were measured at baseline, and weeks 3 and 8. Differences were assessed by multiple linear regression adjusted for baseline and key prognostic variables. Registration ISRCTN 12580546.

Results: At week 8, platelet count was higher with cilostazol vs. no cilostazol (mean difference, MD 35.73, 95% confidence intervals, 95% CI 2.81–68.66, $p = 0.033$), but no significant differences were noted for hemoglobin levels or platelet function. At week 8, BP did not differ between the treatment groups, whilst heart rate was higher in those taking cilostazol vs. no cilostazol (MD 6.42, 95% CI 1.17–11.68, $p = 0.017$). Buckberg index (subendocardial perfusion) was lower in those randomized to cilostazol vs. no cilostazol and in those randomized to both drugs vs. either drug. Whilst ISMN significantly increased unadjusted augmentation index (arterial stiffness, MD 21.19, 95% CI 9.08–33.31, $p = 0.001$), in isolation both drugs non-significantly reduced augmentation index adjusted for heart rate.

Conclusions: Cilostazol increased heart rate and platelet count, and reduced Buckberg index, whilst both drugs may individually reduce arterial stiffness adjusted for heart rate. Neither drug had clinically significant effects on hemoglobin or platelet function over 8 weeks. Further assessment of the safety and efficacy of these medications following lacunar ischaemic stroke is warranted.

Keywords: cilostazol, isosorbide mononitrate, blood pressure, safety, platelets, lacunar stroke, randomized clinical trial

INTRODUCTION

Cerebral small vessel disease (SVD) is a common cause of stroke—both “lacunar” ischaemic and haemorrhagic stroke—cognitive impairment and dementia (1). SVD is a disorder of the small perforating arterioles of the brain involving endothelial dysfunction, inflammation (2), and blood-brain barrier breakdown (3). However, there are no specific treatments for either primary or secondary prevention of SVD and its associated clinical manifestations (4). Two medications with potential beneficial mechanisms of action have been highlighted for potential repurposing: cilostazol (a phosphodiesterase 3' inhibitor used in stroke prevention in the Asia-Pacific Region) and isosorbide mononitrate (ISMN, a nitric oxide donor widely used in ischaemic heart disease). Little is known about the safety and efficacy of these drugs in SVD, particularly in combination, and yet their effects may be synergistic (4). As a mild antiplatelet, cilostazol can cause bleeding sufficient to result in anemia. Further, cilostazol can rarely cause thrombocythaemia (5). Both drugs can lower peripheral blood pressure (BP) and increase heart rate (5, 6), but data regarding their effects on central hemodynamics following ischaemic lacunar stroke are lacking.

The Lacunar Intervention Trial-1 (LACI-1) tested cilostazol and ISMN, alone and in combination, for tolerability in patients with prior lacunar ischaemic stroke (7). Overall, the medications were well-tolerated by participants (8). As both drugs may influence platelet count and hemoglobin level in addition to hemodynamics, we sought to assess these important safety outcomes.

METHODS

Population

LACI-1 was a phase IIa, partial factorial, dose-escalation, prospective, randomized, open-label, blinded endpoint (PROBE) trial. Details regarding the trial protocol and statistical analysis plan are available (7), and the main results have been presented and published (8, 9). In summary, LACI-1 recruited 57 patients from stroke centers in Edinburgh and Nottingham, UK, with clinically confirmed lacunar ischaemic stroke, without dependency and able to consent themselves, and randomized them to one of four groups for 9 weeks: ISMN 25 mg twice daily; cilostazol 100 mg twice daily; both ISMN and cilostazol

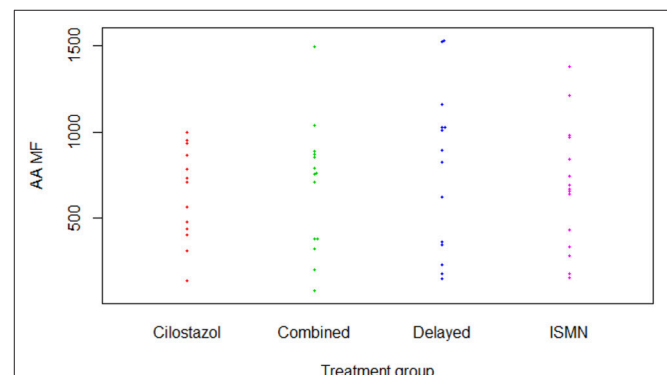


FIGURE 1 | P-selectin surface expression in response to arachidonic acid (Aspirin test). AA, Arachidonic acid; ISMN, isosorbide mononitrate; MF, median fluorescence.

started immediately; or both medications with a 3-week delayed start, thus providing a drug-free control period (see **Figure 1** in main paper) (8). Patients were contacted on alternate weeks to enquire about symptoms (headache, nausea, diarrhea, vomiting, and bleeding) using a structured questionnaire. All patients continued to take guideline secondary stroke prevention medications including statins and antihypertensive treatment where appropriate. Hematology and haemodynamic measures were assessed blind to treatment allocation.

All patients provided written informed consent. LACI-1 was approved by the Scotland A Research Ethics Committee (15/SS/0154) and registered (ISRCTN 12580546).

Hematology and Platelet Function Testing

Full blood counts were taken at baseline, and at weeks 3 and 8: hemoglobin (g/L); and platelet count ($\times 10^9/L$). Platelet function was assessed with measurement of surface expression of P-selectin (CD63P) using kits sensitive to aspirin (arachidonic acid) or clopidogrel (adenosine diphosphate) at the same timepoints (10). An unstimulated sample provided baseline expression data at each timepoint. Median fluorescence (MF) was recorded for platelet surface expression of P-selectin for each sample using flow cytometry. Platelet P-selectin expression was chosen since blood samples can be obtained and fixed at multiple clinical sites then transported for measurement at a central core laboratory.

Haemodynamic Measures

Hemodynamics were measured at baseline and at weeks 3 and 8. Peripheral blood pressure (BP, mmHg) and heart rate (bpm)

Abbreviations: Bpm, beats per minute; BP, blood pressure; CI, confidence interval; FBC, full blood count; ISMN, isosorbide mononitrate; MD, mean difference; SVD, small vessel disease.

TABLE 1 | Baseline characteristics of LACI-1 participants.

	All	Both delayed	ISMN	Cilostazol	Both immediate
Patients	57	15	15	13	14
Age (years)*	66.1 (11.1)	63.4 (11.5)	62.2 (11.0)	75.8 (8.7)	64.4 (8.1)
Sex, female	18 (31.6%)	6 (40.0%)	4 (26.7%)	5 (38.5%)	3 (21.4%)
Onset to randomization (days)	202.6 (256.2)	153.3 (180.4)	137.5 (214.2)	279.2 (324.7)	254.0 (290.7)
Systolic BP (mmHg)	147.3 (20.5)	141.8 (19.6)	150.9 (19.0)	146.1 (21.3)	150.4 (22.9)
Diastolic BP (mmHg)	83.3 (12.6)	82.9 (14.3)	86.6 (11.5)	79.3 (12.0)	83.7 (12.6)
Past medical history (%)					
Treated hypertension	42 (73.7%)	11 (73.3%)	11 (73.3%)	12 (92.3%)	8 (57.1%)
Treated hyperlipidaemia	48 (84.2%)	11 (73.3%)	12 (80.0%)	13 (100.0%)	12 (85.7%)
Diabetes	11 (19.3%)	3 (20.0%)	3 (20.0%)	2 (15.4%)	3 (21.4%)
Atrial fibrillation	0	0	0	0	0
Myocardial infarction	1 (1.8%)	1 (6.7%)	0	0	0
Previous stroke	6 (10.5%)	1 (6.7%)	2 (13.3%)	1 (7.7%)	2 (14.3%)
Smoking	26 (45.6%)	10 (66.7%)	6 (40.0%)	6 (46.2%)	4 (28.6%)
Patient status					
mRS, baseline [6]	1.0 [0.0, 1.0]	1.0 [0.0, 2.0]	1.0 [1.0, 1.0]	1.0 [1.0, 1.0]	1.0 [0.0, 1.0]
Current NIHSS [42]	0.0 [0.0, 1.0]	0.0 [0.0, 1.0]	0.0 [0.0, 1.0]	0.0 [0.0, 1.0]	0.5 [0.0, 1.0]

BP, blood pressure; ISMN, isosorbide mononitrate; mRS, modified Rankin Scale; NIHSS, National Institute of Health Stroke Scale.

*Significant difference between the treatment groups ($p < 0.05$), comparisons done and Kruskal-Wallis tests.

were measured three times sitting and three times standing at each visit using a validated monitor. Central hemodynamics were measured in duplicate using the SphygmoCor device at the same timepoints: mean arterial pressure (MAP); Augmentation index (%)—a measure of arterial stiffness; Buckberg index (%)—a measure of subendocardial perfusion; and pulse wave velocity (m/s)—a measure of arterial stiffness, assessed using non-invasive tonometry measurements taken at the radial and carotid arteries.

Sample Size and Statistics

The sample size calculation for LACI-1 was based on the ability to detect a difference of 90 vs. 55% (i.e., an absolute difference of 35%) between those reaching target dose on one drug vs. both drugs. For 80% power, significance 0.05, a sample size of 55 was needed.

Data are number (%), mean (standard deviation, SD), and median [interquartile quartiles, IQR]. Baseline differences between treatment groups were assessed using chi-square and Kruskal-Wallis tests. Differences in hemodynamics and hematological measures were assessed by multiple linear regression, adjusted for baseline values, age, SVD imaging score and time to randomization. Haemodynamic measures were also adjusted for baseline systolic BP. As heart rate can lead to spurious results, Augmentation index (%) was measured unadjusted and normalized to heart rate 75 bpm as is standard practice. The resultant mean difference (MD) with 95% confidence intervals (CI) are presented with significance set at $p < 0.05$. Analyses were performed using SAS.

RESULTS

In total, 57 patients were recruited at mean 203 [median 256] days after their index stroke with a mean age of 66 (11) years

and 18 (32%) were female (Table 1). Most participants (97%) were on clopidogrel for stroke secondary prevention (guideline therapy in the UK), the remainder on aspirin. Apart from the cilostazol group being slightly older, baseline characteristics were well-balanced across the treatment groups. One participant in the delayed start group withdrew during follow-up.

Hematology and Platelet Function Testing

There were no differences in hemoglobin at week 8 between treatment groups (Table 2). Platelet count was slightly higher in those on cilostazol $286.8 \times 10^9/L$ vs. no cilostazol $249.1 \times 10^9/L$ (MD 35.73, 95% CI 2.81 to 68.66, $p = 0.033$). No differences were noted in platelet function between treatment groups in aspirin or clopidogrel tests (Figures 1, 2). There was no difference in bruising or bleeding with either medication in isolation or combination during the study.

Hemodynamics

Full haemodynamic data were available for 56 participants. Baseline peripheral BP and heart rate did not differ between treatment groups (Table 1). At week 8, BP did not significantly differ between the treatment groups, whilst heart rate was significantly higher in those taking cilostazol 82.8 bpm vs. no cilostazol 74.5 bpm (MD 6.42, 95% CI 1.17 to 11.68, $p = 0.017$, Table 3). Central MAP did not differ between treatment groups at week 8. Buckberg index (subendocardial perfusion) was reduced in those randomized to cilostazol 142.2% vs. no cilostazol 160.7% (MD -10.81 , 95% CI -21.15 to -0.47 , $p = 0.040$) and in those randomized to both drugs 148.9% vs. either drug 159.9% (MD -11.37 , 95% CI -21.01 to -1.72 , $p = 0.021$). Unadjusted Augmentation index was significantly higher (i.e., increased arterial stiffness) in those randomized to ISMN 123.8% vs. no ISMN 119.8% (MD 21.19, 95% CI 9.08 to 33.31, $p = 0.001$).

TABLE 2 | Hematology and platelet function testing at week 8 by treatment group.

Week 8	Both delayed N = 14	ISMN N = 15	Cilostazol N = 13	Both immediate N = 14	Cilostazol vs. none (2 + 3 vs. 1 + 4*)	ISMN vs. none (1 + 3 vs. 2 + 4*)	Cil + ISMN vs. one or other (3 + 4 vs. 1 + 2)
Full blood count, adjusted for baseline	Week 3 (4*)	Week 8 (4)	Week 8 (1)	Week 8 (2)	Week 8 (3)	MD (95% CI)	p-value
Hemoglobin (g/L), mean (SD)	133.0 (12.2)	136.2 (13.5)	145.9 (12.0)	130.8 (9.5)	137.1 (14.6)	−3.7 (−8.4, 1.0)	0.12
Platelet count ($\times 10^9/L$), mean (SD)	260.3 (47.1)	258.4 (56.1)	238.6 (45.5)	289.5 (61.4)	284.3 (57.8)	35.7 (2.8, 68.7)	0.033
Platelet function, adjusted for baseline							
Unstimulated median fluorescence, mean (SD)	87.0 (29.0)	80.4 (29.1)	86.1 (29.0)	75.9 (27.3)	83.7 (33.8)	−2.9 (−15.1, 9.3)	0.64
AA median fluorescence, mean (SD)	741.0 (395.0)	775.4 (474.4)	675.2 (364.1)	636.4 (272.4)	679.6 (376.6)	−83.6 (−256.5, 89.4)	0.34
ADP median fluorescence, mean (SD)	519.3 (234.5)	502.1 (242.8)	454.9 (238.8)	518.9 (179.5)	451.7 (176.5)	−1.3 (−77.6, 75.0)	0.97
						−0.5 (−80.1, 79.1)	0.99
						109.7 (−54.0, 273.5)	0.88
						11.9 (−60.2, 84.1)	0.75

AA, arachidonic acid (aspirin test); ADP, adenosine diphosphate (clopidogrel test); CI, confidence intervals; ISMN, isosorbide mononitrate; MD, mean difference; SD, standard deviation.

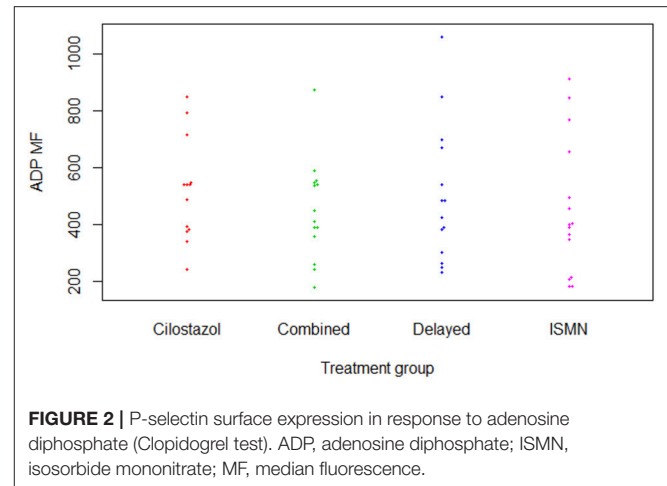


FIGURE 2 | P-selectin surface expression in response to adenosine diphosphate (Clopidogrel test). ADP, adenosine diphosphate; ISMN, isosorbide mononitrate; MF, median fluorescence.

In contrast, when adjusted for heart rate there was a tendency toward lower Augmentation index (i.e., less arterial stiffness) in those randomized to cilostazol 18.7% vs. no cilostazol 20.6% (MD -4.79 , 95% CI -9.72 to 0.15 , $p = 0.057$) and ISMN 16.1% vs. no ISMN 23.5% (MD -4.74 , 95% CI -9.78 to 0.30 , $p = 0.066$). No differences in pulse wave velocity were seen.

DISCUSSION

In this secondary analysis of the LACI-1 trial—the first trial to assess cilostazol and/or ISMN in lacunar ischaemic stroke patients, and the first trial to assess both together in any ischaemic stroke—we have demonstrated that cilostazol and ISMN in isolation and in combination do not influence hemoglobin levels or platelet function in the short-term when given in addition to usual secondary stroke prevention therapy. Platelet count was significantly higher in those randomized to cilostazol. Cilostazol alone and both drugs in combination, reduced Buckberg index (subendocardial perfusion), whilst cilostazol increased heart rate. Both drugs in isolation may reduce arterial stiffness when adjusted for heart rate.

Due to its mild antiplatelet effects, cilostazol can uncommonly ($\geq 1/100$ to $< 1/10$) cause bleeding sufficient to lead to anemia according to the summary of product characteristics (SmPC) (5). Although we have a small population, it is reassuring that hemoglobin was stable between treatment groups during the trial given that all participants were already on guideline antiplatelet therapy. The increase in platelet count seen with cilostazol at 8 weeks needs further investigation, especially since thrombocythaemia, is known to occur rarely ($\geq 1/10,000$ to $< 1/1,000$) (5). The lack of any difference in platelet function between the treatment groups is of further reassurance.

ISMN is known to lower BP and increase heart rate and so can commonly lead to postural dizziness ($\geq 1/100$ to $< 1/10$) and rarely syncope (6). Cilostazol can increase heart rate and, if co-administered with BP-lowering medication, an additive hypotensive effect with reflex tachycardia is reported (5). Neither symptom were apparent across the trial population (8). Importantly, despite cilostazol increasing heart rate in

TABLE 3 | Peripheral and central hemodynamics by treatment group.

	Both delayed N = 14		ISMN N = 15		Cilostazol N = 13		Both immediate N = 14		Cilostazol vs. none (2 + 3 vs. 1 + 4*)		ISMN vs. none (1 + 3 vs. 2 + 4*)		Cil + ISMN vs. one or other (3 + 4 vs. 1 + 2)	
	Week 3 (4*)	Week 8 (4)	Week 8 (1)	Week 8 (2)	Week 8 (3)	Week 8 (3)	Week 8 (3)	Week 8 (3)	MD (95% CI)	p-value	MD (95% CI)	p-value	MD (95% CI)	p-value
Peripheral hemodynamics, adjusted for baseline														
Systolic (mmHg), mean (SD)	134.8 (12.4)	131.4 (19.0)	144.1 (16.5)	146.7 (19.4)	139.9 (20.7)	139.9 (20.7)	139.9 (20.7)	139.9 (20.7)	-1.11 (-8.38, 6.16)	0.765	-1.06 (-8.52, 6.40)	0.780	-4.91 (-11.71, 1.88)	0.156
Diastolic (mmHg), mean (SD)	80.4 (9.7)	78.0 (10.8)	84.9 (7.6)	81.3 (11.2)	79.8 (10.5)	79.8 (10.5)	79.8 (10.5)	79.8 (10.5)	-1.63 (-5.84, 2.58)	0.448	-0.65 (-4.96, 3.66)	0.768	-2.56 (-6.50, 1.38)	0.202
Heart rate, mean (SD)	74.3 (9.3)	79.5 (11.2)	74.7 (12.5)	80.6 (15.0)	84.8 (15.1)	84.8 (15.1)	84.8 (15.1)	84.8 (15.1)	6.42 (1.17, 11.68)	0.017	0.06 (-5.50, 5.62)	0.984	3.13 (-1.93, 8.20)	0.225
Central hemodynamics, adjusted for baseline														
Pulse wave velocity (m/s), mean (SD)	8.4 (1.3)	8.7 (1.4)	8.7 (1.6)	8.6 (1.3)	8.2 (1.3)	8.2 (1.3)	8.2 (1.3)	8.2 (1.3)	-0.34 (-0.99, 0.30)	0.296	-0.14 (-0.84, 0.55)	0.686	0.00 (-0.64, 0.64)	0.996
Augmentation index 75 (%), mean (SD)	24.0 (10.6)	16.2 (12.4)	17.5 (12.9)	23.0 (10.6)	14.7 (10.5)	14.7 (10.5)	14.7 (10.5)	14.7 (10.5)	-4.79 (-9.72, 0.15)	0.057	-4.74 (-9.78, 0.30)	0.066	0.09 (-4.76, 4.94)	0.970
Augmentation index (%), mean (SD)	118.6 (28.3)	123.3 (23.2)	131.1 (16.8)	121.1 (18.9)	133.1 (25.0)	133.1 (25.0)	133.1 (25.0)	133.1 (25.0)	3.46 (-8.65, 15.57)	0.575	21.19 (9.08, 33.31)	0.001	0.97 (-10.77, 12.71)	0.871
Central blood pressure (mmHg), mean (SD)	99.0 (14.6)	95.4 (12.7)	101.2 (12.4)	103.1 (11.8)	98.8 (11.7)	98.8 (11.7)	98.8 (11.7)	98.8 (11.7)	-2.03 (-8.23, 4.17)	0.521	-4.74 (-10.67, 1.19)	0.117	-3.36 (-9.12, 2.40)	0.253
Buckberg index (%), mean (SD)	154.4 (21.5)	164.8 (22.2)	166.6 (25.2)	152.2 (31.4)	132.9 (22.7)	132.9 (22.7)	132.9 (22.7)	132.9 (22.7)	-10.81 (-21.15, -0.47)	0.040	6.75 (-3.59, 17.09)	0.201	-11.37 (-21.01, -1.72)	0.021

CI, confidence intervals; ISMN, isosorbide mononitrate; MD, mean difference; SD, standard deviation. Augmentation index 75: normalized to heart rate 75 bpm.

our population, no significant hypotensive effect was seen in combination with participants' pre-prescribed antihypertensives (74% were on antihypertensives at randomization) or ISMN. Central haemodynamic data regarding cilostazol and/or ISMN in the context of lacunar ischaemic stroke are lacking. Buckberg index is a marker of subendocardial perfusion, which is reduced with increased heart rate (11). Cilostazol and both drugs in combination reduced Buckberg index, which may be due to their underlying effects on heart rate, or may reflect that the patients allocated to cilostazol were older than those in other allocated groups. ISMN was associated with increased Augmentation index (a marker of arterial stiffness) unadjusted for heart rate, but when Augmentation index was adjusted for heart rate, cilostazol and ISMN in isolation both non-significantly reduced arterial stiffness. Given that small vessel stiffness is implicated in the pathophysiology of cerebral SVD (12), medications that reduce arterial stiffness may be of benefit.

The strengths of this LACI-1 substudy include using data from the first randomized controlled trial assessing both cilostazol and ISMN in lacunar ischaemic stroke patients. There are, however, limitations. First, the sample size was small and the study was not powered to look for differences in hematological or haemodynamic secondary outcomes, therefore some findings may represent chance. Second, the treatment duration was relatively short and so we cannot comment on the longer-term effects of these medications on hematological markers or hemodynamics. Third, those who were randomized to cilostazol were older which may explain some of the reported differences in these outcomes. Last, there was no formal control group throughout the trial, rather the delayed start group represented a drug-free control period. This gave the opportunity to establish whether starting one drug first over the other impacted upon side-effects, whilst still providing a control group for the first 3 weeks of the study.

In summary, cilostazol and ISMN were safe in isolation and combination in the short- to medium-term in this small population following lacunar ischaemic stroke. Further data from larger trials are required to establish the longer term effects of these medications on safety and efficacy following lacunar ischaemic stroke. As such, the LACI-2 study is testing their effects on stroke recurrence, cognitive function, imaging features of SVD and safety when given for 12 months in patients with lacunar ischaemic stroke (ISRCTN14911850).

DATA AVAILABILITY

The datasets generated for this study are available on request to the corresponding author.

ETHICS STATEMENT

LACI-1 was approved by the Scotland A Research Ethics Committee (15/SS/0154) and registered (ISRCTN 12580546).

AUTHOR CONTRIBUTIONS

JA: recruitment, data collection, analysis, and manuscript preparation. GB and ZL: recruitment, data collection, analysis, and manuscript editing. KF and LW: statistical analysis, manuscript preparation, and editing. JM: platelet function testing. FD and NS: study design, supervision, study set up, data collection, SAE adjudication, and manuscript editing. PB: trial conception, design, management, supervision, data collection and analysis, and manuscript editing. JW: trial conception, design, funding, supervision, data collection, analysis, manuscript editing, and overall guarantor.

FUNDING

LACI-1 is funded by the Alzheimer's Society Ref: 252 (AS-PG-14-033). Additional support is provided by the European Union Horizon 2020 project No 666881, SVDs@Target (GB), the Stroke Association Princess Margaret Research Development

Fellowship scheme (GB), the Stroke Association Garfield Weston Foundation Stroke Association Senior Clinical Lectureship (FD), NHS Research Scotland (FD), NHS Lothian Research and Development Office and the Scottish Funding Council through the Scottish Imaging Network, A Platform for Scientific Excellence (SINAPSE) Collaboration. Funding is gratefully acknowledged from the Foundation Leducq (ref no. 16 CVD 05) and Edinburgh and Lothians Health Foundation. JA and LW are supported, in part, by the National Institutes of Health Research (NIHR) HTA TARDIS and BHF RIGHT-2 trials. ZL and KF are supported, in part, by the NIHR HTA TICH-2 trial. PB is Stroke Association Professor of Stroke Medicine, and is a NIHR Senior Investigator. LACI-1 was adopted by the NIHR CRN.

ACKNOWLEDGMENTS

Data contributing to this manuscript were presented, in part, as posters at the European Stroke Organization Conference (ESOC) in Gothenburg, Sweden May 2018: Appleton et al. (13, 14).

REFERENCES

- Wardlaw JM, Smith C, Dichgans M. Small vessel disease: mechanisms and clinical implications. *Lancet Neurol.* (2019) 18: 684–96. doi: 10.1016/S1474-4422(19)30079-1
- Wiseman S, Marlborough F, Doubal F, Webb DJ, Wardlaw J. Blood markers of coagulation, fibrinolysis, endothelial dysfunction and inflammation in lacunar stroke versus non-lacunar stroke and non-stroke: systematic review and meta-analysis. *Cerebrovasc Dis.* (2014) 37:64–75. doi: 10.1159/000356789
- Wardlaw JM, Makin SJ, Valdés Hernández MC, Armitage PA, Heye AK, Chappell FM, et al. Blood-brain barrier failure as a core mechanism in cerebral small vessel disease and dementia: evidence from a cohort study. *Alzheimer Dement.* (2017) 13:634–43. doi: 10.1016/j.jalz.2016.09.006
- Bath P, Wardlaw J. Pharmacological treatment and prevention of cerebral small vessel disease: a review of potential interventions. *Stroke.* (2015) 46:769–78. doi: 10.1111/ijis.12466
- European Medicines Agency. *Cilostazol—Summary of Product Characteristics.* (2016). Available online at: <https://www.medicines.org.uk/emc/product/3379/smpc> (accessed September 1, 2018).
- SmPC. *Isosorbide Mononitrate—Summary of Product Characteristics.* (2014). Available online at: <https://www.medicines.org.uk/emc/product/6115/smpc> (accessed September 1, 2018).
- Blair GW, Appleton JP, Law ZK, Doubal F, Flaherty K, Dooley R, et al. Preventing cognitive decline and dementia from cerebral small vessel disease: the LACI-1 trial. protocol and statistical analysis plan of a phase IIa dose escalation trial testing tolerability, safety and effect on intermediary endpoints of isosorbide mononitrate and cilostazol, separately and in combination. *Int J Stroke.* (2018) 13:530–8. doi: 10.1177/1747493017731947
- Blair GW, Appleton JP, Flaherty K, Doubal F, Sprigg N, Dooley R, et al. Tolerability, safety and intermediary pharmacological effects of cilostazol and isosorbide mononitrate, alone and combined, in patients with lacunar ischaemic stroke: the LACunar Intervention-1 (LACI-1) trial, a randomised clinical trial. *EclinicalMedicine.* (in press). doi: 10.1016/j.eclinm.2019.04.001
- Blair GW, Appleton JP, Flaherty K, Sprigg N, Doubal F, Boyd J, et al. Preventing cognitive decline and dementia from cerebral small vessel disease: the LACI-1 trial. *Int J Stroke.* (2017) 12 (5 Suppl. 2):15.
- Bath PM, May J, Flaherty K, Woodhouse LJ, Dovlatova N, Fox SC, et al. Remote assessment of platelet function in patients with acute stroke or transient ischaemic attack. *Stroke Res Treat.* (2017) 2017:7365684. doi: 10.1155/2017/7365684
- Buckberg GD, Fixler DE, Archie JP, Hoffman JL. Experimental subendocardial ischemia in dogs with normal coronary arteries. *Circ Res.* (1972) 30:67–81. doi: 10.1161/01.RES.30.1.67
- Del Bene A, Makin SD, Doubal FN, Wardlaw JM. Do risk factors for lacunar ischaemic stroke vary with the location or appearance of the lacunar infarct? *Cerebrovasc Dis.* (2012) 33:21.
- Appleton JP, Flaherty K, Blair GW, Law ZK, Doubal F, Sprigg N, et al. Platelet and haemoglobin levels in patients on isosorbide mononitrate and/or cilostazol with lacunar ischaemic stroke: data from the LACI-1 trial. *Eur Stroke J.* (2018) 3:488–9.
- Appleton JP, Blair GW, Flaherty K, Law ZK, Doubal F, Sprigg N, et al. Peripheral and central haemodynamics in patients on isosorbide mononitrate and/or cilostazol with lacunar ischaemic stroke: data from the LACI-1 trial. *Eur Stroke J.* (2018) 3:489.

Conflict of Interest Statement: The authors declare that the research was conducted in the absence of any commercial or financial relationships that could be construed as a potential conflict of interest.

Copyright © 2019 Appleton, Blair, Flaherty, Law, May, Woodhouse, Doubal, Sprigg, Bath and Wardlaw. This is an open-access article distributed under the terms of the Creative Commons Attribution License (CC BY). The use, distribution or reproduction in other forums is permitted, provided the original author(s) and the copyright owner(s) are credited and that the original publication in this journal is cited, in accordance with accepted academic practice. No use, distribution or reproduction is permitted which does not comply with these terms.



Alteration of the Cortex Shape as a Proxy of White Matter Swelling in Severe Cerebral Small Vessel Disease

François De Guio^{1,2}, David Germanaud^{3,4,5†}, Julien Lefèvre^{6†}, Clara Fischer⁷, Jean-François Mangin⁷, Hugues Chabriat^{1,2,8} and Eric Jouvent^{1,2,8*}

¹ Université Paris Diderot, UMR-S 1161 INSERM, Paris, France, ² DHU NeuroVasc Sorbonne Paris Cité, Paris, France, ³ Université de Paris, Inserm, NeuroDiderot, inDev Team, Paris, France, ⁴ CEA, NeuroSpin, UNIACT, Gif-sur-Yvette, France, ⁵ AP-HP, Hôpital Robert-Debré, Service de Neurologie Pédiatrique et des Maladies métaboliques, Paris, France, ⁶ Institut de Neurosciences de la Timone, CNRS UMR7289, Aix-Marseille University, Marseille, France, ⁷ UNATI, NeuroSpin, I2BM/DSV, CEA, Paris Saclay University, Paris, France, ⁸ AP-HP, Lariboisière Hospital, Department of Neurology, Paris, France

OPEN ACCESS

Edited by:

Hugh Markus,
University of Cambridge,
United Kingdom

Reviewed by:

Muhib Khan,
Michigan State University,
United States
Suyash P. Awate,
Indian Institute of Technology Bombay,
India

*Correspondence:

Eric Jouvent
eric.jouvent@aphp.fr

[†]These authors have contributed
equally to this work

Specialty section:

This article was submitted to
Stroke,
a section of the journal
Frontiers in Neurology

Received: 15 December 2018

Accepted: 27 June 2019

Published: 10 July 2019

Citation:

De Guio F, Germanaud D, Lefèvre J, Fischer C, Mangin J-F, Chabriat H and Jouvent E (2019) Alteration of the Cortex Shape as a Proxy of White Matter Swelling in Severe Cerebral Small Vessel Disease. *Front. Neurol.* 10:753. doi: 10.3389/fneur.2019.00753

CADASIL is a monogenic small vessel disease characterized by the accumulation of brain tissue lesions of microvascular origin leading to strokes and cognitive deficits. Both cortical and parenchymal alterations have been described using various MRI markers. However, relationships between cortical and subcortical alterations remain largely unexplored. While brain atrophy is a preponderant feature in cerebral small vessel disease, recent results in CADASIL suggest slightly larger brain volumes and increased white matter water content at early stages of the disease by comparison to controls. We hypothesized in this study that increased water content in gyral white matter balances expected brain atrophy. Direct white matter volume computation is challenging in these patients given widespread subcortical alterations. Instead, our approach was that a gyral white matter swelling would translate into a modification of the shape of cortical gyri. Our goal was then to assess the relationship between subcortical lesions and possible alteration of the cortex shape. More specifically, aims of this work were to assess 1) morphometric differences of the cortex shape between CADASIL patients and controls 2) the relationship between the cortex shape and the volume of white matter hyperintensities (WMH), a reflect of white matter alterations. Twenty-one patients at the early stage of the disease and 28 age- and sex-matched controls were included. Cortical surfaces were reconstructed from 3D-T1-weighted images. Folding power assessed from spectral analysis of gyrification and cortical morphometry using curvedness and shape index were computed as proxies of the cortex shape. Influence of segmentation errors were evaluated through the simulation of WMH in controls. As a result, patients had larger folding power and curvedness compared to controls. They also presented lower shape indices both related to sulci and gyri. In patients, the volume of WMH was associated with decreased gyral shape index. These results suggest that the cortex shape of CADASIL patients is different compared to controls and that the enlargement of gyri is related to the extent of white matter alterations. The study of the cortex shape might be another way to evaluate subcortical swelling or atrophy in various neurological disorders.

Keywords: cortex, shape, white matter hyperintensities, small vessel disease, CADASIL

INTRODUCTION

CADASIL (Cerebral Autosomal Dominant Arteriopathy with Subcortical Infarcts and Leukoencephalopathy) is a monogenic brain disorder, due to *NOTCH3* mutations, characterized after a normal brain development, by the accumulation of brain tissue lesions of microvascular origin as soon as the 3rd or 4th decade (1). While the accumulation of tissue lesions is usually expected to be associated with the development of brain atrophy in cerebral small vessel disease, we recently observed in patients at early stage of the disease that brain volume did not differ from that of age- and sex-matched healthy individuals (2). We also found with the use of T1 and T2* relaxometry that the white matter water content was presumably increased in patients, particularly in gyral juxtacortical areas (3), which led us to hypothesize that brain volume loss might be absent or masked by an increase of white matter water content (swelling) at the initial stage of the disorder.

Given that tissue lesions accumulate mainly in deep brain areas, while the increase of white matter water content seems to predominate in certain juxtacortical areas, we aimed to determine whether the gyral white matter was actually increased when compared to age- and sex-matched controls. Unfortunately, the gray to white matter tissue contrast may be altered in CADASIL (4) and the segmentation of gyral white matter is hampered by the presence of extensive white matter lesions and the difficulty to distinguish gyral vs. sulcal regions. Hence, a reliable comparison of white matter volume with that of controls is difficult. Another pathway to test the hypothesis of a gyral white matter swelling is to consider the shape of the cortex as a proxy of its underlying white matter, given that the gyrification pattern is sensitive to geometrical and mechanical perturbations (5). In the present study, we hypothesized that a gyral white matter swelling would translate into a modification of the shape of cortical gyri. As schematized in **Figure 1**, the white matter beneath the gyri was supposed to be enlarged, making the cortical gyri more sharpened and wide as constrained by the meningeal envelope and the skull (6).

While these fine shape alterations are out of reach of advanced computational tools such as cortical thickness estimation, gyrification indices or sulcal morphometry previously used in CADASIL (7, 8) (**Figure 1**), it can be captured by using local curvature-based descriptors such as the curvedness and the shape index that have recently emerged and bring additional information on the 3-D cortical morphology (**Figure 2**). For example, as illustrated in **Figure 1**, sulcal depth or sulcal width are thought to be insensitive measures of a gyral white matter swelling by contrast to the curvedness and shape index which are based on the local curvature of the cortical surface. More specifically, both descriptors derived from surrogates of the two local principal curvatures, the curvedness representing the local bending intensity (sharpness), while the shape index describing the local aspect of the surface (from pit to saddle shape). Computation of those metrics has been notably used to quantify morphological changes in the developing brain (9–11). Another new approach is to apply a Fourier-like analysis to the variations of the curvature on a cortical mesh (12). This spectral analysis

of gyrification (SPANGY) provides a frequency analysis of the folding pattern that has been used to quantify morphological changes coming with size variations among healthy adults and between microcephalic patients (13).

Finally, to ensure that these potential cortical alterations are actually secondary to the disease evolution and not due to innate differences with controls, we tested the relationships between cortical metrics and white matter hyperintensities (WMH), a well admitted reflect of white matter alterations in this disorder.

The aims of this work were then to (1) detect subtle morphometric differences between CADASIL patients and age- and sex-matched controls using geometrical and spectral descriptors of the cortex shape (2) if present, to infer the relationship between cortex shape changes in patients and the volume of WMH.

We included in our analysis other factors that may impact the cortex shape to better highlight the independent effect of WMH. Thus, volume of lacunes were computed given their potential role in cortical thinning and on macroscopic cortical abnormalities through secondary cortical neurodegeneration (14, 15). Also, we paid a particular attention to brain tissue segmentation errors that could bias the measurement of curvature-based descriptors. To that purpose, a simulation was performed to generate WMH in cerebral images obtained in the control population as these lesions were supposed to interfere with shape measurements.

MATERIALS AND METHODS

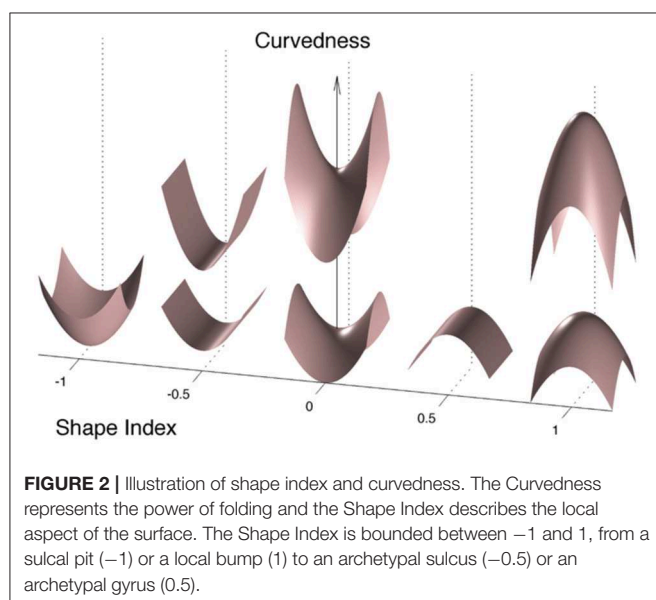
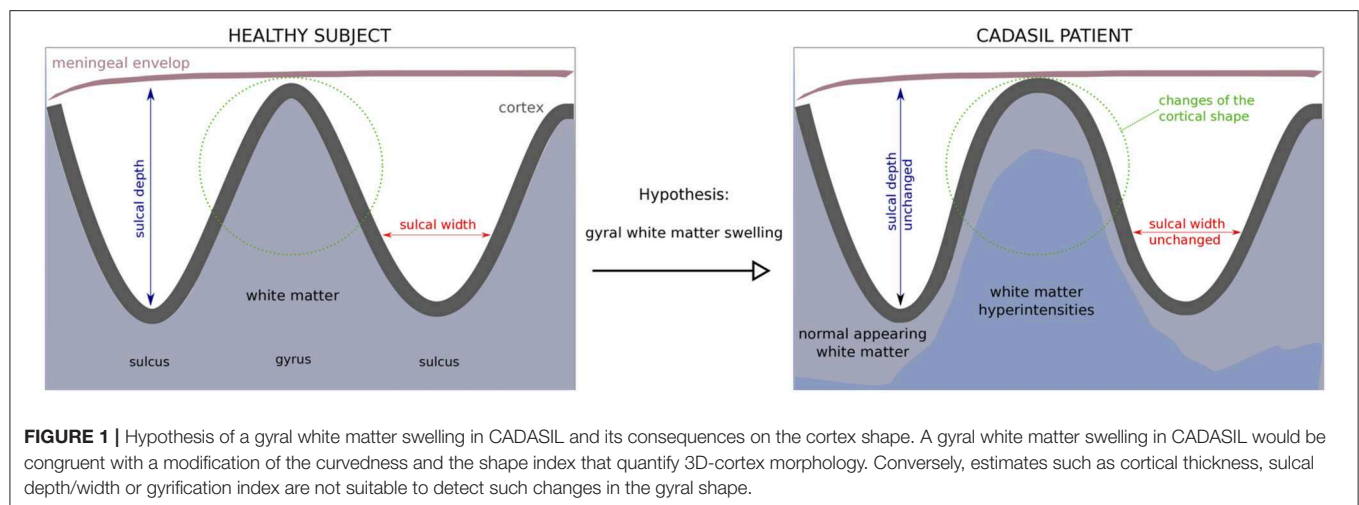
Participants

Non-demented non-disabled (MMSE score ≥ 24 and modified Rankin's scale ≤ 1) adult CADASIL patients at the early clinical stage of the disease were recruited from the CADASIL cohort followed in the National Referral Center for this disorder. Controls were drawn from a local database of healthy volunteers free of any known history of neurological disorder and without symptoms of cognitive impairment or disability as evaluated by a structured interview. Twenty-one patients and 28 controls having good image and cortical surface reconstruction qualities were included in this study.

This study was carried out in accordance with the recommendations of the ethics committee of DRCD (Département de la Recherche Clinique et du Développement) of AP-HP (Assistance Publique-Hôpitaux de Paris) with written informed consent from all subjects. All subjects gave written informed consent in accordance with the Declaration of Helsinki. The protocol was approved by the DRCD of AP-HP.

Magnetic Resonance Imaging Protocol

3D T₁-weighted images used for cortical surface reconstruction were obtained at 3 Tesla with a Tim-Trio MRI scanner (Siemens Healthcare, Erlangen, Germany) equipped with a 12-channel head coil, using a standard sagittal magnetization-prepared rapid acquisition gradient echo (MPRAGE) sequence (in plane resolution: $1 \times 1 \text{ mm}^2$, slice thickness = 1.1 mm, TR = 2,300 ms, TE = 2.98 ms, TI = 900 ms, FA = 9°, BW = 238 Hz/pixel, time of acquisition = 7'45 min). Volumes of lacunes and of WMH of presumed vascular origin were



determined from 3D T1-weighted and FLAIR images obtained within 6 months on a 1.5T Signa scanner (GE Healthcare, Milwaukee, Wisconsin).

Image Processing

The analysis was restricted to the left hemisphere. All subjects were right-handed.

Subcortical Lesion Quantification

Delineation of WMH and of lacunes was performed according to the STRIVE criteria (16). Masks of WMH and of lacunes were obtained for each patient from FLAIR and 3DT1 sequences, respectively. The volume of WMH and of lacunes was determined by multiplying the number of voxels in WMH mask or in lacunes mask by voxel size as previously reported (7).

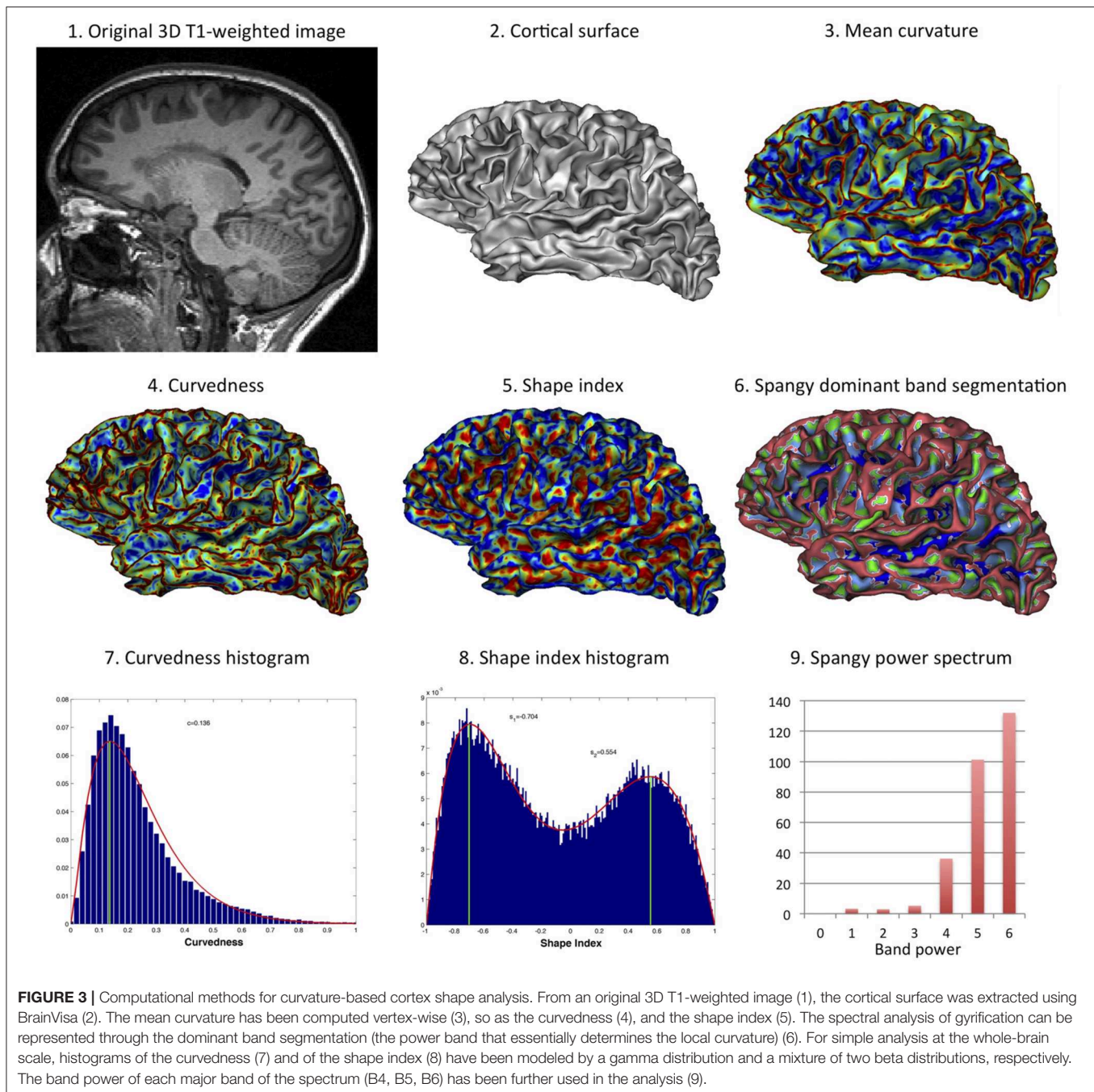
Cortical Surface Reconstruction and Global Morphometry

The Morphologist pipeline of BrainVISA (<http://www.brainvisa.info>) was used to automatically segment the left cortical surfaces (mesh of the gray-white interface) from 3D T1-weighted images (17). In patients, prior to segmentation, masks of WMH were registered to 3D T1-weighted images and, as previously reported (8), voxel intensity inside WMH was set up to an average intensity close to that of normal-appearing white matter to overcome segmentation difficulties possibly induced by WMH in patients. For each subject, BrainVISA was also used to compute the left brain volume BV defined as the sum of gray matter and white matter volumes, the left surface area SA , the hemispheric hull area HA that is the morphological closing of the hemispheric mask, and the total volume inside the hull HV . The global gyrification index (GGI) was defined as the ratio of surface area to hull area ($GGI = SA / HA$) and the spherical gyrification index (SGI) was calculated as the ratio of surface area to the area of a sphere of volume equals to the brain volume ($SGI = SA / 4\pi * (3BV/4\pi)^{2/3}$) (18). The normalized brain volume was computed as the ratio of both hemispheres BV to HV .

Curvature-Based Cortex Shape Analysis

Figure 3 illustrates the various computational methods used for cortex shape analysis.

The spectral analysis of gyrification was performed using the Spangy method (12). Briefly, the method consists in the spectral analysis of the mean curvature spatial variations taken as a proxy of the cortical folding pattern. It achieves a quantitative analysis of cortical folding pattern both in the frequency domain thanks to a band power spectrum and in the image domain where each piece of sulcus is associated with its characteristic frequency band. The analyzed folding power (AFP) is a global characteristic of the hemispheric gyrification, very correlated to the sum of mean curvatures squared. This power is divided into 7 spectral bands with bandwidths of



increasing (doubling) spatial frequency. The 4th, 5th, and 6th bands (B4, B5, and B6 respectively) gather more than 95% of total power and are associated with the variations of curvature related to the sulcal pattern (12). One of the interesting property of this spectrum is that variations in AFP may not divide equally between the 3 sulcal bands: for instance the increase in power that comes with increased brain size mainly add to the high frequency bands (to B6 more than B5 but not to B4) (12, 13).

Curvedness (CVD) and shape index (SI) were computed vertex-wise in each left cortical surface as follows, given the two

principal curvatures k_1 and k_2 :

$$SI = \frac{2}{\pi} \tan^{-1} \frac{k_2 + k_1}{k_2 - k_1}; \quad CVD = \sqrt{\frac{k_2^2 + k_1^2}{2}}$$

The meaning of what shape index and curvedness represent is proposed in **Figure 2**. Curvedness represents the local bending intensity (positive value), while shape index is a scale-invariant value canonically normalized between -1 and $+1$ that describes the local aspect of the surface. Sulci and gyri correspond to a value below -0.5 and above 0.5 , respectively. As previously

described (11), histograms of curvedness and shape index have characteristic shapes that can be summarized at the hemispheric scale by a few parameters (see **Figure 3**). Curvedness distribution was modeled by a gamma distribution from which the peak c was extracted as a global measure of the folding intensity. To obtain a dimensionless parameter as all the gyrification metrics we use otherwise, the normalized curvedness was defined as the product of c and $BV^{1/3}$. The shape index distribution was modeled by a mixture of 2 beta distributions characterized by 2 parameters: the peaks $s1$ and $s2$ which represented the shape modes of sulci and gyri, respectively.

As segmentation errors were recurrent on the medial face of the cortical surface of patients due to periventricular WMH, we defined a lateral face by delineating a curve separating medial and lateral faces using Surfpaint Toolbox (19) in Anatomist (<http://www.brainvisa.info>). The morphometric descriptors of the cortex shape were computed on lateral faces only.

Effect of WMH-Induced Segmentation Errors

As we could not totally exclude that some WMH were not properly masked due to, for example, an imperfect registration between FLAIR and 3D T1-weighted images, we also tested the effect of adding simulated WMH in the white matter of controls as previously done (4). The idea was to differentiate the potential effect of WMH on the cortex shape in the disease from the effect of segmentation errors induced by WMH. To do this, patients were ordered according to their volume of WMH and one patient in two ($N = 11$) were selected. The 11 patients were sex- and age-matched to 11 controls. Then, 3D T1-weighted images of patients were non-linearly co-registered to 3D T1-weighted images of matched controls using FNIRT from FSL (www.fmrib.ox.ac.uk/fsl) (20). The matrix transform was applied to the mask of WMH so that the mask of WMH was registered in the controls space. Finally, mean gray level inside simulated WMH was set up to the mean gray level of the cortex for each subject (i.e., a very unfavorable setting for automatic segmentation algorithms) and gaussian noise was added to simulate a more realistic brain tissue. Thus, the simulation of WMH in the white matter of controls was supposed to produce much more segmentation errors than in the original conditions given that whole WMH of patients were transposed into controls brain, sometimes in regions very close to the cortex. T1-weighted images of controls including simulated WMH were *de novo* processed with BrainVISA to create new cortical surfaces prone to segmentation errors, from which curvedness and shape index were computed again.

Statistical Analyses

Statistical analyses were conducted using the R software (<http://www.r-project.org/>). Between-group comparisons were performed using t -tests or X^2 tests according to variable type and linear regression models including age, gender and brain volume as covariates (**Table 1**). Permutation tests were also used as a non-parametric alternative to compare morphometric outcomes. Finally, linear regression models were used in patients only to

assess the links between morphometric parameters and WMH, independently of age and gender.

To test the effect of segmentation errors on morphometric measurements, we used a Wilcoxon signed-rank test as samples were small ($N = 11$) and paired between one control subject and one control subject with simulated WMH (**Table 2**).

RESULTS

Effect of the Disease on the Cortex Shape

Clinical characteristics of the two groups and results of global measurements, spectral and morphometric analyses of the cortex shape are summarized in **Table 1**. Age and gender did not differ between the 2 groups conversely to educational level. Patients had similar brain volume, normalized brain volume and gyrification indices than healthy individuals, i.e., there was no significant atrophy of the brain parenchyma nor modification in gyrification intensity of the brain cortex (amount of buried cortical surface).

By contrast, the spectral and curvature-based morphometric analyses revealed significant differences between groups using either simple t -tests or linear models to adjust for potential confounders. Patients showed a higher total folding power (AFP) than controls. This increase in power divided up between the three sulcal bands, yet the difference between patient and control was significant only for B5 and B6. This indicates that the cortical folding of CADASIL patients required more high frequency components than the cortex of controls. Consistently, we found an increased curvedness c in patients, reflecting a more bended, sharper folding. The shape index SI brought complementary information: the shape of both sulci and gyri were different as $s1$ and $s2$ were smaller in patients compared to controls. Schematically, sulci were narrower while gyri were widened in patients (**Figure 2**). In terms of estimate accuracy, fitting errors for the gamma distribution of c and the beta distributions of $s1$ and $s2$ were <2 and 0.7% for both groups.

Relationships Between Cortex Shape and the Volume of WMH

To determine whether potential differences in cortex shape were actually related to disease related mechanisms, we tested via a linear model the association between each cortex morphometric descriptor (AFP , c , $s1$, $s2$) and the volume of WMH, independently of age, gender, and other imaging parameters known to alter the cortex in CADASIL, namely the volume of lacune and normalized brain volume. There were no significant associations between AFP , c or $s1$ and the volume of WMH. Gyral shape index descriptor $s2$ was found to decrease with increasing volume of WMH (estimate = -1.79 , std. error = 0.69 , $p = 0.02$).

Influence of Segmentation Errors on the Results

We have simulated WMH in T1-weighted images of controls to disentangle the effect of the disease from the effect of WMH-induced segmentation errors. As it can be observed in **Figure 4**, simulated WMH induce segmentation errors visible as holes and interruptions in the 3D mesh representative of the cortical

TABLE 1 | Clinical characteristics of participants and results of global measurements, spectral, and morphometric analyses of the cortex shape.

	CADASIL patients	Healthy controls	p-value
Number of subjects	21	28	
Clinical characteristics			
Gender, number of women (%)	13 (62%)	14 (50%)	0.59
Age, mean \pm sd, range	54.5 \pm 11.7, 32.1–74.5	53.8 \pm 11.2, 30.1–71.4	0.83 ^a
Level of education, mean \pm sd (years)	10.7 \pm 3.0	13.5 \pm 3.5	0.003^a
MMSE, mean, median, range	28.3, 29, 24–30	29.0, 29, 26–30	0.16 ^a
Global measurements (mean \pm sd)			
Normalized brain volume	0.76 \pm 0.03	0.76 \pm 0.03	0.98 ^a
L brain (GM + WM) volume, in cm ³	486.6 \pm 49.8	506.6 \pm 45.4	0.16 ^a
Global gyration index (GGI)	1.28 \pm 0.08	1.29 \pm 0.04	0.66 ^a /0.88 ^b
Spherical gyration index (SGI)	2.87 \pm 0.23	2.89 \pm 0.11	0.67 ^a /0.98 ^b
Volume of WMH, mean \pm sd, range, in cm ³	75.2 \pm 55.6, 7.2–251.5	No significant lesions	–
Volume of lacunes*, mean \pm sd, range, in mm ³	467 \pm 451, 14–1,356	No lacunes	–
Spectral analysis (mean \pm sd)			
Analyzed folding power <i>AFP</i>	303.0 \pm 22.1	294.2 \pm 15.0	0.13 ^a /0.19 ^b / 0.0005^c
B4 power	38.1 \pm 2.2	36.8 \pm 2.7	0.09 ^a /0.14 ^b /0.08 ^c
B5 power	104.1 \pm 7.1	101.7 \pm 4.8	0.18 ^a /0.15 ^b / 0.01^c
B6 power	146.5 \pm 15.1	145.0 \pm 11.4	0.69 ^a /0.79 ^b / 0.04^c
Morphometric analysis (mean \pm sd)			
Normalized curvedness <i>c</i>	11.6 \pm 0.7	11.1 \pm 0.4	0.003^a / <0.0001^b / <0.0001^c
Sulcal shape index <i>s1</i>	–0.707 \pm 0.008	–0.696 \pm 0.007	<0.0001^a / <0.0001^b / <0.0001^c
Gyral shape index <i>s2</i>	0.550 \pm 0.016	0.565 \pm 0.010	0.0006^a / <0.0005^b / 0.0003^c

^at-test; ^basymptotic two-sample Fisher-Pitman permutation test; ^clinear model with adjustment for age, sex and brain volume; MMSE: Mini Mental State Examination; GM: gray matter; WM: white matter; WMH: White matter hyperintensities; *computed in 12/21 (57%) having lacunes. Bold values means significant between-group differences ($p < 0.05$).

TABLE 2 | Mean observed effects of the disease and of WMH-induced segmentation errors.

Morphometric parameter	MRD Cadasil – Controls	p-value ^a	MRD Controls _{WMH} – Controls	p-value ^b
Normalized curvedness <i>c</i>	4.9%	0.003	0.9%	0.01
Sulcal shape index <i>s1</i>	–1.5%	<0.0001	–0.5%	0.03
Gyral shape index <i>s2</i>	–2.7%	0.0006	–1.2%	0.07

MRD Cadasil–Controls: mean relative difference of morphometric parameters in Cadasil ($N = 21$) vs. Controls subjects ($N = 28$).

MRD Controls_{WMH}–Controls: mean relative difference of morphometric parameters in Controls with simulated WMH and segmentation errors ($N = 11$) vs. Controls subjects ($N = 11$).

^at-test; ^bWilcoxon signed-rank test.

surface. These errors were visually obvious which was expected since this simulation was supposed to provide an upper bound of the effects of segmentation errors in our data.

At the group level (11 controls vs. the same 11 controls with simulated WMH), we found a significant but small effect on *c* and *s1* (Table 2). In average, when adding WMH from different lesion loads sampled from the patient's group, *c* was increased by 0.9% while *s1* was decreased by 0.5%. By comparison, the difference between patient and control groups is 5 or 3 times greater for *c* and *s1* respectively, while expected to be less affected by WMH induced segmentation errors than by simulated ones. There was

no significant effect of simulated WMH on *s2* (Table 2), the parameter that has been found related to the volume of WMH in patients.

DISCUSSION

In the present study, we found that the cortex of CADASIL patients was characterized by a surface that is more sharp and more bended through both the spectral and geometrical analyses, with a difference in global shape of folds toward somehow “tightened” sulci and “expanded” gyri. Also, the level of alteration of the gyral shape descriptor was significantly associated with the extent of WMH that reflects the amount of white matter tissue changes in CADASIL. Altogether, these results support the hypothesis of a gyral white matter swelling.

Our main hypothesis to explain these results is mechanical: the white matter swelling would be “pushing” the cortex so that its shape is slightly modified. As represented in Figure 1, the cortex expansion might be limited by the meningeal envelope, favoring the shape alteration in the tangential direction. One can figure out this diffuse and global mechanism by imagining an increase in the white matter volume inside a gyrus beneath the cortex. As a consequence of increased pressure, the gyrus expands (decreased positive *s2*) and adjacent sulci tighten (decreased negative *s1*) due to lateral compression. This hypothesis could be modeled by a combination of the recent mechanical model by Tallinen et al. (5) and the model by Nie et al. (6) that is able to reproduce the

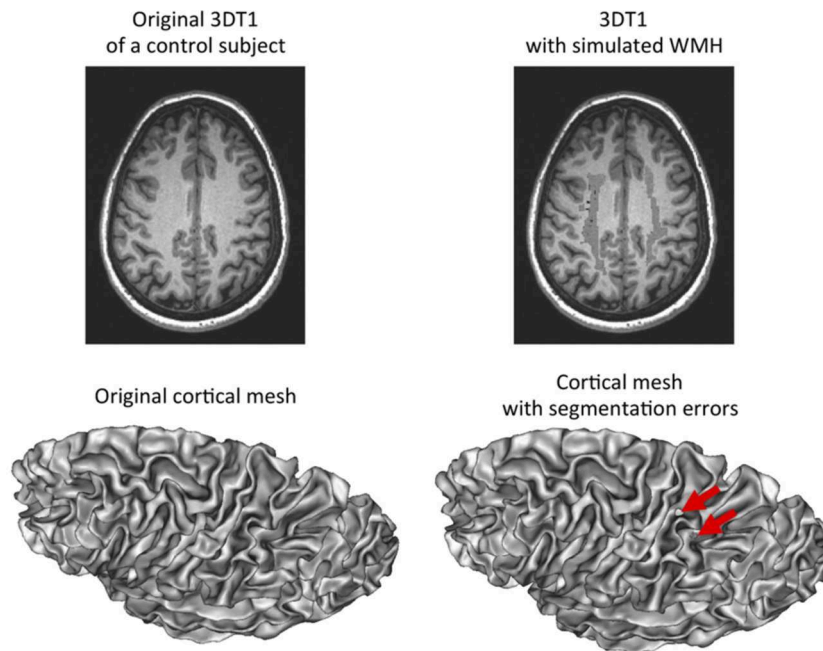


FIGURE 4 | Simulation of white matter hypointensities in control subjects to induce segmentation errors. Left: original 3D T1-weighted image of a control subject with corresponding cortical surface. Right: same 3D T1-weighted image after addition of white matter hypointensities taken from an age-matched CADASIL patient after non-linear registration. The corresponding cortical surface presents with holes in the mesh as a result of segmentation errors due to the presence of white matter hypointensities close to the cortex and with similar gray-level values.

interaction between gray matter and meninges. As for the spectral parameters, the global increase in *AFP* may be due to sharper sulci bank and gyri edges that generate more high frequency component in the spectral decomposition, resulting in more *B5* and *B6* power that are not explained in our data by an increased in cortical surface buried in *B5* and *B6*-associated pieces of sulci (data not shown). Indeed in Fourier-like decomposition, higher frequencies not only contribute to periodic patterning but also to sharpness rendering. Another explanation is that the small increase in global folding power really divides-up into the three sulcal bands because it is a global effect not related to an increase in gyrification complexity nor an extension of the folding pattern.

By simulating WMH in cerebral images of controls, we have shown that segmentation errors due to uncorrected WMH near the cortex could slightly change the values of some descriptors of the cortex shape we used. However, these changes were non-significant (*s2*) or much smaller (*c*, *s1*) than the differences observed between groups. These results were convincing given that the simulated WMH produce much more obvious errors than our original data. Therefore, we could conclude that the observed differences were mainly driven by the disease while we could not exclude a small effect of segmentation errors on *c* and *s1*.

Our study owns some limitations and questions still open to interpretation. First, direct involvement of the cortex microstructure could also be involved in the alteration of the cortex shape aside with gyri white matter swelling. Yet, no significant differences of cortical thickness have been reported in this cohort of paucisymptomatic CADASIL patients compared to

age- and sex-matched controls (21). Similarly, no visible cortical infarcts have been detected. Second, there was a significant statistical association between *s2* and the volume of WMH that we assumed to reflect the effect of white matter swelling on cortex shape, but we did not truly measure the volume of white matter. In fact, we considered global volumetric methods inappropriate to accurately detect a change at the group level. More, even after correction there may be still uncorrected WMH in T1-weighted images due to imperfect registration from FLAIR to T1-weighted images that may corrupt the white matter volume measurement. Ultimately, we found a similar normalized brain volume between groups, which is in favor of a swelling mechanism that would balance the expected cerebral atrophy observed in sporadic small vessel diseases (22). Longitudinal MRI follow-up and evaluation of the metrics presently used to characterize the cortex shape may be a future step to better understand the course of those alterations. Additional sources of data may also be helpful to decipher these mechanisms. For example, combining cortex shape analysis and structural connectome analysis derived by reconstructing fiber pathways with diffusion MRI may reveal some relationships between connected areas. Also, region-based analysis with dedicated methods could be useful to characterize local alterations in cortex shape and determine whether some regions are more affected than others (23).

In conclusion, the shape of the cortex of CADASIL patients is altered compared to age- and sex-matched controls at an early stage of the disease. This cortical alteration is partly associated to the swelling of the underlying white matter. More generally, the study of the cortex shape might be another way to evaluate

subcortical swelling or atrophy in some pathological conditions strongly affecting subcortical tissues. New computational tools assessing cortical shape may help revealing subtle preclinical structural changes where global measurements might fail. Future studies are needed to assess the association between metrics of cortex shape and cognitive scores and clinical outcomes.

ETHICS STATEMENT

This study was carried out in accordance with the recommendations of Good Clinical Practice and applicable local regulations with written informed consent from all subjects. All subjects gave written informed consent in accordance with the Declaration of Helsinki. The protocol was approved by a local ethics committee (Ile de France VII, No. CPP09-012).

AUTHOR CONTRIBUTIONS

FD and EJ: study concept and design. EJ: acquisition of data. FD, DG, JL, CF, and EJ: analysis and interpretation of the data. FD

and EJ: drafting of the manuscript. HC and EJ: study supervision. All authors: critical revision of the manuscript.

FUNDING

This work was funded by Leducq foundation, Avenir foundation, PLAGNIOL foundation, NRJ foundation, CADASIL France association and by the Agence Nationale de la Recherche (Commissariat General à l'Investissement) RHU TRT_cSVD. This work was also partially funded by ANR-12-JS03-001-01 (MODEGY) and by the Human Brain Project, funded from the European Union's Horizon 2020 Framework Programme for Research and Innovation under the Specific Grant Agreements No. 785907 (SGA2) and No: 604102 (SGA1), and by the FRM DIC20161236445.

ACKNOWLEDGMENTS

The authors thank all patients for their collaboration on this study.

REFERENCES

- Chabriat H, Joutel A, Dichgans M, Tournier-Lasserre E, Bousser MG. Cadasil. *Lancet Neurol.* (2009) 8:643–53. doi: 10.1016/S1474-4422(09)70127-9
- De Guio F, Mangin JF, Duering M, Ropele S, Chabriat H, Jouvent E. White matter edema at the early stage of cerebral autosomal-dominant arteriopathy with subcortical infarcts and leukoencephalopathy. *Stroke J Cereb Circ.* (2015) 46:258–61. doi: 10.1161/STROKEAHA.114.07018
- De Guio F, Vignaud A, Chabriat H, Jouvent E. Different types of white matter hyperintensities in CADASIL: insights from 7-Tesla MRI. *J Cereb Blood Flow Metab.* (2017) 38:1654–63. doi: 10.1177/0271678X17690164
- De Guio F, Reyes S, Duering M, Pirpamer L, Chabriat H, Jouvent E. Decreased T1 contrast between gray matter and normal-appearing white matter in CADASIL. *AJNR Am J Neuroradiol.* (2014) 35:72–76. doi: 10.3174/ajnr.A3639
- Tallinen T, Chung JY, Rousseau F, Girard N, Lefèvre J, Mahadevan L. On the growth and form of cortical convolutions. *Nat Phys.* (2016) 12:588–93. doi: 10.1038/nphys3632
- Nie J, Guo L, Li G, Faraco C, Stephen Miller L, Liu T. A computational model of cerebral cortex folding. *J Theor Biol.* (2010) 264:467–78. doi: 10.1016/j.jtbi.2010.02.002
- Jouvent E, Mangin JF, Porcher R, Viswanathan A, O'Sullivan M, Guichard JP, et al. Cortical changes in cerebral small vessel diseases: a 3D MRI study of cortical morphology in CADASIL. *Brain J Neurol.* (2008) 131:2201–8. doi: 10.1093/brain/awn129
- Jouvent E, Mangin JF, Duchesnay E, Porcher R, Duering M, Mewald Y, et al. Longitudinal changes of cortical morphology in CADASIL. *Neurobiol Aging.* (2012) 33:1002.e29–36. doi: 10.1016/j.neurobiolaging.2011.09.013
- Awate SP, Win L, Yushkevich P, Schultz RT, Gee JC. 3D cerebral cortical morphometry in autism: increased folding in children and adolescents in frontal, parietal, and temporal lobes. *Med Image Comput Comput Assist Interv.* (2008) 11:559–67. doi: 10.1007/978-3-540-85988-8_67
- Hu HH, Chen HY, Hung CI, Guo WY, Wu YT. Shape and curvedness analysis of brain morphology using human fetal magnetic resonance images in utero. *Brain Struct Funct.* (2013) 218:1451–62. doi: 10.1007/s00429-012-0469-3
- Lefèvre J, Germanaud D, Dubois J, Rousseau F, de Macedo Santos I, Angleys H, et al. Are developmental trajectories of cortical folding comparable between cross-sectional datasets of fetuses and preterm newborns? *Cereb Cortex NYN.* (2016) 26:3023–35. doi: 10.1093/cercor/bhv123
- Germanaud D, Lefèvre J, Toro R, Fischer C, Dubois J, Hertz-Pannier L, et al. Larger is twistier: spectral analysis of gyrification (SPANGY) applied to adult brain size polymorphism. *Neuroimage.* (2012) 63:1257–72. doi: 10.1016/j.neuroimage.2012.07.053
- Germanaud D, Lefèvre J, Fischer C, Bintner M, Curie A, des Portes V, et al. Simplified gyral pattern in severe developmental microcephalies? New insights from allometric modeling for spatial and spectral analysis of gyrification. *Neuroimage.* (2014) 102(Pt 2):317–31. doi: 10.1016/j.neuroimage.2014.07.057
- Duering M, Righart R, Csanadi E, Jouvent E, Herve D, Chabriat H, et al. Incident subcortical infarcts induce focal thinning in connected cortical regions. *Neurology.* (2012) 79:2025–8. doi: 10.1212/WNL.0b013e3182749f39
- Lyoubi-Idrissi A, De Guio F, Chabriat H, Jouvent E. Focal macroscopic cortical lesions in cerebral autosomal-dominant arteriopathy with subcortical infarcts and leukoencephalopathy. *Stroke.* (2017) 48:1408–11. doi: 10.1161/STROKEAHA.116.015724
- Wardlaw JM, Smith EE, Biessels GJ, Cordonnier C, Fazekas F, Frayne R, et al. Neuroimaging standards for research into small vessel disease and its contribution to ageing and neurodegeneration. *Lancet Neurol.* (2013) 12:822–38. doi: 10.1016/S1474-4422(13)70124-8
- Mangin JF, Riviere D, Cachia A, Duchesnay E, Cointepas Y, Papadopoulos-Orfanos D, et al. A framework to study the cortical folding patterns. *Neuroimage.* (2004) 23(Suppl. 1):S129–38. doi: 10.1016/j.neuroimage.2004.07.019
- Paus T, Bernard M, Chakravarty MM, Davey Smith G, Gillis J, Lourdasamy A, et al. KCTD8 gene and brain growth in adverse intrauterine environment: a genome-wide association study. *Cereb Cortex NYN.* 1991. (2012) 22:2634–42. doi: 10.1093/cercor/bhr350
- Le Troter A, Auzias G, Coulon O. Automatic sulcal line extraction on cortical surfaces using geodesic path density maps. *Neuroimage.* (2012) 61:941–9. doi: 10.1016/j.neuroimage.2012.04.021
- Jenkinson M, Beckmann CF, Behrens TE, Woolrich MW, Smith SM. FSL. *Neuroimage.* (2012) 62:782–90. doi: 10.1016/j.neuroimage.2011.09.015

21. De Guio F, Reyes S, Vignaud A, Duering M, Ropele S, Duchesnay E, et al. *In vivo* high-resolution 7 Tesla MRI shows early and diffuse cortical alterations in CADASIL. *PLoS ONE*. (2014) 9:e106311. doi: 10.1371/journal.pone.0106311
22. Smith EE, O'Donnell M, Dagenais G, Lear SA, Wielgosz A, Sharma M, et al. Early cerebral small vessel disease and brain volume, cognition, and gait. *Ann Neurol*. (2015) 77:251–61. doi: 10.1002/ana.24320
23. Awate SP, Leahy RM, Joshi AA. Kernel methods for riemannian analysis of robust descriptors of the cerebral cortex. *Inf Process Med Imaging Proc Conf*. (2017) 10265:28–40. doi: 10.1007/978-3-319-59050-9_3

Conflict of Interest Statement: The authors declare that the research was conducted in the absence of any commercial or financial relationships that could be construed as a potential conflict of interest.

Copyright © 2019 De Guio, Germanaud, Lefèvre, Fischer, Mangin, Chabriat and Jouvent. This is an open-access article distributed under the terms of the Creative Commons Attribution License (CC BY). The use, distribution or reproduction in other forums is permitted, provided the original author(s) and the copyright owner(s) are credited and that the original publication in this journal is cited, in accordance with accepted academic practice. No use, distribution or reproduction is permitted which does not comply with these terms.



Spatial Gradient of Microstructural Changes in Normal-Appearing White Matter in Tracts Affected by White Matter Hyperintensities in Older Age

Susana Muñoz Maniega^{1,2,3*†}, Rozanna Meijboom^{1,2,3,4†}, Francesca M. Chappell^{1,5}, Maria del C. Valdés Hernández^{1,2,3}, John M. Starr^{3,5‡}, Mark E. Bastin^{1,5}, Ian J. Deary^{5,6} and Joanna M. Wardlaw^{1,2,5}

OPEN ACCESS

Edited by:

Eric Jouvent,
Université Sorbonne Paris Cité, France

Reviewed by:

Anne-Katrin Giese,
Massachusetts General Hospital,
Harvard Medical School,
United States
Yael D. Reijmer,
University Medical Center
Utrecht, Netherlands

*Correspondence:

Susana Muñoz Maniega
s.m.maniega@ed.ac.uk

[†]These authors have contributed
equally to this work

[‡]Deceased 8 Dec, 2018

Specialty section:

This article was submitted to
Stroke,
a section of the journal
Frontiers in Neurology

Received: 26 March 2019

Accepted: 08 July 2019

Published: 25 July 2019

Citation:

Muñoz Maniega S, Meijboom R, Chappell FM, Valdés Hernández MdC, Starr JM, Bastin ME, Deary IJ and Wardlaw JM (2019) Spatial Gradient of Microstructural Changes in Normal-Appearing White Matter in Tracts Affected by White Matter Hyperintensities in Older Age. *Front. Neurol.* 10:784. doi: 10.3389/fneur.2019.00784

¹ Neuroimaging Sciences, Centre for Clinical Brain Sciences, University of Edinburgh, Edinburgh, United Kingdom, ² UK Dementia Research Institute at the University of Edinburgh, Edinburgh, United Kingdom, ³ Alzheimer Scotland Dementia Research Centre, University of Edinburgh, Edinburgh, United Kingdom, ⁴ Department of Radiology and Nuclear Medicine, Erasmus MC–University Medical Centre Rotterdam, Rotterdam, Netherlands, ⁵ Centre for Cognitive Ageing and Cognitive Epidemiology, University of Edinburgh, Edinburgh, United Kingdom, ⁶ Department of Psychology, University of Edinburgh, Edinburgh, United Kingdom

Background and Purpose: White matter hyperintensities (WMH) are commonly seen on structural MRI of older adults and are a manifestation of underlying and adjacent tissue damage. WMH may contribute to cortical disconnection and cognitive dysfunction, but it is unclear how WMH affect intersecting or nearby white matter tract integrity. This study investigated the effects of WMH on tract microstructure by determining the spatial distribution of water diffusion characteristics in white matter tract areas adjacent to both intersecting and nearby WMH.

Methods: We used diffusion and structural MRI data from 52 representative participants from the Lothian Birth Cohort 1936 (72.2 ± 0.7 years) including a range of WMH burden. We segmented WMH, reconstructed 18 main white matter tracts using automated quantitative tractography and identified intersections between tracts and WMH. We measured mean diffusivity (MD) and fractional anisotropy (FA) in tract tissue at 2 mm incremental distances from tract-intersecting and non-intersecting (nearby) WMH.

Results: We observed a spatial gradient of FA and MD abnormalities for most white matter tracts which diminished with a similar distance pattern for tract-intersecting and nearby WMH. Overall, FA was higher, while MD was lower around nearby WMH compared with tract-intersecting WMH. However, for some tracts, FA was lower in areas immediately surrounding nearby WMH, although with faster normalization than in FA values surrounding tract-intersecting WMH.

Conclusion: WMH have similar effects on tract infrastructure, whether they be intersecting or nearby. However, the observed differences in tract water diffusion properties around WMH suggest that degenerative processes in small vessel disease

may propagate further along the tract for intersecting WMH, while in some areas of the brain there is a larger and more localized accumulation of axonal damage in tract tissue nearby a non-connected WMH. Longitudinal studies should address differential effects of intersecting vs. nearby WMH progression and how they contribute to cognitive aging.

Keywords: brain, aging, diffusion MRI, white matter hyperintensities, tractography, cerebral small vessel disease

INTRODUCTION

White matter hyperintensities (WMH), or leukoaraiosis, are routinely found in brain magnetic resonance imaging (MRI) scans of older people and have been described as white matter (WM) degeneration characterized by axonal loss, demyelination and gliosis, on neuropathological examination (1). The presence of WMH contributes to cortical “disconnection” (2, 3) and cognitive and functional decline (4–6). Several studies have observed associations between WMH volume within specific WM tracts and cognition (7, 8), suggesting that the presence of WMH affects the performance of WM pathways. The influence of WMH on WM tracts can be explored further by assessing, not just the extent of the observable damage in the tract, but also the invisible changes in tract tissue close to WMH.

Diffusion MRI (dMRI) allows the assessment of microstructural quality of WM *in-vivo* through the tissue diffusion properties. Fractional anisotropy (FA) is an indicator of the degree of directionality of the water diffusion within the tissue, while mean diffusivity (MD) reflects the degree of diffusion in all directions. These parameters can therefore be used to assess changes in structural barriers within WM, such as axonal membranes or myelin (9). Histology studies of WM have shown that reduced axonal density, and anomalies in the myelin sheaths underlie abnormalities observed in these water diffusion parameters (10, 11).

Previous dMRI studies of whole-brain normal-appearing white matter (NAWM) have observed gradual changes of FA and MD with distance from WMH and described them as a “penumbra” effect of WMH on NAWM (12, 13). A similar distance pattern of NAWM tissue damage has been observed within the corticospinal tract, caused by the WMH that crossed the tract, as well as by nearby WMH, outside the tract (14).

In the current study, we used dMRI tractography (15) to reconstruct 18 of the main WM pathways of the brain. We measured FA and MD within these tracts to investigate how the presence of WMH affects the integrity of surrounding NAWM in tracts segmented in a group of older age subjects.

METHODS

Participants

The LBC1936 comprises a group of community-dwelling individuals born in 1936, most of whom took part in the Scottish Mental Survey of 1947. At ~70 years of age, the LBC1936 participants were recruited for follow-up cognitive and other medical and psycho-social assessments (16, 17). During a second wave of this longitudinal study, at ~73 years of age,

700 participants underwent comprehensive MRI to assess brain structure (18). Written informed consent was obtained from all participants under protocols approved by the National Health Service Ethics Committees.

The current study used imaging data from the second wave of the LBC1936. A sample was chosen with three requirements: it represented all levels of WMH burden, each participant had available structural and diffusion MRI data, and participants did not have a history of stroke (self-reported). We selected the participants in recruitment order, blind to any other medical or imaging data. In order to create a sample representative of all levels of WMH burden, participants were selected based on Fazekas score (19), as we have previously shown that, there is a strong correlation between Fazekas score and WMH volume (20). A sample of 60 participants, with 10 participants per Fazekas total score of 1–6 (sum of deep + periventricular 0–3 scores) was intended. However, only eight participants with a Fazekas score of 6 were selected, as all other participants with this score had a history of stroke. We completed the sample with an additional case for Fazekas scores 2 and 3, as these were the most frequent scores observed in the LBC1936. The final sample therefore consisted of ten participants per Fazekas scores 1, 4 and 5; 11 participants per Fazekas scores 2 and 3; and eight participants with a Fazekas score of 6.

Imaging Acquisition

All MRI data were acquired using the same GE Signa Horizon HDxt 1.5T clinical scanner (General Electric, Milwaukee, WI, USA), with a self-shielding gradient set at a maximum of 33 mT/m and an 8-channel phased-array head coil. The full details of the imaging protocol can be found in Wardlaw et al. (18). Briefly, the MRI examination comprised a high-resolution 3D T1-weighted (T1W), T2W, T2*-weighted (T2*W) and FLAIR structural scans, as well as dMRI. The dMRI protocol consisted of seven T2W volumes ($b = 0 \text{ s/mm}^2$) and sets of diffusion-weighted ($b = 1,000 \text{ s/mm}^2$) single-shot, spin-echo, echo-planar (EP) volumes acquired with diffusion gradients applied in 64 non-collinear directions (21). All sequences, except for the T1W, were acquired in the axial plane with a field-of-view (FOV) of $256 \times 256 \text{ mm}$, contiguous slice locations, and image matrices and slice thicknesses designed to give 2 mm isotropic voxels for dMRI, and voxel dimensions of $1 \times 1 \times 2 \text{ mm}$ for T2W and T2*W, and $1 \times 1 \times 4 \text{ mm}$ for FLAIR. The high-resolution 3D T1W scan was acquired in the coronal plane with a FOV of $256 \times 256 \text{ mm}$ and voxel dimensions of $1 \times 1 \times 1.3 \text{ mm}$.

Visual Scoring of White Matter Hyperintensities

WMH were defined according to the STRIVE criteria (22). All assessments used validated visual or computational methods and were performed blind to all patient demographic, clinical and tractography characteristics. A qualitative assessment of WMH load was performed by an expert neuroradiologist who scored hyperintensities on the FLAIR and T2W scans using the Fazekas scale, after training on a standard data set. A second consultant neuroradiologist cross-checked a random sample of 10% of ratings, all scans with stroke lesions, and any scans where the first rater was uncertain. The final measurements were those agreed as discussed amongst the two neuroradiologists. A total score ranging from 0 to 6 was obtained by summing the periventricular and deep WMH Fazekas scores. The Fazekas scale is one of the most widely used visual rating scales and has been in use for over two decades (19).

Whole Brain WMH and NAWM Segmentation

All structural MRI volumes were registered to the corresponding T2W volume using rigid body registration (23). Whole brain NAWM and WMH tissue masks were obtained using the multispectral coloring modulation and variance identification (MCMxxxVI) method (24). In brief, T2*W and FLAIR volumes were mapped into red-green color space and fused; the minimum variance quantization clustering technique was then used in the resulting image to reduce the number of color levels, thereby allowing WMH to be separated from other tissues in a reproducible and semiautomatic manner. The same method was used to extract the NAWM from the T1W and T2W volumes. Any silent stroke lesions were identified by a neuroradiologist and excluded from the masks manually by a trained image analyst.

Diffusion Tensor Imaging Analysis and Tractography

dMRI volumes were pre-processed using FSL 4.1 (25). First, brain extraction was performed using BET (26), and second, bulk motion and eddy current induced distortions were removed by registering all volumes to the first T2W EP volume (23). Third, DTIFIT was used to obtain the water diffusion tensor on a voxel-wise level, and to calculate parametric maps of FA and MD from the diffusion tensor eigenvalues. This was followed by automatic tractography using Tracula implemented in Freesurfer5.3 [TRActs Constrained by UnderLying Anatomy; (27)]. Tracula uses global probabilistic tractography (28) and anatomical priors of the white matter pathways derived from a set of training subjects; its accuracy has been evaluated against manual tract labels (27). Registration to the tract atlas containing the priors was performed by affine registration to the MNI125 template (23). We reconstructed the 18 white matter pathways included in Tracula (corpus callosum: forceps major and forceps minor, and bilateral corticospinal tract (CST), inferior longitudinal fasciculus (ILF), uncinate fasciculus (UNC), anterior thalamic radiation (ATR), cingulum: cingulate gyrus

(CCG) and angular bundle (CAB), and superior longitudinal fasciculus: parietal (SLFp) and temporal (SLFt) segments). All white matter tracts were visually inspected and those not following the expected paths were discarded from further analysis. See **Figure 1A** for an example showing the 18 tracts and WMH in a representative participant. The tract masks were binarized after applying a threshold of 1% to the tract posterior probability.

WM Tract-WMH and WM Tract-NAWM Intersections

To obtain the areas of the tracts that intersected with WMH for each individual, we first non-linearly registered the T2W volume to the averaged T2W EP volume (S0) using RNiftyReg (29, 30). This registration was then applied to the whole-brain WMH and NAWM masks created previously in order to overlap them with the Tracula tracts-masks in diffusion space and obtain the intersections. This way the tracts were divided into *tract-WMH* (as the intersection between the tract and the whole-brain WMH mask) and *tract-NAWM* (as the intersection between the tract and the whole-brain NAWM), see example in **Figure 1B**. These were subsequently overlaid onto the FA and MD parametric maps for quantitative measurements. Averages of FA and MD values from each tract area (WMH and NAWM) were obtained. Please note that not all tracts had a tract-WMH intersection, and the area of WMH overlap varied for different tracts and between participants. The percentages of overlap were quantified as the tract-WMH percentage volume (% WMHvol) for each individual WM tract and for all WM tracts combined. These were calculated by dividing the tract-WMH volume by the total WM tract volume (tract-WMH plus tract-NAWM).

Spatial Analysis of Tracts Spatial Contours of Tract-WMH

We assessed how the intersection or proximity of the WMH was associated with changes in tract integrity by creating approximately equidistant 3D contours around the tract-WMH, which propagated into the tract-NAWM for each tract. To achieve this, we dilated the tract-WMH masks in 3D by 2 mm increments (1 voxel in dMRI-space) up to 10 mm, and then subtracted from each dilated ROI the previous ones. That is, the tract-WMH mask was subtracted from the 2 mm ROI to obtain a contour at about 2 mm from the WMH edge; the tract-WMH and 2 mm ROI were subtracted from the 4 mm ROI to obtain a contour at about 4 mm from the WMH edge, and so on (the distances quoted are approximate as they are limited by the finite voxel size). For each contour, only the voxels overlapping with the tract-NAWM were kept for each tract, so no other tissues were included. See “WMH1” in **Figure 1C** for a graphical representation of this approach and **Figure 1D** for an example of contours in the SLFt. Means of FA and MD were obtained for each contour for parametric assessment of the effects of tract-WMH.

Nearby-WMH

The spatial analysis was repeated for WMH that were nearby, but that did not intersect the tract, to assess their association

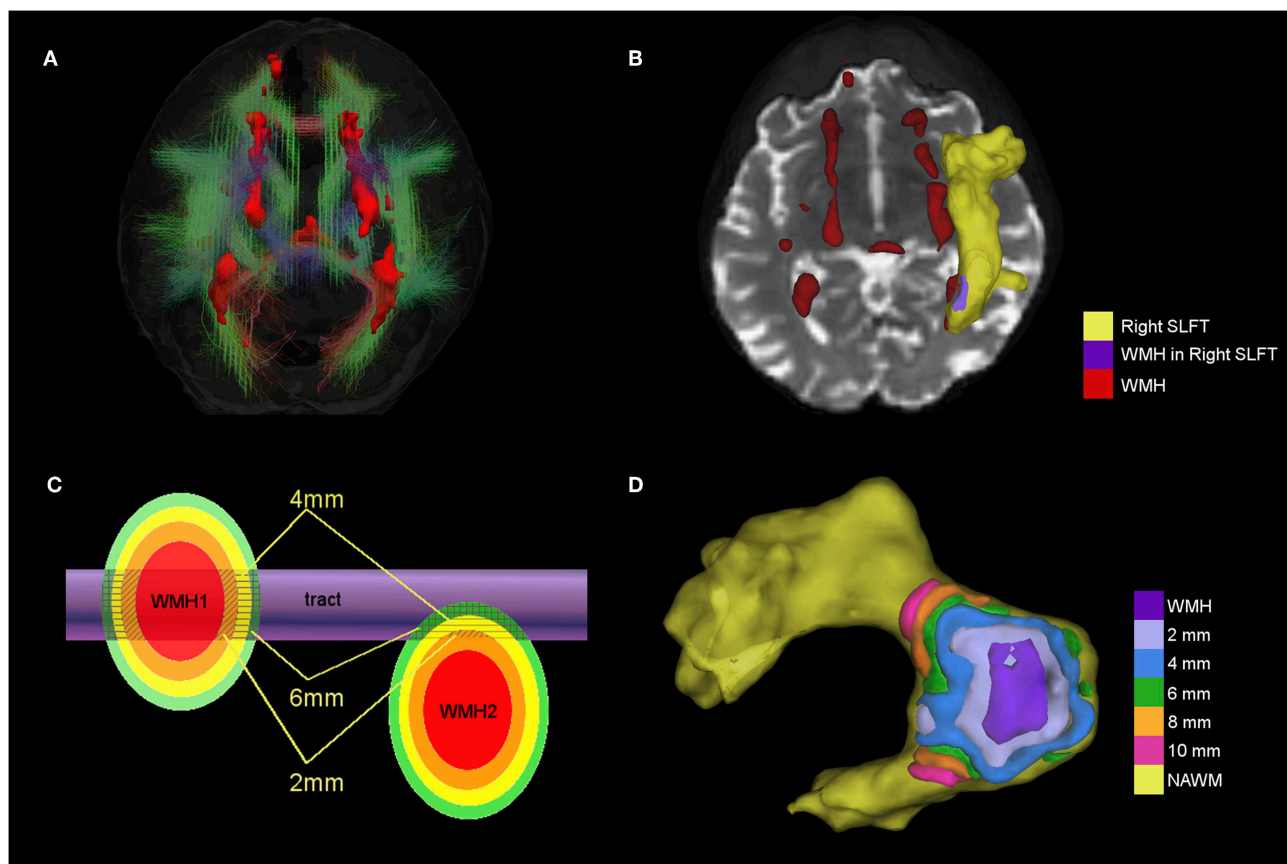


FIGURE 1 | (A) 3D view of 18 tracts (streamlines) and WMH (red surface) from a participant with a total Fazekas score of 3. Streamlines are color-coded according to the main direction of the middle segment of the tract (red = x axis, green = y axis and blue = z axis). **(B)** Example showing the superior longitudinal fasciculus temporal ending (SLFt) as a yellow surface and the area where the SLFt intersects with WMH in purple. Remaining WMH are shown in red. **(C)** Schematic figure of the spatial analysis of the effects of tract-WMH (WMH1) and the nearby-WMH (WMH2) showing 2, 4, and 6 mm contours around the WMH. Average FA and MD are measured only where the contours intersect with tract-NAWM (patterned areas). **(D)** Example of the spatial analysis contours for tract-WMH in the SLFt; the tract-WMH area (purple) is dilated by 2 mm at a time to create surface contours within the tract-NAWM at different distances from the WMH edge.

with changes in the WM tract. We considered only those nearby-WMH for which any of the 2–10 mm contours intersected with the tract-NAWM (see “WMH2” in **Figure 1C**). Any voxel already belonging to a WMH-tract contour was automatically excluded from the nearby-WMH contours, to ensure the areas measured were not connected to an intersecting WMH. Means of FA and MD were obtained for each nearby-WMH contour that intersected with an individual tract-NAWM.

Statistical Analyses

All statistical analyses were performed in R v.3.5 with packages *car* (31) and *lmerTest* (32). Plots were made with *ggplot2* (33). Analyses were performed including all tracts within a model, and also for each individual tract.

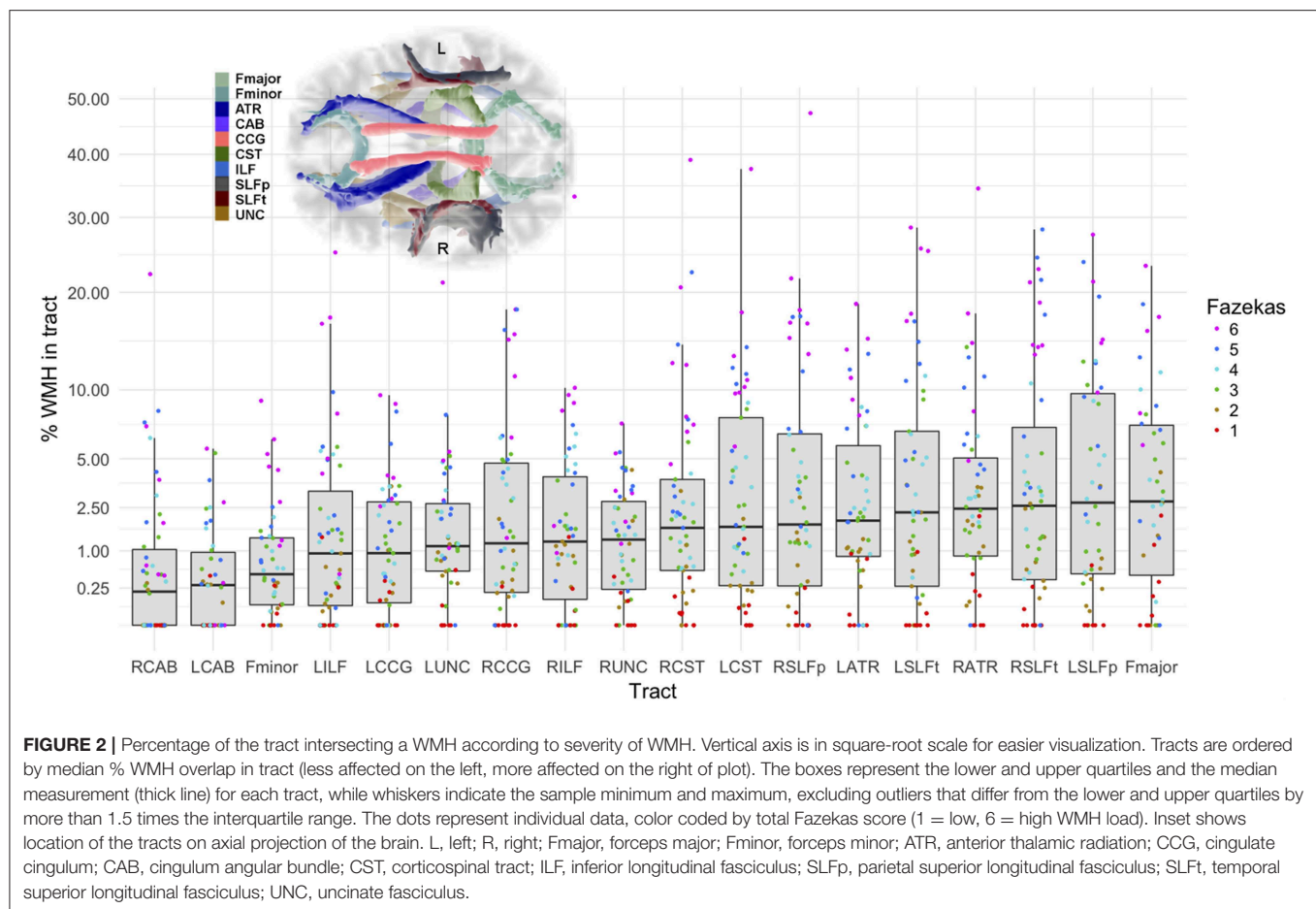
We are aware of the problem of multiple comparison, and so, for transparency, we report all *p*-values and coefficients estimated from the models. Methods for correcting for multiple comparison, such as Bonferroni, can be overly conservative and difficult to interpret where variables are highly correlated (such as brain MRI biomarkers), and therefore we chose not to apply any

correction here; however to provide a compromise between Type I and Type II errors, we interpret results as significant if $p < 0.01$.

Water Diffusion in Tract-NAWM Spatial Contours for Tract-WMH

We assessed the spatial changes of FA and MD values with distance from the tract-WMH with a repeated-measurements linear mixed model for each parameter, with the repeats being FA or MD obtained in tract-WMH, and tract-NAWM at 2, 4, 6, 8 and 10 mm from the tract-WMH. As the trajectories of FA and MD show an asymptotic relationship of water diffusion with distance (**Figures 3A,B**), $\log(\text{distance}+1)$ was used as fixed effect (with tract-WMH coded as 0 mm). The model including all tracts was a three-level model, with the measurements for each tract included in the model as repeats at each distance. A model with random intercept and slope for both participant and tract gave the best fit (lowest Bayesian information criterion) and residual distribution.

The analysis was repeated for each tract separately, with $\log(\text{distance}+1)$ as fixed effect and random intercept



and slope for participant. Type III Wald F tests with Kenward-Roger df approximation were used to obtain F and *p*-values.

Water Diffusion in Tract-NAWM Spatial Contours for Nearby-WMH

FA and MD values for spatial distances at 2, 4, 6, 8, and 10 mm from nearby-WMH were measured for all tracts. We then assessed the effect of the two types of WMH (tract or nearby) on the water diffusion measurements in NAWM spatial contours. The value of WMH was not available for nearby-WMH, hence we compare the trajectories between tract-WMH and nearby-WMH for distances 2–10 mm only. We used a repeated-measure linear mixed model with distance and WMH type as fixed effects; the interaction of distance and WMH type was included as fixed effect only if it improved the model (lowest Bayesian information criterion). The best fitting model for both FA and MD included $\log(\text{distance})$, WMH type (tract-WMH and nearby WMH), and random intercept and slope for both participant and tract.

The analysis was repeated for each tract separately, with $\log(\text{distance})$ and WMH type as fixed effects and random intercept and slope for participant. The interaction term [$\log(\text{distance})$:WMH type] was included in the model for those tracts that showed an improvement in model fit with this term.

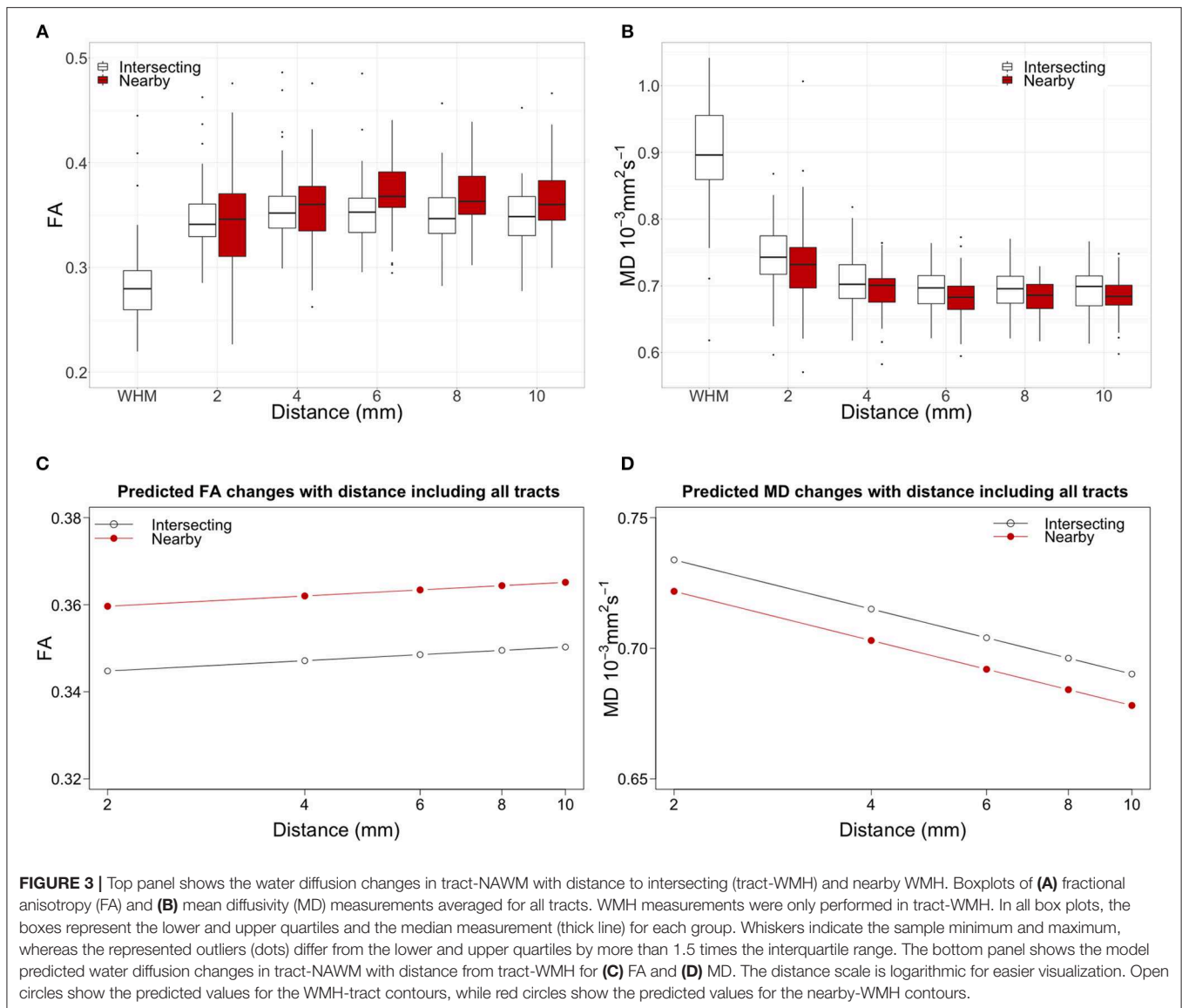
Type III Wald F tests with Kenward-Roger df approximation were used to obtain F and *p*-values.

RESULTS

Participant Demographics

Data from 52 participants (27 male) with a mean age of 72.2 (standard deviation 0.7) years were used for analysis (Table 1). Out of the 60 participants in the initial sample, Tracula failed to produce viable tractography outputs in six participants, one participant's WMH were too small to be segmented, while another participant's WMH did not intersect with any of the tracts of interest, and they were therefore excluded from the analysis. One participant had a silent stroke lesion, which was excluded from the tissue segmentation masks.

Participants varied in Fazekas score, with seven participants with a total Fazekas score of 1; nine participants with a score of 2; 10 participants with a score of 3; nine participants with each scores of 4 and 5; and eight participants with a Fazekas score of 6. Consequently, there was also a variation in number of tracts affected by WMH, but most participants ($N = 46$) had at least 8 tracts intersecting WMH. The corticospinal tracts had the highest percentage of participants with WMH intersecting the tract, followed by the anterior thalamic radiations and right



temporal superior longitudinal fasciculus (Table 1). The lowest percentage of participants with a WMH was observed for the bilateral cingulum angular bundle.

Tract-WMH Percentage Volumes

Median tract-WMH volumes ranged from 0.2 to 2.8% of total WM tract volume, with maximum overlaps seen up to 47% (see Figure 2 and Supplementary Table 1). The forceps major of the corpus callosum, the superior longitudinal fasciculus segments and the anterior thalamic radiations presented the largest median overlap with WMH, while the cingulate angular bundles and forceps minor presented the lowest overlap.

Water Diffusion in Tract-WMH and Tract-NAWM Spatial Contours

All Tracts

We observed some outliers in the model caused by CSF contamination in some NAWM contours. Contours with

$MD > 10^{-3} \text{ mm}^2/\text{s}$ were therefore excluded from analysis as we found in this population MD is unlikely to be over this value in white matter (13).

Results from the repeated-measurements linear mixed model including all WM tracts showed that FA increases significantly [estimate = 0.024, $F_{(1,27.3)} = 53.1$, $p < 0.001$], while MD decreases significantly [estimate = -0.085 , $F_{(1,42.1)} = 199.1$, $p < 0.001$], and logarithmically, with the distance from the WMH (Table 2, top section).

Figures 3A,B show in white the boxplots for FA and MD measured in tract-WMH (intersecting) and each distance to tract-WMH, including results for all WM tracts. The open circles in Figures 3C,D show the models predicted water diffusion changes in tract-NAWM with distance from tract-WMH.

Individual Tracts

FA increases significantly with distance for all tracts except for the bilateral CAB and ILE, while MD decreases significantly with

distance all tracts (Table 3). Supplementary Figure 1 shows plots of the changes for individual tracts for each participant.

Water Diffusion in Tract-NAWM Spatial Contours: Tract-WMH and Nearby-WMH Compared All Tracts

Figures 3A,B show the changes of water diffusion parameters with distance to the intersecting WMH (white boxplots) compared with those of nearby WMH (red boxplots). For both types of WMH the parameters show similar trajectories, for FA and MD. Figures 3C,D show the predicted values obtained by fitted models for both FA and MD.

TABLE 1 | Percentage of WM tracts affected by WMH.

WM tract	% N with WMH in tract
Anterior thalamic radiation L	84.6
Anterior thalamic radiation R	82.7
Cingulate cingulum L	75.0
Cingulate cingulum R	78.9
Cingulum angular bundle L	46.2
Cingulum angular bundle R	50.0
Corticospinal tract L	94.2
Corticospinal tract R	92.3
Inferior longitudinal fasciculus L	78.9
Inferior longitudinal fasciculus R	76.9
Forceps Major	67.3
Forceps Minor	75.0
Superior longitudinal fasciculus, parietal L	76.9
Superior longitudinal fasciculus, parietal R	76.9
Superior longitudinal fasciculus, temporal L	78.9
Superior longitudinal fasciculus, temporal R	84.6
Uncinate fasciculus L	76.9
Uncinate fasciculus R	82.7

WM, white matter; L, left; R, right; WMH, white matter hyperintensity.

% of N with a WMH tract, excluding participants without a WMH in that tract and those that were excluded after data quality assessment.

Table 2 bottom section shows the results from the models. For FA, the statistical model showed significant effects for WMH type [estimate = 0.015, $F_{(1,6513.9)} = 81.1$, $p < 0.001$], with higher FA for nearby-WMH contours than for the same distance tract-WMH contours. The effect of distance was not significant [estimate = 0.003, $F_{(1,26.0)} = 0.39$, $p = 0.540$].

For MD, we observed a significant effect of WMH type [estimate = -0.012, $F_{(1,6510.8)} = 81.9$, $p < 0.001$], with higher MD for tract-WMH contours than for the equivalent nearby-WMH contours. The log(distance) effect was also significant [estimate = -0.027, $F_{(1,38.1)} = 91.5$, $p < 0.001$], indicating a decrease of MD with distance from the WMH.

Individual Tracts

Figure 4 shows the measured FA and MD averaged for all participants, plotted against distance from intersecting and nearby WMH for each individual tract. The pattern of diffusion changes with distance varied slightly between tracts. Tracts in Figure 4 are ordered by increasing median % WMH overlap in tract, as per Figure 2. There was no observable trend in the patterns of changes according to the %WMH in the tract.

Table 4 shows the results from the models. A significant increase of FA with Log(distance) was observed for F Minor, bilateral CCG and right CST, and significant decrease in right ILF. Additionally, FA was significantly lower for nearby WMH type in the F Minor, left CST and right ATR, and significantly higher for the F Major, left ATR, and bilateral CAB, CCG, and UNC.

A significant decrease of MD with Log(distance) was observed for all tracts, except for the left CAB and left UNC. Additionally, a significantly lower MD for the contours of nearby vs. intersecting WMH type was observed for the bilateral ATR, left CAB, left CST and bilateral UNC, while MD was significantly higher for nearby vs. intersecting WMH type in bilateral SLFt.

The interaction term log(distance):WMH type was significant and improved the model in F Minor, left CST, right ATR and right UNC for FA, and in right UNC for MD.

DISCUSSION

This is the largest study to date quantitatively describing changes in the microstructure of main brain WM tracts with distance

TABLE 2 | Results from the repeated-measures linear mixed model analysis for the full models including all tracts.

Outcome variable	Predictor	Estimate	Std. error	Df.res	F	p
TRACT-WMH SPATIAL CONTOURS						
FA	Log(distance+1)	0.024	0.003	27.3	53.1	<0.001
MD	Log(distance+1)	-0.085	0.006	42.1	199.1	<0.001
TRACT-WMH vs. NEARBY-WMH						
FA	Log(distance)	0.003	0.006	26.0	0.39	0.540
	WMH "nearby"	0.015	0.002	6513.9	81.1	<0.001
MD	Log(distance)	-0.027	0.003	33.2	91.5	<0.001
	WMH "nearby"	-0.012	0.001	6510.8	81.9	<0.001

Top section shows the results for water diffusion in tract-WMH spatial contours; bottom section shows the results for the models including tract-WMH and nearby-WMH contours. WMH, white matter hyperintensity; FA, fractional anisotropy; MD, mean diffusivity in (10^{-3} mm²/s).

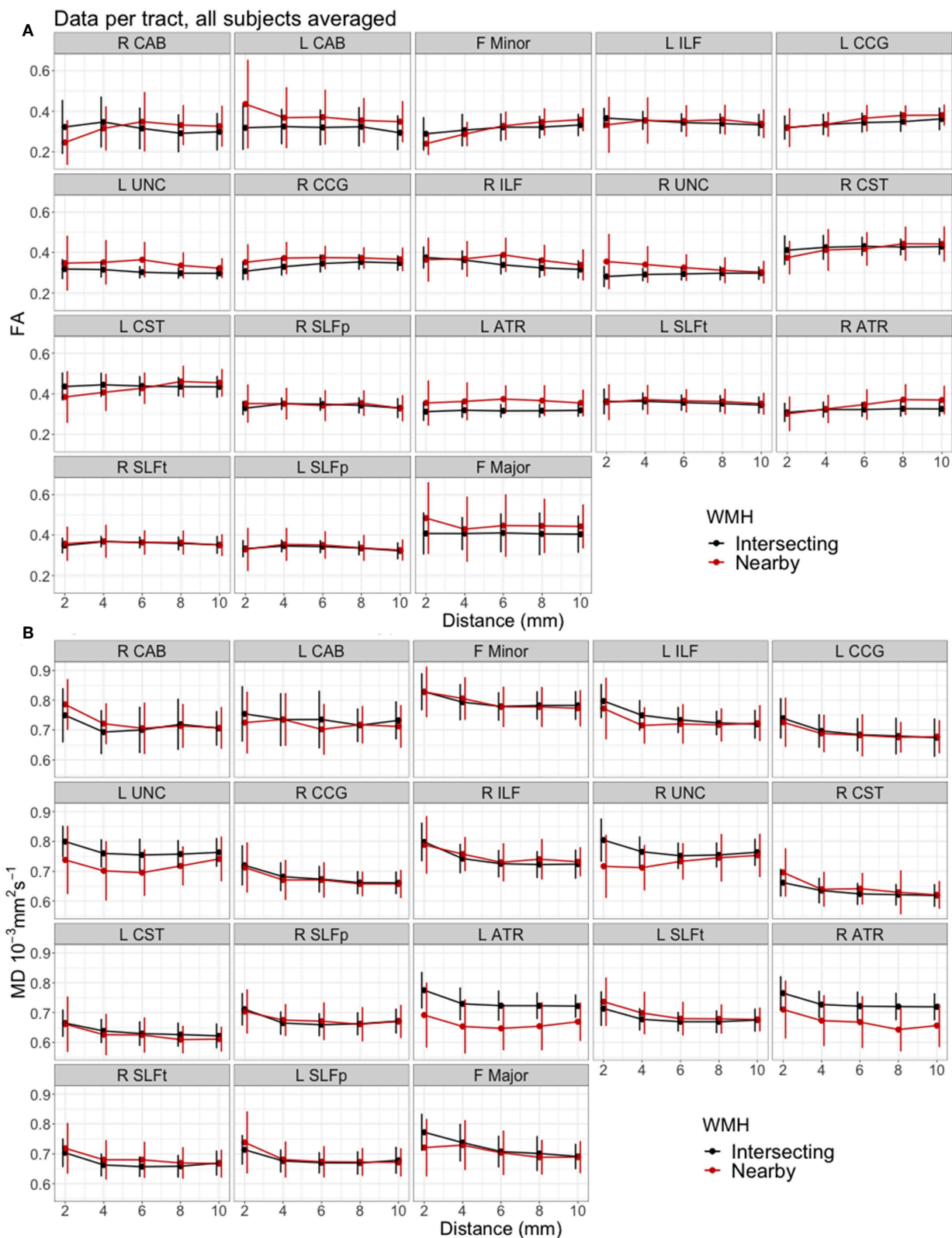


FIGURE 4 | Mean water diffusion changes in tract-NAWM with distance to intersecting (tract-WMH) and nearby WMH, for each individual tract. **(A)** Fractional anisotropy (FA), **(B)** mean diffusivity (MD). Error bars show standard deviation. Tracts are ordered by median % WMH overlap in tract, as in **Figure 2**. L, left; R, right; F, forceps; ATR, anterior thalamic radiation; CCG, cingulate cingulum; CAB, cingulum angular bundle; CST, corticospinal tract; ILF, inferior longitudinal fasciculus; SLFp, parietal superior longitudinal fasciculus; SLFt, temporal superior longitudinal fasciculus; UNC, uncinate fasciculus.

TABLE 3 | Results from the repeated-measures linear mixed model analysis for the analysis of water diffusion in tract-WMH spatial contours in individual tracts.

Outcome	FA					MD				
	Log(distance+1)					Log(distance+1)				
	Predictor									
Tract	Estimate	Std. error	Df.res	F	p	Estimate	Std. error	Df.res	F	p
F Major	0.034	0.007	33	20.8	<0.001	−0.126	0.007	33	300.1	<0.001
F Minor	0.040	0.006	35	52.4	<0.001	−0.076	0.007	35	121.1	<0.001
L ATR	0.033	0.003	42	114.8	<0.001	−0.105	0.007	42	259.1	<0.001
L CAB	0.000	0.013	16	0.0	0.999	−0.044	0.013	16	12.2	0.003
L CCG	0.037	0.005	34	66.4	<0.001	−0.076	0.008	34	100.1	0.000
L CST	0.022	0.006	44	13.8	0.001	−0.059	0.005	44	170.7	<0.001
L ILF	0.010	0.005	39	3.9	0.057	−0.112	0.009	39	161.7	<0.001
L SLFp	0.017	0.004	38	16.5	<0.001	−0.078	0.006	38	164.5	<0.001
L SLFt	0.020	0.003	40	34.0	<0.001	−0.087	0.006	40	198.6	<0.001
L UNC	0.023	0.003	37	51.4	<0.001	−0.100	0.007	37	209.7	<0.001
R ATR	0.040	0.004	42	106.8	<0.001	−0.094	0.007	42	203.7	<0.001
R CAB	0.013	0.012	20	1.1	0.310	−0.059	0.019	20	10.1	0.005
R CCG	0.036	0.004	28	75.1	<0.001	−0.085	0.009	28	97.6	<0.001
R CST	0.034	0.005	47	54.5	<0.001	−0.070	0.006	47	142.9	<0.001
R ILF	−0.001	0.004	38	0.0	0.834	−0.114	0.007	38	240.7	<0.001
R SLFp	0.024	0.004	38	28.7	<0.001	−0.088	0.006	38	185.7	<0.001
R SLFt	0.027	0.004	42	46.3	<0.001	−0.084	0.005	42	250.1	<0.001
R UNC	0.033	0.004	37	60.2	<0.001	−0.083	0.009	37	86.2	<0.001

FA, fractional anisotropy; MD, mean diffusivity in (10^{-3} mm²/s); L, left; R, right; F, forceps; ATR, anterior thalamic radiation; CCG, cingulate cingulum; CAB, cingulum angular bundle; CST, corticospinal tract; ILF, inferior longitudinal fasciculus; SLFp, parietal superior longitudinal fasciculus; SLFt, temporal superior longitudinal fasciculus; UNC, uncinat fasciculus.

from intersecting WMH. We observed a pattern of decreasing abnormalities as we moved further away from the intersecting WMH and along the WM tract. A similar distance pattern of abnormalities was observed in WM tract tissue at specific distances away from nearby WMH that were not directly connected to the tract. This indicates that microstructural tissue changes in WM tracts spread beyond the visible damage of the WMH, and also suggests that WMH have similar effects on tracts whether they are intersecting or nearby the tract.

A few studies of brain aging have specifically analyzed the structure of WM tracts intersecting with WMH (14, 34–37). They generally found the largest rates of WMH overlap in the anterior thalamic radiation, inferior longitudinal fasciculus, forceps major, posterior thalamic radiation and the inferior fronto-occipital fasciculus. We found similar rates of overlap for the forceps major and anterior thalamic radiation, but also observed large overlap in other tracts, such as in the parietal and temporal superior longitudinal fasciculi (median 2.0–2.7%, with several subjects with >25%), and with WMH affecting tracts in either brain hemisphere to a similar level (**Figure 2**). Differences in the overlap patterns with previous studies could be due to different tractography or registration methods employed, or by the different age ranges of the samples, as the prevalence of WMH is highly dependent on age (38). All the participants in our study were born in the same year, and therefore very close in age at time of MRI scanning, minimizing the effect of age on other results. However, we aimed to include participants to represent the whole range of WMH burden (Fazekas scores). As expected,

the distribution of Fazekas scores in **Figure 2** shows that those with lower Fazekas scores tend to have less WMH overlap in all tracts.

The incidence of WMH in specific tracts was not reported in previous studies, however the patterns of overlap that we observe agree with previous analyses on the distribution of WMH (39, 40). The CST had the highest percentage of participants with a WMH in this tract (>92%; **Table 1**), with a median WMH volume of 1.7%. The high incidence may be explained by the proximity of this tract to the lateral ventricles, and the common occurrence of periventricular WMH (41). Similarly, due to the typical pattern of distribution of WMH, the percentages of participants with a WMH in the forceps minor and the uncinat fasciculus, both tracts prominently passing through periventricular areas, were high (75–82.7%), but with smaller WMH volumes (median 0.5–1.3%). Additionally, we observed that the cingulum angular bundle was least often affected by WMH (46.2–50%). This might be explained by the smaller size of this tract, or because its section within the periventricular area is mostly located medially of the posterior part of the lateral ventricle, whereas periventricular WMH are mainly observed lateral to the anterior or posterior ends of the lateral ventricles (41). It can also be noted from **Figure 2**, that most participants with a low total Fazekas score did not have WMH overlapping with the cingulum angular bundle, while other tracts do overlap with WMH at all Fazekas scores, suggesting that the cingulum angular bundle is affected only in persons with more severe WMH.

TABLE 4 | Results from the repeated-measures linear mixed model analysis for the analysis of water diffusion in tract-WMH and nearby-WMH contours for individual tracts.

Predictor	Log(distance)					WMH “nearby”					Log(distance): WMH “nearby”				
Tract	Estimate	Std. error	Df.res	F	p	Estimate	Std. error	Df.res	F	p	Estimate	Std. error	Df.res	F	p
Outcome		FA													
F Major	−0.005	0.011	33.9	0.2	0.681	0.039	0.011	256.2	13.0	0.000					
F Minor	0.029	0.007	79.6	15.8	0.000	−0.085	0.015	325.7	32.9	0.000	0.049	0.008	325.3	33.8	< 0.001
L ATR	0.004	0.007	44.2	0.3	0.595	0.045	0.005	346.4	72.4	0.000					
L CAB	−0.030	0.020	32.2	2.3	0.139	0.042	0.013	156.0	10.9	0.001					
L CCG	0.035	0.006	40.9	31.6	0.000	0.015	0.005	326.3	8.8	0.003					
L CST	−0.003	0.009	70.2	0.1	0.716	−0.099	0.019	352.6	27.4	0.000	0.053	0.0102	349.4	26.6	< 0.001
L ILF	−0.014	0.007	43.0	4.0	0.053	0.005	0.006	281.5	0.8	0.361					
L SLFp	−0.006	0.006	40.4	0.8	0.371	0.004	0.004	306.1	0.7	0.417					
L SLFt	−0.008	0.006	42.7	1.7	0.198	0.006	0.004	325.0	2.7	0.104					
L UNC	−0.017	0.007	40.0	5.3	0.026	0.038	0.006	305.1	46.4	0.000					
R ATR	0.010	0.007	75.1	1.9	0.171	−0.045	0.016	351.8	7.3	0.007	0.039	0.009	347.2	18.3	< 0.001
R CAB	0.005	0.015	36.1	0.1	0.728	0.046	0.013	212.8	12.2	0.001					
R CCG	0.018	0.005	39.3	12.4	0.001	0.036	0.005	306.3	44.1	0.000					
R CST	0.025	0.007	48.6	12.4	0.001	−0.001	0.005	372.4	0.0	0.852					
R ILF	−0.029	0.006	43.4	25.6	0.000	0.019	0.006	292.7	11.5	0.001					
R SLFp	−0.002	0.005	40.4	0.2	0.661	0.002	0.005	318.4	0.3	0.608					
R SLFt	0.000	0.005	45.5	0.0	0.976	0.004	0.004	344.6	1.1	0.300					
R UNC	0.012	0.008	66.2	2.1	0.150	0.120	0.019	312.8	41.1	0.000	−0.050	0.010	313.3	25.0	< 0.001
Outcome		MD													
F Major	−0.044	0.006	33.8	48.9	0.000	−0.010	0.006	258.7	2.7	0.099					
F Minor	−0.034	0.004	38.3	82.7	0.000	0.005	0.004	310.5	1.3	0.262					
L ATR	−0.024	0.006	43.5	15.9	0.000	−0.071	0.005	345.0	168.0	0.000					
L CAB	−0.018	0.012	30.4	2.4	0.134	−0.031	0.011	175.6	7.1	0.008					
L CCG	−0.036	0.006	40.6	36.8	0.000	−0.004	0.005	321.1	0.7	0.398					
L CST	−0.027	0.004	46.1	49.7	0.000	−0.013	0.004	336.6	13.1	0.000					
L ILF	−0.041	0.006	42.9	53.3	0.000	−0.011	0.005	279.6	5.8	0.016					
L SLFp	−0.028	0.005	40.4	35.7	0.000	0.004	0.003	303.6	1.2	0.283					
L SLFt	−0.031	0.004	42.3	54.4	0.000	0.011	0.004	326.0	10.3	0.001					
L UNC	−0.013	0.006	39.4	4.9	0.033	−0.044	0.005	302.9	67.3	0.000					
R ATR	−0.029	0.005	42.4	38.1	0.000	−0.059	0.005	333.0	147.0	0.000					
R CAB	−0.030	0.010	34.5	9.9	0.003	0.002	0.010	219.2	0.0	0.859					
R CCG	−0.035	0.005	39.9	48.9	0.000	−0.012	0.005	305.1	5.9	0.016					
R CST	−0.031	0.004	47.3	71.3	0.000	0.009	0.004	375.0	6.3	0.013					
R ILF	−0.042	0.006	43.8	52.5	0.000	0.010	0.004	285.8	4.5	0.034					
R SLFp	−0.025	0.005	40.5	27.2	0.000	0.007	0.004	312.3	3.4	0.067					
R SLFt	−0.027	0.004	45.2	49.3	0.000	0.013	0.003	340.9	16.1	0.000					
R UNC	−0.030	0.008	73.8	13.5	0.000	−0.144	0.020	309.3	50.5	0.000	0.063	0.011	313.1	33.8	< 0.001

WMH, white matter hyperintensity; FA, fractional anisotropy; MD, mean diffusivity in (10^{-3} mm²/s); L, left; R, right; F, forceps; ATR, anterior thalamic radiation; CCG, cingulate cingulum; CAB, cingulum angular bundle; CST, corticospinal tract; ILF, inferior longitudinal fasciculus; SLFp, parietal superior longitudinal fasciculus; SLFt, temporal superior longitudinal fasciculus; UNC, uncinate fasciculus.

Regarding the microstructural quality of the WM, for the majority of the 18 WM tracts assessed here, we observed the expected pattern with higher MD and lower FA in tract-WMH. Both parameters then normalize as we move away from the visible damage, with FA significantly increasing and MD significantly decreasing as we get 2–10 mm away from the visible WMH. Such microstructural abnormalities may be caused by

a variety of microvascular dysfunctions, resulting in interstitial edema, inflammation, ischemia and damage to the myelin sheath of WM tracts, ultimately leading to visible WMH (42).

These results agree with a similar analysis of tracts crossing through WMH (14), although they are not entirely in line with previous studies conducted by our group of the whole NAWM (13, 43). In our previous analysis, we *qualitatively*

observed a similar distance pattern for whole-brain NAWM up to and including 4 mm distance from WMH edge for FA and 8 mm from WMH edge for MD, but at further distances the abnormalities in the NAWM apparently increased (with reducing FA and increasing MD). This might be explained by the fact that previously we looked at whole-brain NAWM rather than tract specific regions, hence may have found a “location bias” where the WMH contours extended across WM tracts (13). The current study did not suffer from location bias because water diffusion was measured in NAWM contours specifically in the same tract.

Another location effect to be considered is that WMH typically appear in areas of the brain where there is complex white matter fiber architecture (e.g., fiber bundle crossing, bending or kissing), such as periventricular regions. This could in turn affect values of the water diffusion metrics measured in a specific tract (44), and hence the changes observed in contours moving away from the WMH could be caused by the changing fiber architecture, rather than by the WMH. This effect could be mitigated in an individual tract by measuring also the water diffusion parameters in a non-WMH affected tract. However, FA and MD values are relatively specific to each tract system (45), and water diffusion parameters measured along a tract show very specific patterns (46). Hence this correction could only be performed between equivalent contralateral white matter tracts. WMH tend to be quite symmetrical between brain hemispheres (41, 47), even when there is an asymmetry in potential risk factors, such as blood supply (48), and there are typically insufficient equivalent areas of each tract affected by WMH in one hemisphere, but unaffected in the contralateral hemisphere, to perform such a correction. Nevertheless, we performed a supplementary analysis of FA and MD measured in a tract with complex fiber architecture and compared the values measured in equivalent areas in participants with and without WMH. We found that any residual effects of fiber architecture in tract sections equivalent to those surrounding a WMH would not fully account for the changes we observed around a WMH (see **Supplement 1**).

We also measured the diffusion characteristics in areas of tracts that were nearby, but not directly connected to a WMH, to study the effects of these nearby WMH on the tracts. It has been suggested that, from a biological perspective, WMH in a WM tract would influence the tissue integrity along the rest of the tract more strongly than a nearby (non-directly connected) WMH since the interstitial fluid changes and secondary degenerative processes could theoretically propagate more easily along the tract than in adjacent non-tract tissue where cell processes are less well aligned (12, 37). This interpretation was supported by Reginold et al. (14) who analyzed diffusion changes in WM tracts with distance from WMH and reported that CST tracts traversing WMH have worse diffusion characteristics (MD, axial, and radial diffusivity, but not FA) at the same distance from WMH, compared to CST tracts that did not intersect but were close to a WMH, concluding that WMH may be causing abnormalities in NAWM through Wallerian-type degeneration. Our results are consistent with these findings and our plots of FA and MD for the CST in **Figure 4** show similar trajectories to those in Reginold et al. (14). In particular, we also observed higher MD in areas

surrounding tract-WMH compared to nearby-WMH contours (**Table 4**). The changes for FA in this tract were however more complex; **Figure 4A** shows that, for both CST, the areas of the tract nearby, but not directly connected to WMH, had lower FA than areas at similar distance surrounding an intersecting WMH, up to a distance approximately of 6 mm, while at further distances FA was higher for “nearby” contours. Low FA can indicate axonal injury and myelin loss, hence the lower values of FA in the nearby-WMH contours, up to 6 mm, suggest lower quality of the WM in these areas, compared to the intersecting-WMH contours. A similar effect is also observed in other tracts, such as the right CAB, F Minor and the R ATR, indicating that in these tracts the damage is more localized around the nearby-WMH. For both WMH types the FA increased with distance from WMH with a higher gradient for nearby-WMH contours, with FA trends for both WMH types crossing over at 4–6 mm suggesting a faster normalization for nearby-WMH contours in some tracts.

Our analysis including all 18 tracts in the model also supports previous studies (14). Our full model including data from all tracts in **Figure 3** shows that MD was consistently lower, while FA was higher in nearby-WMH contours compared with intersecting WMH contours. For both WMH types, MD decreased while FA increased with distance from WMH. The estimated differences observed for both type of WMH were small but significant for both FA and MD. Our results may support the hypothesis that age-related WM damage propagates further along tract axons, potentially through enabling propagation of interstitial fluid or through Wallerian-type degeneration, as previous studies suggested. However, the larger accumulation of damage around the nearby WMH (lower FA) in some tracts, may suggest that different mechanisms of tissue damage propagation also play a role. For example, age-related WMH are associated with other small vessel disease (SVD) features, such as widening of perivascular spaces (1, 49, 50), that reflect microvascular dysfunction including abnormal blood-brain barrier leakage, impaired vasoreactivity and impaired pulsatility. Other SVD studies also found that MD is more abnormal than FA in NAWM adjacent to WMH (51, 52), suggesting other potential channels for the propagation of tissue damage, inducing FA and MD changes, independently of the direct connections of WM tracts. As shown in **Figure 4**, the effects of WMH in WM tracts are variable across the brain. A detailed study of this variation across tracts and locations in the brain could help pinpointing the processes underlying the microstructural changes detected and their effects on cognitive and physical function.

Water diffusion abnormalities within the NAWM are suggestive of tissue damage not yet visible on a lesion level. It is, however, unclear whether the WMH are the cause of the NAWM damage, or whether both are part of the same continuum of tissue damage (53). These water diffusion abnormalities are a precursor to lesion extension or development within the NAWM (53–56), which reflect the general association between higher WMH load, worse NAWM MD and more WMH growth. As lesions are associated with cognitive abnormalities (7, 8, 57), such lesion development in NAWM areas suggests that pre-lesional NAWM water diffusion abnormalities may already play a role

in cognitive functioning (58, 59). Previous studies have found that the rate of WMH growth was heterogeneous, occurring more rapidly within some association and projection tracts compared to other white matter regions (39). A longitudinal study of this growth at the tract level, and with respect to the location of tract-WMH and nearby WMH induced changes in the tract-NAWM, could help explain the patterns of WMH progression.

This study has some limitations. Firstly, it has a relatively small sample, mainly for the individual tract comparisons where there were few cases with WMH in some tracts. However, the current study is the largest to date looking at specific locations of NAWM in WM tracts with distance from the WMH and its results will be used as motivation for investigating WMH-tract interactions in larger samples. The current study can be further extended to focus on relating water diffusion in tract-WMH and tract-NAWM to premorbid cognition, current cognitive functioning, and on the development of water diffusion abnormalities in tract-WMH and tract-NAWM over time. Secondly, the closer spatial contours were not available for every tract as some nearby WMH were too far away for a 2- or 4-mm contour to cross with the tract. This means that there were less data contributing to the calculation of water diffusion for 2 and 4 mm and their measurements might be less accurate than for the tract-WMH contours. However, we used linear mixed models for our analysis, which are less sensitive to missing data and allow the inclusion of location data for all tracts without introducing a bias. Thirdly, water diffusion metrics need to be interpreted with care in regions with complex fiber configurations, such as crossing or bending fibers, which might confound the measured changes in water diffusion metrics. The imaging parameters and methodology used for analyzing the diffusion data might also have a significant effect in such a fine-grained analysis, therefore the patterns of change with distance will need to be corroborated in larger studies.

In conclusion, microstructural changes in tract-NAWM became less pronounced along the tract and further away from the tract-WMH, with a comparable distance pattern away from the nearby (not intersecting) WMH. The observed differences in tissue microstructure between the WM tract areas surrounding intersecting WMH and those surrounding nearby non-intersecting WMH suggest that WM degenerative processes in SVD may propagate further along the tract for intersecting WMH. In some areas of the brain there is a larger and more localized accumulation of axonal damage in tract tissue nearby a non-connected WMH, suggesting that different channels of accumulation of the damage need to be explored. The tissue damage in WM tracts observed beyond visible lesions may contribute to cortical disconnection and changes in cognitive functioning. Our future efforts are aimed at elucidating the relationship between microstructural changes of nearby and intersecting-WMH, tract-NAWM and cognitive functioning at older ages, and at the development of tissue changes in tract-NAWM over time.

DATA AVAILABILITY

The datasets generated for this study are available on request to the corresponding author.

ETHICS STATEMENT

Written informed consent was obtained from all participants under protocols approved by the National Health Service Ethics Committees.

AUTHOR CONTRIBUTIONS

SM and RM conducted the MRI tractography, data processing and statistical analyses, and drafted the initial manuscript. FC assisted with data statistical analysis and interpretation. MV conducted the tissue segmentation analysis. MB designed the MRI protocol and assisted with manuscript. JS, ID, and JW designed and conceived the LBC1936 study and assisted with manuscript. JW performed WMH visual scores and assisted with data interpretation.

ACKNOWLEDGMENTS

This research and LBC1936 phenotype collection were supported by Research Into Ageing and continues as part of The Disconnected Mind project, funded by Age UK, and by the UK Medical Research Council (G0701120, G1001245, and MR/M013111/1). Magnetic Resonance Image acquisition and analyses were conducted at the Brain Research Imaging Centre, Neuroimaging Sciences, University of Edinburgh (www.bric.ed.ac.uk) which is part of SINAPSE (Scottish Imaging Network—A Platform for Scientific Excellence) collaboration (www.sinapse.ac.uk) funded by the Scottish Funding Council and the Chief Scientist Office. This work was supported by the Centre for Cognitive Ageing and Cognitive Epidemiology, funded by the Medical Research Council and the Biotechnology and Biological Sciences Research Council (MR/K026992/1), the Row Fogo Charitable Trust (BRO-D.FID3668413), the European Union Horizon 2020, PHC-03-15, project No 666881, SVDs@Target, the Fondation Leducq Transatlantic Network of Excellence for the Study of Perivascular Spaces in Small Vessel Disease, ref no. 16 CVD 05, and the Medical Research Council UK Dementia Research Institute at the University of Edinburgh. We thank the Lothian Birth Cohort 1936 participants who took part in this study, the Lothian Birth Cohort 1936 research team members, and radiographers at the Brain Research Imaging Centre. A version of this manuscript has been released as a Pre-Print at BioRxiv (2018, doi: 10.1101/412064).

SUPPLEMENTARY MATERIAL

The Supplementary Material for this article can be found online at: <https://www.frontiersin.org/articles/10.3389/fneur.2019.00784/full#supplementary-material>

REFERENCES

- Fazekas F, Kleinert R, Offenbacher H, Schmidt R, Kleinert G, Payer F, et al. Pathologic correlates of incidental MRI white matter signal hyperintensities. *Neurology*. (1993) 43:1683–9. doi: 10.1212/WNL.43.9.1683
- O'Sullivan M, Jones DK, Summers PE, Morris RG, Williams SC, Markus HS. Evidence for cortical “disconnection” as a mechanism of age-related cognitive decline. *Neurology*. (2001) 57:632–8. doi: 10.1212/WNL.57.4.632
- Ritchie SJ, Bastin ME, Tucker-Drob EM, Muñoz Maniega S, Engelhardt LE, Cox SR, et al. Coupled changes in brain white matter microstructure and fluid intelligence in later life. *J Neurosci*. (2015) 35:8672–82. doi: 10.1523/JNEUROSCI.0862-15.2015
- Haynes BI, Bunce D, Kochan NA, Wen W, Brodaty H, Sachdev PS. Associations between reaction time measures and white matter hyperintensities in very old age. *Neuropsychologia*. (2017) 96:249–55. doi: 10.1016/j.neuropsychologia.2017.01.021
- Fernández-Cabello S, Valls-Pedret C, Schurz M, Vidal-Piñero D, Sala-Llanch R, Bargallo N, et al. White matter hyperintensities and cognitive reserve during a working memory task: a functional magnetic resonance imaging study in cognitively normal older adults. *Neurobiol Aging*. (2016) 48:23–33. doi: 10.1016/j.neurobiolaging.2016.08.008
- Ritchie SJ, Dickie DA, Cox SR, Valdes Hernandez Mdel C, Corley J, Royle NA, et al. Brain volumetric changes and cognitive ageing during the eighth decade of life. *Hum Brain Mapp*. (2015) 36:4910–25. doi: 10.1002/hbm.22959
- Reginold W, Luedke AC, Tam A, Itorralba J, Fernandez-Ruiz J, Reginold J, et al. Cognitive function and 3-tesla magnetic resonance imaging tractography of white matter hyperintensities in elderly persons. *Dement Geriatr Cogn Dis Extra*. (2015) 5:387–94. doi: 10.1159/000439045
- Biesbroek J. Impact of strategically located white matter hyperintensities on cognition in memory clinic patients with small vessel disease. *PLoS ONE*. (2016) 11:e016626. doi: 10.1371/journal.pone.0166261
- Beaulieu C. The basis of anisotropic water diffusion in the nervous system—a technical review. *NMR Biomed*. (2002) 15:435–55. doi: 10.1002/nbm.782
- Rodríguez-Cruces R, Concha L. White matter in temporal lobe epilepsy: clinico-pathological correlates of water diffusion abnormalities. *Quant Imaging Med Surg*. (2015) 5:264–78. doi: 10.3978/j.issn.2223-4292.2015.02.06
- Song SK, Sun SW, Ju WK, Lin SJ, Cross AH, Neufeld AH. Diffusion tensor imaging detects and differentiates axon and myelin degeneration in mouse optic nerve after retinal ischemia. *Neuroimage*. (2003) 20:1714–22. doi: 10.1016/j.neuroimage.2003.07.005
- Maillard P, Fletcher E, Harvey D, Carmichael O, Reed B, Mungas D, et al. White matter hyperintensity penumbra. *Stroke*. (2011) 42:1917–22. doi: 10.1161/STROKEAHA.110.609768
- Muñoz Maniega S, Valdés Hernández MC, Clayden JD, Royle NA, Murray C, Morris Z, et al. White matter hyperintensities and normal-appearing white matter integrity in the aging brain. *Neurobiol Aging*. (2015) 36:909–18. doi: 10.1016/j.neurobiolaging.2014.07.048
- Reginold W, Sam K, Poulblanc J, Fisher J, Crawley A, Mikulis DJ. Impact of white matter hyperintensities on surrounding white matter tracts. *Neuroradiology*. (2018) 60:933–44. doi: 10.1007/s00234-018-2053-x
- Mori S, van Zijl PCM. Fiber tracking: principles and strategies—a technical review. *NMR Biomed*. (2002) 15:468–80. doi: 10.1002/nbm.781
- Deary IJ, Gow AJ, Taylor MD, Corley J, Brett C, Wilson V, et al. The lothian birth cohort 1936: a study to examine influences on cognitive ageing from age 11 to age 70 and beyond. *BMC Geriatr*. (2007) 7:28. doi: 10.1186/1471-2318-7-28
- Deary IJ, Gow AJ, Pattie A, Starr JM. Cohort profile: the lothian birth cohorts of 1921 and 1936. *Int J Epidemiol*. (2012) 41:1576–84. doi: 10.1093/ije/dyr197
- Wardlaw JM, Bastin ME, Valdés Hernández MC, Muñoz Maniega S, Royle NA, Morris Z, et al. Brain aging, cognition in youth and old age and vascular disease in the lothian birth cohort 1936: rationale, design and methodology of the imaging protocol. *Int J Stroke*. (2011) 6:547–59. doi: 10.1111/j.1747-4949.2011.00683.x
- Fazekas F, Chawluk JB, Alavi A, Hurtig HI, Zimmerman RA. MR signal abnormalities at 1.5 T in Alzheimer's dementia and normal aging. *AJR Am J Roentgenol*. (1987) 149:351–6. doi: 10.2214/ajr.149.2.351
- Valdés Hernández MC, Morris Z, Dickie DA, Royle NA, Muñoz Maniega S, Aribisala BS, et al. Close correlation between quantitative and qualitative assessments of white matter lesions. *Neuroepidemiology*. (2013) 40:13–22. doi: 10.1159/000341859
- Jones DK, Williams SCR, Gasston D, Horsfield MA, Simmons A, Howard R. Isotropic resolution diffusion tensor imaging with whole brain acquisition in a clinically acceptable time. *Hum Brain Mapp*. (2002) 15:216–30. doi: 10.1002/hbm.10018
- Wardlaw JM, Smith EE, Biessels GJ, Cordonnier C, Fazekas F, Frayne R, et al. Neuroimaging standards for research into small vessel disease and its contribution to ageing and neurodegeneration. *Lancet Neurol*. (2013) 12:822–38. doi: 10.1016/S1474-4422(13)70124-8
- Jenkinson M, Smith S. A global optimisation method for robust affine registration of brain images. *Med Image Anal*. (2001) 5:143–56. doi: 10.1016/S1361-8415(01)00036-6
- Valdés Hernández MC, Ferguson KJ, Chappell FM, Wardlaw JM. New multispectral MRI data fusion technique for white matter lesion segmentation: method and comparison with thresholding in FLAIR images. *Eur Radiol*. (2010) 20:1684–91. doi: 10.1007/s00330-010-1718-6
- Jenkinson M, Beckmann CF, Behrens TEJ, Woolrich MW, Smith SM. FSL. *Neuroimage*. (2012) 62:782–90. doi: 10.1016/j.neuroimage.2011.09.015
- Smith SM. Fast robust automated brain extraction. *Hum Brain Mapp*. (2002) 17:143–55. doi: 10.1002/hbm.10062
- Yendiki A, Panneck P, Srinivasan P, Stevens A, Zöllei L, Augustinack J, et al. Automated probabilistic reconstruction of white-matter pathways in health and disease using an atlas of the underlying anatomy. *Front Neuroinform*. (2011) 5:23. doi: 10.3389/fninf.2011.00023
- Behrens TEJ, Johansen-Berg H, Jbabdi S, Rushworth MFS, Woolrich MW. Probabilistic diffusion tractography with multiple fibre orientations: what can we gain? *Neuroimage*. (2007) 34:144–55. doi: 10.1016/j.neuroimage.2006.09.018
- Modat M, Ridgway GR, Taylor ZA, Lehmann M, Barnes J, Hawkes DJ, et al. Fast free-form deformation using graphics processing units. *Comput Methods Programs Biomed*. (2010) 98:278–84. doi: 10.1016/j.cmpb.2009.09.002
- Clayden J, Modat M, Presles B, Anthopoulos T, Daga P. *RNiftyReg: Image Registration Using The NiftyReg Library*. (2015) Available online at: <http://cran.r-project.org/package=RNiftyReg>
- Fox J, Weisberg S. *An R Companion to Applied Regression*. Thousand Oaks, CA: Sage (2011). Available online at: <http://socserv.socsci.mcmaster.ca/jfox/Books/Companion>
- Kuznetsova A, Brockhoff PB, Christensen RHB. {lmerTest} Package: Tests in Linear Mixed Effects Models. *J Stat Softw*. (2017) 82:1–26. doi: 10.18637/jss.v082.i13
- Wickham H. *ggplot2: Elegant Graphics for Data Analysis*. New York, NY: Springer-Verlag (2016). Available online at: <https://ggplot2-book.org>
- Taylor ANW, Kambeitz-Ilanovic L, Gesierich B, Simon-Vermot L, Franzmeier N, Araque Caballero MÁ, et al. Tract-specific white matter hyperintensities disrupt neural network function in Alzheimer's disease. *Alzheimer's Dement*. (2017) 13:225–35. doi: 10.1016/j.jalz.2016.06.2358
- Maillard P, Seshadri S, Beiser A, Himali J, DeCarli C. Regional vulnerability within white matter tracts to white matter hyperintensities: a diffusion tensor imaging tractography study. *Stroke*. (2015) 46:A221. Available online at: http://stroke.ahajournals.org/content/46/Suppl_1/A221.short (accessed November 17, 2016).
- Seiler S, Fletcher E, Hassan-Ali K, Weinstein M, Beiser A, Himali JJ, et al. Cerebral tract integrity relates to white matter hyperintensities, cortex volume, and cognition. *Neurobiol Aging*. (2018) 72:14–22. doi: 10.1016/j.neurobiolaging.2018.08.005
- Reginold W, Itorralba J, Luedke AC, Fernandez-Ruiz J, Reginold J, Islam O, et al. Tractography at 3T MRI of corpus callosum tracts crossing white matter hyperintensities. *AJNR Am J Neuroradiol*. (2016) 37:1617–22. doi: 10.3174/ajnr.A4788
- de Leeuw FE, de Groot JC, Achten E, Oudkerk M, Ramos LM, Heijboer R, et al. Prevalence of cerebral white matter lesions in elderly people: a population based magnetic resonance imaging study. The rotterdam scan study. *J Neurol Neurosurg Psychiatry*. (2001) 70:9–14. doi: 10.1136/jnnp.70.1.9
- Lambert C, Benjamin P, Zeestraten E, Lawrence AJ, Barrick TR, Markus HS. Longitudinal patterns of leukoaraiosis and brain atrophy in symptomatic small vessel disease. *BRAIN*. (2016) 139:1136–51. doi: 10.1093/brain/aww009

40. Habes M, Erus G, Toledo JB, Zhang T, Bryan N, Launer LJ, et al. White matter hyperintensities and imaging patterns of brain ageing in the general population. *Brain*. (2016) 139:1164–79. doi: 10.1093/brain/aww008
41. Valdés Hernández MC, Maconick LC, Muñoz Maniega S, Wang X, Wiseman S, Armitage PA, et al. A comparison of location of acute symptomatic vs. “silent” small vessel lesions. *Int J Stroke*. (2015) 10:1044–50. doi: 10.1111/ijss.12558
42. Wardlaw JM, Chappell FM, Valdés Hernández MDC, Makin SDJ, Staals J, Shuler K, et al. White matter hyperintensity reduction and outcomes after minor stroke. *Neurology*. (2017) 89:1003–10. doi: 10.1212/WNL.0000000000004328
43. Wardlaw JM, Makin SJ, Valdés Hernández MC, Armitage PA, Heye AK, Chappell FM, et al. Blood-brain barrier failure as a core mechanism in cerebral small vessel disease and dementia: evidence from a cohort study. *Alzheimer's Dement*. (2017) 13:634–43. doi: 10.1016/j.jalz.2016.09.006
44. Vos SB, Jones DK, Jeurissen B, Viergever MA, Leemans A. The influence of complex white matter architecture on the mean diffusivity in diffusion tensor MRI of the human brain. *Neuroimage*. (2012) 59:2208–16. doi: 10.1016/j.neuroimage.2011.09.086
45. Bastin ME, Muñoz Maniega S, Ferguson KJ, Brown LJ, Wardlaw JM, MacLullich AMJ, et al. Quantifying the effects of normal ageing on white matter structure using unsupervised tract shape modelling. *Neuroimage*. (2010) 51:1–10. doi: 10.1016/j.neuroimage.2010.02.036
46. Colby JB, Soderberg L, Lebel C, Dinov ID, Thompson PM, Sowell ER. Along-tract statistics allow for enhanced tractography analysis. *Neuroimage*. (2012) 59:3227–42. doi: 10.1016/j.neuroimage.2011.11.004
47. Ryu W, Schellingerhout D, Ahn H, Park S, Hong K, Jeong S, et al. Hemispheric asymmetry of white matter hyperintensity in association with lacunar infarction. *J Am Heart Assoc*. (2018) 7:e010653. doi: 10.1161/JAHA.118.010653
48. Potter GM, Doubal FN, Jackson CA, Sudlow CLM, Dennis MS, Wardlaw JM. Lack of association of white matter lesions with ipsilateral carotid artery stenosis. *Cerebrovasc Dis*. (2012) 33:378–84. doi: 10.1159/000336762
49. Schmidt R, Schmidt H, Haybaeck J, Loitfelder M, Weis S, Cavalieri M, et al. Heterogeneity in age-related white matter changes. *Acta Neuropathol*. (2011) 122:171–85. doi: 10.1007/s00401-011-0851-x
50. Munoz DG, Hastak SM, Harper B, Lee D, Hachinski VC. Pathologic correlates of increased signals of the centrum ovale on magnetic resonance imaging. *Arch Neurol*. (1993) 50:492–7. doi: 10.1001/archneur.1993.00540050044013
51. MacLullich AMJ, Ferguson KJ, Reid LM, Deary IJ, Starr JM, Seckl JR, et al. Higher systolic blood pressure is associated with increased water diffusivity in normal-appearing white matter. *Stroke*. (2009) 40:3869–71. doi: 10.1161/STROKEAHA.109.547877
52. Muñoz Maniega S, Chappell FM, Valdés Hernández MC, Armitage PA, Makin SD, Heye AK, et al. Integrity of normal-appearing white matter: influence of age, visible lesion burden and hypertension in patients with small-vessel disease. *J Cereb Blood Flow Metab*. (2017) 37:644–56. doi: 10.1177/0271678X16635657
53. Maillard P, Fletcher E, Lockhart SN, Roach AE, Reed B, Mungas D, et al. Carmichael OT. White matter hyperintensities and their penumbra lie along a continuum of injury in the aging brain. *Stroke*. (2014) 45:1721–6. doi: 10.1161/STROKEAHA.113.004084
54. Maillard P, Carmichael O, Harvey D, Fletcher E, Reed B, Mungas D, et al. FLAIR and diffusion MRI signals are independent predictors of white matter hyperintensities. *Am J Neuroradiol*. (2013) 34:54–61. doi: 10.3174/ajnr.A3146
55. de Groot M, Verhaaren BFJ, de Boer R, Klein S, Hofman A, van der Lugt A, et al. Changes in normal-appearing white matter precede development of white matter lesions. *Stroke*. (2013) 44:1037–42. doi: 10.1161/STROKEAHA.112.680223
56. Mayo CD, Mazerolle EL, Ritchie L, Fisk JD, Gawryluk JR. Longitudinal changes in microstructural white matter metrics in Alzheimer's disease. *NeuroImage Clin*. (2017) 13:330–8. doi: 10.1016/j.nicl.2016.12.012
57. Valdés Hernández MC, Booth T, Murray C, Gow AJ, Penke L, Morris Z, et al. Brain white matter damage in aging and cognitive ability in youth and older age. *Neurobiol Aging*. (2013) 34:2740–7. doi: 10.1016/j.neurobiolaging.2013.05.032
58. Jokinen H, Schmidt R, Ropele S, Fazekas F, Gouw AA, Barkhof F, et al. Diffusion changes predict cognitive and functional outcome: the LADIS study. *Ann Neurol*. (2013) 73:576–83. doi: 10.1002/ana.23802
59. Baykara E, Gesierich B, Adam R, Tuladhar AM, Biesbroek JM, Koek HL, et al. A novel imaging marker for small vessel disease based on skeletonization of white matter tracts and diffusion histograms. *Ann Neurol*. (2016) 80:581–92. doi: 10.1002/ana.24758

Conflict of Interest Statement: The authors declare that the research was conducted in the absence of any commercial or financial relationships that could be construed as a potential conflict of interest.

Copyright © 2019 Muñoz Maniega, Meijboom, Chappell, Valdés Hernández, Starr, Bastin, Deary and Wardlaw. This is an open-access article distributed under the terms of the Creative Commons Attribution License (CC BY). The use, distribution or reproduction in other forums is permitted, provided the original author(s) and the copyright owner(s) are credited and that the original publication in this journal is cited, in accordance with accepted academic practice. No use, distribution or reproduction is permitted which does not comply with these terms.



Total Small Vessel Disease Burden Predicts Functional Outcome in Patients With Acute Ischemic Stroke

Ying-chao Huo¹, Qi Li¹, Wen-yu Zhang¹, Ning Zou¹, Rui Li², Si-yuan Huang¹, Hui-qi Wang¹, Kai-yi Song¹, Rong-rong Zhang¹ and Xin-yue Qin^{1*}

¹ Department of Neurology, The First Affiliated Hospital, Chongqing Medical University, Chongqing, China, ² Division of Life Sciences and Medicine, Department of Neurology, The First Affiliated Hospital, University of Science and Technology of China, Hefei, China

OPEN ACCESS

Edited by:

Andreas Charidimou,
Massachusetts General Hospital and
Harvard Medical School,
United States

Reviewed by:

Julie Staals,
Maastricht University Medical
Centre, Netherlands
Gregoire Boulouis,
Université Paris Descartes, France

*Correspondence:

Xin-yue Qin
qinxu2019@sina.com

Specialty section:

This article was submitted to
Stroke,
a section of the journal
Frontiers in Neurology

Received: 16 April 2019

Accepted: 15 July 2019

Published: 06 August 2019

Citation:

Huo Y, Li Q, Zhang W, Zou N, Li R,
Huang S, Wang H, Song K, Zhang R
and Qin X (2019) Total Small Vessel
Disease Burden Predicts Functional
Outcome in Patients With Acute
Ischemic Stroke.
Front. Neurol. 10:808.
doi: 10.3389/fneur.2019.00808

Background: Cerebral small vessel disease (SVD) is generally considered as a cause of stroke, disability, gait disturbances, vascular cognitive impairment, and dementia. The aim of this study was to investigate whether the total SVD burden can be used to predict functional outcome in patients with acute ischemic stroke.

Methods: From April 2017 to January 2018, consecutive patients with acute ischemic stroke who underwent baseline MRI scan were evaluated. The functional outcome was assessed using the modified Rankin Scale (mRS) at 90 days and defined as i) excellent outcome ($mRS \leq 1$) and ii) good outcome ($mRS \leq 2$). Brain MRI was performed and assessed for lacunes, white matter hyperintensities (WMH), and enlarged perivascular spaces (EPVS). The total SVD burden was calculated based on lacunes, WMH, and EPVS and then summed up to generate an ordinal “total SVD burden” (range 0–3). Bivariate logistic regression models were used to identify the association between SVD and functional outcome.

Results: A total of 416 patients were included in the final analysis; 44.0, 33.4, 19.2, and 3.4% of the patients had 0, 1, 2, and 3 features of SVD, respectively. In regard to individual SVD feature, lacunes (OR: 0.48, 95% CI: 0.32–0.71; OR: 0.49, 95% CI: 0.31–0.77) and WMH (OR: 0.53, 95% CI: 0.34–0.82; OR: 0.53, 95% CI: 0.33–0.85) were negatively associated with excellent outcome and good outcome. As to the total burden of SVD, three SVD features had strongest negative associations with functional outcomes (excellent outcome, OR: 0.13, 95% CI: 0.03–0.48; good outcome, OR: 0.18, 95% CI: 0.06–0.54). After adjustment for potential confounders, a high SVD burden (3 features, OR: 0.07, 95% CI: 0.01–0.41) and the score of total SVD burden (OR: 0.64, 95% CI: 0.44–0.93) remained negatively associated with excellent outcome.

Conclusion: Total SVD burden negatively associated with functional outcome at 3 months in patients with acute ischemic stroke and is superior to individual SVD feature in prediction of functional outcome. MRI-based assessment of total SVD burden is highly valuable in clinical management of stroke victims and could help guide the allocation of resources to improve outcome.

Keywords: cerebral small vessel disease, magnetic resonance imaging, excellent outcome, good outcome, acute ischemic stroke

INTRODUCTION

Cerebral small vessel disease (SVD) is prevalent in older people and generally considered as a common cause of stroke, gait disturbances, and vascular cognitive impairment (1, 2). Brain magnetic resonance imaging (MRI) is most commonly used in clinical practice for detection of SVD and also the gold standard imaging for visualization of SVD *in vivo* (3). Imaging features of SVD on MRI encompass lacunes, white matter hyperintensities (WMH), cerebral microbleeds (CMB), and enlarged perivascular spaces (EPVS) (4). Lacunes, WMH and EPVS were associated with increased risk of stroke recurrence, mortality, disability, and worse clinical outcomes (5–9). SVD is thought to be a poor prognostic marker of stroke (10).

Previous studies mainly focused on the effect of individual SVD feature on prognosis of acute ischemic stroke. Whereas, the features of SVD may occur simultaneously in a patient at clinical practice, it seems rather artificial to investigate the presence of only one feature while disregarding the others. Recently, a total SVD score has been proposed and validated (8, 11, 12), assessing the cumulative effect of different SVD features on the whole brain rather than considering individual features separately. Several recent studies have suggested a role for the total SVD score in predicting poor life quality (13), recurrent stroke (8), and mortality (14) after stroke.

However, the information about prognostic implications of the total SVD burden for 90 days functional outcome is scarce. Only two studies had reported the relationship of total SVD burden and 90 days functional outcome among patients with acute ischemic stroke (3, 7), but they just evaluated the combination effect of lacunes and WMH. Whether the total SVD burden is superior to individual SVD feature in prediction of functional outcome after stroke still needs further investigation. Understanding the factors influencing functional outcome is highly valuable in clinical management of stroke victims, and may help to guide rehabilitation strategies to improve outcomes.

Thus, the purpose of our study was to investigate the predictive efficacy of total SVD burden for functional outcome at 90 days after acute ischemic stroke. Since the evaluation of CMB is limited as susceptibility weighted imaging (SWI) and gradient recalled echo (GRE) sequence were not routine sequences of MRI for patients with acute ischemic stroke in most hospitals of China, the use of the total SVD score (11) in clinical practice is limited in China. Therefore, we only chose features of SVD (lacunes, WMH, and EPVS) that were available with routine sequence of MRI, to ensure feasibility of use and transferability of results on clinical practice.

MATERIALS AND METHODS

Study Population

For this retrospective analysis, we used prospectively collected data from a database involving consecutive patients with acute ischemic stroke admitted between April 2017 and January 2018 at the Department of Neurology of First Affiliated Hospital of Chongqing Medical University, a large tertiary medical center in Chongqing. Chongqing is the largest municipality in Southwest

China, with a population of 35 million (15). Acute ischemic stroke was diagnosed if there were new focal neurological deficits explained by relevant lesions detected on diffusion-weighted imaging (DWI) or computed tomography (CT). Patients were eligible for the study if they had cerebral MRI on admission. The exclusion criteria are as follows: 1) patients with contraindication to MRI or with poor quality of MRI; and 2) patients lack of 90-day modified Rankin Scale (mRS) score. All patients underwent standard evaluation, treatment, and rehabilitation that adhered to guidelines for ischemic stroke. The study was approved by the Ethics Committee of The First Affiliated Hospital of Chongqing Medical University, and all participants gave written, informed consent. The study protocol was performed in accordance with the Declaration of Helsinki.

Collection of Demographic and Clinical Data

Clinical data were collected on admission through a specified questionnaire that included demographic data and the presence of vascular risk factors.

Body mass index (BMI) was calculated as weight divided by the square of height. Hypertension was defined as systolic blood pressure ≥ 140 mm Hg and/or diastolic blood pressure ≥ 90 mm Hg, or used antihypertensive drug (16). Diabetes mellitus was defined as fasting plasma glucose level ≥ 7.0 mmol/L, or used hypoglycemic drug/insulin injection (17). Hypercholesterolemia was defined as a low-density lipoprotein cholesterol concentration ≥ 3.4 mmol/L or a total cholesterol concentration ≥ 5.2 mmol/L, or previous diagnosis of hypercholesterolemia with current use of cholesterol-lowering medications (18). Current smoking was defined as consuming ≥ 1 cigarette each day or quit smoking ≤ 1 year; alcohol consumption was defined as alcohol consumption ≥ 8 g every week (19). The definition of coronary heart disease and previous stroke was according to the International Classification of Diseases, 9th version (20).

National Institutes of Health Stroke Scale (NIHSS) score, mRS score, and time from onset to admission were assessed at the time of initial presentation as part of the admission workup. Hospital stay was recorded at discharge. Stroke subtypes were determined based on the modified Trial of Org 10172 in Acute Stroke Treatment (TOAST) criteria: large artery atherosclerosis, cardioembolism, small vessel occlusion, other determined, or undetermined stroke (21).

Outcome Measures

The functional outcome was measured with the mRS at 90 days and defined as i) excellent outcome ($\text{mRS} \leq 1$) and ii) good outcome ($\text{mRS} \leq 2$) (7, 22). We considered the mRS score as dichotomous outcome (0–1: excellent outcome vs. 2–6: disability/death; 0–2: good outcome vs. 3–6: functional dependence/death) and ordinal scale (0–6) (3, 7).

Imaging

Brain MRI was performed on a 3.0-Tesla MRI system scanner (GE Medical Systems, Waukesha, WI, USA), and the images contained T1-weighted, T2-weighted, fluid attenuated inversion

recovery (FLAIR), and DWI sequences. A stroke neurologist (Huo, YC), trained in MRI assessment and blinded to clinical data, rated all the available scans.

Lacunae were defined as rounded or ovoid lesions, >3 and <20 mm diameter, in the basal ganglia, internal capsule, centrum semiovale, or brainstem, of CSF signal intensity on T2 and FLAIR, generally with a hyperintense rim on FLAIR and no increased signal on DWI (4). WMH were diagnosed and scored by the revised version of the visual scale of Fazekas et al. (23). In the Fazekas rating scale, WMH are divided into periventricular white matter hyperintensities (PVWMH) and deep white matter hyperintensities (DWMH) according to anatomic location. PVWMH are scored as follows: none (0, no lesion), mild (1, caps or a pencil-thin lining), moderate (2, smooth halo), and severe (3, irregular lesions extending into the deep white matter). DWMH are scored as follows: none (0, no lesion), mild (1, punctuate foci), moderate (2, beginning confluent foci), and severe (3, large confluent lesions). EPVS were defined as small (<3 mm) punctate (if perpendicular to the plane of scan) or linear (if longitudinal to the plane of scan) lesions with signal intensity similar to that of cerebrospinal fluid on all sequence spaces and without a T2-hyperintense rim on FLAIR imaging (4). EPVS were counted at the level of centrum semiovale (CS) and basal ganglia (BG), respectively, with a validated four-point visual rating scale (0 = none; 1 = 1–10; 2 = 11–20; 3 = 21–40; and 4 = >40) (24). At both levels, we identified the slide in the most affected hemisphere only. Limited intrarater reliability testing (50 scans) showed a good reliability with kappa values of 0.81 for the presence of lacunae, 0.89 for PVWMH, 0.85 for DWMH, and 0.76 for EPVS.

To calculate the total SVD burden, we evaluated lacunae, WMH, and EPVS based on the ordinal scale developed by Klarenbeek et al. (11), which had been validated in several large studies (8, 12–14). A point was awarded if one or more lacunae were present, or WMH were extensive (DWMH Fazekas score 2 or 3, or PVWMH Fazekas score 3), or EPVS in BG were moderate to severe (scored 2–4), respectively. The three sub-scores were then summed up to generate a total SVD burden that ranged from 0 to 3.

Statistical Analysis

Statistical analyses were performed by SPSS 19.0 software (IBM Corp., Armonk, NY, USA) and STATA 12.0 software (STATA Corp., College Station, Texas, USA). The total SVD burden was considered as ordinal scale (0–3), reflecting no features to all three features of SVD. Continuous variables were presented as mean \pm standard deviations (SD) or as median and interquartile range (IQR) as appropriate. In univariate analyses, normally distributed continuous variables were compared with one-way analysis of variance or Student's *t*-test, and the variables not normally distributed were compared with Kruskal–Wallis *H* test or Mann–Whitney *U* test. Categorical variables were presented as percentages and were compared with Pearson's chi square test or Fisher's exact test.

Binary logistic regression was used to analyze the associations between SVD and functional outcomes (excellent outcome and good outcome). Firstly, unadjusted associations of individual

SVD feature and total SVD burden with functional outcomes were analyzed. Secondly, adjusted associations between total burden of SVD and functional outcomes were analyzed. All multivariable analyses were first adjusted for age and sex (Model 1) and additionally adjusted for potential confounders (including age, sex, hypertension, diabetes mellitus, hypercholesterolemia, coronary heart disease, previous stroke, current smoking, alcohol consumption, proximal vessel occlusion, stroke subtype, baseline NIHSS, baseline mRS and hospital stay; Model 2). The results are shown as odds ratio (OR) and 95% confidence intervals (CI). A two-tailed $P < 0.05$ was considered statistically significant.

RESULTS

Characteristics of the Study Population

A total of 557 patients with acute ischemic stroke were screened at baseline, among which 132 patients with contraindication to MRI or with poor quality of MRI and 9 patients lacking 90-day mRS scores were excluded. Finally, 416 patients with acute ischemic stroke were included in the final analysis. There were 278 males (66.8%) and 138 females (33.2%). The average age of the patients was 67 years (age range 19–94). Baseline characteristics of the study population stratified by burden of SVD are presented in **Table 1**. For SVD burden, 183 patients (44.0%) had an SVD burden of 0, showing no signs of lacunae, WMH, and EPVS; 139 patients (33.4%) had 1 feature of SVD; 80 patients (19.2%) presented with 2 features; and 14 patients (3.4%) presented with all 3 features.

Age, the proportion of hypertension, diabetes mellitus, and previous stroke differed significantly with increasing burden (0–3) of SVD ($p < 0.05$, **Table 1**). Sex, BMI, stroke subtype, and the presence of other vascular risk factors showed no differences among groups ($p > 0.05$).

Functional Outcome

A total of 251 (60.3%) patients had excellent outcome ($mRS \leq 1$) and 315 (75.7%) patients had good outcome ($mRS \leq 2$) at 3 months. The incidence of excellent outcome (67.8, 61.2, 48.8, 21.4%, $p_{trend} = 0.001$) and good outcome (80.9, 77.0, 67.5, 42.9%, $p_{trend} = 0.004$) decreased significantly with increasing burden (0–3) of SVD. However, the 90-day mRS score and the proportion of 90-day mortality in patients with increasing SVD burden increased significantly ($p < 0.001$, **Table 1**, **Figure 1**).

Clinical and imaging characteristics of functional outcomes are presented in **Table 2**. Patients with excellent outcome or good outcome were younger and had a lower proportion of diabetes mellitus, coronary heart disease, previous stroke, and proximal vessel occlusion; a lower score of baseline NIHSS; and a shorter time of hospital stay as compared to the patients with disability/death or functional dependence/death ($p < 0.05$). In regard to stroke subtypes, 136 (32.7%) had large artery atherosclerosis, 76 (18.3%) had cardioembolism, and 147 (35.3%) had small vessel occlusion. The distribution of stroke subtypes differed significantly among all groups ($p < 0.001$, **Table 2**).

Logistic regression was used to analyze the associations of individual SVD feature and total burden of SVD with functional outcomes at 90 days; results are presented in **Figure 2**. In regard

TABLE 1 | Baseline characteristics of study population stratified by burden of small vessel disease.

	SVD = 0 (n = 183)	SVD = 1 (n = 139)	SVD = 2 (n = 80)	SVD = 3 (n = 14)	P-value
Demographics					
Age, years, median (IQR)	63 (54 – 69)	69 (60 – 77)	72 (64 – 80)	81 (68 – 83)	0.000
Sex, male, n (%)	114 (62.3)	96 (69.1)	57 (71.3)	11 (78.6)	0.334
BMI, median (IQR)	24.22 (21.94 – 25.84)	23.47 (20.96 – 25.54)	24.10 (21.26 – 25.95)	23.70 (21.61 – 25.05)	0.541
Clinical history					
Hypertension, n (%)	104 (56.8)	107 (77.0)	66 (82.5)	11 (78.6)	0.000
Diabetes mellitus, n (%)	63 (34.4)	73 (52.5)	41 (51.3)	6 (42.9)	0.006
Hypercholesterolemia, n (%)	68 (37.2)	54 (38.8)	37 (46.3)	7 (50.0)	0.461
Previous stroke, n (%)	24 (13.1)	38 (27.3)	22 (27.5)	3 (21.4)	0.004
Proximal vessel occlusion, n (%)	19 (10.4)	18 (12.9)	9 (11.3)	0 (0)	0.506
Thrombolysis, n (%)	14 (7.7)	13 (9.4)	5 (6.3)	1 (7.1)	0.867
Stroke subtype, n (%)					0.052
Large artery atherosclerosis	48 (26.2)	49 (35.3)	33 (41.3)	6 (42.9)	
Cardioembolism	38 (20.8)	27 (19.4)	8 (10.0)	3 (21.4)	
Small vessel occlusion	75 (41.0)	45 (32.4)	25 (31.3)	2 (14.3)	
Undetermined	8 (4.4)	3 (2.2)	1 (1.3)	0 (0.0)	
Other determined	14 (7.7)	15 (10.8)	13 (16.3)	3 (21.4)	
Clinical variables					
Baseline NIHSS, median (IQR)	3 (1 – 7)	4 (2 – 7)	4 (2 – 8)	5 (3 – 8)	0.093
Baseline mRS score, median (IQR)	0 (0 – 0)	0 (0 – 0)	0 (0 – 1)	0 (0 – 2)	0.000
90-day mRS score, median (IQR)	1 (0 – 2)	1 (1 – 2)	2 (1 – 3)	3 (2 – 4)	0.000

SVD, small vessel disease; IQR, interquartile range; BMI, body mass index; NIHSS, National Institute of Health Stroke Scale; mRS, modified Rankin scale.

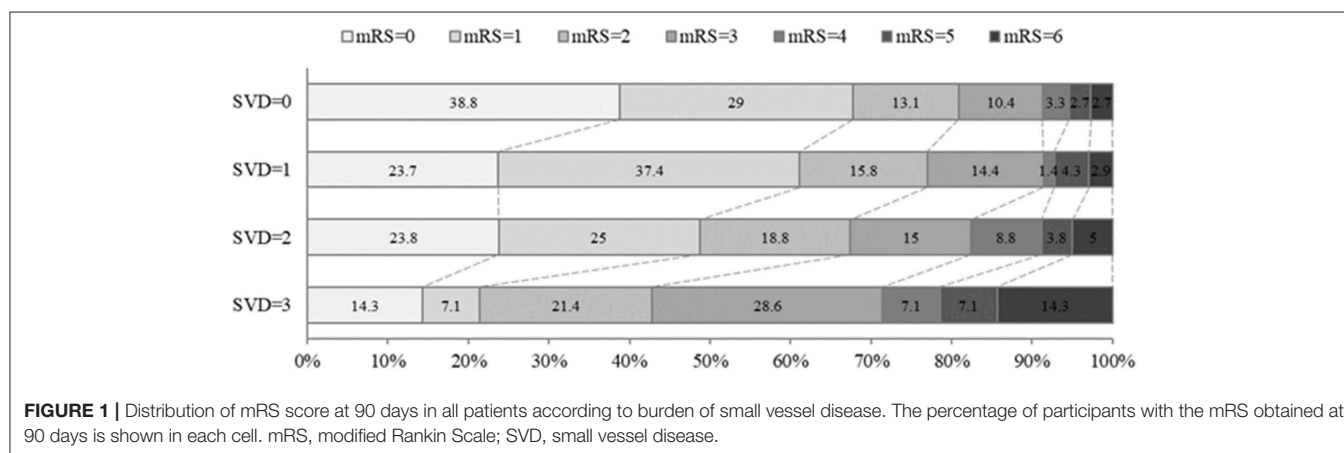


FIGURE 1 | Distribution of mRS score at 90 days in all patients according to burden of small vessel disease. The percentage of participants with the mRS obtained at 90 days is shown in each cell. mRS, modified Rankin Scale; SVD, small vessel disease.

to individual SVD feature, lacunes (OR: 0.48, 95% CI: 0.32–0.71; OR: 0.49, 95% CI: 0.31–0.77) and WMH (OR: 0.53, 95% CI: 0.34–0.82; OR: 0.53, 95% CI: 0.33–0.85) were negatively associated with excellent outcome and good outcome. Further analysis of different location of WMH showed that PVWMH were associated with lower odds of excellent outcome and good outcome than DWMH (**Supplementary Figure 1**). As to the total burden of SVD, 2 SVD features (OR: 0.45, 95% CI: 0.26–0.77; OR: 0.49, 95% CI: 0.27–0.89), 3 SVD features (OR: 0.13, 95% CI: 0.03–0.48; OR: 0.18, 95% CI: 0.06–0.54), and the score of total SVD burden (OR: 0.63, 95% CI: 0.50–0.80; OR: 0.65, 95% CI: 0.50–0.84) were negatively associated with excellent outcome and

good outcome. Among which, three SVD features had strongest negative associations with functional outcomes.

Adjusted associations between total SVD burden and functional outcomes at 90 days are presented in **Table 3**. After adjustment of age and sex, 2 SVD features (OR: 0.46, 95% CI: 0.26–0.82), 3 SVD features (OR: 0.13, 95% CI: 0.03–0.51), and the score of total SVD burden (OR: 0.63, 95% CI: 0.49–0.82) were negatively associated with excellent outcome; 3 SVD features (OR: 0.23, 95% CI: 0.07–0.73) and the score of total SVD burden (OR: 0.70, 95% CI: 0.53–0.93) were negatively associated with good outcome. After adjusting for age, sex, hypertension, diabetes mellitus, hypercholesterolemia, coronary heart disease, previous

TABLE 2 | Clinical and imaging characteristics of the study population based on functional outcomes.

	Functional Outcomes					
	mRS ≤ 1 (<i>n</i> = 251)	mRS ≥ 2 (<i>n</i> = 165)	<i>P</i> -value	mRS ≤ 2 (<i>n</i> = 315)	mRS ≥ 3 (<i>n</i> = 101)	<i>P</i> -value
Demographics						
Age, years, median (IQR)	65 (57 – 74)	68 (60 – 77)	0.043	66 (57 – 74)	71 (60 – 80)	0.006
Sex, male, <i>n</i> (%)	173 (68.9)	105 (63.6)	0.262	212 (67.3)	66 (65.3)	0.717
BMI, median (IQR)	23.88 (21.64 – 25.95)	24.01 (21.25 – 25.71)	0.523	24.06 (21.74 – 25.92)	23.44 (21.22 – 25.46)	0.107
Clinical history						
Hypertension, <i>n</i> (%)	171 (68.1)	117 (70.9)	0.548	220 (69.8)	68 (67.3)	0.634
Diabetes mellitus, <i>n</i> (%)	94 (37.5)	89 (53.9)	0.001	129 (41.0)	54 (53.5)	0.027
Hypercholesterolemia, <i>n</i> (%)	108 (43.0)	58 (35.2)	0.109	129 (41.0)	37 (36.6)	0.441
Coronary heart disease, <i>n</i> (%)	34 (13.5)	37 (22.4)	0.019	45 (14.3)	26 (25.7)	0.008
Previous stroke, <i>n</i> (%)	42 (16.7)	45 (27.3)	0.01	52 (16.5)	35 (34.7)	0.000
Current smoking, <i>n</i> (%)	106 (42.2)	67 (40.6)	0.742	135 (42.9)	38 (37.6)	0.353
Alcohol consumption, <i>n</i> (%)	68 (27.1)	32 (19.4)	0.072	81 (25.7)	19 (18.8)	0.158
Proximal vessel occlusion, <i>n</i> (%)	13 (5.2)	33 (20.0)	0.000	27 (8.6)	19 (18.8)	0.006
Thrombolysis, <i>n</i> (%)	18 (7.2)	15 (9.1)	0.478	24 (7.6)	9 (8.9)	0.676
Stroke subtype, <i>n</i> (%)			0.000			0.000
Large artery atherosclerosis	66 (26.3)	70 (42.4)		90 (28.6)	46 (45.5)	
Cardioembolism	41 (16.3)	35 (21.2)		54 (17.1)	22 (21.8)	
Small vessel occlusion	115 (45.8)	32 (19.4)		133 (42.2)	14 (13.9)	
Undetermined	6 (2.4)	6 (3.6)		8 (2.5)	4 (4.0)	
Other determined	23 (9.2)	22 (13.3)		30 (9.5)	15 (14.9)	
Clinical variables						
Baseline NIHSS, median (IQR)	3 (1 – 5)	7 (4 – 11)	0.000	3 (1 – 5)	8 (5 – 14)	0.000
Hospital stay, day, median (IQR)	12 (9 – 14)	15 (11 – 21)	0.000	12 (10 – 15)	15 (10 – 23)	0.000
Onset to admission time, hour, median (IQR)	17.5 (5.0 – 38.5)	15.3 (5.0 – 40.8)	0.968	17.5 (5.5 – 42.0)	11.8 (4.0 – 36.3)	0.204
SVD						
Lacunes, median (IQR)	0 (0 – 1)	1 (0 – 2)	0.000	0 (0 – 1)	1 (0 – 2)	0.001
WMH, median (IQR)	0 (0 – 0)	0 (0 – 1)	0.004	0 (0 – 0)	0 (0 – 1)	0.008
EPVS, median (IQR)	0 (0 – 0)	0 (0 – 0)	0.353	0 (0 – 0)	0 (0 – 0)	0.630
Total SVD burden, median (IQR)	1 (0 – 1)	1 (0 – 2)	0.000	1 (0 – 1)	1 (0 – 2)	0.003

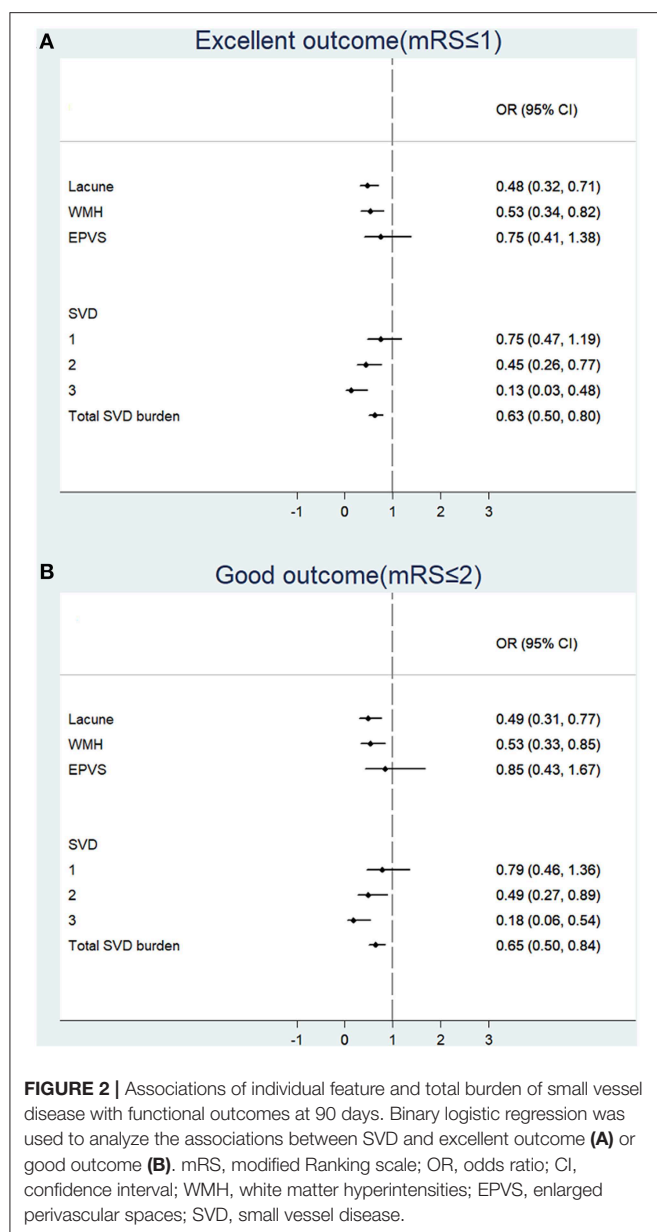
mRS, modified Ranking scale; IQR, interquartile range; BMI, body mass index; NIHSS, National Institute of Health Stroke Scale; SVD, small vessel disease; WMH, white matter hyperintensities; EPVS, enlarged perivascular spaces.

stroke, current smoking, alcohol consumption, proximal vessel occlusion, stroke subtype, baseline NIHSS, baseline mRS, and hospital stay, three SVD features (OR: 0.07, 95% CI: 0.01–0.41) and the score of total SVD burden (OR: 0.64, 95% CI: 0.44–0.93) remained negatively associated with excellent outcome.

DISCUSSION

In the present study, we found that total SVD burden (including lacunes, WMH, and EPVS) negatively affects functional outcome in patients with acute ischemic stroke and is superior to individual SVD feature in prediction of functional outcome. A high SVD burden was associated with a higher mRS score and substantially reduced the chances to have excellent outcome rather than good outcome at 90 days, indicating that a high SVD burden might predict poorer functional outcome.

In our study, lacunes and WMH were related to 90-day functional outcome, which is in accordance with previous results that lacunes and WMH negatively affect clinical outcome in patients with acute ischemic stroke. Lacunes have been reported associated with recurrent stroke and neurological impairment over time (25). Furthermore, two large-scale studies have suggested a role for WMH in predicting early neurological deterioration and disability at 3 months after stroke (6, 26). However, few studies had separately evaluated the impact of PVWMH and DWMH on functional outcome after stroke. We found that PVWMH had stronger association with functional outcome than DWMH, suggesting that PVWMH are more sensitive than DWMH in predicting poor functional outcome after stroke. Previous studies have indicated that PVWMH rather than DWMH were preferentially associated with decline in total cerebral blood flow (27), and thus may be more vulnerable to hemodynamic disturbance and more prone to ischemia owing



to the unstable blood supply of the periventricular watershed area (28). It is speculated that this might be one of the reasons why PVWMH have higher efficacy than DWMH in predicting functional outcome after stroke.

We also analyzed the association between EPVS and functional outcome after stroke. EPVS, the most prevalent feature of SVD in patients with stroke (11), have been reported in relation to increased risk of recurrent ischemic stroke (9, 29). However, no independent association between EPVS and functional outcome was found in our study. Future larger multicenter studies are needed to investigate whether EPVS have a predictive effect on functional outcome in patients with acute ischemic stroke.

SVD features frequently occur together; thus, it is necessary to quantify the total burden of SVD in order to assess the

TABLE 3 | Adjusted associations between total burden of small vessel disease and functional outcomes at 90 days.

SVD	Excellent outcome (mRS ≤ 1) OR (95% CI)		Good outcome (mRS ≤ 2) OR (95% CI)	
	Model 1	Model 2	Model 1	Model 2
0	1	1	1	1
1	0.76 (0.47 – 1.23)	0.93 (0.47 – 1.85)	0.89 (0.51 – 1.57)	1.02 (0.46 – 2.29)
2	0.46 (0.26 – 0.82)	0.57 (0.25 – 1.32)	0.58 (0.31 – 1.09)	0.87 (0.34 – 2.24)
3	0.13 (0.03 – 0.51)	0.07 (0.01 – 0.41)	0.23 (0.07 – 0.73)	0.25 (0.05 – 1.20)
Total SVD burden	0.63 (0.49 – 0.82)	0.64 (0.44 – 0.93)	0.70 (0.53 – 0.93)	0.79 (0.53 – 1.19)

Model 1: Bivariate logistic regression analyses with adjustment for age and sex.

Model 2: Bivariate logistic regression analyses with adjustment for age, sex, hypertension, diabetes mellitus, hypercholesterolemia, coronary heart disease, previous stroke, current smoking, alcohol consumption, proximal vessel occlusion, stroke subtype, baseline NIHSS, baseline mRS, and hospital stay.
mRS, modified Ranking scale; OR, odds ratio; CI, confidence interval; SVD, small vessel disease.

cumulative effect of small vessel injury on the whole brain. We found that the total SVD burden was superior to individual SVD feature in prediction of functional outcome, with three SVD features having the strongest negative association with functional outcome. A high SVD burden (three features) was associated with higher mRS score and substantially reduced the chances to have excellent outcome rather than good outcome at 90 days. Since not all SVD features were combined in our study, the impact of total SVD burden on functional outcome might be underestimated.

The pathogenesis linking total SVD burden and functional outcome after acute ischemic stroke is not entirely clear; various mechanisms might be involved. As total SVD burden indicates the chronic accumulation of small vessel injury, which leads to the decrease of neurological reserve capacity in brain, pre-existing SVD might be a marker of increased susceptibility of brain tissue to ischemia and other injury (1, 10). Besides, a higher burden of SVD and the comorbid brain disease could destroy white matter tissue microstructure and disrupt the network architecture of the brain, thus impairing the plasticity and compensatory mechanisms and slow down the brain's recovery from stroke (30–32). What's more, SVD could affect functional outcome by disrupting motor/cognitive networks that are important for learning and neurorehabilitation (33). Evidence is accumulating that total SVD burden independently contributes to progressive cognitive impairment, dementia, and gait/balance disturbances (34–36). SVD-related cognitive/executive dysfunction may impair not only motor learning but also active participation in rehabilitation and adherence to treatment guidelines, thus leading to poor functional recovery.

Our study has several limitations. First, since the evaluation of CMB is limited as SWI and GRE sequence were not routine sequences of MRI for patients with acute ischemic stroke in most hospitals of China, we only chose SVD features that were available with routine sequence of MRI to ensure feasibility

of use and transferability of results on clinical practice. As not all features of SVD were combined in our study, the impact of total SVD burden on functional outcome might be underestimated. Besides, we acknowledge that our estimation of the total SVD burden still needs further validation in larger, more varied cohorts. Second, severely affected patients who were unable to tolerate MRI and patients who underwent mechanical thrombectomy and evaluated by emergency CT examination usually lack cerebral MRI data or have incomplete MRI data, so they were excluded from the study. This selection bias would probably lead to an underestimation of the association between total SVD burden and function outcome, and might limit the generalizability of the results to all stroke patients. Third, we used qualitative (Fazekas scale) assessment for evaluation of WMH, which is considered not as precise as quantitative (volumetric) assessment. However, as qualitative and quantitative WMH burden assessments have been demonstrated to be highly correlated and comparable in stroke patients (6), quick visual rating is sufficient in WMH evaluation. Despite these limitations, the strengths of our study include relatively large sample size and apprehensive evaluation of three features of SVD with unified rating systems. More importantly, our results are easily transferrable into clinical routine.

In conclusion, our study demonstrated that total SVD burden negatively associated with functional outcome at 3 months in patients with acute ischemic stroke and is superior to individual SVD feature in prediction of functional outcome. MRI-based assessment of total SVD burden might help to identify patients with poor functional outcome. We suggest that caregivers use the knowledge of total SVD burden to provide better and more personalized care, by identifying those patients at higher risk for unfavorable functional outcome and by more clearly assessing the potential of functional recovery.

REFERENCES

1. Wardlaw JM, Smith C, Dichgans M. Mechanisms of sporadic cerebral small vessel disease: insights from neuroimaging. *Lancet Neurol.* (2013) 12:483–97. doi: 10.1016/S1474-4422(13)70060-7
2. Pantoni L. Cerebral small vessel disease: from pathogenesis and clinical characteristics to therapeutic challenges. *Lancet Neurol.* (2010) 9:689–701. doi: 10.1016/S1474-4422(10)70104-6
3. Arba F, Inzitari D, Ali M, Warach SJ, Luby M, Lees KR, et al. Small vessel disease and clinical outcomes after IV rt-PA treatment. *Acta Neurol Scand.* (2017) 136:72–7. doi: 10.1111/ane.12745
4. Wardlaw JM, Smith EE, Biessels GJ, Cordonnier C, Fazekas F, Frayne R, et al. Neuroimaging standards for research into small vessel disease and its contribution to ageing and neurodegeneration. *Lancet Neurol.* (2013) 12:822–38. doi: 10.1016/S1474-4422(13)70124-8
5. Arauz A, Murillo L, Cantú C, Barinagarrementeria F, Higuera J. Prospective study of single and multiple lacunar infarcts using magnetic resonance imaging: risk factors, recurrence, and outcome in 175 consecutive cases. *Stroke.* (2003) 34:2453–8. doi: 10.1161/01.STR.0000090351.41662.91
6. Zerna C, Yu AXY, Modi J, Patel SK, Coulter JJ, Smith EE, et al. Association of white matter hyperintensities with short-term outcomes in patients with minor cerebrovascular events. *Stroke.* (2018) 49:919–23. doi: 10.1161/STROKEAHA.117.017429

DATA AVAILABILITY

The datasets generated for this study are available on request to the corresponding author.

ETHICS STATEMENT

This study was approved by the Ethics Committee of The First Affiliated Hospital of Chongqing Medical University and all participants gave written, informed consent. The study protocol was performed in accordance with the Declaration of Helsinki.

AUTHOR CONTRIBUTIONS

YH and XQ helped in study concept and design. YH, WZ, NZ, SH, HW, and KS collected data. YH drafted the article. YH, QL, RL, and RZ did statistical analysis. QL, RL, and XQ did critical revision of the article. XQ obtained funding and was responsible for the administrative, technical, or material support. All authors have read and approved the final manuscript.

FUNDING

This study was supported by a grant from the National Natural Science Foundation of China (Grant No. 81771275).

SUPPLEMENTARY MATERIAL

The Supplementary Material for this article can be found online at: <https://www.frontiersin.org/articles/10.3389/fneur.2019.00808/full#supplementary-material>

7. Arba F, Palumbo V, Boulanger JM, Pracucci G, Inzitari D, Buchan AM, et al. Leukoaraiosis and lacunes are associated with poor clinical outcomes in ischemic stroke patients treated with intravenous thrombolysis. *Int J Stroke.* (2016) 11:62–7. doi: 10.1177/1747493015607517
8. Lau KK, Li L, Schulz U, Simoni M, Chan KH, Ho SL, et al. Total small vessel disease score and risk of recurrent stroke: validation in 2 large cohorts. *Neurology.* (2017) 88:2260–7. doi: 10.1212/WNL.0000000000004042
9. Lau KK, Li L, Lovelock CE, Zamboni G, Chan TT, Chiang MF, et al. Clinical correlates, ethnic differences, and prognostic implications of perivascular spaces in transient ischemic attack and ischemic stroke. *Stroke.* (2017) 48:1470–7. doi: 10.1161/STROKEAHA.117.016694
10. Kim BJ, Lee SH. Prognostic impact of cerebral small vessel disease on stroke outcome. *J Stroke.* (2015) 17:101–10. doi: 10.5853/jos.2015.17.2.101
11. Klarenbeek P, van Oostenbrugge RJ, Rouhl RP, Knottnerus IL, Staals J. Ambulatory blood pressure in patients with lacunar stroke: association with total MRI burden of cerebral small vessel disease. *Stroke.* (2013) 44:2995–9. doi: 10.1161/STROKEAHA.113.002545
12. Staals J, Makin SD, Doubal FN, Dennis MS, Wardlaw JM. Stroke subtype, vascular risk factors, and total MRI brain small-vessel disease burden. *Neurology.* (2014) 83:1228–34. doi: 10.1212/WNL.0000000000000837
13. Liang Y, Chen YK, Deng M, Mok VCT, Wang DE, Ungvari GS, et al. Association of cerebral small vessel disease burden and health-related quality of life after acute ischemic stroke. *Front Aging Neurosci.* (2017) 9:372. doi: 10.3389/fnagi.2017.00372

14. Song TJ, Kim J, Song D, Yoo J, Lee HS, Kim YJ, et al. Total cerebral small-vessel disease score is associated with mortality during follow-up after acute ischemic stroke. *J Clin Neurol.* (2017) 13:187–95. doi: 10.3988/jcn.2017.13.2.187
15. Zhou R, Zhou H, Cui M, Wang Y, Tan J, Sawmiller D, et al. Association between aortic calcification and the risk of osteoporosis in a Chinese cohort: the chongqing osteoporosis study. *Calcified Tissue Int.* (2013) 93:419–25. doi: 10.1007/s00223-013-9776-9
16. Chobanian AV, Bakris GL, Black HR, Cushman WC, Green LA, Izzo JL Jr, et al. The seventh report of the joint National committee on prevention, detection, evaluation, and treatment of high blood pressure: the JNC 7 report. *JAMA.* (2003) 289:2560–72. doi: 10.1001/jama.289.19.2560
17. Alberti KG, Zimmet PZ. Definition, diagnosis and classification of diabetes mellitus and its complications. Part 1: diagnosis and classification of diabetes mellitus provisional report of a WHO consultation. *Diabet Med.* (1998) 15:539–53. doi: 10.1002/(SICI)1096-9136(199807)15:7<539::AID-DIA668>3.0.CO;2-S
18. Expert Panel on Detection, Evaluation, and Treatment of High Blood Cholesterol in Adults. Executive Summary of the third report of the National cholesterol education program (NCEP) expert panel on detection, evaluation, and treatment of high blood cholesterol in adults (adult treatment panel III). *JAMA.* (2001) 285:2486–97. doi: 10.1001/jama.285.19.2486
19. Zhou S, Zhou R, Zhong T, Li R, Tan J, Zhou H. Association of smoking and alcohol drinking with dementia risk among elderly men in China. *Curr Alzheimer Res.* (2014) 11:899–907. doi: 10.2174/1567205011666141001123356
20. Slee VN. The International classification of diseases: ninth revision (ICD-9). *Ann Intern Med.* (1978) 88:424–6. doi: 10.7326/0003-4819-88-3-424
21. Adams HP Jr, Bendixen BH, Kappelle LJ, Biller J, Love BB, Gordon DL, et al. Classification of subtype of acute ischemic stroke: definitions for use in a multicenter clinical trial: TOAST: trial of org 10172 in acute stroke treatment. *Stroke.* (1993) 24:35–41. doi: 10.1161/01.str.24.1.35
22. Maestrini I, Strbian D, Gautier S, Haapaniemi E, Moulin S, Sairanen T, et al. Higher neutrophil counts before thrombolysis for cerebral ischemia predict worse outcomes. *Neurology.* (2015) 85:1408–16. doi: 10.1212/WNL.0000000000002029
23. Fazekas F, Chawluk JB, Alavi A, Hurtig HI, Zimmerman RA. MR signal abnormalities at 1.5 T in Alzheimer's dementia and normal aging. *AJR Am J Roentgenol.* (1987) 149:351–6. doi: 10.2214/ajr.149.2.351
24. Potter GM, Chappell FM, Morris Z, Wardlaw JM. Cerebral perivascular spaces visible on magnetic resonance imaging: development of a qualitative rating scale and its observer reliability. *Cerebrovasc Dis.* (2015) 39:224–31. doi: 10.1159/000375153
25. van Dijk AC, Fonville S, Zadi T, van Hattem AM, Saiedie G, Koudstaal PJ, et al. Association between arterial calcifications and nonlacunar and lacunar ischemic strokes. *Stroke.* (2014) 45:728–33. doi: 10.1161/STROKEAHA.113.003197
26. Ryu WS, Woo SH, Schellingerhout D, Jang MU, Park KJ, Hong KS, et al. Stroke outcomes are worse with larger leukoaraiosis volumes. *Brain.* (2017) 140:158–70. doi: 10.1093/brain/aww259
27. ten Dam VH, van den Heuvel DM, de Craen AJ, Bollen EL, Murray HM, Westendorp RG, et al. Decline in total cerebral blood flow is linked with increase in periventricular but not deep white matter hyperintensities. *Radiology.* (2007) 243:198–203. doi: 10.1148/radiol.2431052111
28. Kim KW, Macfall JR, Payne ME. Classification of white matter lesions on magnetic resonance imaging in elderly persons. *Biol Psychiatry.* (2008) 64:273–80. doi: 10.1016/j.biopsych.2008.03.024
29. Yang H, Shen R, Jin Z, Li J, Wu Y, Xu Y, et al. Dilated Virchow–Robin spaces in first-ever lacunar stroke patients: Topography and clinical correlations. *J Stroke Cerebrovasc Dis.* (2016) 25:306–11. doi: 10.1016/j.jstrokecerebrovasdis.2015.09.034
30. Helenius J, Mayasi Y, Henninger N. White matter hyperintensity lesion burden is associated with the infarct volume and 90-day outcome in small subcortical infarcts. *Acta Neurol Scand.* (2017) 135:585–92. doi: 10.1111/ane.12670
31. Kim HJ, Im K, Kwon H, Lee JM, Kim C, Kim YJ, et al. Clinical effect of white matter network disruption related to amyloid and small vessel disease. *Neurology.* (2015) 85:63–70. doi: 10.1212/WNL.0000000000001705
32. de Groot M, Ikram MA, Akoudad S, Krestin GP, Hofman A, van der Lugt A, et al. Tract-specific white matter degeneration in aging: the rotterdam study. *Alzheimers Dement.* (2015) 11:321–30. doi: 10.1016/j.jalz.2014.06.011
33. Valdes Hernandez Mdel C, Booth T, Murray C, Gow AJ, Penke L, Morris Z, et al. Brain white matter damage in aging and cognitive ability in youth and older age. *Neurobiol Aging.* (2013) 34:2740–7. doi: 10.1016/j.neurobiolaging.2013.05.032
34. Liu R, Chen H, Qin R, Gu Y, Chen X, Zou J, et al. The altered reconfiguration pattern of brain modular architecture regulates cognitive function in cerebral small vessel disease. *Front Neurol.* (2019) 10:324. doi: 10.3389/fneur.2019.00324
35. Jiang Y, Wang Y, Yuan Z, Xu K, Zhang K, Zhu Z, et al. Total cerebral small vessel disease burden is related to worse performance on the Mini-Mental State Examination and incident dementia: A prospective 5-year follow-up. *J Alzheimers Dis.* (2019) 69:253–62. doi: 10.3233/JAD-181135
36. van der Holst HM, Tuladhar AM, Zerbi V, van Uden IWM, de Laat KF, van Leijssen EMC, et al. White matter changes and gait decline in cerebral small vessel disease. *Neuroimage Clin.* (2018) 17:731–8. doi: 10.1016/j.nicl.2017.12.007

Conflict of Interest Statement: The authors declare that the research was conducted in the absence of any commercial or financial relationships that could be construed as a potential conflict of interest.

Copyright © 2019 Huo, Li, Zhang, Zou, Li, Huang, Wang, Song, Zhang and Qin. This is an open-access article distributed under the terms of the Creative Commons Attribution License (CC BY). The use, distribution or reproduction in other forums is permitted, provided the original author(s) and the copyright owner(s) are credited and that the original publication in this journal is cited, in accordance with accepted academic practice. No use, distribution or reproduction is permitted which does not comply with these terms.



Correlation Between the Number of Lenticulostriate Arteries and Imaging of Cerebral Small Vessel Disease

Yuan-Chang Chen, Xiao-Er Wei, Jing Lu, Rui-Hua Qiao, Xue-Feng Shen and Yue-Hua Li*

Institute of Diagnostic and Interventional Radiology, Shanghai Jiao Tong University Affiliated Sixth People's Hospital, Shanghai, China

OPEN ACCESS

Edited by:

Susanne J. Van Veluw,
Massachusetts General Hospital and
Harvard Medical School,
United States

Reviewed by:

Saima Hilal,
Erasmus Medical Center, Netherlands
Sean Marrelli,
University of Texas, United States

*Correspondence:

Yue-Hua Li
liyuehua_0529@163.com

Specialty section:

This article was submitted to
Stroke,
a section of the journal
Frontiers in Neurology

Received: 26 April 2019

Accepted: 30 July 2019

Published: 12 August 2019

Citation:

Chen Y-C, Wei X-E, Lu J, Qiao R-H,
Shen X-F and Li Y-H (2019)
Correlation Between the Number of
Lenticulostriate Arteries and Imaging
of Cerebral Small Vessel Disease.
Front. Neurol. 10:882.
doi: 10.3389/fneur.2019.00882

Background and purpose: Hypoperfusion plays an important role in the pathophysiology of cerebral small vessel disease (SVD). Lenticulostriate arteries (LSAs) are some of the most important cerebral arterial small vessels. This study aimed to investigate whether the number of LSAs was associated with the cerebral perfusion in SVD patients and determine the correlation between the number of LSAs and SVD severity.

Methods: Five hundred and ninety-four consecutive patients who underwent digital subtraction angiography were enrolled in this study. The number of LSAs was determined. Computed tomography perfusion (CTP) was used to calculate the cerebral blood flow (CBF), cerebral blood volume (CBV), mean transit time (MTT), and time to peak (TTP). Magnetic resonance imaging (MRI) was performed to assess cerebral infarct, cerebral microbleeds (CMBs), white matter hyperintensities (WMHs), enlarged perivascular spaces (EPVSs), and lacunes. An SVD compound score was calculated to express the level of cerebral SVD load.

Results: The SVD scores were negatively correlated with the number of the LSAs ($P < 0.001$, $r_s = -0.44$). The number of LSAs was inversely associated with the presence of any type of SVD ($P < 0.001$). The adjusted ORs of the SVD severity were 0.31 for LSA group 1 (LSA > 20) vs. group 2 (LSA = 10–20) and 0.47 for LSA group 2 (LSA = 10–20) vs. group 3 (LSA < 10). MTT and TTP were significantly higher and CBF was significantly lower when the number of LSAs was between 5 and 10 on each side of the basal ganglia ($P < 0.001$, <0.001 , and <0.001 , respectively). The CBV was slightly lower when the number of LSAs was between 5 and 10, while it was significantly lower when the number was <5 on each side of the basal ganglia ($P < 0.05$, <0.0001 , respectively).

Conclusion: LSA count was lower in SVD patients than the non-SVD participants and there was a positive correlation between the cerebral perfusion and the number of LSAs. The LSA number was negatively associated with SVD severity, hypoperfusion might play an important role. This finding may have potentially important clinical implications for monitoring LSA in SVD patients.

Keywords: intracranial arterial diseases, cerebral small vessel disease, lenticulostriate arteries, magnetic resonance imaging, computed tomography perfusion, digital subtraction angiography

INTRODUCTION

Cerebral small vessel disease (SVD) is an intrinsic disorder of the small vessels of the brain including the small arteries, arterioles, venules, and capillaries (1). There are six closely correlated features of SVD on brain magnetic resonance imaging (MRI), including recent small subcortical infarct, white matter hyperintensities (WMHs), lacunes, cerebral microbleeds (CMBs), enlarged perivascular spaces (EPVSs), and atrophy (2). However, neuroimaging only reveals brain parenchyma lesions and does not directly reflect the processes and severity of SVD.

Cerebral arterial small vessels have two origins: superficially, they stem from the subarachnoid circulation as the terminal vessels of medium-sized arteries; deeper, from the base of the brain, they stem directly from the large vessels as arterial perforators (1). These perforating vessels are essential for maintenance of optimum functioning of the brain's most metabolically active nuclei and complex white matter networks (2). Lenticulostriate arteries (LSAs) are some of the most important vascular structures in the human brain and the sites of many neurologic diseases (3). Ischemic and hemorrhagic cerebral strokes often occur in the areas of the brain supplied by these perforating arteries (4). Lacunar infarcts account for 20% of all strokes, and the basal ganglia are involved in 35–44% of intracerebral hemorrhages (5). Thus, *in vivo* imaging of LSAs could provide important insights and help us understand the pathophysiology and mechanism of SVD. Usually, digital subtraction angiography (DSA) is considered the gold standard when visualizing smaller arteries, including the perforating arteries (5, 6).

Hypoperfusion is suggested to play an important role in the pathophysiology of SVD (7, 8). In addition, hypoperfusion may be particularly detrimental to neurons in the presence of capillary dysfunction or arteriolar disease, owing to concomitant impaired vasoreactivity (9), blood-brain barrier dysfunction (10), and less efficient extraction of oxygen and other diffusible nutrients (11). However, these associations are still debatable (8, 12, 13).

In our previous study (14), we found that the numbers of LSA stems in patients with hypertension were significantly lower than those in non-hypertensive volunteers, determined by 3D-TOF-MRA. Hypertension is one of the most important risk factors for SVD (15). On the basis of these results, we hypothesized that the number of LSAs may be associated with SVD severity. The aim of the current study was to investigate whether the number of LSAs was associated with cerebral perfusion in SVD and to determine the relationship between the number of LSAs and SVD severity.

MATERIALS AND METHODS

Study Population/Patients

Between June 2014 and May 2018, 632 consecutive patients suspected of having arteriostenosis, intracranial aneurysm, arteriovenous malformation, or subarachnoid hemorrhage with corresponding neurological symptoms visited our hospital to undergo DSA. The inclusion criteria were as follows: patients who underwent CT, CTP, MRI, and DSA within 2 weeks of symptom onset; those between 18 and 80 years of age; those

with no critical medical conditions; and those with no history of head trauma or tumors. The exclusion criteria were as follows: patients who did not undergo CT, CTP, and MRI; patients with contraindications for CTP and MRI; those with poor quality imaging data; patients with hemorrhagic stroke (based on CT), acute severe infarction or infarction involving the basal ganglia region (based on DWI), and intracranial aneurysm located in the middle cerebral artery that could have affected the origin of LSA. Any patients with other possible sources of white matter hypoattenuation on a chart review—such as multiple sclerosis, acute disseminated encephalomyelitis (ADEM), vasculitis, or connective tissue diseases—were also excluded. Ultimately, 594 patients were enrolled for further analysis.

This study was carried out in accordance with the recommendations of institutional guidelines. The protocol was approved by the committee of Shanghai Jiao Tong University Affiliated Sixth People's Hospital institutional review board. All subjects provided written informed consent in accordance with the Declaration of Helsinki. This study adhered to standard biosecurity and institutional safety procedures.

DSA Examination

An interventional neuroradiologist performed DSA. Conventional 2D-DSA was performed on a monoplanar digital angiography unit (Axiom Artis VB22N; Siemens, Erlangen, Germany) with a $1,024 \times 1,024$ matrix and a 17–20 cm FOV. The contrast medium was injected at a flow rate of 4–5 mL/s and 2–3 mL/s in two projections; therefore, a total of 10 mL medium was injected into the internal carotid artery, and 7 mL was injected into the vertebral artery. Imaging data were transferred to a workstation (syngoXWP VA70B, Siemens). Then, we counted the number of visible LSA stems. Patients were divided into three groups (1, 2, and 3) according to the number of LSAs on both sides (>20 , $10\text{--}20$, <10) and on one side (>10 , $5\text{--}10$, <5).

MRI Examination and Analysis

MRI scans were performed using a 3.0T MRI system (MAGNETOM Skyra 3.0T, Siemens, Amberg, Germany). MRI images were obtained parallel to the orbitomeatal line, using the following parameters: (i) TR/TE, 5120/62 ms; slice thickness, 4 mm; FOV, 220×220 mm; and three different directions of diffusion gradient and two b values (0 and $1,000 \text{ mm}^2/\text{s}$) for DWI. (ii) TR/TE, 7,500/81 ms; slice thickness, 4 mm; and FOV, and 220×220 mm for FLAIR imaging. (iii) TR/TE, 4,730/72 ms; slice thickness, 4 mm; and FOV, 220×220 mm for T2W. (iv) TR/TE, 28/20 ms; slice thickness, 1 mm; and FOV, 220×220 mm for susceptibility weighted imaging (SWI). No contrast material was administered.

A recent infarct was defined as a hyperintense area on DWI, with a corresponding reduced signal on the apparent diffusion coefficient image, with or without increased signal on T2-weighted imaging or FLAIR, which corresponded with a typical vascular territory. Recent small subcortical infarcts were defined as ovoid or rounded lesions with similar signal characteristics to recent infarcts but were small (>3 mm and <20 mm) in diameter, in the centrum semiovale, internal capsule, basal ganglia, or brainstem, and were carefully distinguished

from WMHs (2). Cortical infarcts were defined as infarcts involving cortical adjacent subcortical tissue, or large (>20 mm) subcortical/striatocapsular lesions (16). Deep and periventricular WMHs were both coded according to the Fazekas scale from 0 to 3, using T2-weighted imaging and FLAIR (17). Lacunes were defined as ovoid or rounded lesions, small (>3 mm and <20 mm) in diameter, in the centrum semiovale, internal capsule, basal ganglia, or brainstem, of cerebrospinal fluid (CSF) signal intensity on T2-weighted imaging and FLAIR, generally with a hyperintense rim on FLAIR and no increased signal on DWI (16). CMBs were defined as small (<5 mm), homogeneous, round foci of low signal intensity on gradient echo images in the cerebellum, brainstem, basal ganglia, white matter, or cortico-subcortical junction, differentiated from vessel flow voids and mineral depositions in the globi pallidi (16). EPVSs were defined as small (<3 mm) punctate (if perpendicular) and linear (if longitudinal to the plane of scan) hyperintensities on T2-weighted imaging in the centrum semiovale or basal ganglia, and they were rated on a validated semiquantitative scale from 0 to 4 (18). In this study, we only counted CMBs and EPVSs in the basal ganglia because in this region, they seem specifically associated with SVD (19, 20).

Determining the Total MRI Burden of SVD

An SVD compound score, expressing the level of cerebral SVD load, was calculated according to the method described below. Based on the recently described score (18), we rated the total MRI burden of SVD on an ordinal scale from 0 to 4 by counting the presence of the following: lacunes and CMBs, which were defined as the presence of one or more lacunes (1 point if present) or any CMB (1 point if present); EPVSs were counted if they were moderate-to-severe (grade 2–4) in the basal ganglia (1 point if present); presence of WMHs was defined as either (early), confluent, deep WMH (Fazekas score 2 or 3) or irregular, periventricular WMH extending into the deep white matter (Fazekas score 3) (1 point if present) (21). The existence of CMBs, high-grade WMHs (HWHs), high-grade EPVSs (HPVSs), and lacunes were determined outside the acute infarct area (based on DWI), and two neurologists who were blinded to patients' clinical information independently investigated these lesions. The interobserver agreement values for the presence of CMBs, HWHs, HPVSs, and lacunes were 0.912, 0.956, 0.938, and 0.888, respectively (all $p < 0.05$). Any disagreement regarding the presence of SVD was resolved by consensus.

CT and CTP Examination

The CT stroke protocol was performed on a Brilliance 256-channel iCT device (Brilliance iCT, Philips Medical Systems, Haifa, Israel). Components included pre- and post-contrast head CT from the skull base to the vertex with the following imaging parameters: 120 kilovolt (peak), 340 mA, 4×5 mm or 8×5 mm collimation, 1 s/rotation, and table speed of 15 mm/rotation. CTP comprised 2 phases with the following parameters: 80 kVp, 190 mA, 3–5 s delay, injection of 0.5 mL/kg (30–50 mL) iohexol (300 mg I/mL, Omnipaque; Nycomed, Princeton, NJ) at 4 mL/s. The initial phase consisted of a 45 s cine scanning at 1 rotation/s.

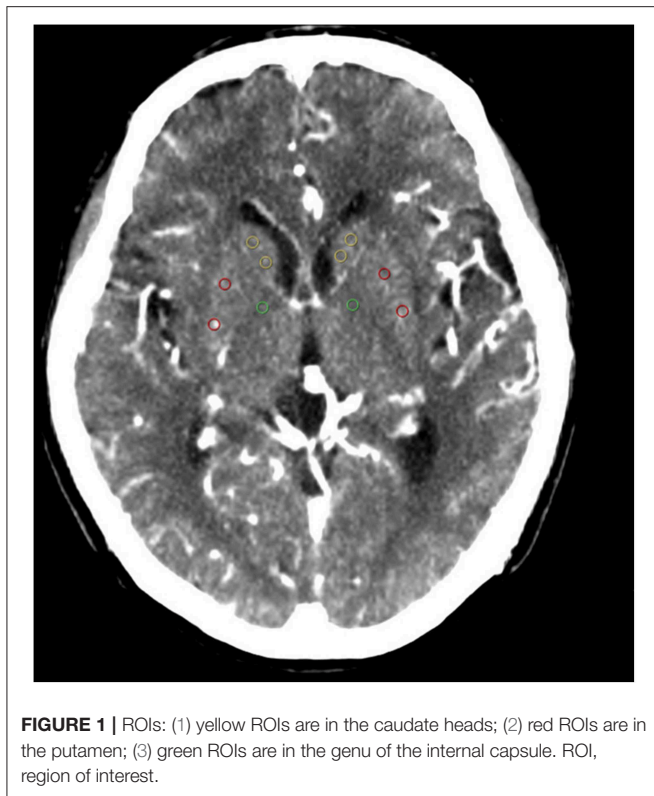
A second phase was added with 1 rotation/s every 15 s for an additional 75 s.

All CTP studies covered a 20–40-mm slab with 4–8 sections measuring 5 mm each, centered between the anterior commissure and the centrum semiovale. Arterial and venous time-enhancement curves were obtained from the anterior cerebral artery and the superior sagittal sinus, respectively. CTP software (Intellispace portal, Philips Medical Systems, Haifa, Israel) was used to calculate the CBF, CBV, MTT, and TTP by deconvolution of 2×2 pixels. Arterial input and venous output functions were obtained from the anterior cerebral artery and from the superior sagittal sinus, respectively. Partial volume averaging of the arterial input curve was corrected by using the venous time-enhancement curve. Perfusion-weighted (PW) maps were calculated by averaging cine images over the duration of the first contrast passage through the brain.

Functional maps (CBF, CBV MTT, and TTP) were imported into custom software (Intellispace portal, Philips Medical Systems, Haifa, Israel) for analysis. The region of interest (ROI) and automatic threshold-based techniques were used to collect data from the functional maps. Analysis was performed at the level of the superior portion of the basal ganglia regions for all patients according to the template shown in **Figure 1**. This region is routinely covered irrespective of the obtained CTP coverage (2–4 cm). Equal sized circular ROI (36 pixels) were placed in the basal ganglia regions on the PW map in every patient. Each ROI was enumerated to provide information on specific locations. Five ROIs were placed as follows: two in the head of the caudate, two in the putamen, and one in the genu of the internal capsule (**Figure 1**). ROI placements were independently verified by an experienced neuroradiologist (blinded to the patient details) to ensure that no CSF or gray matter structures were included. To minimize partial volume effects, we placed the ROIs at least 2 mm from tissue boundaries. CBF and CBV thresholds of $>100 \text{ mL}^{-1} \cdot \text{min}^{-1} \cdot 100 \text{ g}^{-1}$ or $>8 \text{ mL} \cdot 100 \text{ g}^{-1}$, respectively, were applied to perfusion maps to minimize vascular-pixel contribution. A semiautomated threshold technique based on Hounsfield units was used to create a whole gray matter mask on the PW images. This mask was then applied to the functional maps to derive gray matter mean CBF, CBV, MTT, and TTP (22). The values for the 2 ROIs in the head of the caudate and the 2 ROIs in the putamen were averaged before they were entered into the analysis.

Clinical and Laboratory Variables

Patients' data for traditional vascular risk factors (23) and previous episodes of stroke were collected. Hypertension was diagnosed as present when the patient had a resting systolic/diastolic blood pressure of $\geq 140/90$ mm Hg in repeated measurements or had been taking oral antihypertensive agents. Diabetes mellitus was defined as a fasting blood glucose level of ≥ 7.0 mmol/L or treatment with oral hypoglycemic medications or insulin. Hyperlipidemia was defined as a total cholesterol level of ≥ 6.2 mmol/L, a low-density lipoprotein cholesterol level of ≥ 4.1 mmol/L, or if the patient had been treated with lipid-lowering medication after a diagnosis of hyperlipidemia at admission. Current smokers or those who



had stopped smoking within 1 year before the index stroke were considered smokers. Previous stroke was defined if the patient had a previous stroke-like symptom combined with an ischemic lesion confirmed by brain imaging, and a history of TIA was excluded. We further collected data relating to the patients' prior medication; coronary artery disease including history of myocardial infarction, unstable angina, or angiographically confirmed occlusive coronary artery disease, and metabolic syndrome.

Statistical Analyses

Continuous data were analyzed using the analysis of variance (ANOVA) test. Univariate analysis was performed using the χ^2 test for categorical data. A trend χ^2 test and Spearman rank correlation analysis were used to examine evidence of association between the number of LSAs and severity of the MRI makers of SVD. A Mann–Whitney U-test was used to compare the number of LSAs and SVD scores among the different severity groups based on each SVD MRI markers. Multivariate analysis was performed using logistic regression analysis to investigate the association of the number of LSAs with the SVD severity. Multivariate analysis was adjusted for age, sex, hypertension, diabetes mellitus, hyperlipidemia, previous stroke, smoking, coronary artery disease, and metabolic syndrome. The results were expressed as adjusted ORs (multivariate analysis) together with their 95% confidence intervals (CIs). ANOVA was performed to compare the cerebral perfusion in the basal ganglia region with different number of LSAs. A $p < 0.05$ was

TABLE 1 | Baseline characteristics by the number of LSAs.

Number of LSAs (both sides)	>20 (<i>n</i> = 247) <i>n</i> (%)	10–20 (<i>n</i> = 215) <i>n</i> (%)	<10 (<i>n</i> = 132) <i>n</i> (%)	<i>P</i> -value
Demographic data				
Male	154 (42.08)*	133 (36.34)	79 (21.58)	0.89
Female	93 (40.79)	82 (35.96)	53 (23.25)	
Age, years#	58.99 ± 7.30	65.60 ± 10.69	71.70 ± 8.86	<0.001
Risk factors				
Hypertension#	160 (36.45)	164 (37.36)	115 (26.20)	<0.001
Diabetes mellitus	72 (40.22)	66 (36.87)	41 (22.91)	0.91
Hyperlipidemia	25 (34.72)	28 (38.89)	19 (26.39)	0.42
Previous stroke#	31 (25.62)	47 (38.84)	43 (35.54)	<0.001
Smoking#	36 (32.43)	42 (37.84)	33 (29.73)	0.04
Coronary artery disease	39 (34.51)	41 (36.28)	33 (29.20)	0.09
Metabolic syndrome	113 (39.79)	106 (37.32)	65 (22.89)	0.70

LSAs, lenticulostriate arteries. Each baseline characteristic of the study population was compared among the three different LSA number groups on both sides. A $P < 0.05$ was considered significant (#). *The data indicates the number for male participants in the group (LSA > 20) and the data in the bracket indicates the percentage of participants falling into that particular group (LSA > 20/total male participants). Similar for the other data.

considered significant. The statistical packages SPSS 17.0 (IBM Corp., Armonk, NY, USA) was used for the analysis.

RESULTS

The baseline characteristics of the study population ($n = 594$) are presented in **Table 1**. The mean age of patients was 64.21 ± 10.26 years and 61.62% were male. The prevalence of hypertension, previous stroke, smoking, and age were significantly different among the three groups according to LSA number on both sides ($P < 0.001$, <0.001 , $=0.04$, <0.001 , respectively) (**Table 1**). CMBs were found in 28.28% of the subjects, HWHs in 19.02%, HPVSs in 20.20%, and lacunes in 41.59%. Univariate analysis showed that reduction in the number of LSAs on both sides was negatively associated with the presence of each SVD marker ($P < 0.001$). The correlation coefficients (r_s) were -0.67 , -0.51 , -0.42 , and -0.61 for CMBs, HWHs, HPVSs, and lacunes, respectively. The number of the LSAs on both sides was negatively correlated with SVD scores ($P < 0.001$, $r_s = -0.44$) (**Table 2** and **Figure 2**). The adjusted ORs of the SVD severity were 0.31 (95% CI 0.19–0.50, $p < 0.001$) for LSA group 1 (LSA > 20) vs. group 2 (LSA = 10–20) and 0.47 (95% CI 0.30–0.72, $p < 0.001$) for LSA group 2 (LSA = 10–20) vs. group 3 (LSA < 10). MTT and TTP were significantly higher and CBF significantly lower in the LSA group 2 (LSA = 5–10) in each side of the basal ganglia. CBV was slightly lower in LSA group 2 (LSA = 5–10), while it was significantly lower in LSA group 3 (LSA < 5) in each side of the basal ganglia (**Table 3**).

DISCUSSION

In this study, we observed the LSAs by using DSA *in vivo* and found that the number of LSAs was lower in SVD patients

TABLE 2 | Comparison of the number of LSAs according to the presence of SVD and the severity of SVD.

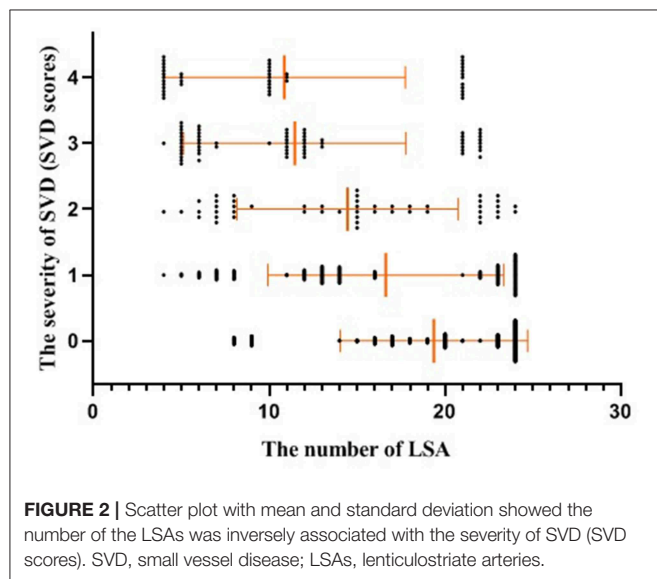
The number of LSA			>20	10–20	<10	P-value	Mean value ± SD	P-value	r _s
CMBs	–	(n = 426)	235 (55.16)*	163 (38.26)	28 (6.57)	<0.001	19.79 ± 4.78	<0.001	–0.67
	+	(n = 168)	12 (7.14)	52 (30.95)	104 (61.90)		9.26 ± 4.69		
HWHs	–	(n = 481)	232 (48.23)	180 (37.42)	69 (14.35)	<0.001	18.57 ± 5.71	<0.001	–0.51
	+	(n = 113)	15 (13.27)	35 (30.97)	63 (55.75)		9.34 ± 5.40		
HPVs	–	(n = 474)	220 (46.41)	174 (36.71)	80 (16.88)	<0.001	18.25 ± 6.01	<0.001	–0.42
	+	(n = 120)	27 (22.50)	41 (34.17)	52 (43.33)		11.15 ± 6.36		
Lacunes	–	(n = 347)	194 (55.91)	136 (39.19)	17 (4.90)	<0.001	20.31 ± 4.43	<0.001	–0.61
	+	(n = 247)	53 (21.46)	79 (31.98)	115 (46.56)		11.90 ± 6.29		
SVD SCORES									
0		(n = 290)	141 (48.62)#	106 (36.55)	43 (14.82)		19.37 ± 5.33		
1		(n = 147)	66 (44.90)	52 (35.37)	29 (19.73)		16.63 ± 6.71		
2		(n = 51)	13 (25.49)	21 (41.18)	17 (33.33)		14.45 ± 6.29		
3		(n = 63)	15 (23.81)	22 (34.92)	26 (41.27)		11.46 ± 6.32		
4		(n = 43)	12 (27.91)	14 (32.56)	17 (39.53)	<0.001	10.86 ± 6.89	<0.001	–0.44

SVD, small vessel disease; LSAs, lenticulostriate arteries; CMB, cerebral microbleed; HWHs, high-grade white matter hyperintensities; HPVVs, high-grade enlarged perivascular spaces; SD, standard deviation; r_s , correlation coefficient.

The number of LSAs was compared according to the presence of each SVD markers, including CMBs, HWHs, HPVVs, and lacunars, and according to the SVD scores (SVD severity). The LSA numbers were analyzed as both categorical variable and continuous variable on both sides.

*The data indicates the number of participants without CMBs in the group (LSA > 20) and the data in the bracket indicates the percentage of participants falling into that particular group (LSA > 20/total participants without CMBs). Similar for the other data.

#The data indicates the number of participants with SVD score = 0 in the group (LSA > 20) and the data in the bracket indicates the percentage of participants falling into that particular group (LSA > 20/total participants with SVD score = 0). Similar for the other data.



than the non-SVD participants. The LSA number had a positive correlation with cerebral perfusion and a negative correlation with SVD severity.

Moody et al. found that brain microvascular density was reduced in subjects with leukoaraiosis (24). Our results indicated that the number of LSAs was low in SVD, which was consistent with their findings. In our patient dataset, presence of hypertension, advanced age, previous strokes, smoking,

and coronary artery disease were higher in the group with fewer LSAs than the group with more LSAs. These results were similar to those reported in previous studies (15). In our previous study (14), we examined 60 patients with hypertension and 60 non-hypertensive volunteers with three dimension-time of flight -magnetic resonance angiography (3D-TOF-MRA) and found that the number of LSA stems was significantly low in hypertensive patients. These findings were likely because of microvascular rarefaction due to hypertension (25). Hypertension alters the structure and function of microcirculation. These changes in the microvascular network lead to a reduction in the number of arterioles or capillaries within the vascular beds of various tissues, known as vascular rarefaction (26).

Additionally, our findings showed that there were significantly fewer visible LSAs in the presence of more severe SVD. We thought that presumably the endothelial-function impairment of small vessels was minor in the early phase of SVD and narrowing of small arterioles may lead to a reduction in CBF (27), while cerebrovascular autoregulation maintains relatively constant CBF over a range of cerebral perfusion pressures (28). However, with SVD progression, diffuse cerebrovascular endothelial failure occurred, vessel walls thickened, and luminal narrowing became more severe, eventually leading to loss of normal autoregulatory ability in these vessels, which could contribute further to tissue damage (29) and concomitant CBF and CBV reduction (30). In the present study, we found that CBF was significantly lower and CBV was slightly lower when the number of LSAs was between 5 and 10; however, CBF and CBV were significantly lower when the number of LSAs was <5. A systematic review showed that CBF

TABLE 3 | Comparison of cerebral perfusion in the basal ganglia regions.

	Left			Right		
	>10 <i>n</i> = 240	5–10 <i>n</i> = 212	<5 <i>n</i> = 142	>10 <i>n</i> = 251	5–10 <i>n</i> = 220	<5 <i>n</i> = 123
Internal capsule						
MMT (s)	3.15 ± 0.23	4.23 ± 0.42*	4.96 ± 0.22*	4.96 ± 0.22	4.29 ± 0.38*	4.98 ± 0.23*
TTP (s)	9.15 ± 0.67	9.84 ± 0.65*	10.86 ± 0.69*	9.18 ± 0.61	9.91 ± 0.55*	10.95 ± 0.77*
CBF (ml 100 g ⁻¹ .min ⁻¹)	47.88 ± 5.01	43.25 ± 5.36*	39.44 ± 4.88*	47.52 ± 4.74	42.68 ± 5.72*	39.64 ± 2.88*
CBV (ml 100 g ⁻¹)	2.49 ± 0.21	2.45 ± 0.18#	2.35 ± 0.28*	2.50 ± 0.23	2.46 ± 0.17#	2.33 ± 0.31*
Head of the caudate						
MMT (s)	3.08 ± 0.13	4.02 ± 0.22*	4.81 ± 0.34*	3.08 ± 0.18	4.06 ± 0.32*	4.88 ± 0.32*
TTP (s)	8.62 ± 0.69	9.60 ± 0.57*	10.48 ± 0.71*	8.67 ± 0.71	9.69 ± 0.53*	10.51 ± 0.57*
CBF (ml 100 g ⁻¹ .min ⁻¹)	69.52 ± 5.48	63.48 ± 7.03*	59.17 ± 6.39*	68.98 ± 6.85	63.42 ± 7.03*	58.27 ± 4.91*
CBV (ml 100 g ⁻¹)	3.59 ± 0.46	3.52 ± 0.38#	3.34 ± 0.31*	3.58 ± 0.48	3.51 ± 0.35#	3.38 ± 0.33*
Putamen						
MMT (s)	3.09 ± 0.12	4.00 ± 0.26*	4.82 ± 0.35*	3.11 ± 0.18	4.03 ± 0.32*	4.89 ± 0.28*
TTP (s)	8.51 ± 0.67	9.50 ± 0.55*	10.34 ± 0.64*	8.61 ± 0.61	9.54 ± 0.52*	10.47 ± 0.68*
CBF (ml 100 g ⁻¹ .min ⁻¹)	76.22 ± 8.26	68.49 ± 8.55*	64.22 ± 7.89*	76.50 ± 8.59	67.40 ± 9.15*	64.01 ± 6.67*
CBV (ml 100 g ⁻¹)	4.07 ± 0.24	4.01 ± 0.30#	3.87 ± 0.35*	4.03 ± 0.25	3.98 ± 0.29#	3.88 ± 0.31*

LSAs, lenticulostriate arteries; MTT, mean transit time; TTP, time to peak; CBF, cerebral blood flow; CBV, cerebral blood volume.

The cerebral perfusion indices were compared among the three LSA groups in three regions of the basal ganglia for each side. **P* < 0.001, #*P* < 0.05.

was negatively related to SVD severity (8). In ischemic lesions caused by SVD, WMH is considered a form of incomplete infarct owing to a state of chronic hypoperfusion of the white matter caused by vessel lumen restriction. Alternatively, occlusion of a small vessel is hypothesized to occur, leading to lacunar infarcts (1). Accordingly, our results may suggest that the LSA number was inversely correlated with SVD severity, and hypoperfusion might play an important role.

In this study, we chose LSA as a marker of SVD, because it has a relatively stable number of branches arising from the middle cerebral artery. The LSA is a terminal artery without collateral branches (31); it arises vertically from the middle cerebral artery, which renders the territory supplied by the LSAs more susceptible to ischemia and leads to high risk of arteriolar necrosis (32). Moreover, the LSAs primarily supply important territories including the basal ganglia and internal capsule, which are vulnerable to ischemia and cause obvious clinical symptoms (31).

The lenticulostriate territory supplies the upper part of the head and the body of the caudate nucleus, putamen, lateral part of the pallidum, superior parts of both the anterior and posterior limbs and genu of the internal capsule, and lateral third of the anterior commissure. We selected the head of the caudate nucleus, putamen, and genu of the internal capsule as ROIs, because these territories were in balance with the territories of other perforating arteries from the internal carotid, anterior cerebral, and anterior choroidal arteries, but not in balance with the territories of the large vessels (32). Perfusion in these regions would not be affected by blood flow in the large vessels.

There are 4 to 12 LSAs that arise from the proximal middle cerebral artery in its horizontal segment, and LSAs

vary from 200 to 400 μm in size (33). The drop in LSA number could reflect rarefaction in the SVD process (26), which might be due to the decrease of the absolute number of LSAs or dip in arterial diameter to below the detection limit. DSA is the gold standard for diagnosis of cerebral vascular disease and the resolution of DSA is 90 μm (34). Hence, we considered that DSA could display most of the LSAs and the low arterial number was mainly due to the lower absolute arterial number. We could not rule out the differences in patient vascular anatomy, but we considered that the distribution of such differences might be random in our participants.

Our study has some limitations. First, a total SVD score was used in this study to evaluate the severity of SVD. Some may argue that there are differences in the underlying pathogenetic mechanisms leading to these different SVD features. However, all of these MRI features are considered to result from disease in the small vessels, and they often co-occur (21). The total SVD score provides a more complete overall view of the impact of SVD on the brain than do the individual MRI features separately. Second, we did not evaluate cerebral atrophy. Because a prior study reported a non-specific association between atrophy and SVD (35), it could have occurred in many other conditions including normal aging. Third, our controls did not represent “healthy” control comparisons, because DSA cannot be performed in completely healthy populations. Fourth, our patient selection favored patients who were comparatively less-disabled and able to undergo MRI. However, both these conditions could have probably led to an underestimation of the association between the total burden of SVD and the number of LSAs. Last, our study had a retrospective design, which is a substantial limitation

for this study type; additionally, it is difficult to ascertain the causation between these factors in this cross-sectional study, so a longitudinal study will be performed in the future to determine if LSA number can be used as a marker for SVD severity.

In conclusion, the number of LSAs was lower in SVD patients and there was a positive correlation between cerebral perfusion and the number of LSAs in SVD. This study has shed light on the association of SVD severity and the number of LSAs, and hypoperfusion might play an important role. This finding may have potential important clinical implications for monitoring LSA in SVD patients.

DATA AVAILABILITY

The datasets generated for this study are available on request to the corresponding author.

ETHICS STATEMENT

This study was carried out in accordance with the recommendations of institutional guidelines given by the committee of Shanghai Jiao Tong University Affiliated Sixth People's Hospital institutional review board, and all subjects provided written informed consent. All subjects gave written informed consent in accordance with the Declaration of Helsinki. The protocol was approved by the committee of Shanghai Jiao

Tong University Affiliated Sixth People's Hospital institutional review board.

AUTHOR CONTRIBUTIONS

Y-HL and Y-CC contributed to the conception and design of the study. Y-CC, R-HQ, and X-FS organized the database. X-EW and JL performed the statistical analysis. Y-CC wrote the first draft of the manuscript. Y-HL, Y-CC, X-EW, and JL wrote sections of the manuscript. All authors contributed to manuscript revision and read and approved the submitted version.

FUNDING

This research was supported by the National Natural Science Foundation of China (Grant No. 81871329), the Shanghai Municipal Education Commission-Gaofeng Clinical Medicine Grant Support (Grant No. 2016427), Clinical Science and Technology innovation project of Shanghai Shen Kang Hospital Development Center (Grant No. SHDC22015038), Shanghai Municipal Science and Technology Commission medical guide project (Grant No. 16411968900), the Shanghai key discipline of medical imaging (Grant No. 2017ZZ02005), the National Natural Science Foundation of China (Grant No. 81471760), the National Natural Science Foundation of China (Grant No. 8167165), and The outstanding Clinical Discipline Project of Shanghai Pudong (Grant No. PWYgy2018-04).

REFERENCES

- Pantoni L. Cerebral small vessel disease: from pathogenesis and clinical characteristics to therapeutic challenges. *Lancet Neurol.* (2010) 9:689–701. doi: 10.1016/S1474-4422(10)70104-6
- Wardlaw JM, Smith C, Dichgans M. Mechanisms of sporadic cerebral small vessel disease: insights from neuroimaging. *Lancet Neurol.* (2013). 12:483–97. doi: 10.1016/S1474-4422(13)70060-7
- Marinkovic S, Gibo H, Milisavljevic M. The surgical anatomy of the relationships between the perforating and the leptomeningeal arteries. *Neurosurgery.* (1996) 39:72–83. doi: 10.1097/00006123-199607000-00016
- Tanriover N, Kawashima M, Rhoton AL, Ulm AJ, Mericle RA. Microsurgical anatomy of the early branches of the middle cerebral artery: morphometric analysis and classification with angiographic correlation. *J Neurosurg.* (2003) 98:1277–90. doi: 10.3171/jns.2003.98.6.1277
- Kang CK, Park CA, Lee H, Kim SH, Park CW, Kim YB, et al. Hypertension correlates with lenticulostriate arteries visualized by 7T magnetic resonance angiography. *Hypertension.* (2009) 54:1050–6. doi: 10.1161/HYPERTENSIONAHA.109.140350
- Harteveld AA, De Cockler LJ, Dieleman N, van der Kolk AG, Zwanenburg JJ, Robe PA, et al. High-resolution postcontrast time-of-flight MR angiography of intracranial perforators at 7.0 Tesla. *PLoS ONE.* 10:e0121051. doi: 10.1371/journal.pone.0121051
- Wolters FJ, Zonneveld HI, Hofman A, van der Lugt A, Koudstaal PJ, Vernooij MW, et al. Cerebral perfusion and the risk of dementia: a population-based study. *Circulation.* (2017) 136:719–28. doi: 10.1161/CIRCULATIONAHA.117.027448
- Shi Y, Thrippleton MJ, Makin SD, Marshall I, Geerlings MI, de Craen AJ, et al. Cerebral blood flow in small vessel disease: a systematic review and meta-analysis. *J Cereb Blood Flow Metab.* (2016) 36:1653–67. doi: 10.1177/0271678X16662891
- Wolters FJ, de Bruijn RF, Hofman A, Koudstaal PJ, Ikram MA, Heart Brain Connection Collaborative Research Group. Cerebral vasoreactivity, apolipoprotein E, and the risk of dementia: a population-based study. *Arterioscler Thromb Vasc Biol.* (2016) 36:204–10. doi: 10.1161/ATVBAHA.115.306768
- Zhao Z, Nelson AR, Betsholtz C, Zlokovic BV. Establishment and dysfunction of the blood-brain barrier. *Cell.* (2015) 163:1064–78. doi: 10.1016/j.cell.2015.10.067
- Østergaard L, Engedal TS, Moreton F, Hansen MB, Wardlaw JM, Dalkara T, et al. Cerebral small vessel disease: capillary pathways to stroke and cognitive decline. *J Cereb Blood Flow Metab.* (2016) 36:302–25. doi: 10.1177/0271678X15606723
- Yata K, Tomimoto H. Chronic cerebral hypoperfusion and dementia. *Neurol Clin Neurosci.* (2014) 2:129–34. doi: 10.1111/ncn3.124
- Gregg NM, Kim AE, Gurol ME, Lopez OL, Aizenstein HJ, Price JC. Incidental cerebral microbleeds and cerebral blood flow in elderly individuals. *JAMA Neurol.* (2015) 72:1021–8. doi: 10.1001/jamaneurol.2015.1359
- Chen YC, Li MH, Li YH, Qiao RH. Analysis of correlation between the number of lenticulostriate arteries and hypertension based on high-resolution MR angiography findings. *Am J Neuroradiol.* (2011) 32:1899–903. doi: 10.3174/ajnr.A2667
- Godin O, Tzourio C, Maillard P, Mazoyer B, Dufouil C. Antihypertensive treatment and change in blood pressure are associated with the progression of white matter lesion volumes: the Three-City (3C)-Dijon magnetic resonance imaging study. *Circulation.* (2011) 123:266–73. doi: 10.1161/CIRCULATIONAHA.110.961052
- Wardlaw JM, Smith EE, Biessels GJ, Cordonnier C, Fazekas F, Frayne R, et al. Neuroimaging standards for research into small vessel disease and its contribution to ageing and neurodegeneration. *Lancet Neurol.* (2013) 12:822–38. doi: 10.1016/S1474-4422(13)70124-8

17. Fazekas F, Chawluk JB, Alavi A, Hurtig HI, Zimmerman RA. MR signal abnormalities at 1.5 T in Alzheimer's dementia and normal aging. *Am J Roentgenol.* (1987) 149:351–6. doi: 10.2214/ajr.149.2.351
18. Doubal FN, MacLulich AM, Ferguson KJ, Dennis MS, Wardlaw JM. Enlarged perivascular spaces on MRI are a feature of cerebral small vessel disease. *Stroke.* (2010) 41:450–4. doi: 10.1161/STROKEAHA.109.564914
19. Staals J, van Oostenbrugge RJ, Knottnerus IL, Rouhl RP, Henskens LH, Lodder J. Brain microbleeds relate to higher ambulatory blood pressure levels in first-ever lacunar stroke patients. *Stroke.* (2009) 40:3264–8. doi: 10.1161/STROKEAHA.109.558049
20. Vernooij MW, van der Lugt A, Ikram MA, Wielopolski PA, Niessen WJ, Hofman A. Prevalence risk factors of cerebral microbleeds: the Rotterdam Scan Study. *Neurology.* (2008) 70:1208–14. doi: 10.1212/01.wnl.0000307750.41970.d9
21. Staals J, Makin SD, Doubal FN, Dennis MS, Wardlaw JM. Stroke subtype, vascular risk factors, and total MRI brain small-vessel disease burden. *Neurology.* (2014) 83:1228–34. doi: 10.1212/WNL.0000000000000837
22. Huynh TJ, Murphy B, Pettersen JA, Tu H, Sahlas DJ, Zhang L. CT perfusion quantification of small-vessel ischemic severity. *Am J Neuroradiol.* (2008) 29:1831–6. doi: 10.3174/ajnr.A1238
23. Kim YD, Jung YH, Saposnik G. Traditional risk factors for stroke in East Asia. *J Stroke.* (2016) 18:273–85. doi: 10.5853/jos.2016.00885
24. Moody DM, Thore CR, Anstrom JA, Challa VR, Langefeld CD, Brown WR. Quantification of afferent vessels shows reduced brain vascular density in subjects with leukoaraiosis. *Radiology.* (2004) 233:883–90. doi: 10.1148/radiol.2333020981
25. Suzuki K, Masawa N, Sakata N, Takatama M. Pathologic evidence of microvascular rarefaction in the brain of renal hypertensive rats. *J Stroke Cerebrovasc Dis.* (2003) 12:8–16. doi: 10.1053/jscd.2003.1
26. Serne EH, de Jongh RT, Eringa EC, IJzerman RG, Stehouwer CD. Microvascular dysfunction: a potential pathophysiological role in the metabolic syndrome. *Hypertension.* (2007) 50:204–11. doi: 10.1161/HYPERTENSIONAHA.107.089680
27. Powers WJ. Cerebral hemodynamics in ischemic cerebrovascular disease. *Ann Neurol.* (1991) 29:231–40. doi: 10.1002/ana.410290302
28. Lee JK, Brady KM, Mytar JO, Kibler KK, Carter EL, Hirsch KG, et al. Cerebral blood flow and cerebrovascular autoregulation in a swine model of pediatric cardiac arrest and hypothermia. *Crit Care Med.* (2011) 39:2337–45. doi: 10.1097/CCM.0b013e318223b910
29. Fernando MS, Simpson JE, Matthews F, Brayne C, Lewis CE, Barber R, et al. White matter lesions in an unselected cohort of the elderly: molecular pathology suggests origin from chronic hypoperfusion injury. *Stroke.* (2006) 37:1391–8. doi: 10.1161/01.STR.0000221308.94473.14
30. Marstrand JR, Garde E, Rostrup E, Ring P, Rosenbaum S, Mortensen EL, et al. Cerebral perfusion and cerebrovascular reactivity are reduced in white matter hyperintensities. *Stroke.* (2002) 33:972–6. doi: 10.1161/01.str.0000012808.81667.4b
31. Liang J, Liu Y, Xu X, Shi C, Luo L. Cerebral perforating artery disease characteristics on high-resolution magnetic resonance imaging. *Clin Neuroradiol.* (2018). doi: 10.1007/s00062-018-0682-4. [Epub ahead of print].
32. Decavel P, Vuillier F, Moulin T. Lenticulostriate infarction. *Front Neurol Neurosci.* (2012) 30:115–9. doi: 10.1159/000333606
33. Leeds NE, Goldberg HI. Lenticulostriate artery abnormalities. Value of direct serial magnification. *Radiology.* (1970) 97:377–83.
34. Gkanatsios NA, Huda W, Peters KR. Effect of radiographic techniques (kVp and mAs) on image quality and patient doses in digital subtraction angiography. *Med Phys.* (2002) 29:1643–50. doi: 10.1118/1.1493213
35. Aribisala BS, Valdés Hernández MC, Royle NA, Morris Z, Muñoz Maniega S, Bastin ME, et al. Brain atrophy associations with white matter lesions in the ageing brain: the Lothian Birth Cohort 1936. *Eur Radiol.* (2013) 23:1084–92. doi: 10.1007/s00330-012-2677-x

Conflict of Interest Statement: The authors declare that the research was conducted in the absence of any commercial or financial relationships that could be construed as a potential conflict of interest.

Copyright © 2019 Chen, Wei, Lu, Qiao, Shen and Li. This is an open-access article distributed under the terms of the Creative Commons Attribution License (CC BY). The use, distribution or reproduction in other forums is permitted, provided the original author(s) and the copyright owner(s) are credited and that the original publication in this journal is cited, in accordance with accepted academic practice. No use, distribution or reproduction is permitted which does not comply with these terms.



Enlarged Perivascular Spaces and Cerebral Small Vessel Disease in Spontaneous Intracerebral Hemorrhage Patients

Xin Wang¹, Hao Feng¹, Yu Wang¹, Jian Zhou² and Xingquan Zhao^{1*}

¹ Department of Neurology, Beijing Tiantan Hospital, Capital Medical University, Beijing, China, ² Department of Radiology, Beijing Tiantan Hospital, Capital Medical University, Beijing, China

OPEN ACCESS

Edited by:

Andreas Charidimou,
Massachusetts General Hospital and
Harvard Medical School,
United States

Reviewed by:

Duangnapa Roongpiboonsopit,
Naresuan University, Thailand
Ellis van Etten,
Leiden University Medical
Center, Netherlands

*Correspondence:

Xingquan Zhao
zxq@vip.163.com

Specialty section:

This article was submitted to
Stroke,
a section of the journal
Frontiers in Neurology

Received: 26 April 2019

Accepted: 30 July 2019

Published: 14 August 2019

Citation:

Wang X, Feng H, Wang Y, Zhou J and
Zhao X (2019) Enlarged Perivascular
Spaces and Cerebral Small Vessel
Disease in Spontaneous Intracerebral
Hemorrhage Patients.
Front. Neurol. 10:881.
doi: 10.3389/fneur.2019.00881

Background: Cerebral small vessel disease (SVD) is associated with cognitive decline, depression, increased mortality, and disability in stroke patients. MRI-visible perivascular spaces (PVS) are a sensitive neuroimaging marker of SVD. We aimed to explore the risk factors and associations with other SVD markers of PVS in two topographical regions (in the basal ganglia [BG] and centrum semiovale [CS]) in a cohort of spontaneous intracerebral hemorrhage (ICH) patients.

Method: We included 306 consecutive patients from a prospective spontaneous ICH cohort. We rated PVS, white matter hyperintensities (WMH), cerebral microbleeds (CMB), and lacunes with validated visual rating scale. We collected clinical information using standardized forms. We predefined severe PVS as score > 2 and examined associations between PVS in both BG and CS regions and clinical and imaging markers of SVD by logistic regression.

Results: In the multivariable logistic regression, increasing age (OR = 1.075; 95% CI = 1.038–1.113, $p < 0.001$), high CS PVS degrees (OR = 6.906; 95% CI = 3.024–15.774, $p < 0.001$), extensive periventricular WMH (OR = 2.878; 95% CI = 1.298–6.379, $p = 0.009$), and the presence of CMB (OR = 4.073, 95% CI = 1.869–8.877, $p < 0.001$) were independently associated with BG PVS severity. Alcohol-drinking habit (OR = 2.805; 95% CI = 1.451–5.422, $p = 0.002$), hyperlipidemia history (OR = 3.782; 95% CI = 1.582–8.783, $p = 0.003$), high BG PVS degrees (OR = 6.293; 95% CI = 2.755–14.371, $p < 0.001$) and the presence of strictly lobar CMB (OR = 2.556, 95% CI = 1.285–5.085, $p = 0.008$) were independent predictors of increased CS PVS severity.

Conclusion: MRI-visible PVS in BG and CS regions are inter-related and have different risk factors in spontaneous ICH patients. Further studies are needed to explore the mechanism and clinical importance of PVS, with possible implications for cerebrovascular disease prevention and effective treatments.

Keywords: cerebral small vessel disease, perivascular spaces, intracerebral hemorrhage, risk factors, MRI

INTRODUCTION

Spontaneous (non-traumatic) intracerebral hemorrhage (ICH) is a devastating neurological disorder resulting from ruptured blood vessels in the brain (1). ICH is the second most common subtype of stroke (10–15%) and accounts for 2 million strokes worldwide each year (2). However, ICH is the most severe subtype of stroke because of its high fatality case rate and poor functional outcome; the median case fatality is 40.4% at 1 month (1).

Perivascular spaces (PVS), or Virchow–Robin spaces, are fluid-containing spaces that surround the walls of arteries, arterioles, veins, and venules as they course from the subarachnoid space into the brain parenchyma (3, 4). PVS are round or linear delineated structures seen on MRI with intensities close to cerebrospinal fluid (CSF) and <3 mm diameter in cross section (3), and are defined as having a diameter “smaller than 3 mm when imaged perpendicular to the course of the vessel” in the STRIVE guidelines to aid the description of cerebral small vessel disease (SVD) features (5).

PVS may function as fluid circulation and drainage pathways for the efficient exchange of essential nutrients and efficient removal of metabolic waste and cell debris through the central nervous system (6). Though the concept of the “glymphatic system” (7) is controversial (6, 8), this perivascular pathway is important for maintaining brain homeostasis. Increasing visibility of PVS on MRI are associated with increasing age, hypertension (9), stroke, other SVD features such as lacunar stroke and white matter hyperintensities (WMH) (10), systemic inflammation (11), multiple sclerosis (4), cognitive impairment, and dementia (12–14).

In ICH patients, hematomas form rapidly after vessel rupture and lead to a sharp increase in intracranial pressure, which causes primary brain injury. Inflammation begins immediately after the hematoma formation and contributes to secondary brain injury. Immune cells recruitment and infiltration into brain parenchyma is the key step of inflammation initiation and progression (15). PVS are specific sites for immune cell accumulation, reaction, and transmigration into the brain parenchyma (e.g., leukocytes, dendritic cells, T-cells, B-cells, and macrophages (16–18)). PVS may provide imaging evidence of vascular and inflammatory changes in the brain after ICH. However, currently there are not many studies that have systematically researched the importance of PVS in spontaneous ICH population (19, 20). Thus, in this study, we aim to investigate the special distribution and severity of PVS in spontaneous ICH patients, and to explore their clinical risk factors and associations with other SVD imaging markers, using structural magnetic resonance imaging (MRI).

MATERIALS AND METHODS

Study Population and Data Collection

For this cross-sectional analysis, we used prospectively collected data from a study of consecutive patients older than 18 years old with spontaneous symptomatic ICH admitted at the Beijing Tiantan Hospital and underwent computed tomography (CT) scans ($N = 883$) from June 2014 to October 2016. Patients were

excluded from the study if they did not undergo MRI scans ($N = 519$). Spontaneous symptomatic ICH was confirmed by non-enhanced CT scans showing parenchymal bleeding. Patients were also excluded if they were diagnosed with secondary ICH ($N = 46$), including brain tumor, head trauma, aneurysm, vascular malformation, hemorrhagic infarction, venous infarction, and Moyamoya disease. Patients underwent MRI scans, but those with poor image quality were also excluded ($N = 12$) as further analysis could not be properly performed.

We finally included 306 patients diagnosed as spontaneous ICH (**Figure 1**). All patients participating in this study provided written informed consent. The Beijing Tiantan Hospital Ethics Committee approved this study. Trained stroke physicians collected detailed patient information by using standard questionnaires at presentation. Age, gender, and clinical history (hypertension, diabetes, hypercholesterolemia, cerebral infarction, intracerebral hemorrhage (ICH), subarachnoid hemorrhage, transient ischemic attack (TIA), atrial fibrillation, myocardial infarction, heart failure and other heart disease, and peripheral vascular disease) were systematically recorded for each patient. Cigarette smoking was classified as never, previous, or current smokers, and alcohol drinking was classified as current drinker or non-drinker. Patients underwent CT, MRI, carotid imaging, and other investigations as required for following ICH treatment.

Brain MRI Acquisition

For all participants, MRI were performed within 6 days of admission. Images were obtained with two 3T MRI scanners, GE Discovery 750 scanner (GE Healthcare, Milwaukee, Wis) and Siemens verio scanner (Siemens, Erlangen, Germany). The MRI ICH protocols are similar in two MRI scanners, including the following sequences: whole brain T1 weighted image (T1W; repetition time/echo time 1,900/9.4 ms; 5 mm slice thickness, 6 mm interslice gap), T2-weighted image (T2W; repetition

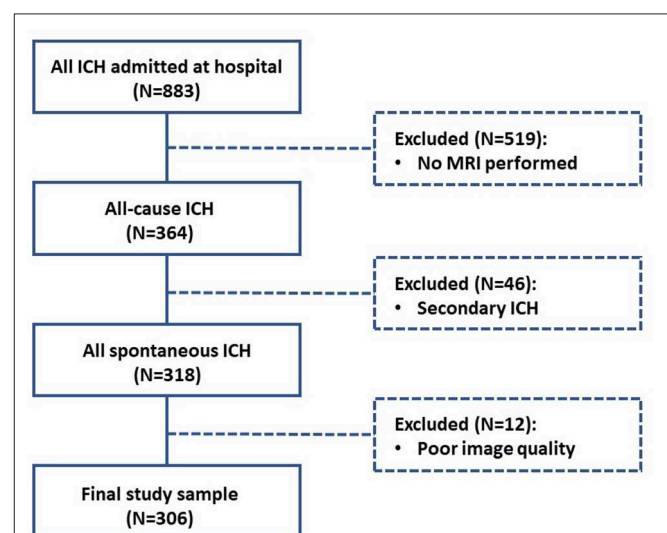


FIGURE 1 | Flow diagram of study enrollment.

time/echo time 6,000/97 ms, 5 mm slice thickness, 6 mm interslice gap), and fluid-attenuated inversion recovery (FLAIR; repetition time/echo time 7,800/91 ms, inversion time 2,200 ms, 5 mm slice thickness, 6 mm interslice gap) and susceptibility-weighted imaging (SWI; repetition time/echo time 28/20 ms, flip angle 15°, 1.6 mm slice thickness, 0.3 mm interslice gap).

Neuroimaging Analysis

All neuroimaging analysis were performed and recorded according to STandards for ReportIng Vascular changes on nEuroimaging (STRIVE) guidelines (5) by trained image analysts blinded to patients' clinical characteristics. PVS were defined as ≤ 3 mm round or linear CSF isointensity lesions and were rated on axial T2W imaging with a validated visual rating scale (10, 21): rated from 0 (none), 1 (1–10), 2 (11–20), 3 (21–40), and 4 (>40) in both the basal ganglia (BG) and centrum semiovale (CS) regions. For both BG and CS regions, after going through all relevant slices for the anatomical area being assessed, we reviewed at least 3 adjacent slices with extensive PVS. One slice with the highest number of PVS was selected and the rating score on this selected slice was recorded. In cases with extensive WMH in the CS region, an estimate was made of the closest PVS rating category, using the appearance of non-involved white matter and cortical gray matter. When background brain parenchyma is asymmetric due to large lobar or deep ICH, PVS were rated in the contralateral hemisphere, and an estimate was made of the closest PVS rating category ipsilateral to the large lesion.

Lacunes were distinguished from PVS by larger size (3–15 mm) on axial FLAIR imaging and defined as a subcortical round or ovoid fluid-filled cavity with a similar signal intensity as CSF (5). WMH are hyperintense lesions on FLAIR and T2W imaging and appear as hypointense on T1W imaging (5). We rated periventricular and deep WMH as 0–3 with the Fazekas scale (22) on FLAIR or T2W imaging. Periventricular WMH was rated from 0 (none), 1 (pencil-thin lining), 2 (smooth halo), and 3 (irregular signal extending to the deep white matter). Deep WMH was rated from 0 (none), 1 (punctate foci), 2 (beginning confluence), and 3 (large confluent areas). Microbleeds were defined as small (generally 2–5 mm in diameter, but up to 10 mm), rounded, or circular areas of signal void on susceptibility sensitive sequences. According to the Microbleed Anatomical Rating Scale (23), microbleeds were classified into deep, lobar, and infratentorial categories. Deep regions included the basal ganglia, thalamus, internal capsule, external capsule, corpus callosum, and deep and periventricular white matter; lobar regions included cortical and subcortical regions; infratentorial regions included the brainstem and cerebellum. We rated the number of microbleeds according to locations separately on SWI imaging and summed them up as total microbleeds. Microbleed mimics were carefully excluded using CT scans or T2W and FLAIR imaging. Basal ganglia calcification can mimic microbleeds and was excluded using CT scans. Mimics of sulcal vessel seen in cross section and partial volume artifact from adjacent bony structures were excluded by careful inspection of adjacent slices and reference to available T2W and FLAIR images.

All MRIs were assessed blinded to clinical information and the other rater's ratings. The interrater Cohen's kappa value for

BG PVS was 0.91 and CS PVS was 0.87, for lacunes was 0.89, for WMH was 0.86–0.89, and for microbleeds was 0.83–0.90.

Statistical Analysis

We classified the PVS burden as high (score 3 and 4) or low (score 0–2) as suggested in previous studies (9, 20). We defined the extensive WMH as irregular periventricular WMH extending into the deep white matter (Fazekas score 3) or early confluent/confluent deep WMH (Fazekas score 2 or 3) as suggested previously (24, 25). Clinical and imaging characteristics of patients with high PVS degree vs. low PVS degree were compared in univariate analyses with the 2-sample *t*-test, Pearson's chi-squared test and Fisher exact test when appropriate. We subsequently evaluated independent predictors of high PVS degree in both BG and CS regions by logistic regression analyses based on univariable analyses results. Logistic regression models were run with a stepwise, forward-elimination method to generate a minimal adjusted model. All tests of significance were 2 tailed. Significance level was set at 0.05 for all analyses. SPSS software (SPSS for Windows, version 22.0, IBM-SPSS, Chicago, IL) was used for all analyses.

RESULTS

Our final cohort included 306 patients with spontaneous ICH. The mean age was 56.00 (± 13.27) years old, ranging from 18 to 86 years old; the proportion of males was 71.57% (219 patients); and more than half of the cohort were current or previous smokers (50.33%) and have the alcohol-drinking habit (50.33%, **Table 1**). In this cohort, 73.20% of patients had been diagnosed as hypertension previously, 13.73% had diabetes mellitus, and 11.11% have hypercholesterolemia problems. No patients had the history of TIA, myocardial infarction, heart failure, or peripheral vascular disease. Nearly 15% of patients had prior cerebral infarction, and seven patients had prior cerebral hemorrhage (seven ICH and one of them also had subarachnoid hemorrhage). Fifteen patients had heart diseases (4.90%); including two patients who had atrial fibrillation (0.65%, **Table 1**).

Table 1 also presents radiological characteristics of all ICH patients. According to the definitions and SVD scales used for visual rating, BG PVS (98.04%), CS PVS (96.41%), and periventricular WMH (95.42%) were the most prevalent, followed by deep WMH (87.25%), presence of microbleeds (50.98%) and lacunes (43.46%). The median BG PVS is 2 (interquartile range: IQR = 1–2) and the median CS PVS is also 2 (IQR = 1–2).

Predictors of Increased BG PVS Severity in Spontaneous ICH Patients

Demographic, vascular, and radiological characteristics of patients with high and low BG PVS degree are compared in **Table 2**. In univariable analyses, high BG PVS degree was significantly associated with increasing age ($p < 0.001$), hyperlipidemia history ($p = 0.034$), and baseline systolic blood pressure ($p = 0.049$). High BG PVS degree was also significantly associated high degree of PVS in CS region ($p < 0.001$), extensive WMH in both periventricular and deep regions (both $p <$

TABLE 1 | Baseline characteristics of all spontaneous ICH patients ($n = 306$).

Characteristics	
DEMOGRAPHICS	
Mean age in years (SD)	56.00 (13.27)
Male gender no. (%)	219 (71.57%)
VASCULAR RISK FACTORS	
Ever-smokers no. (%)	154 (50.33%)
Alcohol drinking no. (%)	154 (50.33%)
Hypertension no. (%)	224 (73.20%)
Diabetes mellitus no. (%)	42 (13.73%)
Hyperlipidemia no. (%)	34 (11.11%)
Prior cerebral infarction no. (%)	44 (14.38%)
Prior intracerebral hemorrhage no. (%)	7 (2.29%)
Prior subarachnoid hemorrhage no. (%)	1 (0.33%)
Atrial fibrillation no. (%)	2 (0.65%)
Other heart disease no. (%)	13 (4.25%)
Mean baseline SBP (SD)	163.58 (24.14)
Mean baseline DBP (SD)	95.38 (17.53)
SVD MARKERS	
Basal ganglia PVS, median (IQR)	2 (1–2)
Rating 0, no. (%)	6 (1.96%)
Rating 1, no. (%)	142 (46.41%)
Rating 2, no. (%)	107 (34.97%)
Rating 3, no. (%)	39 (12.75%)
Rating 4, no. (%)	12 (3.92%)
Centrum semiovale PVS, median (IQR)	2 (1–2)
Rating 0, no. (%)	11 (3.59%)
Rating 1, no. (%)	141 (46.08%)
Rating 2, no. (%)	95 (31.05%)
Rating 3, no. (%)	49 (16.01%)
Rating 4, no. (%)	10 (3.27%)
Periventricular WMH Fazekas score, median (IQR)	2 (1–2)
Grade 0, no. (%)	14 (4.58%)
Grade 1, no. (%)	104 (33.99%)
Grade 2, no. (%)	126 (41.18%)
Grade 3, no. (%)	62 (20.26%)
Deep WMH Fazekas score, median (IQR)	1 (1–2)
Grade 0, no. (%)	39 (12.75%)
Grade 1, no. (%)	116 (37.91%)
Grade 2, no. (%)	114 (37.25%)
Grade 3, no. (%)	37 (12.09%)
Microbleeds, median (IQR)	1 (0–3)
Presence of microbleeds, no. (%)	156 (50.98%)
1 microbleed, no. (%)	58 (18.95%)
2–4 microbleeds, no. (%)	56 (18.30%)
>5 microbleeds, no. (%)	42 (13.73%)
Strictly deep microbleeds, no. (%)	64 (20.92%)
Strictly lobar microbleeds, no. (%)	13 (4.25%)
Lacune, median (IQR)	0 (0–2)
Presence of lacunes, n (%)	133 (43.46%)

DBP, diastolic blood pressure; IQR, interquartile range; PVS, enlarged perivascular spaces; SBP, systolic blood pressure; SD, standard deviation; SVD, small vessel disease; WMH, white matter hyperintensities. Ever smokers indicate current and previous smokers. Other heart disease does not include myocardial infarction and heart failure.

TABLE 2 | Comparison of characteristics between patients with high and low degree of PVS in the BG region.

Characteristic	High BG PVS degree	Low BG PVS degree	p -value
Demographics	(BG PVS > 2, $n = 51$)	(BG PVS ≤ 2, $n = 205$)	
Mean age in years (SD)	64.53 (10.73)	54.29 (13.08)	$p < 0.001$
Male gender no. (%)	39 (76.47%)	180 (70.59%)	$p = 0.395$
VASCULAR RISK FACTORS			
Ever-smokers no. (%)	27 (52.94%)	127 (49.80%)	$p = 0.682$
Alcohol drinking no. (%)	29 (56.86%)	125 (49.02%)	$p = 0.306$
Hypertension no. (%)	38 (74.51%)	186 (72.94%)	$p = 0.817$
Diabetes mellitus no. (%)	6 (11.76%)	36 (14.12%)	$p = 0.656$
Hyperlipidemia no. (%)	10 (19.61%)	24 (9.41%)	$p = 0.034$
Prior cerebral infarction no. (%)	10 (19.61%)	34 (13.33%)	$p = 0.244$
Prior intracerebral hemorrhage no. (%)	1 (1.96%)	6 (2.35%)	$p = 1.000$
Prior subarachnoid hemorrhage no. (%)	1 (1.96%)	0 (0.00%)	$p = 0.167$
Atrial fibrillation no. (%)	1 (1.96%)	1 (0.39%)	$p = 3.060$
Other heart disease no. (%)	2 (3.92%)	11 (4.31%)	$p = 1.000$
Mean baseline SBP (SD)	157.51 (20.41)	164.75 (24.67)	$p = 0.049$
Mean baseline DBP (SD)	91.63 (15.65)	96.13 (17.82)	$p = 0.094$
SVD MARKERS			
CS PVS median (IQR)	2 (1–3)	1 (1–2)	/
High degree CS PVS, no. (%)	20 (39.22%)	39 (15.29%)	$p < 0.001$
Periventricular WMH Fazekas score, median (IQR)	2 (2–3)	2 (1–2)	/
Extensive periventricular WMH (score = 3), no. (%)	24 (47.06%)	38 (14.90%)	$p < 0.001$
Deep WMH Fazekas score, median (IQR)	2 (2–3)	2 (1–2)	/
Extensive deep WMH (score ≥ 2), no. (%)	24 (47.06%)	38 (14.90%)	$p < 0.001$
Microbleeds, median (IQR)	2 (1–7)	0 (0–2)	/
Presence of microbleeds, no. (%)	39 (76.47%)	117 (45.88%)	$p < 0.001$
Strictly deep microbleeds, no. (%)	13 (25.49%)	51 (20.00%)	$p = 0.379$
Strictly lobar microbleeds, no. (%)	2 (3.92%)	11 (4.31%)	$p = 1.000$
Lacunes, median (IQR)	1 (0–3)	0 (0–1)	/
Presence of lacunes, no. (%)	32 (62.75%)	101 (39.61%)	$p = 0.002$

BG, basal ganglia; CS, centrum semiovale; DBP, diastolic blood pressure; IQR, interquartile range; PVS, enlarged perivascular spaces; SBP, systolic blood pressure; SD, standard deviation; SVD, small vessel disease; WMH, white matter hyperintensities. Ever smokers indicate current and previous smokers. Other heart disease does not include myocardial infarction and heart failure. Extensive periventricular WMH indicates periventricular WMH Fazekas score 3 and extensive deep WMH indicates deep Fazekas scores 2–3.

0.001) and presence of lacunes ($p = 0.002$). High degrees of BG PVS were associated with the presence of CMB ($p < 0.001$), but not with strictly deep CMB ($p = 0.379$) or strictly lobar CMB ($p = 1.000$).

In multivariable logistic regression analysis (Table 4), increasing age (OR = 1.075; 95% CI = 1.038–1.113, $p < 0.001$) was an independent predictor of increased BG PVS severity, after adjusting for gender and hypertension. The association between high degrees of BG PVS and high CS PVS degrees (OR = 6.906; 95% CI = 3.024–15.774, $p < 0.001$), extensive WMH in periventricular region (OR = 2.878; 95% CI = 1.298–6.379, $p = 0.009$), the presence of CMB (OR = 4.073, 95% CI = 1.869–8.877, $p < 0.001$) remained significant after adjustment for age, gender, and hypertension.

Predictors of Increased CS PVS Severity in Spontaneous ICH Patients

Demographic, vascular, and radiological characteristics of patients with high and low CS PVS degree are compared in Table 3. In univariable analyses, severe CS PVS were associated with the male gender ($p = 0.030$), an alcohol-drinking habit ($p = 0.007$), and hyperlipidemia history ($p = 0.001$). High degrees of CS PVS were also associated with high degrees of BG PVS ($p < 0.001$) and the presence of strictly lobar CMB ($p = 0.012$).

In multivariable logistic regression analysis (Table 4), an alcohol-drinking habit (OR = 2.805; 95% CI = 1.451–5.422, $p = 0.002$) and hyperlipidemia history (OR = 3.782; 95% CI = 1.582–8.783, $p = 0.003$) were independent predictors of increased CS PVS severity, after adjusting for age, gender, and hypertension. The association between high CS PVS degrees and high BG PVS degrees (OR = 6.293; 95% CI = 2.755–14.371, $p < 0.001$) and the presence of strictly lobar CMB (OR = 2.556, 95% CI = 1.285–5.085, $p = 0.008$) remained significant.

DISCUSSION

In this consecutive cohort of spontaneous ICH patients, we find that MR-visible BG PVS and CS PVS are closely co-associated. BG PVS severity is independently associated with increasing age, extensive periventricular WMH and presence of MB. CS PVS severity is associated with alcohol-drinking habit, hypercholesterolemia history, and the presence of strictly lobar MB.

Our results are in agreement with previous studies that BG and CS PVS are closely co-associated. There was a significant relationship between BG PVS and CS PVS severity in healthy elderly subjects (26) or in patients with acute ischemic stroke (IS) or TIA (10, 13, 27). However, a previous study described no statistically significant association between BG PVS and CS PVS severity in spontaneous ICH patients (19). PVS functions as fluid circulation and drainage pathways for efficient exchange of essential nutrients and efficient removal of metabolic waste and cell debris through the central nervous system, and form part of the glymphatic system (28). Both visibility of BG PVS and CS PVS on MRI could be considered as a marker of dysfunctional perivascular flow, impaired nutrient change and waste flushing (29). In parallel, the arterial wall thickening and stiffening occurring with aging or hypertension impairs normal perivascular fluid flushing, facilitating dilation of PVS (30, 31). The dysfunction of the blood–brain barrier might contribute to

TABLE 3 | Comparison of characteristics between patients with high and low degree of PVS in the CS region.

Characteristic	High CS PVS degree	Low CS PVS degree	p-value
Demographics	(CS PVS > 2, $n = 59$)	(CS PVS ≤ 2, $n = 247$)	
Mean age in years (SD)	54.58 (12.12)	56.34 (13.59)	$p = 0.361$
Male gender no. (%)	49 (83.05%)	170 (68.83%)	$p = 0.030$
VASCULAR RISK FACTORS			
Ever-smokers no. (%)	28 (47.46%)	126 (51.01%)	$p = 0.624$
Alcohol drinking no. (%)	39 (66.10%)	115 (46.56%)	$p = 0.007$
Hypertension no. (%)	42 (71.19%)	182 (73.68%)	$p = 0.697$
Diabetes mellitus no. (%)	11 (18.64%)	31 (12.55%)	$p = 0.222$
Hyperlipidemia no. (%)	14 (23.73%)	20 (8.10%)	$p = 0.001$
Prior cerebral infarction no. (%)	9 (15.25%)	35 (14.17%)	$p = 0.831$
Prior intracerebral hemorrhage no. (%)	2 (3.39%)	5 (2.02%)	$p = 0.528$
Prior subarachnoid hemorrhage no. (%)	1 (1.69%)	0 (0.00%)	$p = 0.93$
Atrial fibrillation no. (%)	1 (1.69%)	1 (0.40%)	$p = 0.349$
Other heart disease no. (%)	3 (5.08%)	10 (4.05%)	$p = 0.723$
Mean baseline SBP (SD)	164.05 (22.90)	163.46 (24.47)	$p = 0.867$
Mean baseline DBP (SD)	98.39 (19.59)	94.66 (16.96)	$p = 0.143$
SVD MARKERS			
BG PVS median (IQR)	2 (1–3)	1 (1–2)	/
High degree BG PVS, no. (%)	20 (33.90%)	31 (12.55%)	$p < 0.001$
Periventricular WMH Fazekas score, median (IQR)	2 (1–2)	2 (1–2)	/
Extensive periventricular WMH (score = 3), no. (%)	9 (15.25%)	53 (21.46%)	$p = 0.287$
Deep WMH Fazekas score, median (IQR)	2 (1–2)	1 (1–2)	/
Extensive deep WMH (score ≥ 2), no. (%)	34 (57.63%)	117 (47.37%)	$p = 0.157$
Microbleeds, median (IQR)	1 (0–2)	1 (0–3)	/
Presence of microbleeds, no. (%)	30 (50.85%)	126 (51.01%)	$p = 0.982$
Strictly deep microbleeds, no. (%)	13 (22.03%)	51 (20.65%)	$p = 0.814$
Strictly lobar microbleeds, no. (%)	6 (10.17%)	7 (2.83%)	$p = 0.012$
Lacunae, median (IQR)	1 (1–2)	0 (0–2)	/
Presence of lacunae, no. (%)	30 (50.85%)	103 (41.70%)	$p = 0.203$

BG, basal ganglia; CS, centrum semiovale; DBP, diastolic blood pressure; IQR, interquartile range; PVS, enlarged perivascular spaces; SBP, systolic blood pressure; SD, standard deviation; SVD, small vessel disease; WMH, white matter hyperintensities. Ever smokers indicate current and previous smokers. Other heart disease does not include myocardial infarction and heart failure. Extensive periventricular WMH indicates periventricular WMH Fazekas score 3 and extensive deep WMH indicates deep Fazekas scores 2–3.

the dilation of PVS in both regions (29). A variety of study groups show advancing age is the strongest independent risk factor for PVS in both BG and CS regions in healthy elderly subjects (9), in IS patients (10), and in patients with CAA-ICH patients (19). Our results are in line with these previous studies that we find BG PVS

TABLE 4 | Univariable and multivariable associations for high degree of BG PVS and high degree of CS PVS.

	Unadjusted OR (95% CI), <i>p</i> -value	Adjusted OR (95% CI), <i>p</i> -value
HIGH DEGREE OF BG PVS		
Age	1.070 (1.041–1.100), <i>p</i> < 0.001	1.075 (1.038–1.113), <i>p</i> < 0.001
High CS PVS degree	3.573 (1.851–6.896), <i>p</i> < 0.001	6.906 (3.024–15.774), <i>p</i> < 0.001
Extensive periventricular WMH	5.076 (2.653–9.713), <i>p</i> < 0.001	2.878 (1.298–6.379), <i>p</i> = 0.009
Presence of microbleeds	3.833 (1.918–7.660), <i>p</i> < 0.001	4.073 (1.869–8.877), <i>p</i> < 0.001
HIGH DEGREE OF CS PVS		
Alcohol drinking	2.792 (1.455–5.358), <i>p</i> = 0.002	2.805 (1.451–5.422), <i>p</i> = 0.002
Hyperlipidemia	3.265 (1.424–7.485), <i>p</i> = 0.005	3.728 (1.582–8.783), <i>p</i> = 0.003
High BG PVS degree	4.299 (2.030–9.102), <i>p</i> < 0.001	6.293 (2.755–14.371), <i>p</i> < 0.001
Strictly lobe microbleeds	2.422 (1.229–4.773), <i>p</i> = 0.011	2.556 (1.285–5.085), <i>p</i> = 0.008

BG, basal ganglia; CI, confidence interval; CS, centrum semiovale; OR, odds ratio; PVS, enlarged perivascular spaces; WMH, white matter hyperintensities. Age effects are presented per year. Multivariable logistic regression model adjusted for age, gender, and hypertension.

is associated with increasing age in this cohort of spontaneous ICH patients, but we did not find the same association between increasing age and CS PVS severity. This difference may relate to different brain integrity status, underlying pathophysiological processes and genotypes among patients (26, 32).

We identified a positive association between BG PVS severity and extensive periventricular WMH in ICH patients after adjusting for age, gender and hypertension. Arba et al. (13) found that in patients with IS or TIA, BG PVS severity was associated with WMH severity in both periventricular and deep regions. In another group of IS and TIA patients, Hurford et al. (33) found severe WMH was independently associated with BG PVS severity, however, they did not specify the WMH regions and used a different WMH visual rating scale. In a large memory clinic cohort, both high degrees of BG PVS and CS PVS were associated with moderate-to-severe WMH after adjustment and they did not specify the periventricular and deep WMH either (34). In the Kashima Scan Study, BG PVS severity was associated with severe WMH but not periventricular WMH (35) in neurologically healthy adults. In a recent published systematic review and meta-analysis about the association between PVS and neuroimaging features, the association between PVS and WMH was not significant in the meta-analysis though the direction is positive (36) and the PVS-WMH associations may reflect differences in population characteristics or shared co-associations. Increased WMH burden is associated with blood-brain barrier dysfunction in patients with SVD (37–39). The blood-brain barrier dysfunction might facilitate dilation of PVS, endothelial dysfunction, and impair further nutrient transport. Endothelial dysfunction blocked oligodendrocyte precursor cell

maturation, thereby causing direct damage to myelin and myelin repairment (40, 41). The blood-brain barrier dysfunction might contribute to both BG PVS severity and extensive periventricular WMH (29).

Our study suggested the association between PVS and CMB varied by regions. We found the BG PVS severity was associated with the presence of CMB (at least one microbleed appearing at any region) and the CS PVS severity as associated with the presence of strictly lobar CMB. Our study agrees with previous studies that CS PVS severity was associated with strictly lobar CMB in neurologically healthy adults (35) and increased lobar CMB count was an independent predictor of high CS PVS degrees in a memory clinic cohort (42). However, in this study we did not find the association between the BG PVS severity and strictly deep CMB observed in previous studies including in ICH patients (19) and in a large memory clinic cohort (34). Currently there were insufficient data to compare PVS and CMB by locations (36), and the association between PVS and CMB in different locations merits attention in future studies.

We identified that current alcohol-drinking status is significantly associated with CS PVS severity in ICH patients after adjusting for age, gender, and hypertension. Other groups have studied alcohol intake and the risk of ICH and SVD. Heavy alcohol intake (more than 300 g alcohol per week) was associated with the spontaneous ICH occurrence at a younger age (43) and deep CMB incident in a population-based study (44). Current alcohol-drinking status was associated with WMH volume in acute ischemic stroke patients (45) and silent brain infarction in community-dwelling elderly people (46). In this study, we recorded the patient current alcohol drinking status instead of alcohol consumed in grams, in accordance with the suggestion that consuming zero standard drinks, daily, minimizes health risks, from the UK's chief medical officer guidelines (47) and the global burden of disease 2016 (48).

We found a positive association between hypercholesterolemia history and severe CS PVS degree in ICH patients; however, a previous study found higher blood total cholesterol levels was inversely associated with PVS severity in CS region in healthy elderly subjects (9). Interestingly, previous studies suggested hypercholesterolemia might play a protective role in SVD features such as WMH and infarction: IS patients and control participants with hypercholesterolemia history had less severe WMH (49); IS patients with high triglyceride levels had less WMH severity (50) and higher blood total cholesterol levels were significantly associated with a lower risk of WMH and lacunar infarction in participants aged 40 and over (51). The link between PVS severity and hypercholesterolemia history or blood cholesterol levels deserves more attention and further investigations.

Major strengths of our study include a large consecutive cohort of spontaneous ICH patients which were reviewed by ICH panel experts; furthermore, we used a highly standardized SVD visual methodology and were blinded to patients' clinical information and risk factor profiles to avoid rating bias. Potential limitations are in the study design. This cohort only consists of patients with spontaneous ICH with good quality MRI scans (after actively excluding patients diagnosed with secondary ICH),

and a potential limitation is the lack of a control group with age-matched healthy patients which might limit the generalizability of the results. Another limitation is that the cohort is not gender balanced; it consists of mainly male patients (72%). We planned to include all unselected consecutive patients referred to the stroke unit who underwent MRI, however, many patients with ICH could not undergo MRI for being too sick or with contraindications, which led to a potential for selection bias. All patients were randomly allocated to two different MRI scanners due to the availability, which might be a potential source of image heterogeneity. However, two scanners have the same field strengths and similar ICH scanning protocols that limit image heterogeneity influencing the ratings. We only rated the PVS in BG and CS regions, however, we did not rate the PVS in the midbrain because there were few numbers of slices on which midbrain PVS appear and its rating agreement was influenced by the limited slice number and partial volume effect. We did not include the hippocampus region because of its visualization on axial images varied and may be confused with normal variants hippocampal fissural cysts as suggested previously (52). However, we rated the BG and CS PVS using a validated scale widely used in stroke and SVD studies (10, 21) and we reviewed all available slices instead of a typical one slice in order to increase rating accuracy. Future validation and confirmation of these results in larger, prospective cohorts will be needed to surmount these sampling biases and current limitations.

The present study provides preliminary evidence for the risk factors and neuroimaging features for MR-visible PVS in spontaneous ICH patients, which are age, periventricular WMH, and presence of microbleeds in the BG region and alcohol-drinking habit, hypercholesterolemia history, and strictly lobar microbleeds in the CS region. These factors have potential applications for PVS in clinical research or clinical trials and may be an efficient way to explore the biological mechanisms underlying PVS in ICH patients. Further studies are needed to explore the mechanism and clinical importance of PVS, with possible implications for cerebrovascular disease prevention.

REFERENCES

- van Asch CJ, Luitse MJ, Rinkel GJ, van der Tweel I, Algra A, Klijn CJ. Incidence, case fatality, and functional outcome of intracerebral haemorrhage over time, according to age, sex, and ethnic origin: a systematic review and meta-analysis. *Lancet Neurol.* (2010) 9:167–76. doi: 10.1016/S1474-4422(09)70340-0
- Qureshi AI, Mendelow AD, Hanley DF. Intracerebral haemorrhage. *Lancet.* (2009) 373:1632–44. doi: 10.1016/S0140-6736(09)60371-8
- Kwee RM, Kwee TC. Virchow-Robin spaces at MR imaging. *Radiographics.* (2007) 27:1071–86. doi: 10.1148/rg.274065722
- Etemadifar M, Hekmatnia A, Tayari N, Kazemi M, Ghazavi A, Akbari M, et al. Features of Virchow-Robin spaces in newly diagnosed multiple sclerosis patients. *Eur J Radiol.* (2011) 80:e104–8. doi: 10.1016/j.ejrad.2010.05.018
- Wardlaw JM, Smith EE, Biessels GJ, Cordonnier C, Fazekas F, Frayne R, et al. Neuroimaging standards for research into small vessel disease and its contribution to ageing and neurodegeneration. *Lancet Neurol.* (2013) 12:822–38. doi: 10.1016/S1474-4422(13)70124-8
- Abbott NJ, Pizzo ME, Preston JE, Janigro D, Thorne RG. The role of brain barriers in fluid movement in the CNS: is there a 'glymphatic' system? *Acta Neuropathol.* (2018) 135:387–407. doi: 10.1007/s00401-018-1812-4
- Nedergaard M. Neuroscience. Garbage truck of the brain. *Science.* (2013) 340:1529–30. doi: 10.1126/science.1240514
- Smith AJ, Verkman AS. The "glymphatic" mechanism for solute clearance in Alzheimer's disease: game changer or unproven speculation? *FASEB J.* (2018) 32:543–51. doi: 10.1096/fj.201700999
- Zhu YC, Tzourio C, Soumare A, Mazoyer B, Dufouil C, Chabriat H. Severity of dilated Virchow-Robin spaces is associated with age, blood pressure, and MRI markers of small vessel disease: a population-based study. *Stroke.* (2010) 41:2483–90. doi: 10.1161/STROKEAHA.110.591586
- Potter GM, Doubal FN, Jackson CA, Chappell FM, Sudlow CL, Dennis MS, et al. Enlarged perivascular spaces and cerebral small vessel disease. *Int J Stroke.* (2015) 10:376–81. doi: 10.1111/ijss.12054
- Aribisala BS, Wiseman S, Morris Z, Valdes-Hernandez MC, Royle NA, Maniega SM, et al. Circulating inflammatory markers are associated with magnetic resonance imaging-visible perivascular spaces but not

DATA AVAILABILITY

All datasets generated for this study are included in the manuscript and/or the supplementary files.

ETHICS STATEMENT

All 306 patients participating in this study provided written informed consent. The Beijing Tiantan Hospital Ethics Committee approved this study.

AUTHOR CONTRIBUTIONS

XW and XZ designed the study and drafted the manuscript. HF and YW collected the clinical data and managed the database. JZ collected the imaging data in this study. All authors approved for the manuscript submitted.

FUNDING

The ICH project was conducted under a China National Key R&D Program Funding (Beijing Municipal Science and Technology Commission, No. Z161100002616008), and supported by National Key Research and Development Program of China (No. 2018YFC1312200), Beijing Municipal Administration of Hospitals' Apex Plan (No. DFL20150501), and National Science and Technology Major Project (2017ZX09304018). XW was supported by China Postdoctoral Science Foundation (No. 2017M620835) and Beijing Postdoctoral Research Foundation (2017-22-119).

ACKNOWLEDGMENTS

We thank all the participants for their important contributions in this study. This manuscript has not been published elsewhere in whole or in part.

- directly with white matter hyperintensities. *Stroke*. (2014) 45:605–7. doi: 10.1161/STROKEAHA.113.004059
12. MacLulich AM, Wardlaw JM, Ferguson KJ, Starr JM, Seckl JR, Deary IJ. Enlarged perivascular spaces are associated with cognitive function in healthy elderly men. *J Neurol Neurosurg Psychiatry*. (2004) 75:1519–23. doi: 10.1136/jnnp.2003.030858
 13. Arba F, Quinn TJ, Hankey GJ, Lees KR, Wardlaw JM, Ali M, et al. Enlarged perivascular spaces and cognitive impairment after stroke and transient ischemic attack. *Int J Stroke*. (2018) 13:47–56. doi: 10.1177/1747493016666091
 14. Banerjee G, Kim HJ, Fox Z, Jager HR, Wilson D, Charidimou A, et al. MRI-visible perivascular space location is associated with Alzheimer's disease independently of amyloid burden. *Brain*. (2017) 140:1107–16. doi: 10.1093/brain/awx003
 15. Chen S, Yang Q, Chen G, Zhang JH. An update on inflammation in the acute phase of intracerebral hemorrhage. *Transl Stroke Res*. (2015) 6:4–8. doi: 10.1007/s12975-014-0384-4
 16. Wuerfel J, Haertel M, Waiczies H, Tysiak E, Bechmann I, Wernecke KD, et al. Perivascular spaces—MRI marker of inflammatory activity in the brain? *Brain*. (2008) 131:2332–40. doi: 10.1093/brain/awn171
 17. Polledo L, Gonzalez J, Benavides J, Martinez-Fernandez B, Ferreras MC, Marin JF. Perivascular inflammatory cells in ovine Visna/maedi encephalitis and their possible role in virus infection and lesion progression. *J Neurovirol*. (2012) 18:532–7. doi: 10.1007/s13365-012-0131-0
 18. Sagar D, Lamontagne A, Foss CA, Khan ZK, Pomper MG, Jain P. Dendritic cell CNS recruitment correlates with disease severity in EAE via CCL2 chemotaxis at the blood-brain barrier through paracellular transmigration and ERK activation. *J Neuroinflammation*. (2012) 9:245. doi: 10.1186/1742-2094-9-245
 19. Charidimou A, Meegahage R, Fox Z, Peeters A, Vandermeeren Y, Laloux P, et al. Enlarged perivascular spaces as a marker of underlying arteriopathy in intracerebral haemorrhage: a multicentre MRI cohort study. *J Neurol Neurosurg Psychiatry*. (2013) 84:624–9. doi: 10.1136/jnnp-2012-304434
 20. Charidimou A, Boulouis G, Pasi M, Auriel E, van Etten ES, Haley K, et al. MRI-visible perivascular spaces in cerebral amyloid angiopathy and hypertensive arteriopathy. *Neurology*. (2017) 88:1157–64. doi: 10.1212/WNL.0000000000003746
 21. Potter GM, Chappell FM, Morris Z, Wardlaw JM. Cerebral perivascular spaces visible on magnetic resonance imaging: development of a qualitative rating scale and its observer reliability. *Cerebrovasc Dis*. (2015) 39:224–31. doi: 10.1159/000375153
 22. Fazekas F, Chawluk JB, Alavi A, Hurtig HI, Zimmerman RA. MR signal abnormalities at 1.5 T in Alzheimer's dementia and normal aging. *AJR Am J Roentgenol*. (1987) 149:351–6. doi: 10.2214/ajr.149.2.351
 23. Gregoire SM, Chaudhary UJ, Brown MM, Yousry TA, Kallis C, Jager HR, et al. The Microbleed Anatomical Rating Scale (MARS): reliability of a tool to map brain microbleeds. *Neurology*. (2009) 73:1759–66. doi: 10.1212/WNL.0b013e3181c34a7d
 24. Staals J, Makin SD, Doubal FN, Dennis MS, Wardlaw JM. Stroke subtype, vascular risk factors, and total MRI brain small-vessel disease burden. *Neurology*. (2014) 83:1228–34. doi: 10.1212/WNL.0000000000000837
 25. Staals J, Booth T, Morris Z, Bastin ME, Gow AJ, Corley J, et al. Total MRI load of cerebral small vessel disease and cognitive ability in older people. *Neurobiol Aging*. (2015) 36:2806–11. doi: 10.1016/j.neurobiolaging.2015.06.024
 26. Duperron MG, Tzourio C, Sargurupremraj M, Mazoyer B, Soumare A, Schilling S, et al. Burden of dilated perivascular spaces, an emerging marker of cerebral small vessel disease, is highly heritable. *Stroke*. (2018) 49:282–7. doi: 10.1161/STROKEAHA.117.019309
 27. Zhang C, Chen Q, Wang Y, Zhao X, Wang C, Liu L, et al. Risk factors of dilated Virchow-Robin spaces are different in various brain regions. *PLoS ONE*. (2014) 9:e105505. doi: 10.1371/journal.pone.0105505
 28. Rasmussen MK, Mestre H, Nedergaard M. The glymphatic pathway in neurological disorders. *Lancet Neurol*. (2018) 17:1016–24. doi: 10.1016/S1474-4422(18)30318-1
 29. Wardlaw JM, Smith C, Dichgans M. Small vessel disease: mechanisms and clinical implications. *Lancet Neurol*. (2019) 18:684–96. doi: 10.1016/S1474-4422(19)30079-1
 30. Iliff JJ, Wang M, Zeppenfeld DM, Venkataraman A, Plog BA, Liao Y, et al. Cerebral arterial pulsation drives paravascular CSF-interstitial fluid exchange in the murine brain. *J Neurosci*. (2013) 33:18190–9. doi: 10.1523/JNEUROSCI.1592-13.2013
 31. Mestre H, Tithof J, Du T, Song W, Peng W, Sweeney AM, et al. Flow of cerebrospinal fluid is driven by arterial pulsations and is reduced in hypertension. *Nat Commun*. (2018) 9:4878. doi: 10.1038/s41467-018-07318-3
 32. Charidimou A, Pantoni L, Love S. The concept of sporadic cerebral small vessel disease: a road map on key definitions and current concepts. *Int J Stroke*. (2016) 11:6–18. doi: 10.1177/1747493015607485
 33. Hurford R, Charidimou A, Fox Z, Cipolletti L, Jager R, Werring DJ. MRI-visible perivascular spaces: relationship to cognition and small vessel disease MRI markers in ischaemic stroke and TIA. *J Neurol Neurosurg Psychiatry*. (2014) 85:522–5. doi: 10.1136/jnnp-2013-305815
 34. Shams S, Martola J, Charidimou A, Larvie M, Granberg T, Shams M, et al. Topography and determinants of magnetic resonance imaging (MRI)-visible perivascular spaces in a large memory clinic cohort. *J Am Heart Assoc*. (2017) 6:e006279. doi: 10.1161/JAHA.117.006279
 35. Yakushiji Y, Charidimou A, Hara M, Noguchi T, Nishihara M, Eriguchi M, et al. Topography and associations of perivascular spaces in healthy adults: the Kashima scan study. *Neurology*. (2014) 83:2116–23. doi: 10.1212/WNL.0000000000001054
 36. Francis F, Ballerini L, Wardlaw JM. Perivascular spaces and their associations with risk factors, clinical disorders and neuroimaging features: a systematic review and meta-analysis. *Int J Stroke*. (2019) 14:359–71. doi: 10.1177/1747493019830321
 37. Huisa BN, Caprihan A, Thompson J, Prestopnik J, Qualls CR, Rosenberg GA. Long-term blood-brain barrier permeability changes in Binswanger disease. *Stroke*. (2015) 46:2413–8. doi: 10.1161/STROKEAHA.115.009589
 38. Munoz Maniega S, Chappell FM, Valdes Hernandez MC, Armitage PA, Makin SD, Heye AK, et al. Integrity of normal-appearing white matter: influence of age, visible lesion burden and hypertension in patients with small-vessel disease. *J Cereb Blood Flow Metab*. (2017) 37:644–56. doi: 10.1177/0271678X16635657
 39. Zhang CE, Wong SM, Uiterwijk R, Backes WH, Jansen JFA, Jeukens C, et al. Blood-brain barrier leakage in relation to white matter hyperintensity volume and cognition in small vessel disease and normal aging. *Brain Imaging Behav*. (2019) 13:389–95. doi: 10.1007/s11682-018-9855-7
 40. Bugiani M, Kevelam SH, Bakels HS, Waisfisz Q, Ceuterick-de Groote C, Niessen HW, et al. Cathepsin A-related arteriopathy with strokes and leukoencephalopathy (CARASAL). *Neurology*. (2016) 87:1777–86. doi: 10.1212/WNL.0000000000003251
 41. Rajani RM, Quick S, Ruigrok SR, Graham D, Harris SE, Verhaaren BFJ, et al. Reversal of endothelial dysfunction reduces white matter vulnerability in cerebral small vessel disease in rats. *Sci Transl Med*. (2018) 10:eam9507. doi: 10.1126/scitranslmed.aam9507
 42. Martinez-Ramirez S, Pontes-Neto OM, Dumas AP, Auriel E, Halpin A, Quimby M, et al. Topography of dilated perivascular spaces in subjects from a memory clinic cohort. *Neurology*. (2013) 80:1551–6. doi: 10.1212/WNL.0b013e31828f1876
 43. Casolla B, Dequatre-Ponchelle N, Rossi C, Henon H, Leys D, Cordonnier C. Heavy alcohol intake and intracerebral hemorrhage: characteristics and effect on outcome. *Neurology*. (2012) 79:1109–15. doi: 10.1212/WNL.0b013e3182698d00
 44. Ding J, Sigurdsson S, Garcia M, Phillips CL, Eiriksdottir G, Gudnason V, et al. Risk factors associated with incident cerebral microbleeds according to location in older people: the age, gene/environment susceptibility (AGES)-Reykjavik study. *JAMA Neurol*. (2015) 72:682–8. doi: 10.1001/jamaneurol.2015.0174
 45. Cloonan L, Fitzpatrick KM, Kanakis AS, Furie KL, Rosand J, Rost NS. Metabolic determinants of white matter hyperintensity burden in patients with ischemic stroke. *Atherosclerosis*. (2015) 240:149–53. doi: 10.1016/j.atherosclerosis.2015.02.052
 46. Fukuda K, Takashima Y, Hashimoto M, Uchino A, Yuzuriha T, Yao H. Early menopause and the risk of silent brain infarction in community-dwelling elderly subjects: the Sefuri brain MRI study. *J Stroke Cerebrovasc Dis*. (2014) 23:817–22. doi: 10.1016/j.jstrokecerebrovasdis.2013.07.005
 47. Burton R, Sheron N. No level of alcohol consumption improves health. *Lancet*. (2018) 392:987–8. doi: 10.1016/S0140-6736(18)31571-X

48. GBD 2016 Alcohol and Drug Use Collaborators. The global burden of disease attributable to alcohol and drug use in 195 countries and territories, 1990–2016: a systematic analysis for the Global Burden of Disease Study 2016. *Lancet Psychiatry*. (2018) 5:987–1012. doi: 10.1016/S2215-0366(18)30337-7
49. Jimenez-Conde J, Biffi A, Rahman R, Kanakis A, Butler C, Sonni S, et al. Hyperlipidemia and reduced white matter hyperintensity volume in patients with ischemic stroke. *Stroke*. (2010) 41:437–42. doi: 10.1161/STROKEAHA.109.563502
50. Ke D, Zhou F, Liang H, Xu Y, Lou H. Hypertriglyceridemia is associated with reduced leukoaraiosis severity in patients with a small vessel stroke. *Behav Neurol*. (2018) 2018:1361780. doi: 10.1155/2018/1361780
51. Ohwaki K, Yano E, Tamura A, Inoue T, Saito I. Hypercholesterolemia is associated with a lower risk of cerebral ischemic small vessel disease detected on brain checkups. *Clin Neurol Neurosurg*. (2013) 115:669–72. doi: 10.1016/j.clineuro.2012.07.025
52. Adams HH, Cavalieri M, Verhaaren BF, Bos D, van der Lugt A, Enzinger C, et al. Rating method for dilated Virchow-Robin spaces on magnetic resonance imaging. *Stroke*. (2013) 44:1732–5. doi: 10.1161/STROKEAHA.111.000620

Conflict of Interest Statement: The authors declare that the research was conducted in the absence of any commercial or financial relationships that could be construed as a potential conflict of interest.

Copyright © 2019 Wang, Feng, Wang, Zhou and Zhao. This is an open-access article distributed under the terms of the Creative Commons Attribution License (CC BY). The use, distribution or reproduction in other forums is permitted, provided the original author(s) and the copyright owner(s) are credited and that the original publication in this journal is cited, in accordance with accepted academic practice. No use, distribution or reproduction is permitted which does not comply with these terms.



Enhanced Effective Connectivity From Ipsilesional to Contralesional M1 in Well-Recovered Subcortical Stroke Patients

Yanmin Peng^{1,2}, Jingchun Liu¹, Minghui Hua^{1,2}, Meng Liang^{1,2*} and Chunshui Yu^{1,2*}

¹ Department of Radiology and Tianjin Key Laboratory of Functional Imaging, Tianjin Medical University General Hospital, Tianjin, China, ² School of Medical Imaging, Tianjin Medical University, Tianjin, China

OPEN ACCESS

Edited by:

Eric Jouvent,
Université Sorbonne Paris Cité, France

Reviewed by:

Laurent Puy,
Centre Hospitalier Régional et
Universitaire de Lille, France
Charlotte Rosso,
Hôpitaux Universitaires Pitié
Salpêtrière, France

*Correspondence:

Meng Liang
liangmeng@tmu.edu.cn
Chunshui Yu
chunshuiyu@tmu.edu.cn

Specialty section:

This article was submitted to
Stroke,
a section of the journal
Frontiers in Neurology

Received: 20 March 2019

Accepted: 05 August 2019

Published: 21 August 2019

Citation:

Peng Y, Liu J, Hua M, Liang M and
Yu C (2019) Enhanced Effective
Connectivity From Ipsilesional to
Contralesional M1 in Well-Recovered
Subcortical Stroke Patients.
Front. Neurol. 10:909.
doi: 10.3389/fneur.2019.00909

Background and Purpose: Interhemispheric imbalance may provide a framework for developing new strategies to facilitate post-stroke motor recovery especially for patients in chronic stage. Using effective connectivity analysis, we aimed to investigate interactions between the bilateral primary motor cortices (M1) and their correlations with motor function and M1-related structural and functional changes in well-recovered patients with chronic subcortical ischemic stroke.

Methods: Twenty subcortical stroke patients and 20 normal controls underwent multimodal magnetic resonance imaging (MRI) examinations. During the movement of the affected hand, functional MRI was used to calculate the M1 activation and M1-M1 effective connectivity. Diffusion tensor imaging was used to compute the fractional anisotropy (FA) of the affected corticospinal tract (CST) and M1-M1 anatomical connection. After intergroup comparisons, we tested whether the altered M1-M1 effective connectivity was correlated with the motor function, M1 activation and FA of the affected CST and M1-M1 anatomical connection in patients.

Results: Compared to normal controls, stroke patients exhibited increased excitatory effective connectivity from ipsilesional to contralesional M1 and increased ipsilesional M1 activation; however, they showed reduced FA values in the affected CST and M1-M1 anatomical connection. The increased effective connectivity was positively correlated with motor score and the FA of the M1-M1 anatomical connection, but not with the M1 activation or the FA of the affected CST in these patients.

Conclusions: These findings suggest that the enhancement of M1-M1 effective connectivity from ipsilesional to contralesional hemisphere depends on the integrity of the underlying M1-M1 anatomical connection (i.e., less deficits of the M1-M1 anatomical connection, greater enhancement of the corresponding effective connectivity), and such M1-M1 effective connectivity enhancement plays a supportive role in motor function in chronic subcortical stroke.

Keywords: brain infarction, motor cortex, motor recovery, magnetic resonance imaging, diffusion tensor imaging

INTRODUCTION

Motor disability is one of the most common deficits after stroke. Post-stroke motor recovery depends mainly on structural damage and functional reorganization of the motor network. The aim of motor rehabilitation is to enhance the beneficial functional reorganization, which could be identified by observing structural and functional changes during spontaneous recovery. In the past decades, neuroimaging studies, especially those with magnetic resonance imaging (MRI), have revealed a variety of structural, functional, connectivity and network changes in the brain after stroke (1–3). However, the clinical importance of these changes depends on their relations to motor recovery and possibilities to be integrated into therapeutic strategies.

In patients with subcortical stroke, structural, and functional changes of the primary motor cortex (M1) have been related to motor recovery. Although more extensive activation in both hemispheres are commonly observed in stroke patients, only normalized ipsilesional M1 activation has been consistently related to motor recovery (4). As the main descending fibers of the M1, the corticospinal tract (CST) damage has been identified as the main cause for motor deficit and the leading barrier for motor recovery (5, 6). Besides the lesion-induced direct damage in the CST, the integrity of transcallosal fibers between the bilateral M1 is also reduced in subcortical stroke (7, 8), which has been correlated with the bilateral recruitment of motor areas (8) and the increase in M1-M1 functional connectivity (9). As a simple method to assess interhemispheric functional interactions, the resting-state functional connectivity between the bilateral M1 experiences a reduction and recovery process, and the normalized or enhanced connectivity has been related to motor recovery (10, 11). In contrast to the lack of directionality of the resting-state functional connectivity, the effective connectivity measures the influence of one brain area exerts over another, can better characterize interhemispheric functional interactions, providing useful information for planning rehabilitation strategies (2).

The model of interhemispheric imbalance is the basis for developing non-invasive brain stimulation (NIBS) strategies to facilitate post-stroke motor recovery (12). On the basis of inhibitory influence from contralesional to ipsilesional M1 (2, 12), these strategies mainly aim to increase ipsilesional M1 excitability and/or reduce contralesional M1 excitability to recover the balance (13, 14). However, inconsistent therapeutic effects on stroke patients (15, 16) indicate the diversity of interhemispheric interactions and the existence of unknown modulators. The diversity of interhemispheric interactions has also been revealed by effective connectivity studies. For example, in patients with subcortical stroke, one study shows additional inhibitory influences from contralesional to ipsilesional M1 (17); however, another study demonstrates a positive influence (18). In addition, M1-M1 effective connectivity changes in subcortical stroke are not isolated from other structural damages and functional reorganization; instead, they are possibly related to structural and functional changes of the M1 (19)—this information is useful in the stratification of patients for suitable interventions.

Although early interventions may be most beneficial by preventing the development of maladaptive reorganization and resulting in greater motor improvement, interventions for chronic stroke patients are also important because a huge number of chronic stroke patients with persistent motor disabilities are waiting for new strategies to improve their impaired motor functions. Examining the relationship between functional reorganization and structural impairment in chronic stroke patients with well recovered motor function may help clarify the beneficial role of the functional reorganization in motor recovery in chronic stage (9, 20). For example, it has been reported that chronic stroke patients with well recovered motor function show reduced cortical thickness but increased task-evoked activation and resting-state neural activity (i.e., regional homogeneity and amplitude of low-frequency fluctuation) and functional connectivity in the ipsilesional M1 (20). Furthermore, in a similar group of patients, we observed that the FA values of the anatomical connections between bilateral M1 and of the CST were reduced but the M1-M1 resting-state functional connectivity was increased, and interestingly, the resting-state functional connectivity was positively correlated with the FA values of these anatomical connections (9). However, it is unclear whether effective connectivity between bilateral M1 plays a similar beneficial role in motor recovery in these patients. Here, we aimed to identify stroke-induced M1-M1 effective connectivity changes in relatively well recovered subcortical stroke patients in chronic stage, and to investigate their functional roles in motor recovery and associations with the ipsilesional M1 activation and the white matter integrity of the affected CST and M1-M1 anatomical connections. Importantly, we directly evaluated the relationship between the M1-M1 effective connectivity and the motor function of these patients.

MATERIALS AND METHODS

Subjects

Twenty well-recovered chronic stroke patients with subcortical infarcts participated in this study. All patients satisfied the inclusion criteria of first-ever ischemic stroke, clear motor deficits at the time of stroke onset, single subcortical lesion involving the motor pathway, right-handed before the stroke [determined using the Chinese edition of the Edinburgh Handedness Inventory (21)], an interval of more than 6 months from stroke onset, well-recovered in motor function with Fugl-Meyer Assessment (FMA) score more than 60 for the affected upper extremity and more than 90 for the whole extremities, and capable of completing neurological and MRI examinations. The exclusion criteria included (1) recurrent stroke, (2) any other brain abnormalities, (3) lacunes and microbleeds based on T1-, T2-, and diffusion-weighted images (DWI), (4) severe white matter hyperintensity manifested as a Fazekas scale (22) score > 1, (5) serious cerebral atrophy and (6) a history of drug dependency or psychiatric disorders. Twenty age-, sex-, and handedness-matched normal volunteers were recruited as controls. This study was approved by the Ethics Committee of Tianjin Medical University General Hospital and informed consent was obtained from each participant before the study.

Parts of these participants have been used in our previous work (9, 20).

Task Design

All subjects performed a block-design motor task (a unilateral voluntary hand-grasping task) with a frequency of 2.4 Hz. The frequency of the task was controlled by a computer. An experimenter inside the scanner room could see the signal on the computer monitor and would lightly touch the foot of the participant. Each participant was instructed to close his fist once perceiving a light touch on the foot. All participants were trained to perform this task until they could perform well the task prior to the formal experiment. Patients with stroke performed the task using the affected hand, but healthy controls used their left hand. Each task block (20 s) was followed by a resting block (20 s), and the cycle was repeated four times. Instructions for the start and the end of each block were given by a visual cue on a screen. The detailed procedures for the task were described previously (20).

Image Acquisition

MRI data were acquired using a Signa HDx 3.0-Tesla scanner (General Electric, Milwaukee, WI). The functional MRI (fMRI) data were acquired by a gradient-echo single-shot echo-planar imaging (SS-EPI) sequence: repetition time/echo time (TR/TE) = 2,000/30 ms; field of view (FOV) = 240 mm × 240 mm; matrix = 64 × 64; slice thickness = 3 mm; 1 mm gap; 38 interleaved transversal slices. The diffusion tensor imaging (DTI) data were obtained using a spin-echo SS-EPI sequence with 30 non-collinear diffusion-sensitized directions and a *b*-value of 1,000 s/mm², and with 3 sets of *b*=0 images. The parameters were TR/TE = 11,000/77.6 ms; FOV = 256 mm × 256 mm; matrix = 128 × 128; slice thickness = 3 mm, no gap; and 50 transversal slices. DWI and conventional MR images (T1- and T2-weighted images) were acquired for brain abnormality assessment. DWI was obtained using the following imaging parameters: TR/TE = 3,000/61 ms; FOV = 240 mm × 240 mm; matrix = 160 × 160; slice thickness = 6 mm; gap = 1.5 mm; and *b* = 1,000 s/mm². Sagittal 3D T1-weighted images were acquired by a brain volume sequence with the following imaging parameters: TR/TE = 7.8/3.0 ms; FOV = 256 × 256 mm; matrix = 256 × 256; inversion time = 450 ms; flip angle = 13°; slice thickness = 1 mm, no gap; and 176 slices.

Image Preprocessing

To facilitate the analysis across patients with lesions on different sides, the imaging data were flipped from left to right along the midline for patients with left-sided lesions. Thus, the right side of the image corresponded to the ipsilesional hemisphere and the left side to the contralesional hemisphere for all patients.

The preprocessing of fMRI data was performed using the Statistical Parametric Mapping (SPM8, <https://www.fil.ion.ucl.ac.uk/spm>). The volumes were corrected for the acquisition time delay between slices and were then realigned across volumes to correct for inter-scan movements. We controlled for head motion with thresholds of 2.5 mm translation in each cardinal direction and 2.5° rotation around each orthogonal axis. The realigned fMRI images were spatially normalized to Montreal

Neurological Institute (MNI) space using the EPI template and were then re-sampled to 3 × 3 × 3 mm³ voxels. The resulting images were smoothed with a Gaussian kernel of 8 mm full-width at half-maximum. A high-pass filter with 128-s cut-off was applied to eliminate signal drifts of each voxel. Head motion effects on fMRI signals were further reduced by regressing out the six head motion parameters from the fMRI time series of each voxel.

The FSL software (<https://fsl.fmrib.ox.ac.uk/fsl/fslwiki/>) was used for DTI data preprocessing, including Eddy-current distortion correction, head motion correction, skull removal, and FA calculation for each voxel in the whole brain. Then, Diffusion Toolkit (<http://www.trackvis.org/dtk/>) was used to track fiber tract of the CST and the M1-M1 fiber tract. Because the white matter integrity can be accurately assessed by FA only in fiber tracts with highly coherent arrangement (6), we only extracted the FA value of the cerebral peduncle for the affected CST and that of the midsagittal slice for the M1-M1 anatomical connection for subsequent analyses. More details about the processing of DTI data were described in our previous study (9).

Task fMRI Analysis

We first created an ipsilesional M1 mask and a contralesional M1 mask as the Brodmann Area 4 in the corresponding hemisphere defined by the Brodmann area atlas available in the software package MRIcron (<https://people.cas.sc.edu/rorden/mricron/>) for the following brain activation analysis and Granger causality analyses. For the brain activation analysis, general linear model (GLM) was used to identify hand motion-induced activation map of each subject, and the contrast maps of all individuals were entered into a two-sample *t*-test to identify voxels within the ipsilesional and contralesional M1 masks that were activated differently between the two groups (*P* < 0.001, uncorrected). The identified voxels with significant intergroup activation difference located within the ipsilesional M1 mask were defined as the seed region for the subsequent effective connectivity analysis. The average activation (i.e., the beta values) of these identified voxels were also extracted from each participant for the subsequent correlation analyses.

Granger Causality Analysis

Granger causality is a widely-used effective connectivity approach to explore the causal relationships between two time series based on their temporal precedence of each other (23). Here, the activity in brain area X can be considered to cause the activity in brain area Y if the blood-oxygen-level dependent (BOLD) signal of the current time point in brain area Y can be predicted using those of the past time points in brain area X. In this study, Granger causality was performed using the bivariate linear autoregressive model implemented in the software package REST (<http://www.restfmri.net/forum/REST-GCA>). In brief, Granger causality from brain area X to brain area Y can be estimated using the following equation:

$$Y_t = \sum_{i=1}^p A_i X_{(t-i)} + \sum_{i=1}^p B_i Y_{(t-i)} + CZ_t + \varepsilon_t \quad (1)$$

where, X_t and Y_t represent the fMRI signals at the time point t in brain areas X and Y , respectively; Z represents covariates (e.g., head motion and global trend); A_i and B_i represent path coefficients and auto regression coefficients at the time lag i . The time series X significantly Granger causes the time series Y if the path coefficient A_i is significantly larger or smaller than zero for at least one time lag. The maximal time lag p represents the model order. As most previous studies (24), we set lag p as 1 in the present study.

A_i can be standardized to Z scores according to the following formula:

$$Z_i = \frac{A_i - m}{s} \quad (2)$$

where m is the global mean (i.e., the mean of all voxels within the whole brain) of A_i , and s is the corresponding standard deviation of A_i . Negative path coefficients A_i mean inhibitory effects and positive path coefficients A_i mean excitatory effects (25).

To investigate Granger causality from the ipsilesional M1 seed region to contralesional M1 voxels, in formula (1), let X be the average time series of the ipsilesional M1 seed region and Y be the time series of a given voxel of the contralesional M1 mask (i.e., Brodmann Area 4), and repeat this estimation for all voxels within this contralesional M1 mask. Therefore, we obtained a map in which the value of each voxel in the contralesional M1 represents the Granger causality value from the seed to this particular voxel. Similarly, Granger causality from every contralesional M1 voxel to the seed can also be obtained by letting X be the time series of a given voxel and Y be the time series of the seed.

The voxel-wise group differences in Granger causality of each direction within the contralesional M1 mask were identified using a two-sample t -test under the threshold of $P < 0.05$ (corrected by voxel-level family wise error, FWE) in SPM8. Finally, the M1-M1 effective connectivity of each direction was represented by the average Granger causality values across all voxels showing significant intergroup differences within the contralesional M1 mask and used in the subsequent correlation analyses.

Statistical Analysis

The average effective connectivity, the average activation, and the FA values of the affect CST and the M1-M1 anatomical connection were compared between patients and controls using a two-sample t -test ($P < 0.05$). Pearson's correlation analyses, after controlling for age, sex, lesion volumes and post-stroke interval, were performed to examine the relationships of the altered M1-M1 effective connectivity with the upper-limb FMA score, the activation of the ipsilesional M1, and the FA of the affected CST and M1-M1 anatomical connection in stroke patients ($P < 0.05$, uncorrected). The normality of these data was checked by one-sample Kolmogorov-Smirnov test. These analyses were performed using an in-house script in MATLAB (R 2015b).

RESULTS

Demographic and Clinical Information

The clinical and demographic data of stroke patients and normal controls are listed in **Table 1**. Compared with normal controls, patients with stroke did not show any significant differences in age ($P = 0.907$) and sex ($P = 0.900$). The duration from stroke onset to the MRI scan ranged 11–64 months (mean value: 31.6 ± 16.54 months). The stroke lesions involved the internal capsule and the surrounding structures such as the thalamus, basal ganglia, and corona radiata; 9 out of 20 patients (i.e., 45%) had infarct lesions in the left hemisphere and 11 (i.e., 55%) in the right hemisphere. The lesion volume (mean \pm standard deviation) is 1077.75 ± 1255.48 mm³ (range: 250–5694 mm³) and the lesion location is shown in **Figure 1**. The motor function of the patients was significantly recovered with an FMA $> 93/100$ for the whole extremities.

Intergroup Comparisons of Imaging Measures of Interest

The voxel-wise comparisons of the hand motion-induced activation within the bilateral M1 masks revealed a cluster in the ipsilesional M1 with significant activation difference between the two groups (peak coordinates = [39, -15, 63]; peak z score = 4.20; cluster size = 28 voxels; $P < 0.001$, uncorrected; **Figure 2A**).

With this cluster as the seed, the voxel-wise Granger causality analysis showed that stroke patients exhibited significantly increased effective connectivity from the seed (the ipsilesional M1) to a cluster of voxels in the contralesional M1 (peak coordinates = [-39, -30, 66]; peak z score = 4.61; cluster size = 12 voxels; $P < 0.05$, FWE corrected; **Figure 2B**) compared to normal controls. However, we did not find any significant intergroup differences in the effective connectivity from contralesional to ipsilesional M1.

TABLE 1 | Demographic and clinical information of patients with stroke and controls.

Variables	Stroke patients (n = 20)	Normal controls (n = 20)	P-value
Age (year)	57.6 \pm 8.5 (42–72)	57.3 \pm 7.5 (47–74)	0.907
Men, n (%)	12 (60%)	11 (55%)	0.900
Duration (months)	31.6 \pm 16.5 (11–64)		
Lesion volume (mm ³)	1077.75 \pm 1255.48 (250–5694)		
Lesion location, n (%)			
Left hemisphere	9 (45%)		
Right hemisphere	11 (55%)		
Fugl-Meyer assessment			
Upper extremity	65.4 \pm 1.0 (62–66)		
Whole extremity	98.9 \pm 2.0 (93–100)		

Data are presented as mean \pm SD (range) for continuous data and n (%) for categorical data.

The average effective connectivity extracted from the voxels within the identified contralesional M1 cluster was significantly increased in patients (shifted from inhibitory in controls to excitatory in patients) ($P = 2.25 \times 10^{-8}$; **Figure 3A**). The average activation (i.e., the beta values) of the ipsilesional M1 cluster (i.e., the seed region) were also significantly increased in patients compared with controls ($P = 2.91 \times 10^{-5}$; **Figure 3B**). In contrast, both the FA values in the affected CST ($P = 0.004$; **Figure 3C**) and the FA values of the M1-M1 anatomical

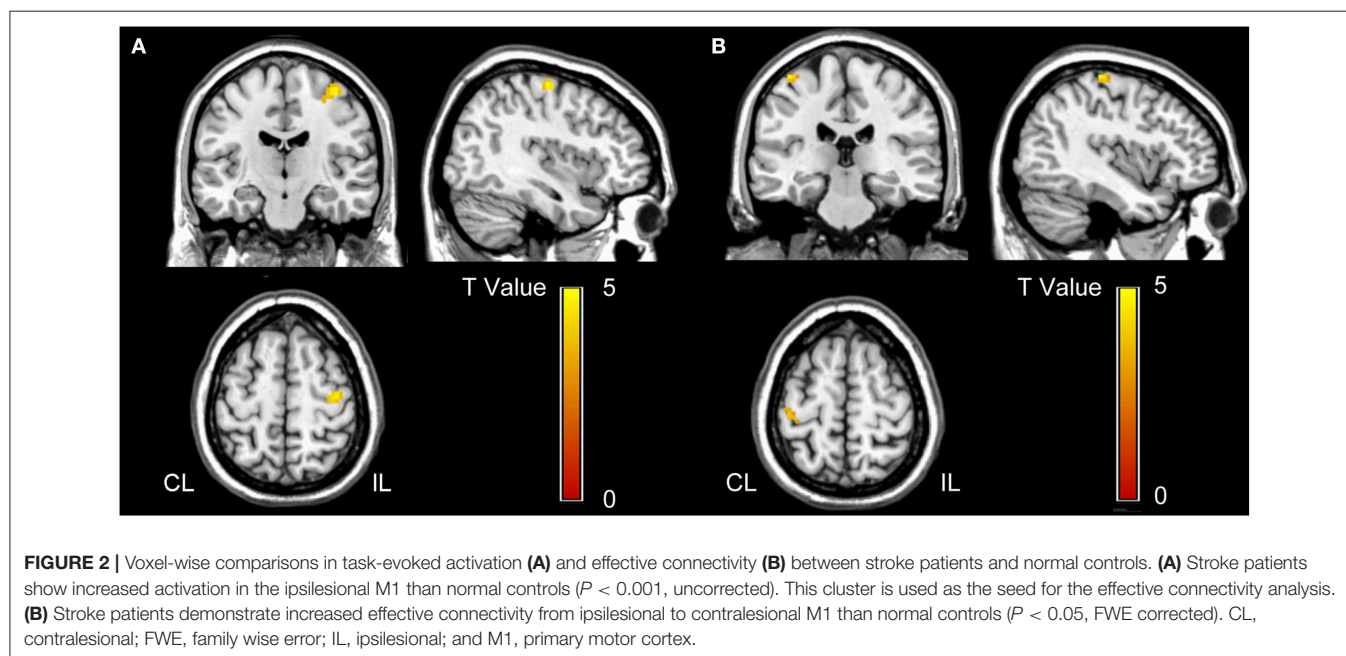
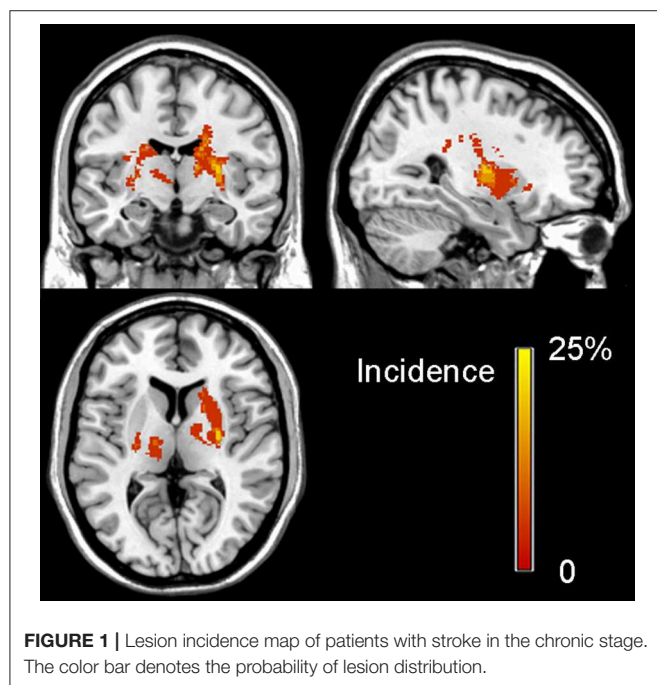
connection were significantly decreased in patients ($P = 0.011$; **Figure 3D**).

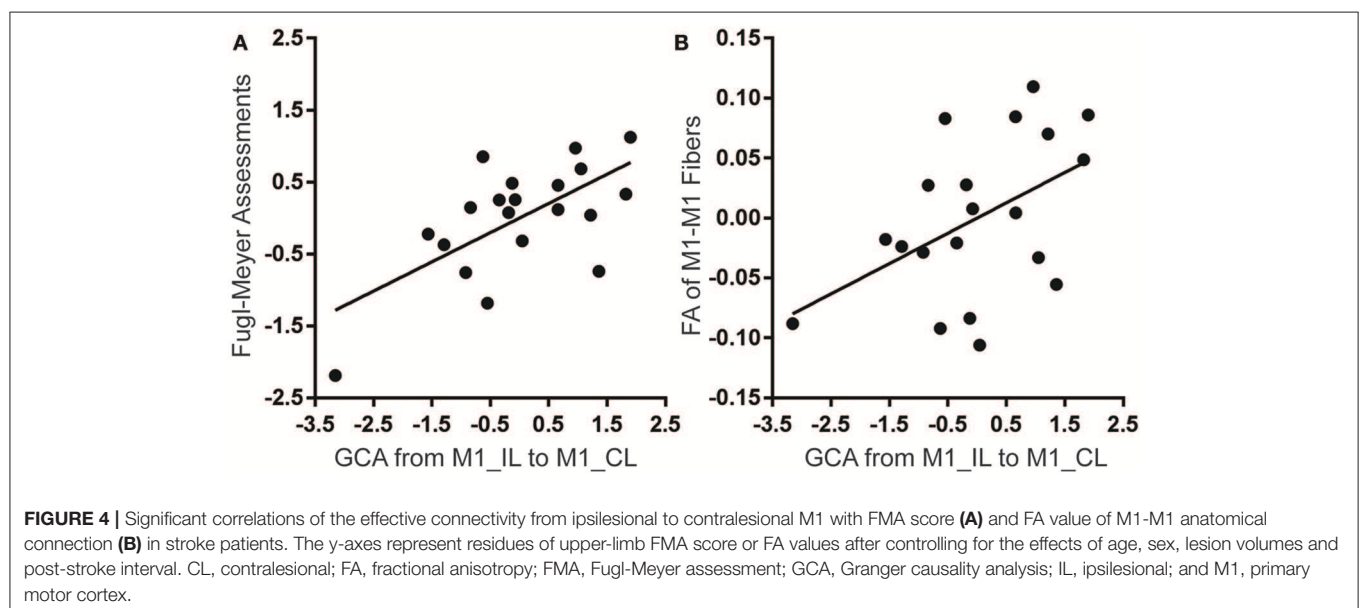
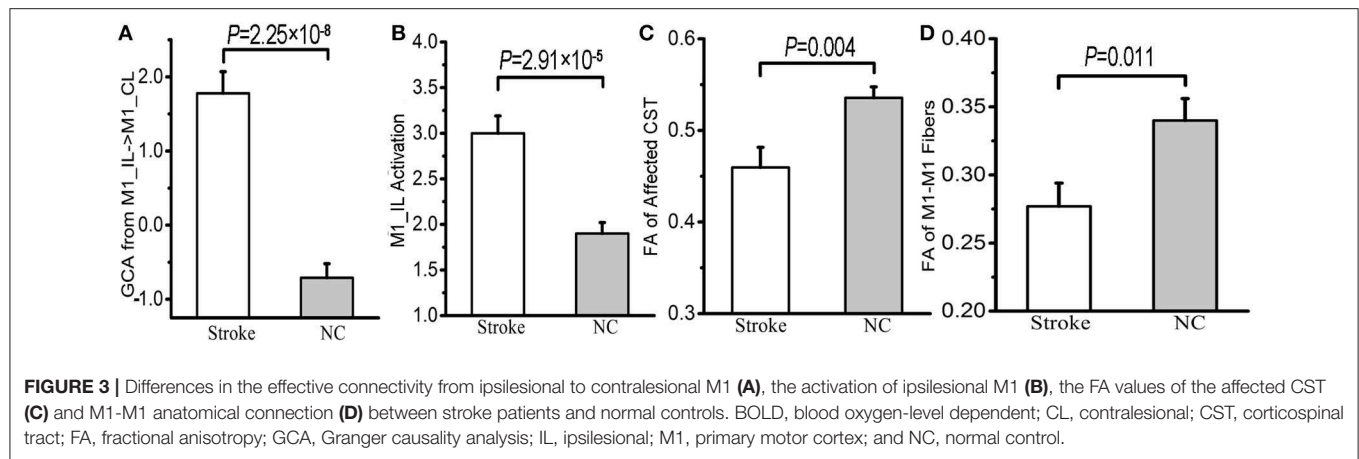
Correlations of M1-M1 Effective Connectivity With Motor Function and Other M1-Related Imaging Measures

When controlling for the effects of sex, age, lesion volume and post-stroke interval, we found that the strengths of the excitatory effective connectivity from ipsilesional to contralesional M1 were positively correlated with the upper limb FMA scores (correlation coefficient = 0.645; $P = 0.002$; **Figure 4A**) and with the FA values of the M1-M1 anatomical connection (correlation coefficient = 0.478; $P = 0.033$; **Figure 4B**) in patients with stroke. However, the strengths of this effective connectivity were not correlated with the FA values of the affected CST (correlation coefficient = 0.200; $P = 0.399$) or the activation of the ipsilesional M1 (correlation coefficient = -0.136 ; $P = 0.569$). After controlling for age, sex, lesion volumes, and post-stroke interval, these data are normally distributed, confirmed by Kolmogorov-Smirnov tests: $Z = 0.452$ ($P = 0.987$) for the M1-M1 effective connectivity, $Z = 0.622$ ($P = 0.834$) for the brain activation, $Z = 0.451$ ($P = 0.987$) for the FA values of the affected CST, and $Z = 0.476$ ($P = 0.977$) for FA values of the M1-M1 anatomical connection, $Z = 0.759$ ($P = 0.613$) for the upper limb FMA scores.

DISCUSSION

In this study, we investigated M1-M1 effective connectivity alterations and their associations with motor function and M1-related activation and connection changes in well-recovered subcortical stroke patients in the chronic stage. Note that, although all patients used in this study were in their chronic stage and well-recovered in motor function, they had clear and





definite motor deficits at the time of stroke onset. Therefore, these patients represent a stroke population with an effective recovery in motor function and thus provide an essential basis for studying neural mechanisms underlying effective motor recovery in stroke patients. We found that the effective connectivity from ipsilesional to contralesional M1 was completely inverted from inhibitory in normal controls to excitatory in stroke patients, and the excitatory connectivity was positively correlated with motor function in these patients, indicating a supportive role in motor recovery. The positive correlation between the effective and anatomical connectivity of the bilateral M1 suggests that the enhancement of the M1-M1 effective connectivity depends on the integrity of the underlying anatomical connection.

In contrast to previous studies showing normalized M1-M1 effective connectivity (18), reduced inhibitory effective connectivity from ipsilesional to contralesional M1 (19), or increased inhibitory effective connectivity from contralesional to ipsilesional M1 (17) in the chronic stage of subcortical stroke, we found increased excitatory effective connectivity from

ipsilesional to contralesional M1 in well-recovered patients with subcortical stroke in the chronic stage. It is noticeable that the patients examined in the previous studies and our present study were at different stages of motor recovery after stroke—Rehme et al. (18), Grefkes et al. (17) and our present study examined, respectively, patients at 2 weeks after stroke, patients with partial motor recovery in an early chronic stage after stroke, and patients with well-recovered motor function in a late chronic stage after stroke. Evidence has suggested that stroke patients at different stages may exhibit different functional changes in the brain. For example, using a rat model of stroke, van Meer (26) found that interhemispheric functional connectivity was reduced and associated with impaired motor performance in the first days after experimental stroke, and then was gradually increased and concomitant to sensorimotor improvements. All these findings suggest the complexity and diversity of interhemispheric functional interactions even in chronic stroke patients at different stages. Both well-recovered characteristic of patients and positive correlation between excitatory connectivity

and motor performance support a beneficial role of the increased excitatory connectivity in motor recovery at least in chronic subcortical stroke patients with a good motor function. Our findings might also imply the importance of incorporating connectivity-based information into the design of more effective NIBS protocols which would be beneficial to the existing great number of stroke patients who have developed into the chronic stage (27, 28). Future studies are needed to identify the suitable NIBS protocols that could enhance the beneficial excitatory effective connectivity from ipsilesional to contralesional M1 to facilitate motor recovery.

The M1-M1 effective connectivity is calculated based on activities of the bilateral M1 during the movement of the affected hand. It is plausible to speculate a correlation between M1-M1 effective connectivity and M1 activation (19). However, we failed to find such a correlation, suggesting different functional meanings of the two measures in terms of motor function. The normalized activation in the ipsilesional M1 has been reported to be an indicator for better motor recovery (4, 17); however, the enhanced excitatory effective connectivity from ipsilesional to contralesional M1 was found to be an indicator for better motor function in the present study. Thus, further clarification of effects of modulating the M1 excitability with NIBS techniques on M1 activation and M1-M1 effective connectivity may help design an appropriate protocol for facilitating motor recovery.

It has been observed a reduced FA of M1-M1 transcallosal fibers in patients with subcortical stroke which has been considered to reflect the pathological process of Wallerian degeneration that is secondary to the direct damage of the CST by stroke lesions (7–9). Furthermore, the FA values of the compromised M1-M1 anatomical connection have found to be negatively correlated with the resting-state M1-M1 functional connectivity in stroke patients, indicating that the increased M1-M1 functional connectivity could compensate for the impaired anatomical connection to some extent (9). In this study, however, we found a positive correlation between the excitatory effective connectivity from ipsilesional to contralesional M1 and the FA of the M1-M1 anatomical connection, suggesting that the severe impairment of the M1-M1 anatomical connection may reduce the potential of the effective connectivity to be reorganized to compensate for motor deficit. Although both enhanced functional (9) and effective connectivity (this study) between the bilateral M1 are associated with motor recovery, they may have different functional meanings in terms of interhemispheric anatomical connection impairment. Our finding also indicates that the assessment of the white matter integrity of M1-M1 transcallosal fibers may be useful in screening patients with less impairment that are more likely to enhance the excitatory effective connectivity from ipsilesional to contralesional M1.

Several limitations in the present study should be noted. Considering differential effects of degree of recovery, post-stroke interval and lesion location on effective connectivity changes of the motor system (17–19), the inclusion of a group of homogeneous well-recovered subcortical stroke patients in the chronic stage in this study may help to identify reliable effective connectivity changes in these specific population of patients. However, our findings cannot be generalized to all

stroke patients. Future studies should investigate the longitudinal effective connectivity changes in a large group of stroke patients with different lesion locations and motor deficits to discern the diversities of the connectivity changes. Although we investigated the influences of M1 activation and M1-related anatomical connection integrity on the increased excitatory effective connectivity from ipsilesional to contralesional M1, we did not explore the relationship between the excitability of the bilateral M1 and the effective connectivity, which may provide information on how to increase the effective connectivity by modulating the M1 excitability via NIBS strategies. Moreover, we included patients with lesions in either the right or the left hemisphere and images of the patients with left-side lesions were flipped in the analyses to increase the statistical power and to facilitate the comparison between patients and controls. However, this procedure might introduce bias to our results due to unmatched hand in the movement task between groups. Finally, this study only focused on the M1-M1 effective connectivity changes to answer the questions of our interest. However, stroke patients may also have effective connectivity changes within the motor system in the same hemisphere or between motor and non-motor systems, and thus systematic investigation of all possible effective connectivity changes after stroke may provide complete understanding of functional reorganization of the brain in stroke patients.

CONCLUSION

In this study, we found a complete inversion of the effective connectivity from ipsilesional to contralesional M1 from inhibitory influence in normal controls to excitatory in stroke patients. The positive correlation between excitatory connectivity and motor function suggests that this excitatory connectivity may facilitate motor recovery. The dependency of the enhancement in this effective connectivity on the integrity of M1-M1 anatomical connection indicates that integrity assessment of M1-M1 connection may help to screen patients with greater potential to motor recovery through enhancing this excitatory effective connectivity. Future studies should clarify the influence of modulating M1 excitability on the effective connectivity from ipsilesional to contralesional M1, which might have clinical significance for facilitating motor recovery in chronic stroke patients.

DATA AVAILABILITY

The datasets analyzed in this manuscript are not publicly available. Requests to access the datasets should be directed to chunshuiyu@tmu.edu.cn.

ETHICS STATEMENT

This study was approved by the Ethics Committee of Tianjin Medical University General Hospital and informed consent was obtained from each participant before the study. All participants in this study provided written informed consent.

AUTHOR CONTRIBUTIONS

YP and MH analyzed the fMRI data and the relationships between the DTI data and fMRI data. YP, ML, and CY wrote the paper. JL analyzed the DTI data. ML and CY designed the study. All authors approved the final version of the paper to be published.

REFERENCES

- Baldassarre A, Ramsey LE, Siegel JS, Shulman GL, Corbetta M. Brain connectivity and neurological disorders after stroke. *Curr Opin Neurol.* (2016) 29:706–13. doi: 10.1097/WCO.00000000000000396
- Grefkes C, Fink GR. Connectivity-based approaches in stroke and recovery of function. *Lancet Neurol.* (2014) 13:206–16. doi: 10.1016/S1474-4422(13)70264-3
- Heiss WD, Kidwell CS. Imaging for prediction of functional outcome and assessment of recovery in ischemic stroke. *Stroke.* (2014) 45:1195–201. doi: 10.1161/STROKEAHA.113.003611
- Rehme AK, Eickhoff SB, Rottschy C, Fink GR, Grefkes C. Activation likelihood estimation meta-analysis of motor-related neural activity after stroke. *NeuroImage.* (2012) 59:2771–82. doi: 10.1016/j.neuroimage.2011.10.023
- Schaechter JD, Fricker ZP, Perdue KL, Helmer KG, Vangel MG, Greve DN, et al. Microstructural status of ipsilesional and contralesional corticospinal tract correlates with motor skill in chronic stroke patients. *Hum Brain Mapp.* (2010) 30:3461–74. doi: 10.1002/hbm.20770
- Yu C, Zhu C, Zhang Y, Chen H, Qin W, Wang M, et al. A longitudinal diffusion tensor imaging study on wallerian degeneration of corticospinal tract after motor pathway stroke. *NeuroImage.* (2009) 47:451–8. doi: 10.1016/j.neuroimage.2009.04.066
- Radlinska BA, Blunk Y, Leppert IR, Minuk J, Pike GB, Thiel A. Changes in callosal motor fiber integrity after subcortical stroke of the pyramidal tract. *J Cereb Blood Flow Metab.* (2012) 32:1515–24. doi: 10.1038/jcbfm.2012.37
- Wang LE, Tittgemeyer M, Imperati D, Diekhoff S, Ameli M, Fink GR, et al. Degeneration of corpus callosum and recovery of motor function after stroke: a multimodal magnetic resonance imaging study. *Hum Brain Mapp.* (2012) 33:2941–56. doi: 10.1002/hbm.21417
- Liu J, Qin W, Zhang J, Zhang X, Yu C. Enhanced interhemispheric functional connectivity compensates for anatomical connection damages in subcortical stroke. *Stroke.* (2015) 46:1045–51. doi: 10.1161/STROKEAHA.114.007044
- Golestani AM, Tymchuk S, Demchuk A, Goodyear BG. Longitudinal evaluation of resting-state fmri after acute stroke with hemiparesis. *Neurorehabil Neural Repair.* (2013) 27:153–63. doi: 10.1177/1545968312457827
- Wang L, Yu C, Chen H, Qin W, He Y, Fan F, et al. Dynamic functional reorganization of the motor execution network after stroke. *Brain A J Neurol.* (2010) 133:1224–38. doi: 10.1093/brain/awq043
- Murase N, Duque J, Mazzocchio R, Cohen LG. Influence of interhemispheric interactions on motor function in chronic stroke[†]. *Ann Neurol.* (2004) 55:400. doi: 10.1002/ana.10848
- Lindenberg R, Renga V, Zhu LL, Nair D, Schlaug G. Bihemispheric brain stimulation facilitates motor recovery in chronic stroke patients (podcast) (e-pub ahead of print) (loe classification). *Neurology.* (2010) 75:2176. doi: 10.1212/WNL.0b013e318202013a
- Schlaug G, Renga V, Nair D. Transcranial direct current stimulation in stroke recovery. *Expert Rev Med Devices.* (2008) 5:759–68. doi: 10.1586/17434440.5.6.759
- Klomjai W, Lackmy-Vallée E, Roche N, Pradat-Diehl P, Marchand-Pauvert V, Katz R. Repetitive transcranial magnetic stimulation and transcranial direct current stimulation in motor rehabilitation after stroke: an update. *Ann Phys Rehabil Med.* (2015) 58:220–4. doi: 10.1016/j.rehab.2015.05.006
- Nathalie K. Non-invasive brain stimulation to enhance post-stroke recovery. *Front Neural Circuits.* (2016) 10:56. doi: 10.3389/fncir.2016.00056

FUNDING

This study was supported by the National Key R&D Program of China (2017YFC0909201), Natural Science Foundation of China (81425013, 81571659, 81601467, and 81601472), and Natural Science Foundation of Tianjin (17ZXMFSY00090, 15JCYBJC55100, and 16JCZDJC36000).

- Grefkes C, Nowak DA, Eickhoff SB, Dafotakis M, Kust J, Karbe H, et al. Cortical connectivity after subcortical stroke assessed with functional magnetic resonance imaging. *Ann Neurol.* (2008) 63:236–46. doi: 10.1002/ana.21228
- Rehme AK, Eickhoff SB, Wang LE, Fink GR, Grefkes C. Dynamic causal modeling of cortical activity from the acute to the chronic stage after stroke. *NeuroImage.* (2011) 55:1147–58. doi: 10.1016/j.neuroimage.2011.01.014
- Volz LJ, Sarfeld AS, Diekhoff S, Rehme AK, Pool EM, Eickhoff SB, et al. Motor cortex excitability and connectivity in chronic stroke: A multimodal model of functional reorganization. *Brain Struct Funct.* (2015) 220:1093–107. doi: 10.1007/s00429-013-0702-8
- Zhang J, Meng L, Qin W, Liu N, Shi FD, Yu C. Structural damage and functional reorganization in ipsilesional m1 in well-recovered patients with subcortical stroke. *Stroke.* (2014) 45:788–93. doi: 10.1161/STROKEAHA.113.003425
- Yang N, Waddington G, Adams R, Han J. Translation, cultural adaption, and test-retest reliability of chinese versions of the edinburgh handedness inventory and waterloo footedness questionnaire. *Laterality.* (2018) 23:255–73. doi: 10.1080/1357650X.2017.1357728
- Fazekas F, Chawluk JB, Alavi A, Hurtig HI, Zimmerman RA. Mr signal abnormalities at 1.5 t in alzheimer's dementia and normal aging. *Am J Roentgenol.* (1987) 149:351–6. doi: 10.2214/ajr.149.2.351
- Zang ZX, Yan CG, Dong ZY, Huang J, Zang YF. Granger causality analysis implementation on matlab: A graphic user interface toolkit for fmri data processing. *J Neurosci Methods.* (2012) 203:418–26. doi: 10.1016/j.jneumeth.2011.10.006
- Palaniyappan L, Simmonite M, White TP, Liddle EB, Liddle PF. Neural primacy of the salience processing system in schizophrenia. *Neuron.* (2013) 79:814–28. doi: 10.1016/j.neuron.2013.06.027
- Hamilton JP, Chen G, Thomason ME, Schwartz ME, Gotlib IH. Investigating neural primacy in major depressive disorder: Multivariate granger causality analysis of resting-state fmri time-series data. *Mol Psychiatry.* (2011) 16:763–72. doi: 10.1038/mp.2010.46
- van Meer MP, Van dMK, Wang K, Otte WM, El BS, Roeling TA, et al. Recovery of sensorimotor function after experimental stroke correlates with restoration of resting-state interhemispheric functional connectivity. *J Neurosci Off J Soc Neurosci.* (2010) 30:3964. doi: 10.1523/JNEUROSCI.5709-09.2010
- Koch PJ, Hummel FC. Toward precision medicine: tailoring interventional strategies based on noninvasive brain stimulation for motor recovery after stroke. *Curr Opin Neurol.* (2017) 30:462. doi: 10.1097/WCO.0000000000000462
- Cárdenas-Morales L, Volz LJ, Michely J, Rehme AK, Pool EM, Nettekoven C, et al. Network connectivity and individual responses to brain stimulation in the human motor system. *Cereb Cortex.* (2014) 24:1697–707. doi: 10.1093/cercor/bht023

Conflict of Interest Statement: The authors declare that the research was conducted in the absence of any commercial or financial relationships that could be construed as a potential conflict of interest.

Copyright © 2019 Peng, Liu, Hua, Liang and Yu. This is an open-access article distributed under the terms of the Creative Commons Attribution License (CC BY). The use, distribution or reproduction in other forums is permitted, provided the original author(s) and the copyright owner(s) are credited and that the original publication in this journal is cited, in accordance with accepted academic practice. No use, distribution or reproduction is permitted which does not comply with these terms.



Cerebral Amyloid Angiopathy Related Inflammation With Prominent Meningeal Involvement. A Report of 2 Cases

Agnès Aghetti^{1,2}, Damien Sène^{3,4}, Marc Polivka⁵, Natalia Shor⁶, Sarah Lechtman^{3,4}, Hugues Chabriat^{1,2,4}, Eric Jouvent^{1,2,4} and Stéphanie Guey^{1,2,4*}

¹ APHP, Lariboisière Hospital, Department of Neurology and DHU NeuroVasc Sorbonne Paris Cité, Paris, France, ² INSERM UMR-S 1141, Paris, France, ³ Department of Internal Medicine, Lariboisière Hospital, AP-HP, Paris, France, ⁴ Univ Paris Diderot, Sorbonne Paris Cité, Paris, France, ⁵ Department of Pathology, Lariboisière Hospital, AP-HP, Paris, France, ⁶ Department of Radiology, La Pitié-Salpêtrière Hospital, AP-HP, Paris, France

OPEN ACCESS

Edited by:

Hugh Markus,
University of Cambridge,
United Kingdom

Reviewed by:

Laurent Puy,
Centre Hospitalier Régional et
Universitaire de Lille, France
John W. Cole,
University of Maryland,
Baltimore, United States

*Correspondence:

Stéphanie Guey
stephanie.guey@aphp.fr

Specialty section:

This article was submitted to
Stroke,
a section of the journal
Frontiers in Neurology

Received: 17 April 2019

Accepted: 28 August 2019

Published: 23 September 2019

Citation:

Aghetti A, Sène D, Polivka M, Shor N,
Lechtman S, Chabriat H, Jouvent E
and Guey S (2019) Cerebral Amyloid
Angiopathy Related Inflammation With
Prominent Meningeal Involvement. A
Report of 2 Cases.
Front. Neurol. 10:984.
doi: 10.3389/fneur.2019.00984

Cerebral amyloid angiopathy related inflammation (CAA-RI) is a rare form of CAA characterized by subacute encephalitic symptoms (cognitive decline, seizures, focal deficits) associated with extensive and confluent white matter lesions co-localizing with lobar microbleeds on brain MRI. We report two cases of unusual CAA-RI mimicking meningoencephalitis but without typical brain lesions on FLAIR and T2* sequences. These 2 cases may extend the clinical spectrum of CAA-RI by suggesting the possible occurrence of quite purely meningeal forms of CAA-RI.

Keywords: cerebral amyloid angiopathy (CAA), cerebral amyloid angiopathy-related inflammation (CAA-RI), xanthochromia, subarachnoid hemorrhage, meningeal inflammation

BACKGROUND

Cerebral amyloid angiopathy related inflammation (CAA-RI) is a very rare disorder resulting from vascular and/or perivascular inflammation in the close vicinity of A β deposits. The clinical presentation of CAA-RI is characterized by acute to subacute encephalitic symptoms (confusion, rapidly cognitive decline, focal neurological deficits, seizures, and/or headaches) (1). The MRI pattern is stereotyped with extensive, confluent, more or less symmetric white matter lesions that most often co-localize with cortical microbleeds. A leptomeningeal or parenchymal contrast enhancement may occasionally occur (2, 3).

We report two cases of CAA-RI with prominent meningeal involvement and no parenchymal lesion on brain MRI, whose diagnosis was long delayed.

CASES DESCRIPTION

Patient 1 was a 60-year old man, without any past medical history, admitted in the emergency room of a nearby hospital in September 2012 for progressively increasing headaches, fever and confusion. The CT scan revealed no parenchymal abnormality. The cerebrospinal fluid examination showed 400 white blood cells/mm³ (95% lymphocytes), with high protein amount (2.4 g/L), normoglycorachia, and xanthochromia.

Patient 2 was a 77-yo women with a past medical history of Grave's disease and pulmonary tuberculosis who was admitted in the emergency room in our hospital in January 2018 with a strikingly similar clinical presentation. CT scans showed no parenchymal abnormality. A lumbar puncture revealed 84 white blood cells (90% lymphocytes) with hyperproteinorachia (3.5 g/L), normoglycorachia, and xanthochromia.

Infectious meningoencephalitis was considered in both cases, and probabilistic antibiotic (Penicillin in patient 1, Penicillin, and Cephalosporin in patient 2) and antiviral (Acyclovir for both patients) treatments were started. Despite full dose treatment, cognitive alterations worsened in both patients, with the occurrence of major psychomotor slowing in patient 1 and of aphasia in patient 2.

Brain MRI was performed, respectively, at day 15 and day 12 after the first symptoms. None of the two patients had large white matter lesions on the FLAIR sequence. Conversely, high intensity signals were observed along cortical sulci in both cases. On T2* sequences, no microbleeds were detected in patient 1, 5 microbleeds were observed in patient 2. By contrast, multiple cortical and subcortical punctuate lesions on diffusion weighted imaging (DWI) sequences were present in both patients (**Figure 1**). There was no parenchymal or meningeal gadolinium enhancement. Angio-MRI was normal in both patients. Conventional angiography (in patient 1) and angio-CTscan (patient 2) did not show any large and medium-sized arteries alterations.

Endocarditis and other sources of cardiac emboli were ruled out with transthoracic and transesophageal echocardiography and blood cultures in both patients. Infections screening was negative both in the blood and in the cerebrospinal

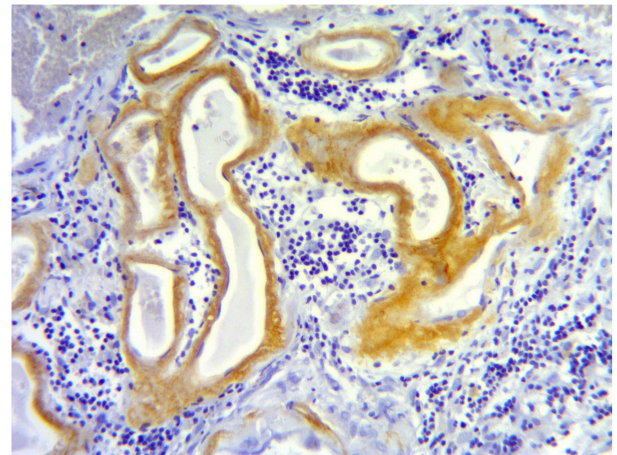


FIGURE 2 | Meningeal biopsy in patient 1. Meningeal tissue section showing Aβ amyloid deposits in the wall of small meningeal arteries (brown staining) and a lymphocytic perivascular infiltrate (dark blue cells).

fluid. Autoimmune and neoplastic etiologies were ruled out by a complete work up, including antinuclear, anti-neutrophil cytoplasmic, anti-cardiolipid, and onconeural antibodies. Thoracoabdominopelvic CTscan was normal in both patients. In addition, Positron Emission Tomography scan with fluorodeoxyglucose, gastric endoscopy, skin and ophthalmologic exams were normal in patient 2. Repeated lumbar punctures showed the persistence of xanthochromia with aseptic pleiocytosis in both cases. The association of diffuse subarachnoid hemorrhage and multiple cortical and subcortical

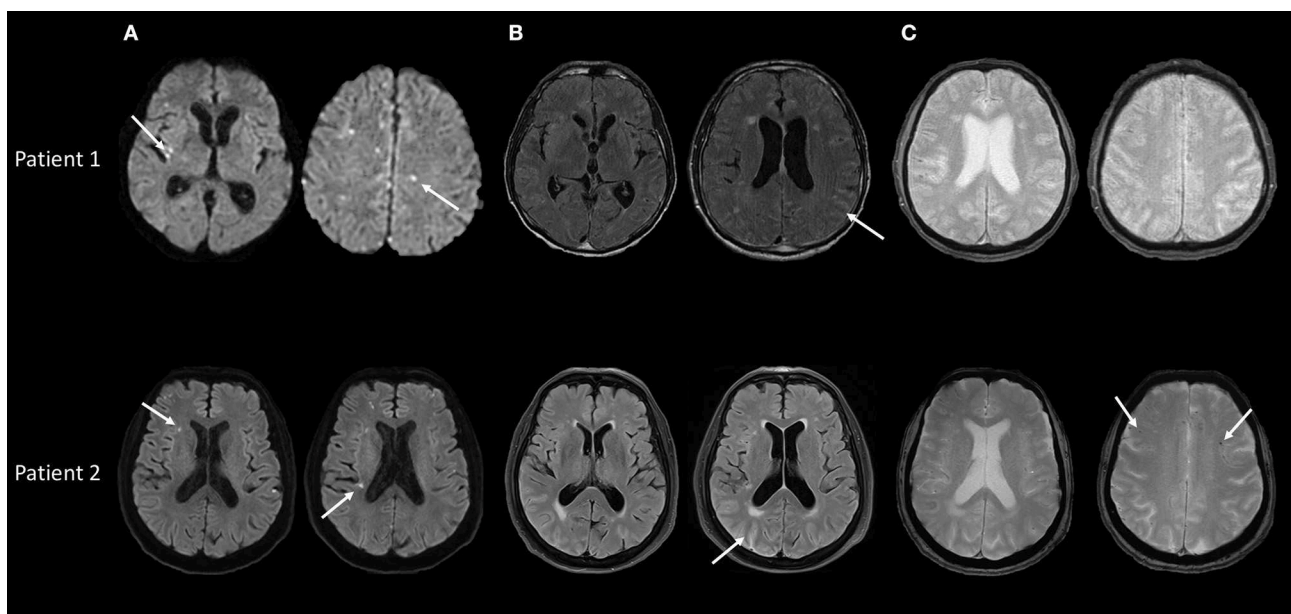


FIGURE 1 | Baseline brain MRI in patients 1 and 2, performed during the first month of the disease. **(A)** Diffusion weighted sequences showing multiple deep and cortical acute microinfarcts in both patients (arrows). **(B)** FLAIR sequences showing no or minimal brain parenchymal lesions but high intensity signal in cortical sulci in patients 1 and 2 (arrows). **(C)** T2* sequences showing doubtful sulcal hypointensities in patient 1 and 5 microbleeds in patient 2 (arrows).



FIGURE 3 | Follow-up brain MRI in the 2 patients. T2* sequences at 1 year after the onset, in patient 1 and patient 2 showing increasing load of superficial microbleeds and hemosiderosis.

microinfarcts finally led to suspect vasculitis involving the small cerebral and meningeal vessels as the potential underlying cause. A brain biopsy was performed in the two patients.

Pathological examination showed vascular amyloid deposits in leptomeningeal and cortical vessels in both patients. In patient 1, a meningeal perivascular lymphocytic and macrophagic inflammation was observed in the close vicinity of amyloid deposits, leading to the diagnosis of CAA-RI (**Figure 2**). Cortical vessels were spared by inflammation. Significant intramural or perivascular inflammation lacked in patient 2, but the tissue was sampled from an area relatively spared by lesions as seen on MRI. Considering the negativity of the complete work-up, the diagnosis of CAA-RI was considered probable for patient 2.

Immunosuppressive treatment was started in both patients, with high-dose parenteral corticosteroids (Methylprednisolone cumulative dose of 3,000 and 1,500 mg for patient 1 and 2, respectively) followed by oral corticoids (1 mg/kg of Prednisone), associated with Cyclophosphamide (one infusion per month for 6 consecutive months). No new DWI lesion was noted on control MRI obtained, respectively, at 1 year after the end of treatment for patient 1 and at 1 month in patient 2. In contrast, on T2* sequences, a large number of microbleeds and several foci of cortical siderosis appeared in both cases as previously reported in cerebral amyloid angiopathy (**Figure 3**). Cerebrospinal fluid examination progressively normalized in both patients. After 2 months, cerebrospinal fluid was acellular and proteinorachia was at 0.5 g/L in patient 1 and 0.3 g/L in patient 2. Patient 1 remained demented with frontal symptoms, apraxia, and disorientation in time and space, whereas patient 2 significantly improved and recovered a full autonomy in daily life. Cognitive assessment obtained at 9 months in patient 2 showed a complete normalization of language but some persisting alterations of executive performances. In addition, Alzheimer's biomarkers

were assessed in the cerebrospinal fluid in patient 2 and showed increased tau protein and reduced beta amyloid 1-42.

DISCUSSION

In the present two cases, the combination of progressive headache associated with fever and confusion, in the total absence of visible parenchymal abnormality on CTscan, but with pleiocytosis in the cerebrospinal fluid led to suspect initially an infectious meningoencephalitis. The clinical worsening under large probabilistic antiviral and antibacterial drugs and negativity of a large work-up led to reconsider the diagnosis in both cases.

Two major features finally contributed to suspect the involvement of small-sized vessels: the presence of multiple microinfarcts on DWI MRI, and the persistence of subarachnoid bleeding over repeated lumbar punctures, while visible vessels were normal on conventional angiography and angioCT, respectively. In both cases, xanthochromia which was present since the first lumbar puncture was overlooked while potentially helpful for diagnosis.

Analysis of brain tissue that showed vascular A β amyloid deposits and peri-vascular inflammation surrounding small meningeal arteries finally led to the diagnosis of CAA-RI in patient 1. In patient 2, although inflammation could not be demonstrated, the exclusion of other etiologies, the detection of CAA on brain biopsy, the favorable outcome under immunosuppressive therapy and mostly, the evolution toward typical imaging features of CAA strongly support the diagnosis of CAA-RI. The patchy and segmental distribution of inflammation may also actually cause false negative results on brain biopsy, as previously reported (3, 4).

These two cases show a presentation strikingly different from the usual MRI pattern of CAA-RI including extensive

and confluent white matter lesions co-localizing with lobar microbleeds (2, 3). In our 2 cases, hemorrhagic alterations mostly involved meningeal vessels, translating into diffuse subarachnoid hemorrhage, while brain parenchyma was only the site of multiple punctuate foci of ischemia. The predominance of inflammation on meningeal arteries may explain this unusual presentation.

Diagnostic criteria have been recently proposed for CAA-RI to avoid brain biopsy in the most typical cases and allow quickly starting immunosuppressive treatments (2, 3). Our two cases do not satisfy these criteria and suggest that the clinical spectrum of CAA-RI is more variable than previously expected. Therefore, brain biopsy should be performed in such atypical cases.

Immunosuppressive drugs are currently used in CAA-RI such as corticosteroids and cyclophosphamide. Such a therapeutic strategy was followed in our two cases. The use of aggressive immunosuppressive treatment allowed to resolve the acute inflammatory stage of the disease but as expected did not alter the chronic course of CAA. In both patients, cortical microbleeds and siderosis, usual markers of CAA, subsequently accumulated during the follow-up

(Figure 3). Paucity of such classical MRI markers at baseline in the two present cases might suggest that these pure meningeal forms of CAA-RI are more likely to occur at early stage of CAA. This point needs to be confirmed by additional reports.

ETHICS STATEMENT

Both patients provided written informed consent for the publication of their clinical data for research via our local written standard protocol.

AUTHOR CONTRIBUTIONS

AA and SG: study design, data collection and interpretation, writing the manuscript. EJ and HC: study design, interpretation of data, revision of the manuscript. MP: pathological data analysis, revision of the manuscript. DS, NS, and SL: data collection and interpretation, revision of the manuscript. AA, SG, DS, MP, NS, SL, HC, and EJ approved the final version of the manuscript.

REFERENCES

- Eng JA, Frosch MP, Choi K, Rebeck GW, Greenberg SM. Clinical manifestations of cerebral amyloid angiopathy-related inflammation. *Ann Neurol*. (2004) 55:250–6. doi: 10.1002/ana.10810
- Chung KK, Anderson NE, Hutchinson D, Synek B, Barber PA. Cerebral amyloid angiopathy related inflammation: three case reports and a review. *J Neurol Neurosurg Psychiatry*. (2011) 82:20–6. doi: 10.1136/jnnp.2009.204180
- Auriel E, Charidimou A, Gurol ME, Ni J, Van Etten ES, Martinez-Ramirez S, et al. Validation of clinico-radiological criteria for the diagnosis of cerebral amyloid angiopathy-related inflammation. *JAMA Neurol*. (2016) 73:197–202. doi: 10.1001/jamaneurol.2015.4078
- Marotti JD, Savitz SI, Kim WK, Williams K, Caplan LR, Joseph JT. Cerebral amyloid angiitis progressing to generalized angiitis

and leucoencephalitis. *Neuropathol Appl Neurobiol*. (2007) 33:475–9. doi: 10.1111/j.1365-2990.2007.00843.x

Conflict of Interest: The authors declare that the research was conducted in the absence of any commercial or financial relationships that could be construed as a potential conflict of interest.

Copyright © 2019 Aghetti, Sène, Polivka, Shor, Lechtman, Chabriet, Jouvent and Guey. This is an open-access article distributed under the terms of the Creative Commons Attribution License (CC BY). The use, distribution or reproduction in other forums is permitted, provided the original author(s) and the copyright owner(s) are credited and that the original publication in this journal is cited, in accordance with accepted academic practice. No use, distribution or reproduction is permitted which does not comply with these terms.



Effects of Dabigatran in Mouse Models of Aging and Cerebral Amyloid Angiopathy

Neethu Michael¹, Mher Mahoney Grigoryan¹, Kelley Kilday², Rachita K. Sumbria^{1,3}, Vitaly Vasilevko², Joanne van Ryn⁴, David H. Cribbs², Annlia Paganini-Hill¹ and Mark J. Fisher^{1,5,6*}

OPEN ACCESS

Edited by:

Andreas Charidimou,
Massachusetts General Hospital and
Harvard Medical School,
United States

Reviewed by:

Susanne J. Van Veluw,
Massachusetts General Hospital and
Harvard Medical School,
United States
Arne Lauer,
University Hospital Frankfurt, Germany
Jan Purucker,
Heidelberg University
Hospital, Germany
Gregoire Boulouis,
Université Paris Descartes, France

*Correspondence:

Mark J. Fisher
mfisher@uci.edu

Specialty section:

This article was submitted to
Stroke,
a section of the journal
Frontiers in Neurology

Received: 03 March 2019

Accepted: 23 August 2019

Published: 27 September 2019

Citation:

Michael N, Grigoryan MM, Kilday K, Sumbria RK, Vasilevko V, van Ryn J, Cribbs DH, Paganini-Hill A and Fisher MJ (2019) Effects of Dabigatran in Mouse Models of Aging and Cerebral Amyloid Angiopathy. *Front. Neurol.* 10:966. doi: 10.3389/fneur.2019.00966

¹ Department of Neurology, University of California, Irvine, Irvine, CA, United States, ² Institute for Memory Impairments and Neurological Disorders, University of California, Irvine, Irvine, CA, United States, ³ Department of Biopharmaceutical Sciences, School of Pharmacy and Health Sciences, Keck Graduate Institute, Claremont, CA, United States, ⁴ Department of Cardiometabolic Research, Boehringer Ingelheim, Hanover, Germany, ⁵ Department of Pathology and Laboratory Medicine, University of California, Irvine, Irvine, CA, United States, ⁶ Department of Anatomy and Neurobiology, University of California, Irvine, Irvine, CA, United States

Oral anticoagulants are a critical component of stroke prevention, but carry a risk of brain hemorrhage. These hemorrhagic complications tend to occur in elderly individuals, especially those with predisposing conditions such as cerebral amyloid angiopathy (CAA). Clinical evidence suggests that non-vitamin K antagonist oral anticoagulants are safer than traditional oral anticoagulants. We analyzed whether the anticoagulant dabigatran produces cerebral microhemorrhage (the pathological substrate of MRI-demonstrable cerebral microbleeds) or intracerebral hemorrhage in aged mice with and without hemorrhage-predisposing angiopathy. We studied aged (22 months old) Tg2576 (a model of CAA) and wild-type (WT) littermate mice. Mice received either dabigatran etexilate (DE) (Tg $N = 7$; WT $N = 10$) or vehicle (Tg $N = 9$; WT $N = 7$) by gavage for 4 weeks. Anticoagulation effects of DE were confirmed using thrombin time assay. No mice experienced intracerebral hemorrhage. Cerebral microhemorrhage analysis, performed using Prussian-blue and H&E staining, showed no significant change in either number or size of cerebral microhemorrhage in DE-treated animals. Analysis of biochemical parameters for endothelial activation (ICAM-1), blood-brain barrier disruption (IgG, claudin-5, fibrinogen), microglial activation (Iba-1), or astrocyte activation (GFAP) showed neither exacerbation nor protective effects of DE in either Tg2576 or WT mice. Our study provides histological and biochemical evidence that aged mice, with or without predisposing factors for brain hemorrhage, tolerate anticoagulation with dabigatran. The absence of dabigatran-induced intracerebral hemorrhage or increased frequency of acute microhemorrhage may provide some reassurance for its use in high-risk patient populations.

Keywords: aging, cerebral amyloid angiopathy, cerebral microhemorrhage, dabigatran, direct thrombin inhibitor, intracerebral hemorrhage

INTRODUCTION

Dabigatran is a direct thrombin inhibitor and is indicated in patients with non-valvular atrial fibrillation for prevention of ischemic stroke (1–3). It is highly selective for thrombin, with rapid and reversible inhibition (4), and has no interaction with other enzymes involved in the coagulation cascade (5). Dabigatran inhibits tissue factor-induced thrombin generation and thrombin-induced platelet aggregation (4). Dabigatran has also shown an anti-inflammatory effect after its long-term treatment in a mouse model of Alzheimer's disease (6). It is not orally absorbed due to its polarity; dabigatran etexilate (DE), the prodrug of dabigatran, can be used orally (5, 7). This prodrug approach allows long-lasting anticoagulation (4) and has no food-drug interactions, and hence does not require routine monitoring (8).

Thrombin is a serine protease in the coagulation cascade which mediates conversion of fibrinogen to fibrin. Thrombin has been implicated in intracerebral hemorrhage (ICH) pathogenesis and mediates inflammation by activating protease-associated receptor-1 (PAR-1) (9, 10). Thrombin expression increases after ICH (11), and upregulation occurs early following ICH. The temporal pattern of thrombin expression is associated with brain edema formation (12). Via PAR signaling, thrombin also affects a wide variety of other disease entities (13), including cancer (14).

Aging and cerebral amyloid angiopathy (CAA) are two major risk factors of ICH (15–19), both of which result in brain microvessels susceptible to develop cerebral microhemorrhages (CMH). CAA is a small vessel disease characterized by deposition of β -amyloid in the cerebral vasculature (20). Spontaneous and anticoagulant-induced CMH are common in both these settings, and current research suggests a link between CMH and increased risk of ICH (21–23).

Thrombin has a pleiotropic role, and selective inhibition of thrombin may have beneficial effects in stroke prevention. Hence, we designed the current study to determine the effects of dabigatran on spontaneous CMH in aged Tg2576 transgenic mice, a model of Alzheimer's disease and CAA (24, 25), with progressive age-related accumulation of A β plaques (26–28). We hypothesized that given its anti-thrombin effect, dabigatran does not increase the number or size of spontaneous CMH. We used Tg2576 and wild-type (WT) littermate mice aged 22 months (comparable to humans aged 60–65 years) to mimic the scenario of elderly patients with predisposing conditions on anticoagulation therapy.

METHODS

Animals

All experimental procedures were approved by the University of California, Irvine, Institutional Animal Care and Use Committee. To study the effect of dabigatran on spontaneous CMH development, we used an amyloid precursor protein transgenic (Tg2576) mouse model that develops CAA and spontaneous CMH and their wild type (WT) littermates. All mice used were 22 months old at the start of the experiment.

Pretreatment With Oral Anticoagulant Dabigatran Etexilate

Dabigatran etexilate (BIBR1048MS, Boehringer Ingelheim, Ingelheim am Rhein, Germany) suspension was freshly prepared by dissolving in a vehicle solution of 0.5% hydroxyethyl cellulose solution in distilled water and using a magnetic stirrer. Four experimental groups were: (1) Tg2576 mice receiving DE (males = 3, females = 4), (2) Tg2576 mice receiving vehicle (males = 7, females = 3), (3) WT mice receiving DE (males = 5, females = 4), and (4) WT mice receiving vehicle (males = 2, females = 5). DE groups received DE doses of 45 mg/kg body weight twice daily on Monday through Friday and a single dose of 60 mg/kg via oral gavage on Saturday and Sunday, for 4 weeks. DE dosing was adapted from previously published work (29). Control mice received equal volume of vehicle solution. All the mice were weighed before starting the oral dosing and were monitored twice a week until the end of experiment.

Determination of Diluted Thrombin Time and Plasma Concentration of Dabigatran

Plasma diluted thrombin time (dTT) and concentration of dabigatran in the plasma were determined using Hemoclot Thrombin Inhibitors (Aniara-Hyphen Biomed, West Chester, OH) and a coagulometer (Thrombostat-2, Behnk Elektronik, Norderstedt, Germany). Blood samples were obtained from a subset of mice at different time points: at baseline ($N = 6$), 0.5 h ($N = 5$), and 1.5 h ($N = 6$) after DE oral dosing, and 1.5 h ($N = 4$) after vehicle oral dosing. After anesthetizing mice with 3% isoflurane, blood samples (70 μ l, 9 vol.) were collected via retro orbital sinus using plain capillary tubes (Fisher brand, Pittsburgh, PA), and were transferred to collection tubes with 3.2% sodium citrate (1 vol., prepared in distilled water). Blood was then centrifuged for 20 min at 2,000 rpm to separate plasma for later use. Plasma dTT analysis was performed following manufacturer's instructions and results were plotted on a calibration curve generated using the calibration plasma samples from the same manufacturer (Aniara-Hyphen Biomed, West Chester, OH). Corresponding dabigatran concentration for the tested plasma was interpolated directly on the calibration curve.

Brain Preparation

Four weeks after the start of DE oral dosing, the mice were anesthetized with a lethal dose of Euthasol (150 mg/kg, i.p.), cardiac perfusion was performed using ice cold phosphate buffered saline (PBS) for 5 min and brains were harvested immediately and processed for histochemical and biochemical analysis. Right brain hemisphere was drop-fixed in 4% paraformaldehyde (PFA) for 24 h and transferred to 15% sucrose solution prepared in PBS. When the brains sank, they were transferred to 30% sucrose solution with 0.01% sodium azide until sectioning. Left hemisphere was flash frozen using dry ice and stored at -80°C for biochemical analysis.

Detection of Cerebral Microhemorrhage

Fixed right brain hemisphere was observed for surface macrohemorrhages. The hemisphere was later sectioned into 40 μ m thick coronal sections using a freezing microtome

(Sliding microtome, ThermoScientific, Grand Island, NY) and the sections were collected in PBS with 0.01% sodium azide. Every 6th section was used for Prussian blue (PB) staining and ~30 sections were analyzed per brain. PB staining was performed as described earlier (25, 30). Stained sections were observed and each CMH was photographed (Olympus BX51 microscope, Infinity 2 Camera and INFINITY ANALYZE, 6.5.0, Lumera Corporation, ON, Canada). CMH were counted at a $\times 20$ magnification by a blinded observer as a collection of red blood cells (RBC) that appear red-orange using hematoxylin and eosin (H&E) stain (≥ 5 RBC) and as clear purple-blue deposits using PB, and total number and size of CMH were determined. A size cut off ($50 \mu\text{m}^2$) was used for considering the PB-stained CMHs. Total CMH positive area was calculated as the sum of the area of each CMH and expressed as a percentage of the total area of the brain analyzed. To determine the total area analyzed, PB-stained slides were scanned using Canon MP250 scanner (Canon, Tokyo, Japan) under 600 dots per inch (DPI), and the area of each individual section was summed using NIH ImageJ software. CMH count, CMH/section (total number of CMH/number of sections), total CMH area, percentage CMH area, and average CMH size were calculated by an observer blinded to genotype and treatment group. Every 7th section (~30 sections/brain) was used for H&E staining as described previously (30), and was performed by the research service core at UCI Medical Center's Department of Pathology & Laboratory Medicine. Stained sections were observed and analyzed as described above for PB staining.

Immunohistochemical Staining

Immunohistochemistry was performed for Iba-1 (microglial/macrophage marker), ICAM-1 (endothelial cell activation marker), IgG (blood-brain barrier (BBB) injury marker), and glial fibrillary acidic protein (GFAP, an astrocyte marker), using one $40 \mu\text{m}$ thick coronal section per mouse, 2–2.4 mm posterior to bregma. Sections were incubated in 0.5% hydrogen peroxide in 0.1 M PBS (pH 7.4) containing 0.3% Triton X-100 (PBST) for 30 min at room temperature to

block endogenous peroxidase activity. After washing with PBST, sections were incubated for 30 min with PBST containing 2% bovine serum albumin to block non-specific protein binding. Sections were then incubated overnight at 4°C with a rabbit antibody against Iba-1 (1:200 dilution; Wako Chemicals USA, Richmond, VA), rabbit monoclonal antibody against ICAM-1 (1:500 dilution Abcam, Cambridge, MA); rabbit anti-mouse IgG antibody (1:200 dilution; Jackson ImmunoResearch, West Grove, PA), or rabbit antibody against GFAP (1:2,000 dilution; Abcam, Cambridge, MA). After washing with PBST, sections were incubated at room temperature for 1 h with biotinylated anti-rabbit IgG (1:500 dilution; Jackson ImmunoResearch, West Grove, PA), followed by 1 h incubation at room temperature with ABC complex, according to manufacturer instructions (Vector Laboratories, Burlingame, CA). Sections were developed with 3,3'-diaminobenzidine (Vector Laboratories, Burlingame, CA). Sixteen images per brain section were acquired randomly at $\times 20$ magnification, and the total positive immunoreactive area (expressed as % of the total area analyzed) was quantified using NIH ImageJ software by an observer blinded to the experimental groups.

Western Blotting

Claudin-5 and fibrinogen were quantified using Western blot. Briefly, frozen left cerebral hemispheres were pulverized, the powder was homogenized in T-PER buffer (Thermo Fisher Scientific, Waltham, MA) with protease inhibitor cocktail (Roche Applied Science, Indianapolis, IN), and soluble fraction was collected after 100,000 g centrifugation for 1 h at 4°C . Protein concentrations for Western blot analysis were determined using the Bradford protein assay, and ~50 μg of protein was resolved on SDS-PAGE 4–12% gel (Invitrogen, Carlsbad, CA). Primary antibodies for claudin-5 (tight junction protein; Abcam, Cambridge, MA) and fibrinogen (a marker of BBB permeability; US Biological, Salem, MA) were used at 1:2,000 dilution, followed by HRP-conjugated donkey anti-rabbit secondary antibody (Jackson Immuno Research, West Grove, PA). NIH ImageJ software was used to quantify Western blot band intensities.

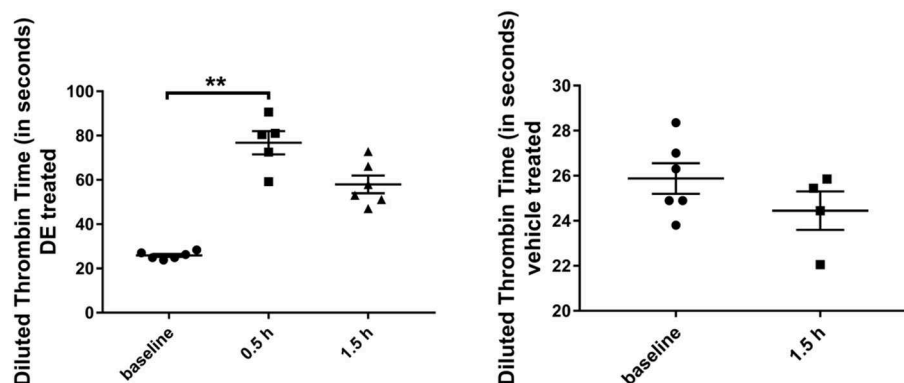


FIGURE 1 | Diluted thrombin time (in seconds) in Tg2576 mice and WT littermates. Increase in diluted thrombin time at 0.5 and 1.5 h time points, compared with the baseline value in DE-treated Tg2576 mice and WT littermates. Statistical tests: Kruskal-Wallis test followed by Dunn's multiple comparison tests. Individual data points are presented with mean and SEM error bars. **Indicates significant difference between means, $p < 0.01$.

Control protein glyceraldehyde 3-phosphate dehydrogenase (GAPDH, Santa Cruz Biotechnology, Dallas, TX) was used to adjust band intensity measurements.

Statistical Analysis

Data are presented as mean \pm SEM. Kruskal-Wallis test followed by Dunn's multiple comparison tests was used for comparison of means. Two-sided $p < 0.05$ was considered statistically significant. Statistical analyses were performed using GraphPad Prism 7.

RESULTS

Survival

We observed high survival rate after DE gavage administration; all mice survived except one mouse from WT DE group, which was euthanized because it demonstrated symptoms of distress. No animals developed ICH.

Diluted Thrombin Time and Plasma Concentration of Dabigatran

In a subset of DE-treated mice analyzed for dTT, an average of 344 ± 38 ng dabigatran/ml (dTT: 76.8 ± 5.2 sec) and an average of 207 ± 29 ng dabigatran/ml (dTT: 57.9 ± 3.9 sec) were detected after 0.5 h ($N = 5$) and 1.5 h ($N = 6$) respectively; this was significantly higher compared with the baseline ($N = 6$) dTT measurements (25.9 ± 0.7 sec, **Figure 1**). In a subset of vehicle-treated mice analyzed, an average dTT of 24.5 ± 0.9 sec was measured 1.5 h ($N = 4$) after the gavage.

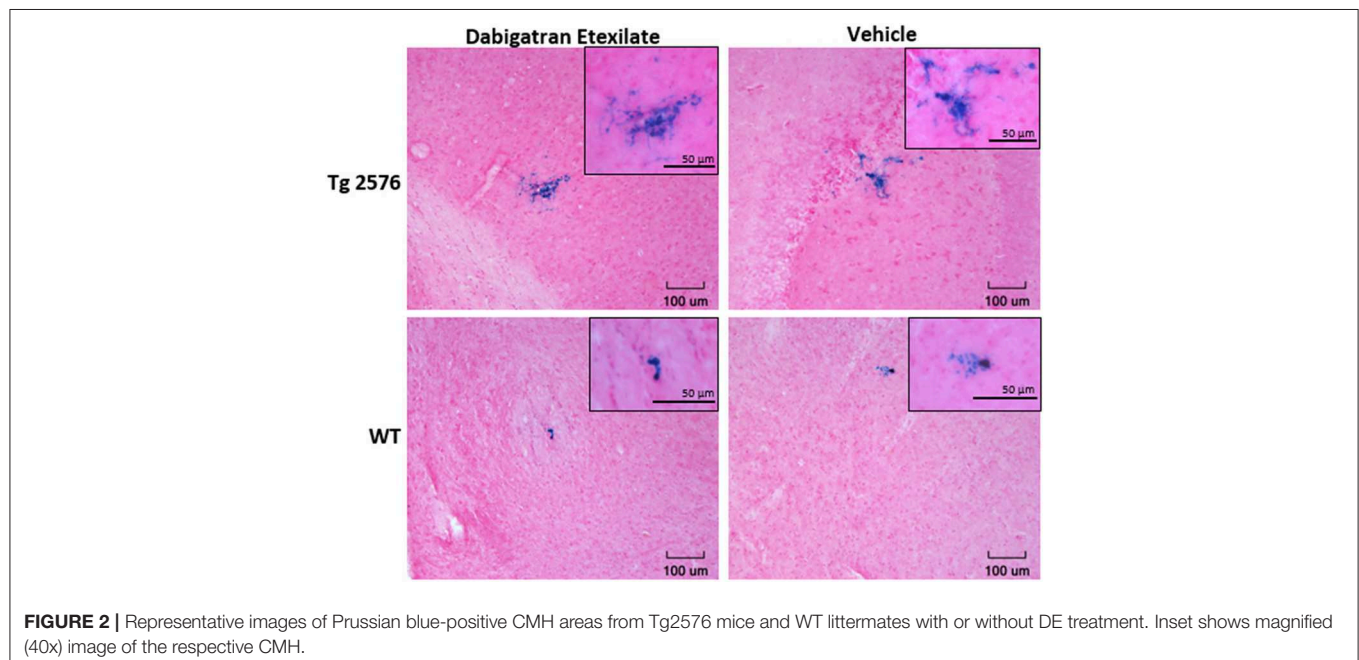
Sub-acute Parenchymal Cerebral Microhemorrhages

Representative examples of PB-positive CMH from vehicle/DE-treated WT/Tg mice are shown in **Figure 2**. As expected, mean

number of CMH (referred as mean CMH) is greater in Tg-vehicle vs. WT-vehicle mice vehicle (14.1 ± 5.5 vs. 4.7 ± 0.9 , $p = 0.3$, **Figure 3**). DE increased mean CMH by $<20\%$ in both Tg and WT mice (16.4 ± 4.0 vs. 14.1 ± 5.5 , $p > 0.99$ in Tg and 5.3 ± 2.2 vs. 4.7 ± 0.9 , $p > 0.99$ in WT). A total of 115 and 141 CMH were analyzed from Tg DE ($N = 7$) and Tg vehicle ($N = 10$) groups, respectively. In Tg mice, other analyzed parameters showed no significant difference in means between the DE-treated and vehicle groups (**Figure 3**): CMH/section (0.51 ± 0.12 vs. 0.48 ± 0.19 , $p > 0.99$), total CMH area ($17,835 \pm 6,351 \mu\text{m}^2$ vs. $11,292 \pm 4,839 \mu\text{m}^2$, $p > 0.99$), %CMH-positive area (0.0025 ± 0.0009 vs. 0.0017 ± 0.0006 , $p > 0.99$), and average CMH size ($962 \pm 193 \mu\text{m}^2$ vs. $668 \pm 119 \mu\text{m}^2$, $p > 0.99$). In WT DE ($N = 9$) and WT vehicle ($N = 7$) groups, 48 and 33 CMH were analyzed, respectively. Similar to Tg2576 mice, WT mice showed no significant difference between the DE and vehicle groups in any of the following analyzed parameters (**Figure 3**): CMH/section (0.16 ± 0.064 vs. 0.16 ± 0.027 , $p > 0.99$), total CMH area ($1,298 \pm 524 \mu\text{m}^2$ vs. $2,855 \pm 835 \mu\text{m}^2$, $p = 0.58$), %CMH-positive area (0.0002 ± 0.0001 vs. 0.0004 ± 0.0001 , $p = 0.62$), and average CMH size ($321 \pm 51 \mu\text{m}^2$ vs. $610 \pm 105 \mu\text{m}^2$, $p = 0.31$). CMH were present in cortical, sub-cortical and cerebellar regions, with cortex having more CMH than other areas across all treatment groups; the exception was WT DE group, in which there was no visible difference among the three regions (One way ANOVA on total CMH present in cortex, sub-cortex and cerebellum: Tg DE: $p = 0.002$; Tg vehicle: $p < 0.0001$; WT DE: $p > 0.8$; WT vehicle: $p = 0.009$).

Acute Parenchymal Cerebral Microhemorrhages

H&E-positive stained acute CMH were relatively few within various groups. None of the 9 WT DE mice and only one



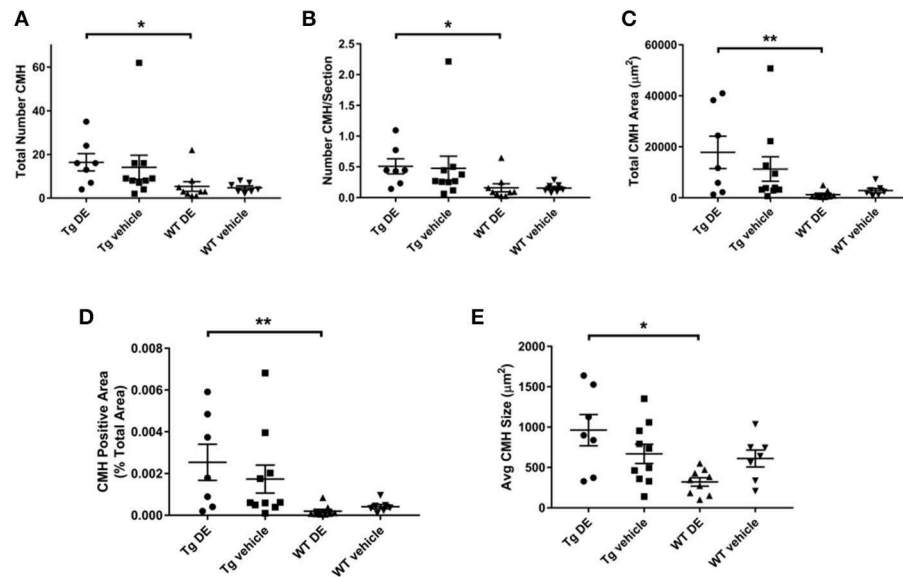


FIGURE 3 | Prussian blue-positive CMH in Tg2576 and WT mice with/without DE. Significant difference in all the CMH parameters [(A) Total number of CMH, (B) Number of CMH per section, (C) Total CMH area, (D) CMH positive area (%), and (E) Average CMH size] of DE-treated Tg2576 mice vs. WT littermates. Statistical tests: Kruskal-Wallis test followed by Dunn's multiple comparison tests. Individual data points are presented with mean and SEM error bars. *Indicates significant difference between means, $p < 0.05$. **Indicates significant difference between means, $p < 0.01$.

of the 7 WT vehicle mice displayed H&E-positive CMH. In Tg2576 mice, three of seven Tg DE mice and six of 10 Tg vehicle mice had H&E-positive CMH. The mean number of CMH did not differ statistically between the DE- and vehicle-treated Tg2576 mice (1.1 ± 0.8 vs. 2.2 ± 0.7 , $p > 0.9$) and DE- and vehicle-treated WT littermates (0 vs. 0.2 ± 0.2 , $p > 0.9$).

Endothelial Activation, Neuroinflammation, and Blood-Brain Barrier

Immunohistochemical analysis of brains revealed no significant difference in the immunoreactivity of brain endothelial activation marker ICAM-1 between the DE- and vehicle-treated Tg2576 mice ($0.5 \pm 0.2\%$ vs. $0.7 \pm 0.1\%$) nor in their WT littermates ($0.3 \pm 0.1\%$ vs. $0.4 \pm 0.1\%$). Similarly, there was no significant difference in the total GFAP- and Iba-1-reactive areas of DE- and vehicle-treated groups of Tg (GFAP: $3.1 \pm 0.5\%$ vs. $2.0 \pm 0.5\%$, Iba-1: $1.8 \pm 0.2\%$ vs. $2.1 \pm 0.2\%$) and WT mice (GFAP: $1.1 \pm 0.2\%$ vs. $1.4 \pm 0.2\%$, Iba-1: $0.8 \pm 0.1\%$ vs. $1.1 \pm 0.2\%$). Neuroinflammatory marker Iba-1 demonstrated a significant difference between the treated and vehicle groups of Tg2576 mice and their WT littermates; astrocyte marker GFAP was significantly different between the treated groups (Figure 4). BBB structure and function assessed by immunohistochemical analysis of IgG and Western blot analysis of fibrinogen and claudin-5 showed no significant difference between DE- and vehicle-treated groups of both Tg (IgG: $1.3 \pm 0.3\%$ vs. $2.3 \pm 0.3\%$, fibrinogen: 0.7 ± 0.2 vs. 0.8 ± 0.3 , claudin-5: 0.5 ± 0.1 vs. 0.7 ± 0.1) and WT mice (IgG: $1.2 \pm 0.2\%$ vs. $1.5 \pm 0.2\%$, fibrinogen: 0.6 ± 0.2 vs. 0.4 ± 0.1 , claudin-5: 0.5 ± 0.1 vs. 0.4 ± 0.1 , Figure 4).

DISCUSSION

The major finding of the current study is that dabigatran does not induce ICH, and neither induces nor enlarges spontaneous CMH in aged Tg2576 mice or their WT littermates. Tg2576 mice, a well-characterized model of Alzheimer's disease and CAA, progressively accumulate CMH with aging (25). In our Tg2576 mice after DE administration for 4 weeks, the mean number and size of CMH did not differ significantly between the treatment and control groups. WT mice also showed no significant effect of DE treatment on CMH formation. As expected, CMH development differed between the Tg2576 mice and WT littermates, as did the Iba-1 and GFAP immunohistochemical parameters. There was no significant difference in various markers for microglial, astrocyte and endothelial activation or BBB integrity between treated and control mice, indicating that inflammation was not induced and that BBB function remained unaltered after DE administration.

Our findings are consistent with prior published work. A cell culture-based study (31) reported a protective effect of dabigatran, inhibiting thrombin-mediated increased permeability of murine brain endothelial cells. We observed no significant increase in size of CMH in our animal models with DE treatment, suggesting a lack of increased vascular disruption with dabigatran. An MRI study (32) found that dabigatran does not promote the formation of cerebral microbleeds (the MRI signature of CMH) and does not induce ICH in APP23 mice (another mouse model of CAA) following 3–4 months of anticoagulation with DE. Our study is consistent with these findings and provides histological evidence for the MRI observations.

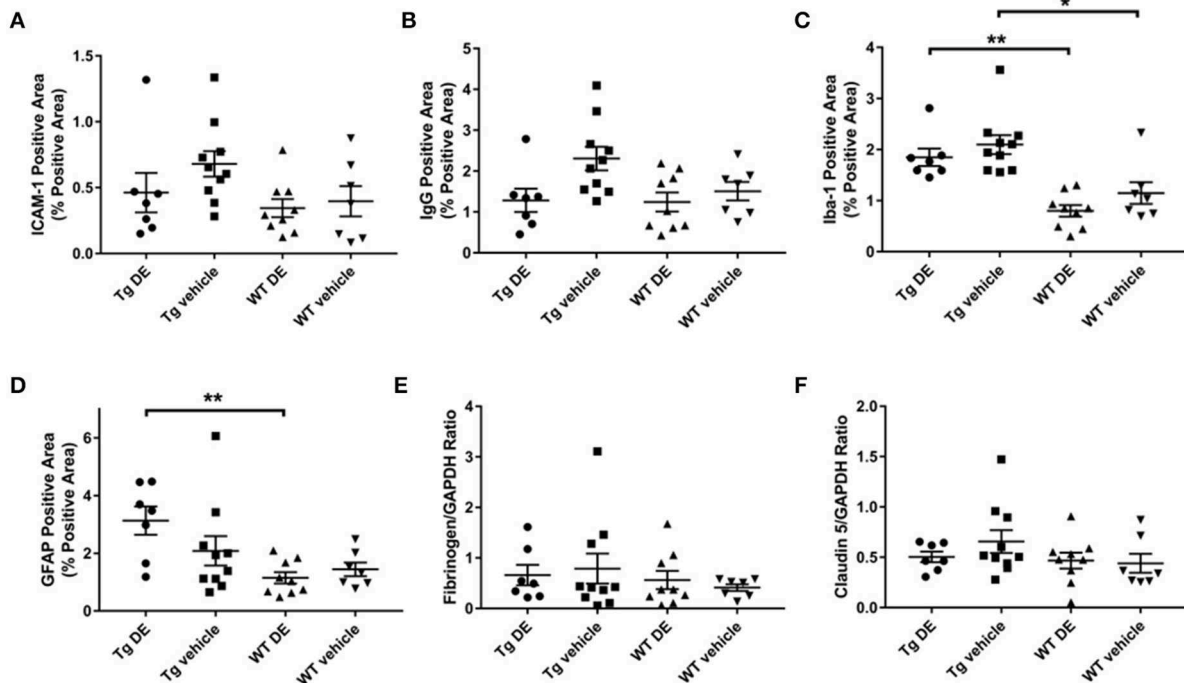


FIGURE 4 | Immunohistochemical (A–D) and Western blot analysis (E–F) of endothelial activation (A), blood-brain barrier structure and function (B,E,F), and neuroinflammation (C,D) in Tg2576 and WT mice with/without DE. Significant difference in Iba-1- (C) and GFAP-positive (D) area of DE-treated Tg2576 mice and WT littermates and in Iba-1-positive area of vehicle-treated Tg2576 mice and WT littermates. Statistical tests: Kruskal-Wallis test followed by Dunn's multiple comparison tests. Individual data points are presented with mean and SEM error bars. *Indicates significant difference between means, $p < 0.05$. **Indicates significant difference between means, $p < 0.01$.

Our study has several limitations. PB staining, used to elucidate CMH development, characterizes CMH accumulated over the lifetime of mice, rather than simply during the 1 month treatment period. As a consequence, PB-stained microhemorrhages do not necessarily indicate lesions that developed during the course of treatment with DE. Thus, H&E stained microhemorrhages may be more meaningful in the context of this study, and it is noteworthy that there was no indication of increased number of H&E-stained lesions associated with DE treatment among either Tg or WT mice. Second, our group sizes were relatively small, and the study was thus not powered to detect some inter-group differences of potential interest. Our study lacked a positive control, i.e., we did not include use of an agent that may be more likely to have hemorrhagic consequences. Note, however, that prior work using warfarin as a positive control has reported findings similar to our own (32). In Marinescu et al., warfarin and dabigatran were administered through drinking water and chow, respectively, which enabled a longer-term treatment compared with our study, in which dabigatran was administered for a shorter period of 1 month via oral gavage. Finally, we did not attempt to distinguish primary microhemorrhages (i.e., due to an initial disruption of microvessel integrity) from secondary hemorrhages (i.e., occurring as a consequence of ischemic injury) (33), a distinction relevant in patients subject to cardiogenic stroke and hemorrhagic transformation (3).

In conclusion, we found no evidence that anticoagulation with dabigatran induces either ICH or CMH in mouse models of aging and CAA. Findings from this study and prior work may provide some reassurance for use of dabigatran in high risk populations. Further *in vivo* studies are needed to determine whether dabigatran may offer a protective effect against brain hemorrhage.

DATA AVAILABILITY

The datasets generated for this study are available on request to the corresponding author.

ETHICS STATEMENT

All experimental procedures were approved by the University of California, Irvine, Institutional Animal Care and Use Committee.

AUTHOR CONTRIBUTIONS

NM was responsible for study concept and design, performing *in vivo* experiments and analytic assays, statistical analysis, data analysis, and interpretation and drafting the manuscript. MG was responsible for performing *in vivo* experiments. KK and VV were responsible for performing histological and biochemical studies. RS was responsible for data interpretation

and critical revision of manuscript. JR was responsible for critical revision of manuscript. DC was responsible for study concept and design, data interpretation, and critical revision of manuscript. AP-H was responsible for study concept and design, assistance with statistical analysis, data interpretation, and critical revision of manuscript. MF was responsible for study concept and design, data interpretation, study supervision and critical revision of manuscript. All authors have read and approved the final manuscript.

REFERENCES

- Hart RG, Pearce LA, Aguilar MI. Meta-analysis: antithrombotic therapy to prevent stroke in patients who have non-valvular atrial fibrillation. *Ann Intern Med.* (2007) 146:857–67. doi: 10.7326/0003-4819-146-12-200706190-00007
- Fisher M. MRI screening for chronic anticoagulation in atrial fibrillation. *Front Neurol.* (2013) 4:137. doi: 10.3389/fneur.2013.00137
- Paciaroni M, Bandini F, Agnelli G, Tsivgoulis G, Yaghi S, Furie KL, et al. Hemorrhagic transformation in patients with acute ischemic stroke and atrial fibrillation: time to initiation of oral anticoagulant therapy and outcomes. *J Am Heart Assoc.* (2018) 7:e010133. doi: 10.1161/JAHA.118.010133
- Wienen W, Stassen JM, Priepke H, Ries UJ, Haul N. *In-vitro* profile and *ex-vivo* anticoagulant activity of the direct thrombin inhibitor dabigatran and its orally active prodrug, dabigatran etexilate. *Thromb Haemost.* (2007) 98:155–62. doi: 10.1160/TH07-03-0183
- Haul NH, Nar H, Priepke H, Ries U, Stassen J-M, Wienen W. Structure-based design of novel potent non-peptide thrombin inhibitors. *J Med Chem.* (2002) 45:1757–66. doi: 10.1021/jm0109513
- Marangoni MN, Braun D, Situ A, Moyano AL, Kalinin S, Polak P, et al. Differential effects on glial activation by a direct versus an indirect thrombin inhibitor. *J Neuroimmunol.* (2016) 297:159–68. doi: 10.1016/j.jneuroim.2016.05.018
- Stangier J. Clinical pharmacokinetics and pharmacodynamics of the oral direct thrombin inhibitor dabigatran etexilate. *Clin Pharmacokinet.* (2008) 47:285–95. doi: 10.2165/00003088-200847050-00001
- Garnock-Jones KP. Dabigatran etexilate: a review of its use in the prevention of stroke and systemic embolism in patients with atrial fibrillation. *Am J Cardiovasc Drugs.* (2011) 11:57–72. doi: 10.2165/11206400-000000000-00000
- Moller T, Hanisch UK, Ransom BR. Thrombin-induced activation of cultured rodent microglia. *J Neurochem.* (2000) 75:1539–47. doi: 10.1046/j.1471-4159.2000.0751539.x
- Noorbakhsh F, Vergnolle N, Hollenberg MD, Power C. Proteinase-activated receptors in the nervous system. *Nat Rev Neurosci.* (2003) 4:981–90. doi: 10.1038/nrn1255
- Wu H, Zhao R, Qi J, Cong Y, Wang D, Liu T, et al. The expression and the role of protease nexin-1 on brain edema after intracerebral hemorrhage. *J Neurol Sci.* (2008) 270:172–83. doi: 10.1016/j.jns.2008.03.010
- Wu H, Zhang Z, Li Y, Zhao R, Li H, Song Y, et al. Time course of upregulation of inflammatory mediators in the hemorrhagic brain in rats: correlation with brain edema. *Neurochem Int.* (2010) 57:248–53. doi: 10.1016/j.neuint.2010.06.002
- Coughlin SR. Protease-activated receptors in hemostasis, thrombosis and vascular biology. *J Thromb Haemost.* (2005) 3:1800–14. doi: 10.1111/j.1538-7836.2005.01377.x
- Palumbo JS, Degen JL. Hemostatic factors in tumor biology. *J Pediatr Hematol Oncol.* (2000) 22:281–7. doi: 10.1097/00043426-200005000-00019
- Fisher M, French S, Ji P, Kim RC. Cerebral microbleeds in the elderly: a pathological analysis. *Stroke.* (2010) 41:2782–5. doi: 10.1161/STROKEAHA.110.593657
- Mehndiratta P, Manjila S, Ostergard T, Eisele S, Cohen ML, Sila C, et al. Cerebral amyloid angiopathy-associated intracerebral hemorrhage: pathology and management. *Neurosurg Focus.* (2012) 32:E7. doi: 10.3171/2012.1.FOCUS11370
- Camacho E, LoPresti MA, Bruce S, Lin D, Abraham M, Appelboom G, et al. The role of age in intracerebral hemorrhages. *J Clin Neurosci.* (2015) 22:1867–70. doi: 10.1016/j.jocn.2015.04.020
- Samarasekera N, Fonville A, Lerpiniere C, Farrall AJ, Wardlaw JM, White PM, et al. Influence of intracerebral hemorrhage location on incidence, characteristics, and outcome: population-based study. *Stroke.* (2015) 46:361–8. doi: 10.1161/STROKEAHA.114.007953
- Stoker TB, Evans NR. Managing risk after intracerebral hemorrhage in concomitant atrial fibrillation and cerebral amyloid angiopathy. *Stroke.* (2016) 47:e190–2. doi: 10.1161/STROKEAHA.116.013323
- Greenberg SM, Charidimou A. Diagnosis of cerebral amyloid angiopathy. *Evol Boston Criteria.* (2018) 49:491–7. doi: 10.1161/STROKEAHA.117.016990
- Naganuma T, Takemoto Y, Shoji T, Ishimura E, Okamura M, Nakatani T. Cerebral microbleeds predict intracerebral hemorrhage in hemodialysis patients. *Stroke.* (2015) 46:2107–12. doi: 10.1161/STROKEAHA.115.009324
- Pasquini M, Benedictus MR, Boulouis G, Rossi C, Dequatre-Ponchelle N, Cordonnier C. Incident cerebral microbleeds in a cohort of intracerebral hemorrhage. *Stroke.* (2016) 47:689–94. doi: 10.1161/STROKEAHA.115.011843
- Wang S, Lv Y, Zheng X, Qiu J, Chen HS. The impact of cerebral microbleeds on intracerebral hemorrhage and poor functional outcome of acute ischemic stroke patients treated with intravenous thrombolysis: a systematic review and meta-analysis. *J Neurol.* (2017) 264:1309–19. doi: 10.1007/s00415-016-8339-1
- Kawarabayashi T, Younkin LH, Saido TC, Shoji M, Ashe KH, Younkin SG. Age-dependent changes in brain, CSF, and plasma amyloid β protein in the Tg2576 transgenic mouse model of alzheimer's disease. *J Neurosci.* (2001) 21:372–81. doi: 10.1523/JNEUROSCI.21-02-0037.2.2001
- Fisher M, Vasilevko V, Passos GF, Ventura C, Quiring D, Cribbs DH. Therapeutic modulation of cerebral microhemorrhage in a mouse model of cerebral amyloid angiopathy. *Stroke.* (2011) 42:3300–3. doi: 10.1161/STROKEAHA.111.626655
- Hsiao K, Chapman P, Nilsen S, Eckman C, Harigaya Y, Younkin S, et al. Correlative memory deficits, A β elevation, and amyloid plaques in transgenic mice. *Science.* (1996) 274:99–102. doi: 10.1126/science.274.5284.99
- Domnitz SB, Robbins EM, Hoang AW, Garcia-Alloza M, Hyman BT, Rebeck GW, et al. Progression of cerebral amyloid angiopathy in transgenic mouse models of Alzheimer Disease. *J Neuropathol Exp Neurol.* (2005) 64:588–94. doi: 10.1097/01.jnen.0000171644.00180.fc
- Milner E, Zhou M-L, Johnson AW, Vellimana AK, Greenberg JK, Holtzman DM, et al. Cerebral amyloid angiopathy increases susceptibility to infarction after focal cerebral ischemia in Tg2576 mice. *Stroke.* (2014) 45:3064–9. doi: 10.1161/STROKEAHA.114.006078

FUNDING

Supported by research grants from Boehringer-Ingelheim (MF) and the National Institutes of Health NS20989 (MF and DC).

ACKNOWLEDGMENTS

We thank Myrna Ayman Mousa and Alexstin Chung Man for their assistance with this study.

29. DeFeo K, Hayes C, Chernick M, Van Ryn J, Gilmour SK. Use of dabigatran etexilate to reduce breast cancer progression. *Cancer Biol Therapy*. (2010) 10:1001–8. doi: 10.4161/cbt.10.10.13236
30. Liu S, Grigoryan MM, Vasilevko V, Sumbria RK, Paganini-Hill A, Cribbs DH, et al. Comparative analysis of H&E and Prussian blue staining in a mouse model of cerebral microbleeds. *J Histochem Cytochem*. (2014) 62:767–73. doi: 10.1369/0022155414546692
31. Hawkins BT, Gu Y-H, Izawa Y, del Zoppo GJ. Dabigatran abrogates brain endothelial cell permeability in response to thrombin. *J Cerebral Blood Flow Metabol*. (2015) 35:985–92. doi: 10.1038/jcbfm.2015.9
32. Marinescu M, Sun L, Fatar M, Neubauer A, Schad L, van Ryn J, et al. Cerebral microbleeds in murine amyloid angiopathy: natural course and anticoagulant effects. *Stroke*. (2017) 48:2248–54. doi: 10.1161/STROKEAHA.117.017994
33. Fisher M. Cerebral microbleeds: where are we now? *Neurology*. (2014) 83:1304–5. doi: 10.1212/WNL.0000000000000871

Conflict of Interest Statement: MF reports grants from Boehringer-Ingelheim (48513359185) and NIH (NS20989) during the conduct of the study, and a grant from Otsuka Pharmaceutical Co. outside the submitted work. JR reports support from Boehringer-Ingelheim. DC reports a grant from NIH (NS20989) during the conduct of this study. RS reports a grant from NIH (AG055949) outside the conduct of this study.

The remaining authors declare that the research was conducted in the absence of any commercial or financial relationships that could be construed as a potential conflict of interest.

Copyright © 2019 Michael, Grigoryan, Kilday, Sumbria, Vasilevko, van Ryn, Cribbs, Paganini-Hill and Fisher. This is an open-access article distributed under the terms of the Creative Commons Attribution License (CC BY). The use, distribution or reproduction in other forums is permitted, provided the original author(s) and the copyright owner(s) are credited and that the original publication in this journal is cited, in accordance with accepted academic practice. No use, distribution or reproduction is permitted which does not comply with these terms.



Underlying Small Vessel Disease Associated With Mixed Cerebral Microbleeds

Clemence Blanc¹, Alain Viguier^{1,2}, Lionel Calviere^{1,2}, Mélanie Planton^{1,2}, Jean François Albucher^{1,2}, Vanessa Rousseau³, Agnès Sommet^{3,4}, Fabrice Bonneville^{2,5}, Jérémie Pariente^{1,2}, Jean Marc Olivot^{1,2} and Nicolas Raposo^{1,2*}

¹ Neurology Department, Hôpital Pierre-Paul Riquet, Centre Hospitalier Universitaire de Toulouse, Toulouse, France, ² Toulouse Neuroimaging Center, Université de Toulouse, Inserm, UPS, Toulouse, France, ³ Epidemiology Department, Centre Hospitalier Universitaire de Toulouse, Toulouse, France, ⁴ Department of Clinical Pharmacology, CIC1436, USMR, Centre Hospitalier Universitaire de Toulouse, Toulouse, France, ⁵ Neuroradiology Department, Hôpital Pierre-Paul Riquet, Centre Hospitalier Universitaire de Toulouse, Toulouse, France

OPEN ACCESS

Edited by:

Andreas Charidimou,
Massachusetts General Hospital,
Harvard Medical School,
United States

Reviewed by:

Duangnapa Roongpiboonsopit,
Naresuan University, Thailand
Mana Shams,
Karolinska Institute (KI), Sweden

*Correspondence:

Nicolas Raposo
raposo.n@chu-toulouse.fr

†ORCID:

Nicolas Raposo
orcid.org/0000-0002-9152-4445

Specialty section:

This article was submitted to
Stroke,
a section of the journal
Frontiers in Neurology

Received: 05 August 2019

Accepted: 08 October 2019

Published: 23 October 2019

Citation:

Blanc C, Viguier A, Calviere L, Planton M, Albucher JF, Rousseau V, Sommet A, Bonneville F, Pariente J, Olivot JM and Raposo N (2019) Underlying Small Vessel Disease Associated With Mixed Cerebral Microbleeds. *Front. Neurol.* 10:1126. doi: 10.3389/fneur.2019.01126

Background and Purpose: Whether patients with both lobar and deep cerebral microbleeds (mixed CMB) have advanced cerebral amyloid angiopathy (CAA), hypertensive angiopathy (HA) or both is uncertain. To get insight into the underlying small vessel disease (SVD) associated with mixed CMB, we explored its association with cortical superficial siderosis (cSS), a key marker of CAA and other MRI markers of SVD in patients with intracerebral hemorrhage (ICH).

Methods: Of 425 consecutive patients with acute ICH who had received brain MRIs, 260 had ≥ 1 CMB and were included in the analysis. They were categorized as strictly lobar CMB (suggesting CAA), strictly deep CMB (suggesting HA) or mixed CMB. Clinical and imaging characteristics were compared (1) between the three CMB groups and (2) within mixed CMB patients according to the symptomatic ICH location.

Results: Overall, 111 (26%) patients had mixed CMB. Compared to strictly lobar CMB ($n = 111$) and strictly deep CMB ($n = 38$), patients with mixed CMB had a more severe burden of lacune, white matter hyperintensities and CMB. cSS was observed in 24.3% of patients with mixed CMB compared to 44.1% in strictly lobar CMB and 10.5% in strictly deep CMB ($p < 0.0001$). Among patients with mixed CMB, 44 (39.6%) had a lobar symptomatic ICH and 67 (60.4%) had a non-lobar ICH. Patients with non-lobar ICH were more likely to have hypertension, whereas those with lobar ICH were more likely to have cSS and chronic lobar ICH and had higher ratio lobar CMB count/total CMB count.

Conclusions: Mixed CMB is frequently encountered in patients with ICH and appears as a heterogeneous group, suggesting that both CAA and HA may be contributing to mixed CMB. Neuroimaging markers including ICH location, cSS, and CMB distribution may indicate the predominant underlying vasculopathy, with potential prognostic implications.

Keywords: intracerebral hemorrhage, cerebral amyloid angiopathy, cerebral microbleeds, cortical superficial siderosis, cerebral small vessel disease, neuroimaging

INTRODUCTION

Hypertensive angiopathy (HA) and cerebral amyloid angiopathy (CAA) are common small vessel diseases (SVDs) that account for most cases of spontaneous intracerebral hemorrhage (ICH) (1), the most severe stroke subtype with high risk of mortality and dementia (2, 3). CAA results from amyloid- β (A β) deposition in the wall of cortical and leptomeningeal vessels and is a common cause of lobar ICH. By contrast, HA is characterized by lipohyalinosis, arteriolosclerosis, and fibrinoid necrosis, predominantly affecting deep perforating arteries, causing deep or infratentorial ICH (4).

Cerebral microbleeds (CMBs) are neuroimaging markers of SVD detected in ~60% of patients with spontaneous ICH (5). The pattern of CMB distribution is suggestive of the underlying SVD (6). Patients with multiple CMB confined to the lobar regions are likely to have CAA (7). Conversely, CMBs are typically located in the deep regions (basal ganglia, thalamus, and brainstem) in HA (8). When patients present with both lobar and deep CMB (i.e., mixed CMB), it is unclear whether they have advanced HA, CAA, or a combination of these two diseases. Understanding the underlying SVD has important clinical implication with regard to the risk of ICH recurrence, anticoagulant strategy, and patient selection for anti-amyloid therapy trials.

In the current study, we aimed to explore the underlying SVD(s) associated with mixed CMB in patients with symptomatic ICH. We investigated the clinical and imaging factors associated with mixed CMB compared to strictly lobar CMB (suggesting CAA) and strictly deep CMB (suggesting HA). We also evaluated whether CMB distribution in patients with mixed CMB may indicate underlying SVD by testing the associations of the ratio lobar / total CMB count with symptomatic lobar ICH and cortical superficial siderosis (cSS), key neuroimaging markers of CAA (7, 9, 10).

MATERIALS AND METHODS

The data that support the findings of this study are available from the corresponding author on reasonable request.

Patient Selection

We conducted a retrospective cross-sectional analysis of data collected prospectively from consecutive patients admitted between December 2011 and January 2016 to Toulouse Hospital stroke center for acute spontaneous ICH who underwent brain MRI. The study was approved by the Toulouse-Purpan Hospital Research Ethics Committee (No. 22-0315). Informed consent was not required because of the retrospective observational design of the study.

Inclusion criteria for this study were as follows: (1) patient with acute spontaneous ICH, (2) MRI of adequate quality performed within 30 days after symptom onset (3) presence of ≥ 1 CMB. Patients with traumatic ICH, secondary causes of ICH, and those without CMB were excluded. To limit diagnostic uncertainty, we also excluded patients with CMB restricted to the cerebellum.

Data Collection

Demographic and clinical data (age, sex, vascular risk factors, anticoagulant, history of symptomatic ICH) were recorded and analyzed. Information on neurological symptoms upon admission was collected.

MRI Acquisition and Analysis

MR images were acquired on 1.5-T or 3-T scanners and included at least T2*-weighted gradient recalled echo (T2*-GRE) and axial fluid-attenuated inversion recovery (FLAIR) sequences, as previously described (11). Among the 260 patients with CMB included in the analysis, 148 (56.9%) underwent a 3-T MRI and 112 (43.1%) a 1.5-T MRI. Among patients with mixed CMB, the proportion of participants who underwent a 3-T MRI (61.3%) was not statistically different from patients with strictly lobar CMB (55.9%; $p = 0.45$) or strictly deep CMB (47.4%; $p = 0.13$). CMB count was similar between patients with 3-T MRI and those with 1.5-T MRI in each CMB group.

The MRI scans were reviewed by the investigators, blinded to all clinical data and in accordance with the Standards for Reporting Vascular Changes on Neuroimaging (STRIVE) recommendations (12). Symptomatic ICH location was categorized as either lobar (cortex or subcortical white matter) or non-lobar (thalamus, basal ganglia, brainstem or cerebellum). ICH volume was calculated using the abc/2 method (13). CMB presence and number were evaluated on the T2*-GRE images according to the current consensus criteria (6). They were classified as lobar (cortical and cortico-subcortical area) or deep (basal ganglia, thalamus, or brainstem). According to CMB distribution, patients were categorized as (1) strictly lobar CMB, (2) strictly deep CMB, or (3) mixed CMB (**Figure 1**). Two trained raters (CB and NR) independently reviewed MR images from 20 randomly selected patients. The inter-rater reliability was excellent for the CMB category ($\kappa = 0.82$). Chronic ICHs were defined as prior symptomatic or asymptomatic ICHs > 5 mm on the T2*-GRE images without acute bleeding identified on MRI scans. Cortical superficial siderosis (cSS) presence and extent were visually assessed according to the consensus recommended criteria (14). Periventricular and deep white matter hyperintensities (WMH) were visually assessed on axial FLAIR images on the 4-point Fazekas' rating scale (15). A total WMH score on a 7-point scale was obtained by adding up the Fazekas' scores in each region.

Statistical Analyses

Baseline clinical and imaging data of patients with mixed CMB were compared to those with (1) strictly lobar CMB and (2) strictly deep CMB. We used χ^2 test (or Fisher test as appropriate) for qualitative variables and Wilcoxon's rank-sum test for quantitative variables.

Multivariable logistic regression models were used to identify factors associated with mixed CMB vs. strictly lobar CMB then vs. strictly deep CMB. We categorized age as <55 vs. ≥ 55 , and total CMB counts using cut points (0, 1, 2–4, ≥ 5). Potential factors were age, hypertension, lobar symptomatic ICH, total CMB count, presence of cSS, chronic lobar ICH,

severe (Fazekas 5 or 6) WMH, and lacunes. Each factor was tested in a univariable model and those with $p < 30\%$ were inserted into multivariable models. Final models were obtained using a backward elimination strategy. All models were adjusted for age and diabetes. The final model contained only factors significant at 5%.

We calculated the ratio lobar/total CMB count (CMB ratio) to assess the predominant CMB distribution (either in lobar or deep regions) in patients with mixed CMB. We explored whether CMB ratio may indicate the underlying SVD in patients with mixed CMB by testing its association with symptomatic ICH location and cSS. Within the mixed CMB group, we compared the clinical

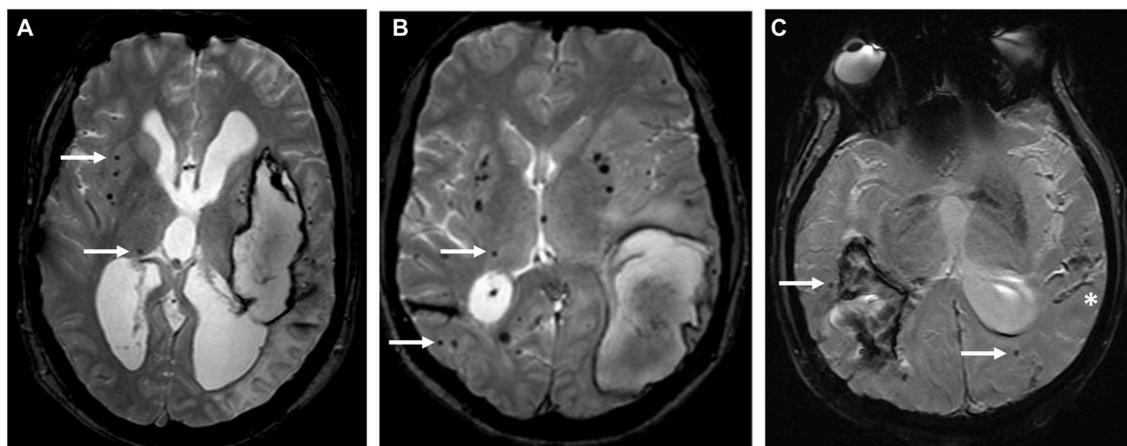


FIGURE 1 | Different distribution patterns of cerebral microbleeds. T2*-GRE MRIs showing the distribution of CMB (white arrows) in three representative cases: **(A)** strictly deep CMB in a patient with deep left ICH, suggesting underlying hypertensive angiopathy, **(B)** mixed CMB with an acute left lobar ICH, **(C)** strictly lobar CMB associated with an acute right lobar ICH and cortical superficial siderosis (*) suggesting underlying CAA.

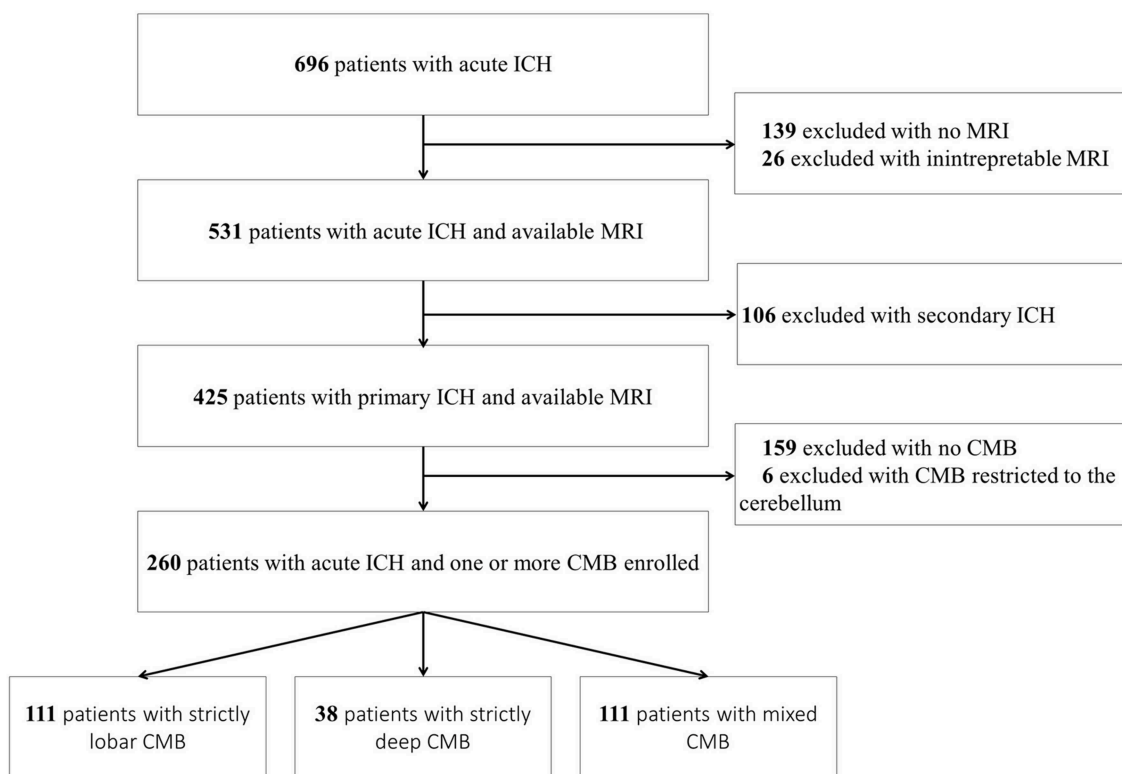


FIGURE 2 | Flow diagram. CMB, cerebral microbleed; ICH, intracerebral hemorrhage.

and imaging characteristics between patients with symptomatic lobar ICH vs. non-lobar ICH. Variables with $p < 30\%$ in the univariable analysis were included in the multivariable model. The model was adjusted for age and diabetes. We also tested the association between CMB ratio (categorized by tertile) and both cSS and symptomatic lobar ICH using χ^2 or Kruskal-Wallis tests.

Statistical testing was conducted at an alpha level of 5% (two-tailed). Data were analyzed using SAS[®] software, version 9.4 (SAS Institute).

RESULTS

Among 696 patients with acute non-traumatic ICH admitted to our stroke unit during the study period, 425 had a primary ICH and interpretable MRI (Figure 2). Of them, 159 [37.4%; 95% confidence interval (CI) 32.8–42.0%] had no CMB, 111 (26.1%; 95% CI 21.9–30.3%) mixed CMB, 111 (26.1%; 95% CI 21.9–30.3%) strictly lobar CMB, and 38 (8.9%; 95% CI 6.2–11.7%) had strictly deep CMB. Six patients had CMB restricted to the cerebellum and were excluded from the analysis.

TABLE 1 | Characteristics and comparison of patients with acute intracerebral hemorrhage according to cerebral microbleeds distribution.

	Mixed CMB (<i>n</i> = 111)	Strictly lobar CMB (<i>n</i> = 111)	Strictly deep CMB (<i>n</i> = 38)
Age, mean \pm SD*	74 \pm 9.8	73.7 \pm 12.8	65.8 \pm 14.9 ^a
Male, No. (%)	64 (57.6)	69 (62.2)	28 (73.7)
Hypertension, No. (%)	82 (73.9)	70 (63.1)	31 (81.6)
Diabetes, No. (%)	16 (14.4)	18 (16.2)	7 (18.4)
Previous symptomatic ICH, No. (%)	9 (8.1)	11 (9.9)	2 (5.2)
Anticoagulant use, No. (%)	27 (24.3)	21 (18.9)	5 (13.2)
NIHSS at admission, median [IQR]*	6 [3–13]	7 [4–15]	7.5 [3–16]
Onset to MRI (days), median [IQR]*	1 [0–4]	1 [0–3]	1 [0–3]
Symptomatic lobar ICH, No. (%)	44 (39.6)	79 (71.2) ^b	5 (13.2) ^a
Presence of cSS, No. (%)	27 (24.3)	49 (44.1) ^a	4 (10.5)
Presence of Disseminated cSS, No. (%)	15 (13.5)	27 (24.3) ^a	1 (2.6)
CMB count, median [IQR]*	11 [6–27]	3 [1–9] ^b	2 [1–4] ^b
Presence of chronic lobar ICH, No. (%)	27 (24.3)	23 (20.7)	1 (2.6) ^a
Fazekas' WMH score/6, median [IQR]*	4 [3–6]	3 [2–4] ^b	3 [2–5] ^b
Presence of lacune, No. (%)	72 (64.8)	31 (27.9) ^b	16 (42.1) ^a

CMB, cerebral microbleed; cSS, cortical superficial siderosis; ICH, intracerebral hemorrhage; NIHSS, National Institute of Health Stroke Score; WMH, white matter hyperintensities.

The *p*-values reported in the strictly lobar CMB column refer to comparison with mixed CMB. The *p*-values reported in the strictly deep CMB column refer to comparison with mixed CMB.

p-values were obtained via χ^2 test or Wilcoxon's rank-sum test (*). ^a $p < 0.05$; ^b $p < 0.001$.

The final cohort consisted of 260 patients with primary ICH who had ≥ 1 CMB (mean age 72.7 \pm 12.2). Baseline clinical and imaging characteristics of patients with mixed CMB, strictly lobar CMB and strictly deep CMB are summarized in Table 1. Location of the symptomatic ICH varied across the three groups ($p < 0.0001$). Patients with strictly lobar CMB had predominantly lobar ICH, whereas those with strictly deep CMB were more likely to have a deep ICH (Figure 3). Presence of both lobar and non-lobar ICH (including acute and chronic ICH) was observed in 17 (15.3%) patients with mixed CMB, compared to 7 (6.3%) patients with strictly lobar CMB ($p = 0.03$) and 1 (2.6%) patient with strictly deep CMB ($p = 0.04$).

Mixed CMB Compared to Strictly Lobar CMB

Compared to patients with strictly lobar CMB, patients with mixed CMB were similar in age and tended to have more frequent history of hypertension ($p = 0.08$). The symptomatic ICH was lobar in 44 (39.6%) patients with mixed CMB compared to 79 (71.2%) patients with strictly lobar CMB ($p < 0.0001$). Patients with mixed CMB were more likely to have lacunes and had a more severe burden of CMB and WMH than those with strictly lobar CMB. Conversely, cSS was more common in patients with strictly lobar CMB than mixed CMB (44.1 vs. 24.3%; $p < 0.002$). Multivariable model shows that compared to strictly lobar CMB, mixed CMB pattern was associated with the presence of severe WMH [odds ratio (OR) 3.38, 95% CI 1.52–7.80, $p = 0.003$], lacunes (OR 3.77, 95% CI 1.83–8.03, $p = 0.0004$), and higher CMB count (OR 7.40, 95% CI 3.96–15.10, $p < 0.0001$). Conversely, strictly lobar CMB pattern was associated with symptomatic lobar ICH (OR 4.71, 95% CI 2.16–10.96, $p = 0.0002$) and cSS (OR 3.09, 95% CI 1.40–7.04, $p = 0.006$).

Mixed CMB Compared to Strictly Deep CMB

Compared to patients with strictly deep CMB, patients with mixed CMB were older but had similar prevalence of hypertension and diabetes. Patients with mixed CMB were more likely to have a symptomatic lobar ICH than those with strictly deep CMB and had a more severe burden of lacunes, CMB, and WMH. Prevalence of cSS did not differ between the two groups. A multivariable model shows that compared to strictly deep CMBs, the pattern of mixed CMB was associated with symptomatic lobar ICH (OR 4.68, 95% CI 1.27–21.68, $p = 0.03$) and higher CMB count (OR 11.69, 95% CI 5.43–29.62, $p < 0.0001$).

Mixed CMB, ICH Location, and Cortical Superficial Siderosis

Among patients with mixed CMB, 44 (39.6%) had a lobar symptomatic ICH and 67 (60.4%) had a non-lobar ICH. The two groups were similar in age (Table 2). Patients with non-lobar ICH and mixed CMB were more likely to be male and to have hypertension, whereas patients with lobar ICH and mixed CMB were more likely to have cSS and chronic lobar ICH. Although total CMB count was similar between

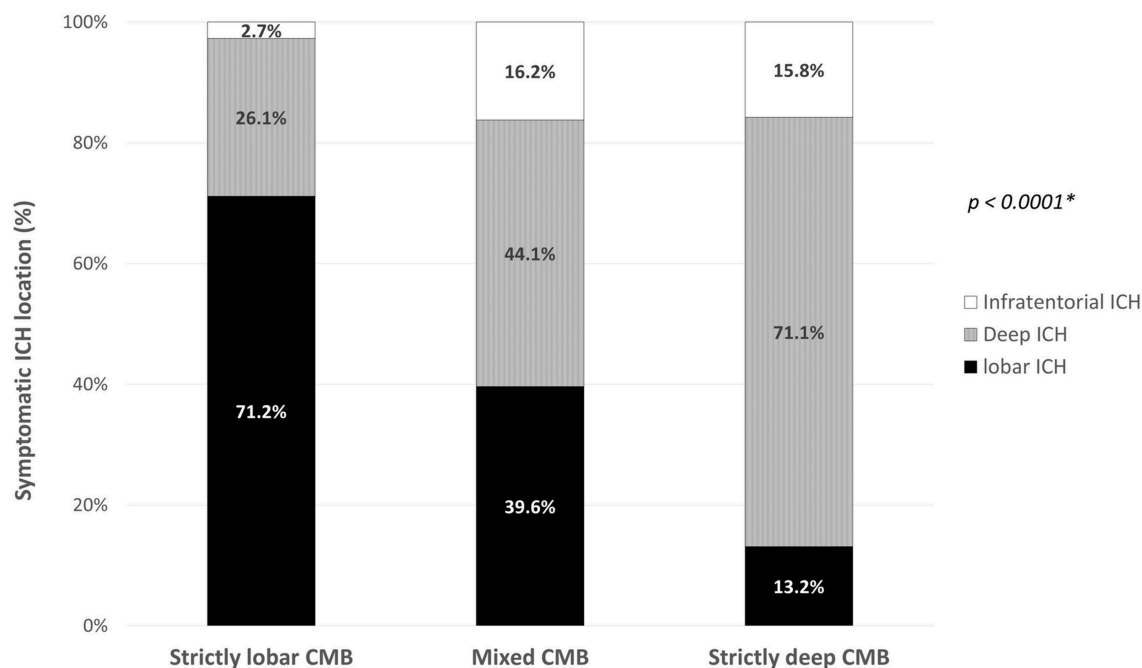


FIGURE 3 | Symptomatic intracerebral hemorrhage location according to the cerebral microbleeds distribution pattern. *global χ^2 test. CMB, cerebral microbleed; ICH, intracerebral hemorrhage.

TABLE 2 | Comparison between patients with lobar and non-lobar symptomatic ICH in subjects with mixed cerebral microbleeds.

	Mixed CMB		p-value
	Lobar ICH	Non-lobar ICH	
No. (%)	44 (39.6)	67 (60.4)	–
Clinical characteristics			
Age, mean \pm SD	75.4 \pm 9.0	73.0 \pm 10.2	0.30*
Male, No. (%)	19 (43.2)	45 (67.2)	0.01
Hypertension, No. (%)	24 (54.6)	58 (86.6)	0.0002
Diabetes, No. (%)	5 (11.4)	11 (16.4)	0.46
Imaging characteristics			
Presence of cSS, No. (%)	17 (38.6)	10 (14.9)	0.004
CMB count, median [IQR]	13 [6–39]	10 [5–24]	0.17*
Lobar CMB count, median [IQR]	10.5 [3–28.5]	4 [2–13]	0.004*
Deep CMB count, median [IQR]	1.5 [1–4]	3 [2–6]	0.008*
Ratio lobar/total CMB, median [IQR]	0.8 [0.5–0.9]	0.5 [0.3–0.6]	<0.0001*
Presence of chronic lobar ICH, No. (%)	15 (34.1)	12 (17.9)	0.05
Severe WMH (Fazekas 5–6), No. (%)	20 (45.5)	30 (44.8)	0.94
Presence of lacune, No. (%)	24 (54.6)	48 (71.6)	0.07

CMB, cerebral microbleed; cSS, cortical superficial siderosis; ICH, intracerebral hemorrhage; WMH, white matter hyperintensities.

p-values were obtained via χ^2 test or Wilcoxon's rank-sum test (*).

the two groups, patients with lobar ICH had higher lobar CMB counts, whereas patients with non-lobar ICH had higher deep CMB counts. Among patients with mixed CMB, the ratio lobar CMB count/total CMB count was higher in patients

with lobar ICH than those with non-lobar ICH. In the multivariable analysis, non-lobar symptomatic ICH location was associated with male gender (OR 3.44 95% CI 1.28–9.91, $p = 0.02$), history of hypertension (OR 7.41, 95% CI 2.57–23.74, $p = 0.0004$), and higher deep CMB counts (OR 2.59, 95% CI 1.50–4.80, $p = 0.001$), whereas lobar ICH location was associated with cSS (OR 3.43, 95% CI 1.18–10.54, $p = 0.03$).

Increasing CMB ratio was associated with increasing prevalence of cSS ($p = 0.03$) and symptomatic lobar ICH ($p < 0.0001$) in patients with mixed CMB (Figure 4).

DISCUSSION

Our study shows that mixed CMB is frequently encountered in subjects with symptomatic ICH and might be due to different degrees of both CAA and HA. Approximately 25% of patients with mixed CMB have cSS and may therefore harbor CAA, as dominant or coexisting underlying SVD. Along with cSS, ICH location and the pattern of CMB distribution may indicate the predominant underlying vasculopathy in patients with mixed CMB.

In our large cohort of patients with primary ICH, 26% had mixed CMB, confirming that mixed hemorrhage distribution is a common condition in adults with symptomatic ICH (16–20). In accordance with previous studies (18), we found that mixed CMB was associated with a more severe burden of SVD including lacunes, CMB, and WMH, compared to patients with strictly lobar and strictly deep CMB. Interestingly, in our cohort, prevalence of hypertension and diabetes was

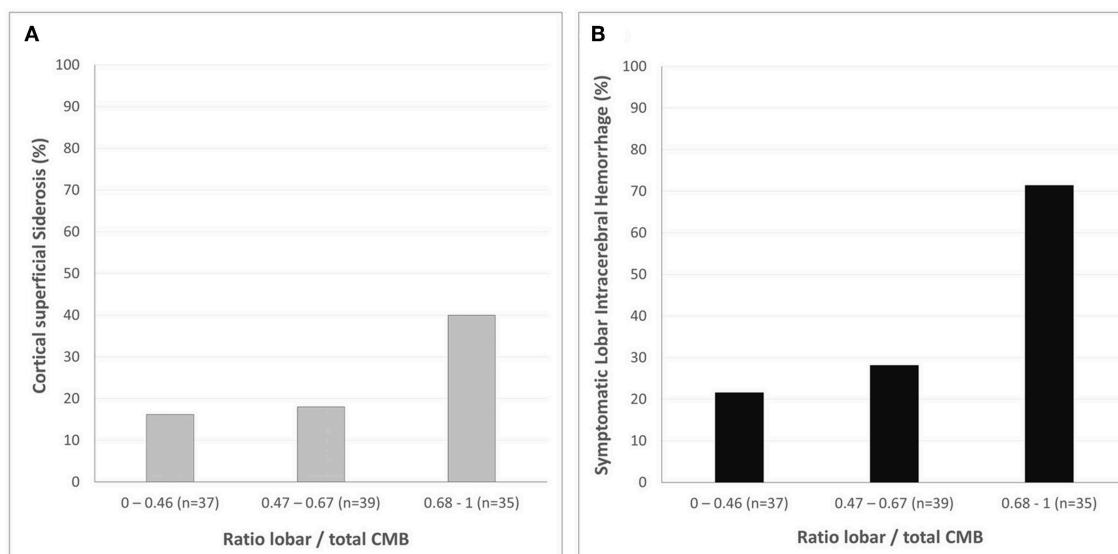


FIGURE 4 | Cerebral microbleeds distribution and markers of CAA in patients with mixed cerebral microbleeds. Prevalence of cortical superficial siderosis (**A**) and symptomatic lobar intracerebral hemorrhage (**B**) according to the ratio lobar/total CMB count (categorized by tertile). Increasing cerebral microbleeds ratio is associated with both cortical superficial siderosis ($p = 0.03$) and lobar intracerebral hemorrhage ($p < 0.0001$).

similar between patients with mixed CMB and the two other groups. The increased severity of SVD associated with mixed CMB may not therefore be driven by vascular risk factors alone.

Whether patients with mixed CMB have advanced HA, CAA, or both is still debated. As both CAA and hypertension are common in the elderly (21, 22), concomitant CAA and HA is a possible hypothesis. Based on post-mortem studies showing that up to 15% of patients with deep ICH had pathological evidence of CAA (23), it has been hypothesized that most patients with mixed CMB would have both CAA and HA. However, it has also been shown that HA could promote lobar CMB, suggesting that patients with mixed CMB may have advanced HA as underlying SVD (8). Results from a recent large imaging study support this hypothesis, showing that patients with mixed ICH are more similar to HA-ICH than CAA-ICH (18).

In our cohort, mixed CMB appears as a relatively heterogeneous group with different ICH subtypes. Most patients with mixed CMB presented with a non-lobar symptomatic ICH and high prevalence of hypertension, suggesting HA as predominant underlying SVD. Nevertheless, cSS was observed in 39% of patients with mixed CMB presenting with a lobar symptomatic ICH, suggesting that a substantial proportion of these patients may have some degree of CAA. A recent amyloid PET study in an Asian ICH population supports this hypothesis (24). Although patients with mixed ICH had overall low burden of amyloid PET, a small subset with mixed ICH who had cSS showed similar high burden of amyloid PET than CAA-ICH.

Interestingly, CMB distribution in patients with mixed CMB may differ according to the ICH location and the presence

of cSS. Increasing lobar/total CMB ratio was associated with symptomatic lobar ICH and cSS, two key neuroimaging markers of CAA. Hence, the ratio lobar/total CMB may be an interesting biomarker that could help to identify underlying CAA in patients with mixed CMB and should be assessed along with cSS.

Our study has limitations, including its retrospective and MRI-based design. This could have led to a selection bias toward the less severe ICH cases, but nonetheless 76% of patients screened for this study underwent MRI and were included in the analysis. Moreover, unlike previous studies (16–20), our “mixed” category referred to mixed CMB instead of mixed hemorrhage (i.e., including symptomatic ICH and CMB). Therefore, our findings are not entirely comparable to these previous reports. However, we designed our study to assess lobar ICH, along with cSS, as imaging marker of CAA (10). In a clinical setting, patients underwent either 1.5-T or 3-T MRI. This could have affected our CMB detection. However, we did not find any difference in MRI field strength between the three groups. Finally, the most important limitation is the lack of pathological examinations. Although patients were subject to rigorous selection criteria to limit diagnostic uncertainty, further studies with MRI and pathological validation are needed to confirm our findings.

In summary, mixed CMB is a frequent condition, observed in ~25% of patients with primary ICH, characterized by a severe burden of SVD. Mixed CMB appears as a heterogeneous vasculopathy that may be due to different degrees of both HA and CAA. Although most subjects with mixed CMB seem to have HA as dominant underlying SVD, 25% of patients with mixed CMB have cSS, suggesting dominant or coexisting CAA. Along with cSS and lobar ICH, a predominantly lobar CMB

distribution (assessed by the ratio lobar/total CMB) may be a useful biomarker to identify underlying CAA in these patients. As CAA is associated with an increased risk of recurrent ICH, these findings may have important prognostic implications.

DATA AVAILABILITY STATEMENT

The datasets generated for this study are available on request to the corresponding author.

ETHICS STATEMENT

The studies involving human participants were reviewed and approved by Toulouse-Purpan Hospital Research Ethics Committee. Written informed consent for participation was not required for this study in accordance with the national legislation and the institutional requirements.

REFERENCES

1. Cordonnier C, Demchuk A, Ziai W, Anderson CS. Intracerebral haemorrhage: current approaches to acute management. *Lancet*. (2018) 392:1257–68. doi: 10.1016/S0140-6736(18)31878-6
2. van Asch CJ, Luitse MJ, Rinkel GJ, van der Tweel I, Algra A, Klijn CJ. Incidence, case fatality, and functional outcome of intracerebral haemorrhage over time, according to age, sex, and ethnic origin: a systematic review and meta-analysis. *Lancet Neurol*. (2010) 9:167–76. doi: 10.1016/S1474-4422(09)70340-0
3. Planton M, Saint-Aubert L, Raposo N, Branchu L, Lyoubi A, Bonneville F, et al. High prevalence of cognitive impairment after intracerebral hemorrhage. *PLoS ONE*. (2017) 12:e0178886. doi: 10.1371/journal.pone.0178886
4. Pantoni L. Cerebral small vessel disease: from pathogenesis and clinical characteristics to therapeutic challenges. *Lancet Neurol*. (2010) 9:689–701. doi: 10.1016/S1474-4422(10)70104-6
5. Cordonnier C, Al-Shahi Salman R, Wardlaw J. Spontaneous brain microbleeds: systematic review, subgroup analyses and standards for study design and reporting. *Brain*. (2007) 130(Pt 8):1988–2003. doi: 10.1093/brain/awl387
6. Greenberg SM, Vernooij MW, Cordonnier C, Viswanathan A, Al-Shahi Salman R, Warach S, et al. Cerebral microbleeds: a guide to detection and interpretation. *Lancet Neurol*. (2009) 8:165–74. doi: 10.1016/S1474-4422(09)70013-4
7. Linn J, Halpin A, Demaerel P, Ruhland J, Giese AD, Dichgans M, et al. Prevalence of superficial siderosis in patients with cerebral amyloid angiopathy. *Neurology*. (2010) 74:1346–50. doi: 10.1212/WNL.0b013e3181dad605
8. Fazekas F, Kleinert R, Roob G, Kleinert G, Kapeller P, Schmidt R, et al. Histopathologic analysis of foci of signal loss on gradient-echo T2*-weighted MR images in patients with spontaneous intracerebral hemorrhage: evidence of microangiopathy-related microbleeds. *Am J Neuroradiol*. (1999) 0:637–42.
9. Raposo N, Calviere L, Cazzola V, Planton M, Patsoura S, Wargny M, et al. Cortical superficial siderosis and acute convexity subarachnoid hemorrhage in cerebral amyloid angiopathy. *Eur J Neurol*. (2018) 25:253–9. doi: 10.1111/ene.13484
10. Knudsen KA, Rosand J, Karluk D, Greenberg SM. Clinical diagnosis of cerebral amyloid angiopathy: validation of the Boston criteria. *Neurology*. (2001) 56:537–9. doi: 10.1212/WNL.56.4.537
11. Revel-Mouroz P, Viguier A, Cazzola V, Calviere L, Patsoura S, Rousseau V, et al. Acute ischaemic lesions are associated with cortical superficial siderosis

AUTHOR CONTRIBUTIONS

NR: conception, design, and supervision. VR: statistical analyses. CB and NR: data collection, writing, and tables and figures. All authors: data analyses and interpretation, review and editing, and read and approved the final manuscript.

FUNDING

NR was supported by a Fulbright Scholarship and received an Arthur Sachs Scholarship from the Harvard University committee on General Scholarship, and a Philippe Foundation research grant.

ACKNOWLEDGMENTS

The authors thank the CHU de Toulouse.

- in spontaneous intracerebral hemorrhage. *Eur J Neurol*. (2019) 26:660–6. doi: 10.1111/ene.13874
12. Wardlaw JM, Smith EE, Biessels GJ, Cordonnier C, Fazekas F, Frayne R, et al. Neuroimaging standards for research into small vessel disease and its contribution to ageing and neurodegeneration. *Lancet Neurol*. (2013) 12:822–38. doi: 10.1016/S1474-4422(13)70124-8
13. Kothari RU, Brott T, Broderick JP, Barsan WG, Sauerbeck LR, Zuccarello M, et al. The ABCs of measuring intracerebral hemorrhage volumes. *Stroke*. (1996) 27:1304–5. doi: 10.1161/01.STR.27.8.1304
14. Charidimou A, Linn J, Vernooij MW, Opherk C, Akoudad S, Baron JC, et al. Cortical superficial siderosis: detection and clinical significance in cerebral amyloid angiopathy and related conditions. *Brain*. (2015) 138(Pt 8):2126–39. doi: 10.1093/brain/awv162
15. Fazekas F, Chawluk JB, Alavi A, Hurtig HI, Zimmerman RA. MR signal abnormalities at 1.5 T in Alzheimer's dementia and normal aging. *Am J Roentgenol*. (1987) 149:351–6. doi: 10.2214/ajr.149.2.351
16. Yakushiji Y, Yokota C, Yamada N, Kuroda Y, Minematsu K. Clinical characteristics by topographical distribution of brain microbleeds, with a particular emphasis on diffuse microbleeds. *J Stroke Cerebrovasc Dis*. (2011) 20:214–21. doi: 10.1016/j.jstrokecerebrovasdis.2009.12.001
17. Haussen DC, Henninger N, Kumar S, Selim M. Statin use and microbleeds in patients with spontaneous intracerebral hemorrhage. *Stroke*. (2012) 43:2677–81. doi: 10.1161/STROKEAHA.112.657486
18. Pasi M, Charidimou A, Boulouis G, Auriel E, Ayres A, Schwab KM, et al. Mixed-location cerebral hemorrhage/microbleeds: underlying microangiopathy and recurrence risk. *Neurology*. (2018) 90:e119–26. doi: 10.1212/WNL.0000000000004797
19. Smith EE, Nandigam KR, Chen YW, Jeng J, Salat D, Halpin A, et al. MRI markers of small vessel disease in lobar and deep hemispheric intracerebral hemorrhage. *Stroke*. (2010) 41:1933–8. doi: 10.1161/STROKEAHA.110.579078
20. Zhang C, Li Z, Wang Y, Zhao X, Wang C, Liu L, et al. Risk factors of cerebral microbleeds in strictly deep or lobar brain regions differed. *J Stroke Cerebrovasc Dis*. (2015) 24:24–30. doi: 10.1016/j.jstrokecerebrovasdis.2014.07.041
21. Neuropathology Group, Medical Research Council Cognitive F, Aging S. Pathological correlates of late-onset dementia in a multicentre, community-based population in England and Wales. Neuropathology Group of the Medical Research Council Cognitive Function and Ageing Study (MRC CFAS). *Lancet*. (2001) 357:169–75. doi: 10.1016/S0140-6736(00)03589-3

22. Yoon SS, Gu Q, Nwankwo T, Wright JD, Hong Y, Burt V. Trends in blood pressure among adults with hypertension: United States, 2003 to 2012. *Hypertension*. (2015) 65:54–61. doi: 10.1161/HYPERTENSIONAHA.114.04012
23. Ritter MA, Droste DW, Hegedus K, Szepesi R, Nabavi DG, Csiba L, et al. Role of cerebral amyloid angiopathy in intracerebral hemorrhage in hypertensive patients. *Neurology*. (2005) 64:1233–7. doi: 10.1212/01.WNL.0000156522.93403.C3
24. Tsai HH, Pasi M, Tsai LK, Chen YF, Lee BC, Tang SC, et al. Microangiopathy underlying mixed-location intracerebral hemorrhages/microbleeds: a PiB-PET study. *Neurology*. (2019) 92:e774–81. doi: 10.1212/WNL.00000000000006953

Conflict of Interest: The authors declare that the research was conducted in the absence of any commercial or financial relationships that could be construed as a potential conflict of interest.

Copyright © 2019 Blanc, Viguier, Calviere, Planton, Albucher, Rousseau, Sommet, Bonneville, Pariente, Olivot and Raposo. This is an open-access article distributed under the terms of the Creative Commons Attribution License (CC BY). The use, distribution or reproduction in other forums is permitted, provided the original author(s) and the copyright owner(s) are credited and that the original publication in this journal is cited, in accordance with accepted academic practice. No use, distribution or reproduction is permitted which does not comply with these terms.



Risk Profile of Ischemic Stroke Caused by Small-Artery Occlusion vs. Deep Intracerebral Hemorrhage

Zimo Chen^{1,2,3,4†}, Jinglin Mo^{1,2,3,4†}, Jie Xu^{1,2,3,4}, Haiqiang Qin^{1,2,3,4}, Huaguang Zheng^{1,2,3,4}, Yuesong Pan^{1,2,3,4}, Xia Meng^{1,2,3,4}, Jing Jing^{1,2,3,4}, Xianglong Xiang^{2,3,4} and Yongjun Wang^{1,2,3,4*}

¹ Department of Neurology, Beijing Tiantan Hospital, Capital Medical University, Beijing, China, ² China National Clinical Research Center for Neurological Diseases, Beijing, China, ³ Center of Stroke, Beijing Institute for Brain Disorders, Beijing, China, ⁴ Beijing Key Laboratory of Translational Medicine for Cerebrovascular Disease, Beijing, China

OPEN ACCESS

Edited by:

Andreas Charidimou,
Massachusetts General Hospital,
Harvard Medical School,
United States

Reviewed by:

Aristeidis H. Katsanos,
McMaster University, Canada
Vasileios-Arsenios Lioutas,
Beth Israel Deaconess Medical
Center, Harvard Medical School,
United States

*Correspondence:

Yongjun Wang
yongjunwang@nrcnd.org.cn

[†]These authors have contributed
equally to this work

Specialty section:

This article was submitted to
Stroke,
a section of the journal
Frontiers in Neurology

Received: 18 August 2019

Accepted: 30 October 2019

Published: 27 November 2019

Citation:

Chen Z, Mo J, Xu J, Qin H, Zheng H,
Pan Y, Meng X, Jing J, Xiang X and
Wang Y (2019) Risk Profile of Ischemic
Stroke Caused by Small-Artery
Occlusion vs. Deep Intracerebral
Hemorrhage. *Front. Neurol.* 10:1213.
doi: 10.3389/fneur.2019.01213

Background: Small-artery occlusion (SAO) subtype accounts for a quarter of the cases of ischemic stroke and is mainly caused by pathological changes in cerebral small vessels, which also involve in deep intracerebral hemorrhage (dICH). However, the factors that drive some cases to SAO and others to dICH remained incompletely defined.

Material and Methods: This study is a cross-sectional study from the China National Stroke Registry that included consecutive patients with ischemic stroke or intracerebral hemorrhage between August 2007 and September 2008. We compared the risk profile between the two subgroups using multivariable logistic regression.

Results: A total of 1,135 patients with SAO stroke and 1,125 dICH patients were included for analyses. Generally, patients with SAO stroke were more likely to be male (odds ratio = 0.74, confidence interval = 0.58–0.94) and have diabetes (0.30, 0.22–0.40), higher atherogenic lipid profiles, higher body mass index (0.96, 0.94–0.99), higher waist/height ratio (0.12, 0.03–0.48), higher platelet count (0.84, 0.77–0.91), and higher proportion of abnormal estimated glomerular filtration rate (<90, ml/min/1.73 m²) (0.77, 0.62–0.95). Conversely, patients with dICH were more likely to have higher blood pressure parameters, inflammation levels (white blood cell count: 1.61, 1.48–1.76; high sensitivity C-reactive protein: 2.07, 1.36–3.16), and high-density lipoprotein-c (1.57, 1.25–1.98).

Conclusions: The risk profile between SAO stroke and dICH were different. Furthermore, despite of traditional indexes, waist/height ratio, platelet count, inflammation levels, lipid profile, and estimated glomerular filtration rate also play important roles in driving arteriosclerosis into opposite ends.

Keywords: cerebrovascular disease, lacunar stroke, intracerebral hemorrhage, risk factor, inflammation

INTRODUCTION

Small-artery occlusion (SAO), a distinct ischemic stroke (IS) subtype resulting in small (<15 mm in axial diameter) subcortical infarcts, is thought to correlate with intrinsic disorders of perforating cerebral arterioles called arteriosclerosis (1), due to multiple risk factors, including age, hypertension, and diabetes (2). Intracranial hemorrhage (ICH) can be classified into deep intracerebral hemorrhage (dICH) and lobar ICH, according to the location of the lesion. dICH

is more likely related to longstanding hypertension (3), which results in hypertensive vasculopathy and causes microscopic degenerative changes in the wall of small-to-medium penetrating vessels (4), while lobar ICH is multimorbid and widely known as cerebral amyloid angiopathy (CAA) related disease (5, 6).

However, SAO stroke and dICH represent opposite ends of the similar pathological process in cerebral small vessels. It was shown that patients with SAO were older and more likely to have diabetes mellitus and higher cholesterol level, while dICH patients tended to be excessive alcohol consumers and have hypertension (7, 8). However, controversy still remained on other risk factors for cerebrovascular disease. It was demonstrated that renal dysfunction led to the thickening of vascular wall in arteriosclerosis (9). Moreover, previous studies have verified that platelet (PLT) also actively participate in the pathology of arteriosclerosis (10). Besides, recent findings provided strong evidence for the inflammatory hypothesis of atherosclerosis (11, 12). However, to date, no evidence has shown the above factors in differentiating SAO stroke and dICH.

Therefore, this investigation focused on more detailed differences and points of controversy between the two groups.

MATERIALS AND METHODS

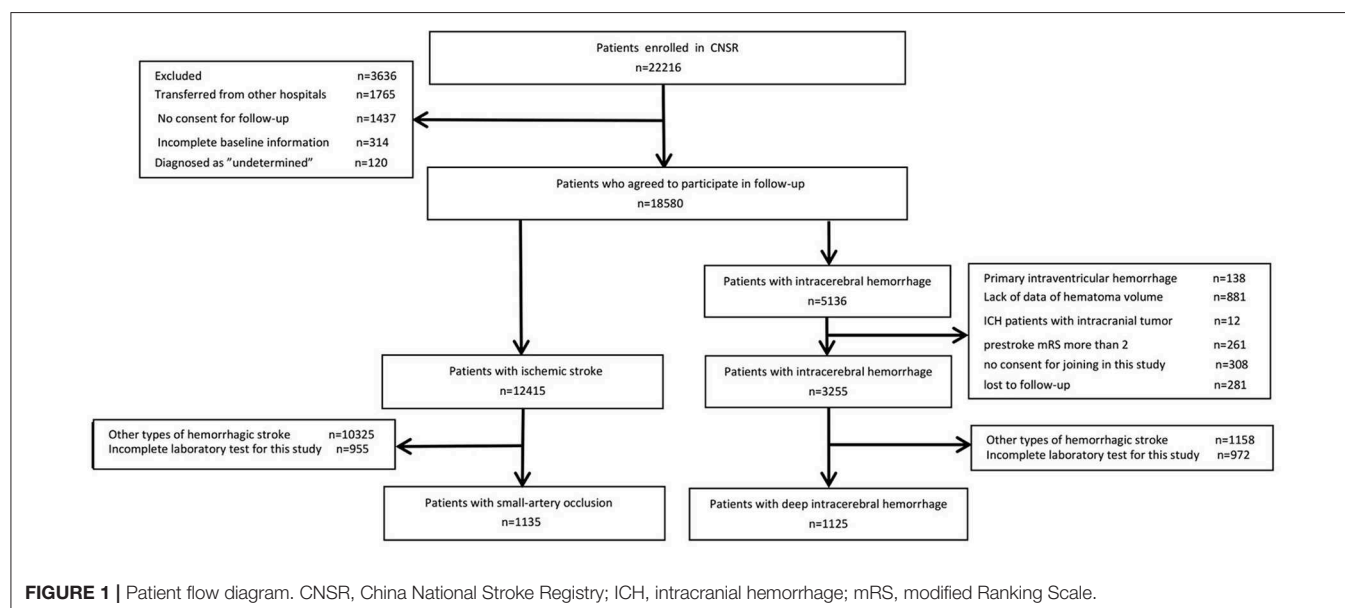
Study Cohort and Population

This is a cross-sectional study from the China National Stroke Registry (CNSR), which consecutively enrolled stroke patients (≥ 18 years) within 14 days after stroke onset from 132 participating hospitals in China. Stroke was defined as acute IS, intracerebral hemorrhage, and subarachnoid hemorrhage according to the World Health Organization criteria. The diagnosis was confirmed by brain computed tomography (CT) or magnetic resonance imaging (MRI) (13). The participating hospitals covered 100 tertiary and 32 secondary urban hospitals from 27 provinces and 4 municipalities in China, including

the Hong Kong region, between September 2007 and August 2008. Written informed consent was issued by all participants. The study was approved by the Central Institutional Review Board at Beijing Tiantan Hospital. Demographic information (age, sex), medical variables [admission systolic blood pressure (SBP), diastolic blood pressure (DBP), pulse pressure (PP), and mean arterial pressure (MAP), reported history of hypertension, history of diabetes mellitus, history of coronary heart disease, history of dyslipidemia, history of anticoagulant drug use, and history of alcohol or tobacco use], and laboratory studies on admission [estimated glomerular filtration rate (eGFR), PLT count, white blood cell (WBC) count, high sensitivity C-reactive protein (hs-CRP) level, triglyceride (TG) level, total cholesterol (TC) level, low-density lipoprotein cholesterol (LDL-c) level, high-density lipoprotein cholesterol (HDL-c) level, waist/height ratio (WHtR), and body mass index (BMI)] were documented in paper-based case report forms.

Defining dICH and SAO

The diagnostic criteria for SAO were defined as follows: patients who had one of the traditional clinical lacunar syndromes (including pure motor stroke, pure sensorimotor stroke, pure sensory stroke, ataxic hemiparesis, or clumsy hand dysarthria) along with brain imaging (CT or MRI) findings (infarction diameter <1.5 cm in the appropriate region) and did not show evidence of cerebral cortical dysfunction. Evidence of cardiac sources of embolism was absent, and large extracranial arteries showed a stenosis of $<50\%$ in an ipsilateral artery (14). ICH was defined according to World Health Organization criteria (13), and dICH was located at the following regions: putamen, caudate nucleus, internal capsule, thalamus, and brain stem. Cortical hemorrhage, deep intracerebral hemorrhage, intraventricular hemorrhage, prestroke modified Ranking Scale >2 , lack of data for hematoma volume, and hemorrhage resulting from trauma, underlying tumor, aneurysm, or arteriovenous malformation were excluded (15).



Risk Factor Definition

Hypertension was defined by SBP ≥ 140 mmHg and/or DBP ≥ 90 mmHg out of the acute phase or the use of pharmacological treatment for hypertension. PP was calculated as SBP–DBP, and MAP was calculated as DBP + 0.33 (SBP–DBP). Other risk factors were defined as follows: dyslipidemia (TC level ≥ 240 mg/dl, HDL-c level < 35 mg/dl, or the use of lipid-lowering agents), diabetes mellitus (fasting blood glucose level ≥ 120 mg/dl or current treatment with antidiabetic drugs), current or previous smoker (an individual who smoked at the time of stroke or had quit smoking within 1 year), or heavy alcohol consumption (≥ 5 standard alcoholic beverages per day). We also collected information on coronary artery disease (medical history of angina, myocardial infarction, coronary artery bypass graft, or percutaneous transluminal coronary angioplasty), and treatment with anticoagulant drugs (previously documented in medical files). The details and definitions have been described previously (16).

Data were obtained from interviews with patients, next of kin, and/or attending physicians or general practitioners. Fasting lipid levels, WBC count, hs-CRP, PLT count, and eGFR measurements

were carried out on venous blood samples obtained within 24 h of stroke occurrence in each participating center, using comparable procedures. eGFR was calculated using the Chronic Kidney Disease Epidemiology Collaboration creatinine equation with an adjusted coefficient of 1.1 for the Asian population (17, 18). BMI was calculated by dividing body weight in kilograms by the square of body length in meters (kg/m^2). WHtR was obtained by dividing the waist circumference (cm) by height (cm). The atherogenic index of plasma (AIP) is defined as the base 10 logarithm of the ratio of the concentration of TG to HDL-c; the non-HDL-c is defined as TC minus HDL-c; the atherogenic index (AI) is defined as the ratio of non-HDL-c to HDL-c; and the lipoprotein combine index (LCI) is defined as the ratio of $\text{TC} \times \text{TG} \times \text{LDL-c}$ to HDL-c (19).

Statistical Analysis

Parametric continuous variables were analyzed by the *t*-test, and results were presented as means with SD. Non-parametric variables were analyzed with the Wilcoxon rank-sum test, and results are presented as medians with interquartile range. Categorical variables are presented as proportions (*n*%), and intergroup differences were tested with the χ^2 test. Multivariable logistic regression was performed including demographic factors (age and sex) as well as a history of hypertension, SBP, DBP, history of diabetes mellitus, history of coronary heart disease, history of hypercholesterolemia, TG, TC, LDL-c, HDL-c, AIP, non-HDL-c, TC/HDL-c, LDL-c/HDL-c, AI, LCI, current or previous smoker, heavy alcohol consumption, BMI, WHtR, eGFR, PLT count, hs-CRP, and WBC count as covariates. SAO group is the reference group in evaluating odds ratios. The covariates above were analyzed by several models to avoid the selected factors concurring with each other. In model of pressure values (SBP, DBP, PP, and MAP), covariates included age, sex, history of coronary heart disease, current or previous smoker, heavy alcohol consumption, history of diabetes mellitus, TG, TC, HDL-c, BMI, PLT count, WBC count, and eGFR. In the model of traditional and nontraditional lipid profiles, covariates included age, sex, SBP, DBP, history of coronary heart disease, current or previous smoker, heavy alcohol consumption, history of diabetes mellitus, TG, TC, HDL-c, BMI, PLT count, WBC count, and eGFR. In the model of CRP, covariates included age, sex, SBP, DBP, history of coronary heart disease, current or previous smoker, heavy alcohol consumption, history of diabetes mellitus, TC, BMI, and eGFR. $P < 0.05$ on a two-sided test was considered as significant. Data were analyzed using SAS 9.4.

RESULTS

Of the 22,216 patients enrolled in the China National Stroke Registry, 18,580 patients had complete baseline information and agreed to participate in follow-up. Among them, 12,415 had IS and 5,136 had ICH. For IS patients, 955 without complete data of laboratory test and 10,325 for other types of IS were further excluded, leaving 1,135 SAO stroke patients included in the final analysis. For patients with ICH, after exclusion for other types of ICH, incomplete data of laboratory test and other reasons, 1,125 dICH patients were included for the comparison with SAO stroke (Figure 1).

TABLE 1 | Characteristics of the study population.

Characteristics	
Age, mean (SD), year	63.0 (12.1)
Sex, male, <i>n</i> (%)	1,436 (63.5)
History of hypertension, <i>n</i> (%)	1,546 (68.4)
Admission SBP, mean (SD), mmHg	158.4 (26)
Admission DBP, mean (SD), mmHg	92.5 (15.5)
Admission PP, mean (SD), mmHg	65.8 (19.5)
Admission MAP, mean (SD), mmHg	114.5 (17.3)
History of diabetes mellitus, <i>n</i> (%)	365 (16.2)
History of coronary heart disease, <i>n</i> (%)	38 (1.7)
History of anticoagulant drug, <i>n</i> (%)	26 (1.2)
Current smoker, <i>n</i> (%)	948 (42.0)
Heavy alcohol consumption, <i>n</i> (%)	79 (3.5)
History of dyslipidemia, <i>n</i> (%)	225 (10.0)
Admission LDL-c, median (IQR), mmol/l	2.7 (2.1–3.3)
Admission TG, median (IQR), mmol/l	1.4 (1.0–2.0)
Admission TC, median (IQR), mmol/l	4.6 (3.9–5.3)
Admission HDL-c, median (IQR), mmol/l	1.2 (1.0–1.4)
AIP, median (IQR)	0.1 –0.1–0.3
non-HDL-C, median (IQR)	3.3 (2.7–4.0)
LDL-c/HDL-c, median (IQR)	2.2 (1.7–2.9)
TC/HDL-c, median (IQR)	3.8 (3.1–4.71)
LCI, median (IQR)	13.8 (7.4–25.6)
AI, median (IQR)	2.8 (2.1–3.7)
BMI, mean (SD), kg/m^2	24.3 (3.9)
WHtR, mean (SD)	0.5 (0.1)
PLT count, median (IQR)	190 (149–232)
WBC count, median (IQR), $10^9/\text{l}$	7.5 (6.1–9.5)
eGFR, median (IQR), $\text{ml}/\text{min}/1.73 \text{ m}^2$	83.5 (67.6–96.8)

SBP, systolic blood pressure; DBP, diastolic blood pressure; PP, pulse pressure; MAP, mean arterial pressure; TG, triglyceride; TC, total cholesterol; LDL-c, low-density lipoprotein cholesterol; HDL-c, high-density lipoprotein cholesterol; AIP, atherogenic index of plasma; LCI, lipoprotein combine index; AI, atherogenic index; BMI, body mass index; WHtR, waist/height ratio; PLT count, platelet count; WBC count, white blood cell count; eGFR, estimated glomerular filtration rate; IQR, interquartile range; SD, standard deviation.

TABLE 2 | Univariable analysis between SAO stroke and dICH.

Risk factors	Univariable Analysis			
	SAO stroke (n = 1,135)	dICH (n = 1,125)	OR (95% CI)	P-value
Age, mean (SD), year	64.2 (11.8)	61.7 (12.3)	0.98 (0.98–0.99)	<0.01
Sex, male, n (%)	757 (66.7)	679 (60.4)	0.76 (0.64–0.90)	<0.01
History of hypertension, n (%)	756 (66.6)	790 (70.2)	1.18 (0.99–1.41)	0.07
Admission SBP, mean (SD), mmHg	150.9 (23.3)	165.9 (26.5)	1.02 (1.02–1.03)	<0.01
Admission DBP, mean (SD), mmHg	87.7 (13.2)	97.3 (16.0)	1.05 (1.04–1.05)	<0.01
Admission PP, mean (SD), mmHg	63.2 (17.9)	68.5 (20.6)	1.01 (1.01–1.02)	<0.01
Admission MAP, mean (SD), mmHg	108.8 (15.0)	102.2 (17.6)	1.04 (1.04–1.05)	<0.01
History of diabetes mellitus, n (%)	227 (24.4)	88 (7.8)	0.26 (0.20–0.34)	<0.01
History of coronary heart disease, n (%)	29 (2.6)	9 (0.8)	0.31 (0.15–0.65)	<0.01
Current smoker, n (%)	504 (44.4)	444 (39.5)	0.82 (0.69–0.97)	<0.01
Alcohol consumption, n (%)	29 (2.6)	50 (4.4)	1.77 (1.11–2.82)	0.02
History of dyslipidemia, n (%)	143 (12.6)	82 (7.3)	0.55 (0.41–0.73)	<0.01
Admission LDL-c, median (IQR), mmol/l	2.8 (2.2–3.3)	2.6 (2.0–3.2)	0.83 (0.76–0.91)	<0.01
Admission TG, median (IQR), mmol/l	1.5 (1.0–2.1)	1.3 (0.9–1.7)	0.85 (0.79–0.91)	<0.01
Admission TC, median (IQR), mmol/l	4.7 (4.0–5.5)	4.5 (3.9–5.2)	0.93 (0.87–0.99)	0.03
Admission HDL-c, median (IQR), mmol/l	1.14 (0.9–1.4)	1.25 (1.0–1.5)	2.04 (1.64–2.54)	<0.01
AIP, median (IQR)	0.1 (–0.1–0.3)	0.00 (–0.2–0.2)	0.28 (0.21–0.38)	<0.01
non-HDL-c, median (IQR)	3.5 (2.8–4.2)	3.2 (2.6–3.9)	0.85 (0.80–0.92)	<0.01
LDL-c/HDL-c, median (IQR)	2.4 (1.9–3.1)	2.1 (1.6–2.7)	0.69 (0.63–0.75)	<0.01
TC/HDL-c, median (IQR)	4.1 (3.3–4.9)	3.5 (2.9–4.3)	0.77 (0.72–0.83)	<0.01
LCI, median (IQR)	16.5 (8.8–29.6)	11.3 (6.2–21.1)	0.99 (0.99–1.00)	<0.01
AI, median (IQR)	3.1 (2.3–3.9)	2.5 (1.9–3.3)	0.77 (0.72–0.83)	<0.01
BMI, mean (SD) (kg/m ²)	24.6 (3.7)	24.1 (4.1)	0.97 (0.95–0.99)	<0.01
WHtR, mean (SD)	0.5 (0.1)	0.5 (0.1)	0.09 (0.03–0.31)	<0.01
PLT count, mean (SD), 10 ¹² /L	197 (3.4)	189 (2.7)		
Q1	269 (23.7)	297 (26.4)	0.92 (0.85–0.99)	0.02
Q2	281 (24.8)	297 (26.4)		
Q3	280 (24.7)	274 (24.4)		
Q4	305 (26.9)	257 (22.8)		
WBC count, median (IQR), 10 ⁹ /L	6.9 (5.8–8.4)	8.5 (6.5–10.9)		
Q1	345 (30.4)	224 (19.9)	1.60 (1.48–1.73)	<0.01
Q2	357 (31.5)	209 (18.6)		
Q3	280 (24.7)	283 (25.2)		
Q4	153 (13.5)	409 (36.4)		
eGFR, median (IQR), ml/min/1.73 m ²	80.7 (60.0–94.1)	85.82 (69.3–99.0)		
eGFR ≥ 90, median (IQR), ml/min/1.73 m ²	372 (32.8)	481 (42.8)	1	
eGFR < 90, median (IQR), ml/min/1.73 m ²	763 (67.2)	644 (57.2)	0.65 (0.55–0.78)	<0.01

SAO, small-artery occlusion; dICH, deep intracerebral hemorrhage; OR, odds ratio; CI, confidence interval; SBP, systolic blood pressure; DBP, diastolic blood pressure; PP, pulse pressure; MAP, mean arterial pressure; TG, triglyceride; TC, total cholesterol; LDL-c, low-density lipoprotein cholesterol; HDL-c, high-density lipoprotein cholesterol; AIP, atherogenic index of plasma; LCI, lipoprotein combine index; AI, atherogenic index; BMI, body mass index; WHtR, waist–height ratio; PLT count, platelet count; WBC count, white blood cell count; eGFR, estimated glomerular filtration rate; IQR, interquartile range; SD, standard deviation.

The average age of the included patients was 63.0 ± 12.1 years (male, 63.54%). Descriptive statistics of the whole study group are summarized in **Table 1**. Univariable and multivariable logistic regression analyses were performed to determine the association of risk factors with stroke type (**Tables 2, 3**). In univariable analysis (**Table 2**), patients with SAO were more likely to be older, male, to smoke, to have history of diabetes, coronary heart disease, and dyslipidemia, to have higher TG, TC, LDL-c, BMI,

WHtR, and PLT count and lower eGFR. Patients with dICH were more likely to be heavy alcohol consumers and have higher SBP, DBP, PP, MAP, HDL-c WBC count, and hs-CRP.

We further performed several models of multivariable analyses in case of the factors concurring with each other. In the model adjusting medical history of hypertension, diabetes mellitus, and dyslipidemia, age, smoking, and heavy alcohol consumption were not consistently significant (**Table S1**). In the

TABLE 3 | Multivariable regression analysis of indexes between SAO stroke and dICH.

Risk factors	Multivariable Analysis OR (95% CI)	P-value
Age	0.99 (0.98–1.00)	0.06
Sex, male	0.74 (0.58–0.94)	0.01
Admission SBP	1.01 (1.01–1.02)	<0.01
Admission DBP	1.03 (1.02–1.04)	<0.01
History of coronary heart disease	0.57 (0.25–1.33)	0.19
Current or previous smoker	0.74 (0.59–0.94)	0.01
Heavy alcohol consumption	1.52 (0.89–2.58)	0.12
History of diabetes mellitus	0.30 (0.22–0.40)	<0.01
Admission TG	0.89 (0.82–0.96)	<0.01
Admission TC	0.89 (0.82–0.97)	<0.01
Admission HDL-c	1.66 (1.30–2.13)	<0.01
BMI	0.96 (0.94–0.99)	<0.01
PLT count	0.84 (0.77–0.91)	<0.01
WBC count	1.61 (1.48–1.76)	<0.01
eGFR	–	
eGFR \geq 90 ml/min/1.73 m ²	1.00	
eGFR < 90 ml/min/1.73 m ²	0.77 (0.62–0.95)	0.02

SAO, small-artery occlusion; dICH, deep intracerebral hemorrhage; OR, odds ratio; CI, confidence interval; SBP, systolic blood pressure; DBP, diastolic blood pressure; TG, triglyceride; TC, total cholesterol; HDL-c, high-density lipoprotein cholesterol; BMI, body mass index; PLT quartiles, platelet quartiles; WBC quartiles, white blood cell quartiles; eGFR, estimated glomerular filtration rate.

model adjusting indexes of pressure and serum lipid instead of the medical histories, compared with univariable analysis, age, history of coronary heart disease, and heavy alcohol consumption were not significant (Table 3). Multivariable models for MAP and PP showed that higher MAP and PP were significantly related to dICH in accord with SBP and DBP (Tables S2, S3). Moreover, in the multivariable model for WHtR instead of BMI, higher WHtR was associated with SAO, which favored the result of BMI (Table S4).

In multivariable analysis models for traditional and non-traditional lipid profile, all results indicated that SAO patients are likely to have higher level of atherogenic lipid profile such as higher LDL-c, TC, and TG, as well as other non-traditional lipid profile such as AIP and lower HDL-c (Figure 2).

On the contrary, higher inflammation levels were associated with higher possibility of dICH. Our results showed that dICH patients have higher WBC count than SAO patients. To consolidate the conclusion, we further performed the subgroup analysis including 449 patients with available value of hs-CRP. Consistently, we found that higher hs-CRP level was associated with dICH (Table S5).

DISCUSSION

The main finding of our study is that SAO stroke and dICH exhibit different risk profiles although they share similar pathophysiological process of cerebral small vessels. In

comparison with previous studies, we included more detailed patient characteristics and found their significant roles in differentiating SAO stroke and dICH, such as traditional and non-traditional lipid profiles, inflammation levels, PLT count, BMI, WHtR, WBC count, hs-CRP, and eGFR in our study, which were rarely analyzed before. Thus, our work provides a more comprehensive view on the impact of risk factors in driving arteriolosclerosis into opposite ends.

In our study, history of hypertension and the specific pressure values (SBP, DBP, PP, and MAP) played a dominant role in dICH, which favored previous findings (7, 8). Contrary to hypertension, diabetes mellitus was associated with SAO stroke, which was also consistent with previous reports (19–21). Furthermore, we observed that elevated PLT count were more strongly associated with SAO stroke. Platelets play a key role in the development of IS via their role in evolution of atherosclerosis (22). In contrast, thrombocytopenia has been found to be associated with spontaneous intracerebral hemorrhage (23). In addition, PLT count have also been recorded as an important index for development and prognosis of ischemic and hemorrhagic stroke (24, 25).

Investigations remain limited by far on BMI or WHtR between SAO and dICH. In accordance with previous studies (26–29), our findings agreed that lower BMI and WHtR were more relevant to dICH. We hypothesize that the adipose tissue may play an important role in shifting the cerebral small vessel disease manifestations toward either ischemia or hemorrhage (28). Furthermore, we compared the role of various blood lipid parameters including traditional (TG, TC, LDL-c, and HDL-c) and non-traditional lipid profiles (AIP, non-HDL-c, TC/HDL-c, LDL/HDL-c, AI, and LCI) between dICH and SAO stroke. Numerous studies focused on the association between lipid profiles and stroke subtypes but yielded conflict results. The China Kadoorie Biobank study with 512,891 participants found that plasma concentrations of LDL-C and TG were positively associated with risk of IS and inversely associated with a risk of ICH. Moreover, plasma concentrations of HDL-C were inversely associated with risk of IS, but not with ICH. Furthermore, the causal relevance of LDL-C for both IS and ICH was confirmed by Mendelian randomization analyses in this study (30). However, two studies enrolled elderly adults and observed no association between LDL-C levels and the risk of ICH (31, 32). In Women's Health Study with 27,937 women enrolled, they reported that low LDL-C levels and low TG levels were associated with increased risk of hemorrhagic stroke, but no association between HDL-C levels and the risk of ICH was found. Most lipid profiles analyzed in our study were shown to significantly participate in differentiating SAO from dICH (33, 34). The analyses demonstrated that ICH patients tend to have lower level of atherogenic lipid profiles. It is supported by the histopathological studies demonstrating that lower cholesterol concentrations may increase permeability of the vessel walls (35, 36), causing arterionecrosis and microaneurysms, which is often found in ICH. AIP was shown to be a better marker to reflect increased cardiovascular disease risk than TC, LDL-c, HDL-c, and other nontraditional lipid profiles (37). Our results also showed

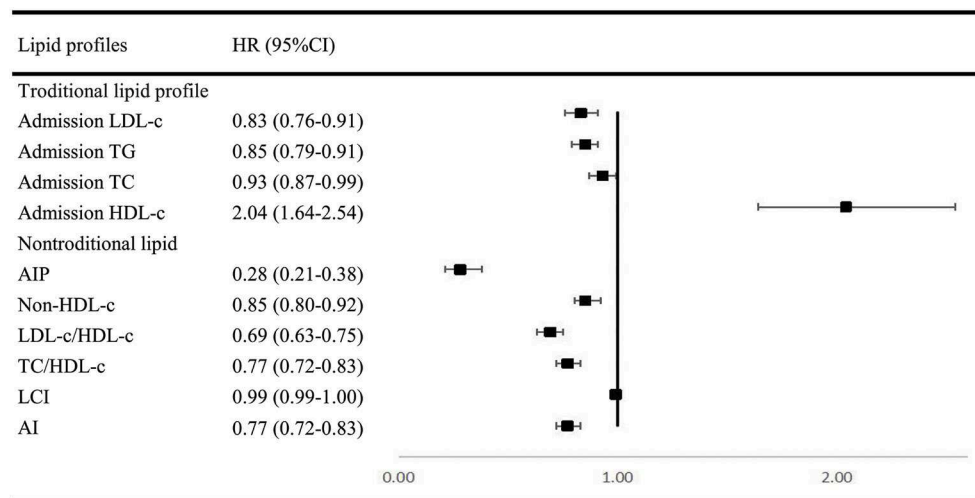


FIGURE 2 | Multivariable regression analysis of lipid profile between SAO stroke and dICH. SAO, small-artery occlusion; dICH, deep intracerebral hemorrhage; OR, odds ratio; CI, confidence interval; TG, triglyceride; TC, total cholesterol; LDL-c, low-density lipoprotein cholesterol; HDL-c, high-density lipoprotein cholesterol; AIP, atherogenic index of plasma; LCI, lipoprotein combine index; AI, atherogenic index.

that AIP may have a better capability in distinguishing SAO from dICH.

Evidence suggested that inflammation played a key role in the pathogenesis of cardiovascular diseases (38), and increased inflammation levels were related to the severity, disability, and mortality of both ischemic and hemorrhagic stroke (39). However, it was rarely considered in analysis as a differential characteristic between dICH and SAO stroke. Previous studies have shown that inflammatory cytokines were involved in the pathogenesis of cerebral small vessel disease and differing inflammatory pathways between ischemic and hemorrhagic manifestations of cerebral small vessel disease (40). As markers of inflammation, the increase in WBC count and hs-CRP was significantly associated with dICH compared with SAO group in our investigation. Thus, we proposed that the intensive systematic inflammation may involve in the weakening of vessel wall and lead to vessel rupture. However, due to the design of this cross-sectional study, it remains unknown whether the observed higher level of hs-CRP in ICH patients results from the inflammation or is just an acute phase reactant.

Our study has several limitations: First, the lack of MRI data about the presence/absence of neuroradiological markers of small vessel disease prevented us from further revealing the differences such as white matter hyperintensities and microbleed between SAO stroke and dICH, and may cause the confounders for selection of cases for the present study. Second, our study is a cross-sectional study, but the indexes such as blood pressure, lipid values, and WBC count were collected at the acute phase of stroke, which cannot fully reflect the long-term behavior. Third, because of the lack of a stroke-free control group, we cannot conclude but speculate that the observed associations might represent the causality in a way, and further relationships need to be investigated

in the future. Fourth, the lack of centralization for biological measures and radiological data may also cause the potential biases. Fifth, our study population is based on Asian population; therefore, the findings may not be generalized directly to all populations. Our study needs to be investigated in a longitudinal prospective cohort to further reveal the association between risk factors and different subtype of stroke occurrence. In addition, elucidating the differences in neuroradiological markers of small vessel disease by MRI is needed to deeply demonstrate the underlying mechanism between SAO and dICH in future investigation.

CONCLUSIONS

On the basis of the traditional risk profiles, this study adds evidence that higher PLT count, higher level of atherogenic lipid profile, and abnormal eGFR were in favor of SAO stroke as compared to dICH. Patients with dICH were more likely to have higher inflammation levels and higher HDL-c.

DATA AVAILABILITY STATEMENT

The datasets generated for this study are available on request to the corresponding author.

ETHICS STATEMENT

The studies involving human participants were reviewed and approved by the ethics committee of Beijing Tiantan Hospital. The patients/participants provided their written informed consent to participate in this study.

AUTHOR CONTRIBUTIONS

YW contributed to the conception and design of the study. ZC and JM contributed to manuscript drafting and critical revisions of the manuscript. JX, HQ, HZ, XM, and JJ contributed to the acquisition and analysis of data. YP and XX contributed to statistical analysis.

FUNDING

The China National Stroke Registry was funded by the Ministry of Sciences and Technology and the Ministry of Health of the People's Republic of China (Grant nos. 2006BA101A11, 2009CB521905, and 200902004) and the National Science Foundation (Grant no. 81071115). The current analysis of the CNSR data were supported by Beijing Novartis Pharma

Co, Ltd. In compliance with the Uniform Requirements, for manuscripts, established by the International Committee of Medical Journal Editors, Novartis did not impose any impediment, directly or indirectly, on the publication of the study's results.

ACKNOWLEDGMENTS

We would like to convey our appreciation to all patients who participated in this study.

SUPPLEMENTARY MATERIAL

The Supplementary Material for this article can be found online at: <https://www.frontiersin.org/articles/10.3389/fneur.2019.01213/full#supplementary-material>

REFERENCES

- Fisher CM. Lacunar strokes and infarcts. A review. *Neurology*. (1982) 32:871–6. doi: 10.1212/WNL.32.8.871
- Wardlaw JM, Smith C, Dichgans M. Mechanisms of sporadic cerebral small vessel disease: insights from neuroimaging. *Lancet Neurol*. (2013) 12:483–97. doi: 10.1016/S1474-4422(13)70060-7
- Ariesen MJ, Claus SP, Rinkel GJE, Algra A. Risk factors for intracerebral hemorrhage in the general population. a systematic review. *Stroke*. (2003) 34:2060–5. doi: 10.1161/01.STR.0000080678.09344.8D
- Fisher CM. Pathological observations in hypertensive cerebral hemorrhage. *J Neuropathol Exp Neurol*. (1971) 30:536. doi: 10.1097/00005072-197107000-00015
- Matsukawa H, Shinoda M, Fujii M, Takahashi O, Yamamoto D, Murakata A, et al. Factors associated with lobar vs. non-lobar intracerebral hemorrhage. *Acta Neurol Scand*. (2012) 126:116–21. doi: 10.1111/j.1600-0404.2011.01615.x
- Rodrigues MA, Samarasekera N, Lerpiniere C, Humphreys C, McCarron MO, White PM, et al. The Edinburgh CT and genetic diagnostic criteria for lobar intracerebral haemorrhage associated with cerebral amyloid angiopathy: model development and diagnostic test accuracy study. *Lancet Neurol*. (2018) 17:232–40. doi: 10.1016/S1474-4422(18)30006-1
- Morotti A, Paciaroni M, Zini A, Silvestrelli G, Del Zotto E, Caso V, et al. Risk profile of symptomatic lacunar stroke versus nonlobar intracerebral hemorrhage. *Stroke*. (2016) 47:2141–3. doi: 10.1161/STROKEAHA.116.013722
- Labovitz DL, Bodenalbala B, Hauser WA, Sacco RL. Lacunar infarct or deep intracerebral hemorrhage. *Neurology*. (2007) 68:606–8. doi: 10.1212/01.wnl.0000254619.98089.43
- Campean V, Neureiter D, Varga I, Runk F, Reiman A, Garlich C, et al. Atherosclerosis and vascular calcification in chronic renal failure. *Kidney Blood Press Res*. (2005) 28:280–9. doi: 10.1159/000090182
- Linden MD, Jackson DE. Platelets: pleiotropic roles in atherogenesis and atherothrombosis. *Int J Biochem Cell Biol*. (2010) 42:1762–6. doi: 10.1016/j.biocel.2010.07.012
- Ridker PM, MacFadyen JG, Everett BM, Libby P, Thuren T, Glynn RJ, CANTOS Trial Group. Relationship of C-reactive protein reduction to cardiovascular event reduction following treatment with canakinumab: a secondary analysis from the CANTOS randomised controlled trial. *Lancet*. (2018) 391:319–28.
- Hansson GK, Libby P. The immune response in atherosclerosis: a double-edged sword. *Nat Rev Immunol*. (2006) 6:508–19. doi: 10.1038/nri1882
- Stroke—1989. Recommendations on stroke prevention, diagnosis, and therapy. Report of the WHO Task Force on Stroke and other Cerebrovascular Disorders. *Stroke*. (1989) 20:1407. doi: 10.1161/01.STR.20.10.1407
- Adams HP Jr, Bendixen BH, Kappelle LJ, Biller J, Love BB, Gordon DL, et al. Classification of subtype of acute ischemic stroke. Definitions for use in a multicenter clinical trial. TOAST. Trial of Org 10172 in Acute Stroke Treatment. *Stroke*. (1993) 24:35–41. doi: 10.1161/01.STR.24.1.35
- Li Z, Zhao X, Wang Y, Wang C, Liu L, Shao X, et al. Association between seizures and outcomes among intracerebral hemorrhage patients: the China National Stroke Registry. *J Stroke Cerebrovasc Dis*. (2015) 24:455–64. doi: 10.1016/j.jstrokecerebrovasdis.2014.09.021
- Wang W, Lu J, Wang Y, Wang C, Wang Y, Hoff K, et al. Clinical characteristics, management, and functional outcomes in Chinese patients within the first year after intracerebral hemorrhage: analysis from China National Stroke Registry. *CNS Neurosci Ther*. (2012) 18:773–80. doi: 10.1111/j.1755-5949.2012.00367.x
- Teo BW, Xu H, Wang D, Li J, Sinha AK, Shuter B, et al. GFR estimating equations in a multiethnic Asian population. *Am J Kidn Dis*. (2011) 58:56–63. doi: 10.1053/j.ajkd.2011.02.393
- Levey AS, de Jong PE, El Nahas M, Astor BC, Matsushita K, Gansevoort RT, et al. The definition, classification, and prognosis of chronic kidney disease: a KDIGO Controversies Conference report. *Kidney Int*. (2011) 80:17–28. doi: 10.1038/ki.2010.483
- Jamrozik K, Broadhurst R, Anderson C, Stewart-Wynne E. The role of lifestyle factors in the etiology of stroke. A population-based case-control study in Perth, Western Australia. *Stroke*. (1994) 25:51–9. doi: 10.1161/01.STR.25.1.51
- Andersen K, Olsen T, Dehlendorff C, Kammersgaard L. Hemorrhagic and ischemic strokes compared: stroke severity, mortality, and risk factors. *Stroke*. (2009) 40:2068–72. doi: 10.1161/STROKEAHA.108.540112
- Kaplan E, Gottesman R, Llinas R, Marsh E. The Association between specific substances of abuse and subcortical intracerebral hemorrhage versus ischemic lacunar infarction. *Front Neurol*. (2014) 5:174. doi: 10.3389/fneur.2014.00174
- del Zoppo GJ. The role of platelets in ischemic stroke. *Neurology*. (1998) 51:9–14. doi: 10.1212/WNL.51.3_Suppl_3.S9
- Rajasee V, Brown DM, Tuhim S. Coagulation abnormalities following primary intracerebral hemorrhage. *J Stroke Cerebrovasc Dis*. (2004) 13:47–51. doi: 10.1016/j.jstrokecerebrovasdis.2004.01.002
- Maydadomac F, Misirli H, Yilmaz M. Prognostic role of mean platelet volume and platelet count in ischemic and hemorrhagic stroke. *J Stroke Cerebrovasc Dis*. (2010) 19:66–72. doi: 10.1016/j.jstrokecerebrovasdis.2009.03.003
- Du J, Wang Q, He B, Liu P, Chen J, Quan H, et al. Association of mean platelet volume and platelet count with the development and prognosis of ischemic and hemorrhagic stroke. *Int J Lab Hematol*. (2016) 38:233–9. doi: 10.1111/ijlh.12474
- Kroll ME, Green J, Beral V, Sudlow CL, Brown A, Kirichek O, et al. Adiposity and ischemic and hemorrhagic stroke: prospective study in women and meta-analysis. *Neurology*. (2016) 87:1473–81. doi: 10.1212/WNL.0000000000003171

27. Bazzano L, Gu D, Whelton MR, Wu X, Chen CS, Duan X, et al. Body mass index and risk of stroke among Chinese men and women. *Ann Neurol.* (2010) 67:11–20. doi: 10.1002/ana.21950
28. Lioutas VA, Beiser A, Himali J, Aparicio H, Romero JR, DeCarli C, et al. Lacunar infarcts and intracerebral hemorrhage differences: a nested case-control analysis in the FHS (Framingham Heart Study). *Stroke.* (2017) 48:486–9. doi: 10.1161/STROKEAHA.116.014839
29. Biffi A, Cortellini L, Nearnberg CM, Ayres AM, Schwab K, Gilson AJ, et al. Body mass index and etiology of intracerebral hemorrhage. *Stroke.* (2011) 42:2526–30. doi: 10.1161/STROKEAHA.111.617225
30. Sun L, Clarke R, Bennett D, Guo Y, Walters RG, Hill M, et al. Causal associations of blood lipids with risk of ischemic stroke and intracerebral hemorrhage in Chinese adults. *Nat Med.* (2019) 25:569–74. doi: 10.1038/s41591-019-0366-x
31. Wieberdink RG, Poels MMF, Vernooij MW, Koudstaal PJ, Hofman A, van der LA, et al. Serum lipid levels and the risk of intracerebral hemorrhage: the Rotterdam Study. *Arterioscler Thromb Vasc Biol.* (2011) 31:2982–9. doi: 10.1161/ATVBAHA.111.234948
32. Bonaventure A, Kurth T, Pico F, Barberger-Gateau P, Ritchie K, Stapf C, et al. Triglycerides and risk of hemorrhagic stroke vs. ischemic vascular events: the Three-City Study. *Atherosclerosis.* (2010) 210:243–8. doi: 10.1016/j.atherosclerosis.2009.10.043
33. Iso H, Jacobs DR, Wentworth D, Neaton JD, Cohen JD. Serum cholesterol levels and six-year mortality from stroke in 350,977 men screened for the multiple risk factor intervention trial. *N Engl J Med.* (1989) 320:904–10. doi: 10.1056/NEJM198904063201405
34. Puddey IB. Low serum cholesterol and the risk of cerebral hemorrhage. *Atherosclerosis.* (1996) 119:1–6. doi: 10.1016/0021-9150(95)05634-3
35. Ooneda G, Yoshida Y, Suzuki K, Shinkai H, Hori S, Kobori K, et al. Smooth muscle cells in the development of plasmatic arterionecrosis, arteriosclerosis and arterial contraction. *Blood Vessels.* (1978) 15:148–56. doi: 10.1159/000158160
36. Konishi M, Iso H, Komachi Y, Iida M, Shimamoto T, Jacobs DR Jr, et al. Associations of serum total cholesterol, different types of stroke, and stenosis distribution of cerebral arteries. The Akita Pathology Study. *Stroke.* (1993) 24:954–64. doi: 10.1161/01.STR.24.7.954
37. Niroumand S, Khajedaluae M, Khademrezaian M, Maryam A, Mohammadreza J, Gholamhasan K, et al. Atherogenic Index of Plasma (AIP): a marker of cardiovascular disease. *Med J Islamic Republic of Iran.* (2015) 29:240.
38. Hansson GK. Mechanisms of disease: inflammation, atherosclerosis, and coronary artery disease. *Nature.* (2005) 306:5.
39. Yu S, Arima H, Heeley E, Delcourt C, Krause M, Peng B, et al. White blood cell count and clinical outcomes after intracerebral hemorrhage: the INTERACT2 trial. *J Neurol Sci.* (2016) 361:112–6. doi: 10.1016/j.jns.2015.12.033
40. Shoamanesh A, Preis SR, Beiser AS, Vasan RS, Benjamin EJ, Kase CS, et al. Inflammatory biomarkers, cerebral microbleeds, and small vessel disease: Framingham Heart Study. *Neurology.* (2015) 84:825–32. doi: 10.1212/WNL.00000000000001279

Conflict of Interest: The authors declare that the research was conducted in the absence of any commercial or financial relationships that could be construed as a potential conflict of interest.

Copyright © 2019 Chen, Mo, Xu, Qin, Zheng, Pan, Meng, Jing, Xiang and Wang. This is an open-access article distributed under the terms of the Creative Commons Attribution License (CC BY). The use, distribution or reproduction in other forums is permitted, provided the original author(s) and the copyright owner(s) are credited and that the original publication in this journal is cited, in accordance with accepted academic practice. No use, distribution or reproduction is permitted which does not comply with these terms.



Application of an Imaging-Based Sum Score for Cerebral Amyloid Angiopathy to the General Population: Risk of Major Neurological Diseases and Mortality

Pinar Yilmaz^{1,2}, Mohammad Arfan Ikram¹, Mohammad Kamran Ikram^{1,3}, Wiro J. Niessen^{2,4}, Anand Viswanathan⁵, Andreas Charidimou⁵ and Meike W. Vernooij^{1,2*}

¹ Department of Epidemiology, Erasmus Medical Center, Rotterdam, Netherlands, ² Department of Radiology and Nuclear Medicine, Erasmus Medical Center, Rotterdam, Netherlands, ³ Department of Neurology, Erasmus Medical Center, Rotterdam, Netherlands, ⁴ Department of Medical Informatics, Erasmus Medical Center, Rotterdam, Netherlands, ⁵ Department of Neurology, Massachusetts General Hospital Stroke Research Center, Harvard Medical School, Boston, MA, United States

OPEN ACCESS

Edited by:

Nishant K. Mishra,
Icahn School of Medicine at Mount
Sinai, United States

Reviewed by:

Cheryl R. McCreary,
University of Calgary, Canada
Mark Fisher,
University of California, Irvine,
United States

*Correspondence:

Meike W. Vernooij
m.vernooi@erasmusmc.nl

Specialty section:

This article was submitted to
Stroke,
a section of the journal
Frontiers in Neurology

Received: 23 August 2019

Accepted: 18 November 2019

Published: 06 December 2019

Citation:

Yilmaz P, Ikram MA, Ikram MK,
Niessen WJ, Viswanathan A,
Charidimou A and Vernooij MW (2019)
Application of an Imaging-Based Sum
Score for Cerebral Amyloid
Angiopathy to the General Population:
Risk of Major Neurological Diseases
and Mortality. *Front. Neurol.* 10:1276.
doi: 10.3389/fneur.2019.01276

Objective: To assess the relation between a sum score of imaging markers indicative of cerebral amyloid angiopathy (CAA) and cognitive impairment, stroke, dementia, and mortality in a general population.

Methods: One thousand six hundred twenty-two stroke-free and dementia-free participants of the population-based Rotterdam Study (mean age 73.1 years, 54.3% women) underwent brain MRI (1.5 tesla) in 2005–2011 and were followed for stroke, dementia and death until 2016–2017. Four MRI markers (strictly lobar cerebral microbleeds, cortical superficial siderosis, centrum semiovale perivascular spaces, and white matter hyperintensities) were combined to construct the CAA sum score, ranging from 0 to 4. Neuropsychological testing measured during the research visit closest to scan date were used to assess general cognitive function and cognitive domains. The associations of the CAA sum score with cognition cross-sectionally and with stroke, dementia, and mortality longitudinally were determined using linear regression and Cox proportional hazard modeling adjusted for age, sex, hypertension, cholesterol, lipid lowering medication, atrial fibrillation, antithrombotic medication and APOE-ε2/ε4 carriership. Additionally, we accounted for competing risks of death due to other causes for stroke and dementia, and calculated absolute risk estimates.

Results: During a mean follow-up of 7.2 years, 62 participants suffered a stroke, 77 developed dementia and 298 died. Participants with a CAA score of 1 showed a lower Mini-Mental-State-Exam (fully-adjusted mean difference -0.21 , 95% CI $(-0.42-0.00)$) compared to a score of 0. In general, for increased CAA scores we saw a lower g-factor. The age and sex-adjusted hazard ratios (HRs) per point increase of the CAA score were 1.41 for stroke (95% CI, 0.99–2.00), 1.19 for dementia (95% CI, 0.86–1.65), and 1.26 for mortality (95% CI, 1.07–1.48). The results for dementia and stroke risk did not differ after correcting for the competing risk of death. For all outcomes, higher CAA scores showed higher absolute risk estimates over 10 years.

Conclusions: Our results suggest that in this community-dwelling population, a higher CAA score is related to cognitive impairment and a higher risk of stroke, dementia, and death. The composite CAA score can be used to practically quantify the severity of vascular brain injury.

Keywords: cerebral small vessel disease, cerebral amyloid angiopathy, sum score, MRI, cognition, stroke, dementia, mortality

INTRODUCTION

Cerebral amyloid angiopathy (CAA) is a frequent form of sporadic cerebral small vessel disease caused by accumulation of amyloid- β in leptomeningeal and cortical vessels and capillaries (1, 2). The pathogenesis of CAA is complex and its consequences can result in cognitive impairment, dementia and stroke with a high recurrence rate of intracerebral hemorrhages (3, 4).

Brain imaging markers that reflect parenchymal damage caused by small vessel brain injury have shown to be useful in a clinical setting to diagnose CAA (2, 5). These markers visible on magnetic resonance imaging (MRI) include lobar cerebral microbleeds (CMB), cortical superficial siderosis (cSS), centrum semiovale perivascular spaces (CSO-PVS) and white matter hyperintensities of presumed vascular origin (henceforth WMH) (6, 7). Several markers individually are thought to reflect different types of small vessel disease. For CAA, cSS has shown to be highly indicative as a marker in not only patient cohorts, but also in population-based studies (8–10). Previous studies have used these individual CAA markers to determine their relation to neurological outcomes (stroke and dementia) and mortality in both healthy and diseased populations (9, 11–13).

Given that shared risk factors and pathophysiological pathways of CAA markers are known to overlap, and that often CAA patients have more than one of the brain imaging markers present, a recent study developed a composite CAA score by combining all four markers (CMB, cSS, CSO-PVS and WMH) (14). The authors concluded that this composite score may better reflect the overall CAA-related small vessel disease burden in the brain. Such composite scores reflecting CAA disease burden could be used in clinical practice or research settings (2, 14).

In a recent study, an association between the proposed CAA sum score and the prediction of dementia conversion in patients with probable CAA in absence of intracranial hemorrhage has been reported (15). Other studies in patients with CAA have shown that higher CAA scores are correlated with reduced global brain connectivity (16), and that patients who first present with transient focal neurological episodes have higher CAA scores than those who first present with cognitive complaints (17). In a patient population with ischemic cardioembolic stroke or transient ischemic attack (TIA) and non-valvular atrial fibrillation, patients who did not show improvement in their cognitive assessment in 12 months also had an increased CAA score (18).

Increasing evidence for the presence of subclinical CAA in the general population has been supported by high prevalence of lobar microbleeds identified in individuals over the age of 60 years, and the link with determinants such as APOE genotype

similar to those found in CAA patients (4, 19–22). Though evidence is at present circumstantial, it is a logical next step to study whether presence of CAA markers in the general population leads to an increased risk of neurological events as well. This was recently shown for presence of microbleeds, with increased risk of cognitive decline, stroke, dementia and mortality (23–26). Despite the clear clinical potential of the developed CAA sum score, its correlations with major neurological outcomes and death have not yet been assessed in a general population. We therefore used data from the population-based Rotterdam Study to investigate the CAA score based on the four imaging markers in relation to cognitive status and risk of stroke, dementia, and mortality.

MATERIALS AND METHODS

Study Participants

This study was conducted in the Rotterdam Study, a prospective population-based cohort study in which participants aged ≥ 45 years and living in the Ommoord district are examined and followed for various diseases (27). Imaging of the brain was incorporated in the study protocol from August 2005 onwards (28). For the present study, eligible participants of the fifth visit of the first wave (Rotterdam Study I-5), and second visit of the second wave (Rotterdam Study II-2) were included. 2015 out of 2,376 eligible participants (84.8%) underwent MRI in the period between 2005 and 2012. Participants were excluded if they had insufficient quality scans or missing sequences for ratings ($n = 108$), scans with missing PVS and CMB ratings ($n = 94$), and scans with MRI-defined large cortical infarcts ($n = 53$). In addition, participants without informed consent to access medical records and hospital discharge letters ($n = 27$) and if diagnosed with stroke or dementia or had incomplete follow-up for stroke and dementia diagnoses at time of MRI scan were excluded ($n = 111$). This resulted in 1,622 participants free from stroke and dementia with brain imaging data available for our analyses (**Supplementary Figure 1**).

The institutional review board (Medical Ethics Committee) approved the Rotterdam Study according to the Population Study Act, executed by the Ministry of Health, Welfare and Sports of the Netherlands. All participants gave written informed consent.

MRI Scan Protocol and Assessment of CAA Imaging Markers

MRI of the brain was performed on a 1.5 tesla MRI scanner (GE-Healthcare). We acquired four high-resolution axial sequences without administering contrast material: T1-weighted sequence,

proton density-weighted sequence, fluid-attenuated inversion recovery sequence and T2*-weighted gradient-recalled-echo sequence. Detailed information of the imaging protocol has been described elsewhere (28).

Trained research physicians rated the presence, number and location of CMB and PVS, and the presence of cSS and cortical infarcts on MRI. CMB were defined as focal areas <10 mm of very low signal intensity and rated on T2*-weighted imaging. We categorized CMB distribution based on their location in the brain into strictly lobar, lobar, and deep microbleeds. Strictly lobar microbleeds restricted to cortical gray matter and subcortical white matter, whereas lobar microbleeds could present with or without deep microbleeds. Cortical superficial siderosis was defined as linear hypointensities with gyriform patterns over the cerebral cortex on T2*-weighted images (8) PVS were defined as linear, ovoid or round-shaped hyperintensities of ≥ 1 and <3 mm and counted in the centrum semiovale, basal ganglia, hippocampi and midbrain on proton density-weighted images (29) PVS were counted on a single, predefined slice in the centrum semiovale (the slice 1 cm above the uppermost part of the lateral ventricles) and basal ganglia (the slice with the anterior commissure). For the hippocampi and midbrain, all PVS were counted in the anatomical areas. For this study we only used CSO-PVS and categorized the PVS in a validated visual rating scale of 0 to 4, defined as 0=no PVS; 1=<10 PVS; 2=11–20 PVS; 3=21–40 PVS and 4=>40 PVS (30).

Quantitative measurements of WMH were obtained using a validated automated segmentation method (31). Intracranial volume (ICV) was defined as the summation of gray matter, white matter, and cerebrospinal fluid. Cortical infarcts were defined as focal lesions with tissue loss showing involvement of cortical gray matter.

CAA Score

A simplified version of the CAA sum score (henceforth referred to as the CAA score) proposed by Charidimou et al. consisted of scoring the presence of strictly lobar CMB, cSS, CSO-PVS, and WMH, with a total score that ranged from 0 to 4 (**Figure 1**) (14). One point was given to the CAA score for presence of strictly lobar microbleeds and another point was given if any cSS was present. PVS categories of ≥ 21 CSO-PVS were awarded with one point to the score. We computed WMH quartiles after dividing total WMH volume by ICV. WMH burden in third or fourth quartiles were awarded with a point to the score.

Modified Boston Criteria Score

In clinical practice, the modified Boston criteria is a tool to aid diagnose of CAA in patients. Therefore, we also explored the application of the modified Boston criteria in our population, and its relation with clinical outcomes. To operationalize this, the modified Boston criteria score was computed as an ordinal score ranging from 0 to 2. One point was given to this score if a single lobar microbleed was present or if cSS was present (representing possible CAA in the modified Boston criteria) (5). Two points were given to the modified Boston score if multiple lobar or cerebellar microbleeds were present or if a single lobar

microbleed and cSS were present (i.e., probable CAA in the modified Boston criteria).

Assessment of Cognitive Functioning

The cognitive assessment at one time-point, during the research visit closest to MRI date, included Mini-Mental State Examination (MMSE), letter-digit-substitution task (LDST), word fluency test (WFT), Stroop test, 15-word verbal learning test (15-WLT) and Perdue Pegboard test. For global cognition, we computed a standardized composite score (g-factor) with principal component analysis on the adjusted Stroop interference subtask, LDST, WFT, delayed recall of the 15-WLT, and Perdue Pegboard). The g-factor explained 43.1% of the total variance in cognitive test scores in our population. We combined different tests to construct compound scores for executive function (average Z-score of Stroop interference subtask, LDST, and WFT), information processing speed (average Z-score of Stroop reading and color-naming subtask, and LDST), memory (average Z-score of immediate and delayed recall of the 15-WLT), and motor speed (average Z-score of Perdue Pegboard test). New Z-scores were calculated for each compound score.

The median time between cognitive assessment and the MRI scan was 0.4 years (interquartile range: 0.1–1.0 years).

Assessment of Stroke

History of stroke was assessed at study entry using home interviews and reviewing medical records. Stroke was defined as a syndrome of rapidly advancing clinical signs of focal or global disturbance of cerebral function lasting ≥ 24 h or cause death with no apparent cause other than of vascular origin, in accordance with World Health Organization criteria. Continuous monitoring for occurrence of stroke was realized through automated linkage of general practitioners' (GPs) files with the study database (32). Regular checking of medical files by contacting their treating physicians were done for participants who moved out of the district or into nursing homes. Research physicians reviewed all potential stroke cases using hospital discharge letters, information from GPs and from nursing home physicians. An experienced vascular neurologist verified the stroke diagnoses, these were classified as ischemic or hemorrhagic based on neuroimaging reports or hospital discharge letters and unspecified if these were absent.

Follow-up started on the date that participants received brain imaging. Participants were followed until date of stroke occurrence, date of death, date of last contact in case of loss to follow-up, or January 1st 2016, whichever came first. Follow-up was complete for 11564.8 (96.9%) of potential person-years.

Assessment of Dementia

Participants were screened for dementia at baseline and during visits to the study center for incident and prevalent dementia. They underwent the MMSE and the Geriatric Mental Schedule (GMS). Subjects with MMSE<26 or GMS score>0 underwent further investigation and informant interview including the Cambridge Examination for Mental Disorders of the Elderly. Standard criteria were used for dementia (Diagnostic and Statistical Manual of Mental Disorders, version III, Revised),

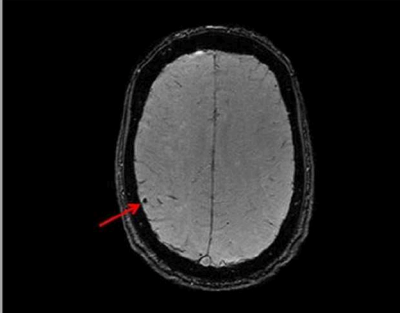
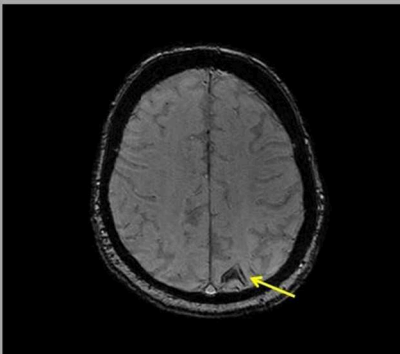
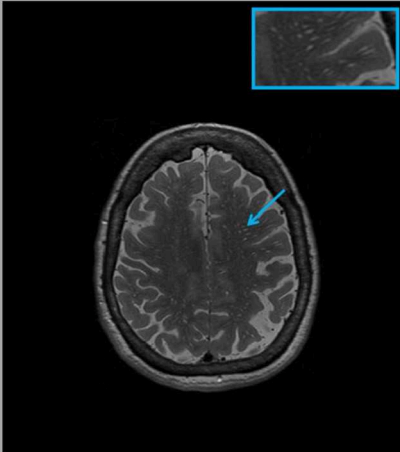
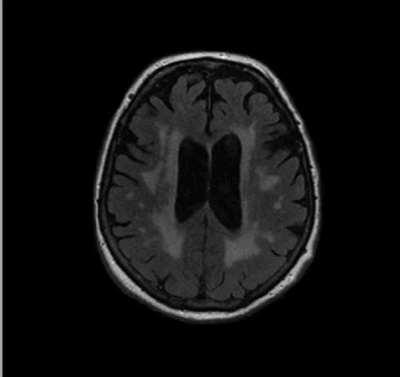
MRI marker definitions, categories, and points	MRI examples of CAA markers
<p><u>Strictly lobar cerebral microbleeds</u></p> <ul style="list-style-type: none"> Focal areas <10 mm of very low signal intensity, rated on T2*-weighted imaging and restricted to cortical gray matter and subcortical white matter. Presence of ≥ 1 strictly lobar microbleed(s): 1 point. 	
<p><u>Cortical superficial siderosis</u></p> <ul style="list-style-type: none"> Linear hypointensities with gyriform patterns over the cerebral cortex on T2*-weighted images. Presence of cortical superficial siderosis: 1 point. 	
<p><u>Perivascular spaces in centrum semiovale</u></p> <ul style="list-style-type: none"> Linear, ovoid or round-shaped hyperintensities of ≥ 1 mm and <3 mm on proton density-weighted images. Presence of ≥ 21 perivascular spaces in centrum semiovale: 1 point. Figure demonstrates perivascular spaces of various sizes bilaterally in the centrum semiovale. The arrow is pointing to a cluster of perivascular spaces in left centrum semiovale and the box in the top left corner is zoomed in to show this region in detail. 	
<p><u>White matter hyperintensities</u></p> <ul style="list-style-type: none"> Quantitative measurements of hyperintensities on fluid-attenuated inversion recovery sequence with validated automated segmentation method.(31) White matter hyperintensities were divided by intracranial volume and quartiles computed. White matter hyperintensities in 3rd and 4th quartiles: 1 point. 	

FIGURE 1 | Magnetic Resonance Imaging (MRI) features of the cerebral amyloid angiopathy (CAA) score.

Alzheimer's disease (National Institute of Neurological and Communicative Disorders and Stroke-Alzheimer's Disease and Related Disorders Association), and vascular dementia (National Institute of Neurological Disorders and Stroke and Association Internationale pour la Recherche et l'Enseignement en Neurosciences). Continuous monitoring for dementia was accomplished through electronic linkage of the center with medical records from GPs and the regional institute for outpatient mental health care. Cognitive testing and clinical neuroimaging were used, if available, to diagnose dementia subtypes. Final diagnosis was made according to international criteria and established by a consensus panel led by a consultant neurologist (33).

Incident dementia follow-up started on the date that participants came for brain MRI. Follow-up of dementia was until January 1st 2016, participants were censored at date of dementia diagnosis, death, loss to follow-up, whichever came first. Until January 1st 2016, follow-up was complete for 11273.6 (94.9%) of potential person-years.

Assessment of Mortality

Information on vital status of participants was collected from municipal health authorities in Rotterdam and updated for all-cause mortality on a monthly basis in the Rotterdam Study. Continuous reporting for incident events was achieved through automatic linkage of GPs files and verified by checking medical records to gather information on cause of death.

Participants were followed up from date of MRI scan until date of death, loss to follow-up or June 16th 2017, whichever came first. Follow-up was complete for 12110.2 (100%) of potential person-years.

Assessments of Covariates

Participants were interviewed during center visits preceding brain MRI, and underwent laboratory and physical examinations for information on demographic, genetic and cardiovascular risk factors.

History of TIA and coronary heart disease, atrial fibrillation, diabetes mellitus, hypertension, serum total cholesterol, blood pressure and antithrombotic and lipid lowering medication, smoking, *APOE*- ϵ 2/ ϵ 4 carriership, and education were used as covariates in this study. Definitions of included variables are presented in the online-only **Supplementary Material**.

Statistical Analysis

Differences in baseline variables between CAA scores were assessed using chi-square test, Fisher's exact test or ANOVA. 5-fold multiple imputations were used for missing covariates [ranging from 0.001% (hypertension) to 10.6% (atrial fibrillation)] based on determinants, outcome status, and follow-up time. Distribution of covariates in imputed and non-imputed datasets showed no differences.

CAA scores of 3 and 4 occurred infrequently and were therefore combined. We investigated the CAA score and modified Boston criteria score in an ordinal manner and continuously in our analyses. Superficial siderosis and WMH were the strongest determinants amongst the individual CAA

markers. We evaluated the dependency of the score on cSS and WMH by separately excluding one of the markers from the score, resulting in a maximum score of 3 in repeated analyses.

Multiple linear regression models were applied to investigate the cross-sectional association between the combined CAA score and cognitive functioning. Cox proportional-hazards models were used to investigate the association between the combined CAA score, the modified Boston criteria score and individual CAA markers with the risk of stroke, dementia, or mortality. All models were corrected for age and sex (model 1). Additionally, we corrected for hypertension, cholesterol, lipid lowering and antithrombotic medication, history of atrial fibrillation, and *APOE*- ϵ 2/ ϵ 4 carriership based on literature (model 2) (1, 3). The proportional-hazards assumption was tested using Schoenfeld residuals and no violations were identified. Further, Fine-Gray modeling was used to perform competing risk analyses by modeling subdistribution hazards to assess mortality as a competing risk for stroke and dementia (34). Goodness-of-fit tests revealed no linear, quadratic or log time-varying effects of categorical and continuous CAA score ($p > 0.1$ for all analyses) for the Fine-Gray models. After adjusting for model 2, absolute risks of stroke and dementia were estimated up to 10 years with Fine-Gray modeling and for mortality with Cox modeling according to the CAA score. We used bootstrap resampling ($n = 5,000$) to estimate confidence intervals of the absolute risk estimates. Models did not converge for 1-year absolute risk estimates of stroke and dementia and 2-year risk estimates of stroke, due to low number of incident events and were excluded.

We studied the relation of the CAA score with subgroups of the neurological outcomes and mortality, namely ischemic and hemorrhagic stroke, Alzheimer's disease, and cardiovascular mortality. Finally, we explored non-linear effects of age in our models by adding age-squared or natural cubic splines with 3 degrees of freedom.

All analyses were performed using statistical software packages SPSS (version 24.0) and R using *cmprsk* (35), *riskRegression* (36), and *nlme* (37) packages (version 3.5.2, R Foundation for Statistical Computing, R Core Team (38), Vienna, Austria). The significance threshold was set at $P < 0.05$. The Strengthening the Reporting of Observational Studies in Epidemiology statement was used as guideline (39).

RESULTS

Baseline Characteristics

Characteristics of the study population are shown in **Table 1**. Of the total of 1,622 participants, 54.3% were women and the average age at baseline was 73.1 years (SD 7.6). The majority of the participants had a CAA score of 1 ($n = 753$) and only one participant had a score of 4. More men than women had scores of 1 and 2, and women more often had CAA scores of 0 and 3 ($p = 0.002$). The MMSE score ranged between 12.0 and 30.0 (median 28.0). Mean follow-up time was 7.2 years for stroke, dementia and death. In our study, 62 participants suffered from a stroke, 77 developed dementia and 298 died.

TABLE 1 | Baseline characteristics of the study population.

	All participants, <i>N</i> = 1622
Age, years	73.1 (7.6)
Female sex, <i>n</i>	880 (54.3)
History of transient ischemic attack, <i>n</i>	110 (6.8)
History of coronary heart disease, <i>n</i>	146 (9.0)
History of atrial fibrillation [†] , <i>n</i>	86 (5.9)
History of diabetes mellitus [†] , <i>n</i>	185 (11.6)
Hypertension [†] , <i>n</i>	1,276 (78.8)
Systolic blood pressure [†] , mmHg	148.5 (20.7)
Diastolic blood pressure [†] , mmHg	82.5 (10.8)
Body mass index, kg/m ²	27.4 (3.8)
Total cholesterol [†] , mmol/L	5.5 (1.0)
Blood pressure lowering medication [†] , <i>n</i>	756 (46.7)
Antithrombotic medication [†] , <i>n</i>	454 (28.1)
Serum lipid lowering medication [†] , <i>n</i>	441 (27.3)
Smoking status [†] , <i>n</i>	
Never	513 (31.9)
Current	221 (13.7)
Former	875 (54.4)
APOE-ε2/ε4 carrier [†] , <i>n</i>	643 (40.5)
Education [†] , years	12.3 (3.7)
Imaging markers	
Strictly lobar cerebral microbleeds, <i>n</i>	284 (17.5)
Cortical superficial siderosis, <i>n</i>	10 (0.6)
Centrum semiovale perivascular spaces, <i>n</i>	1,490 (93.0)
0	113 (7.0)
≤10	1,120 (69.1)
≥11–20	316 (19.5)
≥21–40	73 (4.5)
WMH, mL*	4.4 [2.4–9.1]
First quartile	0.4–2.4
Second quartile	2.5–4.4
Third quartile	4.5–9.1
Fourth quartile	9.2–135.1

Non-imputed values are means (standard deviation) or numbers (valid percentages).

*Intracranial volume-corrected white matter hyperintensities (WMH) shown in median and interquartile range with separate quartile ranges.

[†]Data was missing for the following variables: history of atrial fibrillation (10.6%), history of diabetes mellitus (1.8%), hypertension (0.1%), systolic blood pressure (0.1%), diastolic blood pressure (0.5%), total cholesterol (0.4%), smoking status (0.8%), blood pressure lowering medication (0.2%), antithrombotic medication (0.6%), serum lipid lowering medication (0.5%), APOE-ε2/ε4 carriership (2.2%), and education (1.9%).

Association of CAA Score With Cognitive Functioning

Participants with a CAA score of 1 showed a significant lower MMSE after adjustments for cardiovascular factors and APOE-ε2/ε4 carriership compared to those with a score of 0 (mean difference −0.21, 95% CI (−0.42–0.00), **Figure 2**). An increasing CAA score related to a lower g-factor, yet none of the associations with g-factor were significant.

Overall, the associations of cognitive domains were also not significant, only for the memory domain, having a CAA score of 1 compared to a score of 0 showed a significant impairment persisting after further adjustments in model 2 (**Figure 3**).

Association of CAA Score With Stroke, Dementia, and Mortality

Higher CAA scores were related to higher HRs for stroke, dementia and mortality (**Table 2**). After further adjustments in model 2, having a score of 1 remained significant for stroke. Risk for developing dementia was highest for participants with CAA scores of 3–4 and remained significant after correction in model 2 [HR 3.25, 95% CI (1.00–10.54)]. When comparing subjects with a CAA score of 2 compared to a score of 0, associations were seen with mortality after additional adjustments for cardiovascular risk factors and APOE-ε2/ε4 carriership.

Excluding cSS from the combined CAA score attenuated associations of the scores for all outcomes and only remained significant for score 1 and MMSE and score 1 and stroke after further adjustments (model 2, **Table 3** and **Supplementary Table 2**). After excluding WMH from the CAA score, all associations again attenuated and none remained significant (**Supplementary Tables 3, 4**).

Association of the Modified Boston Criteria Score With Stroke, Dementia, and Mortality

The modified Boston criteria score showed higher risk for developing dementia with a score of 2 (probable CAA) and for death with a score of 1 (possible CAA) after adjusting for cardiovascular risk factors and APOE-ε2/ε4 carriership (**Supplementary Table 5**). The HRs of the Boston criteria score were lower compared to the CAA score, particularly for stroke.

Association of Individual CAA MRI Markers With Stroke, Dementia, and Mortality

CSO-PVS, cSS, and WMH were related to all outcomes (**Table 4**). Strictly lobar microbleeds were only related with mortality. Ten participants had superficial siderosis and this marker showed the highest risk among all markers for all outcomes. Participants with cSS had a 2.2–5.5 times higher risk of developing an event in our population. These relations remained significant for stroke and mortality after correcting for cardiovascular risk factors and APOE-ε2/ε4 carriership. Other significant associations were found for WMH and stroke (model 2).

Association of CAA Score With Stroke and Dementia Adjusted for the Competing Risk of Mortality and Absolute Risk Estimations for All Outcomes

The associations between the CAA score and stroke and dementia slightly attenuated after correcting for the competing risk of death (**Table 5**).

For all outcomes over 10 years, higher CAA scores noted increased risk estimates (**Figure 4**).

Subgroup and sensitivity analyses are presented in the online **Supplementary Material**.

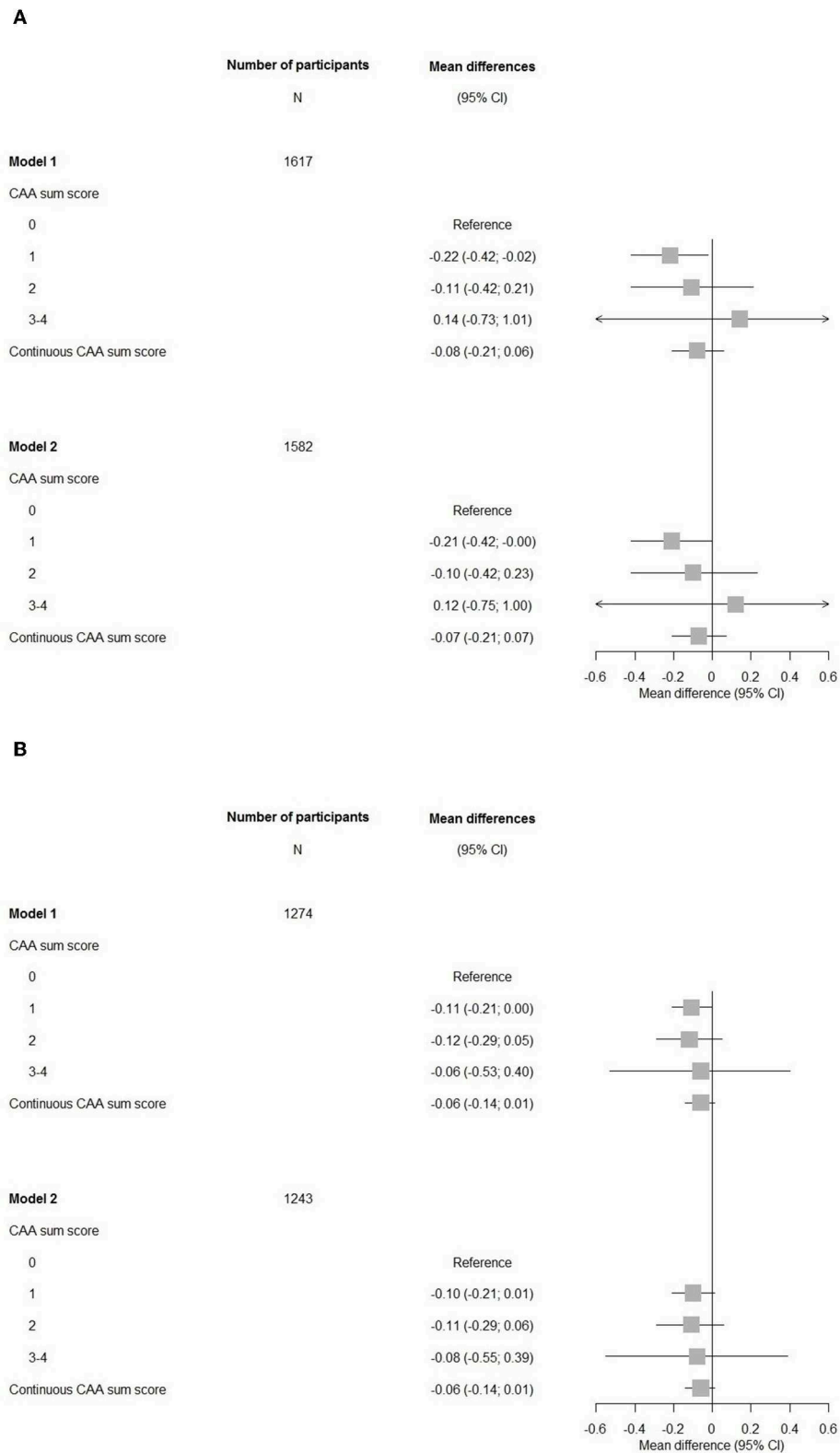
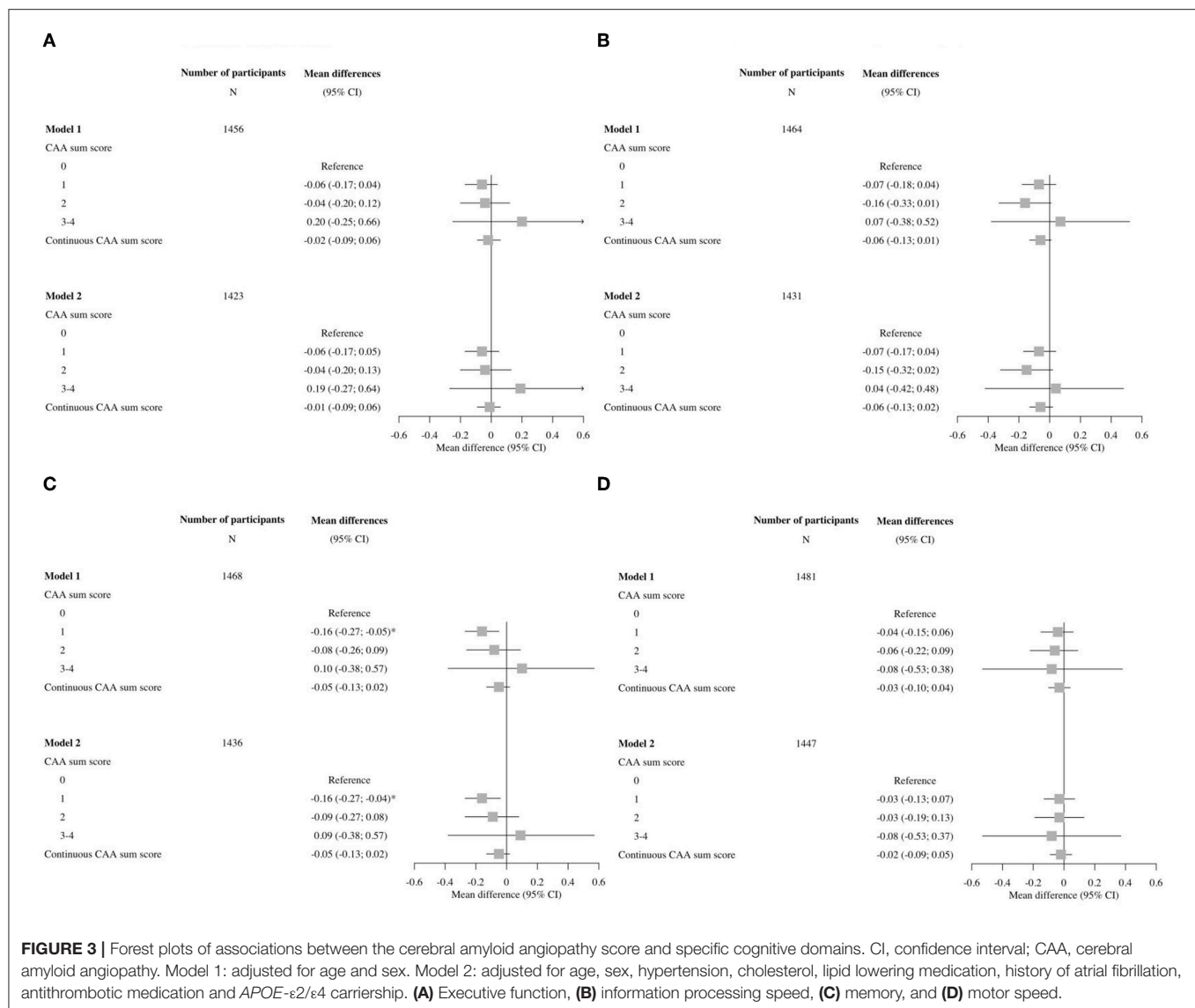


FIGURE 2 | Forest plots of associations between the cerebral amyloid angiopathy score and cognitive measures. CI, confidence interval; CAA, cerebral amyloid angiopathy. Model 1: adjusted for age and sex. Model 2: adjusted for age, sex, hypertension, cholesterol, lipid lowering medication, history of atrial fibrillation, antithrombotic medication, and *APOE*- $\epsilon 2/\epsilon 4$ carriership. **(A)** Mini-Mental State Examination. **(B)** G-factor.



DISCUSSION

We found that a higher imaging-based CAA score relates to cognitive impairment and a higher risk of stroke, dementia, and mortality in our community-dwelling population. Our study is the first study to apply the proposed CAA sum score in a non-diseased population.

Previous studies have investigated the CAA score in patients with CAA (or probable CAA), ischemic cardioembolic stroke, or TIA with non-valvular atrial fibrillation (14–18). Patients with an ischemic cardioembolic stroke or TIA with atrial fibrillation were also more likely to have higher CAA scores and persistent cognitive impairment over a 12-month period (18). They found the CAA score to be associated to cognitive impairment, although the sample size of the study was small ($N = 117$). We found a relation with having a CAA score of 1 and a significant lower MMSE and a significant impairment of the memory domain with

a trend of an increasing CAA score leading to a lower g-factor. Even though these observations were cross-sectional and overall not significant, they were in the direction of our hypothesis. Lower test scores for memory, executive function and processing speed have previously been described in patients with CAA without dementia (40). The pattern we observed for cognitive impairment in our population could have several explanations. Application of the CAA score to a general population could reflect non-CAA etiology compared to applying the score in a population with CAA patients and not lead to the expected pattern of cognitive impairment as seen in CAA pathology. Another explanation could be the long latency period of CAA for cognitive changes in a subclinical population.

In our study, of all the outcomes, dementia had the strongest association with the CAA score after adjusting for cardiovascular factors and *APOE*- $\epsilon 2/\epsilon 4$ carriership [HR 3.25, 95% CI (1.00–10.54)]. The study by Banerjee et al. (18) also examined the

TABLE 2 | The association of the cerebral amyloid angiopathy score with stroke, dementia, and mortality.

	N	n	Stroke HR (95%CI)	n	Dementia HR (95%CI)	n	Mortality HR (95%CI)
Model 1							
CAA score							
0	666	14	1.00 (reference)	20	1.00 (reference)	76	1.00 (reference)
1	753	38	2.22 (1.17–4.21)*	45	1.45 (0.83–2.51)	162	1.34 (1.00–1.78)*
2	185	9	2.08 (0.86–5.02)	8	0.86 (0.37–2.02)	53	1.66 (1.15–2.40)*
3–4	18	1	2.04 (0.26–15.95)	4	4.61 (1.51–14.08)*	7	1.70 (0.77–3.74)
Continuous CAA score	1,622	62	1.41 (0.99–2.00)	77	1.19 (0.86–1.65)	298	1.26 (1.07–1.48)*
Model 2[‡]							
CAA score							
0	651	13	1.00 (reference)	18	1.00 (reference)	75	1.00 (reference)
1	738	38	2.18 (1.13–4.22)*	44	1.52 (0.85–2.72)	160	1.28 (0.96–1.71)
2	180	9	2.01 (0.82–4.92)	8	0.90 (0.38–2.15)	51	1.49 (1.02–2.17)*
3–4	18	1	1.48 (0.18–11.89)	4	3.25 (1.00–10.54)*	7	1.34 (0.60–3.00)
Continuous CAA score	1,587	61	1.33 (0.93–1.89)	74	1.16 (0.84–1.60)	293	1.18 (1.00–1.39)*

N, number of participants; n, number of events; HR, hazard ratio; CI, confidence interval; CAA, cerebral amyloid angiopathy.

Model 1: adjusted for age and sex.

Model 2: adjusted for age, sex, hypertension, cholesterol, lipid lowering medication, history of atrial fibrillation, antithrombotic medication, and APOE-ε2/ε4 carriership.

[‡]Data missing for APOE-ε2/ε4 carriership n = 35.

*P < 0.05.

TABLE 3 | The association of cerebral amyloid angiopathy score excluding cortical superficial siderosis with stroke, dementia and mortality.

	N	n	Stroke HR (95%CI)	n	Dementia HR (95%CI)	n	Mortality HR (95%CI)
Model 1							
CAA score excluding cSS							
0	667	15	1.00 (reference)	20	1.00 (reference)	77	1.00 (reference)
1	755	38	2.05 (1.09–3.82)*	45	1.44 (0.83–2.50)	162	1.32 (0.99–1.75)
2–3	200	9	1.73 (0.72–4.12)	12	1.18 (0.56–2.53)	59	1.62 (1.13–2.32)*
Continuous CAA score excluding cSS	1,622	62	1.37 (0.94–2.02)	77	1.12 (0.79–1.59)	298	1.27 (1.07–1.52)*
Model 2[‡]							
CAA score excluding cSS							
0	652	14	1.00 (reference)	18	1.00 (reference)	76	1.00 (reference)
1	740	38	2.00 (1.05–3.80)*	44	1.50 (0.84–2.68)	160	1.26 (0.95–1.68)
2–3	195	9	1.60 (0.66–3.88)	12	1.18 (0.54–2.57)	57	1.43 (0.99–2.06)
Continuous CAA score excluding cSS	1,587	61	1.31 (0.89–1.94)	74	1.11 (0.78–1.59)	293	1.20 (1.00–1.44)

N, number of participants; n, number of events; HR, hazard ratio; CI, confidence interval; CAA, cerebral amyloid angiopathy; cSS, cortical superficial siderosis.

Model 1: adjusted for age and sex.

Model 2: adjusted for age, sex, hypertension, cholesterol, lipid lowering medication, history of atrial fibrillation, antithrombotic medication and APOE-ε2/ε4 carriership.

[‡]Data missing for APOE-ε2/ε4 carriership n = 35.

*P < 0.05.

cerebral small vessel disease (CSVD) score in patients with atrial fibrillation-related ischemic stroke or TIA. The CSVD score is a more well-known sum score to capture the global burden of small vessel disease in the brain (41). Previously, we also investigated the CSVD score in the general population and found that stroke was correlated strongest with this score amongst the

outcomes for stroke, dementia and mortality in our population [adjusted for the Framingham Stroke Risk Profile, HR 3.47 (1.33–9.06)] (42). Since it is hypothesized that composite scores reflect the overall disease burden better, this can indicate that different combinations of individual markers reflect different pathological mechanisms even when markers co-occur in the

TABLE 4 | The association of cerebral amyloid angiopathy MRI markers with stroke, dementia and mortality.

	<i>N</i>	<i>n</i>	Stroke HR (95%CI)	<i>n</i>	Dementia HR (95%CI)	<i>n</i>	Mortality HR (95%CI)
Strictly lobar cerebral microbleeds							
None ^a			1.00 (reference)		1.00 (reference)		1.00 (reference)
≥1, model 1	284	8	0.64 (0.30–1.34)	15	0.96 (0.54–1.70)	67	1.17 (0.89–1.54)
≥1, model 2 [†]	277	8	0.61 (0.29–1.30)	15	0.95 (0.54–1.69)	65	1.10 (0.83–1.46)
Cortical superficial siderosis							
None			1.00 (reference)		1.00 (reference)		1.00 (reference)
Present, model 1	10	3	7.11 (2.17–23.33)*	3	4.88 (1.51–15.78)*	8	2.66 (1.31–5.43)*
Present, model 2 [†]	10	3	5.49 (1.56–19.35)*	3	3.07 (0.90–10.42)	8	2.16 (1.03–4.54)*
Centrum semiovale perivascular spaces							
≤20			1.00 (reference)		1.00 (reference)		1.00 (reference)
≥21, model 1	73	4	1.34 (0.49–3.70)	5	1.19 (0.48–2.95)	20	1.18 (0.74–1.87)
≥21, model 2 [†]	72	4	1.27 (0.46–3.53)	5	1.14 (0.46–2.86)	20	1.18 (0.74–1.88)
White matter hyperintensities							
1st and 2nd quartiles			1.00 (reference)		1.00 (reference)		1.00 (reference)
3rd and 4th quartiles, model 1	811	44	2.29 (1.27–4.13)*	51	1.35 (0.81–2.25)	195	1.34 (1.04–1.72)*
3rd and 4th quartiles, model 2 [†]	794	44	2.19 (1.19–4.02)*	50	1.35 (0.79–2.30)	191	1.24 (0.96–1.60)

MRI, magnetic resonance imaging; *N*, number of participants; *n*, number of events; HR, hazard ratio; CI, confidence interval.

Model 1: adjusted for age and sex.

Model 2: adjusted for age, sex, hypertension, cholesterol, lipid lowering medication, history of atrial fibrillation, antithrombotic medication and APOE-ε2/ε4 carriership.

^aNone strictly microbleeds include no microbleeds and microbleeds at other locations like deep and infratentorial microbleeds.

[†]Data missing for APOE-ε2/ε4 carriership *n* = 35.

**P* < 0.05.

TABLE 5 | The association of cerebral amyloid angiopathy score with stroke and dementia after adjusting for the competing risk of mortality.

	<i>N</i>	<i>n</i>	Stroke sHR (95%CI)	<i>n</i>	Dementia sHR (95%CI)
Model 1					
CAA score					
0	666	14	1.00 (reference)	20	1.00 (reference)
1	753	38	2.19 (1.14–4.22)*	45	1.39 (0.78–2.47)
2	185	9	2.00 (0.81–4.95)	8	1.24 (0.34–1.95)
3–4	18	1	2.02 (0.27–15.37)	4	4.56 (1.30–16.07)
Continuous CAA score	1,622	62	1.39 (1.01–1.90)*	77	1.17 (0.81–1.67)
Model 2[†]					
CAA score					
0	651	13	1.00 (reference)	18	1.00 (reference)
1	738	38	2.17 (1.09–4.30)*	44	1.46 (0.79–2.69)
2	180	9	1.93 (0.77–4.84)	8	0.85 (0.34–2.12)
3–4	18	1	1.59 (0.21–12.09)	4	3.40 (0.87–13.29)
Continuous CAA score	1,587	61	1.32 (0.96–1.82)	74	1.14 (0.80–1.64)

N, number of participants; *n*, number of events; sHR, subdistribution hazard ratio; CI, confidence interval; CAA, cerebral amyloid angiopathy.

Model 1: adjusted for age and sex.

Model 2: adjusted for age, sex, hypertension, cholesterol, lipid lowering medication, history of atrial fibrillation, antithrombotic medication and APOE-ε2/ε4 carriership.

[†]Data missing for APOE-ε2/ε4 carriership *n* = 35.

**P* < 0.05.

disease spectrum. CSVD is a spectrum referring to a group of pathological processes with different mechanisms affecting small arteries, veins and capillaries in the brain (43). Since these pathologies partially co-occur and lead to similar markers in different types of CSVD, there might be an overlap between CSVD types and with CSVD and CAA scores and we might not capture the pure disease type. Yet, depending on the setting, to distinguish the pure disease type would be more desirable for a clinical setting and to capture broad CSVD would be more useful in a population-based setting. Conversely, CSVD, and CAA scores are more likely to reach a ceiling effect within patient populations, losing the granularity of individual markers, whereas in a population-based setting they may better capture the cumulative effect and variability of subclinical disease. Another way these scores could assist, is to detangle individual and shared underlying mechanisms of CSVD biomarkers. Moreover, reliable identification of asymptomatic CSVD with specific markers could aid in selecting high risk individuals, monitoring CSVD progression and predicting conversion of individuals from asymptomatic to symptomatic CSVD (44).

Interestingly, we found no relation of strictly lobar microbleeds with stroke and dementia, whereas we previously found this in a larger population with microbleeds (23, 24). There are several possible explanations for this. Firstly, the definitions used for microbleeds differ, i.e., we separately categorized strictly lobar microbleeds in the current study whereas in previous studies “CAA-related” microbleeds were defined, which include lobar microbleeds with or without cerebellar microbleeds.

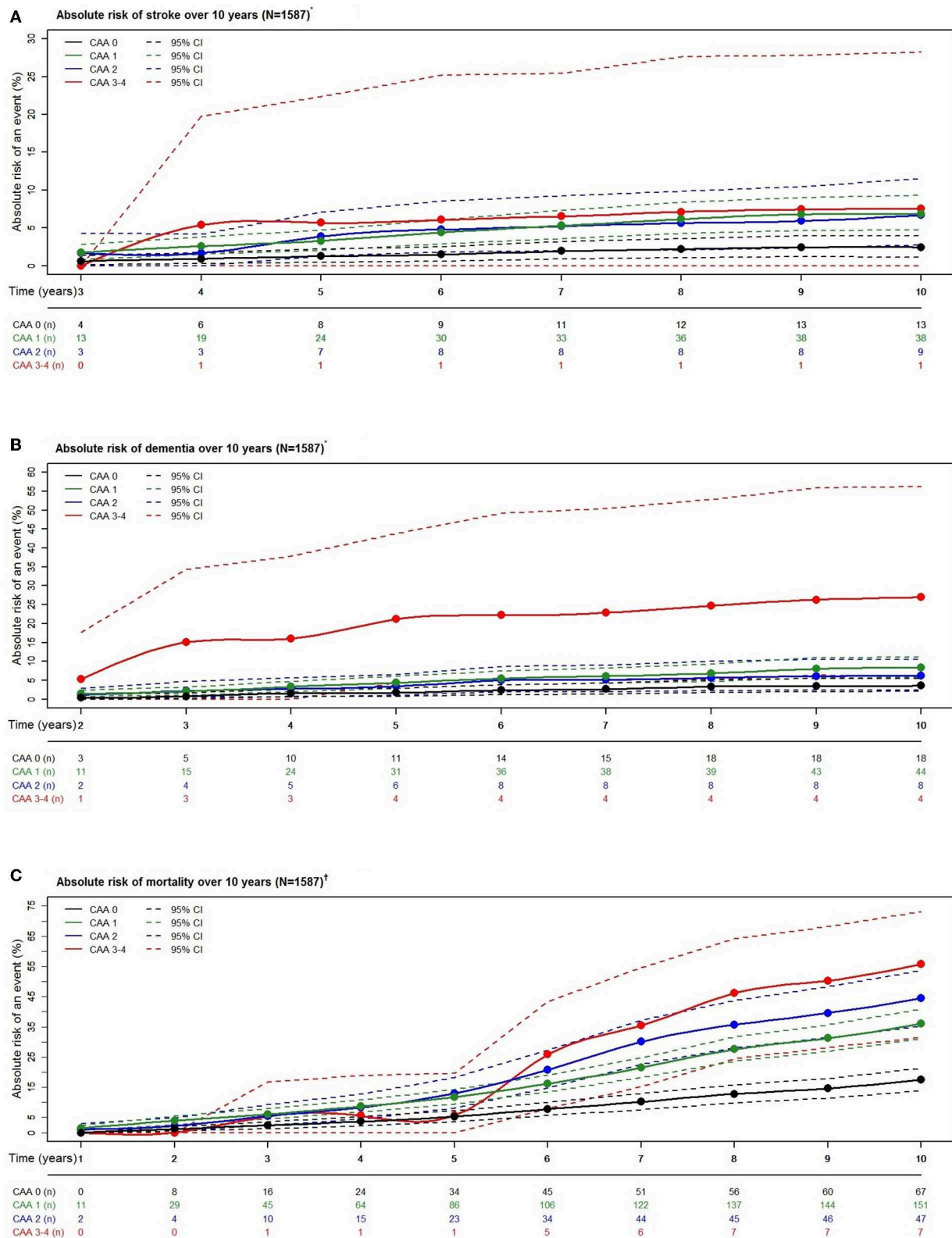


FIGURE 4 | Absolute risk estimates of stroke (A), dementia (B), and mortality (C) according to cerebral amyloid angiopathy score category over a period of 10 years. N, number of participants; n, number of events. *Estimates calculated with competing risk modeling. †Estimates calculated with Cox modeling. ††Adjusted for age, sex, hypertension, cholesterol, lipid lowering medication, history of atrial fibrillation, antithrombotic medication, and APOE-ε2/ε4 carriership.

Secondly, we observed a small number of events per outcome for the presence of strictly lobar microbleeds. The third explanation is that microbleeds might be more acute markers and its subclinical impact varies over time. Another study found that while presence of strictly lobar microbleeds reflects CAA in individuals without intracerebral hemorrhage, the diagnostic accuracy of lobar microbleeds in the general population was limited (45).

The modified Boston criteria are diagnostic criteria often used in clinical practice and applied to identify other CAA biomarkers in research (5). Application of these criteria in a non-selected population should not be compared to its use in a clinical setting, but we consider it of value to compare the performance of the CAA score to the modified Boston criteria in terms of risk prediction. In our population-based study, we found that the CAA score estimated the relative risks for major neurological outcomes and death better than the modified Boston criteria. Recently, a review that summarized the validation of the Boston criteria for probable CAA concluded that in a community-based cohort the sensitivity was very low relative to hospital-based cohorts (5, 45). This finding assumes that the current set of criteria is insufficient to adequately identify probable CAA in a subclinical setting. Presumably, CAA pathology has a latent period during which CAA-related damage advances prior to becoming severe enough to be diagnosed (5). Improving the Boston criteria by incorporating non-hemorrhagic imaging markers to better reflect CAA pathology on imaging is currently a key issue for the future directions in diagnosis of CAA (2, 5). Examples of such imaging markers are CSO-PVS, WMH and cortical microinfarcts, or more advanced imaging markers derived from diffusion tensor imaging (5, 7). The diagnostic accuracy of the CAA score in combination with pathological verification and the added value of new markers should be evaluated to establish its practical use in research and in clinics.

The strengths of our study are the longitudinal population-based design and extensive data collection. However, several limitations should also be considered. First, the CAA sum score proposed by Charimidou et al. (14) used visual ratings of WMH, whereas we used quantitative WMH volumes. Despite this, quantitative and qualitative WMH assessments have been shown to be acceptable in a population-based setting (46). Although, we used our volumetric WMH data to approximate the Fazekas scale, for clinical use a semi-quantitative rating with the Fazekas scale would be more practical, as described in the original CAA score (14, 47). Second, our CAA score was defined as a simple addition of dichotomized imaging markers with certain thresholds, which presume arbitrary cut-offs and may not reflect true biological processes. Specifically, cut-offs based on counts could depend on imaging techniques or scanner parameters, for example markers like CMB and PVS. Potentially, using other methods to combine imaging biomarkers, e.g., using machine learning techniques, could have led to more informative markers and increased statistical power. Yet, point-based scores such as the CAA sum score are likely to be more practical in clinical and trial settings. Third, the CAA score had an uneven distribution with fewer

events in participants with CAA scores of 3–4 due to the small numbers of events in the long-term follow-up. Fourth, we investigated cognitive deterioration in a cross-sectional design with MMSE and g-factor which are crude global measures of cognition. Longitudinal research will provide more robust results and gain more insight in these findings. Also, healthier participants without subjective memory complaints are more likely to receive cognitive retesting during the study follow-up which may have led to selection bias and influenced our results. Nonetheless, in that case our results presumptively would be biased toward the null. Fifth, although we aimed to address potential confounders based on the literature, residual confounding and unmeasured confounders may have affected our results to some extent. Sixth, a definitive diagnosis of CAA relies on pathological examination, yet obtaining pathological confirmation was not feasible in our population-based setting. Lastly, the majority of our population is Caucasian and generalizability of our study results to other ethnicities is therefore limited.

CONCLUSIONS

The results of this study in a community-dwelling population indicate that a higher CAA score is related to cognitive impairment and a higher risk of stroke, dementia, and mortality. Our findings suggest that the practical use of the CAA score to quantify the severity of vascular brain injury in an elderly population could further assist etiologic or predictive research purposes. Further evaluation of the score is needed to establish its application in clinical practice.

DATA AVAILABILITY STATEMENT

Data can be obtained upon request. Requests should be directed toward the management team of the Rotterdam Study (secretariat.epi@erasmusmc.nl), which has a protocol for approving data requests. Because of restrictions based on privacy regulations and informed consent of the participants, data cannot be made freely available in a public repository.

ETHICS STATEMENT

The studies involving human participants were reviewed and approved by The institutional review board (Medical Ethics Committee) approved the Rotterdam Study according to the Population Study Act, executed by the Ministry of Health, Welfare and Sports of the Netherlands. The participants provided their written informed consent to participate in this study.

AUTHOR CONTRIBUTIONS

PY, AC, AV, and MV: conception and design of the research. PY, MKI, MAI, and MV: acquisition of the data. PY, MAI, AC, AV, and MV: analysis and interpretation of the data. PY: drafting the manuscript. PY, MAI, MKI, WN, AV, AC, and MV: critical revision of the manuscript. PY, MAI, MKI,

WN, AV, AC, and MV: final approval of the version to be published.

FUNDING

The Rotterdam Study was supported by the Erasmus MC and Erasmus University Rotterdam; the Netherlands Organization for Scientific Research; the Netherlands Organization for Health Research and Development; the Research Institute for Diseases in the Elderly; the Netherlands Genomics Initiative; the Ministry of Education, Culture and Science; the Ministry of Health Welfare

and Sports; the European Commission; and the Municipality of Rotterdam. The funding sources had no involvement in the collection, analysis, writing, interpretation, or the decision to submit the paper for publication.

SUPPLEMENTARY MATERIAL

The Supplementary Material for this article can be found online at: <https://www.frontiersin.org/articles/10.3389/fneur.2019.01276/full#supplementary-material>

REFERENCES

- Charidimou A, Boulouis G, Gurol ME, Ayata C, Bacskaï BJ, Frosch MP, et al. Emerging concepts in sporadic cerebral amyloid angiopathy. *Brain*. (2017) 140:1829–50. doi: 10.1093/brain/awx047
- Banerjee G, Carare R, Cordonnier C, Greenberg SM, Schneider JA, Smith EE, et al. The increasing impact of cerebral amyloid angiopathy: essential new insights for clinical practice. *J Neurol Neurosurg Psychiatry*. (2017) 88:982–94. doi: 10.1136/jnnp-2016-314697
- Wermer MJH, Greenberg SM. The growing clinical spectrum of cerebral amyloid angiopathy. *Curr Opin Neurol*. (2018) 31:28–35. doi: 10.1097/WCO.0000000000000510
- Boyle PA, Yu L, Nag S, Leurgans S, Wilson RS, Bennett DA, et al. Cerebral amyloid angiopathy and cognitive outcomes in community-based older persons. *Neurology*. (2015) 85:1930–6. doi: 10.1212/WNL.0000000000002175
- Greenberg SM, Charidimou A. diagnosis of cerebral amyloid angiopathy: evolution of the boston criteria. *Stroke*. (2018) 49:491–7. doi: 10.1161/STROKEAHA.117.016990
- Wardlaw JM, Smith EE, Biessels GJ, Cordonnier C, Fazekas F, Frayne R, et al. Neuroimaging standards for research into small vessel disease and its contribution to ageing and neurodegeneration. *Lancet Neurol*. (2013) 12:822–38. doi: 10.1016/S1474-4422(13)70124-8
- Boulouis G, Charidimou A, Greenberg SM. Sporadic cerebral amyloid angiopathy: pathophysiology, neuroimaging features, and clinical implications. *Semin Neurol*. (2016) 36:233–43. doi: 10.1055/s-0036-1581993
- Vernooij MW, Ikram MA, Hofman A, Krestin GP, Breteler MMB, van der Lugt A. Superficial siderosis in the general population. *Neurology*. (2009) 73:202–5. doi: 10.1212/WNL.0b013e3181ae7c5e
- Charidimou A, Linn J, Vernooij MW, Opherk C, Akoudad S, Baron JC, et al. Cortical superficial siderosis: detection and clinical significance in cerebral amyloid angiopathy and related conditions. *Brain*. (2015) 138:2126–39. doi: 10.1093/brain/awv162
- Wollenweber FA, Baykara E, Zedde M, Gesierich B, Achmüller M, Jouvent E, et al. Cortical superficial siderosis in different types of cerebral small vessel disease. *Stroke*. (2017) 48:1404–7. doi: 10.1161/STROKEAHA.117.016833
- Yates PA, Villemagne VL, Ellis KA, Desmond PM, Masters CL, Rowe CC. Cerebral microbleeds: a review of clinical, genetic, and neuroimaging associations. *Front Neurol*. (2014) 4:205. doi: 10.3389/fneur.2013.00205
- Gutierrez J, Elkind MSV, Dong C, Di Tullio M, Rundek T, Sacco RL, et al. Brain perivascular spaces as biomarkers of vascular risk: results from the northern manhattan study. *AJNR Am J Neuroradiol*. (2017) 38:862–7. doi: 10.3174/ajnr.A5129
- DeBette S, Markus HS. The clinical importance of white matter hyperintensities on brain magnetic resonance imaging: systematic review and meta-analysis. *BMJ*. (2010) 341:c3666. doi: 10.1136/bmj.c3666
- Charidimou A, Martinez-Ramirez S, Reijmer YD, Oliveira-Filho J, Lauer A, Roongpiboonsopit D, et al. Total magnetic resonance imaging burden of small vessel disease in cerebral amyloid angiopathy: an imaging-pathologic study of concept validation. *JAMA Neurol*. (2016) 73:994–1001. doi: 10.1001/jamaneurol.2016.0832
- Xiong L, Boulouis G, Charidimou A, Roongpiboonsopit D, Jessel MJ, Pasi M, et al. Dementia incidence and predictors in cerebral amyloid angiopathy patients without intracerebral hemorrhage. *J Cereb Blood Flow Metab*. (2018) 38:241–9. doi: 10.1177/0271678X17700435
- Valenti R, Reijmer YD, Charidimou A, Boulouis G, Martinez SR, Xiong L, et al. Total small vessel disease burden and brain network efficiency in cerebral amyloid angiopathy. *J Neurol Sci*. (2017) 382:10–2. doi: 10.1016/j.jns.2017.09.015
- Boulouis G, Charidimou A, Jessel MJ, Xiong L, Roongpiboonsopit D, Fotiadis P, et al. Small vessel disease burden in cerebral amyloid angiopathy without symptomatic hemorrhage. *Neurology*. (2017) 88:878–84. doi: 10.1212/WNL.0000000000003655
- Banerjee G, Chan E, Ambler G, Wilson D, Cipolotti L, Shakeshaft C, et al. Effect of small-vessel disease on cognitive trajectory after atrial fibrillation-related ischaemic stroke or TIA. *J Neurol*. (2019) 266:1250–9. doi: 10.1007/s00415-019-09256-6
- Vernooij MW, van der Lugt A, Ikram MA, Wielopolski PA, Niessen WJ, Hofman A, et al. Prevalence and risk factors of cerebral microbleeds: the Rotterdam scan study. *Neurology*. (2008) 70:1208–14. doi: 10.1212/01.wnl.0000307750.41970.d9
- Sveinbjornsdottir S, Sigurdsson S, Aspelund T, Kjartansson O, Eiriksdottir G, Valtysdottir B, et al. Cerebral microbleeds in the population based AGES-Reykjavik study: prevalence and location. *J Neurol Neurosurg Psychiatry*. (2008) 79:1002–6. doi: 10.1136/jnnp.2007.121913
- Arvanitakis Z, Leurgans SE, Wang Z, Wilson RS, Bennett DA, Schneider JA. Cerebral amyloid angiopathy pathology and cognitive domains in older persons. *Ann Neurol*. (2011) 69:320–7. doi: 10.1002/ana.22112
- Yu L, Boyle PA, Nag S, Leurgans S, Buchman AS, Wilson RS, et al. APOE and cerebral amyloid angiopathy in community-dwelling older persons. *Neurobiol Aging*. (2015) 36:2946–53. doi: 10.1016/j.neurobiolaging.2015.08.008
- Akoudad S, Portegies MLP, Koudstaal PJ, Hofman A, van der Lugt A, Ikram MA, et al. Cerebral microbleeds are associated with an increased risk of stroke the Rotterdam study. *Circulation*. (2015) 132:509–16. doi: 10.1161/CIRCULATIONAHA.115.016261
- Akoudad S, Wolters FJ, Viswanathan A, de Bruijn RF, van der Lugt A, Hofman A, et al. Association of cerebral microbleeds with cognitive decline and dementia. *JAMA Neurol*. (2016) 73:934–43. doi: 10.1001/jamaneurol.2016.1017
- Akoudad S, Ikram MA, Koudstaal PJ, Hofman A, van der Lugt A, Vernooij MW. Cerebral microbleeds and the risk of mortality in the general population. *Eur J Epidemiol*. (2013) 28:815–21. doi: 10.1007/s10654-013-9854-3
- Ding J, Sigurdsson S, Jonsson PV, Eiriksdottir G, Meirelles O, Kjartansson O, et al. Space and location of cerebral microbleeds, cognitive decline, and dementia in the community. *Neurology*. (2017) 88:2089–97. doi: 10.1212/WNL.0000000000003983
- Ikram MA, Brusselle GGO, Murad SD, van Duijn CM, Franco OH, Goedegeure A, et al. The Rotterdam study: 2018 update on objectives, design and main results. *Eur J Epidemiol*. (2017) 32:807–50. doi: 10.1007/s10654-017-0321-4
- Ikram MA, van der Lugt A, Niessen WJ, Koudstaal PJ, Krestin GP, Hofman A, et al. The Rotterdam scan study: design update 2016 and main findings. *Eur J Epidemiol*. (2015) 30:1299–315. doi: 10.1007/s10654-015-0105-7

29. Adams HH, Hilal S, Schwingenschuh P, Wittfeld K, van der Lee SJ, DeCarli C, et al. A priori collaboration in population imaging: the uniform neuro-imaging of Virchow-Robin spaces enlargement consortium. *Alzheimers Dement (Amst)*. (2015) 1:513–20. doi: 10.1016/j.dadm.2015.10.004
30. Doubal FN, MacLulich AM, Ferguson KJ, Dennis MS, Wardlaw JM. Enlarged perivascular spaces on MRI are a feature of cerebral small vessel disease. *Stroke*. (2010) 41:450–4. doi: 10.1161/STROKEAHA.109.564914
31. de Boer R, Vrooman HA, Ikram MA, Vernooij MW, Breteler MM, van der Lugt A, et al. Accuracy and reproducibility study of automatic MRI brain tissue segmentation methods. *Neuroimage*. (2010) 51:1047–56. doi: 10.1016/j.neuroimage.2010.03.012
32. Wieberdink RG, Ikram MA, Hofman A, Koudstaal PJ, Breteler MM. Trends in stroke incidence rates and stroke risk factors in Rotterdam, the Netherlands from 1990 to 2008. *Eur J Epidemiol*. (2012) 27:287–95. doi: 10.1007/s10654-012-9673-y
33. de Bruijn RF, Bos MJ, Portegies ML, Hofman A, Franco OH, Koudstaal PJ, et al. The potential for prevention of dementia across two decades: the prospective, population-based Rotterdam study. *BMC Med*. (2015) 13:132. doi: 10.1186/s12916-015-0377-5
34. Fine JP, Gray RJ. A proportional hazards model for the subdistribution of a competing risk. *J Am Stat Assoc*. (1999) 94:496–509. doi: 10.1080/01621459.1999.10474144
35. Gray B. *Subdistribution Analysis of Competing Risks*. Version 2.2–7. Vienna: R Foundation for Statistical Computing.
36. Gerds TA, Blanche P, Mortensen R, Tollenaar N, Brusch Mogensen U, Ozenne B. *Risk Regression Models and Prediction Scores for Survival Analysis With Competing Risks*. Version 1.4.3. Vienna: R Foundation for Statistical Computing.
37. Inoue E. *NRI for Risk Prediction Models with Time to Event and Binary Response Data*. Version 1.4. Vienna: R Foundation for Statistical Computing.
38. R Core Team. *R: A Language and Environment for Statistical Computing*. Vienna: R Foundation for Statistical Computing (2019).
39. von Elm E, Altman DG, Egger M, Pocock SJ, Gøtzsche PC, Vandenbroucke JP. The strengthening of reporting of observational studies in epidemiology (STROBE) statement: guidelines for reporting observational studies. *Lancet*. (2007) 370:1453–7. doi: 10.1016/S0140-6736(07)61602-X
40. Case NF, Charlton A, Zwiers A, Batool S, McCreary CR, Hogan DB, et al. Cerebral amyloid angiopathy is associated with executive dysfunction and mild cognitive impairment. *Stroke*. (2016) 47:2010–6. doi: 10.1161/STROKEAHA.116.012999
41. Staals J, Booth T, Morris Z, Bastin ME, Gow AJ, Corley J, et al. Total MRI load of cerebral small vessel disease and cognitive ability in older people. *Neurobiol Aging*. (2015) 36:2806–11. doi: 10.1016/j.neurobiolaging.2015.06.024
42. Yilmaz P, Ikram MK, Niessen WJ, Ikram MA, Vernooij MW. Practical small vessel disease score relates to stroke, dementia, and death the Rotterdam study. *Stroke*. (2018) 49:2857–65. doi: 10.1161/STROKEAHA.118.022485
43. Pantoni L. Cerebral small vessel disease: from pathogenesis and clinical characteristics to therapeutic challenges. *Lancet Neurol*. (2010) 9:689–701. doi: 10.1016/S1474-4422(10)70104-6
44. Das AS, Regenhardt RW, Vernooij MW, Blacker D, Charidimou A, Viswanathan A. Asymptomatic cerebral small vessel disease: insights from population-based studies. *J Stroke*. (2019) 21:121–38. doi: 10.5853/jos.2018.03608
45. Martinez-Ramirez S, Romero JR, Shoamanesh A, McKee AC, Van Etten E, Pontes-Neto O, et al. Diagnostic value of lobar microbleeds in individuals without intracerebral hemorrhage. *Alzheimers Dement*. (2015) 11:1480–8. doi: 10.1016/j.jalz.2015.04.009
46. Valdes Hernandez Mdel C, Morris Z, Dickie DA, Royle NA, Munoz Maniega S, Aribisala BS, et al. Close correlation between quantitative and qualitative assessments of white matter lesions. *Neuroepidemiology*. (2013) 40:13–22. doi: 10.1159/000341859
47. Fazekas F, Chawluk JB, Alavi A, Hurtig HI, Zimmerman RA. MR signal abnormalities at 1.5 T in Alzheimer's dementia and normal aging. *AJR Am J Roentgenol*. (1987) 149:351–6. doi: 10.2214/ajr.149.2.351

Conflict of Interest: The authors declare that the research was conducted in the absence of any commercial or financial relationships that could be construed as a potential conflict of interest.

Copyright © 2019 Yilmaz, Ikram, Ikram, Niessen, Viswanathan, Charidimou and Vernooij. This is an open-access article distributed under the terms of the Creative Commons Attribution License (CC BY). The use, distribution or reproduction in other forums is permitted, provided the original author(s) and the copyright owner(s) are credited and that the original publication in this journal is cited, in accordance with accepted academic practice. No use, distribution or reproduction is permitted which does not comply with these terms.

Advantages of publishing in Frontiers



OPEN ACCESS

Articles are free to read
for greatest visibility
and readership



FAST PUBLICATION

Around 90 days
from submission
to decision



HIGH QUALITY PEER-REVIEW

Rigorous, collaborative,
and constructive
peer-review



TRANSPARENT PEER-REVIEW

Editors and reviewers
acknowledged by name
on published articles

Frontiers

Avenue du Tribunal-Fédéral 34
1005 Lausanne | Switzerland

Visit us: www.frontiersin.org

Contact us: info@frontiersin.org | +41 21 510 17 00



REPRODUCIBILITY OF RESEARCH

Support open data
and methods to enhance
research reproducibility



DIGITAL PUBLISHING

Articles designed
for optimal readership
across devices



FOLLOW US

@frontiersin



IMPACT METRICS

Advanced article metrics
track visibility across
digital media



EXTENSIVE PROMOTION

Marketing
and promotion
of impactful research



LOOP RESEARCH NETWORK

Our network
increases your
article's readership